Part I. Tectonic Evolution of the Northern Gulf of California, Mexico, Deduced from Conjugate Rifted Margins of the Upper Delfín Basin
Part II. Active Folding and Seismic Hazard in Central Los Angeles, California

Thesis by

Michael E. Oskin

In Partial Fulfillment of the Requirements

for the Degree of

Doctor of Philosophy

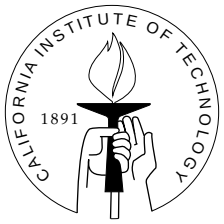

California Institute of Technology

Pasadena, California

2002

(Submitted October 9, 2001)

Acknowledgments

Caltech is a strange, intense, and exceptional place, full of really great people, many of whom I owe a great debt of gratitude. The California Institute of Technology and especially the Division of Geological and Planetary Sciences are unparalleled places to pursue scientific discovery. I would like to thank the community here for the collective effort that makes this such a special place.

I would foremost like to thank my advisors, Joann Stock and Kerry Sieh, who have guided, supported and inspired me through my development as a scientist here at Caltech. It would be impossible here to thank Joann and Kerry for everything that they have done for me over these past six years. If I were to select an experience from each, however, it would be the following. From Kerry, an infectious sense of excitement for scientific research and a commitment to a free exchange of ideas. From Joann, an appreciation for the many dimensions and implications of a scientific problem, and an unlimited capacity and inspiration for hard work–especially under the intense desert sun! From both Kerry and Joann, a great sense of humor, an open-door policy of advising, and many, many, many great conversations over the years. It has been a great pleasure to work with both of you.

There are many people without whom the work that has led to this thesis would have been impossible. Arturo Martín-Barajas has been an invaluable scientific colleague and sponsor of my field work in Mexico. I could not have begun to navigate the Canal de Infernillo (Little Hell Channel) to Isla Tiburón without the great efforts by Arturo to obtain permission every year, starting months in advance. Ernesto Molina-Villabosa has been my Cumcaác (Seri Indian) guide every year that I have worked on Isla Tiburón. I could not have approached fieldwork on the exposed, western coastline of the island without Ernesto's immense wisdom and skill as a boat pilot. Very simply, when the going got rough, Ernesto always knew what to do. My

life was in very good hands. Thank you, my friend.

Many people have assisted me with my fieldwork in northwest Mexico. Becky Oskin (then known as Becky Charlton) conducted initial reconnaissance of the Sonoran coastal area in 1997 with Joann Stock and Gordon Gastil. Claudia Lewis and Arturo accompanied me on the first reconnaissance trip to Isla Tiburón in 1998, where we identified much of the geology that comprises the core of this thesis. Claudia's encouragement (see quote) was greatly appreciated. Lesley Perg has been a frequent companion on my travels to the coastal desert of Baja California and Sonora since 1995. Together, we have endured many experiences, from the dangerous to the bizarre. Scott Dobner weathered three long months and over 4000 km of driving during my 1998 season of reconnaissance fieldwork over a 100 km length of both coastlines of the northern Gulf of California. Scott's endurance is amazing. Naomi Marks endured dawn-to-past-dark fieldwork in Baja California and each day wisely marked and then relocated our field vehicle by GPS in the dark. Matt Bachman, Robert Houston, and Jason Wise each endured weeks of dawn-to-dusk fieldwork under the blazing sun on Isla Tiburón and on the unpredictable waters of the Gulf of California. I also owe thanks to the Prescott College Field Station at Bahía Kino, Sonora–especially Ed Boyer and Tad Phister–who welcomed and guided me when I was a stranger to fieldwork in Sonora.

Many other colleagues at Caltech and elsewhere, too many to comprehensively list here, have contributed to the development of this thesis through their discussion, support, and friendship. This study is built on a strong foundation established by prior work in the Puertecitos Volcanic Province of Baja California by Arturo Martín, Claudia Lewis, Elizabeth Nagy, and Joann Stock. Discussions and samples provided by Claudia and Elizabeth Nagy and discussions with Joe Kirschvink, John Eiler, Jason Saleeby, and Brian Wernicke contributed greatly to the development of the data set and ideas presented here. I would like to thank Gary Axen, Lee Silver, Paul Umhoefer, Francisco Paz, Jaime Roldán-Quintana, Carlos Gonzales-León, Thierry Calmus, Martin Valencia, J.C. Ingle, Ana Luisa Carreño, Luis Delgado-Argote, Jorge

Ledesma, John Holt, Patricia Persaud, Jane Dmochowski, and probably many others for discussions of the Geology of the Gulf of California over the years. I would also like to thank the community of scientists at the Southern California Earthquake Center for collaboration on the problems of seismic hazard in the Los Angeles region– especially Andrew Meigs, Karl Mueller, Robert Yeats, John Shaw, Doug Yule, and others of the Geology group. Suefawn Barnett, Evelina Cui, Donna Sackett, Jean Grinols, Marcia Hudson, Carolyn Porter, and many others provided an efficient and invaluable support structure here at the Caltech GPS division. Terry Gennaro has expertly maintained field vehicles and equipment here and has gone through extra effort to accommodate my travels south of the border. Joanne Giberson and Tony Soeller provided a supportive environment at the Caltech GIS lab, and Jim O'Donnell has built one of the most amazing geology library collections at any university I have ever visited.

Finally, I am incredibly indebted to my friends and family, who have supported me through the long years of my education at U.C.L.A. and Caltech. I would like to thank my parents, Marilyn and Robert, for their love and unbending support. I would also like to thank my brothers, Mark and Peter, and my grandparents, Dorothy and Roy, for their love and inspiration. Lastly, I would like to express my deepest love and gratitude to my wife, Becky, who has stood closely by me through the years of hard work leading to this day. We have followed a long road from the our first days together here at Caltech as first-year graduate students. Of everything that I have gained during my time here, you, Becky, are by far and away the best.

Abstract

Part I of this thesis addresses the tectonic evolution of the Pacific–North America plate boundary through northwest Mexico and its implications for rifting processes. Offset ignimbrites support 255±10 km of opening across the Upper Delfín basin of the northern Gulf of California. Additional deformation from the continental margins supports 296±17 km total plate boundary displacement between coastal Sonora and the Main Gulf Escarpment in Baja California, of which at least 276±13 km occurred since ∼6 Ma. This strain history requires that the plate boundary localized into the the northern Gulf of California during latest Miocene time. Only a narrow width of upper continental crust foundered into the Upper Delfín basin, such that most of the crust between Isla Tiburón and Baja California must be new transitional oceanic crust and possibly lower continental crust contributed by inflow from the rift flanks. Extension of the margins of the Upper and Lower Delfín basins is <40% in most places, though the whole crustal column may have been thinned by a factor of two, further supporting that lower crustal flow has operated here. Opening of the Upper Delfín basin was accompanied by a steady or increased strain rate on its continental margins, contrary to the expected rheology of a narrow continental rift. Reevaluation of a critical deposit of marine rocks on Isla Tiburón indicates that initial marine incursion in the northern Gulf of California also occurred during latest Miocene time. Together, these records suggest that opening of the Upper Delfín basin was an abrupt event, accompanied by a localized zone of intense extension, marine incursion, and a rapid increase in strain rate. Continental rupture in the Upper Delfín basin does not appear to have been a response to crustal weakening by intracontinental extension, but rather may have resulted from a significant increase in strain rate, brought on by a change in boundary forces. Part II of this thesis develops methods to estimate seismic hazard from blind reverse faults by analysis of fault-related folding of Late

Quaternary strata, with application to the Elysian Park anticline of Los Angeles, California.

Contents

List of Tables

List of Figures

You can shoot me if they're different.

— *Claudia Lewis,*
During field reconnaissance of
ignimbrites on western Isla Tiburón.

Chapter 1

Introduction

1.1 Introduction

The Pacific-North America plate boundary of southwestern North America (Fig. 1.1) represents the most influential example of a continental transform margin. Early kinematic models of continental transform plate boundaries [*Larson et al.*, 1968; *Atwater*, 1970], translation of continental slivers [*Coney*, 1989], and the mechanics of continental transform systems [*Thatcher*, 1975] developed from the concentrated study of the geology of this margin. While a basic model for the development of the Pacific-North America transform plate boundary here remains well-accepted [*Atwater*, 1970], reconciliation is still often lacking between plate boundary deformation measured on the continents and plate movements recorded by seafloor spreading [*Stock and Molnar*, 1988]. Reconciliation of these records is possible with sufficient geologic records of continental strain, as shown for the Pacific-North America plate boundary of central California [*Dickinson and Wernicke*, 1997; *Atwater and Stock*, 1998]. Combination of continental and oceanic strain records such as these provides new insight into the role of continental crust in plate tectonics and the relationship between competing buoyancy and plate boundary forces that drive deformation of continental lithosphere. Closing the discrepancy between plate motions as measured from seafloor spreading and geological records of continental deformation thus addresses fundamental problems in the study of plate tectonics and continental dynamics.

The Pacific–North America plate boundary of southwestern North America also represents a premiere natural laboratory for the study of seismic hazards. Beginning with the recognition by *Reid* [1910] that the 1906 San Francisco earthquake was produced by motion on the San Andreas fault, many of the methods to evaluate these hazards have been developed through study of this plate boundary [*Sieh*, 1978; *Shaw and Shearer*, 1999, for example]. Neotectonic studies here have recognized the importance of diffuse continental deformation to the distribution of seismicity. A consequence of diffuse tectonic deformation is that minor faults with low strain rates, if located beneath urban areas, pose significant seismic hazards. Recent damaging

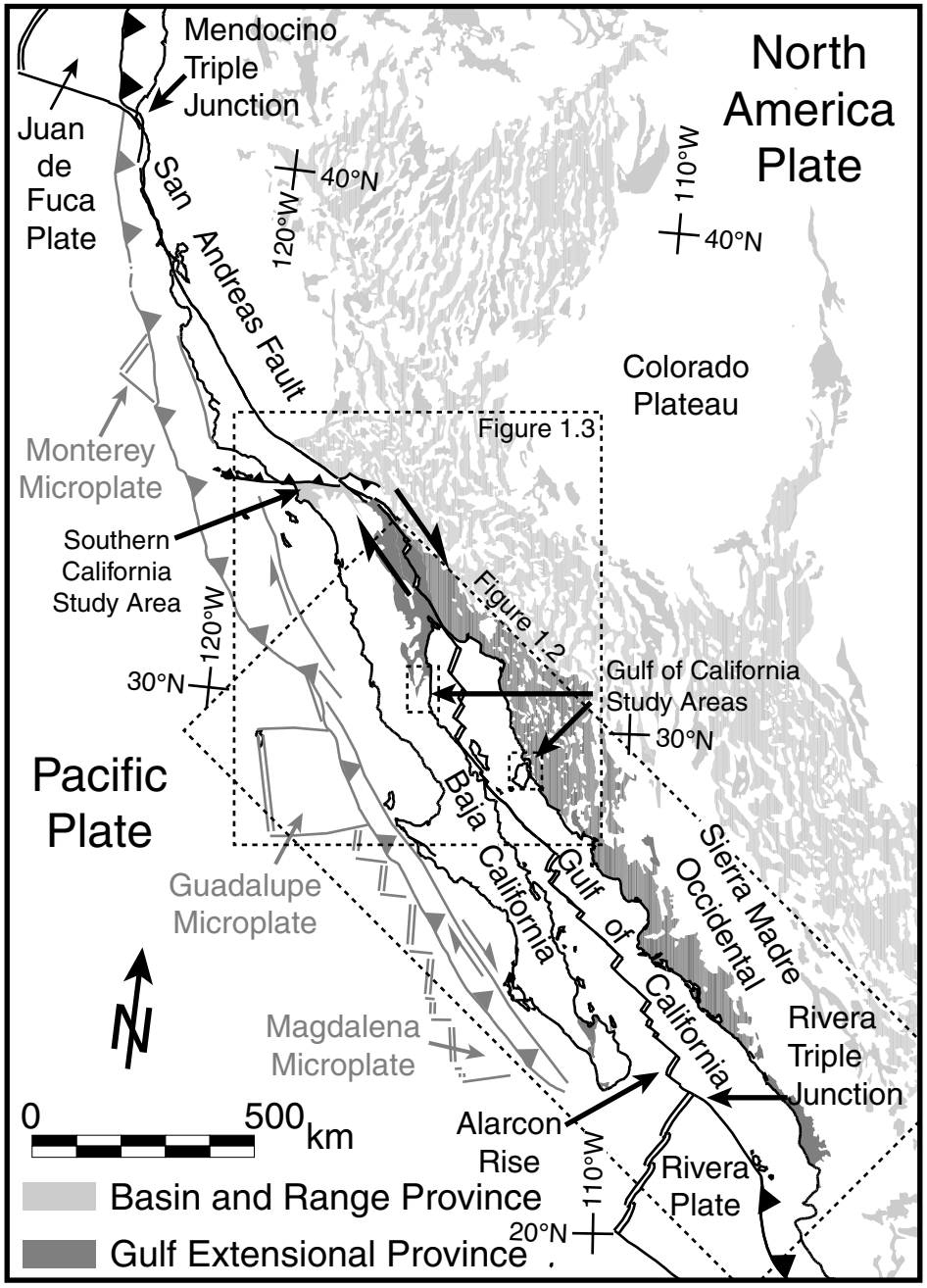

Figure 1.1. Tectonic map of southwestern North America. Derived from the Tectonic Map of North America [*Muehlberger et al.*, 1996]. Shaded areas represent basins of the Basin and Range province (light grey) and the Gulf Extensional Province (dark grey). Present-day plates and plate boundaries shown as dark lines. Inactive microplates and plate boundaries shown as grey lines.

large earthquakes on poorly characterized faults within the urban areas of California have underscored the need to fully account for a complex plate boundary zone to compute seismic hazard. Often, deformation rates are known to higher confidence than the locations of faults that accommodate this deformation [*Walls et al.*, 1998; *Argus et al.*, 1999].

1.2 Purpose of study

This thesis addresses two aspects of the geological constraint of crustal strain along the Pacific–North America plate boundary. Part I of this thesis addresses the development of the Pacific–North America plate boundary through southern California and northwest Mexico. In this region, the timing and amount of rifting of Baja California away from North America contributes a large part of the uncertainty in closure between the continental and seafloor records for Pacific–North America plate boundary motion. Tectonic reconstruction of the Gulf of California is currently limited by a dearth of youthful, high-precision cross-gulf tie points. This problem is addressed here with a new set of Mid to Late Miocene cross-gulf geologic tie points that constrain both the magnitude and rate of dextral shear in the Gulf. A set of four pyroclastic flow (ignimbrite) sequences, comprising nine separate cooling units, are correlated lithologically, geochemically, and paleomagnetically from the Puertecitos Volcanic Province of Baja California across the Gulf to Isla Tiburón and the adjacent coast of Sonora. Comparison of the distribution and facies of these ignimbrite sequences indicate a close match between opposing margins of the Gulf of California at ∼6 Ma and 12.6 Ma. These data provide new, independent constraints on the strain budget and kinematic development of the Pacific–North America plate boundary in the Gulf of California.

Part II of this thesis is a study of the neotectonic development of a reverse fault system beneath central Los Angeles, California (Fig. 1.1). Oblique convergence along the Pacific-North America plate boundary through the Transverse Ranges of southern

California is manifested here by secondary reverse faulting (Fig. 1.1). This study addresses a segment of this fault system where fault-related folding has obscured structures that accommodate compression. This analysis of fault-related folding of Late Quaternary strata overlying the Elysian Park anticline provides a direct measure of the rate and style of deformation of the otherwise inaccessible Elysian Park fault.

1.3 Geologic setting of the Pacific-North America plate boundary

1.3.1 Plate tectonic constraints

From Mesozoic until Middle Miocene time, the geology of southwestern North America was dominated by subduction of a series of oceanic plates west of California [*Atwater*, 1970]. During Oligocene time, the Farallon plate subducted eastward beneath North America, forming a continuous subduction zone from Canada through southern Mexico [*Atwater*, 1989]. Starting in earliest Miocene time, the Farallon-Pacific spreading center impinged on the western margin of North America, beginning at about the latitude of southern California [*Atwater*, 1970, approximately 34° on Fig. 1.1]. The intersection of these plates formed a pair of triple junctions bounding the newly formed Pacific-North America transform boundary. These triple junctions diverged by northwestward relative motion of the Pacific Plate and by progressive fragmentation and capture of pieces of the Farallon plate [*Atwater*, 1989]. Inactive remnants of some of these microplates remain now attached to the Pacific Plate offshore of central and Baja California (Fig. 1.1). During Early- to Mid-Miocene time, Pacific-North American transform motion was restricted to the coastal margin of southern California and northern Baja California [*Atwater*, 1989]. West of southern and central Baja California subduction of the Guadalupe and Magdelena microplates maintained a volcanic arc centered near the present-day eastern shore of the Gulf [*Hausback*, 1984]. Cessation of spreading at the Guadalupe-Pacific rise at

12.5 Ma marks the onset of the Pacific-North America transform boundary along the full length of Baja California [*Mammerickx and Klitgord*, 1982].

1.3.2 Opening of the Gulf of California

The Gulf of California currently forms the southern half of the Pacific–North America transform plate boundary between the Mendocino and Rivera triple junctions (Fig. 1.1). Initiation of the plate boundary in the Gulf of California followed cessation of subduction and microplate capture offshore of the Pacific coast of southern Baja California sometime after ∼12.5 Ma [*Lonsdale*, 1989]. However, only 300 to 350 km of the expected 500 to 600 km of transform offset between the Pacific and North American plates has been accommodated within the Gulf, with the remainder partitioned on faults west of Baja California [*Stock and Hodges*, 1989] and/or in the Mexican Basin and Range Province [*Gans*, 1997]. Transfer of Baja California to the Pacific Plate is evident by 3.5 Ma from the formation of magnetically lineated oceanic crust at the Alarcón Rise in the mouth of the Gulf (*Lonsdale* [1989]; Fig. 1.1). The timing, partitioning, and magnitude of plate boundary slip between 12.5 and 3.5 Ma, and any amount of pre-12.5 Ma strike-slip, is not constrained from within the Gulf of California or its surrounding extensional Province (Fig. 1.1).

In a plate tectonic context, faulting today within the Gulf of California represents a relatively mature stage of development of the Pacific–North America transform plate boundary. Early transform motion on this plate boundary was partitioned over a broad zone from the Pacific coast and continental borderland west of Baja California to the Basin and Range province of central Mexico [*Spencer and Normark*, 1979; *Stock and Hodges*, 1989, and Fig. 1.1]. Localization of plate boundary motion in the Gulf sometime after 12.5 Ma has led to oblique continental rifting and the formation of new ocean floor [*Lonsdale*, 1989, and Fig. 1.2]. The modern plate boundary in the Gulf of California is dominated by long transform faults separated by narrow submarine basins [*Lonsdale*, 1989, and Figs. 1.2 and 1.3]. Magnetic lineations in youthful oceanic crust forming at the Alarcón rise indicate that more than 95% of

Pacific–North America plate motion is currently accommodated on the Gulf fault system [*DeMets and Dixon*, 1999; *Dixon et al.*, 2000, and Fig. 1.2]. The northern and central gulf is characterized by thick sediment cover and complex patterns faults and magnetic anomalies [*Lonsdale*, 1991]. However, since most of the length of the Baja California Peninsula remains unfaulted during Tertiary time, the full rate of seafloor spreading at the Alarcón Rise must be translated northwestward through the Gulf of California fault systems [*Dickinson*, 1996].

With adequate geologic control, fundamental tectonic problems such as the role of pre-existing weaknesses and strain partitioning in localizing crustal deformation may be addressed from the geologic record in the Gulf of California. It remains unclear, however, whether localization of transform motion within the Gulf was a gradual process beginning at 12.5 Ma, or an abrupt transition some 5 to 7 Myr later. Commonly it has been assumed that Baja California was transferred to the Pacific Plate at or near the full plate motion rate, sufficient to open the Gulf at 5.5 to 6 Ma [*Curray et al.*, 1982; *Lonsdale*, 1989; *Dickinson*, 1996]. The evidence for these models is less than conclusive. Dextral displacement on the southern San Andreas fault system, and extension and marine deposition in the Gulf region began as early as 12 Ma [*Stock and Hodges*, 1989; *Weldon et al.*, 1993; *Lee et al.*, 1996; *Helenes and Carreño*, 1999]. Full Pacific-North America plate motion may not have been carried in the Gulf until 1 Ma [*DeMets*, 1995].

1.3.3 Existing cross-Gulf geologic tie points

Several basement geologic relationships indicate approximately 300 km of opening of the northern Gulf of California (Fig. 1.3). The oldest of these is a Paleozoic stratigraphic transition between miogeoclinal and eugeoclinal facies at the southwestern margin of North America. *Gastil et al.* [1991] correlated a southeast-trending facies transition in northeastern Baja California with a similar-aged east-trending transition in southern Sonora. Detailed correlation of this transition is complicated by intrusion of the Peninsular Ranges Batholith, tectonic intercalation of syn-batholithic strata

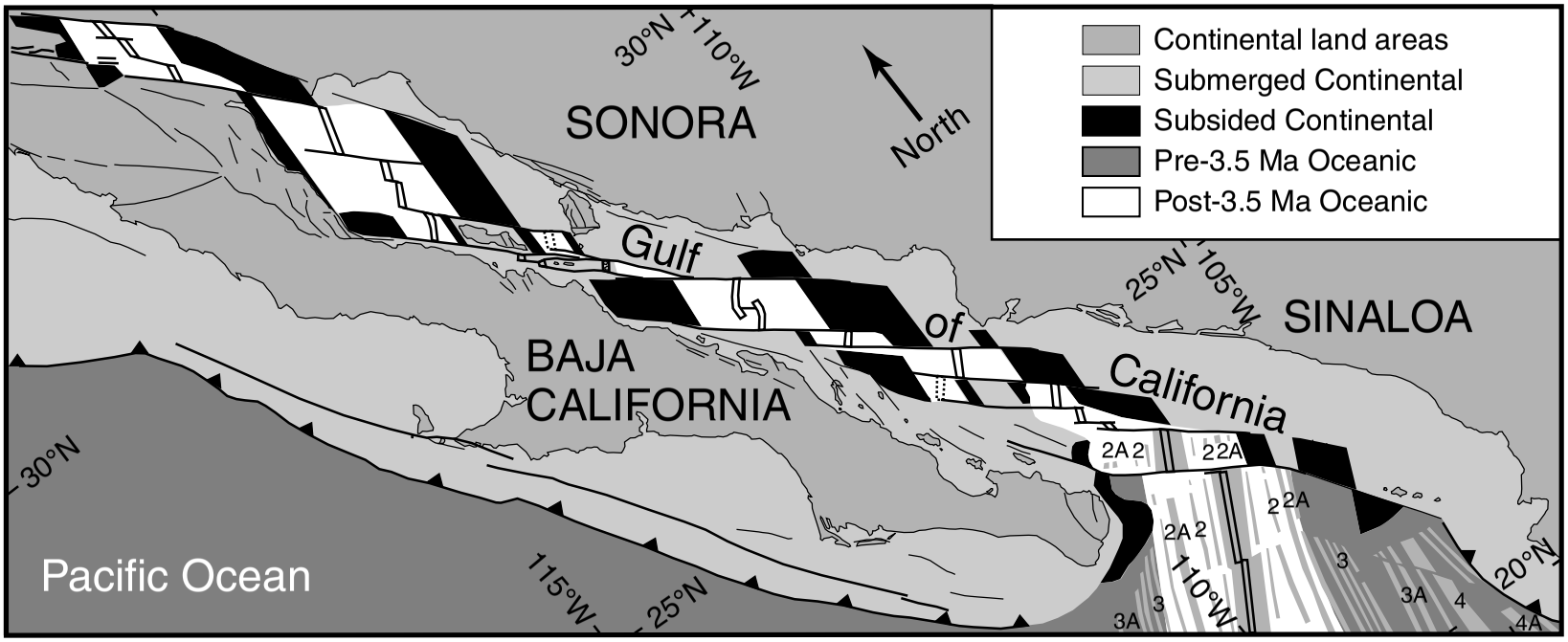

Figure 1.2. Continental and oceanic crust of northwestern Mexico and southern California. Reproduced from Figs. 2 and 8 of *Lonsdale* [1989]. Magnetic anomalies (thin gray lines) shown for oceanic crust generated at the east Pacific Rise. Approximately 180 km of seafloor spreading has occurred at the mouth of the Gulf of California. The remaining seafloor of the Gulf of California is proposed here to comprise subsided and submerged continental crust.

[*Gastil et al.*, 1975], and by a change in trend of the facies boundary coincident with the Gulf of California. Compositional trends within the Mesozoic Peninsular Ranges Batholith correlate to similar trends the coastal Sonoran Batholith [*Silver and Chappell*, 1988]. Unfortunately, the trend of this batholith and the trend of gulf are similar, complicating precise correlation of opposite margins. Also, the age of these basement tie points does not constrain the temporal development of the Gulf.

A second set of cross-gulf tie points is preserved as two well-correlated fluvial systems that originated in central and northern Sonora and crossed the position of the northern Gulf of California during Tertiary time (Fig. 1.3). The first of these is the Eocene Poway Conglomerate, which carried distinctive Jurassic volcanic clasts from northern Sonora across the eroded Peninsular Range Batholith and out to the Pacific Ocean near San Diego, California [*Abbott and Smith*, 1989]. The second of these is a pre-15 Ma conglomerate that carried distinctive Permian fusulinid-bearing limestone clasts from central Sonora to the Santa Rosa Basin area of northern Baja California [*Gastil et al.*, 1973; *Bryant*, 1986]. Both of these correlated fluvial systems are offset approximately 300 km dextrally across the Gulf of California and indicate that this offset occurred in Late Tertiary time.

1.3.4 Potential new cross-Gulf geologic tie points

The published geology of conjugate rifted margins of the northern Gulf of California presents several possibilities for precise temporal constraints on the development of the Gulf rift. As described previously, existing correlation of basement geology and Tertiary-age conglomerate deposits indicates ∼300 km total displacement for this area [*Gastil et al.*, 1973; *Silver and Chappell*, 1988; *Gastil et al.*, 1991, see Fig. 1.3]. In addition, younger pre- and syn-rift volcanic deposits of the Puertecitos Volcanic Province (PVP) of northern Baja California comprise a well-dated Mid- to Late Miocene stratigraphic sequence adjacent to the Gulf [*Stock*, 1989; *Stock et al.*, 1991; *Lewis*, 1996; *Nagy et al.*, 1999, Fig. 1.4]. Contained within these units are a series of extensive ignimbrite sequences deposited at 12.6 Ma, ∼6 Ma, and 3 to 2 Ma.

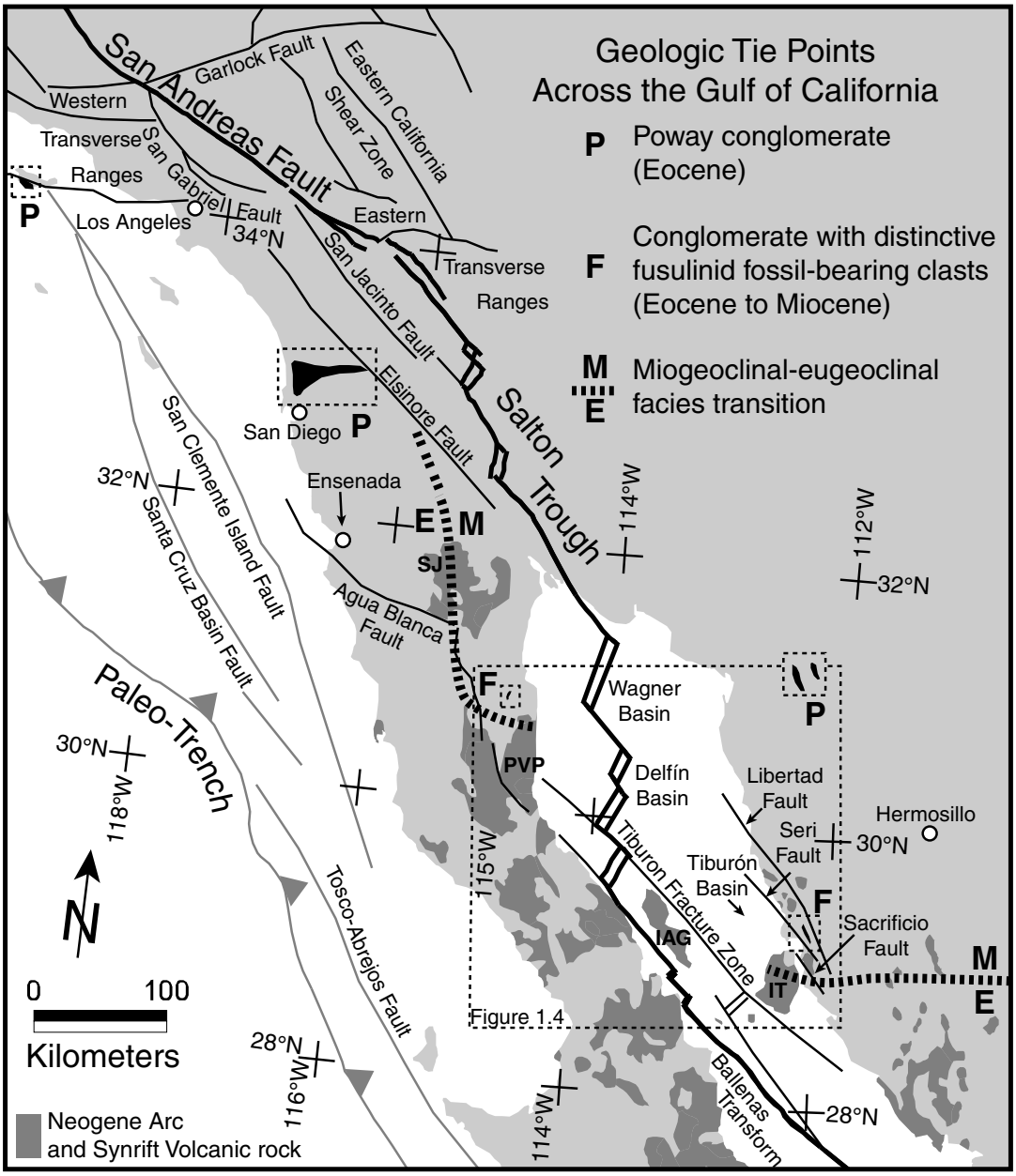

Figure 1.3. Tectonic elements of southern California and the northern Gulf of California. Faults and areas of Neogene arc and syn-rift volcanic rock from *Muehlberger et al.* [1996]. Neogene arc not shown north of 32°N. Present-day plate boundary shown as a heavy black line. Other faults of the plate-boundary zone shown as thin black lines. Grey fault lines show older plate boundaries along the Pacific coast of Baja California and southern California. Black patches indicate outcrops of distinctive conglomerates that correlate across the northern Gulf of California. Poway conglomerate outcrops (P) from *Abbott and Smith* [1989]. Conglomerate with distinctive fusilinid clasts (F) from *Gastil and Krummenacher* [1976] and *Bryant* [1986]. Miogeoclinal-eugeoclinal facies transition in pre-batholithic rocks (M:E) from *Gastil et al.* [1991]. CM, Chocolate Mountains; MB, Monte Blanco Dome [*Axen et al.*, 2000]; SJ, Sierra Juárez; PVP, Puertecitos Volcanic Province; IAG, Isla Angel de La Guarda; IT, Isla Tiburón. A-A' and B-B' are locations of cross sections on Fig. 5.23.

Detailed mapping in the northern PVP indicates sources for these deposits near the present-day western shore of the Gulf of California [*Stock et al.*, 1991; *Martín-Barajas and Stock*, 1993; *Lewis*, 1994; *Nagy*, 1997]. These widespread ignimbrite deposits, with eastern sources, comprise ideal candidates for cross-gulf correlation [*Stock et al.*, 1999; *Nagy et al.*, 1999]. A likely target for correlation is the coastal area of central Sonora, located ∼300 km southeast of the Puertecitos area. Reconnaissance mapping of coastal Sonora by *Gastil and Krummenacher* [1976] indicated a similar, extensive Mid- to Late-Miocene volcanic cover adjacent to the eastern shoreline of the Gulf of California.

1.4 Overview of thesis

Part I of this thesis is comprised of seven chapters. Chapters 2 and 3 compile the geology of correlative conjugate margins of the northern Gulf of California. The stratigraphy of these areas is grouped into simplified framework. Four sets of correlative pyroclastic flow deposits are recognized in these study areas. Much of Chapter 2 summarizes detailed studies of parts of northeastern Baja California by *Bryant* [1986], *Stock* [1993], *Martín-Barajas and Stock* [1993], *Lewis* [1994], and *Nagy* [1997] (Fig. 1.4). These studies are combined with new reconnaissance investigations to produce a new geologic map of the northeastern Baja California continental margin of the northern Gulf of California. Chapter 3 describes new reconnaissance-level and detailed mapping of the central-western Sonora continental margin of the northern Gulf of California. The stratigraphy of the Sonora margin is described under the simplified framework established for Baja California. Preliminary correlations of pyroclastic flow deposits from Baja California to Isla Tiburón and coastal Sonora are established by lithologic and stratigraphic similarity.

Chapters 4 and 5 form the core of part I of this thesis. These chapters describe geochemical and paleomagnetic tests that confirm correlation of pyroclastic flow deposits from Baja California to Isla Tiburón and coastal Sonora. The distribution of these

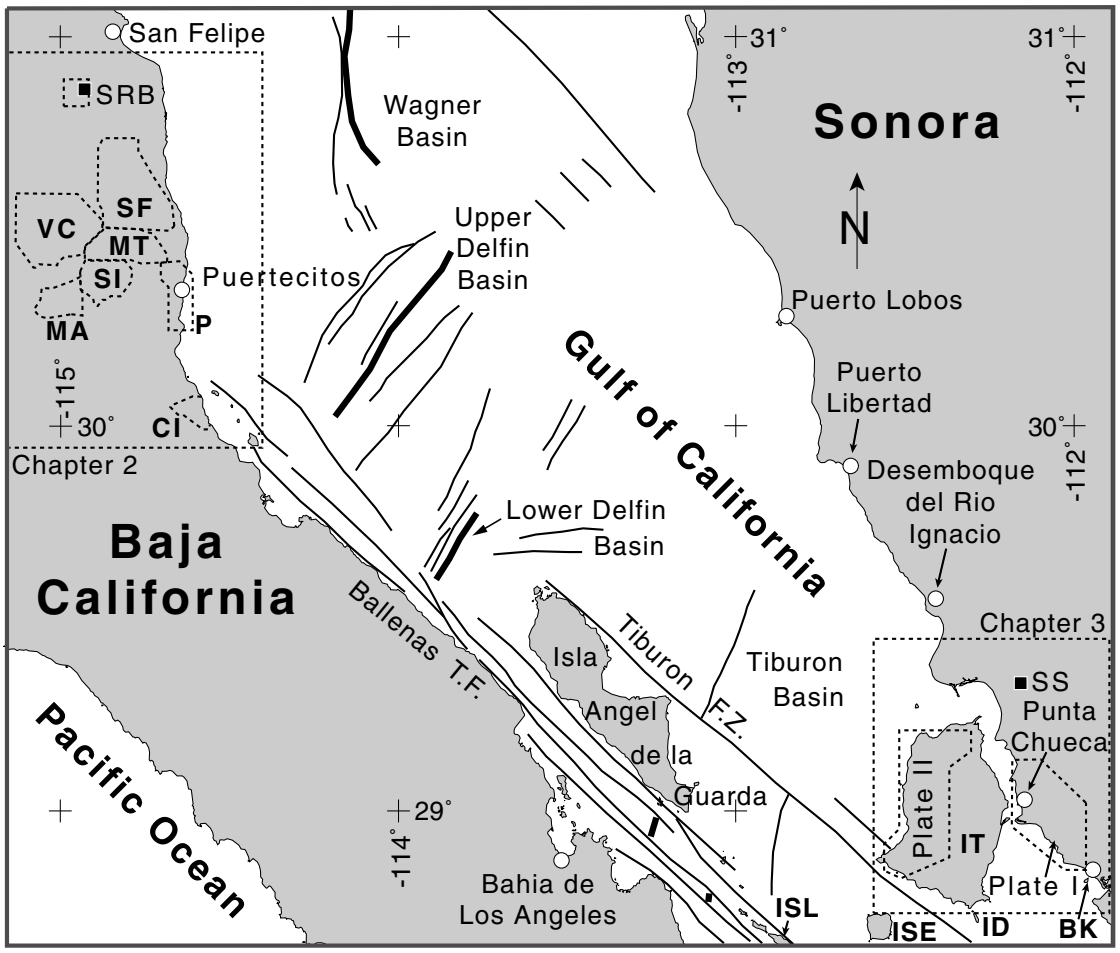

Figure 1.4. Index map of the northern Gulf of California. Marine faults from *Fenby and Gastil* [1991]. Areas of reconnaissance mapping for this study shown by large dashed boxes. Areas of detailed mapping shown by smaller dashed lines. SRB, Santa Rosa Basin [*Bryant*, 1986]; SF, Sierra San Fermín [*Lewis*, 1994]; VC, Valle Chico [*Stock*, 1993]; MT, Arroyo Matomí Transect [*Stock et al.*, 1991, *and unpublished mapping*]; SI, Santa Isabel Wash [*Nagy*, 1997]; P, Puertecitos [*Martín-Barajas and Stock*, 1993]. MA, Mesa El Avion [*Stock, unpublished mapping*]; CI, Cinco Islas (Plate IV and Chapter 7 of this thesis). Plate II (western Isla Tiburón) and Plate I (coastal Sonora) are included as separate sheets with this thesis. IT, Isla Tiburón; ISL, Isla San Lorenzo; ISE, Isla San Esteban; ID, Isla Datil; BK, Bahía Kino.

pyroclastic flow deposits and other volcanic and sedimentary facies relationships are then examined to build a set of offset features on conjugate margins of the northern Gulf of California. Map-view restoration of these features defines the rate and timing of displacement across the northern Gulf of California in Chapter 4. This chapter was published as *Rapid localization of Pacific–North America plate motion in the Gulf of California* in the May, 2001 issue of *Geology*. The implications of these reconstructions for the strain budget and tectonic evolution of the Pacific-North America plate boundary are addressed in Chapter 5.

Chapter 6 builds on the correlation presented in Chapters 4 and 5 to explore the kinematic history of localization of the Pacific–North America plate boundary. Normal faulting on both margins of the northern Gulf of California displays a constant long-term rate of continental extension. Quaternary scarps on most major fault systems indicate that this extension continues into the present, coeval with formation of new transitional oceanic crust at the plate boundary in the Gulf of California. In two localities where the syn-rift volcanic sequence preserves a higher-resolution record of rifting, preliminary evidence suggests a period of more rapid extension during the initial opening of the Gulf of California.

Two chapters conclude part I of this thesis. Chapter 7 focuses on the geology of Cinco Islas, Baja California. The geology of this small area helps to define the tectonic setting of the location where Isla Angel de La Guarda was detached from Baja California (Fig. 1.4). This island forms a 30 x 70 km continental microplate within the evolving plate boundary in the Gulf of California. Chapter 8 proposes a revised history of marine incursion into the Gulf of California. A reappraisal of marine deposition on southwest Isla Tiburón combined with a review of other age constraints strongly suggests that initial marine incursion into the northern Gulf of California was coincident with localization of the Pacific-North America plate boundary here.

Part II comprises the final chapter of this thesis. Chapter 9 appeared as *Active parasitic folds on the Elysian Park anticline: Implications for seismic hazard in central Los Angeles* in the May, 2000 issue of the *Geological Society of America Bulletin*. This

article is reprinted here with permission from the Geological Society of America.

Chapter 2

Geology of the northeastern Baja California continental margin

2.1 Abstract

The stratigraphy of the Baja California continental margin of the Upper Delfín basin is divided here into six partially interfingering stratigraphic groups corresponding to time periods prior to and during rifting in the Gulf of California extensional province. Group one encompasses the basement rocks, which are dominantly plutons of the Peninsular Ranges Batholith with lesser amounts of host metamorphosed sedimentary rocks. Group two rocks nonconformably overlie the basement as a thin, discontinuous veneer of Eocene through Mid-Miocene fluvial, lacustrine, and aeolian sedimentary rock. These deposits grade upward and laterally into lava flows, intrusions, and volcaniclastic deposits of the Middle Miocene volcanic arc that comprise group three. Lithologic group four contains only the Tuff of San Felipe, a 12.6 Ma ignimbrite of regional extent in northeastern Baja California. Group five is an assemblage of volcanic, volcaniclastic, and fluvial deposits deposited synchronously with rifting in the Gulf of California Extensional Province. Group five is capped by an extensive series of 6-7 Ma ignimbrites designated here as the Tuffs of the Northern Puertecitos Volcanic Province. Group six contains a younger syn-rift volcanic and fluvial assemblage similar to group five, and also includes marine deposits of the Gulf of California. Two regional-scale stratigraphic relationships of pre-rift and syn-rift ignimbrite deposits are identified for correlation to the conjugate rifted margin of the Upper Delfín basin in western Sonora. The first of these relationships is distribution and facies of the Tuff of San Felipe which centered on a region of thick, densely-welded outcrops in the northern Sierra San Fermín and the adjacent Sierra San Felipe (30.7°N, 114.8°W). The second relationship is the distribution and source of the Tuffs of the Northern Puertecitos Volcanic Province. These tuffs crop out adjacent to ∼40 km of the coastline of the Gulf of California from Puertecitos to the northern Sierra San Fermín. Thick, higher-grade deposits of the Tuffs of Mesa Cuadrada and the Tuffs of Arroyo El Canelo (both part of the Tuffs of the Northern Puertecitos Volcanic Province) appear to be centered on a vent or vents at the eastern

end of Arroyo Matomí and the eastern coast of Baja California (30.5°N, -114.7°W).

2.2 Introduction

This chapter and Chapter 3 introduce the geology of conjugate rifted continental margins of the Northern Gulf of California. This chapter summarizes the geology of northeastern Baja California in order to match this region to the conjugate rifted margin of coastal Sonora. Prior to the opening of the Gulf of California, volcanic and sedimentary rocks deposited on the conjugate rift margins should share similar lithologies and paleogeographic distributions. Restoration of displacement across the northern Gulf of California must reasonably match the distribution of pre-rift volcanic and sedimentary deposits and explain the distribution of syn-rift deposits. This chapter contains a complete stratigraphic overview of the northeastern Baja California continental margin between 30° and 31° N latitude (Fig. 2.1 and Table 2.2). Particular attention is given here to the lithology and facies distribution of several widespread silicic ignimbrites of the Puertecitos Volcanic Province that will be shown to correlate to western Sonora and Isla Tiburón in Chapters 3, 4, and 5.

2.3 Geologic mapping of northeastern Baja California

Much of the geology of northeastern Baja California is known only in reconnaissance (Figs. 1.4 and 2.1). *Gastil et al.* [1975] first published a reconnaissance geologic map of the state of Baja California Norte and described Tertiary sedimentary and volcanic strata of the study area. Since this work, several detailed studies of northeastern Baja California have significantly refined the stratigraphic and tectonic knowledge of the study region [*Bryant*, 1986; *Stock et al.*, 1991; *Stock*, 1993; *Martín-Barajas and Stock*, 1993; *Lewis*, 1994; *Nagy*, 1997]. New reconnaissance-scale field investigations and inspection of Landsat imagery link together these areas of detailed work into a

Figure 2.1. (next page) Geologic map of northeastern Baja California. See text for discussion of stratigraphic groups depicted here. Stratigraphic relationships of these groups are shown in Fig. 2.2. Geology based on detailed mapping of areas shown on Fig. 1.4 and *Gastil et al.* [1975], field reconnaissance in the Sierra San Felipe, and interpretation of a Landsat image (path 38 row 39) and aerial photography of the Puertecitos Volcanic Province. Asterisks mark locations of group 6 (late syn-rift) andesitic volcanoes. This map and also Figs. 2.3 and 2.5 through 2.8 are universal transverse Mercator projection, zone 11. Group 6 andesitic volcanic centers: B, Unnamed Quaternary basaltic andesite of Santa Isabel Wash; F, Pico San Fermín; G, Pico de Los Gemelos; H, Pico Los Heme; P, Volcán Prieto. S.I. and SIW, Santa Isabel Wash; MA, Mesa El Avión; Oc., Arroyo El Oculto.

new reconnaissance geologic map (Fig. 2.1).

The limits of the northeastern Baja California study area (Fig. 2.1) were selected by multiple criteria. The eastern boundary of the study area is the shoreline of the Gulf of California. The northern boundary of the study area corresponds approximately with latitude 31°00′, which is sufficient to enclose the northern extent of the ignimbrite deposits of interest. The western extent of the study area encompasses the Main Gulf escarpment fault system, which separates the stable interior of Baja California from the Gulf Extensional Province [*Gastil et al.*, 1975]. The southern boundary of the study area encloses the Puertecitos Volcanic Province. Much of the interior of the Puertecitos Volcanic Province is mapped in reconnaissance only (Fig. 1.4). In this region, nearly flat-lying strata complicate reconnaissance mapping because many important stratigraphic relationships are difficult to resolve on steep canyon walls using overhead imagery. Additional detailed fieldwork is required here to completely document the geology of this area. Fortunately, detailed studies of the northern Puertecitos Volcanic Province constrain the important volcanic deposits and structural relationships necessary for correlation across the northern Gulf of California.

Figure 2.1.

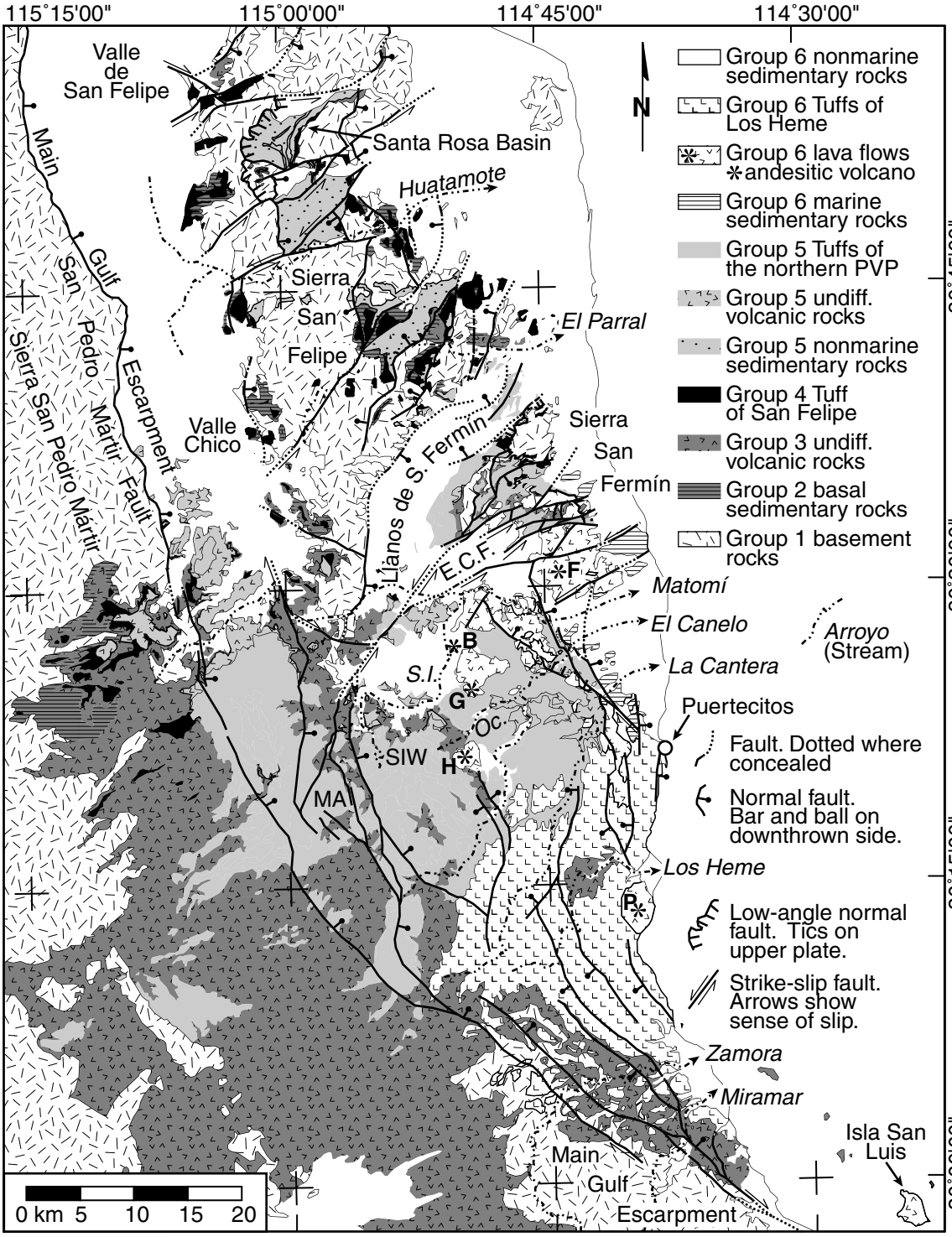
115˚15'00"
115˚00'00"
114˚45'00"
114˚30'00"
30˚45'00"
30˚30'00"
30˚15'00"
30˚00'00"
N
Valle de San Felipe
Santa Rosa Basin
Huatamote
Main Gulf Escarpment
San Pedro Mártir Fault
Sierra San Pedro Mártir
Sierra San Felipe
El Parral
Valle Chico
Llanos de S. Fermín
Sierra San Fermín
E.C.F.
F
Matomí
El Canelo
B
S.I.
La Cantera
G
Puertecitos
Oc.
SIW
H
MA
Los Heme
P
Zamora
Miramar
Isla San Luis
Main Gulf Escarpment
0 km 5 10 15 20
Group 6 nonmarine sedimentary rocks
Group 6 Tuffs of Los Heme
Group 6 lava flows ✻andesitic volcano
Group 6 marine sedimentary rocks
Group 5 Tuffs of the northern PVP
Group 5 undiff. volcanic rocks
Group 5 nonmarine sedimentary rocks
Group 4 Tuff of San Felipe
Group 3 undiff. volcanic rocks
Group 2 basal sedimentary rocks
Group 1 basement rocks
Arroyo (Stream)
Fault. Dotted where concealed
Normal fault. Bar and ball on downthrown side.
Low-angle normal fault. Tics on upper plate.
Strike-slip fault. Arrows show sense of slip.

2.4 Stratigraphy of northeastern Baja California

2.4.1 Stratigraphic framework

To simplify description of the geology of conjugate margins of the northern Gulf of California, the regional stratigraphy is divided into six groups. These groups encompass six partially interfingering stratigraphic-tectonic packages corresponding to time periods prior to and during Gulf rifting (Fig. 2.2). This stratigraphic framework is based on previous groupings used by *Nagy et al.* [1999]. Cross-references of these groups with mapping by previous authors is compiled into Table 2.2, located at the end of this chapter.

Lithologic groups one, two, and three contain strata from intervals prior to Neogene rifting in the Gulf of California region. Group one encompasses the basement rocks, which are dominantly plutons of the Peninsular Ranges Batholith with lesser amounts of host metamorphosed sedimentary rocks. Group two rocks nonconformably overlie the basement as a thin, discontinuous veneer of Eocene through Mid-Miocene fluvial, lacustrine, and aeolian sedimentary rock. These deposits grade upward and laterally into lava flows, intrusions, and volcaniclastic deposits of the Middle Miocene volcanic arc that comprise group three.

Lithologic group four contains only the Tuff of San Felipe, a 12.6 Ma ignimbrite of regional extent in northeastern Baja California [*Stock et al.*, 1999, Fig. 2.1]. This distinctive ignimbrite is allotted a separate group because of its stratigraphic position marking the transition from the Mid to Late Miocene arc volcanism to rifting, volcanism, and sedimentation related to formation of the Gulf Extensional Province [*Stock*, 1993; *Lewis*, 1994].

Lithologic groups five and six were deposited synchronously with rifting in the Gulf of California Extensional Province. Group five is an assemblage of volcanic, volcaniclastic, and fluvial deposits. This group is capped by an extensive series of 6-7 Ma ignimbrites that form much of the volcanic cover of the northern Puertecitos Volcanic Province (Fig. 2.1). Group six contains a younger volcanic and fluvial

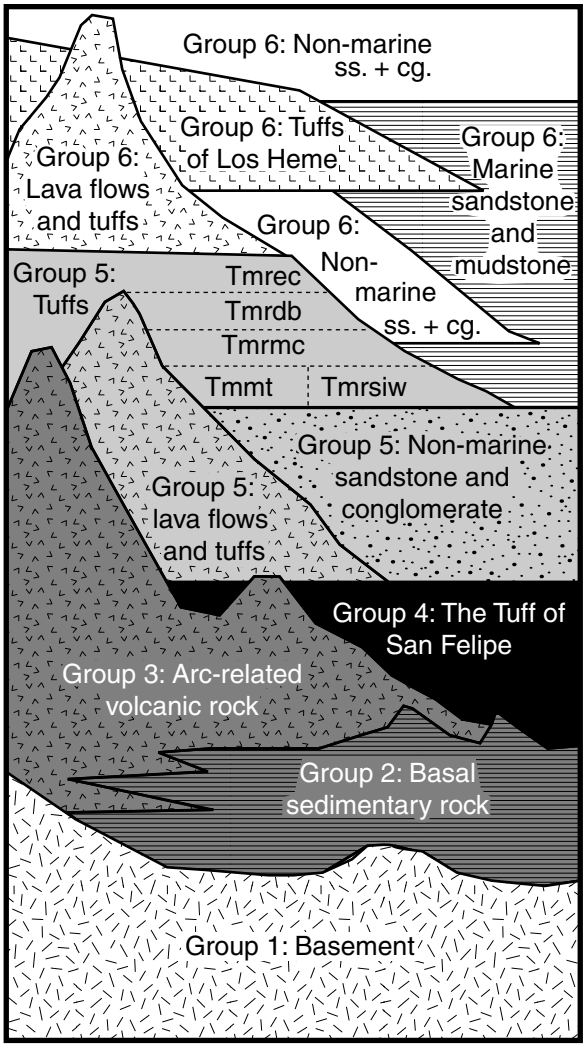

Figure 2.2. Schematic stratigraphic column of northeastern Baja California. See text for discussion of stratigraphic groups depicted here. Group 5 tuffs are collectively named the Tuffs of the Northern Puertecitos Volcanic Province. Five ignimbrites that comprise the Tuffs of the Northern Puertecitos Volcanic Province are divided by dashed lines. Tmmt, Tuffs of Mesa Matomí; Tmrsiw, Tuffs of Santa Isabel Wash; Tmrmc, Tuffs of Mesa Cuadrada; Tmrdb, Tuffs of Dead Battery Canyon; Tmrec, Tuffs of Arroyo El Canelo.

assemblage similar to group five, and also includes marine deposits of the Gulf of California.

2.4.2 Group 1: Basement complex

The Peninsular Ranges Batholith dominates the basement geology of northeastern Baja California, obscuring much of the prior geologic history of the region. This batholith was emplaced during Jurassic through Cretaceous time as a volcanic arc at the western margin of North America [*Gastil et al.*, 1975]. Exposures of pre-batholithic basement are not known in the study area. Isotopic studies of the batholith intrusions and the provenance of pre-batholithic sedimentary strata indicate that the basement beneath the study area is probably rifted Proterozoic North American continental crust [*DePaolo*, 1981; *Silver and Chappell*, 1988; *Gastil et al.*, 1991; *Rothstein*, 1997]. The oldest exposed host rocks for the batholithic intrusions consist of a Neoproterozoic through Jurassic siliciclastic and carbonate passive margin sedimentary sequence [*Gastil et al.*, 1991]. Within the Gulf extensional province of Baja California, these strata are generally preserved as steeply-dipping, isoclinally folded intrabatholithic screens metamorphosed to amphibolite (andalusite-staurolite to sillimanite) grade [*Gastil et al.*, 1975; *Rothstein*, 1997]. The youngest metasedimentary basement of northern Baja California comprises syn-intrusive volcaniclastic deposits of the Cretaceous Alisitos Formation, exposed west of the Main Gulf Escarpment [*Gastil et al.*, 1975]. Within the study region, some metasedimentary deposits may record a Jurassic and Cretaceous marine back-arc basin [*Gastil*, 1993; *Phillips*, 1993] that was closed in Mid Cretaceous time.

Basement is exposed heterogeneously in the study area (Fig. 2.1). Within the PVP, a thick Tertiary volcaniclastic section covers basement [*Gastil et al.*, 1975]. North of the PVP, basement is extensively exposed in the Sierra San Pedro Mártir and Sierra San Felipe. In the Sierra San Fermín, adjacent to the Gulf of California, exposures are about equally divided between basement and Tertiary volcanic cover [*Lewis*, 1994]. The transition between thick Tertiary volcanic cover and basement

exposures corresponds approximately to the position of Arroyo Matomí (Fig. 2.1). Basement lithologies are dominantly tonalite composition, with lesser amounts of granodiorite, granite, and gabbro [*Gastil et al.*, 1975]. *Stock* [1993] and *Nagy* [1997] report garnet-bearing, two-mica granite from the southern Sierra San Felipe and Santa Isabel Wash areas ($^{6}96^{500}$,$^{33}\,68^{000}$, all locations in the Baja California study area are universal transverse mercator projection, zone 11, NAD27 datum). *Bryant* [1986] reports tonalite and granodiorite in plutonic contact nonconformably beneath sediments of the Santa Rosa basin ($^{6}93^{000}$,$^{34}\,17^{000}$). Detailed mapping of some of the larger metasedimentary exposures reveals a variety of lithologies. *Stock* [1993], *Lewis* [1994], and *Nagy* [1997] report marble, quartzite, pelitic schist, calc-silicate schist, and amphibolite from vertically-foliated metamorphic screens in the southernmost Sierra San Felipe ($^{6}98^{000}$,$^{33}\,76^{800}$), central Sierra San Fermín ($^{7}79^{000}$,$^{33}\,82^{800}$), and Santa Isabel Wash ($^{6}96^{400}$,$^{33}\,67^{800}$). *Schmidt* [2000] reports amphibolite, quartzite, and metavolcanic rocks from the southern Sierra San Pedro Mártir. *Anderson* [1993] reports quartzite from the San Felipe area ($^{7}05^{000}$,$^{34}\,36^{000}$, ∼15 km north of Fig. 2.1) that may correlate with Neoproterozoic deposits in Sonora. New reconnaissance mapping near Arroyo Huatamote also reveals a marble and calc-silicate metamorphic screen ($^{6}94^{600}$,$^{34}\,07^{300}$). *Rothstein* [1997] classified most outcrops of the pre-batholithic basement north of the PVP as miogeoclinal strata, similar to exposures mapped by *Anderson* [1993] near San Felipe.

Isotopic measurements of the age of basement are sparse in the study area, and age designations rely in part on correlations to more studied regions of southern California. *Krummenacher et al.* [1975] report K-Ar ages from 120 to 75 Ma on hornblende and 115 to 65 Ma on biotite across northern Baja California and Southern California. *Silver et al.* [1979] and *Silver and Chappell* [1988] report U-Pb zircon ages from 140 to 90 Ma in southern California. Both of these studies describe younger crystallization ages in the eastern part of the batholith. *Schmidt* [2000] reports U-Pb ages of 100 to 137 Ma from plutons and ∼164 Ma for orthogneiss from the southern Sierra San Pedro Mártir. *Ortega-Rivera et al.* [1997] reports a U-Pb zircon and

monazite crystallization ages of 93–98 Ma for emplacement of the San Pedro Mártir pluton located at the northwest corner of Fig. 2.1. Ages of the pre-batholithic rocks east of the Main Gulf Escarpment are even less well constrained, except in a few localities where fossils are preserved. *Buch and Delattre* [1993] and *Phillips* [1993] report Permian, Triassic, and Mid Cretaceous fossils from metamorphic rocks near El Mármol, ($^{7}21^{000}$,$^{33}\,17^{000}$). *Gastil et al.* [1981] report late Paleozoic crinoidal limestone from the Sierras Pintas, located ∼50 km northwest of the area enclosed by Fig. 2.1.

2.4.3 Group 2: Tertiary basal sedimentary rocks

Group two sedimentary deposits nonconformably and unconformably overlie the group one basement complex. Strata of group two comprise a variety of fine- to coarse-grained colluvial, fluvial, lacustrine, and eolian deposits. Clast composition dominantly reflects the local basement substrate, with the exception of rare fluvial conglomerates containing exotic lithologies. Group two basal sedimentary rocks are recognized regionally across northeastern Baja California and the Peninsular Ranges. *Gabb* [1882] first proposed the name Mesa Formation to describe the combined basal sedimentary rocks and overlying volcaniclastic strata at Rancho de Los Martires (Sierra San Pedro Mártir?). *Dorsey and Burns* [1994] restricted the Mesa Formation to the dominantly locally-derived basal sedimentary rocks, and assigned the overlying volcaniclastic strata to the Comondú formation. Groups two and three reflect this same division within the study area.

Within the Baja California study area, group two forms a thin sedimentary veneer. The basal contact on basement (group one) is an irregular erosional surface and weathering horizon. Group two strata vary from 0 to 120 meters in thickness. Discontinuous colluvial and fluvial facies characterize the basal deposits of group two strata, and are commonly buttressed against local paleo-relief. Tabular-bedded sandstones, mudstones, and cross-bedded eolian sandstones are more evenly distributed in the upper sections of group two. The upper contact of group two sedimentary rocks with group three volcaniclastic strata is gradational and laterally interfingering. Towards

Figure 2.3. (next page) Outcrop map of stratigraphic groups 1, 2, and 3 in northeastern Baja California. See Figs. 1.4 and 2.1 for mapping sources. Facies distribution of group 2 divided into aeolian, fluvial, and playa-dominated depositional environments. A distinctive fluvial conglomerate containing clasts of extra-regional lithologies [*Bryant*, 1986] is shown as a paleo-terrrace isolated from younger group 2 and group 3 deposits. Facies distribution of group three deposits shown as the distribution known group 3 vents (asterisks) and the northern limit of the stratovolcano volcaniclastic facies of the Puertecitos Volcanic Province. Outcrops of the basaltic facies of group three (see text) are present north of this line and as undifferentiated outcrops within the Pueretecitos Volcanic Province.

the northern end of the Baja California study area, group three is absent, and group two sedimentary rocks are overlain directly by the Tuff of San Felipe (group four) or younger deposits.

The lithologies of group two strata within the Baja California study area define four distinct facies (Fig. 2.3). The most common facies are the basal weathering profile above group one basement and an extensive cover of eolian sands. Fluvial and lacustrine facies are present to lesser extent. The basal weathering profile facies are recognized by immature, poorly-bedded fluvial sandstone, grus, and basement breccia overlying a 5 to 10 meter thickness of weathered basement. Where the overlying sedimentary rocks are absent, the weathered basement surface may be recognized by rounded corestones exhumed from the weathering profile. Medium- to fine-grained, poorly indurated eolian deposits form the most common facies of upper group two strata in the study area, and are present everywhere from southern Valle Chico [*Stock*, 1993] and the Sierra San Fermín [*Lewis*, 1994] to the Santa Rosa Basin [*Bryant*, 1986]. Medium- to coarse-grained, moderately indurate tabular sandstone and conglomerate interfinger locally throughout these eolian sand deposits. Between Arroyo Huatamote and the Santa Rosa Basin, fluvial deposits are the dominant facies, with local deposits of eolian sandstone. Mudstone with authigenic gypsum, siltstone with mud cracks, and laminated fine-grained sandstone comprise a lacustrine/playa facies exposed within the central Sierra San Felipe adjacent to Arroyo Huatamote ($^{6}94^{150}$,$^{34}\,07^{550}$, Fig. 2.3).

A fluvial conglomerate containing a distinctive, exotic clast assemblage comprises

Figure 2.3.

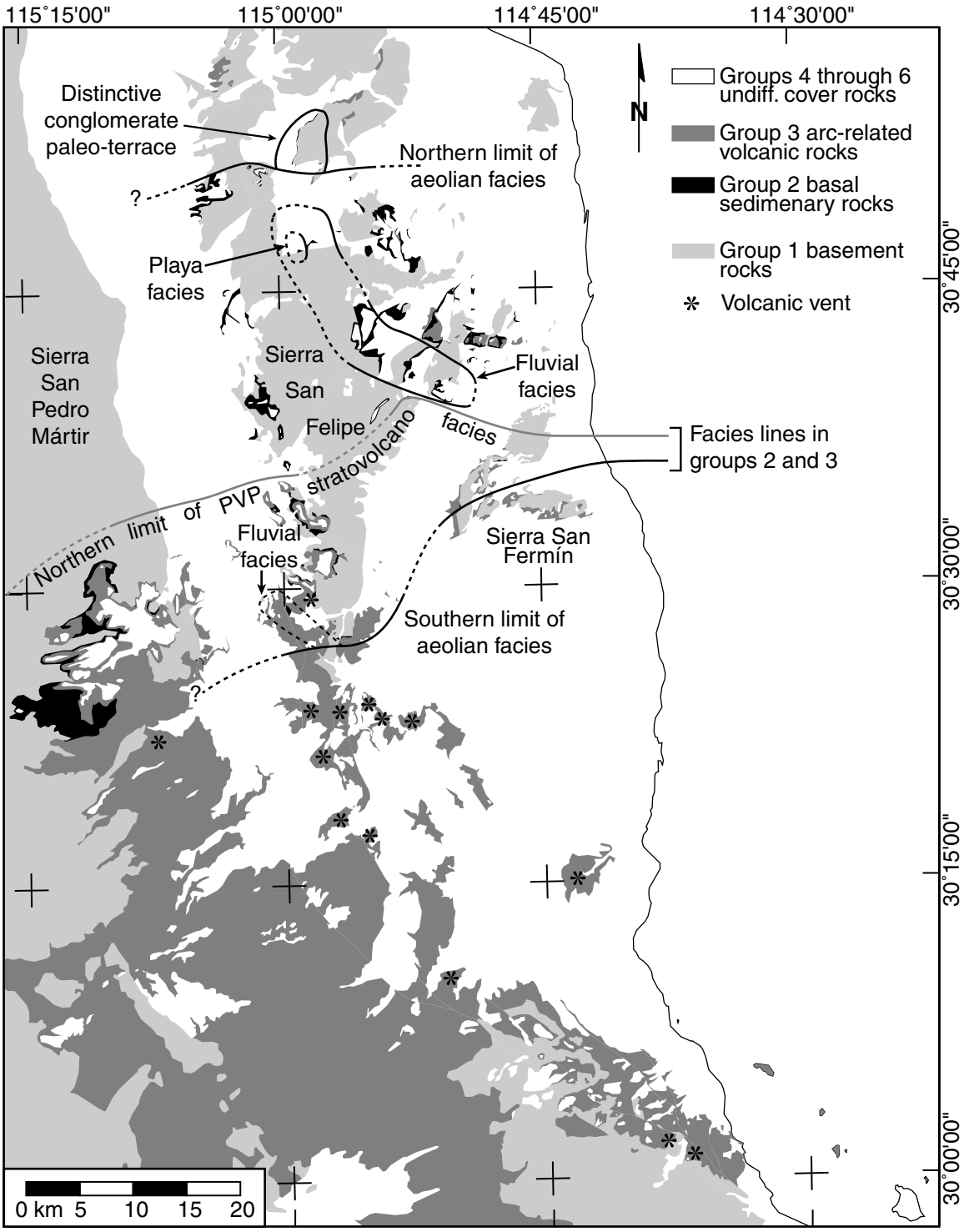
115˚15'00"
115˚00'00"
114˚45'00"
114˚30'00"
30˚45'00"
30˚30'00"
30˚15'00"
30˚00'00"
N
Groups 4 through 6 undiff. cover rocks
Group 3 arc-related volcanic rocks
Group 2 basal sedimenary rocks
Group 1 basement rocks
Volcanic vent
Distinctive conglomerate paleo-terrace
Northern limit of aeolian facies
?
Playa facies
Sierra San Pedro Mártir
Sierra San Felipe stratovolcano
Fluvial facies
Facies lines in groups 2 and 3
Northern limit of PVP
Fluvial facies
Sierra San Fermín
Southern limit of aeolian facies
?
0 km 5 10 15 20

group two strata at the base of the Santa Rosa basin (Figs. 2.3 and 2.4). This conglomerate contains a diverse assemblage of volcanic and sedimentary lithologies exotic to Baja California [*Bryant*, 1986]. From the presence of distinctive limestone clasts containing Permian fusilinid fossils, *Gastil et al.* [1973] correlated this conglomerate with a similar deposit in the Sierra Seri of coastal Sonora and estimated 300 km of dextral offset across the Gulf of California. Locally derived basement clasts and basalt boulders are also present in this deposit in the Santa Rosa basin. Stratigraphic relationships at the southern end of the basin indicate that this conglomerate formed an older terrace deposit during deposition of adjacent fluvial, eolian, and lacustrine deposits that are also mapped within group two (Fig. 2.4). Exotic clasts from the Santa Rosa basin conglomerate are recycled within these younger group two deposits, although the distinctive limestone clasts are not present in the younger strata.

Determination of the age of group two strata is problematic. Most likely, these strata are of Oligocene (?) to Mid-Miocene age [*Dorsey and Burns*, 1994], although similar strata northwest of the study area are as old as Cretaceous [*Minch*, 1979]. The oldest group two deposits must post-date Cretaceous intrusions of the Peninsular Ranges Batholith that form group one. Cooling ages on basement outcrops in the Sierra El Mayor (Fig. 1.3) record 3 to 4 km of denudation between 45 and 33 Ma [*Axen et al.*, 2000]. In Baja California, known Eocene and older Tertiary marine sedimentary deposits are restricted to the western slope of the Peninsula [*Minch*, 1979; *Gastil et al.*, 1975]. Together, these data suggest that the basal unconformity/nonconformity between group one and group two in the study area formed during early Tertiary time, and that an Eocene age is probably the oldest possible age for group two strata. Upper group two strata are overlain by, and laterally equivalent to, Miocene volcaniclastic strata of group three. In the Sierra San Fermín ($^{7}11^{670}$,$^{33}\,87^{600}$), southern Valle Chico ($^{6}97^{100}$,$^{33}\,78^{810}$) and Arroyo Huatamote ($^{6}97^{200}$,$^{34}\,09^{140}$) group two strata are intercalated with group three basalt. The oldest ages of intercalated and overlying volcanic flows are 20–21 Ma [*Lewis*, 1994; *Stock*, 1989, Table 2.2]. The youngest conformable overlying unit observed is group four, the 12.5 Ma Tuff of San Felipe [*Stock et al.*,

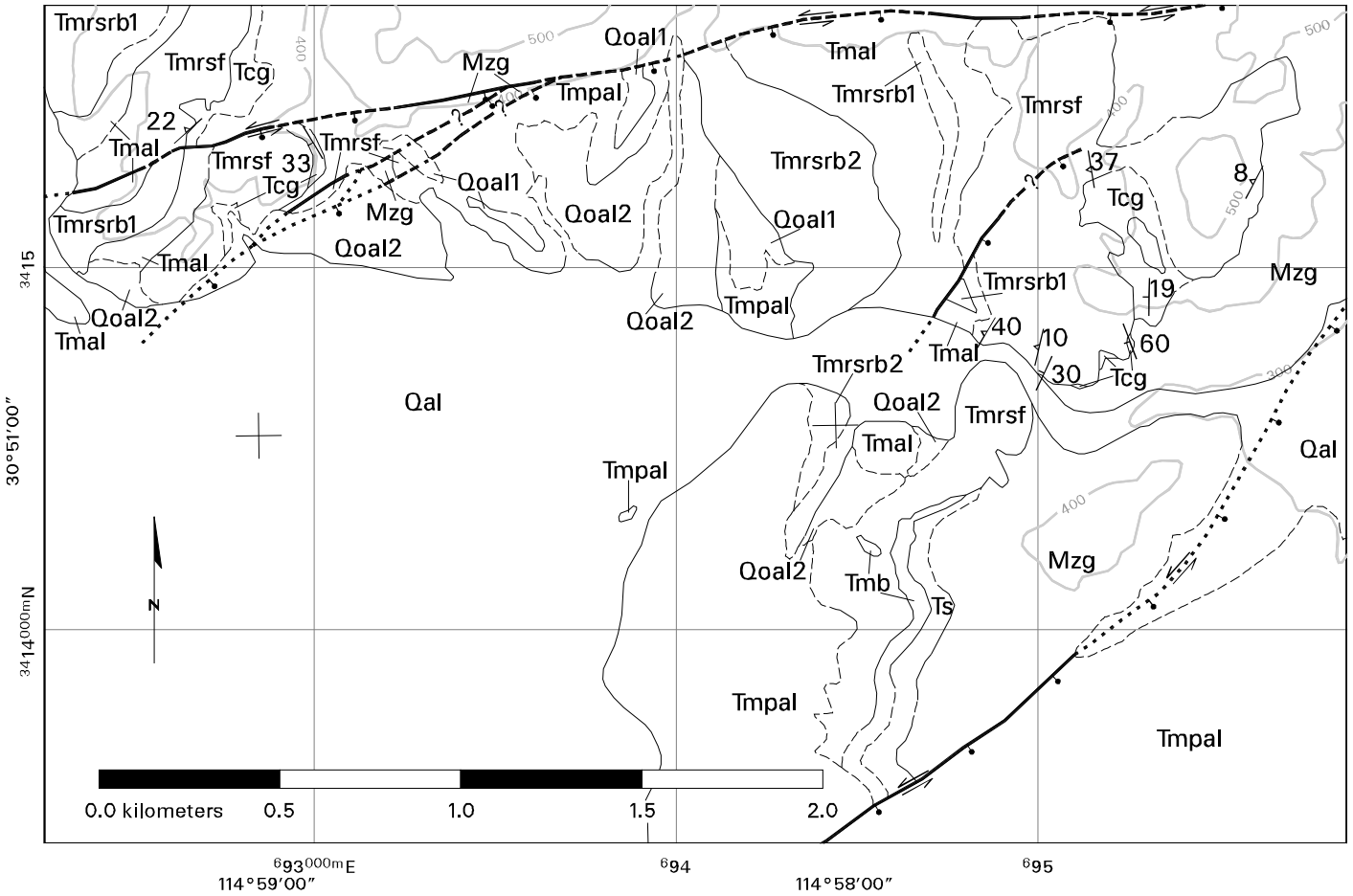

Figure 2.4. Geologic map of southern Santa Rosa Basin (mapping by the author; continues on next page). The geology here illustrates several important relationships. Two types of group two strata are mapped. Outcrops of a distinctive conglomerate (Tcg) with clasts exotic to this field area lie north of outcrops of locally-derived fluvial and eolian strata (Ts). These strata are overlain by group four, the Tuff of San Felipe (Tmrsf). This ignimbrite fills a paleocanyon cut through group two strata into group one bedrock near the transition of the underlying group two strata. Thinner deposits of the Tuff of San Felipe overlying the conglomerate (Tcg) indicate that this conglomerate formed an elevated terrace during deposition of the adjacent sandstones and basalt (Ts and Tmb). Two generations of synrift basin fill overlie the Tuff of San Felipe here. The older of these volcanic (Tmrsrb1 and Tmrsrb2) and fluvial (Tmal) deposits filled the Santa Rosa basin [*Bryant*, 1986]. The younger basin-fill deposit (Tmpal) cross-cuts the older basin-fill with a slight angular unconformity. These later deposits are probably fill of the Huatamote basin, which lies south of the Santa Rosa basin.

Figure 2.4. (continued)

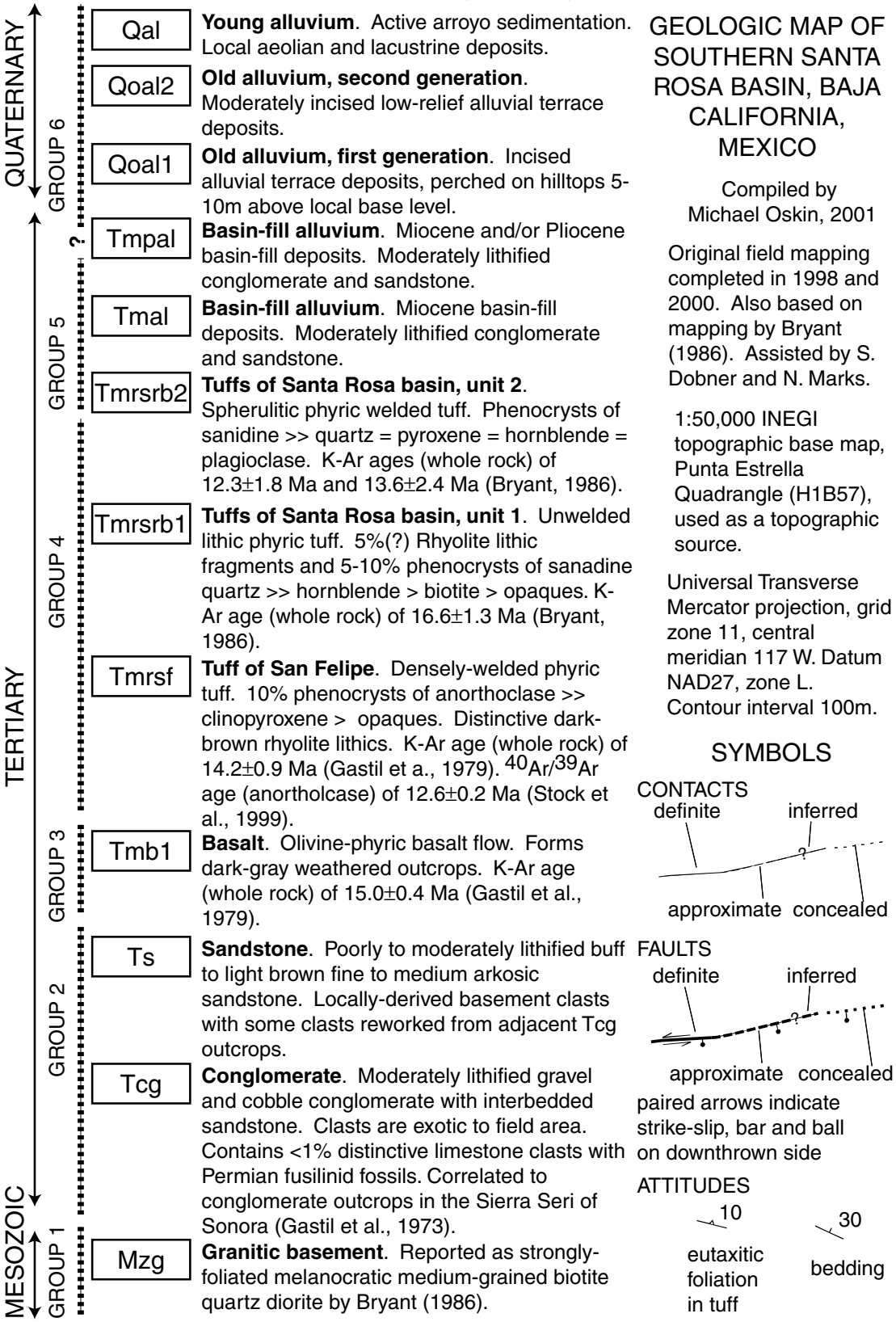

1999]. These relationships indicate that group two depositional systems were active synchronously with deposition of group three strata in other parts of the study area.

2.4.4 Group 3: Miocene volcanic arc

Extensive volcanic and volcaniclastic deposits of dominantly andesitic composition comprise the first volumetrically significant lithologic group overlying the basement nonconformity in northeastern Baja California. These deposits form part of a belt of calc-alkaline volcanic rocks located adjacent to the eastern shoreline of the Baja California peninsula [*Gastil et al.*, 1979; *Sawlan and Smith*, 1984, Fig. 2.3]. In southern Baja California, equivalent deposits are known as the Comondú formation and comprise a continuous volcanic pile up to 2 km thick extending from Lat. 28° to Lat. 25° [*Hausback*, 1984]. Proximal facies of the volcanic arc in southern Baja California lie adjacent to the Gulf shoreline, with more distal facies deposited westward across the Peninsula [*Hausback*, 1984]. In contrast, group three deposits of northeastern Baja California surround isolated volcanic edifices [*Gastil et al.*, 1975; *Sawlan*, 1991] present from the center of the peninsula to the eastern shore. Unlike the continuous belt of arc volcanic rocks present in Baja California Sur, volcanic rocks of this age in northern Baja California are mainly preserved in discrete volcanic provinces such as at Puertecitos and the southern Sierra Juarez [*Gastil et al.*, 1975, Figs. 1.3 and 2.3]. Within the study area, group three deposits overlie a veneer of group two sedimentary rocks or basement. Over much of the study area, the presence of the distinctive welded Tuff of San Felipe (Group 4) marks the transition to syn-rift group 5 and 6 strata. Elsewhere, unconformable contacts with overlying deposits are used to divide group three from younger syn-rift volcanic and sedimentary strata. In cases where both rift-related tilting and the Tuff of San Felipe are absent, the division between Group three and Group five or six mafic- to intermediate-composition volcanic rocks may be difficult to detect in the field.

Within the Baja California study area, group three is divided into two distinctive facies (Fig. 2.3). The more voluminous stratovolcano facies is concentrated at the

PVP (Fig. 2.3). These deposits, andesitic to dacitic flows and intrusions, proximal to medial debris apron, lava, pyroclastic flows, and distal volcaniclastic deposits comprise facies derived from andesitic to dacitic stratovolcanoes. The second, basaltic facies comprises small-volume basalt and basaltic andesite intrusions and flows distributed throughout the study area.

Deposits of the stratovolcano facies reach a composite thickness of up to 500 m within the PVP [*Nagy et al.*, 1999], where eroded stratovolcano edifices with up to 500 m of additional relief are present locally [*Gastil et al.*, 1975]. Individual flow fields and dome complexes of the stratovolcano facies range in volume up to $\sim$20 km^3 (e.g., the Tombstone Dacite of *Nagy et al.* [1999]). Separation of stratovolcano facies into vent, proximal-medial, and distal facies is incomplete in the study region, although some vent localities are known from areas of detailed mapping [*Martín-Barajas and Stock*, 1993; *Nagy*, 1997; *Gastil et al.*, 1975, Chapter 7 of this thesis; Fig. 2.3]. West of the PVP, a westward-fining apron of volcaniclastic conglomerate and sandstone comformably overlies group two strata [*Dorsey and Burns*, 1994]. Volcaniclastic deposits of the stratovolcano facies thin much more abruptly north of the Puertecitos Volcanic Province, and pinch out completely in the northern Sierra San Fermín and adjacent parts of the Sierra San Felipe (Fig. 2.3).

The lithology and distribution of the basaltic facies of group three contrast with the lithology and distribution of the stratovolcano facies. Flows of the basaltic facies seldom exceed 10 meters thickness. Isolated deposits of cinders that may indicate proximity to a vent are mapped together with the flows. Few vent areas have been identified for these deposits, but the distribution of individual flows suggests a similarly widespread distribution of sources. The intercalation of the basaltic facies and the stratovolcano facies of group three with group two sedimentary strata indicates that these groups represent depositional systems that coexisted in the study area (Fig. 2.2).

The ages of group three strata in the study area show two overlapping distributions that correspond to the facies divisions defined above. The broadest range of ages is

measured from the basaltic facies. The oldest ages are 20.5 ± 0.36 Ma from basalt in the Southern Valle Chico [*Stock*, 1989], and 21 ± 1 Ma from basalt in the central Sierra San Fermín [*Lewis*, 1996]. The youngest ages measured for group three strata are also from a basalt that erupted in southern Valle Chico at 12.70 ± 0.24 Ma. Ages spanning this range for the basaltic facies are known from throughout the study area (Table 2.2). Age determinations for the stratovolcano facies span a slightly more restricted range, from 14 to 20 Ma (Table 2.2). Deposits of this facies in the Puertecitos Volcanic Province cluster even more closely at 15 to 18 Ma, and may indicate a pulse of activity in this region during this time interval. In most localities between Arroyo Matomí and the Santa Rosa Basin, group three strata are overlain by the ∼12.6 Ma Tuff of San Felipe [*Stock et al.*, 1999]. Outliers of the Tuff of San Felipe also cap thick group three deposits within the Puertecitos Volcanic Province [*Stock*, 1993; *Nagy*, 1997, *Stock, unpublished mapping*, Fig. 2.1].

Arc volcanism in northern Baja California occurred during a short interval of Early to Mid-Miocene time [*Gastil et al.*, 1975; *Sawlan*, 1991, Table 2.2]. Older ages on volcanic rocks east of the Gulf indicate that the locus of the arc shifted westward near the end of Early Tertiary time [*Gastil et al.*, 1981]. The limited distribution of the stratovolcano facies in northern Gulf of California may reflect a short residence time of the arc here [*Sawlan*, 1991] which is supported by clustered ages measured for the PVP (Table 2.2). This contrasts with the presence of more extensive arc deposits and a longer duration of volcanism (24 to 12 Ma) in southern Baja California [*Hausback*, 1984; *Sawlan and Smith*, 1984; *Gastil et al.*, 1979].

2.4.5 Group 4: The Tuff of San Felipe

Lithologic group four consists of a single volcanic unit, the Tuff of San Felipe. This welded ash-flow tuff is assigned its own group to reflect its unique transitional stratigraphic position and widespread occurrence in the study area between Early to Middle-Miocene volcanic arc deposits and younger syn-rift deposits. The significance of the Tuff of San Felipe as a stratigraphic marker was recognized by *Stock* [1993]

and *Lewis* [1994] who correlated the deposit from the Main Gulf Escarpment eastward to the coastal plain (Figs. 1.4 and 2.1). *Stock et al.* [1999] compiled lithologic, petrographic, geochemical, paleomagnetic, and geochronologic data for the Tuff of San Felipe and correlated this unique deposit across an 1800 km^2 area of northeastern Baja California (Figs. 2.1 and 2.5).

Contacts of the Tuff of San Felipe upon group two or group three strata are commonly disconformable. The Tuff of San Felipe is preserved discontinuously within the Puertecitos Volcanic Province where it occupies canyons cut westward across group three volcaniclastic deposits (Fig. 2.5). North of the Puertecitos Volcanic Province, the Tuff of San Felipe is deposited on group two sedimentary rocks and group one basement. Although erosion is often evident where the Tuff of San Felipe contacts group three strata and occasionally evident where in contact with group two strata, evidence for regional tilting or faulting prior to deposition of the Tuff of San Felipe has not been proven in the study area. *Lewis* [1994] reported one location in the Siera San Fermín where group three strata (Tmvs) were tilted up to 80° prior to deposition of the Tuff of San Felipe. Non-tectonic angular discordance between cross-stratified eolian sandstone of group two and the Tuff of San Felipe is commonly observed throughout much of the Sierra San Fermín and Sierra San Felipe.

Angular contact relationships with younger group five and six strata are common throughout the study area and indicate rifting after deposition of the Tuff of San Felipe [*Stock and Hodges*, 1989; *Lewis*, 1994; *Nagy*, 1997; *Stock et al.*, 1999]. Within the Puertecitos Volcanic Province, the Tuff of San Felipe underlies synrift volcanic and volcaniclastic deposits [*Stock*, 1989; *Nagy et al.*, 1999]. North of the Puertecitos Volcanic Province and Mesa Cuadrada, the Tuff of San Felipe caps tilted mesas on the west side of the Sierra San Felipe without evidence for later deposition [*Stock*, 1993; *Lewis*, 1994; *Stock et al.*, 1999, Fig. 2.1]. Elsewhere in the Sierra San Felipe, sedimentary rift basin deposits overlie the Tuff of San Felipe, such as in the Cañon el Parral area [*Lewis*, 1994], Arroyo Huatamote, and the Santa Rosa Basin (*Bryant* [1986], with correlation by *Stock et al.* [1999]).

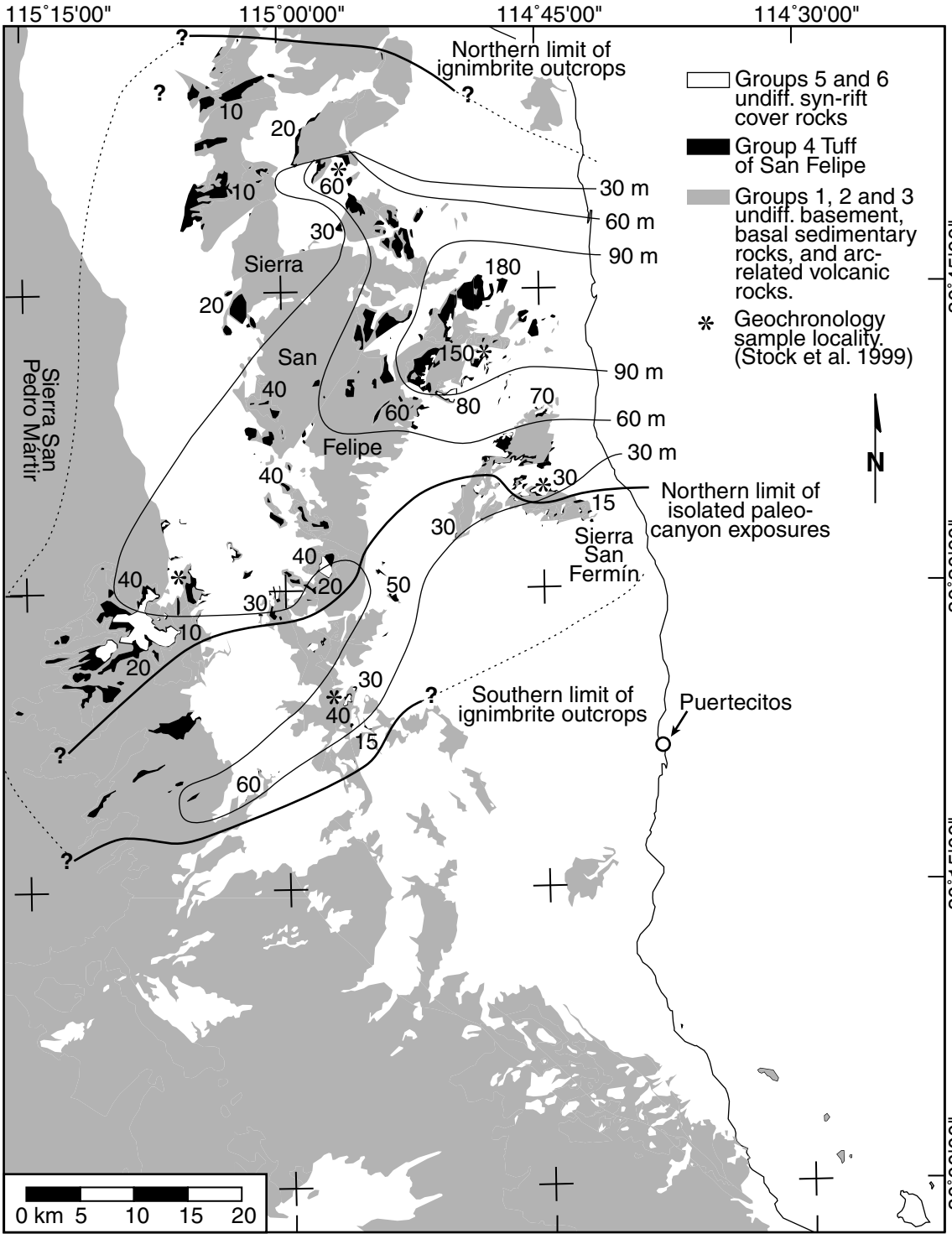

Figure 2.5. The Tuff of San Felipe in northeastern Baja California. Outcrops are depicted in black, stratigraphic thickness measurements (in meters) are depicted by numbers, isopachs of the Tuff of San Felipe are depicted by thin black lines and labelled with values in meters. Isolated paleocanyon exposures occur over the southern quarter of the total outcrop area of the ignimbrite. Isopachs are contoured at 30 m intervals up to 90 m.

The Tuff of San Felipe may be recognized in the field by several characteristic lithologic features. The tuff is everywhere densely welded, with 10–15% anorthoclase phenocrysts, <1% augite phenocrysts, rare accidental lithic fragments, and distinctive, rare to uncommon dark inclusions of rhyolite. These inclusions contain 20% phenocrysts (alkali feldspar $\gg$ clinopyroxene $>$ fayalite) and form pods up to 40 cm in length. Typical outcrops of the base of the tuff have a dark brown to black vitrophyre at the base, grading into densely welded, red to orange eutaxitically foliated tuff. In the thicker deposits, the vitrophyre grades into densely welded, red to light purple rheomorphic tuff with lithophysae up to 50 cm long. The remaining thickness of tuff is generally light-colored and vapor-phase recrystallized. Non-welded airfall ash up to 1 m thick may be present beneath thicker sections of the Tuff of San Felipe. The total outcrop area and volume of the Tuff of San Felipe in Baja California may be as much as 3,400 km^2 and 120 km^3 in Baja California (Table 2.1). This estimate does not account for 10% to 80% extension of the study area [*Stock and Hodges*, 1990; *Lewis and Stock*, 1998b].

Table 2.1. Volume calculations of tuffs in northeastern Baja California.

contour interval (m)	Area[1] (km^2)	Multiplier[2] (km)	Volume (km^3)
	Tuff of San Felipe (Max 180 m)		
0 m	3354.4	0.015	50.3
30 m	1394.1	0.03	41.8
60 m	542.3	0.03	16.3
90 m	215.6	0.045	9.7
Volume of the Tuff of San Felipe in Baja California:			118.1
	Tuffs of Mesa Cuadrada (Max 110 m)		
0 m	1790.2	0.015	26.9
0 m	-3	0.015	0.0
30 m	1313.8	0.03	39.4
30 m	-31.2	0.03	-0.9
30 m	-13.3	0.03	-0.4
60 m	883.9	0.03	26.5
60 m	-62.5	0.03	-1.9
60 m	-22.9	0.03	-0.7
60 m	48.4	0.03	1.5
90 m	32.4	0.022	0.7
90 m	39.8	0.022	0.9
90 m	241.9	0.022	5.2
90 m	13.7	0.022	0.3
Volume of the Tuffs of Mesa Cuadrada in Baja California:			97.4
	Tuffs of Dead Battery Canyon (Max: 74 m)		
0 m	110.8	0.015	1.7
30 m	27.2	0.03	0.8
60 m	15.2	0.020	0.3
Volume of the Tuffs of Dead Battery Canyon in Baja California:			2.8
	Tuffs of Arroyo El Canelo (Max 325 m)		
0 m	587.4	0.015	8.8
30 m	290	0.03	8.7
60 m	233.4	0.03	7.0
90 m	178.1	0.093	16.6
Volume of the Tuffs of Arroyo El Canelo in Baja California:			41.1

[1] The areas of closed internal contours shown as negative values. Area measurements do not account for extension of the outcrop area after deposition and may overestimate the volume of tuffs by up to a factor of 2.

[2] 0 m contour multiplied at $\frac{1}{2}$ contour interval (15 m). Each complete contour above 0 m multiplied at 1 contour interval or (30 m). Final contour interval multiplied at $\frac{1}{2}$ contour interval $+\frac{1}{3}$ remaining thickness.

Samples of the Tuff of San Felipe have been dated from several localities in the study area (Figure 2.5). *Stock et al.* [1999] summarized these ages and determined that emplacement of the Tuff of San Felipe at about 12.6 Ma is in best agreement with isotopic age determinations of the tuff and bounding volcanic strata. A problematic older age of 13.3 ± 0.5 Ma from the Sierra San Fermín is attributed to possible xenocrystic contamination from rhyolite inclusions described above [*Lewis*, 1996]. Petrographic examination of these inclusions reveals a very similar phenocryst assemblage to the Tuff of San Felipe and evidence for plastic flow and disaggregation, consistent with the possibility for xenocrystic contamination. These distinctive inclusions have not been dated separately.

The Tuff of San Felipe in Baja California is distributed in a semicircular region centered at the northern end of the Sierra San Fermín. Thickness and welding grade increase towards this area, where up to 180 m of tuff with rheomorphic texture is present (Fig. 2.5). *Lewis* [1996] proposed a vent location for the Tuff of San Felipe in this area. Based upon its wide distribution and distinctive characteristics, *Stock et al.* [1999] proposed that the Tuff of San Felipe may be present and recognized on the opposite rifted margin of the Gulf of California. In Chapter 3, the Tuff of San Felipe is shown to indeed correlate across the Gulf of California to Isla Tiburón and the adjacent coast of Sonora. Salient lithologic, paleomagnetic, and geochemical characteristics of the Tuff of San Felipe used to confirm correlation are discussed separately in Chapters 4 and 5.

2.4.6 Group 5: Early syn-rift deposits

Rifting that ultimately led to formation of the Gulf of California caused a pronounced change in sedimentary and volcanic deposition in northeastern Baja California. Group five comprises an early syn-rift sequence of volcanic and non-marine sedimentary strata. Rift-related bimodal volcanism in the northern Puertecitos Volcanic Province generated an abundance and variety of flows and pyroclastic deposits that covered most of the pre-existing arc strata [*Martín-Barajas et al.*, 1995]. A few

isolated eroded cores of stratovolcanoes were left standing above the level of extensive synrift ignimbrite sheets [*Gastil et al.*, 1975]. North of the PVP, fault-generated topographic relief produced an abundance of locally-derived conglomerate and sandstone that filled adjacent rift basins [*Gastil et al.*, 1975; *Lewis*, 1994; *Bryant*, 1986]. Group five strata may be most easily differentiated from older deposits by the presence of extensive rhyolitic ash-flow tuffs and proximal rift basin conglomerates and breccias. Often, the stratigraphic succession of group five deposits shows evidence for rifting such as internal angular unconformities and angular contacts with older strata. Group five is differentiated from group six by a pulse of ignimbrite volcanism from the northern Puertecitos Volcanic Province at ∼6 Ma [*Nagy et al.*, 1999]. These eruptions left a mantle of distinctive ash-flow tuffs throughout the southern half of the study area that are useful as structural markers [*Stock and Hodges*, 1990; *Lewis and Stock*, 1998b]. These ignimbrite deposits also pre-date marine deposition in the study area [*Martín-Barajas and Stock*, 1993; *Lewis*, 1994]. In the northern part of the study area synrift sedimentary deposits form continuous sections lacking these marker beds.

Sedimentary Strata

Group five syn-rift clastic strata comprise nonmarine conglomerate and sandstone. Over much of the study area it is likely that rift basin formation has continued to the present, burying older syn-rift strata. Exposures of syn-rift sedimentary deposits are shown in Figs. 2.1 and 2.6. These deposits occupy a chain of fragmented syn-rift sedimentary basins located within the Sierra San Felipe where later faulting has uplifted and exposed older syn-rift strata.

The best studied of the early syn-rift basins in the study area is the Santa Rosa basin [*Bryant*, 1986, Figs. 2.1 and 2.6]. Here, a tilted section of conglomeratic strata was deposited on a conformable section of older fluvial conglomerate (group two), basalt and andesite flows (group three) and the Tuff of San Felipe (group four). Group five strata in the Santa Rosa basin contain boulder conglomerate interstrati-

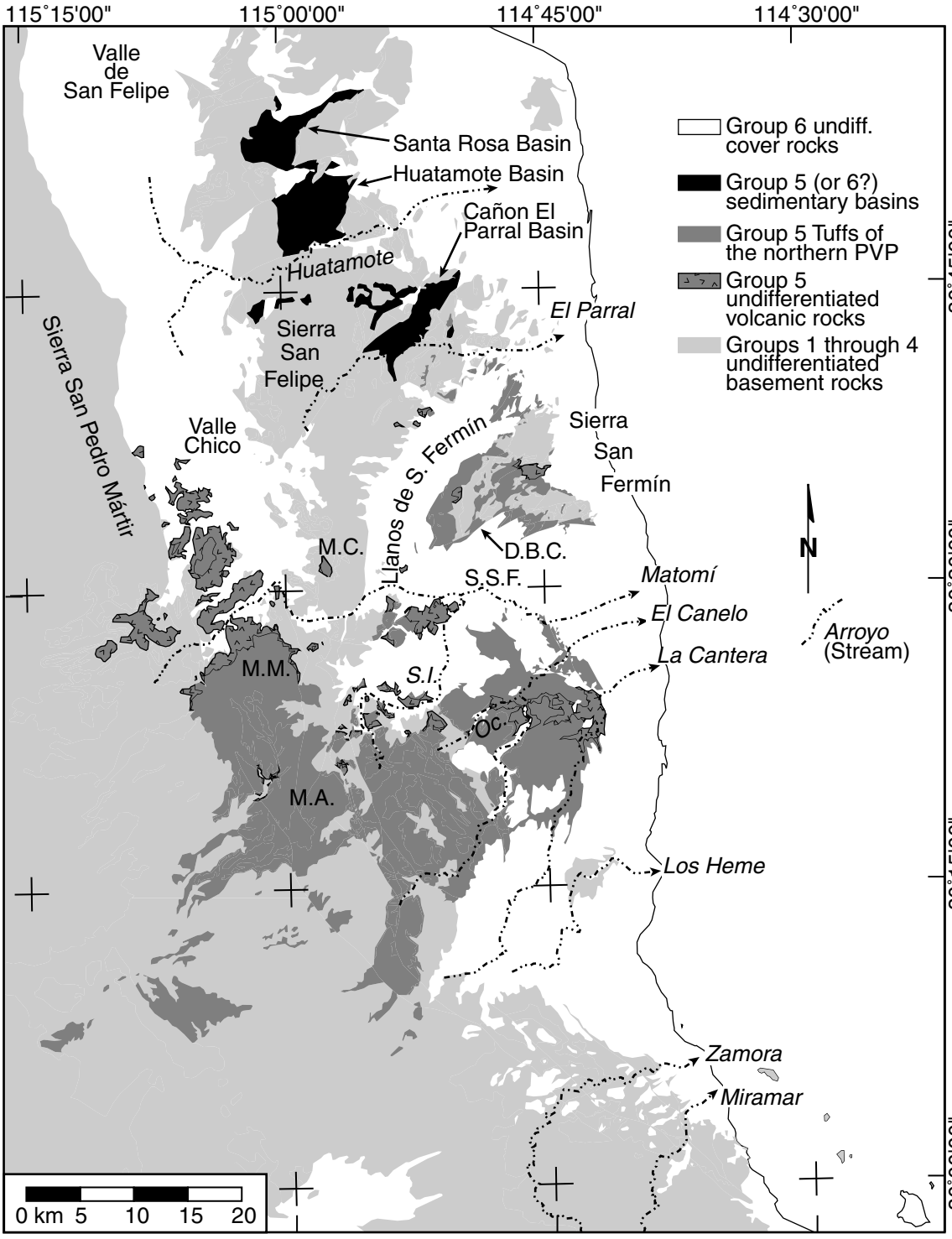

Figure 2.6. Early syn-rift (group 5) deposits of northeastern Baja California. Syn-rift sedimentary basin fill (black) and volcanic rocks (grey with pattern) are depicted where known or suspected to be older than the Tuffs of the Northern Puertecitos Volcanic Province (solid grey). The Huatamote Basin and the Cañon el Parral basin may be all or part group six age. Abbreviations refer to locations described in text: S.I. Santa Isabel Wash; Oc., Arroyo el Oculto; M.C., Mesa Cuadrada; M.M., Mesa Matomí; M.A., Mesa el Avión; D.B.C., Dead Battery Canyon; S.S.F., Southern Sierra San Fermín.

fied with conglomeratic sandstone [*Bryant*, 1986]. These strata contain clasts of the Tuff of San Felipe and group three volcanic rocks and are interpreted as alluvial fan deposits. Finer-grained non-marine conglomerate and sandstone become predominant up-section. The total exposed basin fill covers an area of 30 km^2 in the central Sierra San Felipe (Fig. 2.1). The western exposures of basin fill rest against basement along a gently inclined low-angle (18° to 20°) normal fault with up to 5 km of throw [*Bryant*, 1986]. An interstratified basalt flow dated at 8.9 ± 1.2 Ma (K–Ar on plagioclase, *Bryant* [1986]) indicates that the lower part of Santa Rosa Basin section is of group five age.

South of the Santa Rosa basin, the Huatamote basin (new name) occupies a similar structural position within the central Sierra San Felipe (Figs. 2.1 and 2.6). Reconnaissance mapping indicates that the Tuff of San Felipe (group four) was erosionally removed from some areas prior to deposition of coarse clastic syn-rift deposits. Group two sandstones and lacustrine deposits are preserved unconformably beneath group five strata. This contact is marked by an irregular and abrupt transition to coarse-grained group five conglomerates north of Arroyo Huatamote. The Huatamote basin fill preserves no volcanic units useful for dating deposition here. However, truncation of the Santa Rosa basin deposits by deposits of the Huatamote basin (unit Tmpal, Fig. 2.4) indicates that the Huatamote basin is younger than the adjacent Santa Rosa Basin. The distinctive ignimbrites that mark the top of group five in the Puertecitos Volcanic Province do not crop out as far north as Arroyo Huatamote (Fig. 2.1). Therefore, all or part of the Huatamote basin strata may be part of group six rather than group five.

The Cañon el Parral and southern Sierra San Fermín regions also contain areas of uplifted non-marine conglomerate interbedded with sandstone and mudstone [*Lewis*, 1994]. Some mapped exposures of basin fill here overlie distinctive ∼6 Ma rhyolite ignimbrites that mark the upper part of group five, and thus at least some of these deposits are assigned to group six (see below). Air-photo inspection of interior (western) areas of the Cañon el Parral basin (new name) indicates that sedimentary rocks

there are deposited directly upon the Tuff of San Felipe (group four) and thus may be of group five age.

Volcanic Strata

Group five volcanic strata form the majority of exposures in the northern Puertecitos Volcanic Province. These strata are subdivided into two facies (Fig. 2.6). Distinctive, regionally correlative ignimbrites of the northern Puertecitos Volcanic Province are mapped separately from lava flows and local pyroclastic deposits. Bedded rhyolitic pyroclastic deposits comprise the greatest volume of group five materials mapped in the PVP, where sections of ash-flow tuff may exceed 300 m thickness and cap a ∼2,000 km^2 area of mesas and plateaus. Individual welded ash-flow tuffs of this series form regionally correlative marker horizons [*Stock and Hodges*, 1989; *Lewis*, 1996; *Nagy et al.*, 1999, Figs. 2.1, 2.7, and 2.8]. Several of these units are thickest adjacent to the west coast of the Gulf of California [*Lewis*, 1994; *Nagy*, 1997] and will be shown in later chapters to correlate across the Gulf of California to Isla Tiburón. Lithologic characteristics of these ash-flow tuffs are summarized separately below.

The age of group five strata is defined between the onset of rifting in the study area up to and including deposition of the extensive rhyolite ignimbrites at ∼6 Ma in the northern Puertecitos Volcanic Province [*Nagy et al.*, 1999]. The ∼12.6 Ma Tuff of San Felipe (group four) predates rifting [*Stock and Hodges*, 1989; *Stock et al.*, 1999] and provides the lower age constraint on group five strata. 100 km north of the study area, in the southern Sierra Juarez, *Lee et al.* [1996] constrained extension to have begun between 15.98 ± 0.13 Ma and 10.96 ± 0.05 Ma. Assuming that the timing of extension is the same in the study area as in the southern Sierra Juárez, these data together constrain the onset of rifting and the lower age of group five in the study area to 11–12.6 Ma [*Stock et al.*, 1999]. The uppermost welded ash-flow tuff of group five is the Flagpole member of the Tuffs of Arroyo El Canelo (Flagpole Tuff of *Nagy et al.* [1999]). The main member of the Tuffs of Arroyo El Canelo was dated as 6.1 ± 0.3 Ma by *Nagy et al.* [1999] and the lowest member of the Tuff of Arroyo El Canelo

was dated at 6.4 ± 0.04 Ma by *Martín-Barajas et al.* [1995] and 6.4 ± 0.1 Ma by *Nagy et al.* [1999]. These constrain the age of group five strata as between 12.6 Ma and 6 Ma. Ages of interstratified volcanic units agree with these constraints (Table 2.2).

2.4.7 Tuffs of the northern Puertecitos Volcanic Province

The Tuffs of the northern Puertecitos Volcanic Province form a set of marker beds that correlate over the southern half of the Baja California study area and comprise the uppermost group five strata (Figs. 2.2 and 2.6). These tuffs are subdivided into five eruptive sequences. Three of these sequences, the Tuffs of Mesa Cuadrada, the Tuffs of Dead Battery Canyon, and the Tuffs of Arroyo El Canelo, will be shown to correlate across the Gulf of California to Isla Tiburón in later chapters. Together, the Tuffs of the northern Puertecitos Volcanic Province comprise over 100 km^3 erupted from 6.7 to 6.1 Ma, covering ∼2,000 km^2 of northeastern Baja California with up to 300 m of pyroclastic material (Figs. 2.7 and 2.8; Table 2.1).

Tuffs of Santa Isabel Wash

The lowermost tuffs of the northern Puertecitos Volcanic Province are two local sequences of pyroclastic flow deposits located at Santa Isabel Wash ('SI' on Fig. 2.6) and Mesa Matomí ('MM' on Fig. 2.6). The following description is from *Nagy* [1997] and *Nagy et al.* [1999]. The Tuffs of Santa Isabel Wash are weakly indurated, crystal-rich (plagioclase + anorthoclase ≫ olivine ≈ clinopyroxene ≈ Fe–Ti Oxides) pumice- and lithic-lapilli pyroclastic flow deposits. A variety of volcanic and granitic lithic fragments are present in the Tuffs of Santa Isabel Wash. Pale blue-grey and pale purple fine-grained volcanic lithics fragments are distinctive in these tuffs. The lowermost cooling unit of the Tuffs of Santa Isabel Wash is a non-welded pumice-flow and air-fall deposit up to 30 m thick. This unit is overlain by up to four ash-flow tuff cooling units with moderately- to densely-welded bases and less-welded to non-welded

upper sections. The composite thickness of the Tuffs of Santa Isabel Wash ranges from 70 m at the southern limit of detailed mapping to 140 m near Arroyo Matomí. The Tuffs of Santa Isabel Wash have been recognized only in the Santa Isabel Wash area of the northern PVP. $^{40}Ar/^{39}Ar$ isotopic dates determined by *Nagy et al.* [1999] indicate that the Tuffs of Santa Isabel Wash erupted at ∼6.6 ± 0.2 Ma (Table 2.2). Identical paleomagnetic remanance measured for all four ash-flow tuff cooling units *Nagy* [2000] suggests that these were erupted over a time period less than the 10^3 to 10^4 yr time scale of secular variation [*Butler*, 1992; *Merrill and McElhinny*, 1983].

Tuffs of Matomí

The Tuffs of Matomí (Tmmt of *Stock* [1989] and *Stock* [1993]) are a package of unwelded pumice lapilli tuffs that crop out on Mesa Matomí and Mesa Cuadrada at the southern end of Valle Chico. The following description is from *Stock* [1989]. Individual pyroclastic flow units that make up the Tuffs of Matomí range from 2.5 m to 37 m thickness, and the composite thickness of the tuffs ranges from 20 m to 180 m. The unit fills constructional relief formed of group three and group five andesite and group four (The Tuff of San Felipe). The Tuffs of Matomí are not mapped east of Mesa Cuadrada ('MC' on Fig. 2.6). However, non-welded pumice-flow deposits similar to the Tuffs of Matomí, in the same stratigraphic position in the Sierra San Fermín, are mapped as unit Tmr3a [*Lewis*, 1994]. The Tuffs of Matomí are undated but are overlain comformably by unit Tmr3 of the Tuffs of Mesa Cuadrada which has been dated at ∼6.3 ± 0.2 Ma in several localities (Table 2.2).

Tuffs of Mesa Cuadrada

The Tuffs of Mesa Cuadrada (new name) comprise two distinctive cooling units, Tmr3 and Tmr4 [*Stock*, 1989; *Lewis*, 1996; *Nagy et al.*, 1999, Fig. 2.7]. Parallel changes in thickness and welding grade, and the absence of intervening erosion supports grouping of these units into a single eruptive sequence [*Lewis*, 1994]. Tmr3 is a non-welded to partially-welded ash-flow tuff characterized by 5–10% cm-sized vol-

Figure 2.7. (next page) Distribution of the Tuffs of Mesa Cuadrada in northeastern California. Ignimbrite outcrops are depicted as solid grey. Numbers represent the combined stratigraphic thickness of cooling units Tmr3 and Tmr4. Thicknesses from the interior of the Puertecitos Volcanic Province estimated from topographic maps. Proposed group five caldera walls are hypothesized in areas of abrupt thickness changes that occur within the group five ignimbrite section. These areas define a possible caldera structure centered on the eastern part of Arroyo Matomí. 30 m isopach contour interval.

canic lithics and 10–15% phenocrysts (alkali feldspar $\gg$ augite $\approx$ quartz $>$ biotite $\approx$ Fe–Ti oxides $>$ basaltic hornblende $\approx$ fayalite $\approx$ zircon). Matrix material of Tmr3 is dominantly glass spicules with up to 10% pumice lapilli. Typical deposits of Tmr3 weather orange, with a light grayish purple fresh surface. Progressively more welded sections appear bright orange to red, with a dark-brown indurated vitrophyre near the base. Tmr4 is a densely welded ash-flow tuff characterized by distinctive welding zonation, 1–3% phenocrysts (plagioclase $>$ pyroxene $>$ quartz) and 1% volcanic lithic inclusions. Glass spicules dominate the matrix material, lending the tuff an even porcelainous texture. Basal Tmr4 commonly includes a thin ($<$1 m) layer of yellow ash and pumice, grading upwards into brown to black vitrophyre with pumice fiamme. A sharp break separates the black vitrophyre from a zone of densely welded red tuff. This is capped by vapor-phase altered light purple welded tuff. Thicker sections of Tmr4 near Dead Battery Canyon ('DBC' on Fig. 2.6) and Santa Isabel Wash display spherulitic crystal growths in the basal welded zones, and are capped by an additional zone of non-welded tuff.

Combined thickness of the Tuffs of Mesa Cuadrada in Baja California ranges from zero to over 100 m (Fig. 2.7). Tmr3 is everywhere at least 50% thicker than the overlying Tmr4 cooling unit except where Tmr3 fills in paleotopography. The thickest sections of the Tuffs of Mesa Cuadrada (Fig. 2.7 are located on Mesa el Avión [*Stock, unpublished mapping*], adjacent to Santa Isabel Wash [*Nagy*, 1997] and in the central Sierra San Fermín [*Lewis*, 1994]. Between these areas, abundant coalesced rhyolite domes and younger welded tuffs bury the Tuffs of Mesa Cuadrada [*Lewis*, 1994; *Nagy*, 1997]. Abrupt thickening of cooling unit Tmr4 from 5 m to 80

Figure 2.7.

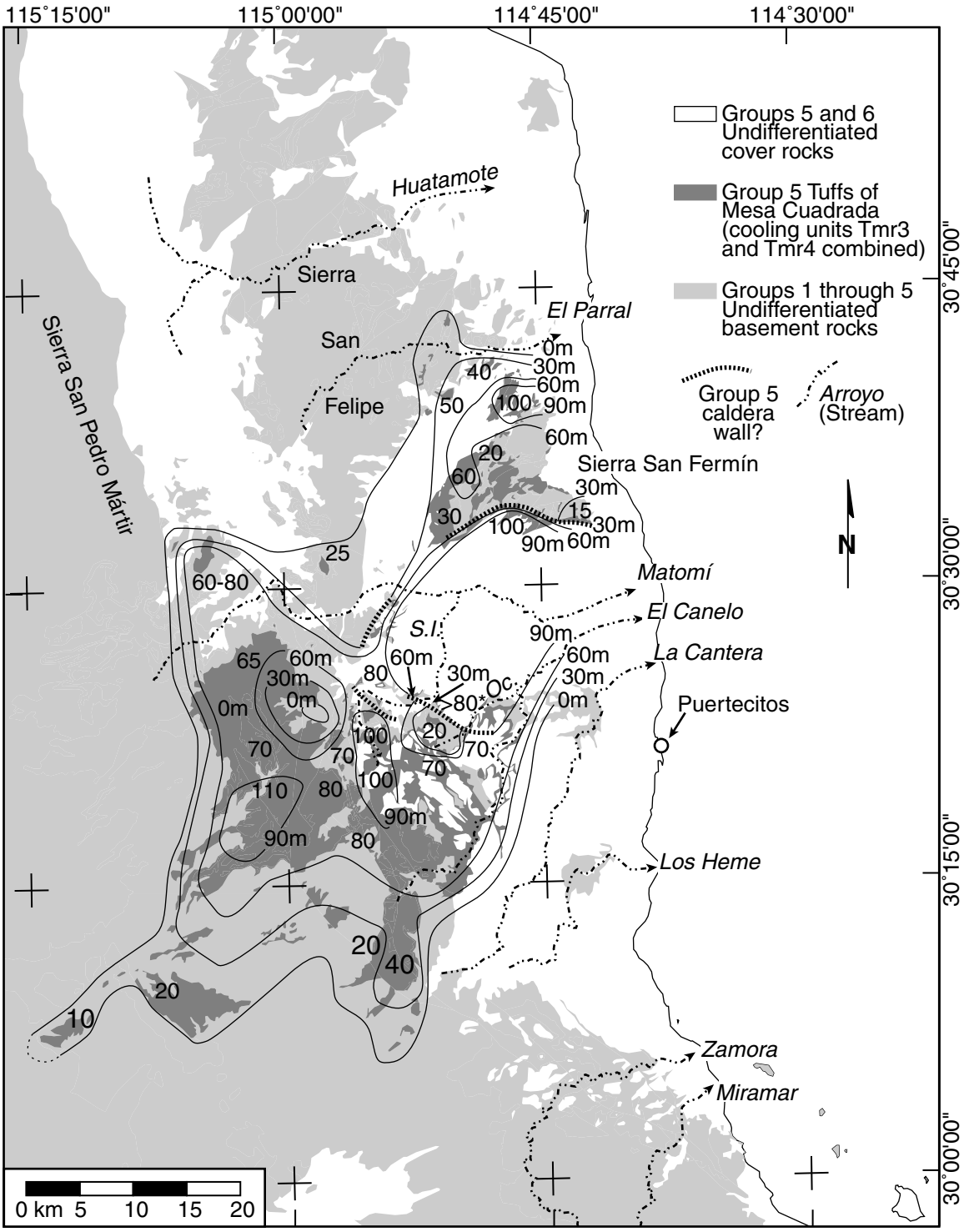
115°15'00"
115°00'00"
114°45'00"
114°30'00"
30°45'00"
30°30'00"
30°15'00"
30°00'00"
Groups 5 and 6 Undifferentiated cover rocks
Group 5 Tuffs of Mesa Cuadrada (cooling units Tmr3 and Tmr4 combined)
Groups 1 through 5 Undifferentiated basement rocks
Group 5 caldera wall?
Arroyo (Stream)
Huatamote
Sierra San Pedro Mártir
Sierra San Felipe
El Parral
Sierra San Fermín
Matomí
El Canelo
La Cantera
Puertecitos
Los Heme
Zamora
Miramar
S.I.
N
0 km 5 10 15 20

m across an escarpment adjacent to Santa Isabel Wash ($^{7}06^{000}$,$^{33}\,64^{000}$, *Nagy* [1997]; Fig. 2.7) may indicate a collapse feature formed during an earlier eruption. This feature may have formed during eruption of the Tmr3 cooling unit of the Tuffs of Mesa Cuadrada. Exposures of Tmr3 on the higher (west) side of this escarpment are commonly over 100 m thick and fill paleotopography. Exposures of Tmr3 are the same thickness or thinner on the lower (east) side of the escarpment ($^{7}06^{960}$,$^{33}\,60^{720}$ and $^{7}09^{170}$,$^{33}\,62^{450}$, *Nagy* [1997]). The Tuffs of Mesa Cuadrada covered up to 1800 km^2 of the northern Puertecitos Volcanic province with approximately 100 km^3 of pyroclastic deposits (Fig. 2.7, Table 2.1).

Local non- to moderately-welded pyroclastic deposits commonly underlie the Tuffs of Mesa Cuadrada. *Lewis* [1994] mapped unit Tmr3a in the southern Sierra San Fermín and *Nagy* [1997] describes unit Tmr3-type 1 from Santa Isabel Wash. Paleomagnetic data indicate that these units do not correlate [*Nagy*, 2000, also see Chapter 5]. A thin (1 to 2 m), welded tuff (unit Tmr3-4) is locally visible between the Tmr3 and Tmr4 cooling units in the Santa Isabel Wash and Sierra San Fermín [*Nagy*, 1997; *Lewis*, 1994].

The age of the Tuffs of Mesa Cuadrada is measured from several localities in the study area as $\sim$6.3 $\pm$ 0.2 Ma (Table 2.2). Ages are determined from the abundant alkali feldspar in Tmr3. The overlying Tmr4 deposit has not been directly dated because of the dearth of phenocrysts present in this unit. Stratigraphic evidence suggests that Tmr4 erupted soon after Tmr3; thus, the age of $\sim$6.3 Ma is adopted for the combined Tuffs of Mesa Cuadrada. A consistent, 10–15° difference in paleomagnetic remanence direction occurs between Tmr3 and Tmr4 [*Lewis and Stock*, 1998a; *Nagy*, 2000]. This difference suggests that the time interval between eruption of cooling unit Tmr3 and cooling unit Tmr4 was on the order of at least the 10^3 year scale of secular variation [*Butler*, 1992; *Merrill and McElhinny*, 1983]. Paleomagnetic remanence directions for units Tmr3a [*Lewis*, 1994] and Tmr3 type 1 [*Nagy*, 1997] are dissimilar, proving that these lower deposits do not correlate [*Nagy*, 2000].

Tuffs of Dead Battery Canyon

The Tuffs of Dead Battery Canyon form an isolated stack of two welded ash-flow tuffs in the southern Sierra San Fermín [*Lewis*, 1996]. Two nearly identical cooling units, Tmr5 and Tmr6, comprise the Tuffs of Dead Battery Canyon exposed in a series of east-tilted fault blocks at the type locality (Fig. 2.8). Based upon similar lithology and conformable contact relationships, *Lewis* [1994] suggested that these ignimbrites may comprise an uppermost product of the same eruptions that produced Tmr3 and Tmr4 of the Tuffs of Mesa Cuadrada. The following descriptions are from *Lewis* [1994] and *Lewis* [1996]. Cooling unit Tmr5 is characterized by ∼3% cm-sized pumice and 5–10% phenocrysts (feldspar ≫ Fe–Ti oxides > clinopyroxene). Tmr5 is comprised of a base of indurated, dark reddish-brown porcelainous welded tuff, capped by light purple vapor-phase altered tuff. Tmr6 contains 10–15% phenocrysts (feldspar ≫ Fe-Ti oxides > clinopyroxene ≈ basaltic hornblende) and up to 10% flattened pumice. *Lewis* [1994] and *Lewis* [1996] also noted a trace amount of tourmaline phenocrysts in Tmr6, but additional petrographic observations of Tmr6 for this study did not encounter this phenocryst phase. Like Tmr5, Tmr6 is also composed of a base of indurate dark reddish-brown porcelainous welded tuff, capped by lighter-colored vapor-phase altered zones. Additional outcrops of plagioclase-phyric welded tuff mapped as Tmr4a [*Lewis*, 1994] on the western side of the Sierra San Fermín are included here with the Tuffs of Dead Battery Canyon. The thickness of the Tuffs of Dead Battery Canyon measured at the type locality is 36 m of Tmr5 and 38 m of Tmr6, for 74 m total [*Lewis*, 1994]. The combined area and volume of these outcrops, including deposits that probably underlie the Llanos de San Fermín, is approximately 110 km^2 and 3 km^3 (Fig. 2.8, Table 2.1). Tmr5 has not been dated, but it is younger than the 6.3 ± 0.2 Ma Tuffs of Mesa Cuadrada and it is overlain with a slight angular unconformity by a non-welded sequence of pyroclastic deposits (Tmr7) dated at 6.3 ± 0.4 Ma [*Lewis*, 1994]. The Tuffs of Dead Battery Canyon are also overlain by *Lewis* [1994]'s Tmr8, which may be a northernmost equivelant of the Tuffs of Arroyo

Figure 2.8. (next page) Distribution of the Tuff of Dead Battery Canyon and the Tuffs of Arroyo El Canelo in northeastern Baja California. Outcrops of the Tuffs of Dead Battery Canon shown in black and outcrops of the Tuffs of Arroyo El Canelo shown in grey. Numbers represent stratigraphic thickness of these units in meters. Thickness estimates combine all cooling units (see text for a definition of these cooling units). Proposed caldera wall features correspond to abrupt thinning of these ignimbrites from >30 m to <5 m thickness.

El Canelo which were dated at 6.1 ± 0.5 Ma by *Nagy et al.* [1999]. Conformable contacts and bracketing strata suggest that the Tuffs of Dead Battery Canyon are probably very close in age and may deposited by the same eruptions that produced the underlying Tuffs of Mesa Cuadrada.

Tuffs of Arroyo El Canelo

The Tuffs of Arroyo El Canelo comprise a complexly zoned unit present in the coastal areas adjacent to Arroyo Matomí. *Stock et al.* [1991] named the Tuffs of Arroyo El Canelo for a sequence of high-grade welded ignimbrites that crop out in Arroyo El Canelo and Arroyo Matomí, northeast of the town of Puertecitos (Fig. 2.8). Six cooling units of the Tuff of Arroyo El Canelo were measured by *Martín-Barajas and Stock* [1993] at the type locality in Arroyo La Cantera (Fig. 2.8). *Nagy* [1997] mapped a similar sequence of units in the Santa Isabel Wash region (Fig. 2.8). The Tuff of Arroyo El Canelo is defined here based upon the exposures in the Santa Isabel Wash region, where these tuffs are best exposed in relation to other group five units [*Nagy et al.*, 1999]. Many of the tuffs designated as cooling units of the Tuffs of Arroyo El Canelo in this study were given separate names by *Nagy et al.* [1999]. These units are the Tuff of Arroyo El Oculto, Tuff of Arroyo El Canelo (with an internal cooling break), the Bighorn Sheep Tuff, and the Flagpole Tuff. Since the distribution of these units is closely related in the study area and, as will be shown in Chapters 3 and 5, similarly related on Isla Tiburón, these ash-flow deposits are grouped together here as the Tuffs of Arroyo El Canelo. The combined area and distribution of the Tuffs of Arroyo El Canelo in Baja California is estimated at approximately 600 km^2 and 40 km^3, respectively (Fig. 2.8, Table 2.1). These estimates do not account for significant

Figure 2.8.

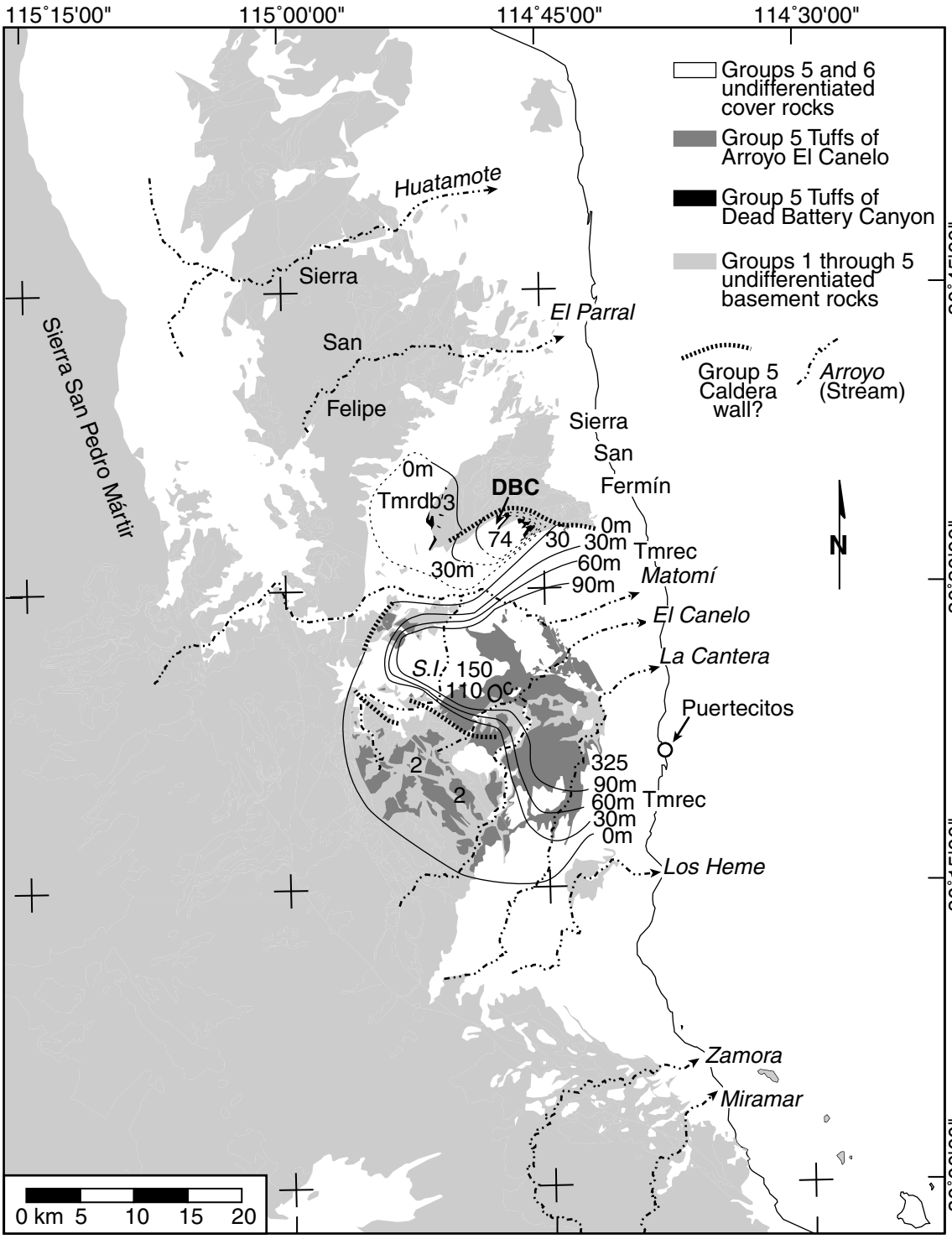
115°15'00"
115°00'00"
114°45'00"
114°30'00"
30°45'00"
30°30'00"
30°15'00"
30°00'00"
Groups 5 and 6 undifferentiated cover rocks
Group 5 Tuffs of Arroyo El Canelo
Group 5 Tuffs of Dead Battery Canyon
Groups 1 through 5 undifferentiated basement rocks
Group 5 Caldera wall?
Arroyo (Stream)
Huatamote
Sierra San Pedro Mártir
Sierra
San Felipe
El Parral
Sierra San Fermín
DBC
Tmrdb
3
0m
74
30
30m
60m
90m
Tmrec
Matomí
El Canelo
La Cantera
Puertecitos
S.I.
150
110
2
325
Los Heme
Zamora
Miramar
N
0 km 5 10 15 20

(100%?) extension of the Arroyo Matomí area described by *Stock et al.* [1991].

The El Oculto member of the Tuffs of Arroyo El Canelo is a non-welded lithic-rich devitrified ash-flow tuff with 2% phenocrysts (plagioclase + anorthoclase(?) > orthopyroxene). The El Oculto member is typically thin (0-2 m thick) and has a distinctive bright-white weathered surface. Thicker sections of 20–30 m near Arroyo El Oculto [*Nagy*, 1997] display a densely welded interior zone, up to decimeter-sized lithic fragments, and lithic-concentration zones. *Nagy et al.* [1999] obtained an inverse isochron $^{40}Ar/^{39}Ar$ age of 6.4 ± 0.1 Ma for the El Oculto member. This unit is correlated to unit t14 which forms the base of the Tuff of Arroyo El Canelo in the Arroyo Matomí area and which is also crystal poor, light-colored, nonwelded and devitrified [*Stock et al.*, 1991; *Nagy*, 1997]. *Martín-Barajas and Stock* [1993]'s unit t1 is a non-welded lithic-rich ash-flow tuff at Arroyo La Cantera that occupies a similar stratigraphic position to the El Oculto member but contains 25–30% phenocrysts. The relationship of unit t1 to the El Oculto member is unclear.

The main (El Canelo) member of the Tuffs of Arroyo El Canelo comprises multiple cooling units of densely welded lithic-phyric ash-flow tuff. These units are characterized by 3-10% phenocrysts (plagioclase + anorthoclase ≫ orthopyroxene ≈ Fe–Ti oxides > hornblende), a dark-purple matrix of welded glass, and distinctive pumice fiamme up to 50 cm in length. The base of the tuff is characterized by dense, dark-purple indurated vitrophyre with cm-scale variations in phenocryst concentration and black fiamme. Above the basal densely welded zones, phenocryst concentration levels out at ∼10% and replacement of the pumice by light-colored vapor-phase crystals form white pods that sharply contrast with the dark-purple glassy matrix. Thick sections of the El Canelo member in the eastern part of Santa Isabel Wash and adjacent to Arroyo Matomí display extremely thin (<1 cm) fiamme with rheomorphic flow lineations. Cooling breaks in the El Canelo member are distinguished by a volcanic lithic concentration zone overlain by a thin non-welded dark-colored glass and/or a dark purple indurated vitrophyre. *Nagy et al.* [1999] determined an age of 6.1 ± 0.5 Ma for the El Canelo member at Santa Isabel Wash.

The main (El Canelo) member of the Tuffs of Arroyo El Canelo ranges from less than 5 m to over 200 m thickness in the study area. Two cooling units, 80 m and 40 m thick, are mapped as the Tuff of Arroyo El Canelo in the eastern Santa Isabel Wash area [*Nagy*, 1997, $^{7}07^{000},^{33}66^{000}$]. These units are mapped in continuity with unit t12 of the Tuff of Arroyo El Canelo adjacent to Arroyo Matomí [*Stock et al.*, 1991; *Nagy et al.*, 1999, $^{7}12^{000},^{33}70^{000}$] where multiple cooling breaks are observed. At Arroyo La Cantera ($^{7}19^{200},^{33}59^{200}$), units tmc2 and tmc3 of the Tuffs of Arroyo El Canelo [*Martín-Barajas et al.*, 1995] comprise 225 m of welded tuff correlated here to the main member. The main member of Tuffs of Arroyo El Canelo thins dramatically in the western part of the Santa Isabel Wash area, forming a thin (<5 m) densely welded single (or possibly compound) cooling unit that caps the group five volcaniclastic section here. In the southern Sierra San Fermín, *Lewis* [1994]'s Tmr8 is a complexly zoned welded tuff up to 30 m thick with a light-purple glassy matrix, vapor-phase altered fiamme, and lithic concentration zones. Tmr8 is tentatively correlated to the main member of the Tuffs of Arroyo El Canelo.

The Bighorn Sheep member and the Flagpole member are the uppermost cooling units of the Tuffs of Arroyo El Canelo. These units were first described in the Santa Isabel Wash area by *Nagy* [1997]. The following descriptions are from *Nagy* [1997] and *Nagy et al.* [1999]. The Bighorn Sheep member is a weakly-indurated crystal- and lithic-rich pyroclastic flow deposit. The concentration of lithic fragments ranges from 2% to up to 50%, and they average 2–3 cm size. Elongate dark pumice or scoria may be up to 50 cm in length and comprise up to 100% of the unit locally. Matrix material, where present, consists of pale pink/purple, or yellow devitrified ash and 5–10 phenocrysts (plagioclase + anorthoclase(?) > Fe–Ti oxides > altered mafic silicates (pyroxene?)). The distribution of the Bighorn Sheep member is erratic at the 100 m-scale and its thickness ranges from 0–15 m. The Flagpole member is an indurate densely welded dark-purple to dark-orange crystal-rich ash-flow tuff. Its appearance is similar to that of the underlying El Canelo member, with large vapor-phase replaced fiamme and cm-scale variation in phenocryst abundance in the

basal welded vitrophyre. The presence of trace amounts of fayalite distinguishes this capping unit from the underlying members of the Tuffs of Arroyo El Canelo at Santa Isabel Wash. Possible correlatives to the Bighorn and Flagpole members are unit t9 from Arroyo Matomí [*Stock et al.*, 1991] and units tmc4 and tmc5 from Arroyo La Cantera [*Martín-Barajas et al.*, 1995]. However, fayalite is not described from these tuffs and these may comprise additional cooling units of the underlying El Canelo member.

The Tuffs of Arroyo El Canelo are the highest ignimbrites of group five. The distribution of these tuffs is centered on a probable vent area at the eastern end of Arroyo Matmoí [*Stock et al.*, 1991]. Very high-grade welding, rheomorphic flow, and intercalated lithic breccias present here support deposition in an intracaldera setting [*Stock et al.*, 1991]. The Tuffs of Arroyo El Canelo thin abruptly and pinch out in the Santa Isabel Wash region (Fig. 2.8). Outflow sheets of these tuffs pinch out more gradually against paleotopography south of Arroyo La Cantera [*Martín-Barajas and Stock*, 1993]. Tmr8, which is tentatively correlated to the Tuffs of Arroyo El Canelo, is restricted in distribution to the southern Sierra San Fermín. The Tuffs of Arroyo El Canelo have not been identified further north despite all of the detailed mapping that has been conducted.

2.4.8 Group 6: Late syn-rift deposits

Group six comprises a continuation of group five syn-rift sedimentary deposits, but with the addition of marine strata of the Gulf of California. The base of group six is defined by the extensive Tuffs of the Northern Puertecitos Volcanic Province of group five which covered much of the southern part of the study area during latest Miocene time. Where these tuffs are not present, the base of group six may be difficult to differentiate from underlying group five. Group six syn-rift strata include present-day sedimentary and volcanic rocks, and thus the age of group six spans from latest Miocene/earliest Pliocene to Late Quaternary time. Volcanic strata of group six (Fig. 2.1) are similar to those of group five and include flows of a range of compositions.

Group six also includes a Late Pliocene to Early Pleistocene sequence of welded rhyolitic ignimbrites (Fig. 2.1) known as the Tuffs of Los Heme [*Martín-Barajas and Stock*, 1993] and the correlative Tuffs of Mesa El Tábano [*Stock et al.*, 1991; *Lewis*, 1996]. Sedimentary strata of group six include non-marine breccia, conglomerate, and sandstone as well as marine sedimentary rocks (Fig. 2.1).

Nonmarine clastic sedimentary deposits of group six age are common throughout the study area. Exposures of this type include areas of uplifted sedimentary deposits in the Cañon el Parral basin (Fig. 2.6) and the southern Sierra San Fermín (*Lewis* [1994]; 'SSF' on Fig. 2.6). Present-day analogs to these basins are Valle Chico-Valle de San Felipe and the Llanos de San Fermín (Fig. 2.6). Transitional marine-nonmarine conditions are present on the coastal plain east of the Sierra San Felipe, the Sierra San Fermín, and the PVP where alluvial fans prograde into the Gulf of California to form deltas, and littoral and eolian processes combine to redistribute these sediments.

Marine sedimentary deposits are preserved in an uplifted marginal basin adjacent to the east side of the Sierra San Fermín extending southward to Puertecitos [*Lewis*, 1994; *Martín-Barajas and Stock*, 1993, Fig. 2.1]. *Martín-Barajas et al.* [1997] summarized the stratigraphy here and designated these deposits as the Puertecitos Formation. This formation records two marine transgressions that post-date the 6.1 $\pm$ 0.5 Ma Tuffs of Arroyo El Canelo. Both sequences exhibit sedimentological characteristics of a shallow marine, intertidal to subtidal environment with local progradation of alluvial fans and fan-deltas [*Martín-Barajas et al.*, 1997]. Isotopic ages from the Tuff of Valle Curbina, a non-welded ash-flow tuff and partially water-lain air-fall tuff, date the base of the second transgression at 3.27 Ma [*Lewis*, 1994]. Primary volcaniclastic input increased during deposition of the second sequence coeval with eruption of the Tuffs of Los Heme to the south [*Martín-Barajas et al.*, 1995, 1997].

Volcanic deposits of group six are concentrated in the southeastern corner of the study area (Fig. 2.1). This area of the Puertecitos Volcanic Province hosted waning volcansim surrounding the eastern end of Arroyo Matomí during Early Pliocene time and the formation of a new eruptive center for the Tuffs of Arroyo Los Heme further

to the southeast. Volcanism at the eastern end of Arroyo Matomi formed a thick accumulation of coelesced rhyolite domes [*Martín-Barajas and Stock*, 1993] and three andesite volcanoes: Pico Los Heme, Pico Los Gemelos (both from *Nagy et al.* [1999]; 'H' and 'G' on Fig. 2.1), and Pico San Fermín (*Lewis* [1994]; 'F' on Fig. 2.1). A basaltic andesite flow south of Arroyo Matomí ('B' on Fig. 2.1) dated at 0.7 Ma records the most recent volcanism here [*Martín-Barajas et al.*, 1995]. The Los Heme eruptive center, located to the southeast offshore of Puertecitos [*Martín-Barajas et al.*, 1997], started to erupt during mid-Pliocene time. The Tuffs of Los Heme form a stack of up to 28 densely welded cooling units increasing in thickness and number towards this eruptive center [*Martín-Barajas et al.*, 1995]. Scattered basaltic andesite cinder cones are interstratified at an unconformity within the Tuffs of Los Heme [*Martín-Barajas and Stock*, 1993, also Chapter 7 of this thesis]. Volcán Prieto, a 10 km^2 basaltic andesite volcano ('P' on Fig. 2.1) dated at 2.6 $\pm$ 0.1 Ma [*Martín-Barajas et al.*, 1995] is the largest of these basaltic andesite eruptive centers. The youngest volcanism in the Puertecitos Volcanic Province is a series of Late Pleistocene and Holocene rhyolite lava domes and airfall deposits erupted from Isla San Luis (*Paz-Moreno and Demant* [1999]; *Hausback et al.* [2000]; Fig. 2.1).

2.5 Discussion

The following sections apply the stratigraphic framework (groups 1–6) to present a concise geologic summary of the northeastern Baja California continental margin. These descriptions and interpretations are first presented on a range-by-range basis below and then summarized at the conclusion of this chapter. Following this chapter, the characteristics of the volcaniclastic stratigraphy of the conjugate Sonoran margin are described in Chapter 3. These observations are synthesized into a paleogeographic restoration of the Gulf of California rift in Chapter 5.

2.5.1 Sierra San Felipe

This range at the northern end of the Baja California margin study area is comprised of basement outcrops with a thin sedimentary and volcanic cover. Group 2 fluvial and eolian sedimentary rocks define an Early Miocene low-relief surface with scattered basement outcrops, sand dune fields, and shallow closed basins (Fig. 2.3). A fluvial system that deposited exotic clasts from Sonora appears to have been isolated as a terrace deposit by middle Miocene time (Figs. 2.3 and 2.4). Deposits from the group 3 volcanic arc are limited to scattered basalt flows intercalated with these sedimentary rocks and a northward-thinning wedge of volcaniclastic debris derived from intermediate-composition volcanoes in the Puertecitos Volcanic Province (Fig. 2.3). The Tuff of San Felipe comprises the majority of volcanic outcrops in the Sierra San Felipe (Fig. 2.5). This ash-flow tuff formed a once-continuous sheet over most of the range south of 31° latitude. Deposits of high-grade Tuff of San Felipe up to 180 m thick ponded over fluvial and eolian group 2 deposits near the present coastline of the Gulf of California. Thin (10–40 m thick) deposits of the Tuff of San Felipe form a ubiquitous mesa-capping unit along the crest of the range. Synrift sedimentary deposits are confined to a string of small basins in the central reach of the Sierra San Felipe (Fig. 2.6). Synrift volcanic deposits are limited to thin deposits of the Tuffs of Mesa Cuadrada on Mesa Cuadrada and adjacent to the northern Sierra San Fermín (Fig. 2.7). Two partially welded synrift pyroclastic flows are present in the Santa Rosa Basin [*Bryant*, 1986, also Fig. 2.4] and appear unrelated to synrift volcanic strata exposed elsewhere in the study area.

2.5.2 Sierra San Fermín

The stratigraphy of this range is transitional between the thin volcanic and sedimentary cover of the Sierra San Felipe and the thick volcanic cover of the northern Puertecitos Volcanic Province [*Lewis*, 1994]. Group 2 sedimentary rocks intercalated with volcaniclastic deposits and basalt flows overlie basement in the northern part of

the range (Fig. 2.3). A thicker wedge of volcaniclastic material overlies basement to the south (Fig. 2.3). The Tuff of San Felipe thickens from 15 m at the southern end of the range to over 70 m in the north with a concurrent increase in welding grade and abundance of dark-colored volcanic inclusions (Fig. 2.5). This ignimbrite covered a low-relief surface in the northern part of the range and is restricted to paleocanyons cut into group three volcaniclastic deposits in the central and southern areas. Early synrift andesite crops out in the central-northern part of the range. Most of the Sierra San Fermín is capped by the Tuffs of Mesa Cuadrada (Fig. 2.7). Tmr3 is over 100 m thick and partially welded in the central and northern Sierra San Fermín and much thinner in the intervening part of the range. Tmr4 forms a 1–5 m thick welded deposit capping the central and northern parts of the range and thickens abruptly to 70 m in the east-central and southern Sierra San Fermín. The Tuffs of Mesa Cuadrada pinch out in the northernmost Sierra San Fermín and parts of the adjacent Sierra San Felipe. The Tuffs of Dead Battery Canyon also appear as a 3 m thick veneer in the east-central part of the range and thicken abruptly to 74 m (combined thickness of units Tmr5 and Tmr6) to the south.

Abrupt thickness changes in the Tuffs of Mesa Cuadrada and the Tuffs of Dead Battery Canyon occur adjacent to the El Coloradito Fault (Fig. 2.1), an oblique left-lateral fault zone that may have excised a caldera ring fracture system here [*Lewis*, 1996, Figs. 2.7 and 2.8]. This gradient marks the appearance of a 20 to 600 m section of rhyolite domes and lava flows that cover most of the tuff outcrops and may be post-caldera fill following eruption of the Tuffs of Mesa Cuadrada and the Tuffs of Dead Battery Canyon. Unit Tmr8, a 10–30 m thick densely welded tuff intercalated with these rhyolite lava flows, may be a northernmost equivalent of the Tuffs of Arroyo El Canelo. Late synrift marine strata are exposed in fault blocks along the eastern range-front of the Sierra San Fermín, and fluvial conglomerate fills fault-bounded basins at the northern and southern ends of the range.

2.5.3 Southern Valle Chico

This region comprises the western, interior area of the northern Puertecitos Volcanic Province. Here, a thick (up to 300 m) section of Early- to Mid-Miocene arc volcanic rocks (group 3, Fig. 2.3) is overlain by ash-flow tuffs and synrift lava flows [*Stock*, 1989]. These strata crop out at the southern end of the Sierra San Pedro Mártir Fault, which bounds the western edge of the Gulf Extensional Province here (Fig. 2.1). In the southern Sierra San Pedro Mártir, group 3 volcaniclastic deposits thin northward beneath a 10 m- to 30 m–thick cover of the Tuff of San Felipe, similar to exposures in the adjacent Sierra San Felipe [*Stock*, 1993; *Schmidt*, 2000, and Fig. 2.5]. Group 3 volcanic rocks become more abundant and proximal to the south, whereas the Tuff of San Felipe appears to pinch out here. A chain of synrift andesite volcanoes and related pyroclastic deposits is preserved as a series of ridges extending eastward from the Sierra San Pedro Mártir. These are overlain by rhyolite lava domes and non-welded pyroclastic deposits of the Tuffs of Matomí. The uppermost Tuffs of Matomí may correlate to unit Tmr3a of the Sierra San Fermín [*Lewis*, 1994]. Tmr3 and Tmr4 of the Tuffs of Mesa Cuadrada (Fig. 2.7) form a mesa-capping sequence in the northwestern Puertecitos Volcanic province. Tmr3 thins northward from 54 m thick on Mesa Matomí to 20 m thick on Mesa Cuadrada. Cooling unit Tmr4 forms a thin (<10 m) veneer capping these areas.

2.5.4 Santa Isabel Wash and Mesa El Avión

The Santa Isabel Wash and Mesa El Avión areas [*Nagy*, 1997, *Stock, unpublished mapping*] comprise the central-northern Puertecitos Volcanic Province. This region preserves a similar volcanic sequence as the adjacent Mesa Matomí and Mesa Cuadrada [*Nagy et al.*, 1999]. Here, lava flows, vents, and associated volcaniclastic deposits of the Early- to Mid-Miocene arc exceed 500 m thickness [*Nagy*, 1997, and Fig. 2.3]. Paleocanyons inset into this section contain 15–30 m of the Tuff of San Felipe (Fig. 2.5). Deposits derived from an early synrift andesite volcano (Pico Del

Toro) overlie the Tuff of San Felipe and are, in turn, overlain by the Tuffs of the Northern Puertecitos Volcanic Province (Fig. 2.1).

The Tuffs of Santa Isabel Wash form one of the stratigraphically lowest units of the Tuffs of the Northern Puertecitos Volcanic Province. The Tuffs of Santa Isabel Wash, which are collectively up to 140 m thick, appear to be restricted to the Santa Isabel Wash area of the northern Puertecitos Volcanic Province. The Tuffs of Mesa Cuadrada overlie the Tuffs of Santa Isabel Wash here. Cooling unit Tmr3 is commonly over 100 m thick and fills paleotopography formed by older volcanic centers. Cooling unit Tmr4 ranges from 3 to 5 m thick in the north, thickening slightly (to 10-20 m) in the south. To the east, cooling unit Tmr4 thickens abruptly to 70 m across a prominent, northwest-trending, 200 to 300 m-high escarpment [*Nagy*, 1997]. Map relations and structural evidence suggest that this escarpment formed during eruption of the Tuffs of Mesa Cuadrada. A thin (1–2 m thick) single densely welded cooling unit of the Tuffs of Arroyo El Canelo (or possibly a compound cooling unit, *Nagy, pers. comm.*, 1999) caps the central and western parts of the northern Puertecitos Volcanic Province. The Tuffs of Arroyo El Canelo also thicken abruptly across the northwest-trending escarpment, splitting into four distinct cooling units (Tmrao, Tmrec with an internal cooling break, Tmrbs, and Tmrfp) with an aggregate thickness exceeding 75 m and evidence for high-grade welding and rheomorphic flow [*Nagy*, 1997]. Northeast of the escarpment, a Late Miocene rhyolite lava dome (Picacho El Canelo) and three Late Miocene or younger andesite volcanoes (Picacho El Gemelo, 'Ugly Mountain,' and Picacho Los Heme) overlie the Tuffs of Arroyo El Canelo [*Nagy*, 1997].

2.5.5 Arroyo Matomí–Puertecitos

The Arroyo Matomí–Puertecitos region preserves a complex stratigraphy of synrift volcanic deposits, including the probable eruptive centers for the Tuffs of the Northern Puertecitos Province [*Stock et al.*, 1991, and Figs. 2.1, 2.7, and 2.8]. Basement is exposed at the western end of Arroyo Matomí where its channel crosses the southern end of the Sierra San Felipe. Here, a 50 m+ thick section of Tmr4 of the Tuffs of

Mesa Cuadrada and a similarly thick section of the Tuffs of Arroyo El Canelo overlie tilted and faulted group three volcaniclastic strata and the Tuff of San Felipe (*Stock et al.* [1991]; *Stock* [1993], with correlation by *Nagy* [1997]). Tmr4 from this area is much thicker than on nearby Mesa Cuadrada. Similar abrupt thickness changes in the Tuffs of Mesa Cuadrada are seen at Santa Isabel Wash and the Southern Sierra San Fermín (Fig. 2.7). These abrupt thickness changes may reflect underlying topographic relief caused by subsidence due to a prior eruption (e.g., Tmr3). Adjacent to Arroyo Matomí and extending eastward toward the coastline, there are rhyolite lava flows both above and below high-grade deposits of the Tuff of Arroyo El Canelo. These high-grade deposits are interpreted as caldera fill [*Stock et al.*, 1991]. The associated rhyolite lavas here comprise coalesced domes and flows extending from the Southern Sierra San Fermín [*Lewis*, 1994] to Santa Isabel Wash [*Nagy*, 1997] and the town of Puertecitos [*Martín-Barajas and Stock*, 1993]. This region of concentrated Late Miocene volcanic activity during and just after eruption of the Tuffs of the Northern Puertecitos Volcanic Province is interpreted to be the source area for these ignimbrites. A section of the Plio-Pleistocene Tuffs of Arroyo Los Heme [*Martín-Barajas et al.*, 1995] caps the synrift volcanic sequence here. Pliocene marine strata crop out adjacent to the mountain front both north and south of Arroyo Matomí (Fig. 2.1).

2.6 Summary

In summary, the Baja California margin study area comprises a southward-thickening wedge of volcanic and sedimentary strata (groups 2–6) overlying Mesozoic and older bedrock (group 1). The lowest strata of this wedge are a thin veneer of fluvial and eolian sandstones, including a distinctive conglomerate with clasts derived from Sonora (group 2). These strata are intercalated with Early- to Mid-Miocene volcanic and volcaniclastic deposits (group 3). These deposits are comprised of scattered basalt flows in the northern part of the study area and culminate in a 500 m+

thick distal to proximal volcaniclastic apron and associated andesitic stratovolcanoes in the northern Puertecitos Volcanic Province. The Tuff of San Felipe (group 4) disconformably overlies all older units. This widespread welded tuff covers a 3,300 km^2 area encompassing the Sierra San Felipe, Sierra San Pedro Mártir, Sierra San Fermín and the northern Puertecitos Volcanic Province. Early syn-rift volcanic rocks (group 5) formed widely scattered rhyolite and andesite flows throughout the study area, with a concentration of andesite and rhyolite in the southern Valle Chico area. The 6.1 to 6.7 Ma Tuffs of the Northern Puertecitos Volcanic Province (top of group 5) cover most of the central part of the Baja California margin study area from the northern and western Puertecitos Volcanic Province to the southernmost Sierra San Felipe and the Sierra San Fermín. The thickest and highest grade outcrops of these ignimbrites occur within a ∼25 km–diameter area centered on the eastern end of Arroyo Matomí. Late syn-rift volcanism (group 6) is confined to areas adjacent to the Gulf of California coastline near the outlet of Arroyo Matomí. The most widespread group six volcanic rocks are the Plio-Pleistocene Tuffs of Arroyo Los Heme, which crop out over the eastern half of the Puertecitos Volcanic Province. Syn-rift basin deposits include non-marine alluvial fill of Valle Chico and the Llanos de San Fermín, as well a chain of uplifted basin deposits that crop out in the Sierra San Fermín and Sierra San Felipe. Marine and non-marine sedimentary deposits form a coastal plain extending eastward from the Sierra San Felipe, Sierra San Fermín, and the outlet of Arroyo Matomí.

Two regional-scale stratigraphic relationships of pre-rift and syn-rift ignimbrite deposits are key for correlation to the conjugate rifted margin in Sonora. The first of these relationships is distribution and facies of the Tuff of San Felipe. Regional mapping of the Tuff of San Felipe indicates that the source of this unit was likely to be most proximal to the northern Sierra San Fermín and the adjacent Sierra San Felipe as suggested by *Lewis* [1996] and *Stock et al.* [1999]. However, a vent for the Tuff of San Felipe was not encountered in Baja California. The second key regional-scale relationship is the distribution and source of the Tuffs of the Northern

Puertecitos Volcanic Province. These tuffs cover a ∼2,000 km^2 area of northeastern Baja California and crop out adjacent to ∼40 km of the coastline of the Gulf of California from Puertecitos to the northern Sierra San Fermín. Thick, higher-grade deposits of the Tuffs of Mesa Cuadrada and the Tuffs of Arroyo El Canelo (both part of the Tuffs of the northern Puertecitos Volcanic Province) appear to be centered on a vent or vents at the eastern end of Arroyo Matomí.

Table 2.2. Compilation of mapped units of northeastern Baja California and western Sonora into stratigraphic groups 1–6

Location	Mapped Units[1]
	Group 1: Basement Complex
Southern Valle Chico[2]	m, c, q, p, a: Metasedimentary rocks g: Granitic rocks
Sierra San Felipe	pbs, sch: Metasedimentary rocks[3] t, gb: tonalite, gabbro[3] Kgd, Kqd: Granodiorite, Quartz-Diorite[4] Mzg: Undifferentiated granitic rocks[5]
Sierra San Fermín[6]	mm: Metasedimentary rocks g: Granitic rocks
Arroyo Matomí[7]	not exposed
Santa Isabel Wash[8]	Pz: Metasedimentary rocks Mg: Granitic rocks
Puertecitos[9]	not exposed
Cinco Islas[10]	Mzm: Metasedimentary rocks of the Olvidada Formation
Isla Tiburón[11]	MzPzm: Metasedimentary rocks Mzg: Granitic rocks
Coastal Sonora[12]	MzPzm: Metasedimentary rocks Mzg: Granitic rocks
	Group 2: Tertiary Basal Sedimentary Rocks
Southern Valle Chico[2]	Tc: Fluvial conglomerate Ts: Sandstone
Sierra San Felipe	Tmf: Fluvial deposits[3] Tos: Old conglomerate (with distinctive clasts)[4] Tcg, Ts: Conglomerate (with distinctive clasts), sandstone[5]
Sierra San Fermín[6]	Ts: Sandstone
Arroyo Matomí[7]	not exposed
Santa Isabel Wash[8]	not exposed (base of Tmvs?)
Puertecitos[9]	not exposed
Cinco Islas[10]	Tcg: Conglomerate

Compilation of mapped units of northeastern Baja California and western Sonora into stratigraphic groups 1–6, continued

Location	Mapped Units[1]
	Group 2: Tertiary Basal Sedimentary Rocks (continued)
Isla Tiburón[11]	Tcg: Conglomerate
Coastal Sonora[13]	T1c: Conglomerate (with distinctive clasts)
	Group 3: Miocene volcanic arc
Southern Valle Chico[2]	Mb1: Basalt, 20.5±0.36 K–Ar on whole rock Mb2: Basalt, 19.56±0.42 K–Ar on whole rock Mb3: Basalt, 17.03±0.26 K–Ar on whole rock Mvb: Breccia, 16.82±0.26 K–Ar on whole rock Mvs: Volcaniclastic sediments, 16.75±0.28 K–Ar on biotite Mtt: *Tuffs of Toronja Hill* Mb4: Basalt, 14.53±0.22 K–Ar on whole rock Mb5: Basalt, 12.70±0.24 K–Ar on whole rock
Sierra San Felipe	Tmb: Basalt, 15.0±0.4[14] Tmb, Tma, Tmv: Basalt, andesite, and undifferentiated volcanic rock[3] Tmb1: Basalt[5]
Sierra San Fermín[6]	Tmb1: Basalt, 21±1 K–Ar on whole rock Tmb2: Basalt Tmvs: Volcaniclastic sediments, pyroclastic flows, epiclastic deposits
Arroyo Matomí[7]	Tmvs: Volcaniclastic sediments, pyroclastic flows, epiclastic deposits
Santa Isabel Wash[8]	Tmvs: Volcaniclastic sediments, pyroclastic flows, epiclastic deposits Tmrb: *Biotite Tuff*, 17±2.4 $^{40}Ar/^{39}Ar$ on biotite Tmbk: *Klondike Canyon Basalt*, 17.1±2.4 $^{40}Ar/^{39}Ar$ on plagioclase Tmbl: *Land of the Lost Basalt*, 16.3±1.0 $^{40}Ar/^{39}Ar$ on plagioclase Tmdt: *Tombstone Dacite*, 15.5±0.7 to 16.7±1.0 $^{40}Ar/^{39}Ar$ on plagioclase
Puertecitos[9]	Tma: Andesite, pyroclastic flows and epicalstic deposits, 15.9±0.2, 16.3±0.1 $^{40}Ar/^{39}Ar$ on hornblende

Compilation of mapped units of northeastern Baja California and western Sonora into stratigraphic groups 1–6, continued

Location	Mapped Units[1]
	Group 3: Miocene volcanic arc (continued)
Cinco Islas[10]	Tmv: Volcaniclastic sediments, pyroclastic flows, epiclastic deposits Tmva, Tmla, Tmua: Andesite
Isla Tiburón[11]	Tmvs: Volcaniclastic sediments, pyroclastic flows, epiclastic deposits Tmb1, Tmrf1: Basalt, Rhyolite lava Tma, Tma1, Tma1d: Andesite Tmvlc: *La Cruz Volcanic Sequence* (basalt, volcaniclastic redbeds, rhyolite lava(?) and pyroclastic flows(?)) Tmrcc: *Tuffs of Cerro Colorado*, 9.58±2.66 Ma, $^{40}Ar/^{39}Ar$ on alkali feldspar Tmrk: *Tuff of the Sierra Kunkaak*
Coastal Sonora[12]	Tmvs: Volcaniclastic sediments, pyroclastic flows, epiclastic deposits Tmb1, Tma1: Basalt, Andesite Tmrj: *Tuffs of Pico Johnson*
	Group 4: Tuff of San Felipe
Southern Valle Chico[2]	Mr1: *Rhyolite Tuff #1*
Sierra San Felipe	Tmr1: Ash-flow rhyolite, 12.2±0.9 K–Ar on whole rock[4] Tmrsf: *Tuff of San Felipe*, 12.43±0.14 $^{40}Ar/^{39}Ar$ on alkali feldspar[15]
Sierra San Fermín[6]	Tmr1: *Rhyolite Tuff #1*, 13.5±0.5, (10.6±0.1) $^{40}Ar/^{39}Ar$ on alkali feldspar
Arroyo Matomí[7]	Tmr1: *Rhyolite Tuff #1*
Santa Isabel Wash[8]	Tmrs: *Tuff of San Felipe*, 12.7±0.5 $^{40}Ar/^{39}Ar$ on alkali feldspar
Puertecitos[9]	not exposed/not present
Cinco Islas[10]	not present
Isla Tiburón[11]	Tmrsf: *Tuff of San Felipe*, 12.96±3.67, (9.66±1.31) $^{40}Ar/^{39}Ar$ on alkali feldspar
Coastal Sonora[12]	Tmrsf: *Tuff of San Felipe*, 13.86±2.21 $^{40}Ar/^{39}Ar$ on alkali feldspar

Compilation of mapped units of northeastern Baja California and western Sonora into stratigraphic groups 1–6, continued

Location	Mapped Units[1]
	Group 5: Early syn-rift deposits[16]
Southern Valle Chico[2]	Ma2: Andesite, 6.47±0.5, K–Ar on alkali feldspar Mr2: Rhyolite flows, 5.80±0.5 $^{40}Ar/^{39}Ar$ on alkali feldspar Tmyt: Non-welded yellow tuffs
Sierra San Felipe	Tmb2: Basalt, 8.9±1.2, K–Ar on plagioclase[3] Tmt: Rhyolitic tuff, 16.6±1.3, K–Ar on whole rock[4] Tmr2: Spherulitic welded tuff, 12.3±1.8, 13.6±2.4, K–Ar on whole rock[4] Tmrsrb1, Tmrsrb2: *Tuffs of Santa Rosa Basin*, equivalent to Tmt and Tmr2 above[5] Tmf: fluvial deposits[3] Tmm, Tmf1, Tmf2, Tmf3: Monolithologic megabreccia, alluvial fan deposits[4] Tmal, Tmpal: fluvial deposits[5]
Sierra San Fermín[6]	Tma2: Andesite, 11.7±0.6 wr Tmr2: Rhyolite flows Tmyt: Non-welded yellow tuffs Tmr9: Rhyolite flows (lower)
Arroyo Matomí[7]	f1, f2: Rhyolite flows.
Santa Isabel Wash[8]	Tmat: *Pico del Toro Andesite*, 9.3±0.8 $^{40}Ar/^{39}Ar$ on plagioclase
Puertecitos[9]	Tmrl: Lower rhyolite flows
Cinco Islas[10]	not present(?)
Isla Tiburón[11]	Tmb2, Tma2, Tmrf2: Basalt, andesite, and rhyolite flows Tm Tmal, Tmpal: Fluvial conglomerate and non-welded pyroclastic deposits
Coastal Sonora[12]	Tmrpc: *Tuffs of Punta Chueca* Tmb2, Tmrf2: Basalt, Rhyolite flows Tmpal: Fluvial conglomerate

Compilation of mapped units of northeastern Baja California and western Sonora into stratigraphic groups 1–6, continued

Location	Mapped Units[1]
	Tuffs of the Northern Puertecitos Volcanic Province[16]
Southern Valle Chico[2]	Mmt: *Tuffs of Matomí* Mr3: *Rhyolite Tuff #3*, 6.07±0.20, 6.14±0.16 K–Ar on alkali feldspar Mr4: *Rhyolite Tuff #4*
Sierra San Felipe	not present, except adjacent to the Sierra San Fermín (see below) and southern Valle Chico (see above)
Sierra San Fermín[6]	Tmr3a: *Rhyolite Tuff #3a* Tmr3b: *Rhyolite tuff #3b*, 6.5±0.2, 6.7±0.2 ^{40}Ar/^{39}Ar on alkali feldspar Tmr4: *Rhyolite Tuff #4* Tmr5: *Rhyolite Tuff #5* Tmr6: *Rhyolite Tuff #6* Tmr7: *Rhyolite Tuff #7*, 6.4±0.3, ^{40}Ar/^{39}Ar on alkali feldspar Tmr8: *Rhyolite Tuff #8*
Arroyo Matomí[7]	t2: *Rhyolite Tuff #4*[17] t3: *Tuffs of Arroyo El Canelo*[17] t12, t14, t9: *Tuffs of Arroyo El Canelo*
Santa Isabel Wash[8]	Tmrw: *Tuffs of Santa Isabel Wash*, 6.5±0.3, 6.6±0.5, 6.7±0.3 ^{40}Ar/^{39}Ar on plagioclase Tmr3–I: *Rhyolite Tuff #3–I* Tmr3–II: *Rhyolite Tuff #3–II*, 6.2±0.1, 6.5±0.2, 6.4±0.2 ^{40}Ar/^{39}Ar on alkali feldspar Tmr4: *Rhyolite Tuff #4* Tmra: *Tuff of Arroyo El Oculto*, 6.4±0.3 ^{40}Ar/^{39}Ar on alkali feldspar Tmre: *Tuff of Arroyo El Canelo*, 6.1±0.5 ^{40}Ar/^{39}Ar on plagioclase Tmrb: *Bighorn Sheep Tuff* Tmrf: *Flagpole Tuff*
Puertecitos[9]	Tmrc: *Tuffs of Arroyo El Canelo*
Cinco Islas[10]	not present

Compilation of mapped units of northeastern Baja California and western Sonora into stratigraphic groups 1–6, continued

Location	Mapped Units[1]
	Tuffs of the Northern Puertecitos Volcanic Province (continued)[16]
Isla Tiburón[11]	Tmr3a: *Tuffs of Mesa Cuadrada, Tmr3a member* Tmr3: *Tuffs of Mesa Cuadrada, Tmr3 member*, 5.7±0.6 K–Ar on alkali feldspar[14], 5.33±2.18, 6.15±1.03 $^{40}Ar/^{39}Ar$ on alkali feldspar Tmr4: *Tuffs of Mesa Cuadrada, Tmr4 member* Tmr5: *Tuffs of Dead Battery Canyon, Tmr5 member* Tmrao: *Tuffs of Arroyo El Canelo, El Oculto Member* Tmrec: Tmrec1, Tmrec2: *Tuffs of Arroyo El Canelo, El Canelo Members* Tmrfp: *Tuffs of Arroyo El Canelo, Flagpole Member*
Coastal Sonora[12]	not present
	Group 6: Late syn-rift deposits
Southern Valle Chico[2]	PQl: Lacustrine limestone Qoal, Qal: Alluvium
Sierra San Felipe	Tpf, Qf, Qal: Alluvium[3] Tpm: Marine sediments[3] Tmpal, Qoal, Qal: Alluvium[5]
Sierra San Fermín[6]	Tmr9: Rhyolite flows (upper) Tpet: *Tuffs of Mesa El Tabano* (6.2±0.3), (5.6±0.2) $^{40}Ar/^{39}Ar$ on plagioclase Tpa: andesite (5.7±0.2) $^{40}Ar/^{39}Ar$ on whole rock Tpm, Tpsc, Tpsb: Marine sediments (*Puertecitos Formation*) Tpsa: Marine volcanic sandstone, (4.5±0.3), 3.2±0.7 $^{40}Ar/^{39}Ar$ on plagioclase from interbedded tuff Ps, Qoal, Qal: Alluvium
Arroyo Matomí[7]	f4, f11, r6: Rhyolite flows t8: *Tuffs of Mesa El Tabano* Pmw, Pmy: Marine sediments Ps, QPal, Qoal, Qf, Qal: Alluvium
Santa Isabel Wash[8]	Tmag: *Pico de los Gemelos Andesite* Tmrc: *Picacho Canelo Rhyolite* (flow), 6.0±0.4, 5.9±0.8 $^{40}Ar/^{39}Ar$on alkali feldspar Tmau: *Ugly Mountain Andesite* Tmah: *Low Heme Andesite* Qoal, Qal: Alluvium

Compilation of mapped units of northeastern Baja California and western Sonora into stratigraphic groups 1–6, continued

Location	Mapped Units[1]
	Group 6: Late syn-rift deposits (continued)
Puertecitos[9]	Tmru: Rhyolite flows, 5.80±0.03 $^{40}Ar/^{39}Ar$ on whole rock Tba: Andesite, 5.1±0.3 $^{40}Ar/^{39}Ar$ on whole rock Tph: *Tuffs of Los Heme*, 2.7±0.4, 3.36±0.03 $^{40}Ar/^{39}Ar$ on plagioclase Tpvc: *Tuff of Valle Curbina*, 3.5±0.1 $^{40}Ar/^{39}Ar$ on plagioclase Tpet: *Tuffs of Mesa El Tábano* Tpa: *Andesite of Volcan Prieto*, 2.6±0.1 $^{40}Ar/^{39}Ar$ on whole rock Tms, Pms: *Puertecitos Formation* marine deposits Qal: Alluvium
Cinco Islas[10]	Tprh: *Tuffs of Los Heme* Tpb, Tpbc: Basalt Tmpal, Qoal, Qal: Alluvium
Isla Tiburón[11]	Tmprsz: *Tuffs of Arroyo Sauzal*, 5.67±0.17 K–Ar on alkali feldspar[18], 6.67±0.83, 5.40±3.90, 6.40±1.63, $^{40}Ar/^{39}Ar$ on alkali feldspar Tprcs: *Rhyodacite of Cerro Starship*, $(11.2\pm1.3)^{14}$, 3.7 ± 0.9^{14}, 4.16 ± 1.81^{18}, K–Ar on plagioclase Tprbv: *Tuffs of Bahia Vaporeta* Tpdcc: *Cerro Colorado Dacite* Tpth: *Hipat Tuffs* Tmpm, Qm: Marine sediments, terraces Tmpal, Qoal, Qal: Alluvium
Coastal Sonora[12]	Tmpal, Qoal, Qal: Alluvium

[1]Named units *emphasized*. Anomalous or otherwise suspect dates enclosed in parentheses. All ages in millions of years.

[2]*Stock* [1993] and *Stock* [1989].

[3]*Gastil et al.* [1975].

[4]*Bryant* [1986].

[5]Fig. 2.4.

[6]*Lewis* [1994] and *Lewis* [1996].

[7]*Stock et al.* [1991].

[8]*Nagy* [1997] and *Nagy et al.* [1999].

[9]*Martín-Barajas and Stock* [1993], *Martín-Barajas et al.* [1995], and *Martín-Barajas et al.* [1997].

[10]See Plate IV and chapter 7 of this thesis.

[11]See Plate II and chapter 3 of this thesis.

[12]See Plate I and chapter 3 of this thesis.

[13]*Gastil and Krummenacher* [1976].

[14]*Gastil et al.* [1979].

[15]*Stock et al.* [1999].

[16]The Tuffs of the Northern Puertecitos Volcanic Province, which form the uppermost deposits of group 5, are listed separately here for clarity.

[17]With correlation by *Nagy* [1997].

[18]*Gastil et al.* [1999].

Chapter 3
Geology of the western Sonoran continental margin

3.1 Abstract

Geologic investigations of Isla Tiburón and western Sonora encountered a similar stratigraphy to that described for the conjugate rift margin of the Upper Delfín basin in northeastern Baja California. The rocks of the Sonoran margin are divided here into six partially interfingering stratigraphic groups in the same manner as for Baja California. Group one encompasses the basement rocks of the Sonoran coastal batholith and host metamorphosed sedimentary rocks. Group two basal sedimentary rocks are mostly absent from the Sonoran margin except for a distinctive fluvial conglomerate described by *Gastil et al.* [1973] for the Sierra Seri. Lava flows, intrusions, and volcaniclastic deposits of the Middle Miocene volcanic arc comprise group three. Unique volcanic sections within group three delineate separate stratigraphic domains that are juxtaposed by faulting in coastal Sonora and Isla Tiburón. Lithologic group four contains correlative deposits of the Tuff of San Felipe, a 12.6 Ma ignimbrite. Part of the vent for the Tuff of San Felipe is identified near Punta Chueca, Sonora (29.0°N, 112.2°W). Syn-rift volcanic, volcaniclastic, and fluvial deposits are divided into groups five and six. On western Isla Tiburón, group five is capped by correlative outcrops of the Tuffs of the Northern Puertecitos Volcanic Province. Group six contains a younger syn-rift volcanic and fluvial assemblage similar to group five, and also includes marine deposits of the Gulf of California. As in Baja California, regional-scale stratigraphic relationships of the Tuff of San Felipe and the Tuffs of the Northern Puertecitos Volcanic Province are identified for correlation to the conjugate rifted margin of the Upper Delfín basin. The Tuff of San Felipe fills a series of west-trending paleocanyons that crop out over a north-south distance of 30 km adjacent to the western coastline of Isla Tiburón. Higher-grade densely welded outcrops of the Tuff of San Felipe occur in coastal Sonora and on the northern areas of Isla Tiburón. The Tuffs of the Northern Puertecitos Volcanic Province are restricted to the western and northern areas of Isla Tiburón.

3.2 Introduction

This chapter is the second of two chapters that introduce the geology of conjugate rifted continental margins of the Upper Delfín basin in the Gulf of California. This chapter summarizes the geology of central western Sonora in order to match this region to its conjugate rifted margin in northeastern Baja California. Prior to opening of the Gulf of California, volcanic and sedimentary rocks deposited on the conjugate rift margins should share similar lithologies and paleogeographic distributions. Restoration of displacement across this segment of the rift must reasonably match the distribution of pre-rift volcanic and sedimentary deposits and explain the distribution of syn-rift deposits. This chapter contains an explanation of new geologic mapping and a complete stratigraphic overview of central coastal Sonora and Isla Tiburón between 28°45′ and 29°25′ latitude (Plates I and II, Fig. 3.1 and Table 2.2 located at the end of chapter 2). Particular attention is given here to the lithology and facies distribution of several widespread silicic ignimbrites ro establish their correlation to the Puertecitos Volcanic Province of Baja California.

3.3 Geologic mapping of coastal Sonora and Isla Tiburón

3.3.1 Reconnaissance investigations

Reconnaissance geologic investigations conducted over the central-western coastline of Sonora, Mexico, sought to identify matching pyroclastic flow deposits to the Puertecitos Volcanic Province and the Sierra San Felipe of Baja California. Earlier reconnaissance mapping by *Gastil and Krummenacher* [1976] guided selection of the central region of the Sonoran coastline for initial study. *Gastil et al.* [1973] and *Gastil and Krummenacher* [1976] correlated a distinctive conglomerate from the Sierra Seri in coastal Sonora to the Santa Rosa Basin in Baja California (Fig. 1.4). This cor-

relation suggested the possibility of matching the younger, voluminous Tuff of San Felipe and the ash-flow tuffs of the northern Puertecitos Volcanic Province to this same region of coastal Sonora [*Stock et al.*, 1999; *Nagy et al.*, 1999]. Accessible outcrops of ash-flow tuffs mapped by *Gastil and Krummenacher* [1976] were assessed for litholigic similarity to the distinctive tuffs mapped in northeastern Baja California (Fig. 2.1). These investigations from Puerto Lobos in the north to Bahía Kino in the south (Fig. 1.4) spanned the entire length of earlier mapping by *Gastil and Krummenacher* [1976].

Potentially correlative outcrops of the Tuff of San Felipe and the Tuffs of the northern Puertecitos Volcanic Province were found in coastal Sonora and Isla Tiburón. Outcrops of the Tuff of San Felipe up to 135 m thickness were found along a 25 km length of the Sierra Seri between Punta Chueca and Bahia Kino (Fig. 3.1). On the western side of Isla Tiburón, a 300 m thick section of ash-flow tuffs contains correlatives to the Tuff of San Felipe overlain by correlatives to the Tuffs of the northern Puertecitos Volcanic Province. Inspection of Landsat Thematic Mapper imagery of Isla Tiburon revealed that the potentially correlative section here is present in the Sierra Menor and Sierra Alta on the western half of the island. Additional isolated outcrops are present in the Sierra Kunkaak on the northeastern part of the island (Fig. 3.1).

3.3.2 Detailed geologic mapping

Areas for detailed study were chosen to encompass the extent of potentially correlative ash-flow tuffs on Isla Tiburón and mainland coastal Sonora (Plates I and II, Figs. 1.4 and 3.1). Field studies of tuff outcrops on mainland Sonora concentrate on the facies and depositional relationships of the Tuff of San Felipe. Possible vent and near-vent facies of this pre-rift deposit in this region indicate displacement between Isla Tiburón and Coastal Sonora. Outcrops of a thick and possibly complete section of tuffs on western Isla Tiburón matching the northern Puertecitos Volcanic Province were selected for more intensive field study. The unusual position of western

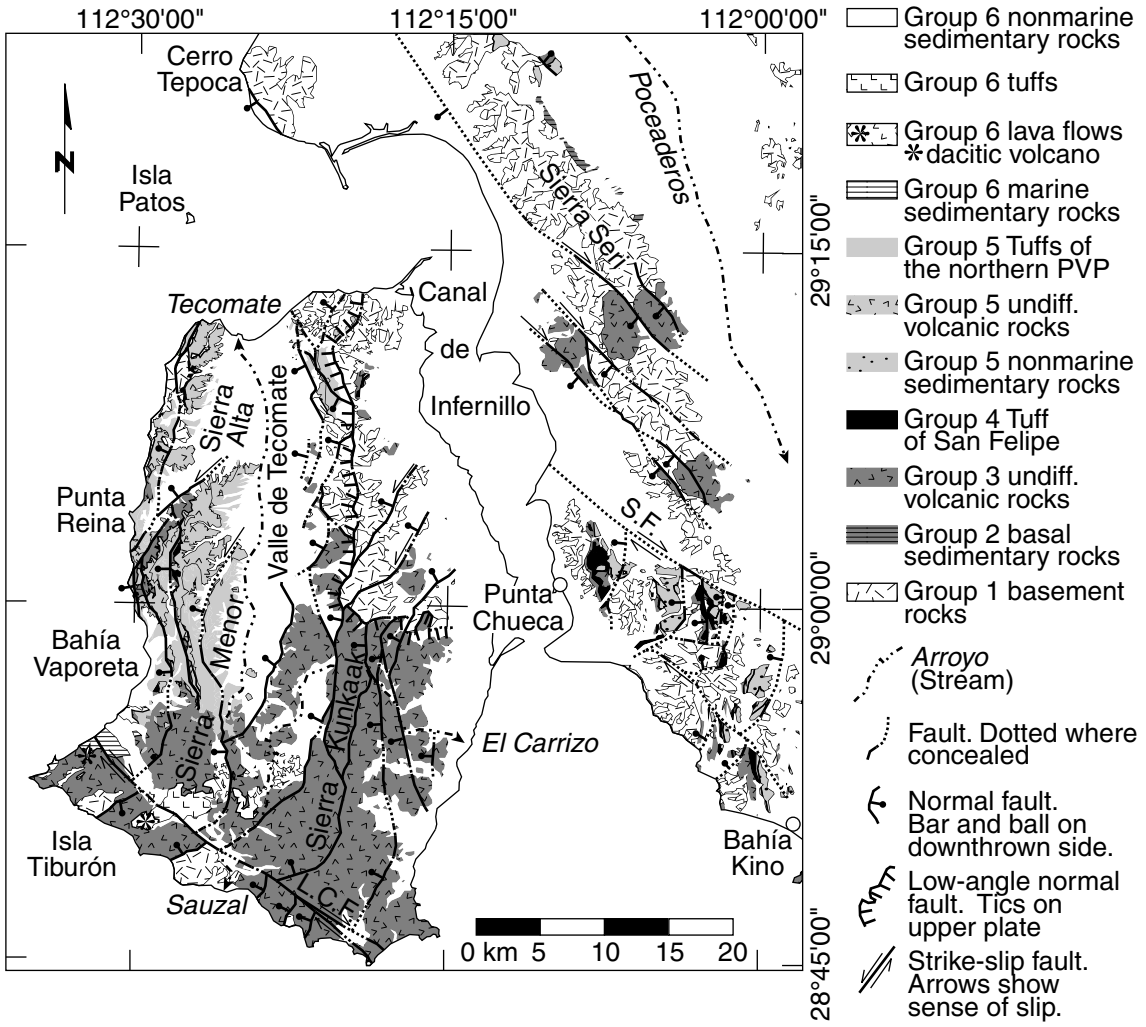

Figure 3.1. Geologic map of coastal Sonora and Isla Tiburón. Mapping generalized from plate I, plate II, *Gastil and Krummenacher* [1976], and *Gastil et al.* [1999] with additional field reconnaissance. A georeferenced Landsat Thematic Mapper image (path 36, row 40) was used as a base map. See text for discussion of the lithologic groups presented here. This map and figures 3.2–3.6 are universal transverse Mercator projection, zone 12.

Isla Tiburón closely adjacent to the deep basins of the northern Gulf of California provides exceptional potential for matching its geology to the conjugate rifted margin of Baja California.

Detailed geologic mapping of the coastal Sonora and western Isla Tiburón study areas each was limited by significant cartographic, access, and time constraints. The geology of coastal Sonora was mapped directly onto 1:50,000 topographic base maps published by the Mexican government (Plate I). No 1:50,000 maps are published for Isla Tiburón, and map sheets that cover both the mainland and the island show only mainland areas. A pair of lower-quality 1:250,000 topographic maps include the island, but these were unsuitable for detailed geologic mapping. Aerial photographs obtained from the Mexican cartographic agency (INEGI) cover both the island and mainland areas as separate flight lines. These photographs, printed at a scale of approximately 1:50,000, were used as field base maps for geologic mapping of Isla Tiburon (Fig. 3.1, Plate II). The final geologic map was composed in Arc/Info GIS (geographical information system) from a georeferenced mosaic of these photographs at 2 meter pixel resolution. This mosaic was generated in ENVI (Environment for Visualizing Images) software using a 30-meter-pixel Landsat Thematic Mapper image (path 36, row 40) as a base, georeferenced to a 90-meter-pixel digital elevation model provided by *National Imagery and Mapping Agency* [1993]. Absolute locations on this mosaic are accurate at the 100-meter level, while local relative positions (within 1000 meters) are probably accurate to 10 meters. Local distortions are present in areas of high topographic relief or at photograph boundaries.

Access to all areas of the mainland required permission of landowners. The coastal Sonora map area includes several ranchos, small parcels near the town of Bahia Kino, and tribal lands of the Seri (Kunkaak) Indian tribe. Permission to access Seri lands is obtained from the Seri governor at home in Punta Chueca or at an office in Bahía Kino. Access to ranchos and other parcels required locating and obtaining permission of individual owners or operators. Permission to enter Rancho Sacrificio, a hunting rancho located northeast of Punta Chueca, was obtained from a ranch house located

one kilometer east of the coastal road. Other ranch houses are located on the Valle de Kino road east of the Sierra Seri. Several poorly maintained ranch roads cross the Sierra Seri between Punta Chueca and Bahia Kino and provide access to interior areas. Most of the reconnaissance mapping of the coastal area relies on detailed observations near these access ways. Remote and fenced-in regions were mapped from air-photo and Landsat image interpretation.

Access to western Isla Tiburón is controlled by the weather and by hunting interests. Trophy bighorn sheep hunting from December through February closes the entire island and much of the mainland ranch lands. From mid-November through early March the western shoreline of Isla Tiburón is exposed to a strong prevailing northwest wind and waves, making boat landings impossible. Temperatures in excess of 38°C (100°F) begin as early as mid-April and are common by the beginning of May. Ideal combinations of sea conditions and weather occur from late March through early May. Access to the interior of the island by a 4-wheel drive vehicle owned by the Seri Tribe is possible during times of rough seas. All fieldwork presented here was performed by boat access to the shoreline of Isla Tiburón (Plate II). Campsites (*Campos*) with safe landings during moderate wave action are located at Bahía Vaporeta on the western shore and Arroyo Tecomate on the northern shore (Plate II). Other areas of western Isla Tiburón could only be accessed during calm days.

Detailed geologic mapping of Isla Tiburón concentrated on the western coast of the island (Figs. 1.4 and 3.1). This area presented a well-exposed north-south transect of volcanic strata to match with the conjugate rifted margin in Baja California. Interior areas of the southern and northeastern parts of the island were explored in order to assess important stratigraphic features identified by initial reconnaissance studies. Areas bordering the interior valley of the island (Valle Tecomate) were mapped primarily by air-photo and Landsat interpretation. Fortunately, stratigraphic and structural complexity appear most commonly near the western coastline of Isla Tiburón while much of the interior area of the Sierra Menor and Sierra Alta consists of sim-

ple, well-exposed block faulted ridges (Plate II). Field reconnaissance of the Sierra Kunkaak revealed a thick section of non-correlative volcanic rocks. Some of these strata were encountered near the northeastern edge of the detailed map area. The relationship of the Sierra Kunkaak to the correlative sections and regional stratigraphy is discussed in greater detail below.

Landsat Thematic Mapper imagery was used to identify volcanic lithologies for initial reconnaissance studies as well as for detailed mapping of interior areas of Isla Tiburón. A simple false color composite image was interpreted, using Band 7 (2.08–2.35 μm, reflected IR) for red, Band 4 (0.76–0.90 μm, reflected IR) for green, and Band 1 (0.45–0.52 μm, blue-green) for blue. A gaussian stretch was applied to the image to enhance contrast of volcanic strata. Empirical, map-view correlation to areas of known lithology enabled mapping of individual units into inaccessible regions. Lava flow compositions were also estimated by reflectance in bands 4 and 7, which most likely indicates Fe content and mineralogy [*Hook et al.*, 1998]. Andesite flows showed a strong signature of hematite, reflecting strongly in both bands 4 and 7 as an orange hue in the false color image. The reflectance of unaltered dacitic and rhyolitic compositions was weaker in band 7 and sharply diminished band 4. These lithologies trended towards darker red to black in the false color image.

Hydrothermal alteration, which most affects bands 1 and 4 [*Sabins*, 1996], and scattering, which affects all bands [*Clark*, 1998], appear to most strongly affect rhyolitic compositions. Hydrothermal alteration was manifested by blue-green hues on the false color image, whereas scattering was manifested by pastel colors and white. Partially welded ash-flow tuffs displayed a characteristic stratigraphic sequence on the false-color image with a red to green base capped by lighter green and white. This sequence is interpreted here as a strongly welded base dominated by reflectance of Fe minerals (red). This is overlain by hydrothermally altered welded to partially-welded tuff (green). Scattering by non-welded tuff or intensively vapor-phase recrystalized tuff is manifested by lighter green to white hues. Basalt, which was typically non-reflective in the false-color image, sometimes showed reflectance in band 1 corre-

sponding to weathered outcrops.

3.4 Stratigraphy of coastal Sonora and Isla Tiburón

3.4.1 Stratigraphic framework

The stratigraphy of coastal Sonora and Isla Tiburón closely resembles that of northeastern Baja California [*Gastil and Krummenacher*, 1977]. The same framework outlined above for Baja California is applied here to the Sonoran margin. *Gastil and Krummenacher* [1976] relied on relative tilting to discriminate between five differently aged volcanic stratigraphic packages. Since different areas of coastal Sonora and Isla Tiburón have been subject to differing degrees and style of tectonism, these age groupings show considerable overlap in K–Ar ages [*Gastil and Krummenacher*, 1977]. Detailed field study has revealed that *Gastil and Krummenacher* [1976] mapped regionally correlative units into multiple groups in different areas. For these reasons, a detailed correlation of the *Gastil and Krummenacher* [1976] map to the stratigraphic framework used in this study is possible only on a range-by-range basis (Table 3.3, located at the end of this chapter). These correlations will be discussed in the following descriptions of the stratigraphy of Isla Tiburón and coastal Sonora.

3.4.2 Basement complex

Group one basement of Isla Tiburón and coastal Sonora is broadly similar to the basement of northeastern Baja California [*Gastil et al.*, 1978]. Plutons of Mid to Late Cretaceous tonalite and granodiorite intrude metasedimentary and metavolcanic strata of Mesozoic and Paleozoic age. Reconnaissance studies suggest that the basement here is an offset continuation of the Peninsular Ranges Batholith of northern Baja California [*Silver and Chappell*, 1988]. Isotopic studies of plutons in the study area support this correlation [*Valencia-Moreno et al.*, 2000]. Interpretations of the metasedimentary strata of Isla Tiburón and coastal Sonora have differed due to lack

of age control. Strata of coastal Sonora and Isla Tiburón may correlate with outcrops of an east-west trending Paleozoic miogeoclinal to eugeoclinal facies transition, located in central Sonora, and with equivalent metasedimentary strata in northeastern Baja California [*Gastil et al.*, 1991]. Alternatively, the metasedimentary strata of Isla Tiburón and coastal Sonora may be a remnant of a Late Paleozoic to Early Mesozoic oceanic basin [*Dickinson and Lawton*, 2001] or back-arc basin [*Radelli*, 1989; *Gastil et al.*, 1981].

Plutonic basement exposures in the study area are not differentiated by lithology and are mapped as unit Mzg (Plates I and II). Metasedimentary and metavolcanic strata were similarly grouped together as unit MzPzm in the map areas (Plates I and II). *Gastil and Krummenacher* [1976] distinguished basement lithologies in the study areas. Field checking of basement lithologies mapped by *Gastil and Krummenacher* [1976] revealed that plutonic lithologies are generally mapped accurately while metamorphic lithologies displayed considerable heterogeneity at the outcrop scale that is not represented in their reconnaissance study.

Outcrops of basement dominate the coastal Sonora study area (Fig. 3.2, Plate I). These outcrops are tonalite to granodiorite near Bahia Kino, with a mixture of plutonic and metamorphic lithologies towards the northwest part of the map area. *Gastil and Krummenacher* [1977] describe tonalite adjacent to Bahía Kino and at Cerro Buenanoche (Fig. 3.2). A granodiorite is described from areas inland from Punta Chueca ($^{3}93^{000}$,$^{32}\,08^{800}$; all locations in the Sonora study area are UTM zone 12). Closer to the village of Punta Chueca, metavolcanic rocks ($^{3}89^{740}$,$^{32}\,09^{280}$), and mixed metacarbonate rock and metachert ($^{3}86^{670}$,$^{32}\,14^{000}$) are described by *Gastil et al.* [1981]. *Valencia-Moreno et al.* [2000] also describe metacarbonate rocks from the coastal region.

On Isla Tiburón, basement is exposed in two distinctive belts. On the southern part of the island and the adjacent island of Isla Datil, tonalite and metasedimentary strata are exposed in a series of northwest-tilted blocks [*Gastil and Krummenacher*, 1976, also Fig. 3.1]. This belt of basement oucrops is separated across the La Cruz

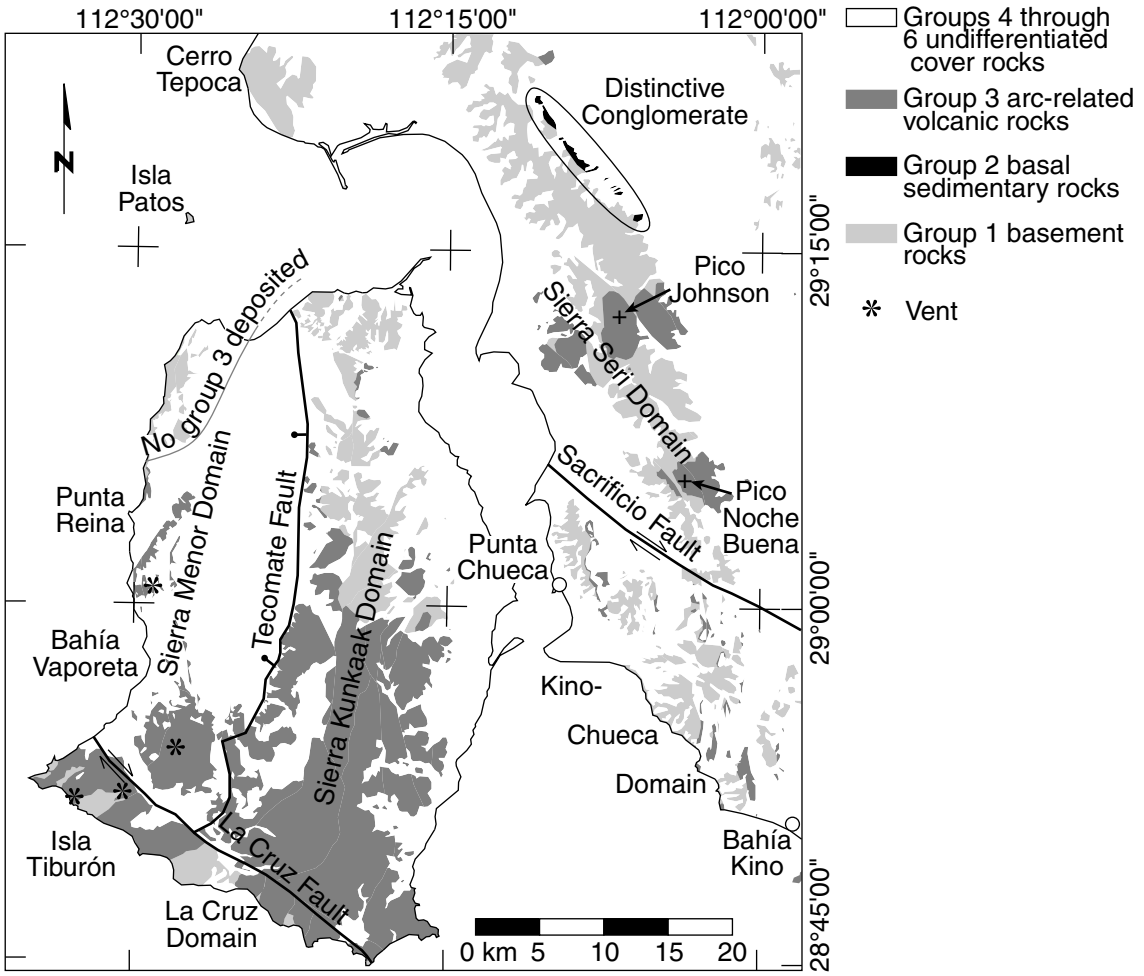

Figure 3.2. Outcrops of stratigraphic groups 1, 2, and 3 in coastal Sonora and Isla Tiburón. Distinctive conglomerate outcrops of *Gastil et al.* [1973] and *Gastil and Krummenacher* [1976] are circled in the northwest corner of map. Five domains of group three volcanic arc strata are shown with boundary structures. On Isla Tiburón, the Sierra Menor domain is separated by the Tecomate basin from the Sierra Kunkaak. The Tecomate fault is shown in a simplified form here. The La Cruz domain spans the southwest shoreline of Isla Tiburón and is separated from adjacent domains by the La Cruz fault. On coastal Sonora, the Kino–Chueca domain and the Sierra Seri domain are separated by the Sacrificio fault. See text for discussion of the stratigraphy of these domains. Grey line denotes an area of northwest Isla Tiburón where no group three rocks were deposited.

fault from the central area of Isla Tiburón where exposure levels do not reveal basement at the surface. Near Punta Reina basement is exposed on the coast beneath east-tilted volcanic strata of the Sierra Alta (Fig. 3.1, Plate II). Basement also appears at approximately this latitude in the Sierra Kunkaak on the eastern side of Isla Tiburón [*Gastil and Krummenacher*, 1976, also Fig. 3.1]. Basement in coastal exposures on the northwest shoreline of Isla Tiburón comprises a steeply-tilted section of pelitic shales, metachert, and possibly metabasalt. Metachert, metacarbonate rocks, thinly-bedded quartzite, pelitic shales and phyllites are also observed in the northern Sierra Kunkaak ($^{3}72^{310}$,$^{32}\,28^{270}$).

Similar to the Baja California study area, the age and composition of pre-batholithic basement is unknown from the study area. The relationship of the Peninsular Ranges Batholith to the Proterozoic margin of North America is exposed 100 km north of the study area, inland of Puerto Libertad [*Gastil and Krummenacher*, 1976]. In this region, Mesozoic plutons are in tectonic and intrusive contact with Neoproterozoic to Paleozoic carbonate rocks that overlie Proterozoic crystalline basement of the Caborca Terrane [*Gastil et al.*, 1981]. Within the study area, ages of metasedimentary and metavolcanic strata are known only from Isla Dátil (also called Isla Turner), a small island located 2 km south of the southernmost point on Isla Tiburon ($3^{73}640, 31^{78}720$). Here, *Poole et al.* [1993] report Ordovician fossils from a section of metamorphosed deep-water shale. Isotopic age determinations indicate Mid to Late Cretaceous plutonic basement in the coastal Sonora and Isla Tiburón areas [*Gastil and Krummenacher*, 1977; *Silver and Chappell*, 1988].

3.4.3 Tertiary basal sedimentary rocks

Group two sedimentary deposits unconformably or nonconformably overlie group one basement and underlie later volcaniclastic strata of group three or group four. These strata are absent from most basement-cover contacts in the Sonoran margin study area except for outcrops in the Sierra Seri (Fig. 3.2). These outcrops correlate to a conglomerate with distinctive fusulinid fossil-bearing clasts present in the Santa

Rosa Basin of Baja California [*Gastil et al.*, 1973]. Outcrop patterns of this conglomerate in the Sierra Seri suggest that this deposit filled a 15 km-wide paleo-valley cut into Mesozoic basement (group one). *Gastil and Krummenacher* [1976] mapped these deposits as unit T1c. Field observations from other parts of the study area revealed additional group two deposits at only one locality within the Sierra Alta area of Isla Tiburón (Fig. 3.1). In this locality, a 3 m thick conglomerate consisting of locally derived clasts of metamorphic rocks fills a 100 m wide paleocanyon. Other regions of the study area mapped as T1c or T1s by *Gastil and Krummenacher* [1976] were remapped as younger syn-rift alluvial deposits (Plate II).

The age of group two strata is best constrained from correlation to Baja California. No other strata cap the distinctive conglomerate outcrops in the Sierra Seri and therefore their upper age limit cannot be constrained from observations in Sonora [*Gastil and Krummenacher*, 1976, also Fig. 3.1]. Correlation of this conglomerate to Baja California indicates a range of possible ages from Eocene through middle Miocene for these deposits in Sonora (Chapter 2). The conglomerate-filled channel mapped as Tcg in the Sierra Alta is overlain by the 12.6 Ma Tuff of San Felipe (Plate II) similar to group two deposits of northeastern Baja California.

3.4.4 Miocene volcanic arc

Early to Middle Miocene volcanic deposits of dominantly andesitic composition crop out extensively throughout the Isla Tiburón and coastal Sonora study areas (Figs. 3.1 and 3.2). Similar to deposits of this age in Baja California, these form part of a Miocene volcanic arc that stretched from northeastern Baja California through central Mexico [*Sawlan*, 1991]. The majority of outcrops in the study areas are volcaniclastic deposits and associated lava flows formed proximal to volcanic centers. Where exposed, the base of group three rests unconformably or nonconformably on basement (group one). Group three is overlain conformably and disconformably by the Tuff of San Felipe (group four) and unconformably by group five and group six synrift strata. Ages of group three strata are based primarily on prior isotopic age de-

terminations by *Gastil and Krummenacher* [1977] and on stratigraphic relationships.

The volcanic and volcanclastic deposits of group three are divided into tectono-stratigraphic packages that distinguish five separate structural domains within the Sonoran margin study area (Fig. 3.2). These domains have been separated and juxtaposed by rift-related faulting. The stratigraphy of each of these domains is described in the following paragraphs. The juxtaposition and origin of these domains and development of the bounding structures will be addressed in chapter 6. The Sierra Menor domain and the Sierra Kunkaak domain on Isla Tiburón define the principal western and eastern fault block mountain ranges, respectively. The La Cruz domain is bounded on the north by the La Cruz fault, a northwest-striking strike-slip fault first mapped by *Gastil and Krummenacher* [1976]). The Kino–Chueca domain lies along the Sonoran coastline between Bahía Kino and Punta Chueca, and the Sierra Seri domain bounds the Kino–Chueca domain to the northeast. The distinctive volcanic stratigraphy of these domains probably developed prior to rifting of the Gulf of California.

Sierra Menor Domain

Group three deposits of the Sierra Menor comprise andesite lava and proximal andesitic debris-flow deposits. The overall pattern of deposition suggests the existence of a volcanic center in the area of the southern Sierra Menor ($^{3}59^{000}$,$^{31}\,98^{000}$). At this center, massive andesite bodies make up the bulk of exposures. These deposits formed a paleotopographic high which blocked deposition of later rift-related ignimbrites (see following sections). Proximal andesitic debris flow deposits and block-and-ash breccias are encountered south and southeast of these andesite flows ($^{3}64^{550}$,$^{31}\,94^{210}$). Additional volcaniclastic conglomerates and debris-flow breccias intercalated with andesite lava flows crop out periodically at the base of a 200–300 meter thick synrift volcanic section in the central Sierra Menor (e.g., at $^{3}57^{900}$,$^{32}\,05^{380}$, and $^{3}58^{220}$,$^{32}\,03^{940}$). Group three deposits of the Sierra Menor domain become dominantly volcaniclastic in the northern Sierra Menor and pinch out in the Sierra Alta ($^{3}54^{900}$,$^{32}\,19^{200}$), where

younger synrift volcanic rocks rest directly upon basement.

Only two isotopic ages exist for group three strata of the Sierra Menor domain. Both of these ages are suspect due to uncertain sample localities. *Gastil and Krummenacher* [1977] reported K-Ar ages of 10.9±2.3 Ma from plagioclase and 15.3±1.3 Ma from hornblende from a sample from central western Isla Tiburón ($^{3}55^{070}$,$^{32}\,07^{140}$). Unfortunately, the sample locality is denoted in an area of marine and fluvial terraces [*Gastil and Krummenacher*, 1976]. There are both group three and synrift andesite lava flows in the vicinity of this locality that may have been sampled by *Gastil and Krummenacher* [1977]. *Smith et al.* [1985] report an age of 12.9±0.5 Ma from an andesitic breccia from southwestern Isla Tiburón. This breccia was originally interpreted as a primary volcaniclastic deposit intercalated with Middle Miocene marine strata. *Neuhaus* [1989] revised the stratigraphic position of this breccia as below the marine deposits. New observations of the geology of this area denote a landslide breccia (unit Tmbr, Plate II) underlain by andesitic debris flow deposits (unit Tmvs, Plate II). The clast dated by *Smith et al.* [1985] may have come from either of these deposits.

Group three deposits of the Sierra Menor domain are mapped as several separate units. *Gastil and Krummenacher* [1977] mapped andesite lava flows as unit T2 and volcaniclastic deposits as units T1 and T3. Most of this domain is remapped in detail on Plate II. Andesite lava flows of group three of the Sierra Menor domain are denoted as unit Tma1 where the age is known to pre-date the 12.6 Ma Tuff of San Felipe, and as unit Tma where these deposits are undifferentiated from synrift andesite lava flows. Volcaniclastic deposits of group three of the Sierra Menor are mapped as unit Tmvs.

Sierra Kunkaak Domain

Very little information is known about the geology of the Sierra Kunkaak domain. This area was not mapped in detail as part of this study. The only published information on the Sierra Kunkaak is from *Gastil and Krummenacher* [1976] who mapped

volcaniclastic deposits as units T2, T3 and T4 and denote the general strike and dip of these strata. A single day of reconnaissance investigation of the southern part of the Sierra Kunkaak domain from Arroyo El Carrizo (Fig. 3.1) revealed a variety of volcaniclastic deposits intercalated with lava flows. The base of the section here is a sequence of andesite lava flows and volcaniclastic debris-flow deposits similar to the Sierra Menor domain. Above these deposits lies the Tuff of the Sierra Kunkaak (new name, unit Tmtk). This welded tuff with a red glassy matrix and 50% angular aphanitic orange volcanic lithic fragments is distinctive to the Sierra Kunkaak. On aerial photographs and Landsat imagery, this welded lithic tuff forms a distinctive unit that crops out throughout the Sierra Kunkaak and may exceed 200 m thickness in the central part of the range. The stratigraphically highest part of the volcanic section exposed in Arroyo el Carrizo comprises a 20 m-thick fluvial conglomerate, a pair of 5 to 10 m-thick rhyolite lava flows, and a thin (<5 m) non-welded pumice flow.

Basement outcrops dominate the northern Sierra Kunkaak [*Gastil and Krummenacher*, 1976]. Field mapping of the northern Sierra Kunkaak ($^{3}71^{980}$,^{32} 27^{330}) revealed an outcrop of welded andesitic lithic tuff identical to the tuff of the Sierra Kunkaak from Arroyo El Carrizo. This deposit of lithic tuff (unit Tmtk) is overlain unconformably by a rhyolite lava flow (unit Tmrf1) and the 12.6 Ma Tuff of San Felipe (unit Tmrsf, group 4). This locality provides the only age control on group three deposits of the Sierra Kunkaak domain. No other age determinations or detailed lithologic descriptions of strata from this part of Isla Tiburón are published. The ages of younger volcanic deposits from the central and southern Sierra Kunkaak and relationships of these deposits to rifting are unknown.

La Cruz Domain

The La Cruz domain of group three deposits forms a distinctive terrane on the southern edge of Isla Tiburón. This domain is separated from the rest of Isla Tiburón by the La Cruz fault, a strike-slip fault that strikes parallel to the Tiburón Fracture Zone (Figs. 1.4 and 3.1). In this region, up to 500 m of middle Miocene lava flows and

volcaniclastic deposits and underlying basement are faulted into a series of southeast-tilted blocks [*Gastil and Krummenacher*, 1976; *Neuhaus*, 1989; *Gastil et al.*, 1999, also Plate II]. *Gastil and Krummenacher* [1976] mapped the volcanic deposits of the La Cruz domain as units T1, T2, T3, and T5. Units T1, T2, and T3 comprise group three of this study. Unit T5 corresponds to a synrift andesite volcano and associated pyroclastic deposits that form part of group six described later in this chapter.

Gastil et al. [1999] subdivided group three strata of the western part of La Cruz domain into units M1-M6. The base of this section consists of thinly bedded lacustrine chert and carbonate rocks interbedded with fluvial arkose and conglomerate (unit M1a of *Gastil et al.* [1999]). Basaltic to andesitic flows and breccias with red volcanic sandstone and tephra overlie these basal sedimentary rocks (units M1b-M5 of *Gastil et al.* [1999]). A dacite lava (unit M6 of *Gastil et al.* [1999]) caps the group three section here. Group three deposits of the La Cruz domain on Plate II were not mapped in as much detail as shown by *Neuhaus* [1989] or *Gastil et al.* [1999]. Unit M4, a latite dome flow [*Neuhaus*, 1989], is mapped as unit Tmlf on Plate II. Other group three units of the western area of the La Cruz domain (M1-M3, M5, and M6 of *Gastil et al.* [1999]) are mapped as unit Tmvlc on Plate II.

Reconnaissance investigations of the central and eastern areas of the La Cruz domain reveal additional volcanic lithologies not present on the western part of the island. These silicic volcanic deposits may have been emplaced during rifting. However, unlike the sedimentary and volcanic deposits of group six from this area, the lithologies described here are confined to the La Cruz block and tentatively included with group three. Two densely welded rhyolitic ignimbrites designated the Tuffs of Cerro Colorado (new name) are mapped as unit Tmrcc ($^{3}54^{770}$,$^{31}\,91^{030}$). The Tuffs of Cerro Colorado are each approximately 15 meters thick and unconformably overlie tilted Tmvlc basalt. The lower member of the Tuffs Cerro Colorado (5% volcanic lithic fragments, 20% phenocrysts: alkali-feldspar $\gg$ pyroxene $\approx$ hornblende $\gg$ olivine) appears similar to unit Tmr3 of the Tuffs of Mesa Cuadrada. Southeast of Punta Sauzal, an undated rhyolite lava flow 40 m thick conformably overlies basalt and red

volcanic sandstone of unit Tmvlc. Fault repetition of this unit forms several prominent headlands on the southern coast of Isla Tiburón ($^{3}65^{250}$,^{31} 83^{770}; $^{3}67^{530}$,^{31} 82^{020}; $^{3}71^{020}$,^{31} 81^{400}). At Ensenada de la Cruz, near the southeastern tip of Isla Tiburón, this rhyolite lava flow is capped by non-welded pumice flows, a 5 m-thick perlitic rhyolite flow, volcaniclastic sandstone, and a 4 m-thick densely welded tuff (5% volcanic lithic fragments, 35% phenocrysts: alkali-feldspar $\geq$ pyroxene $>$ plagioclase) ($^{3}68^{150}$,^{31} 82^{640}).

Several isotopic ages exist for lava flows from the La Cruz domain. *Gastil et al.* [1999] compiled several ages for group three strata of the southwestern part of Isla Tiburón. In this area, unit Tmvlc (units M1-M3, M5 and M6 of *Gastil et al.* [1999]) ranges from 21.0±0.5 Ma to 15.2±0.5 Ma (K-Ar). Unit Tmlf (unit M4 of *Gastil et al.* [1999]) was dated at 17.4±0.4 Ma by *Neuhaus* [1989]. The welded tuff that caps the volcanic section at Ensenada de la Cruz was dated here as 11.25±1.98 Ma (Table 3.1). The lower member of the Tuffs of Cerro Colorado was dated to test for correlation to unit Tmr3 of the Tuffs of Mesa Cuadrada. The 9.58±2.66 Ma (Table 3.1) age of this unit does not support correlation of these outcrops to the Tuffs of Mesa Cuadrada. This result is consistent with observations that the Tuffs of Mesa Cuadrada pinch out further to the north on Isla Tiburón.

Kino-Chueca Domain

The Kino–Chueca domain forms a belt of north to northeast-trending ridges on the Sonoran mainland adjacent to the Gulf of California (Plate I). In the southern and central parts of this region, a 20 to 80 meter thick section of group three lava flows and volcaniclastic deposits nonconformably overlies basement and is conformably overlain by the Tuff of San Felipe (group 4). *Gastil and Krummenacher* [1976] map these deposits and the overlying Tuff of San Felipe as units T1, T2, and T3. A consistent stratigraphy of group three characteristizes of the southern part of the Kino–Chueca domain. The lowest units are basalt (unit Tmb1) and a pair of andesite flows (unit Tma1). The lower of these andesite flows contains abundant (20%) distinctive horn-

Table 3.1. New geochronologic data from Isla Tiburón and coastal Sonora, from *Stock and Oskin, in prep.*

Unit	UTM east	UTM north	Sample number	Mineral[a]	Ca/K[b]	n/n$_0$[c]	Age[d] ($\pm 2\sigma$)	$^{40}Ar/^{36}Ar$[e] ($\pm 1\sigma$)	MSWD[e]	95% crit. MSWD[f]
Tmvlc[g]	$^{3}68^{150}$	$^{31}82^{640}$	TIB-98-02	Anorthoclase	0.06–0.27	10/10	11.25 ± 1.98	Total gas age		
						10/10	11.27 ± 1.79	Error weighted mean age		
						10/10	11.51 ± 1.62	% ^{39}Ar weighted mean age		
Tmrcc	$^{3}54^{770}$	$^{31}91^{030}$	TIB-98-25	Anorthoclase	0.12–0.35	7/7	9.58 ± 2.66	Total gas age		
						7/7	11.99 ± 2.75	Error weighted mean age		
						7/7	10.98 ± 2.38	% ^{39}Ar weighted mean age		
Tmprsz1	$^{3}65^{000}$	$^{31}95^{910}$	SZ-98-08	Anorthoclase	0.05–0.09	9/9	5.40 ± 3.90	Total gas age		
						9/9	6.55 ± 3.65	Error weighted mean age		
						9/9	6.31 ± 3.53	% ^{39}Ar weighted mean age		
Tmprsz1	$^{3}49^{630}$	$^{31}97^{550}$	TIB-98-11	Anorthoclase[h]	0.04–0.07	10/10	6.40 ± 1.63	Total gas age		
					(3.9–6.4)[h]	10/10	6.66 ± 1.46	Error weighted mean age		
						10/10	6.49 ± 1.32	% ^{39}Ar weighted mean age		
Tmprsz1	$^{3}50^{530}$	$^{31}98^{140}$	SWT-99-28	Anorthoclase	0.04–0.08	9/9	6.67 ± 0.83	306 ± 105	1.93	0.24–2.29
						9/9	7.14 ± 1.36	Total gas age		
						9/9	6.56 ± 1.29	Error weighted mean age		
						9/9	6.96 ± 1.18	% ^{39}Ar weighted mean age		
Tmpm[i]	$^{3}50^{520}$	$^{31}98^{130}$	SWT-99-25	Anorthoclase	0.05–0.27	10/10	12.84 ± 0.40	269 ± 16	0.82	0.27–2.19
						10/10	12.58 ± 1.17	Total gas age		
						10/10	12.41 ± 1.14	Error weighted mean age		
						10/10	12.48 ± 1.10	% ^{39}Ar weighted mean age		

Unit	UTM east	UTM north	Sample number	Mineral[a]	Ca/K[b]	n/n$_0$[c]	Age[d] ($\pm 2\sigma$)	$^{40}Ar/^{36}Ar$[e] ($\pm 1\sigma$)	MSWD[e]	95% crit. MSWD[f]
Tmrsf	$^{3}57^{730}$	$^{32}05^{760}$	TIB-98-23	Anorthoclase	0.06–0.28	8/8	9.66 ± 1.31	Total gas age		
						8/8	10.23 ± 1.56	Error weighted mean age		
						8/8	10.69 ± 1.48	% ^{39}Ar weighted mean age		
Tmrsf	$^{3}56^{740}$	$^{32}03^{790}$	BV-99-30	Anorthoclase	0.05–0.24	10/10	12.96 ± 3.67	294 ± 19	0.26	0.27–2.19
						10/10	11.56 ± 10.40	Total gas age		
						10/10	12.26 ± 9.60	Error weighted mean age		
						10/10	12.63 ± 9.02	% ^{39}Ar weighted mean age		
Tmrsf	$^{4}00^{250}$	$^{31}94^{900}$	BK-99-05	Anorthoclase	0.06–0.27	10/10	13.86 ± 2.21	367 ± 118	0.14	0.27–2.19
						10/10	14.93 ± 2.21	Total gas age		
						10/10	14.79 ± 4.11	Error weighted mean age		
						10/10	14.45 ± 3.92	% ^{39}Ar weighted mean age		
Tmr3	$^{3}58^{080}$	$^{32}06^{340}$	TIB-98-12	Anorthoclase[h]	0.04–0.06	10/10	5.33 ± 2.18	Total gas age		
					(28–29)[h]	10/10	6.16 ± 2.28	Error weighted mean age		
						10/10	5.17 ± 2.24	% ^{39}Ar weighted mean age		
Tmr3	$^{3}59^{090}$	$^{32}00^{240}$	BV-99-08	Anorthoclase	0.04–1.29	10/10	6.15 ± 1.03	367 ± 90	1.22	0.27–2.19
						10/10	6.91 ± 2.71	Total gas age		
						10/10	6.10 ± 2.38	Error weighted mean age		
						10/10	6.77 ± 2.17	% ^{39}Ar weighted mean age		

[a] Based on representative microprobe analysis.
[b] Average microprobe analyses of crystal separates used to determine the relative purity of mineral concentrations. See Appendix B for analyses.
[c] Number of aliquots included in calculation over total. Each aliquot is 6 to 8 crystals.
[d] Ages reported in Ma.
[e] Reported for inverse isochron ages.
[f] After *Mahon* [1996].
[g] Welded tuff of Ensenada de La Cruz, capping Tmvlc section.
[h] Plagioclase also present.
[i] Rhyolite tuff clast from marine conglomerate.

blende phenocrysts up to 3 cm long. This sequence is well exposed at Cat Canyon, 3 km north of Bahía Kino ($^{4}02^{220}$,^{31} 94^{770}). The basalt pinches out towards the central area of the domain, whereas outcrops of the distinctive andesite remain abundant. Throughout the southern half of the Kino–Chueca domain volcanic sandstone, conglomerate, and/or debris-flow breccia (unit Tmvs) overlie these lava flows. Group three deposits are thin to absent in most of the northern part of the Kino–Chueca domain. This region corresponds to the position of intracaldera facies of the Tuff of San Felipe and most outcrops of volcanic rocks in this area are high-grade tuff of San Felipe nonconformably overlying basement. One locality near Punta Chueca preserves a section of the distinctive andesite overlain by basalt and capped by the Tuff of San Felipe ($^{3}98^{700}$,^{32} 06^{740}). At the northern end of the Kino–Chueca domain, group three deposits comprise a 5 m thick volcaniclastic debris-flow capped by an andesite lava flow and overlain by the Tuff of San Felipe ($^{3}89^{440}$,^{32} 13^{820}).

Gastil and Krummenacher [1977] report two K-Ar ages from the Kino–Chueca domain. A separate of hornblende from an andesite north of Bahía Kino (Sample S3G-764, misidentified as a dacite?) yielded an age of 17.8±0.8 Ma. A separate of hornblende from an andesite from the central part of the Kino–Chueca domain yielded an age of 21.0±0.8 Ma (Sample S2K-31). Overall, these isotopic ages reported for the Kino–Chueca domain agree with the stratigraphic position of group three deposits beneath outcrops of the 12.6 Ma Tuff of San Felipe.

Sierra Seri Domain

The Sierra Seri domain of group three deposits forms a northwest-trending mountain range adjacent to the Sonoran coastline and northeast of the Kino–Chueca domain. The boundary between the Sierra Seri and Kino–Chueca domains is the Sacrificio fault (Fig. 3.1), a northwest-striking structure. This fault is probably part of a series of northwest-striking faults proposed to have accommodated right-lateral strike-slip displacement along the Sonoran coastline [*Gastil and Krummenacher*, 1977]. The southern part of the Sierra Seri domain is cut by three additional northwest-striking

faults of this series with west-side-down normal separation and probable strike-slip displacement (Fig. 3.1). In this area, a section of group three volcanic deposits up to 300 m thick is mapped as units T1-T3 and T4 by *Gastil and Krummenacher* [1976]. The northern part of the Sierra Seri domain comprises a single fault block capped by outcrops of the distinctive conglomerate of *Gastil et al.* [1973]. Volcanic rocks appear to be absent from this region of the Sierra Seri [*Gastil and Krummenacher*, 1976]. Volcanic rocks crop out further north in the Sierra Seri and Rio San Ignacio areas [*Gastil and Krummenacher*, 1976], outside the region of detailed studies described here.

The group three volcanic section of the Sierra Seri domain was investigated at Pico Noche Buena and in the foothills of Pico Johnson (Fig. 3.2). The base of the section comprises 20 meters of volcaniclastic sandstones and conglomerate (unit Tmvs) overlain by 50 meters of andesite lava flows (unit Tma1). This basal section is similar to group three deposits of the other domains described above. The upper part of the volcanic section is formed of an additional 100 to 200 meters of the rhyolites of Pico Johnson (new name, unit Tmrj). These rhyolites form a distinctive stack of five to ten 20 m thick densely welded ignimbrite cooling units separated by thin non-welded ash deposits and rhyolite lava flows. The lithology of these deposits (15% phenocrysts: plagioclase $>$ quartz $\gg$ pyroxene) is distinct from the Tuff of San Felipe and the Tuffs of the northern Puertecitos Volcanic Province.

Gastil and Krummenacher [1977] report two K-Ar ages from the Sierra Seri domain. Plagioclase from andesite outcrops northwest of Pico Noche Buena (sample S2G-17) yielded an age of 12.3$\pm$2.9 Ma. Plagioclase from rhyolite outcrops northeast of Pico Johnson yielded an age of 12.7$\pm$1.1 Ma (sample S2G-21). These isotopic ages indicate that the rocks are younger than adjacent outcrops of distinctive conglomerate of *Gastil et al.* [1973] which is overlain by a 15.0$\pm$0.4 Ma basalt in the Santa Rosa basin of Baja California [*Gastil et al.*, 1979].

3.4.5 Group 4: The Tuff of San Felipe

The Tuff of San Felipe is assigned to a separate lithologic group (group four) to reflect its significance as a stratigraphic marker. Outcrops here correlated to the Tuff of San Felipe, densely welded rhyolite ignimbrite, are common to the Kino–Chueca domain of coastal Sonora and the western and northern region of Isla Tiburón (Figure 3.3, plates I and II). *Gastil and Krummenacher* [1976] included the Tuff of San Felipe variably into units T1, T2, or T4 and did not regionally correlate tuff exposures. Distinctive lithic and phenocryst content and textural characteristics were used to correlate and map exposures of the Tuff of San Felipe (unit Tmrsf). Geochemical and paleomagnetic tests were applied to verify correlation (see chapters 4 and 5). Similar to its exposures in Baja California, the Tuff of San Felipe in Sonora occupies a transitional stratigraphic position disconformably above group three deposits of the Middle Miocene volcanic arc and unconformably beneath group five and group six synrift deposits. A likely eruptive center for the Tuff of San Felipe is located near the coastline of mainland Sonora (Plate I, Fig. 3.3).

Exposures of the Tuff of San Felipe on Isla Tiburón fill a series of west-trending paleocanyons. The maximum thickness of the Tuff of San Felipe preserved as paleocanyon fill ranges from 50 to 85 meters in the central part of the Sierra Menor, the Sierra Alta, and the northern Sierra Kunkaak (Fig. 3.3). Discontinuous outcrops of the Tuff of San Felipe up to 10 meters thick are deposited against a paleotopographic high of group three andesite in the southern Sierra Menor. Exposures of the Tuff of San Felipe on Isla Tiburón are densely welded with a 20 cm to 50 cm black to dark brown vitrophyre overlain by vapor-phase recrystallized welded tuff. Welding grade, as indicated by the aspect ratio of fiamme, increases from south to north from the Sierra Menor to the Sierra Alta. Very high-grade Tuff of San Felipe with rheomorphic texture occurs in the northern Sierra Kunkaak. The size and abundance of distinctive dark-colored lithic inclusions increases with welding grade as it does in the Tuff of San Felipe in Baja California. The area and volume of the Tuff of San Felipe on Isla

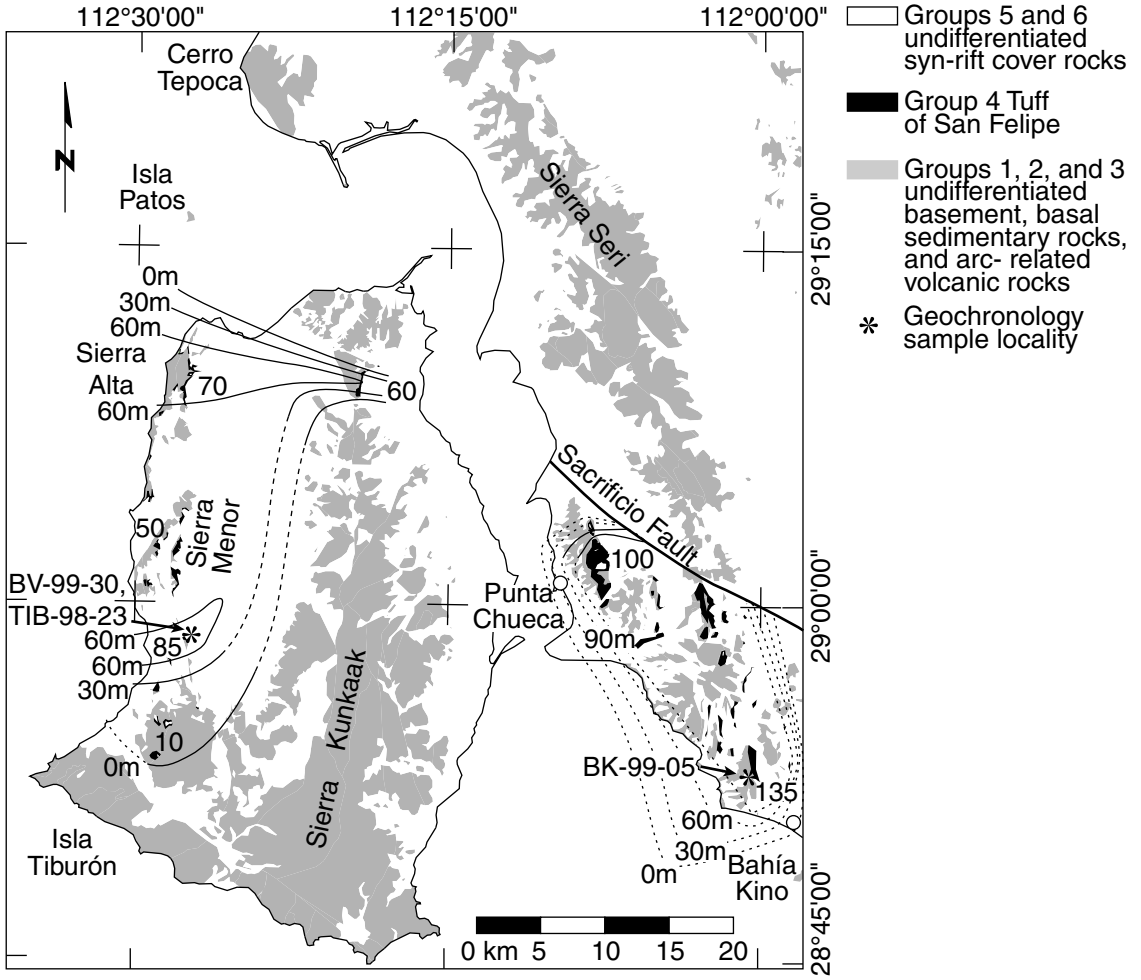

Figure 3.3. The Tuff of San Felipe in coastal Sonora and Isla Tiburón. Thickness measurements in meters shown as numbers. Isopachs of tuff thickness shown as thin black lines. Dashed and dotted lines reflect uncertainty in isopach positions used to calculate tuff volumes (Table 3.2). 30 m contour interval. Outcrops of the Tuff of San Felipe on Isla Tiburón fill west-trending paleocanyons. Thicker outcrops of the Tuff of San Felipe on coastal Sonora are related to a probable vent located east of Punta Chueca. The eastern boundary of these isopachs was arbitrarily placed east of all mapped outcrops of the Tuff of San Felipe on coastal Sonora. Additional deposits of the Tuff of San Felipe probably exist east of the map area.

Tiburón is estimated as 440 km^2 and 17 km^3 (Table 3.2). This estimate does not include moderate extension that has taken place on Isla Tiburón since emplacement of the Tuff of San Felipe.

Table 3.2. Volume calculations of tuffs in coastal Sonora and Isla Tiburón.

Contour interval (m)	Area[1] (km^2)	Multiplier[2] (km)	Volume (km^3)
		Tuff of San Felipe	
		Isla Tiburón, Max Thickness: 85 m	
0 m	441.9	0.015	6.6
30 m	303.5	0.03	9.1
60 m	41.2	0.023	1.0
60 m	16.4	0.023	0.4
Volume of the Tuff of San Felipe on Isla Tiburón:			17.1
		Coastal Sonora, Max Thickness: 135 m	
0 m	334.2	0.015	5.0
30 m	277.9	0.03	8.3
60 m	220.9	0.03	6.6
90 m	174.1	0.030	5.2
Volume of the Tuff of San Felipe in coastal Sonora (west of 112°W):			25.2
		Tuffs of Mesa Cuadrada	
		Max Thickness: 190 m	
0 m	368.4	0.015	5.5
0 m	-12.2	0.015	-0.2
0 m	-1.9	0.015	0.0
30 m	262.9	0.03	7.9
30 m	-10.9	0.03	-0.3
60 m	164.1	0.03	4.9
90 m	5.2	0.048	0.3
90 m	82.1	0.048	4.0
Volume of the Tuffs of Mesa Cuadrada on Isla Tiburón:			22.0

Contour interval (m)	Area[1] (km^2)	Multiplier[2] (km)	Volume (km^3)
	Tuffs of Dead Battery Canyon		
	Max Thickness: 38 m		
0 m	52.5	0.015	0.8
30 m	9.5	0.018	0.2
Volume of the Tuffs of Dead Battery Canyon on Isla Tiburón:			1.0
	Tuffs of Arroyo El Canelo		
	Max Thickness: 60 m		
0 m	169.5	0.015	2.5
0 m	-16.8	0.015	-0.3
30 m	169.5	0.03	5.1
30 m	45.9	0.03	1.4
60 m	7.7	0.015	0.1
Volume of the Tuffs of Arroyo El Canelo on Isla Tiburón:			8.9

[1] The areas of closed internal contours shown as negative values. Area measurements do not account for extension of the outcrop area after deposition and may overestimate the volume of tuffs by up to a factor of 2.

[2] 0 m contour multiplied at $\frac{1}{2}$ contour interval (15 m). Each complete contour above 0 m multiplied at 1 contour interval or (30 m). Final contour interval multiplied at $\frac{1}{2}$ contour interval $+\frac{1}{3}$ remaining thickness.

High grade welded Tuff of San Felipe over 100 meters thick forms a belt of exposures on the mainland coast of Sonora. A stratigraphic section of the Tuff of San Felipe at Cat Canyon, 3 km north of Bahía Kino ($^{4}02^{350}$,^{31} 95^{740}), reveals a 135 m thick section of ignimbrite very similar to thick deposits of the Tuff of San Felipe in Baja California. The base of the Tuff of San Felipe at Cat Canyon rests on a 75 cm thick block-and-ash deposit with altered andesite clasts in a matrix of white volcanic ash. Above this block-and-ash deposit, a 1 m thick black vitrophyre forms the base of the Tuff of San Felipe. Overlying the vitrophyre, a 25-meter section of high-grade rheomorphic tuff with abundant decimeter to centimeter-sized lithophysae completes the densely welded base of the ignimbrite. Spherulitic recrystallization increases upsection such that pyroclastic texture is completely obscured for the upper 100 meters of tuff exposure. Welding grade of the Tuff of San Felipe increases from south to the

north on mainland Sonora. Rheomorphic flow texture is indicated by rolled lithic clasts embedded in the ignimbrite near Bahía Kino. Flow features increase in grade to include meter-scale rheomorphic folding in ignimbrite exposures midway between Punta Chueca and Bahía Kino. The highest-grade rheomorphic texture is expressed by 2- to 5-meter amplitude recumbent rheomorphic folds found in possible intra-caldera facies of the Tuff of San Felipe located near Punta Chueca ($^{3}96^{290}$,$^{32}\,10^{300}$). The volume of the Tuff of San Felipe in coastal Sonora is estimated as 25 km^3 (Table 3.2). This estimate does not account for substantial extension in this region that has tilted outcrops in excess of 70° in some localities (Plate I). Also, there is an unknown but possibly large volume of the Tuff of San Felipe east of the map area.

A portion of the likely vent of the Tuff of San Felipe crops out at the northern end of the mainland coastal Sonora outcrop belt, inland of Punta Chueca (Fig. 3.3). Here, moderate to large-magnitude northwest-directed extension has exposed very high-grade densely welded outcrops of the Tuff of San Felipe that may be caldera-fill deposits (Plate I). These deposits are capped by a 100 to 200 m-thick section of the Tuffs of Punta Chueca (new name). The Tuffs of Punta Chueca are non-welded pyroclastic deposits (unit Tmrpc of group 5) interstratified with and capped by basalt flows (unit Tmb2 of group 5). The Tuffs of Punta Chueca may represent additional caldera-fill deposits. Abrupt thickness changes of the Tuffs of Punta Chueca support deposition in a fault-controlled depression. A possible caldera ring fracture corresponds to an abrupt thinning of the Tuffs of Punta Chueca north of the town of Punta Chueca ($^{3}89^{700}$,$^{32}\,13^{680}$). The large volume of the Tuff of San Felipe (over 160 km^2, Tables 2.1 and 3.2) probably requires a larger source than the extent of collapse indicated by Tuffs of Punta Chueca, suggesting that the Punta Chueca region represents a small part of a larger eruptive center.

The age of Tuff of San Felipe is well constrained from both Baja California and Sonora. *Stock et al.* [1999] summarized the isotopic age of the Tuff of San Felipe in Baja California as ∼12.6 Ma. Additional age determinations of three samples of the Tuff of San Felipe from Sonora confirm correlation of the Tuff of San Felipe.

New isotopic age data are described completely in Chapter 5 and Appendix C. To summarize these results, the Tuff of San Felipe on Isla Tiburón yielded ages of 9.66 ± 1.31 Ma and 12.96 ± 3.67 Ma and the Tuff of San Felipe on coastal mainland Sonora yielded an age of 13.86 ± 2.21 Ma (Table 3.1). *Gastil and Krummenacher* [1977] did not date the Tuff of San Felipe in Sonora.

3.4.6 Group 5: Early syn-rift deposits

Group five rocks record the onset of rift-related deposition on the Sonoran margin of the Gulf of California. The stratigraphic position of these deposits appears to be the same as for the northeastern Baja California margin. Emplacement of the Tuff of San Felipe (group four) disconformably upon group three strata of the Middle Miocene arc indicates that rifting was not underway in coastal Sonora prior to 12.6 Ma. Deposits of group five strata typically form an angular unconformity with the Tuff of San Felipe and indicate the inception of rifting in Mid to Late Miocene time. As in northeastern Baja California, group five comprises an early synrift sequence of volcanic and non-marine sedimentary strata. Rift-related bimodal volcanism beginning in Late Miocene time deposited a variety of lava flows and pyroclastic deposits on the western part of Isla Tiburón. These deposits culminate in a section of ignimbrites up to 300 meters thick that correlate to the Tuffs of the northern Puertecitos Volcanic Province. The top of these ignimbrites divides group five from group six sedimentary and volcanic deposits. The following paragraphs discuss the late Miocene record of volcanic and fluvial group five deposition. The correlative exposures of the Tuffs of the northern Puertecitos Volcanic Province on western Isla Tiburón will be described separately in a following section.

Sedimentary strata

Similar to synrift deposits of Baja California, group five sedimentary rocks of the Sonoran margin record formation of rift basins that filled with fluvial deposits.

The principal rift basins of group five age in the Sonoran margin study area are the Valle de Tecomate, which forms the central valley of Isla Tiburón, and the Canal de Infernillo, the channel between Isla Tiburón and mainland coastal Sonora (Fig. 3.1). Early rift-related deposits from these two basins have been uplifted and exposed on the basin margins in the Sierra Menor ($^{3}58^{100}$,^{32} 04^{700}), the northern Sierra Kunkaak ($^{3}69^{200}$,^{32} 27^{600}), and in the Kino–Chueca domain of coastal Sonora ($^{3}95^{800}$,^{32} 08^{800} and $^{4}02^{400}$,^{32} 02^{600}). Where synrift sedimentary strata are definitely overlain by the Tuffs of the northern Puertecitos Volcanic Provice these deposits are mapped as unit Tmal. Non-marine conglomerates of the Canal de Infernillo basin are not overlain by the Tuffs of the northern Puertecitos Volcanic Province and thus may be in part or entirely of group six age. These deposits are mapped as unit Tmpal. Middle Miocene 'proto-Gulf' marine deposits that crop out on southwest Isla Tiburón are documented by *Gastil and Krummenacher* [1976] and *Gastil et al.* [1999]. These strata are shown in Chapters 6 and 8 to have been deposited in a strike-slip basin of latest Miocene to early Pliocene age. These deposits are classified as group six synrift strata and will be described further below.

Volcanic strata

Volcanic flows and pyroclastic deposits of group five are common in the Sonoran margin study area. In the central and southern parts of the Kino-Chueca domain of mainland coastal Sonora, rhyolite lava flows (unit Tmrf2) and non-welded pyroclastic deposits (unit Tmrpc) conformably overlie the Tuff of San Felipe and are unconformably overlain by synrift fluvial conglomerates (Plate I). Basalt flows (unit Tmb2) also crop out at this same stratigraphic position in the northern part of the Kino-Chueca domain. Rhyolite lava flows capped by a basalt flow overlie outcrops of the Tuff of San Felipe in the northern Sierra Kunkaak (unit Tmrf2 and unit Tmb2, $^{3}72^{130}$,^{32} 26^{350}). A 300 m thick, east-tilted section of early synrift volcanic deposits fills a half-graben basin on western Isla Tiburón (Fig. 3.1). These deposits include basaltic, andesitic, and rhyolitic lava flows, and locally reworked pyroclastic deposits,

as well as non-welded pumice flows and welded ignimbrites. Observations of each of these deposits are discussed in a separate section below.

Basalt flows form the stratigraphically lowest set of group five volcanic deposits on western Isla Tiburón (unit Tmb2, Plate II). A stack of nine basalt flows, each 10 meters thick on average, overlies the Tuff of San Felipe in the central Sierra Menor ($^{3}57^{920}$,$^{32}\,05^{980}$). The lowest and uppermost of these flows are nearly identical petrographically (15% glass, 80% microlitic plagioclase and pyroxene, 5% phenocrysts: plagioclase $\approx$ olivine $>$ pyroxene). A 2 m thick horizon of conglomerate containing clasts of granitic basement underlies the uppermost of these basalt flows and at least 15 meters of conglomerate and non-welded pyroclastic deposits overlie the basalt flow section. Similar basalt flows crop out elsewhere in the southern Sierra Menor; these flows are commonly overlain by conglomerate. Vents in the northern Sierra Menor and adjacent parts of the Sierra Alta are a likely source of these basalts, which appear to have flowed into a basin in the central and southern Sierra Menor. At the northern end of the Sierra Menor outcrops of basalt formed a paleotopographic high during later eruptions ($^{3}62^{900}$,$^{32}\,19^{100}$). A basaltic shield volcano with a preserved summit crater is partially covered by later group five volcanic strata in the southern Sierra Alta (units Tmb2 and Tmb2v, $^{3}57^{400}$,$^{32}\,20^{000}$).

Andesite lava flows overlie basaltic vents and flows in the northern Sierra Menor and southern Sierra Alta (unit Tma2, Plate II). Andesite from the coastal side of the Sierra Menor was identified lithologically (for example, sample BV-99-20, 50% phenocrysts: plagioclase $>$ biotite $>$ hornblende), whereas interior outcrops were identified from their morphology and spectral signature on a Landsat image. Flows of andesite formed several paleotopographic highs that blocked deposition of the Tuffs of the northern Puertecitos Volcanic Province ($^{3}56^{130}$,$^{32}\,08^{100}$; $^{3}58^{780}$,$^{32}\,11^{740}$; $^{3}61^{800}$,$^{32}\,09^{770}$). Additional andesites overlie rhyolite lava flows in the northeastern Sierra Alta. *Gastil and Krummenacher* [1977] dated andesite from an isolated hill in the southern Valle de Tecomate as 9.9±1.3 Ma (K-Ar on hornblende, sample S3G-714, $^{3}62^{900}$,$^{32}\,03^{300}$). This same sample is identified as hornblende dacite by *Gastil*

et al. [1979]. This outcrop is here mapped as andesite (unit Tma2, Plate II) based upon spectral similarity to other outcrops of andesite identified from field mapping at the southern end of the Valle de Tecomate.

Rhyolite lavas form the stratigraphically highest group five lava flows on western Isla Tiburón (unit Tmrf2, Plate II). These form a 50 to 100 meter-thick mantle of lava flows in the northern and central Sierra Menor and culminate in a ∼200 m thick accumulation of ash deposits, lava flows, and breccias that crop out in the northern Sierra Alta. A similar thick culmination may exist in the northeastern Sierra Menor where rhyolite lava was inferred from Landsat imagery and aerial photographs.

Non-welded pumice flows and reworked pyroclastic deposits form a thin (0-15 meter) layer above lava flows and conglomerates of group five and beneath the base of the Tuffs of the Northern Puertecitos Volcanic Province. These deposits are mapped as part of unit Tmal. Elsewhere, bedded pumice and ash at this stratigraphic position have been mapped as 'Yellow Tuffs' [*Stock*, 1993; *Lewis*, 1994, unit Tmyt]. Rhyolite vents in the northern Sierra Menor and the Sierra Alta are a possible source for these deposits on Isla Tiburón. The amount and thickness of pumice beds as well as the proportion of primary deposited material increases up-section to the base of unit Tmr3 of the Tuffs of Mesa Cuadrada.

The age of group five strata is best constrained by stratigraphic position between the 12.6 Ma Tuff of San Felipe and ca. 6.2 Ma Tuffs of the northern Puertecitos Volcanic Province. Two isotopic ages of andesite determined by *Gastil and Krummenacher* [1977] may have been acquired from group five volcanic strata. One of these samples is from an isolated hill of andesite (sample S3G-714, 9.9±1.3 Ma K–Ar on hornblende) while the other sample locality is erroneously placed in an area of marine terraces (sample S2K-11, 10.9±2.3 Ma K–Ar on plagioclase, 15.3±1.3 Ma K–Ar on hornblende). An attempt to date an andesite from the central Sierra Menor was unsuccessful (sample BV-99-20, $^{40}Ar/^{39}Ar$ on plagioclase, *Stock and Oskin, in prep.*).

3.4.7 Tuffs of the northern Puertecitos Volcanic Province on Isla Tiburón

The uppermost group five strata of the Sierra Menor and Sierra Alta of western Isla Tiburón comprise correlative deposits of the tuffs of the Northern Puertecitos Volcanic Province of Baja California (Plate II, Figs. 3.4, 3.5, and 3.6). Correlatives to the Tuffs of the Northern Puertecitos Volcanic Province also crop out in the northern Sierra Kunkaak of northeastern Isla Tiburón. Eight separate cooling units of these ignimbrites are grouped into three eruptive sequences. The lowest sequence is the Tuffs of Mesa Cuadrada (Fig. 3.4), which is composed primarily of cooling units Tmr3 and Tmr4 (Plate II). The second eruptive sequence is the Tuffs of Dead Battery Canyon (Fig. 3.5), represented by cooling unit Tmr5 on Isla Tiburón (Plate II). The Tuffs of Dead Battery Canyon may be from a late-stage pyroclastic flow from the same eruptive sequence that produced the Tuffs of Mesa Cuadrada. The highest eruptive sequence is the Tuffs of Arroyo El Canelo (Fig. 3.6), which is composed of the Arroyo Oculto member (Tmrao, Plate II), the main El Canelo member(s) (Tmrec, Tmrec1, and Tmrec2, Plate II), the Bighorn Sheep member (mapped with the main member on Plate II), and the Flagpole member (Tmrfp, Plate II).

Tuffs of Mesa Cuadrada

The Tuffs of Mesa Cuadrada are deposited over most of western Isla Tiburón as a distinctive pair of cooling units: a lower partially- to non-welded lithic phyric cooling unit mapped as Tmr3, and an upper densely welded vitric cooling unit mapped as Tmr4 (see Chapter 2 and Plate II for additional lithologic description). As in Baja California, Tmr3 and Tmr4 display parallel trends in thickness and welding grade, with Tmr3 everywhere at least 50% thicker than Tmr4 except where Tmr3 fills paleotopographic relief. Locally in the central Sierra Menor, A 10–15 m thick partially welded pyroclastic flow, mapped as Tmr3a, forms the base of the Tuffs of Mesa Cuadrada. This unit may correlate to similar deposits mapped as Tmr3a in the

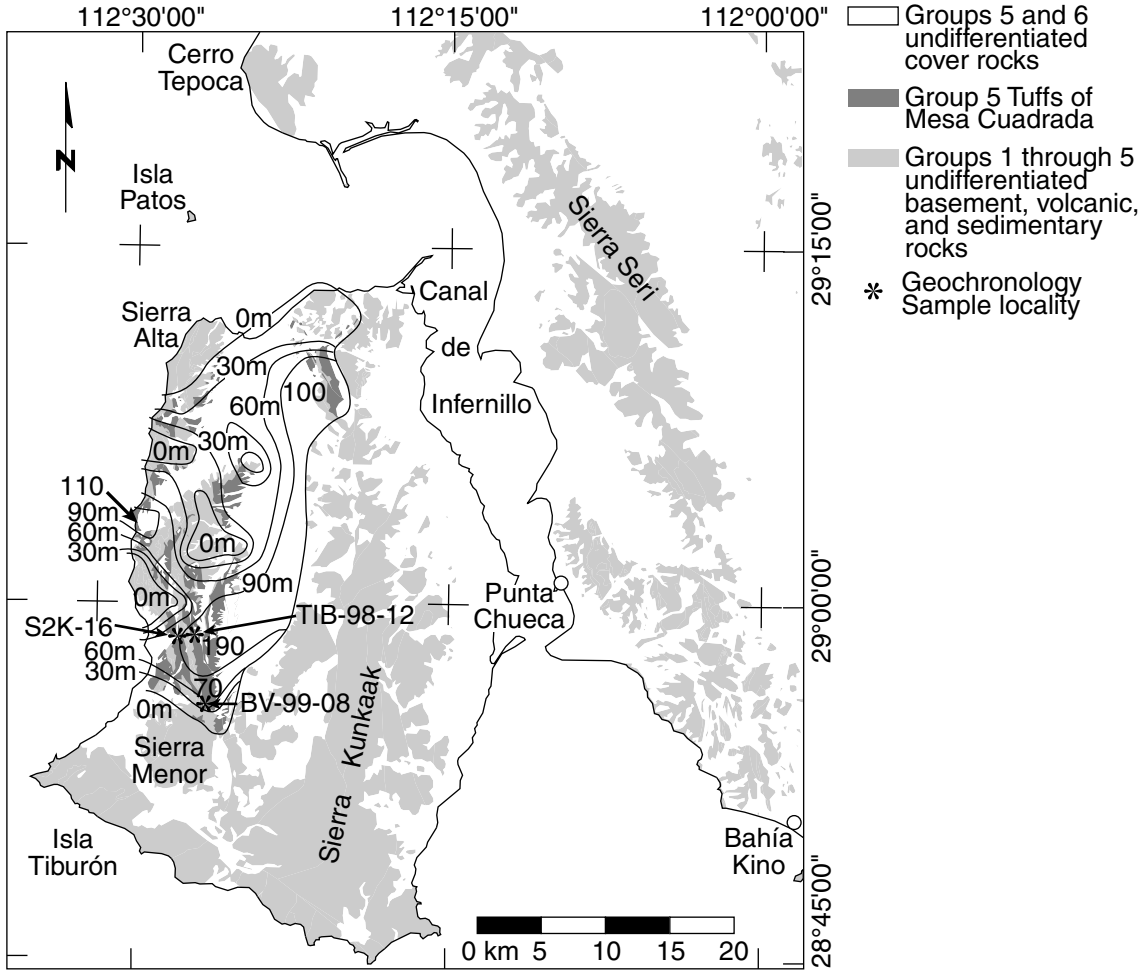

Figure 3.4. Distribution of the Tuffs of Mesa Cuadrada on Isla Tiburón. Numbers denote combined Tmr3 and Tmr4 outcrop thickness measurements (in meters). Isopachs of tuff thickness labelled with 30 m contour interval. Three areas of non-deposition of the Tuffs of Mesa Cuadrada correspond to paleotopographic highs. Adjacent paleocanyons and basins are filled with up to 190 meters of the the Tuffs of Mesa Cuadrada. The eastern edge of tuff distribution was probably the fault-controlled eastern slope of the Tecomate basin (Fig. 3.1). Isopachs of tuff thickness are inferred to terminate against this boundary.

Sierra San Fermín by *Lewis* [1994]. The thickest accumulation of the Tuffs of Mesa Cuadrada occurs in the southern and central Sierra Menor (Plate II). Here, up to 120 meters of Tmr3 and 70 meters of Tmr4 accumulated above older group five sedimentary and volcanic strata. Continuous outcrops of the Tuffs of Mesa Cuadrada form a 9 km-long north-trending ridge in the southern and central Sierra Menor ($^{3}57^{700}$,$^{32}\,09^{100}$ to $^{3}59^{200}$,$^{32}\,00^{000}$). These deposits are buttressed against a paleotopographic high of group three andesite deposits in the southern Sierra Menor and against a paleotopographic high of group five andesite and rhyolite lava flows in the northern Sierra Menor. Deposits of the Tuffs of Mesa Cuadrada fill three paleocanyons on the northwestern part of Isla Tiburón. One of these paleocanyons occurs at the crest of the northern Sierra Menor ($^{3}56^{000}$,$^{32}\,12^{000}$) and a second paleocanyon crops out nearby at Punta Reina ($^{3}54^{000}$,$^{32}\,15^{000}$). A third paleocanyon occurs in the central Sierra Alta ($^{3}57^{000}$,$^{32}\,23^{000}$). The area and volume of the Tuffs of Mesa Cuadrada on Isla Tiburón is estimated as 370 km^2 and over 20 km^3 (Table 3.2). This estimate does not account for moderate extension on Isla Tiburón since emplacement of the Tuffs of Mesa Cuadrada.

Outcrops surrounding the northern Valle de Tecomate record filling of a half-graben during eruption of the Tuffs of Mesa Cuadrada. The northeast slopes of the Sierra Menor and the Sierra Alta are mantled with a westward-thinning section of these ignimbrites. Faulting on the eastern side of the Valle de Tecomate uplifted and exposed a section of basin fill. This section lies tilted to the east at 45° above a gently west-dipping (30°) normal fault at the crest of the northern Sierra Kunkaak (Kunkaak fault, Plate II). The lowest exposures of this basin-fill section record deposition of non-marine conglomerate with a mixture of volcanic and basement clasts (unit Tmal). Emplacement of cooling unit Tmr3 or underlying Tmr3a, if present, marks the beginning of a sequence of volcanic deposits approximately 300 meters thick. The intermediate 200 meters of this section comprises a series of primary and reworked pyroclastic deposits (unit Tmr3t). Sediment input during this time was entirely volcanic and dominantly ash, including ash and pumice beds, cross-bedded

surge deposits, and debris flows with clasts of Tmr3 in an ash matrix. A 20 m thick deposit of densely welded Tmr4 caps this complex volcanic sequence. Following deposition of Tmr4, basin-fill deposition returned to a non-marine conglomerate with mixed volcanic and basement clasts (unit Tmpal). Boulders of Tmr3, probably eroded from the footwall of the Sierra Kunkaak, are present within unit Tmpal near the fault contact with metamorphic basement ($^{3}69^{400}$,^{32} 27^{800}).

Three isotopic ages determined for cooling unit Tmr3 of the Tuffs of Mesa Cuadrada on Isla Tiburón all support correlation of these outcrops to Baja California. An age of 5.7±0.6 Ma on rhyolite from west Isla Tiburón is published in *Gastil et al.* [1979]. The location of this sample (sample #1012, 28°56′00″, 112°29′00″, K–Ar on feldspar) corresponds to sample locality S2K-16 of *Gastil and Krummenacher* [1976]. The locality, age, and lithology of this sample are consistent with Tmr3 mapped at this same locality (Plate II). Two additional $^{40}Ar/^{39}Ar$ ages were obtained on alkali-feldspar from unit Tmr3 to confirm correlation of this unit to the Tuffs of Mesa Cuadrada (Table 3.1). New isotopic ages of 5.33±2.18 Ma and 6.15±1.03 Ma overlap ages of Tmr3 determined for Baja California (*Stock* [1989];*Lewis* [1996]; *Nagy et al.* [1999]; Table 2.2).

Tuffs of Dead Battery Canyon

Outcrops of cooling unit Tmr5 of the Tuffs of Dead Battery Canyon extend from Punta Reina through the central to northern Sierra Menor (Fig. 3.5 and Plate II). As in Baja California, the Tuffs of Dead Battery Canyon cover a limited geographic extent near the center of distribution of the Tuffs of the Northern Puertecitos Volcanic Province. Similar to observations by *Lewis* [1994] in the Sierra San Fermín, the Tuffs of Dead Battery Canyon conformably overlie the Tuffs of Mesa Cuadrada and are unconformably overlain by the Tuffs of Arroyo El Canelo. South of Punta Reina, a paleocanyon cut into the Tuffs of Dead Battery Canyon is filled by the Tuffs of Arroyo El Canelo. A single cooling unit of the Tuffs of Dead Battery Canyon, most likely correlative to Tmr5, is present on Isla Tiburón. This unit on Isla Tiburón

is a moderately- to densely welded ignimbrite, 10 to 35 meters thick, with 5% phenocrysts (plagioclase ≫ clinopyroxene). This unit is compositionally and texturally most similar to cooling unit Tmr5 of the southern Sierra San Fermín [*Lewis*, 1996], although correlation to cooling unit Tmr6 is also possible. The Tuffs of Dead Battery canyon abruptly thin northward against cooling unit Tmr4 of the Tuffs of Mesa Cuadrada at Punta Reina ($^{3}54^{500}$,$^{32}\,16^{140}$). The southern extent of the Tuffs of Dead Battery Canyon is exposed as a gradually thinning section along the crest of the Sierra Menor. Here, Tmr5 is exposed between Tmr4 and the Tuffs of El Canelo. A recognizable welded interval of tuff at the northern end of this ridge ($^{3}58^{000}$,$^{32}\,08^{850}$) thins southward along strike to a 5-meter thick interval of non-welded pumice (Fig. 3.5, Plate II, $^{3}58^{440}$,$^{32}\,06^{600}$). Further south, the Tuffs of Dead Battery Canyon are absent. The total area and volume of the Tuffs of Dead Battery Canyon on Isla Tiburón is estimated as only 50 km^2 and 1 km^3 (Table 3.2).

Outcrops of a section of the Tuffs of the Northern Puertecitos Volcanic Province at Punta Reina and the central Sierra San Fermín constrain the age of the Tuffs of Dead Battery Canyon. Cooling unit Tmr5 of these tuffs overlies the Tuffs of Mesa Cuadrada, as is also mapped in the Sierra San Fermín [*Lewis*, 1994]. In addition, on Isla Tiburón, correlative deposits of the Tuffs of Arroyo El Canelo cap unit Tmr5. This sequence confirms that the Tuffs of Dead Battery Canyon are intermediate in age between the 6.3±0.3 Ma Tuffs of Mesa Cuadrada (see above) and the 6.1±0.5 Ma Tuffs of Arroyo El Canelo [*Nagy et al.*, 1999].

Tuffs of Arroyo El Canelo

The Tuffs of Arroyo El Canelo cap the stratigraphic section of the Sierra Menor. These ignimbrites preserve a sequence of cooling units identical to outcrops mapped in Baja California. The lowest cooling unit of the Tuffs of Arroyo El Canelo on Isla Tiburón is the El Oculto member (Tmrao, Plate II). This non-welded, lithic-rich cooling unit crops out in a restricted area along the coastline south of Punta Reina ($^{3}54^{260}$,$^{32}\,13^{650}$). The base of the El Oculto member includes a 20 meter thick

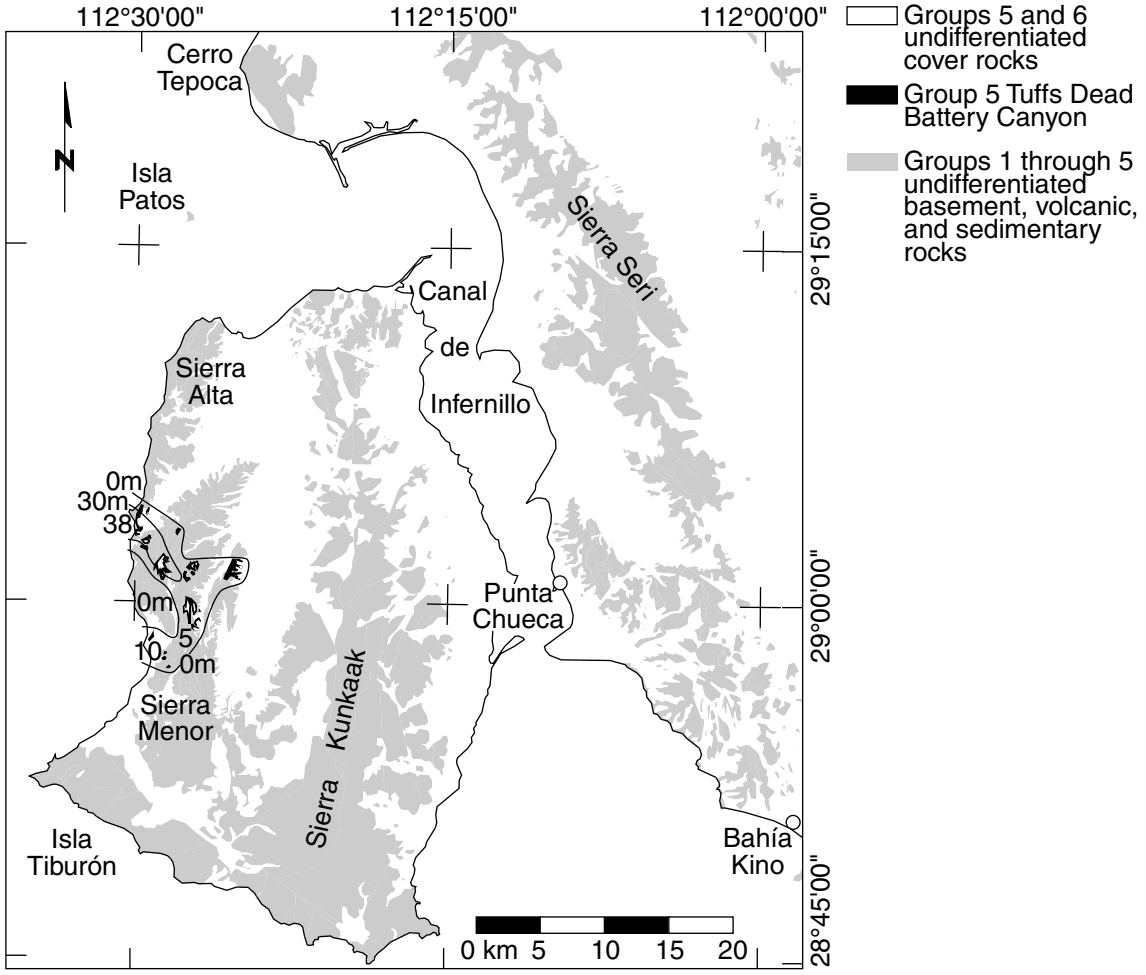

Figure 3.5. Distribution of the Tuffs of Dead Battery Canyon on Isla Tiburón. Numbers denote outcrop thickness measurements (in meters). Isopachs of tuff thickness labelled with 30 m contour interval. Paleotopography and limited tuff volume probably restricted distribution of the Tuffs of Dead Battery Canyon. Enclosed area of zero thickness indicates a paleotopographic high. A paleocanyon located northeast of this high and a basin located southeast of this high each contain eastward-thinning outcrops of the Tuffs of Dead Battery Canyon.

sequence of ash and pumice surge deposits intercalated with volcaniclastic breccia. The El Oculto member fills a paleocanyon whose walls cut down across the Tuffs of Dead Battery Canyon and unit Tmr4 of the Tuffs of Mesa Cuadrada.

One to two main members of the Tuff of Arroyo El Canelo are observed in the Sierra Menor. These members are mapped as units Tmrec1 and Tmrec2 where they are separated by a thin (1 to 2 m) lithic-rich horizon and/or a vitrophyre. At other localities where only one main member unit is present, or the transition between members is welded together and hard to identify, outcrops are mapped as unit Tmrec. The main members of the Tuff of Arroyo El Canelo are characteristically densely welded with 10-15% phenocrysts (plagioclase > pyroxene) and distinctive 5-20 cm long vapor-phase altered pumice. Centimeter-scale variations in phenocryst content are occasionally observed near the base of each member. Thick vapor-phase altered horizons characterize the upper parts of the El Canelo members exposed along the coastline between Punta Reina and Bahia Vaporeta ($^{3}53^{980}$,^{32} 11^{600} to $^{3}54^{900}$,^{32} 07^{000}). Thick deposits of the main members of the Tuff of Arroyo El Canelo in the southwestern Sierra Menor are densely welded, with thin pumice fiamme that display rheomorphic lineations.

The Flagpole member is the uppermost cooling unit of the Tuffs of Arroyo El Canelo. The Bighorn Sheep member, a 1 to 3 m thick lithic tuff, commonly marks the base of the Flagpole member. This transition is mapped with the underlying main member of the Tuffs of Arroyo El Canelo (Plate II). The Flagpole member is found in most outcrop areas of the Tuff of Arroyo el Canelo on Isla Tiburón. It is distinguished from the main member by its thickness (2 to 5 meters) and dense welding, with smaller and less frequent pumice fiamme and the presence of olivine phenocrysts.

The Tuffs of Arroyo El Canelo are preserved further south than the Tuffs of Mesa Cuadrada or the Tuffs of Dead Battery Canyon (Figs. 3.5, and 3.6). At the southern end of the Sierra Menor, the Tuff of Arroyo El Canelo crops out both north and south of a paleotopographic barrier that had blocked deposition of earlier ignimbrites. South

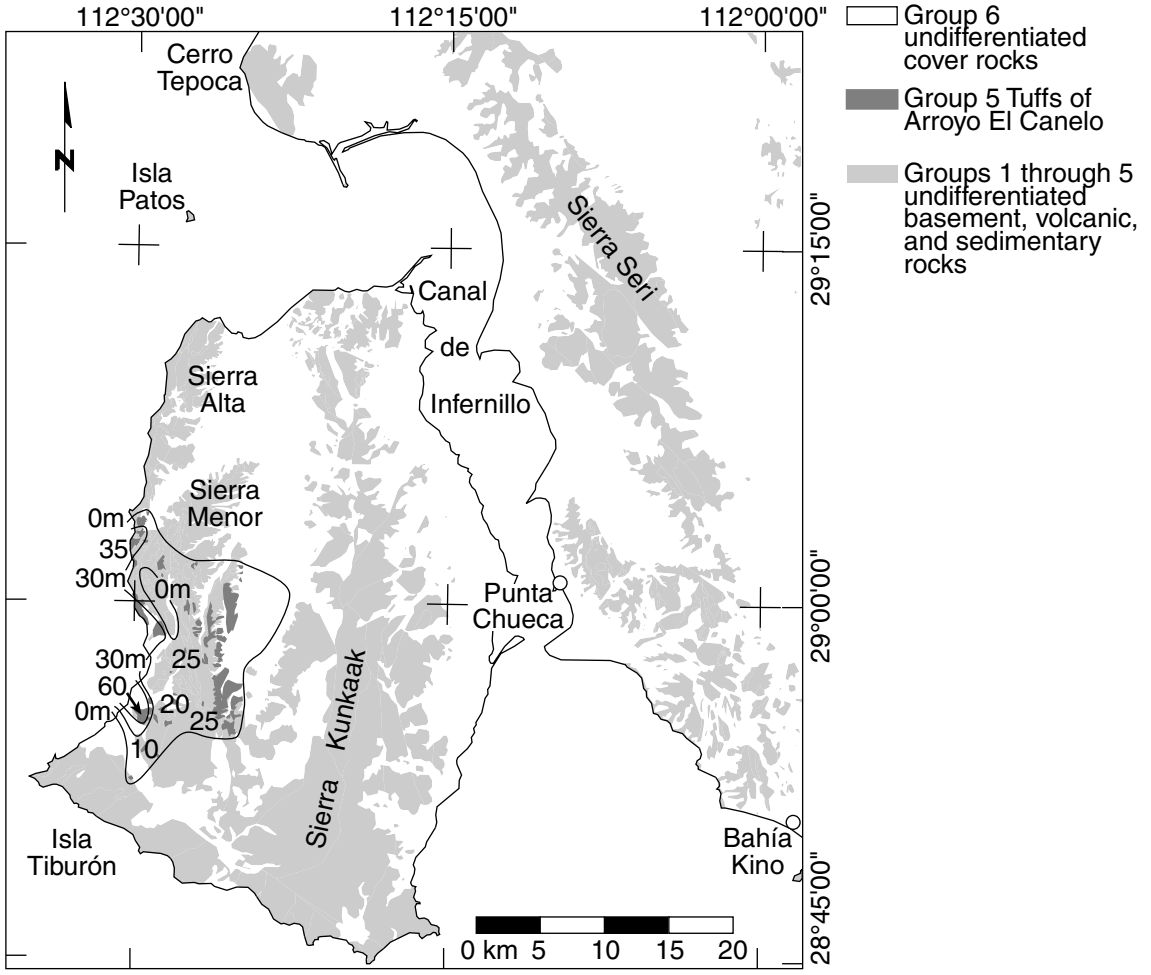

Figure 3.6. Distribution of the Tuffs of Arroyo El Canelo on Isla Tiburón. Numbers denote combined outcrop thickness measurements of all cooling units (in meters). Isopachs of tuff thickness labelled with 30 m contour interval. Enclosed area of non-deposition of the Tuffs of Arroyo El Canelo corresponds to a paleotopographic high. Tuff thickness changes abruptly near the western coastline of Isla Tiburón. The eastern edge of tuff was probably controlled by fault-bounded relief east of the Tecomate basin (Fig. 3.1). Isopachs of tuff thickness are inferred to terminate against this boundary.

of this barrier, the Tuffs of El Canelo are thick and densely welded ($^{3}54^{400}$,$^{32}\,00^{000}$). The Tuffs of Arroyo El Canelo on Isla Tiburón abruptly pinch out northward against the Tuffs of Dead Battery Canyon near Punta Reina and the northern Sierra Menor ($^{3}54^{900}$,$^{32}\,15^{600}$ and $^{3}57^{280}$,$^{32}\,14^{170}$). Combined measured thickness of all members of the Tuffs of Arroyo El Canelo does not appear to exceed 20 meters throughout the interior of the Sierra Menor (Fig. 3.6). However, outcrops adjacent to Valle de Tecomate have not been measured. The thickness of the Tuffs of Arroyo El Canelo reaches at least 60 meters in coastal exposures on Isla Tiburón. These outcrops also display areas of very high-grade welding and steep paleotopography that appears to have developed after deposition of the Tuffs of Mesa Cuadrada and the Tuffs of Dead Battery Canyon. These characteristics are similar to caldera margin areas documented in Baja California and suggest that the present-day western coastline of Isla Tiburón lay near the vent for the Tuffs of Arroyo El Canelo. Alternatively, fault-bounded basin(s) may have controlled deposition of the Tuffs of Arroyo El Canelo near the present-day western coastline of Isla Tiburón. The area and volume of the Tuffs of Arroyo El Canelo on Isla Tiburón is estimated as 170 km^2 and 9 km^3 (Table 3.2).

Dates are reported on the Tuffs of Arroyo El Canelo in Baja California [*Nagy et al.*, 1999; *Martín-Barajas and Stock*, 1993]. These samples yielded ages of 6.4±0.1 Ma for the base of the Tuffs in Arroyo La Cantera and 6.1±0.5 Ma for the main member of the Tuffs of Arroyo El Canelo from Santa Isabel Wash (Fig. 2.1). No age determinations were attempted for samples of the Tuffs of Arroyo El Canelo from Isla Tiburón.

3.4.8 Group 6: Late synrift deposits

Late synrift deposits of Isla Tiburón and Coastal Sonora record a continuation of volcanic and non-marine deposition into marginal rift basins combined with marine incursion into the northern Gulf of California. On Isla Tiburón, group six deposits overlie the 6.1 to 6.3 Ma Tuffs of the Northern Puertecitos Volcanic Province. Group

six deposits filled alluvial valleys in the northern and central-western area of the island. Small-volume lavas and pyroclastic flows are intercalated with both marine and non-marine sedimentary rocks of group six on the southern and southwestern areas of Isla Tiburón. These deposits include the 'proto-Gulf' marine conglomerate of southwestern Isla Tiburón [*Gastil and Krummenacher*, 1977; *Smith*, 1991; *Gastil et al.*, 1999] which is shown to be post-6 Ma age in this study. On the mainland coastal Sonora study area, group six sedimentary rocks are undivided from older synrift sedimentary rocks, except where these younger deposits show geomorphic evidence for deposition during the Quaternary.

Non-marine pre-Quaternary sedimentary rocks of group six crop out throughout the study area. These deposits are mapped as unit Tmpal if they lack geomorphic evidence of depositional setting. Outcrops of Tmpal overlie the Tuffs of the Northern Puertecitos Volcanic Province only in the northern Sierra Kunkaak, where a section of basin fill has been uplifted to the range crest along the Kunkaak low-angle normal fault. Outcrops of Tmpal on southern and southwestern Isla Tiburón may also overlie scattered exposures of the Tuff of Arroyo El Canelo ($^{3}53^{550}$,^{32} 95^{000} and $^{3}53^{930}$,^{31} 95^{780}) and contain intercalated volcanic rocks of group six age (e.g., $^{3}64^{940}$,^{31} 95^{950}). Non-marine basin-filling sedimentary rocks are mapped as unit QTpal where outcrops retain geomorphic evidence of a depositional surface but are stranded as a high-standing thick alluvial terrace. *Gastil and Krummenacher* [1976] mapped outcrops of group six non-marine conglomerates as several different units. They mapped conglomerate exposures of the Kino–Chueca domain of coastal Sonora as units T3, T4x, and Qf. On Isla Tiburón, they mapped exposures of non-marine conglomerate as T3 on southwestern Isla Tiburon, T4y in the northern Sierra Kunkaak, T5 and Qf in central Isla Tiburon, and Qm adjacent to Bahia Vaporeta. Non-marine fluvial conglomerate on southwest Isla Tiburón was mapped as unit Pfc by *Neuhaus* [1989] and unit M11 by *Gastil et al.* [1999].

Exposures of marine pre-Quaternary rocks of group six age are restricted to southwestern Isla Tiburón [*Gastil and Krummenacher*, 1976; *Gastil et al.*, 1999]. These

outcrops (unit Tmpm on Plate II) are a shallow-marine conglomeratic delta-fan deposit [*Cassidy*, 1988]. The conglomerates overlie a landslide breccia (unit Tmbr) which marks the base of the shallow marine basin. This breccia contains monolithologic zones of angular welded tuff clasts intercalated with polylithologic zones of andesitic volcaniclastic breccia. The matrix of unit Tmbr is composed of pulverized angular fragments of breccia lithologies. Volcanic ash and pumice form part of the matrix of the polylithologic breccia. The base of the breccia shows a cm-thick blackened zone of fragmental material with a sheared basal contact that probably formed during emplacement of the breccia as a landslide. Marine rocks on southwest Isla Tiburón are mapped as unit T3m by *Gastil and Krummenacher* [1977], units Mcg and Mss by *Neuhaus* [1989], and unit M8 by *Gastil et al.* [1999]. The underlying breccias were mapped as unit Mbt by *Neuhaus* [1989] and unit M7 by *Gastil et al.* [1999].

The stratigraphically lowest volcaniclastic rocks of group six in the Sonoran margin study area are the Tuffs of Arroyo Sauzal. These ash-flow tuffs comprise four cooling units emplaced into the Sauzal basin ($^{3}56^{000}$,$^{31}\,96^{000}$). Member one of the Tuffs of Arroyo Sauzal is a non-welded to slightly welded ash-flow tuff (20% phenocrysts: alkali-feldspar $\gg$ clinopyroxene $\approx$ hornblende $\gg$ biotite $\approx$ plagioclase $\approx$ zircon) with <1% andesite and crystalline (basement?) lithic fragments. This distinctive unit also crops out beneath the marine sedimentary rocks and above the landslide breccia on southwestern Isla Tiburón ($^{3}50^{730}$,$^{31}\,97^{360}$ and $^{3}49^{650}$,$^{31}\,97^{540}$). Alkali-feldspar separated from member one was dated by K-Ar from southwestern Isla Tiburón at 5.67±0.17 Ma (sample 51A, unit Mr, *Neuhaus* [1989]). Additional samples of this unit from southwestern Isla Tiburón were dated for this study by ^{40}Ar/^{39}Ar as 6.40±1.63 Ma and 6.67±0.83 Ma (Table 3.1). A third sample of member one of the Tuffs of Arroyo Sauzal from southern Isla Tiburón yielded an isotopic age 5.40±3.90 Ma. Members two and three of the Tuffs of Arroyo Sauzal are each 3 meter thick welded ash-flow tuffs that together form a composite unit (Tmprsz2–3) separated from member one by a 15-meter section of non-marine conglomerate. Member

two is a moderately welded ignimbrite with 3% volcanic lithics, 3% pumice fiamme, and 15% phenocrysts (plagioclase $\gg$ clinopyroxene $\approx$ opaques $>$ olivine). Member three is a densely welded ignimbrite with pumice fiamme up to 20 cm long and 20% phenocrysts (plagioclase $>$ alkali-feldspar $\approx$ clinopyroxene $>$ opaques). Outcrops of member four of the Tuffs of Arroyo Sauzal are separated from the top of member three by 3 meters of fluvial conglomerate. Member four is a one meter thick, densely welded ash-flow tuff with 15% pumice fiamme and 3% phenocrysts (alkali-feldspar $\approx$ plagioclase $>$ pyroxene). With the exception of unit Mr/M10 [*Neuhaus*, 1989; *Gastil et al.*, 1999] from southwest Isla Tiburón, the Tuffs of Arroyo Sauzal were not mapped by previous workers.

The Rhyodacite of Cerro Starship caps marine conglomerates on southwestern Isla Tiburón [*Gastil and Krummenacher*, 1976; *Neuhaus*, 1989; *Gastil et al.*, 1999, $^{3}50^{300}$,$^{31}\,97^{300}$]. This flow contains 35% phenocrysts (plagioclase $>$ hornblende $>$ alkali-feldspar $>$ opaques $>$ biotite) and displays macroscopic flow foliation and trachytic alignment of phenocrysts. The Rhyodacite of Cerro Starship was emplaced primarily as a lava flow that erupted from a north-striking dike on the eastern side of Cerro Starship ($^{3}50^{400}$,$^{31}\,97^{190}$). Pyroclastic textures are absent from the main body of the lava flow, and a one- to two-meter–thick block-and-ash deposit underlies the rhyodacite. The Rhyodacite of Cerro Starship was misidentified as an ash-flow tuff by *Gastil and Krummenacher* [1977] and dated by these authors as 11.2±1.3 Ma by K-Ar on plagioclase (sample S2B-27). This date formed the basis of interpretation of marine strata on southwestern Isla Tiburón as evidence for a middle Miocene proto-Gulf of California [*Smith*, 1991]. Attempts to re-date this flow by *Neuhaus* [1989] yielded an age 4.16±1.81 Ma (sample 10W). *Gastil and Krummenacher* [1977] also dated plagioclase by K-Ar from the rhyodacite dike at 3.7±0.9 Ma (sample S2G-13). The older age of 11.2±1.3 Ma for the Rhyodacite of Cerro Starship is discordant with the stratigraphic position of this flow above well-dated outcrops of member one of the Tuffs of Arroyo Sauzal (see above). Thus, the Rhyodacite of Cerro Starship and the underlying marine strata are probably of Early Pliocene age as suggested by the

younger isotopic age determined for the Rhyodacite of Cerro Starship [*Neuhaus*, 1989] and for nearby outcrops of the rhyodacite dike [*Gastil and Krummenacher*, 1977]. An attempt to re-date this flow by $^{40}Ar/^{39}Ar$ on plagioclase produced a large uncertainty [*Stock and Oskin, in prep*]. The Rhyodacite of Cerro Starship was mapped as unit T4x by *Gastil and Krummenacher* [1976], units Mrt (flow) and Mgd (dike) by *Neuhaus* [1989] and units M9 (flow) and M10 (dike) by *Gastil et al.* [1999].

The Tuffs of Bahía Vaporeta form a set of small-volume non-welded to moderately welded pyroclastic flows intercalated with group six non-marine conglomerates exposed along the southwestern shoreline of Isla Tiburón (unit QTprbv). At least three five-meter-thick cooling units are exposed ($^{3}53^{300}$,$^{32}\,00^{280}$). Thin, poorly exposed non-welded pumice flows characterize northern outcrops and a one- to two-meter-thick welded carapace of tuff crops out on southwestern Isla Tiburón ($^{3}52^{630}$,$^{31}\,99^{100}$). The Tuffs of Bahía Vaporeta may be recognized from their distinctive and abundant light- and dark-colored pumice and uncommon (1%) anorthoclase phenocrysts. Outcrops of the Tuffs of Bahía Vaporeta were mapped as Qm by *Gastil and Krummenacher* [1976], unit Mry by *Neuhaus* [1989] and M10 by *Gastil et al.* [1999]. The Tuffs of Bahía Vaporeta have not been dated. These tuffs may be older or younger than the Dacite of Cerro Colorado and the Hipat Tuffs that are described below.

In addition to the Tuffs of Bahía Vaporeta, probably the youngest volcanic rocks on Isla Tiburón are preserved on a prominent volcanic edifice near Punta Colorado ($^{3}54^{630}$,$^{31}\,91^{680}$) and a nearby plateau formed of partially welded to non-welded airfall deposits. These deposits are designated the Dacite of Cerro Colorado (unit Tpdcc) and the Hipat Tuffs (new name, units Tpth1, Tpth2, and Tpth3). The thickness and welding grade of the Hipat Tuffs increases towards the edifice of Dacite of Cerro Colorado, strongly suggesting eruption from a volcano here. The bulk composition of the Hipat Tuffs was determined as dacite by *Neuhaus* [1989]. The volcanic edifice has not been sampled but is assumed to be the same composition as the airfall deposits. The Hipat Tuffs record three pulses of airfall deposition. Unit Tpth1 is a widespread non-welded bedded pumice lapilli and ash deposit up to 20 meters thick.

This unit is draped over paleotopography in the Arroyo Sauzal drainage. Unit Tpth2 and unit Tpth3 are 5- to 10-meter-thick partially welded to non-welded lithic phyric air-fall tuffs dominated by lapilli-sized pumice and containing 15-20% phenocrysts (plagioclase > clinopyroxene > alkali-feldspar). Tpth2 contains one to two prominent red welded bands, whereas Tpth3 contains an equally prominent black welded band. Each of these internal welding zones ranges from 1 to 3 meters thickness. The Dacite of Cerro Colorado and the Hipat Tuffs are mapped as unit T5r by *Gastil and Krummenacher* [1976] and described as unit 12 by *Neuhaus* [1989] and *Gastil et al.* [1999]. Attempts to date the Hipat Tuffs produced large uncertainties. *Neuhaus* [1989] dated a sample by the whole-rock K-Ar method at 5.61±7.89 Ma (sample 239W). An attempt to date plagioclase by the $^{40}Ar/^{39}Ar$ method were unsuccessful [*Stock and Oskin, in prep.*].

Several types of Quaternary deposits are mapped on Isla Tiburón (Plate II) and mainland coastal Sonora (Plate I). Areas of active sedimentary deposition include alluvium (unit Qal), littoral deposits (unit Qli), and colluvial slope-cover (unit Qco). Aeolian deposits stabilized by vegetation (unit Qae) cover some areas adjacent to the coastline. These deposits, where present along the rugged northeast coastline of Isla Tiburón, appear to have been derived from sandy seafloor sediment transported during times of lower sea level. Older Quaternary fluvial deposits are mapped as unit Qoal where these deposits are low (1- to 3-meter-high) terrace deposits likely to be of Quaternary age. Unit QTpal is mapped where thicker, high-standing terraces may pre-date the Quaternary period. Stream terraces were mapped in detail where cut by recent fault movements. Only the more prominent stream terraces are divided from unit Qal in other areas. A string of 3- to 5-meter elevation benches covered with rounded cobbles and sand lies adjacent to the coastline of Bahía Vaporeta (unit Qm). These are interpreted as wave-cut marine terraces that may correspond to a 5±1 m highstand in the Gulf of California during oxygen isotope stage 5e [*Ortlieb*, 1991]. No isotopic age information exists for Quaternary deposits on Isla Tiburón.

3.5 Discussion

In this section, unit distribution and thickness, facies relationships, and paleogeography are discussed on a range-by-range basis for the Sonoran margin study area. There is a similar set of facies relationships for the Tuff of San Felipe and the Tuffs of the Northern Puertecitos Volcanic Province as shown for the northeastern Baja California margin. A likely source area for the Tuff of San Felipe crops out on the coastline of mainland Sonora and appears to be closely related to high-grade exposures of the ignimbrite on northern Isla Tiburón. The Tuffs of the northern Puertecitos Volcanic Province are confined to the western and northern areas of Isla Tiburón. Here, the north to south progression of ignimbrite distribution and facies relationships shares many aspects of the relationships exposed in northeastern Baja California. Characteristics of the volcaniclastic stratigraphy of the Sonoran margin are described below. In Chapter 5 below, these descriptions are synthesized with the geology of northeastern Baja California into a paleogeographic restoration of the Gulf of California rift.

3.5.1 Coastal Sonora

The mainland coastal area of central Sonora (Plate I) contains north- to northwest-trending ridges comprised of basement (group 1) overlain by volcanic and volcaniclastic strata (groups 2–6). This region can be divided into two domains of Miocene volcanic strata. The Sierra Seri domain comprises basal volcaniclastic sandstone capped by a 200 m thick stack of densely welded ash-flow tuffs and rhyolite lava flows. These volcanic strata are tentatively assigned to the Early- to Mid-Miocene arc (group 3) and have no known correlative to the west. Outcrops of a distinctive conglomerate (group 2) in the Sierra Seri correlate to outcrops in the Santa Rosa Basin of Baja California. Outcrop relationships suggest that this conglomerate is younger than the adjacent volcanic section [*Gastil and Krummenacher*, 1976, and Fig. 3.1], although more fieldwork is needed here. The Kino–Chueca domain is separated from the Sierra

Seri domain by the northwest-striking Sacrificio fault. Volcanic strata of the Kino–Chueca domain comprise a basal 5 to 50 m thick section of basalt flows, andesite flows, and volcaniclastic sandstone and conglomerate from the Early- to Mid-Miocene volcanic arc (group 3). These strata are overlain by 100 m to 135 m thick high-grade Tuff of San Felipe (group 4). The highest-grade ignimbrite crops out near Punta Chueca and is capped by the Tuffs of Punta Chueca, a 100 to 200 m thick section of non-welded pyroclastic flows, and by basalt flows. These facies relationships and associated syndepositional faults suggest that the Punta Chueca outcrops comprise part of a caldera formed by eruption of the Tuff of San Felipe. Synrift volcanic deposits (groups 5 or 6) are represented by rhyolite lava flows overlying the Tuff of San Felipe near Bahía Kino. Synrift sedimentary deposits (groups 5 and/or 6) consist of tilted fluvial conglomerate and modern fluvial and marine basin fill.

3.5.2 Sierra Kunkaak

The Sierra Kunkaak of eastern Isla Tiburón are comprised of a thick (500+ m?) and largely unstudied section of probably Early to Mid-Miocene (group 3) lava flows and volcaniclastic deposits [*Gastil and Krummenacher*, 1976]. This section is missing and may have been structurally removed from the northern half of the range, where basement (group 1) exposures predominate. A 3 km wide paleocanyon exposure in the northern Sierra Kunkaak preserves high-grade Tuff of San Felipe intercalated with rhyolite lava flows and capped by a basalt flow. West of this exposure, an eastward-tilted package of synrift basin fill is preserved above the gently west-dipping (30°) Kunkaak normal fault. This section comprises early synrift conglomerates overlain by the Tuffs of Mesa Cuadrada. The ignimbrite section here includes 200 m of primary and reworked pyroclastic deposits overlying a partially-welded 80 m thick section of Tmr3 and underlying a 20 m thick section of Tmr4. Late synrift fluvial conglomerates (group 6) overlie Tmr4 here. Other outcrops of the western range-front of the Sierra Kunkaak (unit Tmvu of Plate I) may also contain the Tuff of San Felipe and/or the Tuffs of the northern Puertecitos Volcanic Province. A pair of incised half-graben

basins within the southwestern Sierra Kunkaak/Arroyo Sauzal area preserves a section of non-marine conglomerate and intercalated late synrift pyroclastic deposits.

3.5.3 Sierra Alta

The Sierra Alta of northwestern Isla Tiburón preserves a discontinuous section of pre-rift strata overlying basement and overlain by approximately 200 m of early synrift lava flows capped by the Tuffs of Mesa Cuadrada. Basement-clast conglomerate (group 2) and the Tuff of San Felipe (group 4) fill west-trending paleocanyons cut into igneous and metamorphic basement (group 1). Outcrops of the Tuff of San Felipe are densely welded deposits up to 70 m thick with abundant dark-colored rhyolite lithic inclusions. Early synrift rhyolite and andesite lava flows with intercalated volcaniclastic deposits overlie the Tuff of San Felipe. Rhyolite lava flows are underlain by block and ash deposits and dikes are associated with andesite flows, suggesting that these flows were erupted locally. The Tuffs of Mesa Cuadrada form a thin to moderately thick (0–50 m) layer on the east side of the range. Tmr3 is poorly welded to non-welded and Tmr4 is densely welded here. Thicker sections of the Tuffs of Mesa Cuadrada are preserved as a paleocanyon fill deposit in the central part of the range.

Located at the southern end of the Sierra Alta, Punta Reina exposes several stratigraphic transitions within both the Early- to Mid-Miocene arc rocks (group 3) and overlying synrift deposits (group 5). Volcaniclastic rocks of the Early- to Mid-Miocene arc appear in the section just north of Punta Reina and thicken southward. Basement is buried from the exposed section at this same location southward and does not reappear until south of the La Cruz fault in southern Isla Tiburón. Two paleocanyons, one cut into basement and the other cut into group three volcaniclastic strata, are filled by up to 30 m of the Tuff of San Felipe. After deposition of the Tuff of San Felipe into these paleocanyons, early synrift andesite flows and volcaniclastic debris flows (group 5) covered the northern paleocanyon. The southern paleocanyon was filled by a $>$ 250 m-thick section of the Tuffs of the Northern Puertecitos Volcanic Province. Within a 2 km north-south distance at Punta Reina, outcrops of the Tuffs of

Dead Battery Canyon and then the Tuffs of Arroyo El Canelo appear stratigraphically above the Tuffs of Mesa Cuadrada. A younger paleocanyon cut across the Tuffs of Mesa Cuadrada and the Tuffs of Dead Battery Canyon is filled by a section of debris flows, ash-flow surge deposits, and other pyroclastic materials of the lowest member of the Tuffs of Arroyo El Canelo. Overall, the Punta Reina area marks an abrupt transition, from a simple section of 0 to 50 m thick deposits of the Tuffs of Mesa Cuadrada in the Sierra Alta, to a complete $>$ 250 m thick section of the Tuffs of the Northern Puertectios Volcanic Province in the central Sierra Menor.

3.5.4 Sierra Menor

The Sierra Menor forms the principal belt of exposures of correlative volcanic deposits adjacent to the western shoreline of Isla Tiburón. The oldest exposed strata here are andesite lava flows and volcaniclastic rocks of the Early to Mid-Miocene arc (group 3). These are exposed in the footwall of larger normal faults in the northern and central parts of the range and in a 10 km diameter area of andesite in the southern part of the range (Plate II). This latter feature appears to have persisted as a paleotopographic high during later depositional episodes. The Tuff of San Felipe crops out periodically in paleocanyons cut into the volcanic and volcaniclastic strata or as isolated ridge-top exposures. The Tuff of San Felipe is typically less than 10 m thick, although local paleocanyon fill deposits reach 85 m thickness in the central part of the range and 50 m thickness east of Punta Reina. Early synrift lava flows are common throughout the range. These are predominantly rhyolite and andesite in the northern half of the Sierra Menor. Basalt flows crop out in central part of the range and at its northeast end. Early synrift conglomerates overlie these basalt flows, defining the base of a 10-km-wide basin in the central Sierra Menor. Most of this basin is filled by a 100 to 250 m thick section of the Tuffs of the Northern Puertecitos Volcanic Province. The Tuffs of Mesa Cuadrada crop out throughout the range and pinch out against paleotopography to the north and south. The Tuffs of Dead Battery canyon are exposed in a 10 km-wide swath extending southeastward

from Punta Reina. Outcrops of the Tuffs of Arroyo El Canelo partially overlie and extend south of exposures of the Tuffs of Dead Battery Canyon. The Tuffs of Arroyo El Canelo cap the stratigraphic section of the central and southern Sierra Menor. In the southwestern part of the Sierra Menor, the Tuffs of Arroyo El Canelo directly overlie older syn-rift or pre-rift strata, including the Tuff of San Felipe. In this area it appears that the Tuff of Arroyo El Canelo surmounted or skirted paleotopography. Thick, densely welded deposits of the Tuff of Arroyo El Canelo near the western shoreline of Isla Tiburón (Fig. 3.6) may represent an equivalent of the intracaldera facies present in the Arroyo Matomí area of Baja California (Fig. 2.8). Late synrift fluvial basin fill deposits are exposed adjacent to the northern and eastern edge of the Sierra Menor. Fluvial and marine deposits fill a fringing basin located at Bahía Vaporeta, west of the central Sierra Menor. A late synrift non-welded pyroclastic flow, the Tuff of Bahía Vaporeta, crops out periodically along the coastline here.

The Sierra Menor of southwestern Isla Tiburón preserves several complex stratigraphic relationships in Early Miocene to Pliocene (or later) volcanic and volcaniclastic rocks. Early to Mid-Miocene volcanic strata (group 3) do not match across the northwest-striking La Cruz fault. Northeast of the La Cruz fault are exposures of andesite and volcaniclastic conglomerates, whereas southwest of the fault, basalt and volcanic sandstone are overlain by scattered andesite lava flows [*Gastil et al.*, 1999]. Outcrops of the Tuff of San Felipe and the Tuffs of the Northern Puertecitos Volcanic Province appear to pinch out against paleotopography north of the La Cruz fault, although isolated outcrops of the Tuff of Arroyo El Canelo may approach the fault zone. The oldest deposits that correlate across the La Cruz fault are a landslide breccia deposit and member one of the Tuffs of Arroyo Sauzal (Plate II). This latest Miocene non-welded ash-flow tuff underlies a small (10 km^2) basin formed adjacent to the La Cruz fault and filled by marine and fluvial conglomerate. The basin deposit is intruded by and overlain by the Early- to Mid-Pliocene Rhyodacite of Cerro Starship. Southeast of Cerro Starship, the Dacite of Cerro Colorado and its associated air-fall deposit, the Hipat Tuffs, form one of the youngest volcanic features on Isla Tiburón.

Cerro Colorado forms a volcanic edifice exceeding 500 m elevation adjacent to the southwestern coastline of Isla Tiburón. The Hipat Tuffs extend northeast of Cerro Colorado, across the La Cruz fault and into the southwestern Sierra Kunkaak. These tuffs are only slightly disrupted by the La Cruz fault.

3.6 Summary

In summary, similar to the northeastern Baja California margin, the Sonoran margin study area contains a southward-thickening wedge of volcanic and sedimentary strata (groups 2–6) overlying Mesozoic and older bedrock (group 1). The lowest strata of this wedge are isolated channel-filling conglomerates (group 2). The largest of these channels, located in the central Sierra Seri of mainland Sonora, contains distinctive clasts that correlate to a similar deposit in the Santa Rosa Basin of Baja California [*Gastil et al.*, 1973]. Early- to Mid-Miocene arc volcanic and volcaniclastic strata (group 3) vary in thickness from zero in the central Sierra Seri, northern Sierra Kunkaak, and the Sierra Alta, to as much as 500 m in the southern Sierra Kunkaak and the southern Sierra Menor. The Tuff of San Felipe (group 4) probably erupted from a caldera located at Punta Chueca, mainland Sonora. Lobes of this ignimbrite flowed southward to Bahía Kino and westward across the northern Sierra Kunkaak, Sierra Alta and the Sierra Menor. Early synrift (group 5) lava flows of varying composition extensively covered the Sierra Alta and the Sierra Menor. Early synrift fluvial conglomerates in the central Sierra Menor and northern Sierra Kunkaak document the formation of rift basins that later filled with the Tuffs of Mesa Cuadrada, the Tuffs of Dead Battery Canyon, and the Tuffs of Arroyo El Canelo. Young synrift volcanic deposits (group 6) are found only in southwestern Isla Tiburón. These Early to Mid-Pliocene lava flows and tuffs bracket the age of a 10 km^2 marine to non-marine basin formed adjacent to the La Cruz fault. Other young synrift sedimentary deposits are found in the north-trending rift basins of the Valle Tecomate and Arroyo Sauzal of central Isla Tiburón, as well as in the Canal de Infernillo located between Isla

Tiburón and mainland Sonora.

Two regional-scale stratigraphic relationships of pre-rift and syn-rift ignimbrite deposits are key for correlation of the geology of coastal Sonora and Isla Tiburón across the northern Gulf of California. These relationships are similar to those described for Baja California in Chapter 2. The first of these relationships is the distribution and facies of the Tuff of San Felipe. The Tuff of San Felipe fills a series of west-trending paleocanyons that crop out over a north-south distance of 30 km adjacent to the the western coastline of Isla Tiburón. Higher-grade densely welded outcrops of the Tuff of San Felipe occur in coastal Sonora and on the northern areas of Isla Tiburón. Outcrops of part of the likely vent area of the Tuff of San Felipe occur near Punta Chueca on the Sonoran mainland. The second key regional-scale relationship is the distribution of the Tuffs of the Northern Puertecitos Volcanic Province. In western Sonora, these tuffs are restricted to a $\sim$400 km^2 area of western and northern Isla Tiburón. These outcrops occur adjacent to $\sim$30 km of the coastline of Isla Tiburón from the La Cruz fault to the northern Sierra Alta. The overall north-south variations in distribution of the Tuffs of Mesa Cuadrada, Tuffs of Dead Battery Canyon, and the Tuffs of Arroyo El Canelo are identical to those seen in Baja California. The Tuffs of Mesa Cuadrada are the most widespread unit. The Tuffs of Dead Battery Canyon are restricted to the central coast of Isla Tiburón. The Tuffs of Arroyo el Canelo are present in the central and southern Sierra Menor. As in Baja California, the distribution of the Tuffs of Arroyo El Canelo is centered southward of the Tuffs of Mesa Cuadrada. Thick, more densely welded deposits of the Tuffs of Mesa Cuadrada and the Tuffs of Arroyo El Canelo appear in the central and coastal regions of Sierra Menor.

Table 3.3. Compilation of mapped units by *Gastil and Krummenacher* [1976] on Isla Tiburón, and coastal Sonora into stratigraphic groups 1–6.

Group	Mapped as Units[1]
	Sierra Alta
Group 1: Basement complex	Ms, Mc, t
Group 2: Tertiary basal sediments	T1s, Base of T4x
Group 3: Miocene volcanic arc	not present
Group 4: Tuff of San Felipe	T1r, Base of T4x
Group 5: Early syn-rift deposits	T1, T4, T4a, T4b, T4d, T4x
Group 5: Tuffs of the Northern Puertecitos Volcanic Province	Top of T4 (T4, T4a, T4b, T4d, T4x)
Group 6: Late syn-rift deposits	al, s
	Sierra Menor
Group 1: Basement complex	not exposed
Group 2: Tertiary basal sediments	not exposed
Group 3: Miocene volcanic arc	Lower T1, (10.9±2.3, K–Ar on plagioclase), 15.3±1.3, K–Ar on hornblende T2 T3, 22.7±1.1, K–Ar on plagioclase, 18.8±2.4, K–Ar on hornblende
Group 4: Tuff of San Felipe	Middle T1 Lower T4x (near coast)
Group 5: Early syn-rift deposits	Upper T1 (near coast) T2, T3 T5 (inland, central to northern area)
Group 5: Tuffs of the Northern Puertecitos Volcanic Province	T3? (unlabelled outcrop), 5.7±0.6, K–Ar on K-feldspar T4, T4x, T4y
Group 6: Late syn-rift deposits	T3m, Qm, T3m, al T5, T5r, T5d (southern area)
	Sierra Kunkaak

Compilation of mapped units by *Gastil and Krummenacher* [1976] on Isla Tiburón, and coastal Sonora into stratigraphic groups 1–6, continued.

Group	Mapped as Units[1]
Group 1: Basement complex	M, Mv, Mc t, gd
Group 2: Tertiary basal sediments	not present(?)
Group 3: Miocene volcanic arc	Lower T1, T1r(?), T1b(?), T2 (northern area) Tv(?), T2, T3, T4b, T4x, T4y, T5d (southern area)
Group 4: Tuff of San Felipe	Middle T1 (northern area)
Group 5: Early syn-rift deposits	T5a (southern area) 9.9±1.3, K–Ar on hornblende Upper T1, T1s, T1c, T3 (northern area)
Group 5: Tuffs of the Northern Puertecitos Volcanic Province	T4, T4x, T4y (northern area)
Group 6: Late syn-rift deposits	al, Qm, Qf T3, T5, T5r (southwestern area)
La Cruz Domain	
Group 1: Basement complex	Ms, gd
Group 2: Tertiary basal sediments	not present(?)
Group 3: Miocene volcanic arc	T1, T1r, T2, T2b, T3
Group 4: Tuff of San Felipe	not present
Group 5: Early syn-rift deposits	T4b, 7.0±0.3, K–Ar on whole rock
Group 5: Tuffs of the Northern Puertecitos Volcanic Province	not present
Group 6: Late syn-rift deposits	T4x, (11.2±1.3, K–Ar on plagioclase), 3.7±0.9, K–Ar on plagioclase T3m, T5r, al, Qm
Kino–Chueca Domain	
Group 1: Basement complex	M, Mc, Ms, Mv, t, gd, d
Group 2: Tertiary basal sediments	not present(?)

Compilation of mapped units by *Gastil and Krummenacher* [1976] on Isla Tiburón, and coastal Sonora into stratigraphic groups 1–6, continued.

Group	Mapped as Units[1]
Group 3: Miocene volcanic arc	Lower T1 (northern area) T2a, 21±0.8, 17.8±0.8, K–Ar on hornblende T1b, T2, T2s
Group 4: Tuff of San Felipe	Upper T1, T2 (northern area) T1r, T2r
Group 5: Early syn-rift deposits	T3, T4, T4x, Qf
Group 5: Tuffs of the Northern Puertecitos Volcanic Province	not present
Group 6: Late syn-rift deposits	T3, T4, T4x, Qf, al
	Sierra Seri
Group 1: Basement complex	M, Ms, ad, gd
Group 2: Tertiary basal sediments	T1c
Group 3: Miocene volcanic arc	Tb, Tv, T1-3, T2, T3 T2a, 12.3±2.9, K–Ar on plagioclase T4x 12.7±1.1, K–Ar on plagioclase
Group 4: Tuff of San Felipe	not present
Group 5: Early syn-rift deposits	not exposed
Group 5: Tuffs of the Northern Puertecitos Volcanic Province	not present
Group 6: Late syn-rift deposits	Qf, al

[1]Anomalous or otherwise suspect dates enclosed in parentheses. All ages in millions of years.

Chapter 4

Rapid localization of Pacific–North America plate motion in the Gulf of California

Michael Oskin, Joann Stock — Division of Geological and Planetary Sciences, California Institute of Technology, Pasadena, California, 91125, USA

Arturo Martín-Barajas — Centro de Investigación Cientifica y Educación Superior de Ensenada, Km 107 Carretera Tijuana-Ensenada, Baja California, Mexico

From *Geology*, vol. 29, no. 5, p. 459–462, Modified with permission of the publisher, the Geological Society of America, Boulder, Colorado, USA.

4.1 Abstract

Correlation of late Miocene volcaniclastic strata across the northern Gulf of California shows that the Pacific–North America plate boundary localized east of the Baja California peninsula ca. 6 Ma. Dextral offset of the 12.6 Ma Tuff of San Felipe and a pair of overlying ca. 6.3 Ma pyroclastic flows indicate at least 255±10 km of displacement along an azimuth of 310°. Isopach and facies trends of the Tuff of San Felipe support no more than a few tens of kilometers of additional dextral displacement between 12.6 and 6.3 Ma. These constraints indicate that nearly all of the dextral displacement between the Pacific and North American plates prior to 6.3 Ma was accommodated outside of the gulf region, and by 4.7 Ma, the plate boundary motion was localized in the Gulf of California. Although continental extension has accounted for a component of plate boundary motion in northwestern Mexico since cessation of subduction offshore of southern Baja California at 12.5 Ma [*Stock and Hodges*, 1989], transfer of Baja California to the Pacific plate was delayed by at least 6–7 m.y.

4.2 Introduction

The Gulf of California is one of a few active examples of the transition from continental rifting to seafloor spreading. The opening of the gulf is directly related to dextral motion on the San Andreas fault [*Larson et al.*, 1968, Fig. 4.1] following the cessation of subduction and microplate capture west of southern Baja California [*Atwater*, 1970; *Mammerickx and Klitgord*, 1982]. However, only 300–350 km of the expected 500–600 km of post-12 Ma displacement between the Pacific and North American plates has been accommodated as transform slip within the gulf, the remainder being partitioned on faults west of Baja California [*Spencer and Normark*, 1979; *Stock and Hodges*, 1989]. Transfer of Baja California to the Pacific Plate by 3.5 Ma is evident from the formation of magnetically lineated oceanic crust at the

Alarcon Rise in the mouth of the gulf [*Lonsdale*, 1989]. The timing and location of plate boundary motion between 12.5 and 3.5 Ma, and any amount of pre-12.5 Ma strike-slip, is not defined from within the gulf or its surrounding extensional province.

From previous studies, it remains unclear whether the northwestward acceleration of Baja California was a gradual process beginning at 12.5 Ma, or an abrupt event 6–7 m.y. later. Commonly, it is assumed that Baja California joined the Pacific plate at or near the full plate motion rate, sufficient to open the gulf at 5 to 6 Ma [*Curray et al.*, 1982; *Dickinson*, 1996]. The evidence for this timing is not conclusive. Dextral displacement on the southern San Andreas fault and extension and marine deposition in the gulf region began as early as 12 Ma [*Stock and Hodges*, 1989; *Weldon et al.*, 1993; *Lee et al.*, 1996; *Helenes and Carreño*, 1999]. Acceleration of Baja California at 3.5 Ma has been proposed [*Lonsdale*, 1989; *Umhoefer et al.*, 1994] and the full Pacific-North America plate motion may not have occurred in the Gulf until 1 Ma [*DeMets*, 1995].

We present a new set of cross-gulf geologic tie points that define the timing, magnitude, and rate of dextral shear in the gulf. Three distinctive pyroclastic flows correlate lithologically, geochemically, and paleomagnetically from the northern Puertecitos Volcanic Province of Baja California, across the gulf to Isla Tiburón and the adjacent coast of Sonora. These units are the 12.6 Ma Tuff of San Felipe [*Stock et al.*, 1999], and a pair of ca. 6.3 Ma tuffs, Tmr3 and Tmr4, that overlie the Tuff of San Felipe [*Stock*, 1989; *Lewis*, 1996; *Nagy et al.*, 1999].

4.3 Tuffs of the Puertecitos Volcanic Province

The Puertecitos Volcanic Province records the transition from the early Miocene andesitic arc to rift-related, bimodal volcanism [*Martín-Barajas et al.*, 1995, Fig. 4.1]. The synrift section here is dominated by a few extensive welded tuffs [*Stock*, 1989, 1993; *Martín-Barajas et al.*, 1995; *Lewis*, 1996; *Nagy et al.*, 1999]. Thickening and facies trends of several of these tuffs indicate vent locations adjacent to the

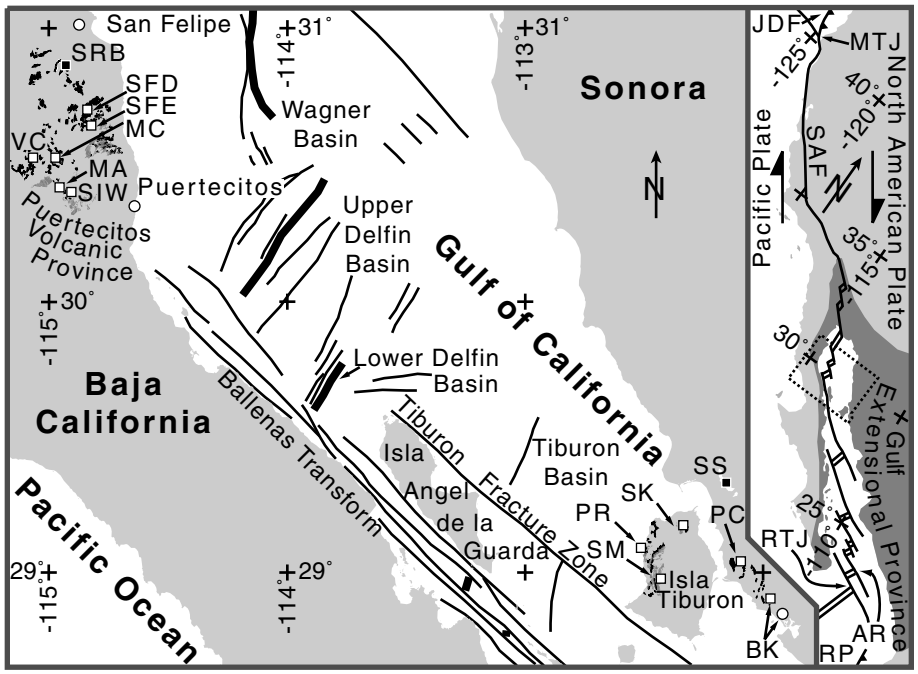

Figure 4.1. Location map of study area. Inset shows part of Pacific-North America plate boundary. AR, Alarcon Rise; JDF, Juan de Fuca plate; MTJ, Mendocino triple junction; RP, Rivera plate; RTJ, Rivera triple junction; SAF, San Andreas fault. Tuff of San Felipe is shown in black, Tmr3 and Tmr4 tuffs are shown in gray. Sample localities are denoted by white squares, towns by white circles: BK, Bahia Kino; SFD and SFE are localities from the Sierra San Fermín; MC, Mesa Cuadrada; MA, Mesa el Avión; PC, Punta Chueca; PR, Punta Reina; SIW, Sierra Santa Isabel; SK, Sierra Kunkaak; SM, Sierra Menor; VC, Valle Chico. Mapping in Baja California was compiled from *Stock et al.* [1991], *Stock* [1993], *Martín-Barajas and Stock* [1993], *Lewis* [1994], and *Nagy* [1997]. Correlative conglomerate locations [*Gastil et al.*, 1973] are denoted by black boxes: SRB, Santa Rosa Basin; SS, Sierra Seri. Marine faults (thin lines) and axes of pull-apart basins (thick lines) are from *Fenby and Gastil* [1991].

modern gulf coastline [*Lewis*, 1994; *Stock et al.*, 1999], making these ideal targets for cross-gulf correlation.

Characteristic lithologic features of the Tuff of San Felipe are dense welding, 3%–15% phenocrysts (anorthoclase $\gg$ Fe-Ti oxides $\approx$ clinopyroxene), rare accidental lithics, and variably abundant distinctive, dark pods of rhyolite with 20% phenocrysts (alkali feldspar $\gg$ Fe-Ti oxides $\approx$ clinopyroxene $>$ fayalite). $^{40}Ar/^{39}Ar$ age determinations suggest that the Tuff of San Felipe is about 12.6 Ma in age [*Stock et al.*, 1999].

The Tmr3 and Tmr4 ignimbrites form a distinctive package of similar extent with parallel changes in thickness and welding grade. Characteristic lithologic features of Tmr3 are partial welding, 5%-10% cm sized, mostly volcanic lithics, and 10%-15% phenocrysts (alkali feldspar $\gg$ magnetite $>$ pyroxene $>$ zircon $\approx$ basaltic hornblende $\approx$ biotite $\approx$ fayalite). $^{40}Ar/^{39}Ar$ age determinations suggest that Tmr3 is about 6.3 Ma in age [*Lewis*, 1996; *Nagy et al.*, 1999]. Tmr4 is a densely welded vitric ash-flow tuff with rare phenocrysts and volcanic lithic inclusions. Tmr4 is undated, but stratigraphic evidence suggests that Tmr3 and Tmr4 together form a single eruptive sequence [*Stock*, 1989; *Lewis*, 1994]. These units are grouped together for correlation (Fig. 4.1).

4.4 Correlation

The likely location of correlative deposits is the coastal region of Sonora and Isla Tiburón. *Gastil and Krummenacher* [1977] identified an extensive cover of volcaniclastic strata here, which they recognized as potentially correlative to the Puertecitos Volcanic Province. Northeastern Baja California and coastal Sonora also share a correlative Tertiary conglomerate [*Gastil et al.*, 1973, Fig. 4.1] and Paleozoic stratigraphic trends [*Gastil et al.*, 1991] supporting $\sim$300 km of separation between these areas.

Our reconnaissance investigations identified ash-flow tuffs lithologically similar to

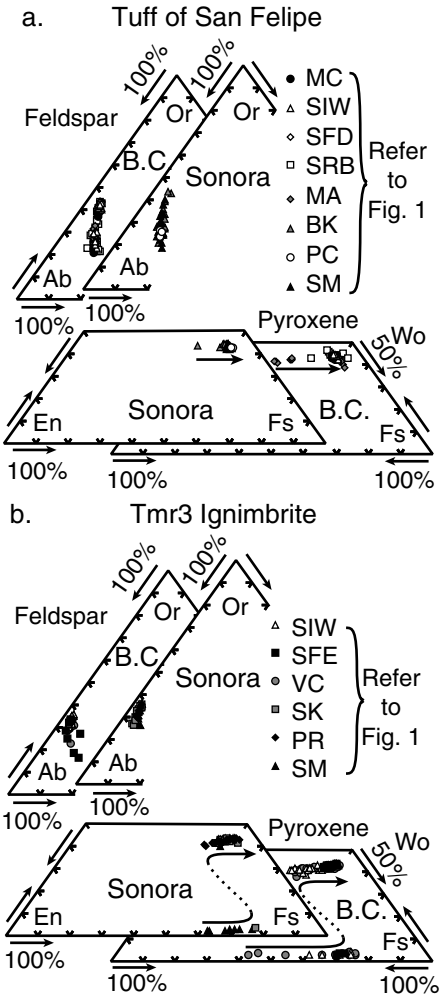

Figure 4.2. Phenocryst compositions from Tuff of San Felipe and Tmr3 ignimbrite. See Figure 4.1 for abbreviations and locations. B.C., Baja California; Ab, albite; Or, orthoclase; En, enstatite; Fs, ferrosilite; Wo, wollastonite. Arrows within pyroxene plots denote zoned phenocryst core to rim compositional trend, dashed across immiscibility gap.

the Tuff of San Felipe, Tmr3, and Tmr4 in coastal Sonora and Isla Tiburón (Fig. 4.1). To confirm correlation, several geochemical tests were applied. Feldspar and pyroxene phenocrysts from the Tuff of San Felipe, Tmr3, and from potential correlative ignimbrites in Sonora were analyzed in thin section by electron microprobe (Fig. 4.2). Both phenocryst composition and zonation are distinctive in these ignimbrites. The phenocrysts of samples from correlated deposits on Isla Tiburón and coastal Sonora are identical to those measured from the Tuff of San Felipe in Baja California (Fig. 4.2, Appendix B). Whole-rock chemical analyses also support correlation (See Table 5.1 in Chapter 5). $^{40}Ar/^{39}$Arage determinations of Sonoran samples are in progress to further validate these correlations.

Paleomagnetic remanence directions also verify the correlation of the tuffs (Fig. 4.3, Table 5.3 in Chapter 5). Remanent magnetic vectors were measured following the procedures outlined in *Stock et al.* [1999]. The Tuff of San Felipe yields a distinctive, low-inclination reversed polarity vector of magnetization [*Stock et al.*, 1999]. Samples of similar tuff from Sonora also yielded low-inclination reversed polarity directions. Tmr3 and Tmr4 from Baja California yield a distinctive pair of moderate-inclination normal polarity vectors. Tmr4 has consistently lower inclination and is counterclockwise to Tmr3. Remanent magnetization of Tmr3 and Tmr4 from Isla Tiburón yield similar vector pairs, supporting correlation of these units.

Thickness and welding grade of the Tuff of San Felipe and the distribution of Tmr3 and Tmr4 are used to match opposite sides of the Gulf of California (Fig. 4.3). The Tuff of San Felipe in Baja California has a semicircular thickness pattern, centered on an area of higher grade, near-vent deposits in the eastern Sierra San Felipe [*Stock et al.*, 1999]. The isopachs of the correlative deposits in Sonora are complex. The thickest deposits and possible intracaldera facies are preserved near the Sonoran coastline. Outcrops on Isla Tiburón fill west-trending paleocanyons, with higher grade deposits present on the northern part of the island. The distribution of Tmr3 and Tmr4 is more uniform and restricted than the Tuff of San Felipe. Thick welded deposits occur in the Sierra Menor on Isla Tiburón and adjacent to an area

covered by younger rhyolitic lava and ignimbrites near the present-day coastline of Baja Califronia ('Covered Area' of Fig. 4.3). Additional deposits of Tmr3 and Tmr4 may exist south of the area of detailed mapping in Baja California.

4.5 Discussion

The identical lithologic, geochemical, and paleomagnetic characteristics of the outcrops in coastal Sonora and Isla Tiburón confirm that these deposits are displaced parts of tuffs known from Baja California. We restore 255±10 km of right slip between Baja California and Sonora, along an azimuth of 310° defined by the Tiburón Fracture Zone and Ballenas Transform (Figs. 4.1 and 4.3). This restoration brings into proximity the correlative ignimbrite outcrops as well as older correlative conglomerates described by *Gastil et al.* [1973]. The map-view restoration (Fig. 4.3) does not account for the effects of additional distributed dextral shear and east-west extension in the study area. The division of slip onto the Ballenas Transform and the Tiburón Fracture Zone (Fig. 4.1) depends upon the restoration of Isla Angel de la Guarda to an uncertain position south of Isla Tiburón [*Lonsdale*, 1989; *Stock*, 2000]. This uncertainty does not affect the summed dextral displacement measured here.

Although a palinspastic reconstruction is beyond the scope of this paper, the map-view restoration defines the strike-slip history in the gulf. Extension in this area during the interval from 12.6 to 6.3 Ma [*Stock and Hodges*, 1989; *Stock et al.*, 1991; *Lewis and Stock*, 1998b; *Nagy*, 2000] was not accompanied by enough dextral shear to significantly displace the Tuff of San Felipe or the older correlative conglomerate of *Gastil et al.* [1973] more than a few tens of kilometers before deposition of Tmr3 and Tmr4. Comparison of the offset of 255±10 km with estimates of plate motion from plate circuit analyses indicates that localization of strike slip into the gulf probably occurred during a short, 1–2 Myr window during late Miocene-early Pliocene time (Table 4.1). This window is largest if the Pacific-North America rate is applied to the gulf. If the spreading rate in the Gulf was 10–15% less than the Pacific-North

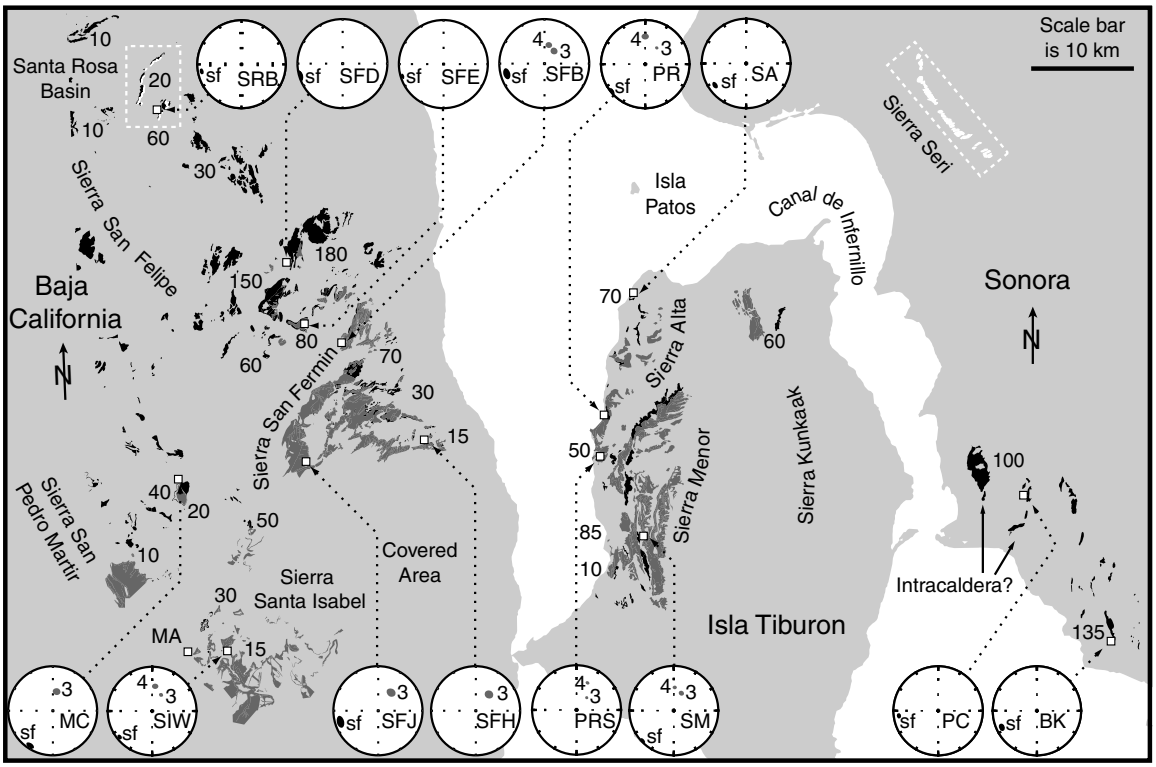

Figure 4.3. Map-view restoration of 255±10 km of transform offset, at azimuth of 310°, across northern Gulf of California. Modern shorelines are shown for reference. Baja California is rotated 2.3° counterclockwise. Correlative, pre-15 Ma conglomerate outcrops (white, surrounded by white-dashed boxes) are from *Gastil and Krummenacher* [1977] and *Bryant* [1986]. Tuff of San Felipe is shown in black, Tmr3 and Tmr4 are shown in gray. See Figure 4.1 for sources of mapping for Baja California. Numbers denote thicknesses in meters of the Tuff of San Felipe. Small white boxes denote sample localities. SFB, SFD, SFE, SFJ, and SFH are localities from Sierra San Fermín; SA, Sierra Alta; PRS, south of Punta Reina. Other abbreviations as in Figure 1. Inclination-declination plots are compilation of primary paleomagnetic remanence directions from Tuff of San Felipe, Tmr3, and Tmr4 from individual localities on both sides of gulf. Data in Baja California are from *Lewis and Stock* [1998a], *Stock et al.* [1999], and *Nagy* [2000]. Shaded ellipses denote area of 95% confidence. Plots are lower hemisphere, equal area projection, with reversed inclination results projected from upper hemisphere. MC is considered unrotated reference locality. All other localities show clockwise vertical-axis rotation.

Table 4.1. Comparison of potential displacement rates across the northern Gulf of California.

Rate[a] (mm/yr)	Time interval[b] (Ma)	Time to 255±10 km[c] (Ma)
Alarcón Rise [*DeMets*, 1995][d]		
47.9±2.1	0–1.03	
41.0±1.9	1.03–3.16[e]	6.1±0.3
Nuvel-1A [*DeMets and Dixon*, 1999][f]		
49.6±0.8	0–3.16[e]	5.1±0.1
Plate Circuit [*Atwater and Stock*, 1998][f]		
∼54	0–5.105	4.7

[a] Rates calculated for a point on the Tiburón Fracture Zone, 28.38°N, 112.5°W.

[b] Interval between magnetic anomalies used to calculate rate.

[c] Time required to accumulate 255 km between Isla Tiburón and the Puertecitos Volcanic Province.

[d] Motion of Baja California relative to North America measured from magnetic anomalies at the Alarcón Rise (Fig. 5.1).

[e] Rate extrapolated to time required to attain displacement of 255 km.

[f] Full Pacific–North America displacement rate.

America rate until 1 Ma [*DeMets*, 1995], then the time to acquire 255±10 km of offset overlaps the age of Tmr3. Significant acceleration of Baja California both at 3.5 Ma and at 1 Ma are incompatible with the total amount of offset recorded since 6.3 Ma.

4.6 Conclusion

The locations of correlative deposits of the 12.6 Ma Tuff of San Felipe, and ca. 6.3 Ma Tmr3 and Tmr4 ignimbrites suggest at least 255±10 km of transform displacement across the northern Gulf of California. These results agree well with models of the San Andreas fault system in southern California that partition significant strike slip into the gulf after 6 Ma [*Crowell*, 1981; *Curray et al.*, 1982; *Matti et al.*, 1992; *Dickinson*, 1996]. Localization of plate boundary slip in the Gulf of California was a rapid transition from extension and minor dextral motion prior to 6.3 Ma, to the principal plate boundary by 4.7 Ma. Transfer of the Baja California peninsula to the Pacific Plate was delayed 6–7 m.y. after microplate capture and initiation of transform faulting west of southern Baja California.

4.7 Acknowledgments

Support was provided by National Science Foundation grants EAR-9614674 and EAR-0001248. We thank R.G. Gastil and C. Lewis for guidance with initial reconnaissance in Sonora, and J. Kirschvink for use of the Caltech Paleomagnetics Laboratory. We also appreciate the support of J. Roldán-Quintana and C. González-León, of the Universidad Nacional Autónoma de México. Permission to enter Isla Tiburón was granted by the Secretaría de Medio Ambiente y Recursos Naturales and the Cumcaác (Seri) Indian Tribe. Prescott College Research Station, Bahia Kino, generously provided logistical support during field studies. We are especially grateful to our Cumcaác guide, Ernesto Molina. S. Dobner, M. Bachman, R. Houston, J. Wise, N. Marks, and L. Perg assisted with field studies. Discussions with G. Axen,

E. Nagy, and C. Lewis, and reviews by J. Vallance and J. Ruiz contributed to the development of this paper. California Institute of Technology, Division of Geological and Planetary Sciences contribution # 8712.

Chapter 5

Miocene to Recent Pacific–North America plate motion and opening of the Upper Delfín basin, northern Gulf of California, Mexico

5.1 Abstract

Correlation of conjugate rifted margins of the Upper Delfín basin constrains the timing of Pacific–North America Plate motion and amount of opening of in the northern Gulf of California. Lithologic, geochemical, paleomagnetic, and geochronologic data from a set of four ignimbrites, consisting of a total of eight distinctive cooling units, are shown to correlate from northeastern Baja California to Isla Tiburón and adjacent areas of western Sonora. These matching ignimbrites are the ∼12.6 Ma Tuff of San Felipe and the 6.1–6.3 Ma Tuffs of Mesa Cuadrada, the Tuffs of Dead Battery Canyon, the Tuffs of Arroyo El Canelo. Offset distributions and facies relationships of these ignimbrites and other strata support 255 ± 10 km of opening between conjugate rifted margins of the Upper Delfín basin. Additional deformation from the continental margins of this basin supports a total of 296 ± 17 km of Pacific–North America Plate motion between coastal Sonora and the Main Gulf Escarpment in Baja California. This measurement is indistinguishable from older conglomerate and basement geologic tie points but requires that at least 276 ± 13 km of displacement has occurred since ∼6 Ma. The restored continental margins of the Upper Delfín supports that only a 15 to 25 km width of upper continental crust has foundered beneath this part of the northern Gulf of California. This result suggests that most of the crust between Isla Tiburón and coastal Sonora is formed of new transitional oceanic crust with a possible contribution from lower continental crust by inflow from the rift flanks. Lower crustal flow was especially likely during initial separation of Baja California from North America prior to arrival of large amounts of sediment from the Colorado River.

5.2 Introduction

The Gulf of California of southwestern North America (Fig. 5.1) presents an exceptional opportunity to examine the formation of a young ocean basin within

an evolving continental orogen. Opening of the Gulf of California is the result of transform motion between the Pacific plate and the North America plate [*Atwater*, 1970]. The tectonic setting of the Gulf of California and southwestern North America is well understood from the perspective of continental geology [*Burchfiel et al.*, 1992; *Stewart*, 1998; *Stock and Hodges*, 1989; *Gastil et al.*, 1991] and from marine plate tectonic studies [*Stock and Molnar*, 1988; *Lonsdale*, 1989; *Atwater and Stock*, 1998]. Opening of the Gulf of California followed the termination of subduction west of Baja California Sur at 12.5 Ma [*Mammerickx and Klitgord*, 1982; *Spencer and Normark*, 1979]. Seafloor spreading at the mouth of the Gulf of California records more than 85% of Pacific-North America plate motion since 3.5 Ma and over 95% of the plate motion since 1 Ma [*DeMets*, 1995; *DeMets and Dixon*, 1999; *Dixon et al.*, 2000].

Continental geologic records define the tectonic history of the Gulf of California prior to 3.5 Ma. Offset basement relationships and Tertiary conglomerates indicate that approximately 300 km of dextral displacement has occurred in the Gulf of California [*Gastil et al.*, 1991, 1973, and Fig. 5.2]. Geologic relationships in southern California indicate that most or all of this displacement occurred after 12.5 Ma [*Crowell*, 1981; *Dickinson*, 1996]. Correlation of syn-rift pyroclastic deposits from the Puertecitos Volcanic Province of Baja California to Isla Tiburón and coastal Sonora supports 255 $\pm$ 10 km of opening of the Upper Delfín basin of the northern Gulf of California. These results suggest that the Pacific–North America plate boundary localized in the Gulf of California during latest Miocene time.

With adequate geologic control, fundamental tectonic problems such as the role of pre-existing weaknesses and strain partitioning in localizing continental rifting may be addressed from the geology of the Gulf of California. Critical geologic parameters from the Gulf of California are the rate of transfer of Baja California to the Pacific plate and the amount of crustal attenuation that accompanied this transfer. Until recently, no record existed that directly measured total offset, offset rate, and crustal attenuation in the Gulf of California.

This paper expands on the initial findings reported by *Oskin et al.* [2001] to docu-

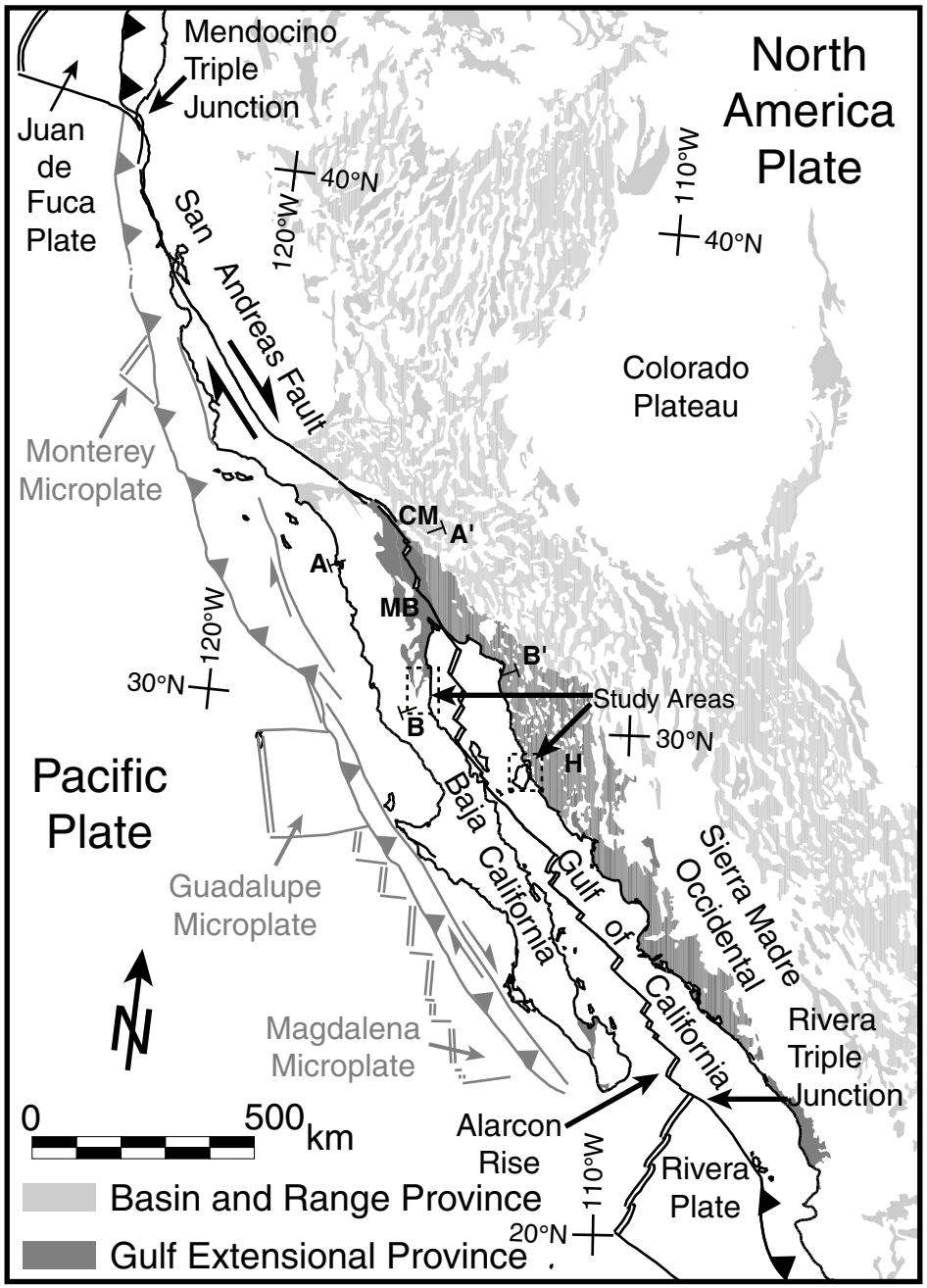

Figure 5.1. Tectonic map of southwestern North America. Derived from the Tectonic Map of North America [*Muehlberger et al.*, 1996]. Shaded areas represent basins of the Basin and Range province (light grey) and the Gulf Extensional Province (dark grey) . Present-day plates and plate boundaries shown as dark lines. Inactive microplates and plate boundaries shown as grey lines. A-A' and B-B' are locations of cross sections on Fig. 5.23. CM, Chocolate Mountains; MB, Monte Blanco Dome [*Axen et al.*, 2000]; H, Hermosillo.

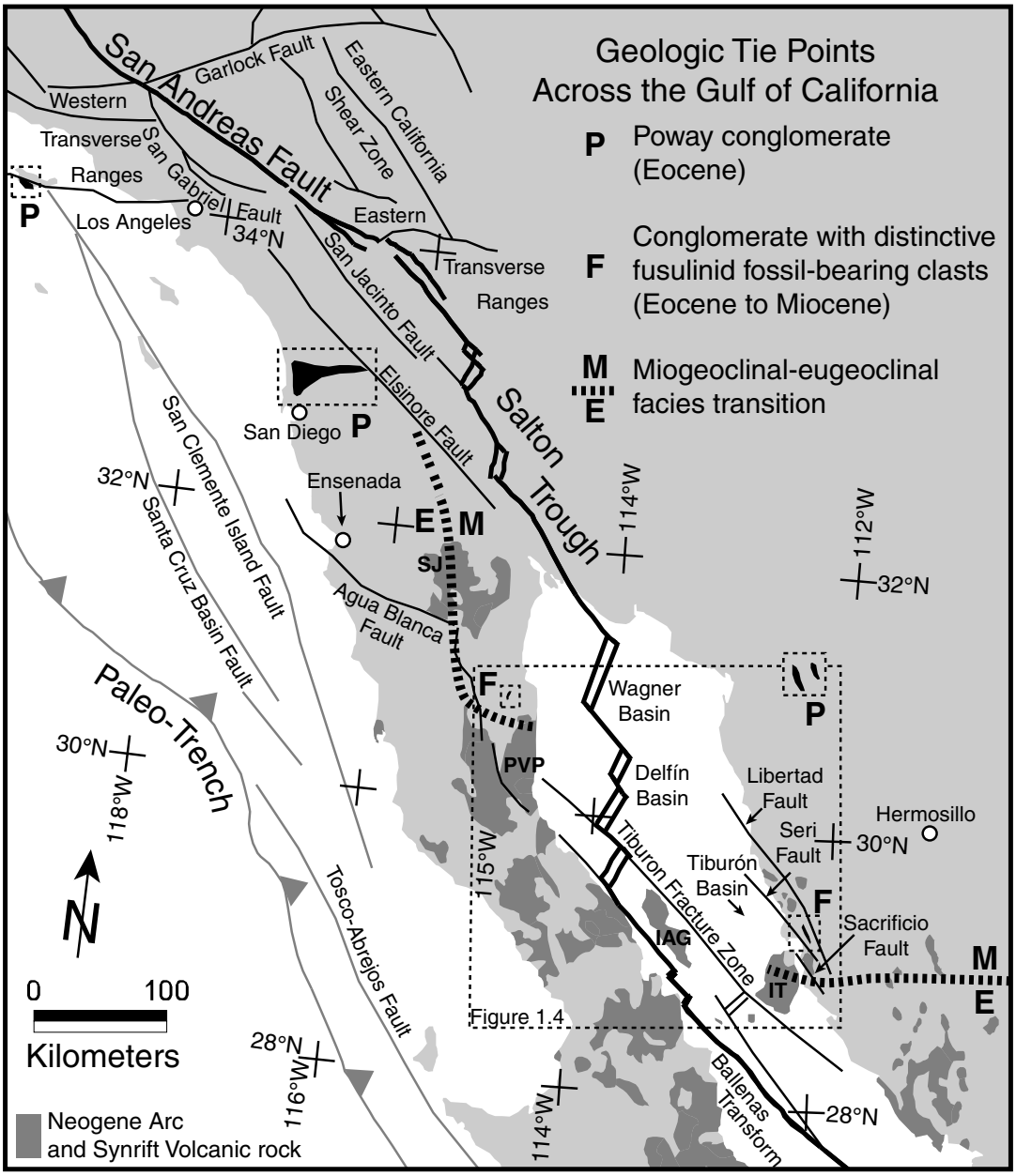

Figure 5.2. Tectonic elements of southern California and the northern Gulf of California. Faults and areas of Neogene arc and syn-rift volcanic rock from [*Muehlberger et al.*, 1996]. Present-day plate boundary shown as a heavy black line. Other faults of the plate-boundary zone shown as thin black lines. Grey fault lines show older plate boundaries along the Pacific coast of Baja California and southern California. Black patches indicate outcrops of distinctive conglomerates that correlate across the northern Gulf of California. Poway conglomerate outcrops (P) from *Abbott and Smith* [1989]. Conglomerate with distinctive fusulinid clasts (F) from *Gastil and Krummenacher* [1976] and *Bryant* [1986]. Miogeoclinal-eugeoclinal facies transition in pre-batholithic rocks (M:E) from *Gastil et al.* [1991]. SJ, Sierra Juárez; PVP, Puertecitos Volcanic Province; IAG, Isla Angel de La Guarda; IT, Isla Tiburón.

ment a complete record of dextral Pacific–North America plate motion in the northern Gulf of California and its surrounding rifted continental margin. A set of four ignimbrites consisting of a total of eight distinctive cooling units are shown to correlate from northeastern Baja California to Isla Tiburón and coastal Sonora. Each of these ignimbrites displays a unique matching distribution in northeastern Baja California and Isla Tiburón. Offset distributions and facies relationships of these ignimbrites and other strata support 255 ± 10 km of the Upper Delfín basin of the northern Gulf of California, as proposed earlier by *Oskin et al.* [2001]. The uncertainty of this geologic tie point is supported by alternative reconstructions. New geologic mapping presented here suggests that an additional 20 ± 10 km of dextral displacement occurred in coastal Sonora sometime after 12.6 Ma. Together with earlier studies of rotational deformation of the continental margin of Baja California by *Lewis and Stock* [1998a], the total opening measured in the northern Gulf of California of 296 ± 17 km is indistinguishable from older conglomerate and basement geologic tie points. Restoration of the conjugate rifted margins of the Upper Delfín basin also constrains the amount of foundered upper continental crust that may underlie this segment of the Gulf of California. This slip history and crustal budget comprise important constraints for the tectonic evolution of southwestern North America and the mechanisms of continental rifting in the northern Gulf of California.

5.3 Geology of northeastern Baja California, Isla Tiburón, and coastal Sonora

5.3.1 Study areas

The geology of conjugate rifted margins of the northern Gulf of California presents several possibilities for precise temporal constraints on the development of the Gulf rift. Existing correlations of basement geology and Tertiary conglomerate deposits indicate ∼300 km total displacement for this area [*Gastil et al.*, 1973; *Silver and*

Chappell, 1988; *Gastil et al.*, 1991, and Fig. 5.2]. Pre- and syn-rift volcanic deposits of the Puertecitos Volcanic Province (PVP) of northern Baja California comprise a well-dated Mid-Miocene to Late Pliocene stratigraphy adjacent to the Gulf of California [*Stock*, 1989; *Stock et al.*, 1991; *Martín-Barajas and Stock*, 1993; *Martín-Barajas et al.*, 1995; *Lewis*, 1996; *Nagy et al.*, 1999, and Fig. 5.3]. Contained within these strata are extensive ignimbrite sequences deposited at 12.6 Ma, ∼6 Ma, and ∼3. Detailed mapping in the northern PVP indicates sources for these deposits near the present-day western shore of the Gulf of California [*Stock et al.*, 1991; *Martín-Barajas et al.*, 1995; *Lewis*, 1994; *Nagy*, 1997]. These widespread ignimbrites, with eastern sources, comprise ideal candidates for cross-gulf correlation [*Stock et al.*, 1999; *Nagy et al.*, 1999]. A likely target for correlation is the coastal area of central Sonora, located ∼300 km southeast of the Puertecitos area. Reconnaissance mapping of coastal Sonora indicates a similar, extensive Mid- to Late-Miocene volcanic cover adjacent to the eastern shoreline of the Gulf of California [*Gastil and Krummenacher*, 1976].

5.3.2 Stratigraphic framework

To simplify description of the geology of conjugate margins of the northern Gulf of California, the regional stratigraphy is divided into six groups. These groups encompass six partially interfingering stratigraphic-tectonic packages corresponding to time periods prior to and during Gulf rifting (Fig. 5.4). This stratigraphic framework is based on previous groupings used by *Nagy et al.* [1999].

Lithologic groups one, two, and three contain strata from intervals prior to Neogene rifting in the Gulf of California region. Group one encompasses the basement rocks, which are dominantly plutons of the Peninsular Ranges Batholith with lesser amounts of host metamorphosed sedimentary rocks [*Gastil et al.*, 1975; *Silver and Chappell*, 1988; *Gastil et al.*, 1991]. Group two rocks nonconformably overlie the basement as a thin, discontinuous veneer of Eocene through Mid-Miocene fluvial, lacustrine, and aeolian sedimentary rock. These deposits grade upward and laterally into lava flows, intrusions, and volcaniclastic rocks of the Middle Miocene volcanic

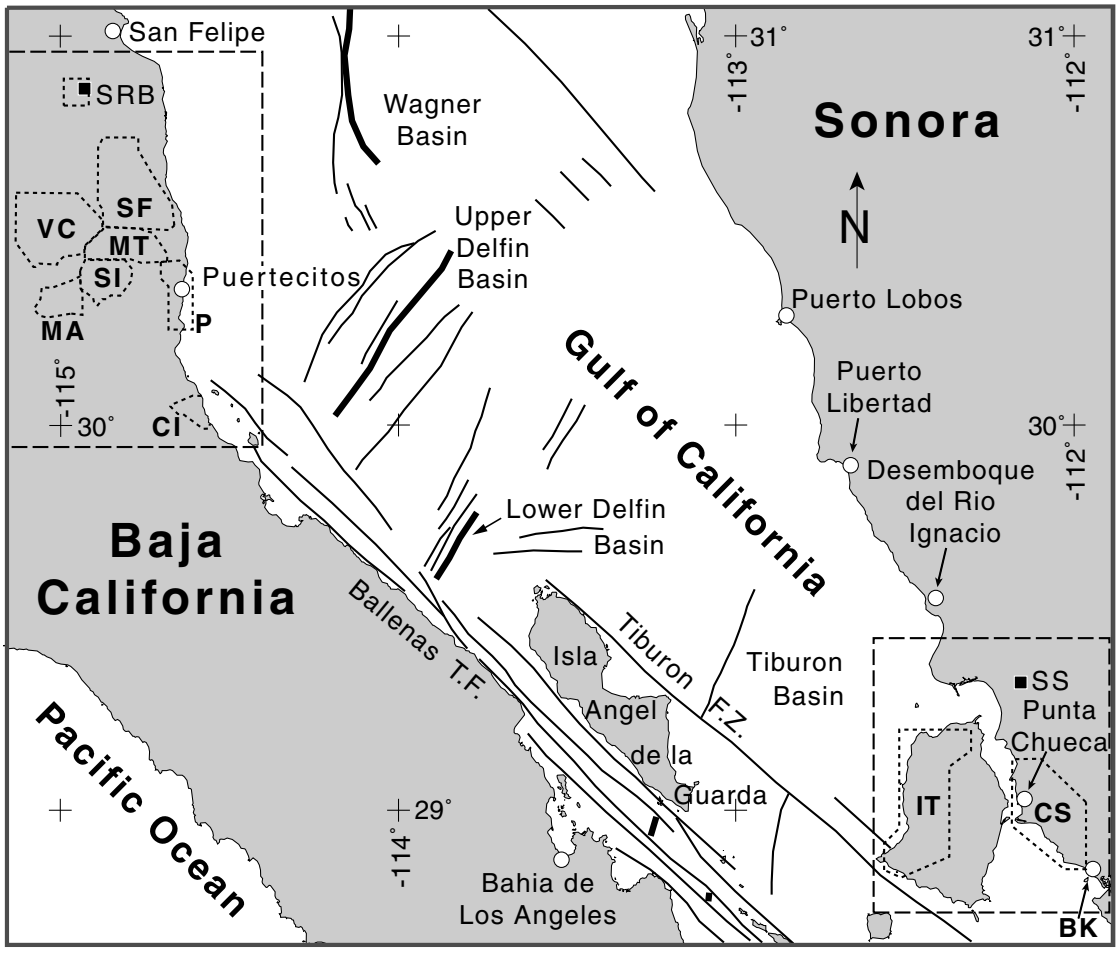

Figure 5.3. Index map of the northern Gulf of California. Marine faults from *Fenby and Gastil* [1991]. Areas of reconnaissance mapping for this study shown by large dashed boxes. Areas of detailed mapping shown by smaller dashed lines. SRB, Santa Rosa Basin [*Bryant*, 1986]; SF, Sierra San Fermín [*Lewis*, 1994]; VC, Valle Chico [*Stock*, 1993]; MT, Arroyo Matomí Transect (*Stock et al.* [1991] and unpublished mapping); SI, Santa Isabel Wash [*Nagy*, 1997]; Puertecitos [*Martín-Barajas and Stock*, 1993]; MA, Mesa El Avión [*Stock, unpublished mapping*]; CI, Cinco Islas (Chapter 7 and Plate IV); CS, Coastal Sonora (Chapter 3 and Plate I); IT, Isla Tiburón (Chapter 3 and Plate II); BK, Bahía Kino.

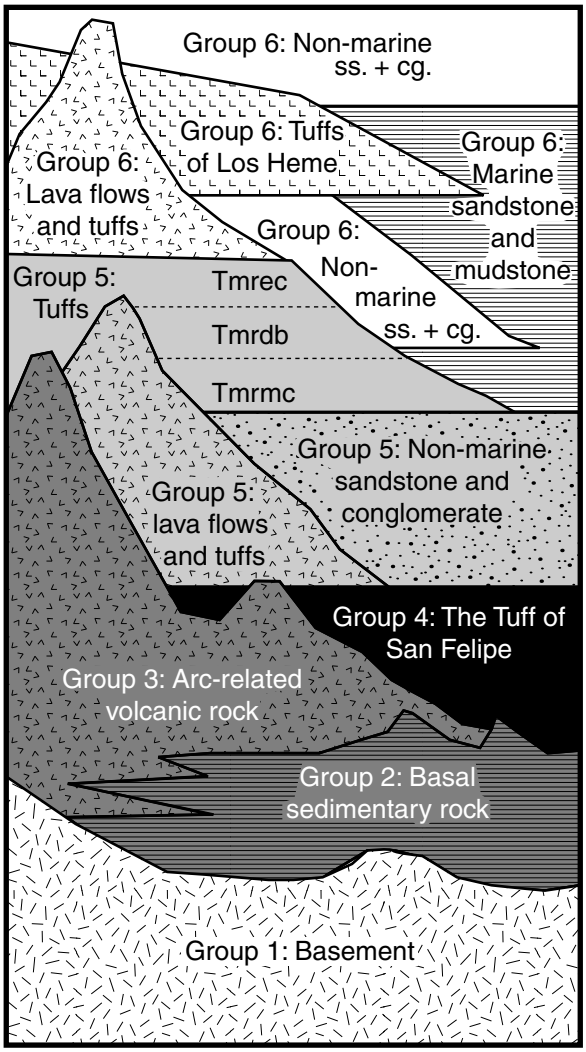

Figure 5.4. Schematic stratigraphic column of northeastern Baja California, Isla Tiburón and coastal Sonora. See text for discussion of stratigraphic groups depicted here. Group 5 tuffs are collectively named the Tuffs of the Northern Puertecitos Volcanic Province. Three ignimbrites of the Tuffs of the Northern Puertecitos Volcanic Province are shown divided by dashed lines. Tmrmc, Tuffs of Mesa Cuadrada; Tmrdb, Tuffs of Dead Battery Canyon; Tmrec, Tuffs of Arroyo El Canelo.

arc that comprise group three [*Dorsey and Burns*, 1994].

Lithologic group four contains only the Tuff of San Felipe, a ∼12.6 Ma ignimbrite of regional extent in northeastern Baja California [*Stock et al.*, 1999]. This distinctive ignimbrite is allotted a separate group because of its stratigraphic position marking the transition from the Mid to Late Miocene volcanic arc to rifting, volcanism, and sedimentation related to formation of the Gulf Extensional Province [*Stock*, 1993; *Lewis*, 1994; *Nagy*, 1997; *Stock et al.*, 1999]. The Tuff of San Felipe is correlated to Isla Tiburón and coastal Sonora by *Oskin et al.* [2001].

Lithologic group five is an assemblage of volcanic, volcaniclastic, and fluvial rocks deposited synchronously with rifting in the Gulf of California Extensional Province. This group is capped by an extensive series of 6-7 Ma ignimbrites that form much of the volcanic cover of the northern Puertecitos Volcanic Province [*Stock*, 1989; *Stock et al.*, 1991; *Stock*, 1993; *Martín-Barajas and Stock*, 1993; *Lewis*, 1996; *Nagy et al.*, 1999]. Three separate sets of group five ignimbrites are recognized both in Baja California and Isla Tiburón. The lowest of these are the Tuffs of Mesa Cuadrada (new name). This unit is comprised of the Tmr3 and Tmr4 ignimbrites which *Oskin et al.* [2001] correlated to Isla Tiburón. The Tuffs of Dead Battery Canyon [*Lewis*, 1996] overlie the Tuffs of Mesa Cuadrada. Two cooling units (Tmr5 and Tmr6) of this tuff are present in Baja California; one of these (Tmr5) is also recognized on Isla Tiburón. The Tuffs of Dead Battery Canyon may be the uppermost deposits from the same eruptions that produced the Tuffs of Mesa Cuadrada [*Lewis*, 1994]. The Tuffs of Arroyo El Canelo [*Stock et al.*, 1991; *Martín-Barajas and Stock*, 1993] cap the group five section (Fig. 5.4). Four distinctive cooling units of the Tuffs of Arroyo El Canelo are recognized in both Baja California and Isla Tiburón. Together, the Tuffs of Mesa Cuadrada, the Tuffs of Dead Battery Canyon, and the Tuffs of Arroyo El Canelo comprise the Tuffs of the Northern Puertecitos Volcanic province (new name).

Group six contains a younger volcanic and fluvial assemblage similar to group five, and also includes marine deposits of the Gulf of California [*Lewis*, 1996; *Stock et al.*, 1991; *Martín-Barajas et al.*, 1997]. The 2.7 Ma to 3.5 Ma Tuffs of Los Heme form

a Late Pliocene composite ignimbrite sheet that covers the southwestern Puertecitos Volcanic Province [*Martín-Barajas et al.*, 1995]. Geologic mapping in Sonora and Isla Tiburón did not correlate these or other group six strata across the Gulf of California.

5.3.3 Geologic mapping

Baja California

Much of the geology of northeastern Baja California is known only in reconnaissance (Figs. 5.3 and 5.5). *Gastil et al.* [1975] first published a reconnaissance geologic map of the state of Baja California Norte and described Tertiary sedimentary and volcanic strata of the study area. Since this work, several detailed studies of northeastern Baja California have significantly refined the stratigraphic and tectonic knowledge of the study region [*Bryant*, 1986; *Stock et al.*, 1991; *Stock*, 1993; *Martín-Barajas and Stock*, 1993; *Lewis*, 1994; *Nagy*, 1997]. New reconnaissance-scale field investigations and inspection of Landsat imagery link together these areas of detailed work into a new reconnaissance geologic map (Fig. 5.5).

The limits of the northeastern Baja California study area (Fig. 5.5) were selected by multiple criteria. The eastern boundary of the study area is the shoreline of the Gulf of California. The northern boundary of the study area corresponds approximately with latitude 31°00′, which is sufficient to enclose the northern extent of the ignimbrite deposits of interest. The western extent of the study area encompasses the Main Gulf escarpment fault system, which separates the stable interior of Baja

Figure 5.5. (next page) Geologic map of northeastern Baja California. See text for discussion of stratigraphic groups depicted here. Stratigraphic relationships of these groups are shown in Fig. 5.4. Geology based on detailed mapping of areas shown on Fig. 5.3 and *Gastil et al.* [1975], field reconnaissance in the Sierra San Felipe, and interpretation of a Landsat image (path 38 row 39) and aerial photography of the Puertecitos Volcanic Province. Asterisks mark locations of group 6 (late syn-rift) andesitic volcanoes: B, Unnamed Quaternary basaltic andesite of Santa Isabel Wash; F, Pico San Fermín; G, Pico de Los Gemelos; H, Pico Los Heme; P, Volcán Prieto. Other locations: S.I. and SIW, Santa Isabel Wash; MA, Mesa El Avión; Oc., Arroyo El Oculto.

Figure 5.5.

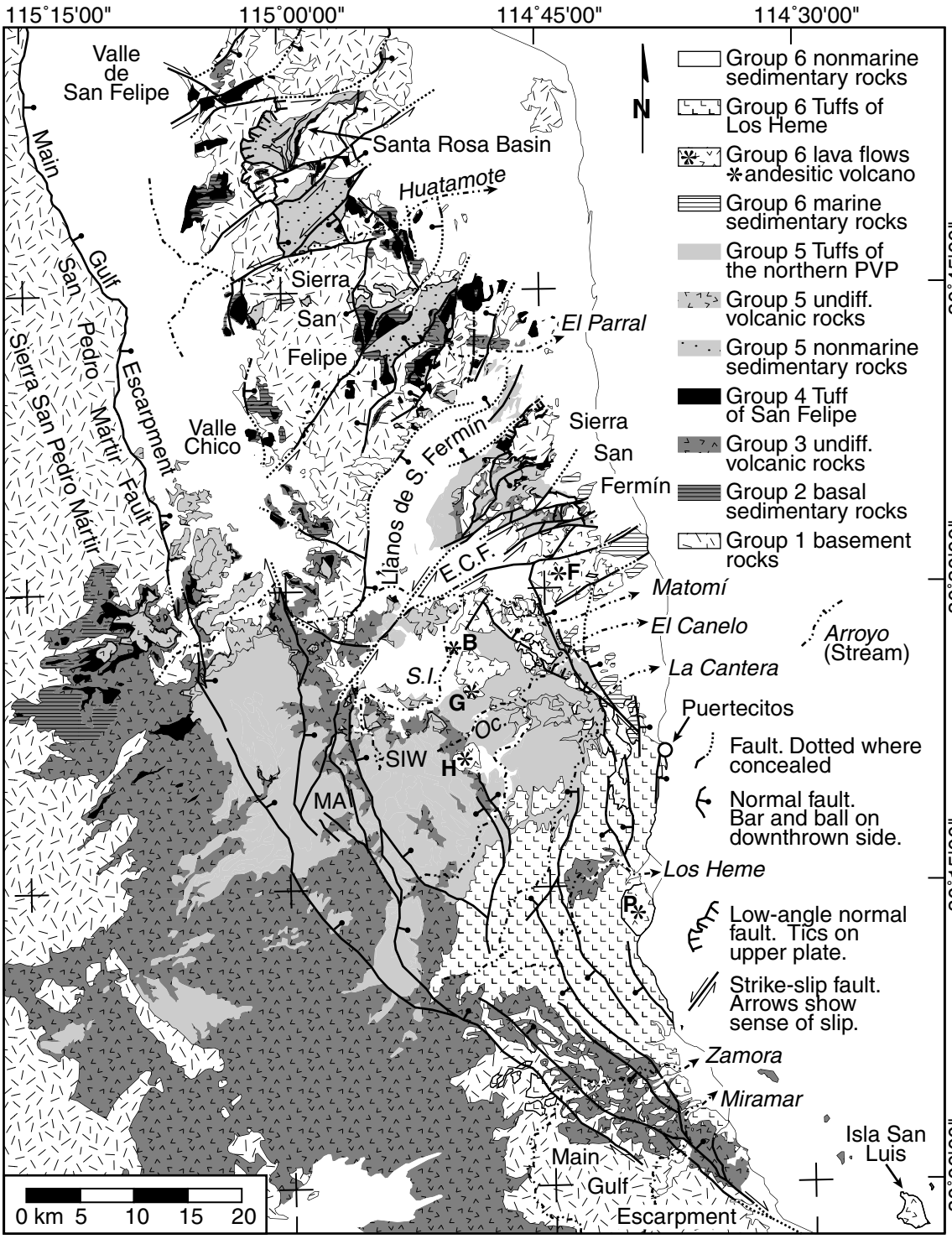
115°15'00"
115°00'00"
114°45'00"
114°30'00"
30°45'00"
30°30'00"
30°15'00"
30°00'00"
N
Valle de San Felipe
Santa Rosa Basin
Huatamote
Main Gulf Escarpment
San Pedro Mártir Fault
Sierra San Pedro Mártir
Sierra San Felipe
El Parral
Valle Chico
Llanos de S. Fermín
Sierra San Fermín
E.C.F.
F
Matomí
El Canelo
B
S.I.
La Cantera
G
Puertecitos
Oc.
SIW
H
MA
Los Heme
P
Zamora
Miramar
Isla San Luis
Main Gulf Escarpment
0 km 5 10 15 20
Group 6 nonmarine sedimentary rocks
Group 6 Tuffs of Los Heme
Group 6 lava flows
andesitic volcano
Group 6 marine sedimentary rocks
Group 5 Tuffs of the northern PVP
Group 5 undiff. volcanic rocks
Group 5 nonmarine sedimentary rocks
Group 4 Tuff of San Felipe
Group 3 undiff. volcanic rocks
Group 2 basal sedimentary rocks
Group 1 basement rocks
Arroyo (Stream)
Fault. Dotted where concealed
Normal fault. Bar and ball on downthrown side.
Low-angle normal fault. Tics on upper plate.
Strike-slip fault. Arrows show sense of slip.

California from the Gulf Extensional Province [*Gastil et al.*, 1975]. The southern boundary of the study area encloses the Puertecitos Volcanic Province. Much of the interior of the Puertecitos Volcanic Province is mapped in reconnaissance only (Fig. 5.3). In this region, nearly flat-lying strata complicate reconnaissance mapping because many important stratigraphic relationships are difficult to resolve on steep canyon walls using overhead imagery. Additional detailed fieldwork is required here to completely document the geology of this area. Fortunately, detailed studies of the northern Puertecitos Volcanic Province constrain the important volcanic deposits and structural relationships necessary for correlation across the northern Gulf of California.

Isla Tiburón and coastal Sonora

Reconnaissance geologic investigations conducted over the central-western coastline of Sonora, Mexico, sought to identify matching ignimbrite units to the Puertecitos Volcanic Province and the Sierra San Felipe of Baja California. Accessible outcrops of ash-flow tuffs mapped by *Gastil and Krummenacher* [1976] were assessed for litholigic similarity to the distinctive tuffs mapped in northeastern Baja California (Fig. 5.5). Potentially correlative outcrops of the Tuff of San Felipe and the Tuffs of the northern Puertecitos Volcanic Province were located on Isla Tiburón and adjacent areas of coastal Sonora (Fig. 5.6). On the western side of Isla Tiburón, a 300 m thick section of ash-flow tuffs contains correlatives to the Tuff of San Felipe overlain by correlatives to the Tuffs of the northern Puertecitos Volcanic Province. Inspection of Landsat Thematic Mapper Imagery of Isla Tiburón revealed that the potentially correlative section here is present in the Sierra Menor and Sierra Alta on the western half of the island. Additional isolated outcrops are present in the Sierra Kunkaak on the northeastern part of the island (Fig. 5.6).

Detailed geologic mapping of Isla Tiburón concentrated on the western coast of the island (Figs. 5.3 and 5.6). This area presented a well-exposed north-south transect of volcanic strata to match with the conjugate rifted margin in Baja California. Inte-

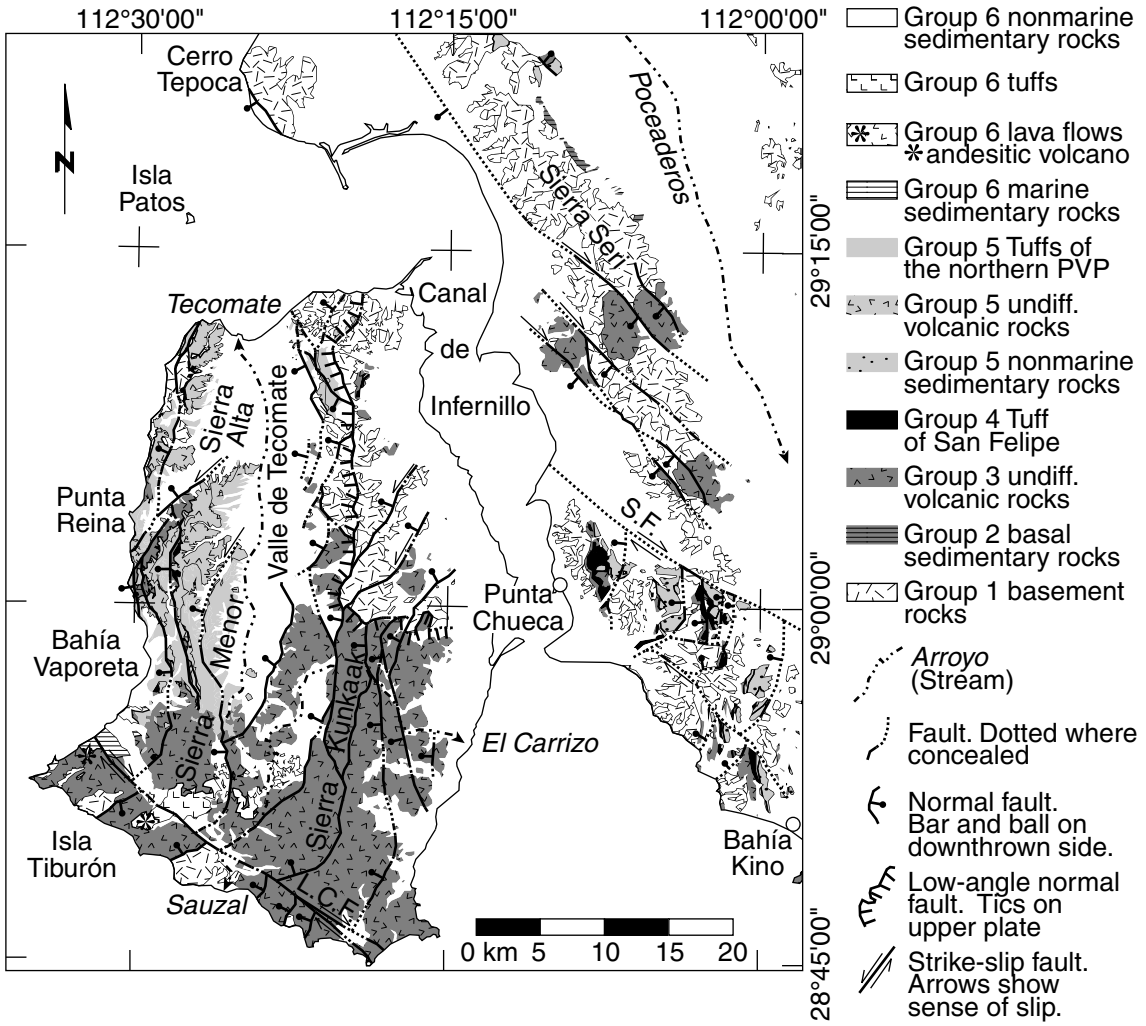

Figure 5.6. Geologic map of coastal Sonora and Isla Tiburón. Mapping generalized from detailed mapping on western Isla Tiburón and coastal Sonora, *Gastil and Krummenacher* [1976], and *Gastil et al.* [1999] with additional field reconnaissance. See text for discussion of the lithologic groups presented here. Stratigraphic relationships of groups 1–6 shown in Fig. 5.4. Georeferenced aerial photographs and a Landsat Thematic Mapper image (path 36, row 40) were used as base maps.

rior areas of the southern and northeastern parts of the island were explored in order to assess important stratigraphic features identified by initial reconnaissance studies. Areas bordering the interior valley of the island (Valle Tecomate) were mapped primarily by air-photo and Landsat image interpretation. Fortunately, stratigraphic and structural complexity appear most commonly near the western coastline of Isla Tiburón while much of the interior area of the Sierra Menor and Sierra Alta consists of structurally simple, well-exposed block faulted ridges.

5.4 Correlation of ash-flow tuffs

Preliminary correlations of ash-flow tuffs were established by lithology and later verified by petrographic examination of phenocryst, glass, pumice, and lithic content. Further geochemical and paleomagnetic tests were applied to the most widespread and stratigraphically simple ignimbrites common to northeastern Baja California and western Sonora [*Oskin et al.*, 2001]. These simple cooling units are the Tuff of San Felipe and Tmr3 and Tmr4 from the Tuffs of Mesa Cuadrada. The Tuffs of Dead Battery Canyon were also analyzed paleomagnetically at two localities in Baja California and one locality on Isla Tiburón (Locations SFI and SFJ, Fig. 5.7; Location PRS, Fig. 5.8). Due to several complexities, the Tuffs of Arroyo El Canelo were avoided for geochemical and paleomagnetic analyses. *Nagy* [1997] reported difficulty recovering core samples and demagnetization paths for the Tuffs of Arroyo El Canelo. Complex and incompletely understood cooling unit stratigraphy for the Tuffs of Arroyo El Canelo in Baja California also complicates interpretation of geochemical data for this unit [*Stock et al.*, 1991; *Martín-Barajas and Stock*, 1993; *Nagy*, 1997]. However, it does appear that much of the zonation of the Tuff of El Canelo is consistent between the Sierra Santa Isabel of Baja California and western Isla Tiburón. Future geochemical tests should reinforce existing lithologic and stratigraphic correlation of this unit.

Figure 5.7. (next page) Measured section and geochemical, paleomagnetic, and geochronology sample localities in northeastern Baja California. Measured section locations (see Fig. 5.9) indicated by circles: AO, Arroyo El Oculto [*Nagy*, 1997]; DBC, Dead Battery Canyon [*Lewis*, 1994]; EC, El Coloradito [*Lewis*, 1994]; LC, Arroyo La Cantera [*Martín-Barajas et al.*, 1995]; MC, Mesa Cuadrada [*Stock*, 1989]; MM, Mesa Matomí [*Stock*, 1989]; SIW, Santa Isabel Wash [*Nagy*, 1997]. Geochemical, paleomagnetic, and geochronology sample localities indicated by asterisks:. MA, Mesa El Avión; MC, Mesa Cuadrada; SFB–SFN, Sierra San Fermín; SIW, Santa Isabel Wash; SRB, Santa Rosa basin; VC, Valle Chico.

5.4.1 Lithology

The Tuff of San Felipe

The Tuff of San Felipe (Fig. 5.9) may be recognized in the field by several characteristic lithologic features [*Stock et al.*, 1999; *Oskin et al.*, 2001]. The tuff is everywhere densely welded, with 10–15% anorthoclase phenocrysts, <1% augite phenocrysts, rare accidental lithics, and distinctive, rare to uncommon dark inclusions of rhyolite. These inclusions contain 20% phenocrysts (alkali feldspar $\gg$ clinopyroxene > fayalite) and form pods up to 40 cm in length. Typical outcrops of the tuff develop a dark brown to black vitrophyre at the base, grading into densely welded, red to orange eutaxitically foliated tuff. In the thicker deposits, the vitrophyre grades into densely welded, red to light purple rheomorphic tuff with lithophysae up to 50 cm long. The remaining thickness of tuff is generally light-colored and vapor-phase recrystallized. Non-welded airfall ash up to 1 m thick may be present beneath thicker sections of the Tuff of San Felipe.

The Tuffs of Mesa Cuadrada

The Tuffs of Mesa Cuadrada (Fig. 5.9) comprise two distinctive cooling units, Tmr3 and Tmr4 [*Stock*, 1989; *Lewis*, 1996; *Nagy et al.*, 1999]. Parallel changes in thickness and welding grade, and the absence of intervening erosion supports grouping of these units into a single eruptive sequence [*Lewis*, 1994]. Tmr3 is a non-welded to partially-welded ash-flow tuff characterized by 5–10% cm-sized volcanic lithic frag-

Figure 5.7.

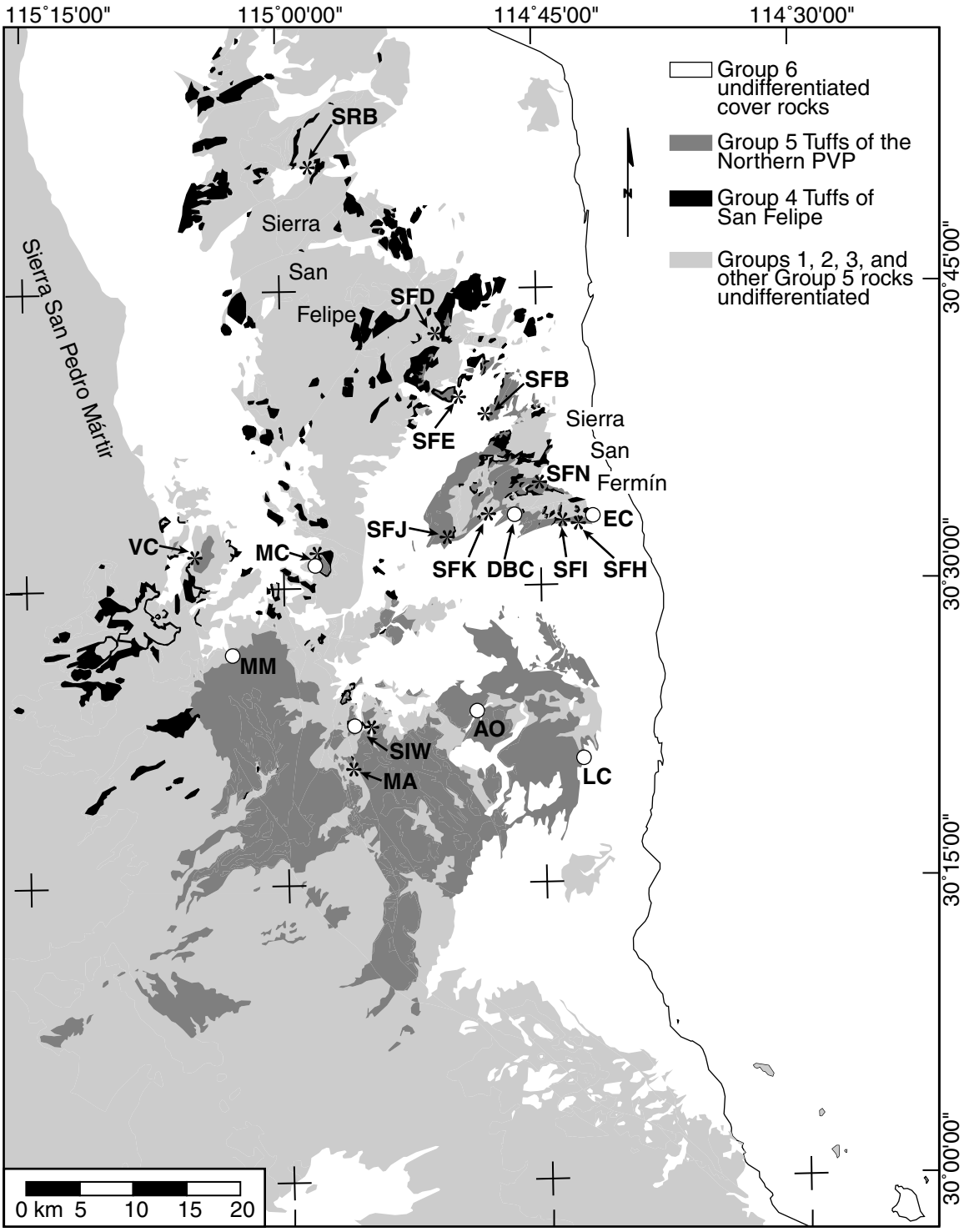
115°15'00"
115°00'00"
114°45'00"
114°30'00"
30°45'00"
30°30'00"
30°15'00"
30°00'00"
Group 6 undifferentiated cover rocks
Group 5 Tuffs of the Northern PVP
Group 4 Tuffs of San Felipe
Groups 1, 2, 3, and other Group 5 rocks undifferentiated
Sierra San Pedro Mártir
Sierra San Felipe
Sierra San Fermín
SRB
SFD
SFB
SFE
SFN
SFJ
SFK
DBC
SFI
SFH
EC
VC
MC
MM
AO
SIW
MA
LC
0 km 5 10 15 20

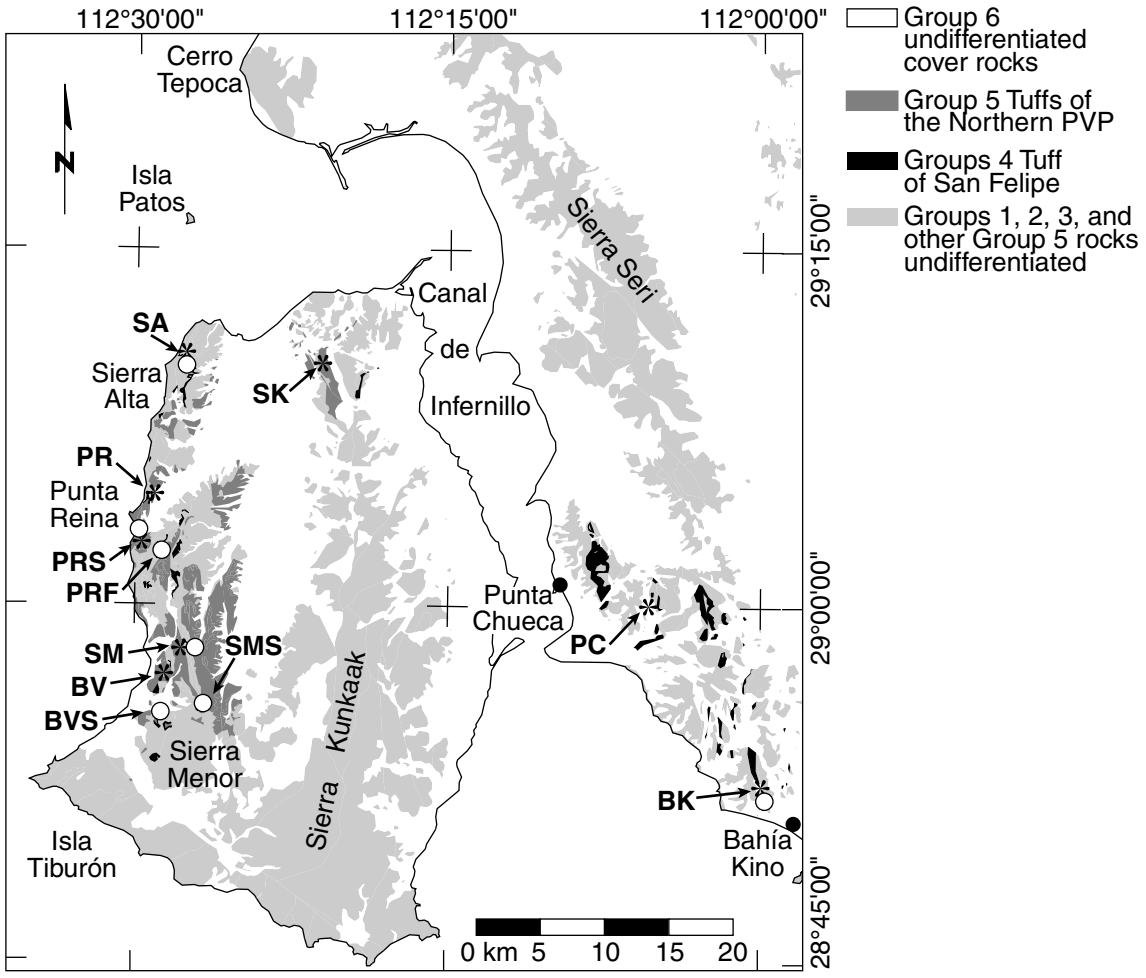

Figure 5.8. Measured section and geochemical, paleomagnetic, and geochronology sample localities in coastal Sonora and Isla Tiburón. Measured section locations (see Fig. 5.9 and Appendix A) indicated by circles. Geochemical, paleomagnetic and geochronology sample localities indicated by asterisks. BK, Bahía Kino; BV, Bahía Vaporeta; BVS, Bahía Vaporeta South; PC, Punta Chueca; PR, Punta Reina; PRF, Punta Reina Footwall; PRS, Punta Reina South; SA, Sierra Alta; SM, Sierra Menor; SMS, Sierra Menor South.

ments and 10–15% phenocrysts (alkali-feldspar ≫ augite ≈ quartz > biotite ≈ Fe–Ti oxides > basaltic hornblende ≈ fayalite ≈ zircon). Matrix material of Tmr3 is dominantly glass shards with up to 10% pumice lapilli. Typical deposits of Tmr3 weather orange, with a light grayish purple fresh surface. Progressively more welded sections appear bright orange to red, with a dark-brown indurated vitrophyre near the base. Tmr4 is a densely welded ash-flow tuff characterized by distinctive welding zonation, 1–3% phenocrysts (plagioclase > pyroxene > quartz) and 1% volcanic lithic fragments. Glass spicules dominate the matrix material, lending the tuff an even porcelainous texture. Basal Tmr4 commonly includes a thin (<1 m) layer of yellow ash and pumice, grading upwards into brown to black vitrophyre with pumice fiamme. A sharp break separates the black vitrophyre from a zone of dense welded red tuff. This is capped by vapor-phase altered light purple welded tuff. Thicker sections of Tmr4 are capped by an additional zone of non-welded tuff.

The Tuffs of Dead Battery Canyon

The Tuffs of Dead Battery Canyon form two nearly identical cooling units, Tmr5 and Tmr6 (Fig. 5.9). The following descriptions are from *Lewis* [1994] and *Lewis* [1996]. Cooling unit Tmr5 is characterized by ∼3% cm-sized pumice and 5–10% phenocrysts (feldspar ≫ Fe–Ti oxides > clinopyroxene). Tmr5 is comprised of a base of indurated, dark reddish-brown porcelainous welded tuff, capped by light purple vapor-phase altered tuff. Tmr6 contains 10–15% phenocrysts (feldspar ≫ Fe-Ti oxides > clinopyroxene ≈ basaltic hornblende) and up to 10% flattened pumice. *Lewis* [1994]

Figure 5.9. (next page) Stratigraphic columns of the Tuff of San Felipe and the Tuffs of the Northern Puertecitos Volcanic Province. See Figs. 5.7 and 5.8 for section locations. Grey bands denote grouping and correlation of ash-flow tuffs. Ash (small filled circles), pumice (ellipses and lenses) and lithic fragments (angular filled blocks) schematically represent the relative concentration of these components in each unit. Welding grade indicated by flattened pumice and a greater concentration of ash and lithic fragments. Measured sections in Baja California are from the references shown beneath each column. Measured section from Isla Tiburón is a composite of Punta Reina localities PRS and PRF located on Fig. 5.8 and described in Appendix A.

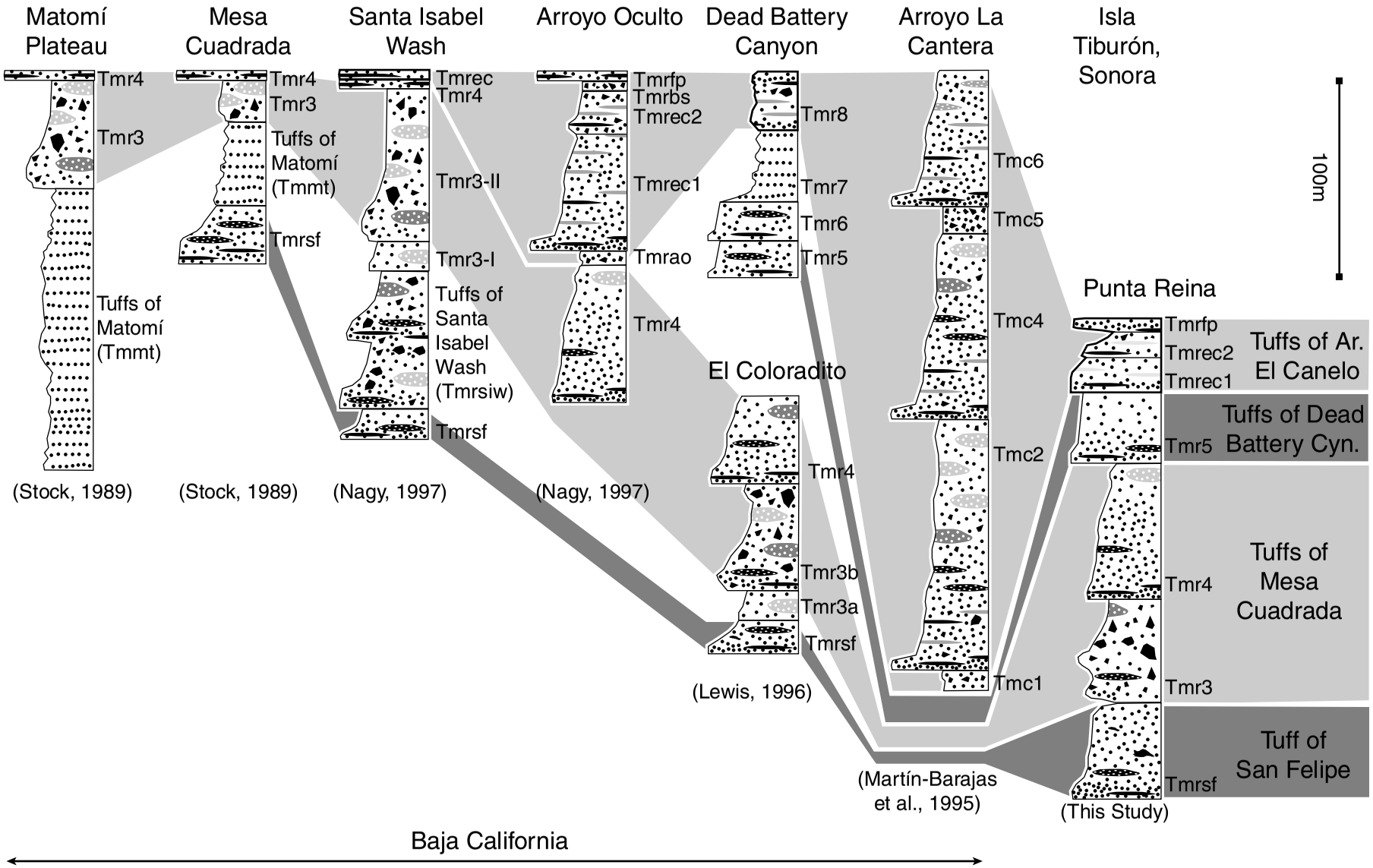
Matomí Plateau
Mesa Cuadrada
Santa Isabel Wash
Arroyo Oculto
Dead Battery Canyon
Arroyo La Cantera
Isla Tiburón, Sonora
Punta Reina
Tmr4
Tmr3
Tuffs of Matomí (Tmmt)
Tmrsf
Tmrec
Tmr3-II
Tmr3-I
Tuffs of Santa Isabel Wash (Tmrsiw)
Tmrfp
Tmrbs
Tmrec2
Tmrec1
Tmrao
Tmr8
Tmr7
Tmr6
Tmr5
El Coloradito
Tmr3b
Tmr3a
Tmc6
Tmc5
Tmc4
Tmc2
Tmc1
Tmrec2
Tmrec1
Tuffs of Ar. El Canelo
Tuffs of Dead Battery Cyn.
Tuffs of Mesa Cuadrada
Tuff of San Felipe
100m
(Stock, 1989)
(Stock, 1989)
(Nagy, 1997)
(Nagy, 1997)
(Lewis, 1996)
(Martín-Barajas et al., 1995)
(This Study)
Baja California

and *Lewis* [1996] also noted a trace amount of tourmaline phenocrysts in Tmr6, but additional petrographic observations of Tmr6 for this study did not encounter this phenocryst phase. Like Tmr5, Tmr6 is also composed of a base of indurate dark reddish-brown porcelainous welded tuff, capped by lighter-colored vapor-phase altered zones. Additional outcrops of plagioclase-phyric welded tuff mapped as Tmr4a [*Lewis*, 1994] on the western side of the Sierra San Fermín are included here with the Tuffs of Dead Battery Canyon. Pumice and phenocryst content of outcrops of the Tuffs of Dead Battery canyon on Isla Tiburón best supports correlation to cooling unit Tmr5.

The Tuffs of Dead Battery Canyon may be an uppermost cooling unit of the Tuffs of Mesa Cuadrada. This possibility was suggested by *Lewis* [1994], who observed that the Tuffs of Dead Battery Canyon are lithologically similar to and conformably overlie Tmr4 in the Sierra San Fermín. Younger units, including a possible correlative to the Tuffs of Arroyo El Canelo (Tmr8, see below) overlie the Tuffs of Dead Battery Canyon with a slight angular unconformity [*Lewis*, 1994]. This same relationship appears on Isla Tiburón south of Punta Reina (Fig. 5.6) where the Tuffs of Dead Battery Canyon conformably overlie the Tuffs of Mesa Cuadrada but are cut by a paleocanyon filled by the El Oculto member of the Tuffs of Arroyo El Canelo.

The Tuffs of Arroyo El Canelo

The Tuffs of Arroyo El Canelo comprise a complexly zoned ignimbrite with at least four distinct cooling units (Fig. 5.9). The Tuffs of Arroyo El Canelo as defined here are based upon the exposures in the Santa Isabel Wash region, where these tuffs are best exposed in relation to other ignimbrites [*Nagy et al.*, 1999]. Many of the tuffs designated as cooling units of the Tuffs of Arroyo El Canelo in this study were given separate names by *Nagy et al.* [1999]. These units are the Tuff of Arroyo El Oculto, Tuff of Arroyo El Canelo (with an internal cooling break), the Bighorn Sheep Tuff, and the Flagpole Tuff.

The El Oculto member of the Tuffs of Arroyo El Canelo is a non-welded lithic-rich devitrified ash-flow tuff with 2% phenocrysts (plagioclase + anorthoclase(?) > or-

thopyroxene). The El Oculto member is typically thin (0-2 m thick) and has a distinctive bright-white weathered surface. Thicker sections described by *Nagy* [1997] display a densely welded interior zone, up to decimeter-sized lithics, and lithic-concentration zones. This unit is correlated by *Nagy et al.* [1999] to unit t14 of *Stock et al.* [1991].

The main (El Canelo) member of the Tuffs of Arroyo El Canelo comprises multiple cooling units of densely welded lithic-phyric ash-flow tuff. These units are characterized by 3-10% phenocrysts (plagioclase + anorthoclase $\gg$ orthopyroxene $\approx$ Fe–Ti oxides > hornblende), a dark-purple matrix of welded glass, and distinctive pumice fiamme up to 50 cm in length. The base of the tuff is characterized by dense, dark-purple indurated vitrophyre with cm-scale variations in phenocryst concentration and black fiamme. Above the basal densely welded zones, phenocryst concentration levels out at $\sim$10% and replacement of the pumice by light-colored vapor-phase crystals form white pods that sharply contrast with the dark-purple glassy matrix. Thick high-grade sections of the El Canelo member display extremely thin (<1 cm) fiamme with rheomorphic flow lineations. Cooling breaks in the El Canelo member are distinguished by a volcanic lithic concentration zone overlain by a thin non-welded dark-colored glass and/or a dark purple indurated vitrophyre. This unit is correlated by *Nagy et al.* [1999] to units t9 and t12 of *Stock et al.* [1991] and units tmc2 and tmc3 of [*Martín-Barajas et al.*, 1995]. *Lewis* [1994]'s Tmr8 is also tentatively correlated to the main member of the Tuffs of Arroyo El Canelo.

The Bighorn Sheep member and the Flagpole member are the uppermost cooling units of the Tuffs of Arroyo El Canelo. The following descriptions are from *Nagy* [1997] and *Nagy et al.* [1999]. The Bighorn Sheep member is a weakly-indurated crystal- and lithic-rich pyroclastic flow deposit. The concentration of lithic fragments ranges from 2% to up to 50%, and they average 2–3 cm size. Elongate dark pumice or scoria may be up to 50 cm in length and comprise up to 100% of the unit locally. Matrix material, where present, consists of pale pink/purple, or yellow devitrified ash and 5–10 phenocrysts (plagioclase + anorthoclase(?) > Fe–Ti oxides > altered mafic silicates (pyroxene?)). The distribution of the Bighorn Sheep member is erratic at

the 100 m-scale and its thickness ranges from 0–15 m. The Flagpole member is a 2–5 m-thick indurate densely welded dark-purple to dark-orange crystal-rich ash-flow tuff. Its appearance is similar to that of the underlying El Canelo member, with large vapor-phase replaced fiamme and cm-scale variation in phenocryst abundance in the basal welded vitrophyre. The presence of trace amounts of fayalite distinguishes this capping unit from the underlying members of the Tuffs of Arroyo El Canelo at Santa Isabel Wash. Possible correlatives to the Bighorn and Flagpole members are unit t9 of *Stock et al.* [1991] and units tmc4 and tmc5 of [*Martín-Barajas et al.*, 1995]. However, fayalite is not described from these tuffs and these may comprise additional cooling units of the underlying El Canelo member.

5.4.2 Major and trace element analyses

Major and trace element analyses provide a simple test of correlation of ash-flow tuffs across the Gulf of California (Table 5.1). However, this test should not produce identical data for every sample locality within a single ignimbrite. Composition variations within a pyroclastic flow may arise from variations within the magma source [*Wilson and Hildreth*, 1997, for example], mechanical separation of ash-flow components during emplacement [*Branney and Kokelaar*, 1992], and transport of mobile elements by hydrothermal processes during cooling of the ash-flow deposit [*Weaver et al.*, 1990, for example]. To minimize these effects, samples of minimally altered vitrophyre from the base of each unit were analyzed where possible. Whole-rock chemical analyses were carried out on one sample each of units Tmr3 and Tmr4 of the Tuffs of Mesa Cuadrada from Isla Tiburón and Baja California (Table 5.1). One sample of the Tuff of San Felipe from Isla Tiburón and one sample from mainland coastal Sonora were also analyzed for comparison to four analyses of the Tuff of San Felipe from Baja California first published in *Stock et al.* [1999].

Table 5.1. Major and trace-element analyses from correlative tuffs.[1]

	Tuff of San Felipe			Tmr3		Tmr4		Other
	Coastal Sonora[2]	Isla Tiburón[3]	Baja California[4]	S. San Fermín[5]	Isla Tiburón[6]	S. San Fermín[7]	Isla Tiburón[8]	PVP Rhyolites[9]
SiO_2	76.57	76.5	74.9–75.9	75.9	75.88	74.33	76.24	70.5–76.4
TiO_2	0.13	0.12	0.14–0.15	0.13	0.14	0.16	0.16	0.17–0.45
Al_2O_3	12.67	12.62	12.2–12.6	12.45	12.29	12.79	12.78	12.8–15.2
Fe_2O_3*	1.81	1.75	1.83–1.91	1.8	1.88	1.37	1.36	0.65–3.26
MnO	0.04	0.04	0.03–0.04	0.03	1.03	0.03	0.03	0.00–0.10
MgO	0.18	0.08	0.17–0.36	0.67	0.19	0.34	0.32	0.14–1.54
CaO	1.13	0.69	0.45–2.02	0.65	0.62	3.44	0.96	0.88–3.22
Na_2O	4.72	4.38	3.68–3.93	3.88	4.24	3.82	3.78	3.70–5.15
K_2O	2.58	3.9	4.94-5.41	4.31	4.34	3.95	4.54	2.73–4.25
P_2O_5	0.01	0.01	0.02–0.05	0.01	0.01	0.06	0.02	0.02–0.10
Total	99.84	100.07		99.83	99.63	100.28	100.17	
Y	51.8	52.6	48.1–51.9	53.6	55.4	26.7	27.6	20–57
U	5	5	4–5	4	4	3	4	0–4
Rb	176.3	195.4	166–188	155.6	149.8	124.9	129.9	80–127
Th	17	18	16–18	12	12	10	10	4–13
Pb	28	25	27–28	29	19	23	15	8–28
Ga	21	22	0–20	23	23	16	16	16–21
Nb	24.6	25	22.5–24.4	20.5	21.1	11.9	12.6	7.6–19.5
Zr	315	321	384–402	329	320	168	177	98–432
Sr	90	35	19–60	65	44	88	68	72–263
Zn	91	85	57–76	107	109	68	42	24–80
Ni	2	1	8–9	1	2	1	1	3–16
Cr	2	6	0–2	0	4	2	6	0–8
V	2	2	7–58	4	2	3	3	0–42
Ce	123	127	111–120	94	94	56	57	20–87
Ba	78	39	52–56	428	460	1093	996	705–1184
La	54	56	54–56	43	38	27	26	13–44

[1] Major- and trace-element analyses (XRF) were done at the University of Massachusetts, Amherst and are reported on a volatile-free, oxidized basis. See *Rhodes* [1988] for typical values of analytical precision from this facility. Oxides reported in wt. %, trace elements reported in ppm. Reprinted from *Oskin et al.* [2001]

[2] Sample number BK-99-05, 28.880°N, 112.001°W.

[3] Sample number BV-99-30, 28.979°N, 112.458°W.

[4] Range of values for samples of the Tuff of San Felipe from Baja California [*Stock et al.*, 1999].

[5] Sample number SF-92-64, 30.594°N, 114.756°W.

[6] Sample number BV-99-08, 28.917°N, 112.447°W.

[7] Sample number SF-92-101, 30.566°N, 114.790°W.

[8] Sample number TIB-98-17, 28.979°N, 112.476°W.

[9] Range of values for other high-SiO_2 rhyolite samples from the Puertecitos area reported by *Martín-Barajas et al.* [1995].

Major element compositions of ash-flow tuffs are similar for all units measured and thus not very useful for testing correlation. The SiO_2 content of the Tuff of San Felipe for Baja California samples ranges from 74.9 to 75.8% and K_2O + Na_2O varies from 8.6 to 9.2% [*Stock et al.*, 1999]. Samples of the Tuff of San Felipe from Sonora and Isla Tiburón contained 76.5 and 76.6% SiO_2 and 7.3 and 8.3% K_2O + Na_2O, respectively. Samples of the Tuffs of Mesa Cuadrada overlap these ranges of SiO_2 and alkali content. Major elements present in minerals that form spherulites and lithophysae within stratigraphically higher sections of the sampled ash-flow tuffs show a greater range of variability between correlated samples. These elements (Si, Al, Ca, Na, and K) form quartz, feldspar, and calcite that comprise crystal structures produced by vapor-phase alteration during cooling of tuffs. Other major element analyses (Fe, Mn and Ti) are consistent and similar for samples of the Tuff of San Felipe and the Tuffs of Mesa Cuadrada. Of all major element analyses, only Fe content may confidently discriminate between cooling units Tmr3 and Tmr4 of the Tuffs of Mesa Cuadrada.

Trace element measurements display a restricted and reproducible range of compositions and a positive test of correlation (Table 5.1). Most of the measured trace element concentrations are similar for correlated ash-flow tuffs and also unique to each unit (e.g., Y, Rb, Th, Ga, Nb, Zr, Zn, Ce, and La). Other trace elements show a wide variability within duplicate analyses and are thus less reliable indicators of correlation (e.g., Pb, Sr, and Ba). Remaining trace elements are present in low concentrations for all samples (e.g., U, Ni, Cr, and V).

The concentrations of trace elements in the Tuff of San Felipe and the Tuffs of Mesa Cuadrada distinguish these units other syn-rift high-silica rhyolites of the northern Puertecitos Volcanic Province. A range of measurements obtained by *Martín-Barajas et al.* [1995] for rhyolites with >70% SiO_2 is shown in the right-hand column of Table 5.1. *Stock et al.* [1999] document that the abundance of Nb, Ce, Rb, and La are higher for the Tuff of San Felipe than for any other silicic rocks measured by *Martín-Barajas et al.* [1995]. Cooling unit Tmr3 of the Tuffs of Mesa Cuadrada is similarly high

in these trace elements but with concentrations distinct from the Tuff of San Felipe (Table 5.1). Trace element composition of cooling unit Tmr4 of the Tuffs of Mesa Cuadrada falls within the range of values measured for other high-silica rhyolites of the northern Puertecitos Volcanic Province.

5.4.3 Phenocryst chemistry

Phenocryst chemistry and zonation provide an additional test of correlation of ash-flow tuffs across the northern Gulf of California. Feldspar and pyroxene phenocrysts from the Tuff of San Felipe and unit Tmr3 of the Tuffs of Mesa Cuadrada were analyzed by electron microprobe on thin sections (Figs. 5.10 and 5.11, Appendix B). Fayalite phenocrysts in Tmr3 samples were also analyzed (Appendix B). Cooling unit Tmr4 of the Tuffs of Mesa Cuadrada was not analyzed because of its extremely low phenocryst content. Both major element concentrations (Fig. 5.10) and minor element concentrations (Fig. 5.11) are consistent between correlated ash-flow tuffs.

Phenocrysts of the Tuff of San Felipe

Electron microprobe analyses were carried out on five samples of the Tuff of San Felipe from Baja California and three samples of correlated ignimbrite from Isla Tiburón and Coastal Sonora (Figs. 5.10 and 5.11). Feldspars from the Tuff of San Felipe are anorthoclase and range from $Ab_{52}An_5Or_{43}$ to $Ab_{67}An_{15}Or_{18}$. These values are within the range of compositions ($Ab_{47}An_4Or_{49}$ to $Ab_{69}An_7Or_{24}$) measured by *Stock et al.* [1999]. This full range of compositions is present in most crystals. Cryptoperthitic texture is rarely visible as differential reflectance under the microprobe SEM, and lamellae correspond to the end-members described above. Of the minor elements measured for feldspars of the Tuff of San Felipe, Fe is consistently present at 0.3 wt.% and Ba is present just at the detection limit, if at all (Fig. 5.11). Rare plagioclase was also measured. Plagioclase compositions are highly variable, suggesting that these crystals are probably xenocrystic. Anorthoclase phenocrysts are identical

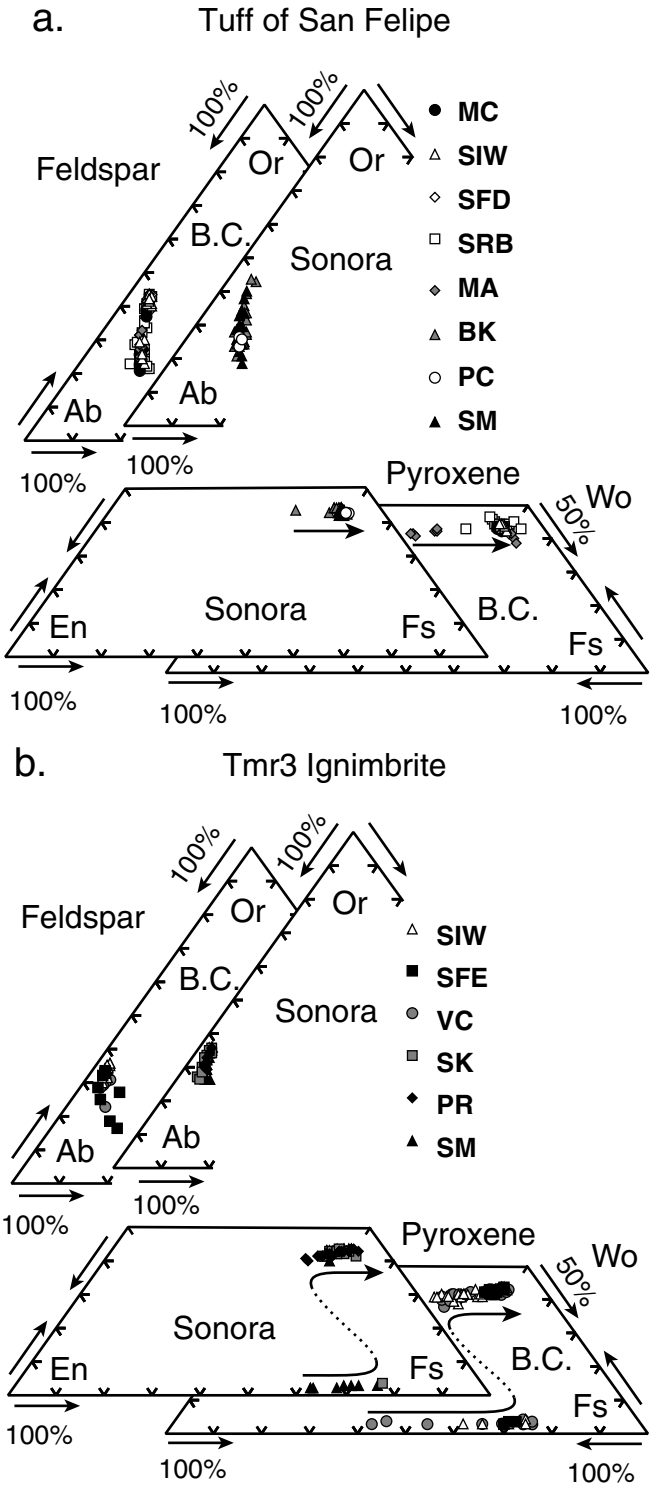

Figure 5.10. Phenocryst major-element compositions from the Tuff of San Felipe and cooling unit Tmr3 of the Tuffs of Mesa Cuadrada. See Figs. 5.7 and 5.8 for abbreviations and locations. B.C., Baja California; Ab, albite; Or, orthoclase; En, enstatite; Fs, ferrosilite; Wo, Wwollastonite. Arrows within pyroxene plots denote phenocryst core-to-rim compositional trend, dashed line across immiscibility gap. Reproduced from *Oskin et al.* [2001].

for samples of the Tuff of San Felipe from each side of the Gulf of California.

Pyroxene phenocrysts of the Tuff of San Felipe show distinctive composition and zonation of major and minor elements (Fig. 5.10 and 5.11). Most pyroxenes (80 to 90% of those observed in thin section) are unzoned green Fe-rich augite ($En_7Fs_{48}Wo_{45}$) with consistent minor-element composition (0.3% Na, 0.2% Ti, 0.4% Al, and 1.0% Mn). Cores of zoned pyroxenes are brown-colored magnesian augite (up to En_{30}) with higher Al content, lower Na content, and variable Mn content. Zoned pyroxene cores are often oxidized. Two orthopyroxene xenocrysts were also measured, each of a distinct composition. Overall, pyroxene chemistry and zonation are identical for samples collected from opposite sides of the Gulf of California and support correlation of these deposits.

Phenocrysts of Tmr3

Compositions of phenocrysts from Tmr3 were measured in three samples from Baja California and three samples from Isla Tiburón (Figs. 5.10 and 5.11). Feldspar phenocrysts from Tmr3 were sanidine and anorthoclase with compositions similar to feldspars from the Tuff of San Felipe ($Ab_{60}An_3Or_{37}$ to $Ab_{72}An_{13}Or_{15}$). Minor element compositions of Tmr3 feldspar are distinctive, however, with 0.2 wt.% Fe and 0.3 wt.% Ba (Fig. 5.11). Feldspar phenocrysts from samples from Isla Tiburón are identical to samples from Baja California.

Pyroxene phenocrysts of Tmr3 also show distinctive composition and zonation of major and minor elements (Figs. 5.10 and 5.11). Most pyroxenes observed in thin section (90%) were unzoned. Measurements of these phenocrysts indicate Fe-rich augite ($En_7Fs_{48}Wo_{45}$) with distinct minor-element composition (0.4% Na, 0.3% Ti,

Figure 5.11. (next three pages) Phenocryst minor element compositions from the Tuff of San Felipe and cooling unit Tmr3 of the Tuffs of Mesa Cuadrada. 5.11a, Feldspar FeO, BaO; 5.11b, pyroxene NaO, TiO_2; 5.11c, pyroxene Al_2O_3, MnO. Each graph is a normalized histogram of minor element concentrations in individual electron microprobe measurements. Pyroxene core compositions shown as dashed lines. Data from Tmr3 type I shown as dotted lines.

Figure 5.11a.

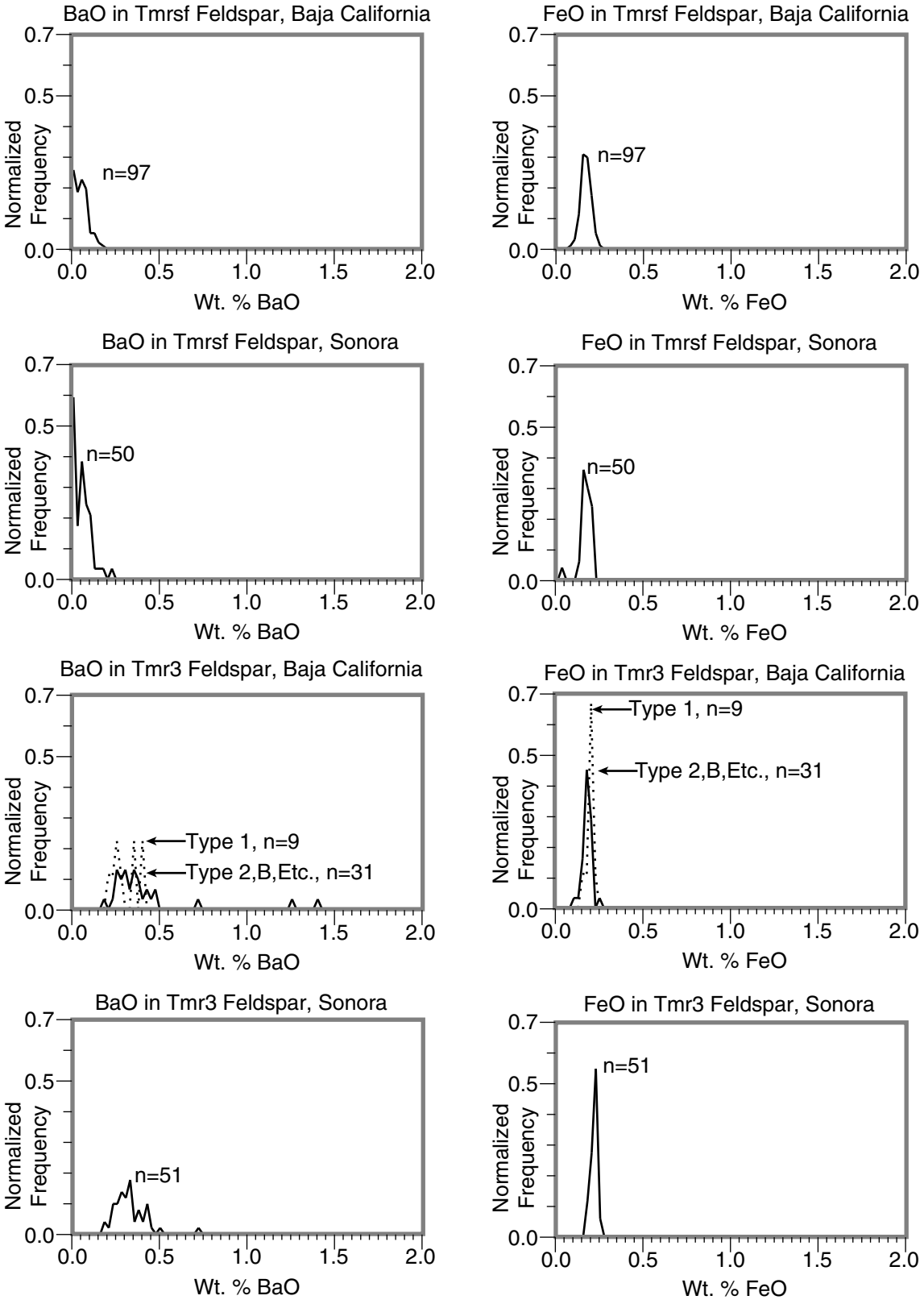
BaO in Tmrsf Feldspar, Baja California
FeO in Tmrsf Feldspar, Baja California
BaO in Tmrsf Feldspar, Sonora
FeO in Tmrsf Feldspar, Sonora
BaO in Tmr3 Feldspar, Baja California
FeO in Tmr3 Feldspar, Baja California
BaO in Tmr3 Feldspar, Sonora
FeO in Tmr3 Feldspar, Sonora
Normalized Frequency
Wt. % BaO
Wt. % FeO
n=97
n=50
n=51
Type 1, n=9
Type 2,B,Etc., n=31
0.0
0.5
1.0
1.5
2.0
0.7

Figure 5.11b.

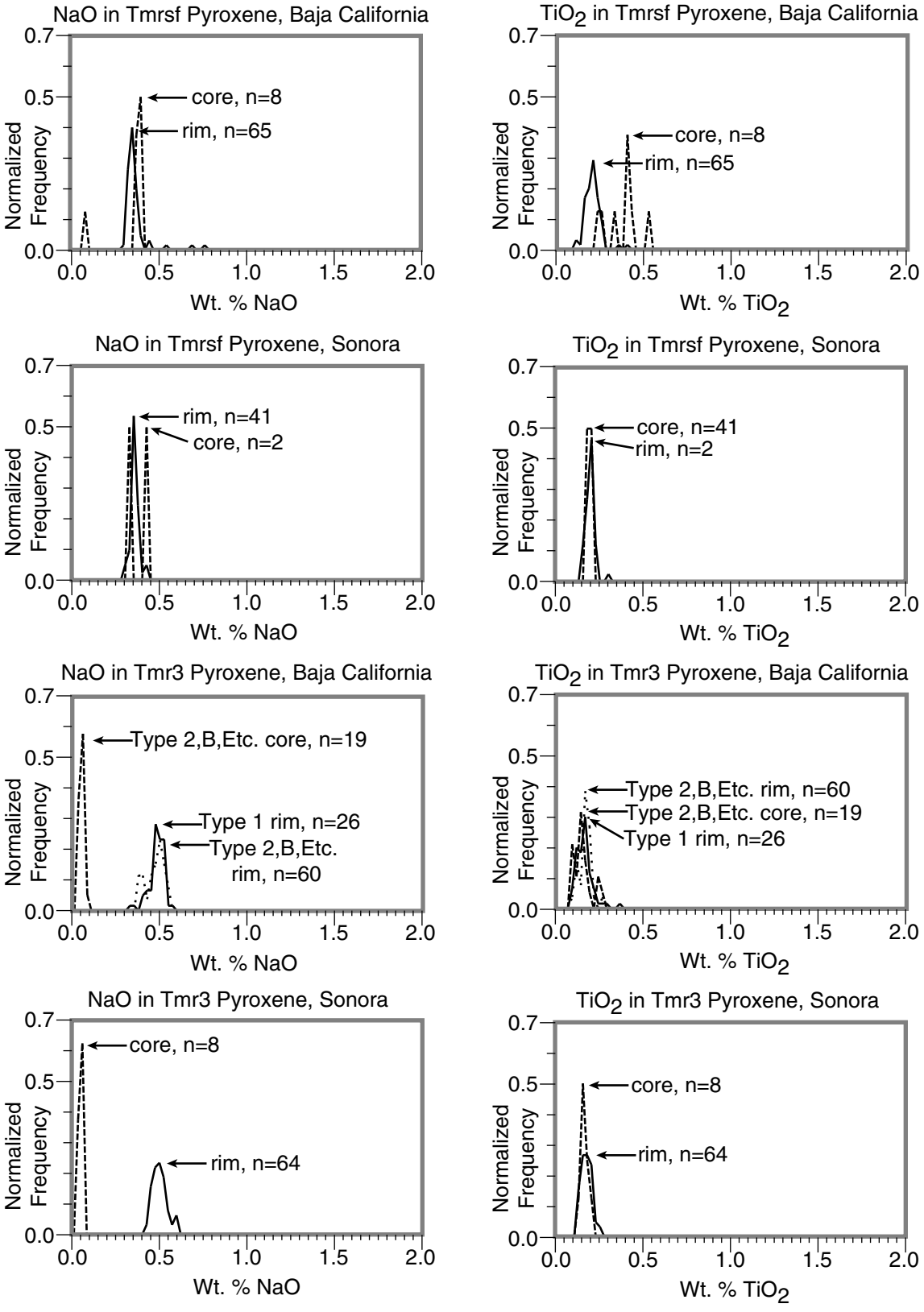
NaO in Tmrsf Pyroxene, Baja California
core, n=8
rim, n=65
Normalized Frequency
Wt. % NaO
TiO2 in Tmrsf Pyroxene, Baja California
core, n=8
rim, n=65
Normalized Frequency
Wt. % TiO2
NaO in Tmrsf Pyroxene, Sonora
rim, n=41
core, n=2
Normalized Frequency
Wt. % NaO
TiO2 in Tmrsf Pyroxene, Sonora
core, n=41
rim, n=2
Normalized Frequency
Wt. % TiO2
NaO in Tmr3 Pyroxene, Baja California
Type 2,B,Etc. core, n=19
Type 1 rim, n=26
Type 2,B,Etc.
rim, n=60
Normalized Frequency
Wt. % NaO
TiO2 in Tmr3 Pyroxene, Baja California
Type 2,B,Etc. rim, n=60
Type 2,B,Etc. core, n=19
Type 1 rim, n=26
Normalized Frequency
Wt. % TiO2
NaO in Tmr3 Pyroxene, Sonora
core, n=8
rim, n=64
Normalized Frequency
Wt. % NaO
TiO2 in Tmr3 Pyroxene, Sonora
core, n=8
rim, n=64
Normalized Frequency
Wt. % TiO2

Figure 5.11c.

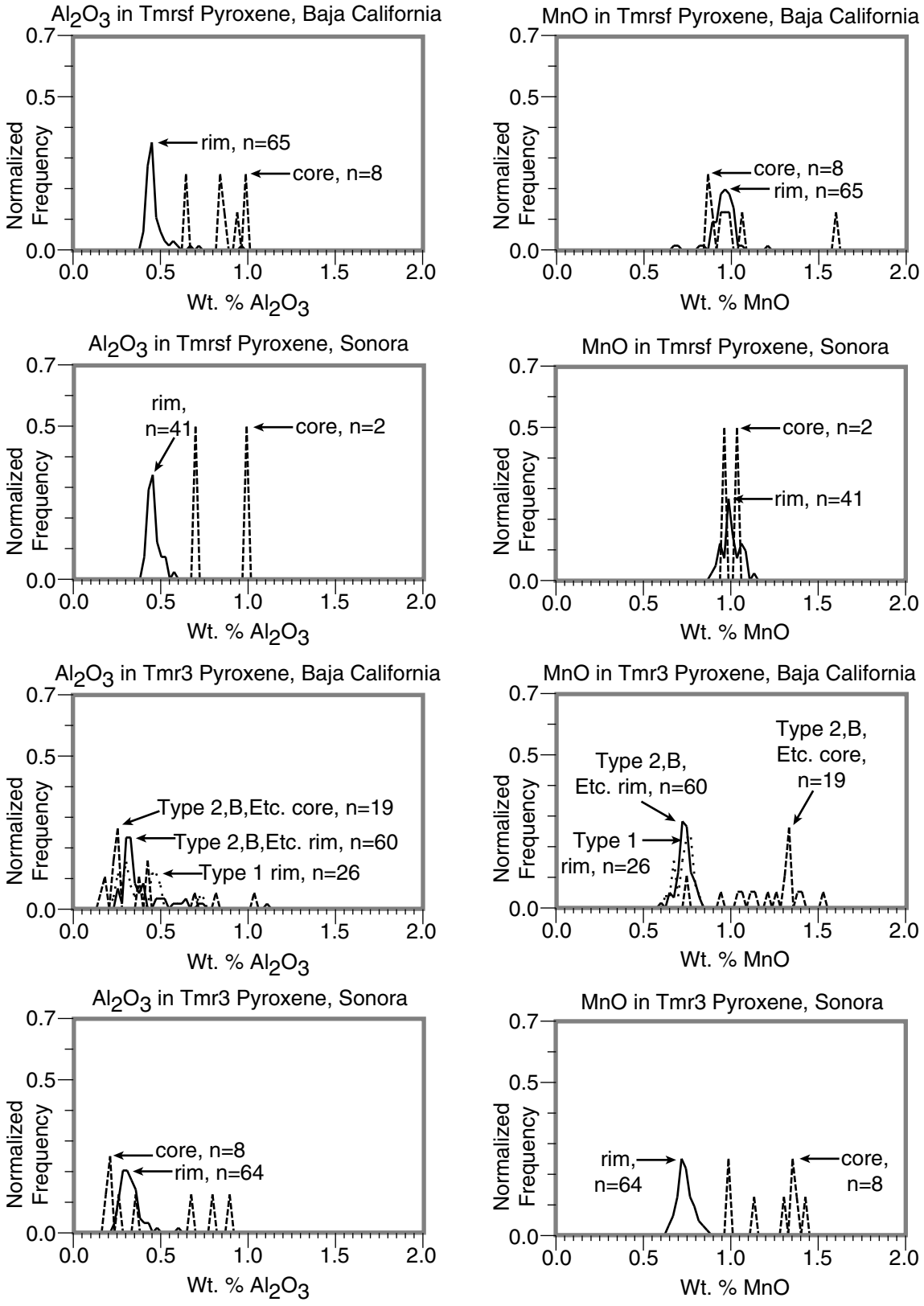
Al2O3 in Tmrsf Pyroxene, Baja California
MnO in Tmrsf Pyroxene, Baja California
Al2O3 in Tmrsf Pyroxene, Sonora
MnO in Tmrsf Pyroxene, Sonora
Al2O3 in Tmr3 Pyroxene, Baja California
MnO in Tmr3 Pyroxene, Baja California
Al2O3 in Tmr3 Pyroxene, Sonora
MnO in Tmr3 Pyroxene, Sonora
Normalized Frequency
Wt. % Al2O3
Wt. % MnO
rim, n=65
core, n=8
rim, n=41
core, n=2
Type 2,B,Etc. core, n=19
Type 2,B,Etc. rim, n=60
Type 1 rim, n=26
Type 2,B, Etc. rim, n=60
Type 2,B, Etc. core, n=19
Type 1 rim, n=26
rim, n=64
0.0
0.5
1.0
1.5
2.0
0.7

0.3% Al, and 0.7% Mn). Core compositions of zoned pyroxenes from Tmr3 are unusual. The most primitive cores are brown-colored Fe-rich enstatite ($En_{57}Fs_{40}Wo_3$) to ferrosilite ($En_{20}Fs_{76}Wo_4$). These orthopyroxene cores are surrounded by brown to green-colored Fe-rich augite ranging from En_{25} to En_7. Compositions intermediate between Wo_4 and Wo_{44} are not present. Exsolution lamellae of orthopyroxene and clinopyroxene form a comb-like boundary between core and rim compositions. Pyroxene phenocrysts in unit Tmr3 are also zoned in terms of minor elements (Fig. 5.11). Three orthopyroxene xenocrysts were also measured, each of a distinct composition. The unusual zoned pyroxenes of the Tmr3 member of the Tuffs of Mesa Cuadrada are identical for samples collected from opposite sides of the Gulf of California and support correlation of these deposits.

Fayalite phenocrysts of Tmr3 were also analyzed by electron microprobe (Appendix B). These phenocrysts contain very little Mg. Oxide totals seldom reached 100%, reflecting oxidation of these phenocrysts to iddingsite. Fayalite phenocrysts were encountered in many, but not all samples of Tmr3. Fayalite is most abundant in samples from the northern Sierra Kunkaak and the Sierra San Fermín. Fayalite is also present in samples from the southern Sierra Menor and the Sierra Santa Isabel. No fayalite was found in Tmr3 from Punta Reina and southern Valle Chico. These variations in fayalite concentration are geographically similar on opposite sides of the Gulf of California. Fayalite abundance is highest in the north, absent in middle reaches of tuff exposure and present to a minor degree in southerly outcrops. These transitions occur across a continuous belt of outcrops in the Sierra Menor. The systematic variation in % fayalite in Tmr3 most likely reflects small variations in the magma source such as have been documented from ignimbrites elsewhere [*Wilson and Hildreth*, 1997, for example].

5.4.4 Geochronology

Isotopic ages are an important test of correlation of ash-flow tuffs across the Gulf of California. Both the Tuff of San Felipe and unit Tmr3 of the Tuffs of Mesa Cuadrada

have been dated in several localities in Baja California [*Stock et al.*, 1999; *Nagy et al.*, 1999, and references therein]. New $^{40}Ar/^{39}Ar$ geochronology of three samples of the Tuff of San Felipe and two samples of unit Tmr3, presented here, confirms correlation of these ash-flow tuffs on both sides of the Gulf of California (Table 5.2). Procedures of $^{40}Ar/^{39}Ar$ dating employed for this study are described in appendix C.

Alkali feldspar was prepared from five samples of correlated ash-flow tuffs. Both the Tuff of San Felipe and unit Tmr3 of the Tuffs of Mesa Cuadrada contain abundant (10%) alkali feldspar. Measurements of Ar isotopes were made at the Massachusetts Institute of Technology CLAIR laboratory by Dr. Joann Stock. Laser fusion was used to release Ar from the sample. 6 to 8 crystals of alkali feldspar were placed in each sample well. Ten sample wells were measured for each sample.

Isotopic ages of correlative ash-flow tuffs of Isla Tiburón and coastal Sonora are consistent with the correlation of these to deposits in Baja California (Table 5.2). Isotopic ages of Tuff of San Felipe samples from coastal Sonora and Isla Tiburón overlap the range of ages cited for this deposit in Baja California [*Stock et al.*, 1999]. One sample (TIB-98-23) does not overlap the ∼12.6 Ma average age cited by *Stock et al.* [1999]. Samples of unit Tmr3 from the Tuffs of Mesa Cuadrada all overlap isotopic ages of ∼6.3 Ma for Tmr3 from Baja California. A sample of rhyolite from western Isla Tiburón dated by *Gastil et al.* [1979] at 5.7 ± 0.6 Ma (Sample #1012, K–Ar on feldspar) also appears to be from unit Tmr3.

5.4.5 Paleomagnetism

Paleomagnetic remanence directions measured on samples of the Tuff of San Felipe, Tuffs of Mesa Cuadrada, and the Tuffs of Dead Battery Canyon from Isla Tiburón and coastal Sonora match those of samples from the same units in Baja California (Fig. 5.12, Table 5.3). Each of these tuffs preserves a unique thermoremanent magnetization (TRM) direction or set of directions for multiple cooling units [*Lewis and Stock*, 1998a; *Stock et al.*, 1999; *Nagy*, 2000]. Sampling methods and analysis are described in appendix D. To match preserved remanence directions, a structural cor-

Table 5.2. New geochronologic data from correlative tuffs on Isla Tiburón and Sonora.

Unit	UTM east	UTM north	Sample number	Mineral[a]	Ca/K[b]	n/n$_0$[c]	Age[d] ($\pm 2\sigma$)	$^{40}Ar/^{36}Ar$[e] ($\pm 1\sigma$)	MSWD[e]	95% crit. MSWD[f]
Tmrsf	$^{3}57^{730}$	$^{32}05^{760}$	TIB-98-23	Anorthoclase	0.06–0.28	8/8	9.66 ± 1.31	Total gas age		
						8/8	10.23 ± 1.56	Error weighted mean age		
						8/8	10.69 ± 1.48	% ^{39}Ar weighted mean age		
Tmrsf	$^{3}56^{740}$	$^{32}03^{790}$	BV-99-30	Anorthoclase	0.05–0.24	10/10	12.96 ± 3.67	294 ± 19	0.26	0.27–2.19
						10/10	11.56 ± 10.40	Total gas age		
						10/10	12.26 ± 9.60	Error weighted mean age		
						10/10	12.63 ± 9.02	% ^{39}Ar weighted mean age		
Tmrsf	$^{4}00^{250}$	$^{31}94^{900}$	BK-99-05	Anorthoclase	0.06–0.27	10/10	13.86 ± 2.21	367 ± 118	0.14	0.27–2.19
						10/10	14.93 ± 2.21	Total gas age		
						10/10	14.79 ± 4.11	Error weighted mean age		
						10/10	14.45 ± 3.92	% ^{39}Ar weighted mean age		
Tmr3	$^{3}58^{080}$	$^{32}06^{340}$	TIB-98-12	Anorthoclase[h]	0.04–0.06	10/10	5.33 ± 2.18	Total gas age		
					(28–29)[h]	10/10	6.16 ± 2.28	Error weighted mean age		
						10/10	5.17 ± 2.24	% ^{39}Ar weighted mean age		
Tmr3	$^{3}59^{090}$	$^{32}00^{240}$	BV-99-08	Anorthoclase	0.04–1.29	10/10	6.15 ± 1.03	367 ± 90	1.22	0.27–2.19
						10/10	6.91 ± 2.71	Total gas age		
						10/10	6.10 ± 2.38	Error weighted mean age		
						10/10	6.77 ± 2.17	% ^{39}Ar weighted mean age		

[a] Based on representative microprobe analysis.
[b] Average microprobe analyses of crystal separates used to determine the relative purity of mineral concentrations. See Appendix B for analyses.
[c] Number of aliquots included in calculation over total. Each aliquot is six to eight crystals.
[d] Ages reported in Ma.
[e] Reported for inverse isochron ages.
[f] After *Mahon* [1996].
[g] Plagioclase also present.

rection for dipping units is applied to each sample locality. This correction does not remove the effect of tectonic vertical-axis rotation of sample localities. Despite this uncertainty, measurements from widely distributed sample localities on both margins of the Gulf of California show similar remanence directions, supporting the lithologic correlations described above. These data also reveal a pattern of clockwise vertical-axis rotation of sample localities on both margins of the Gulf of California. These declination anomalies permit estimation of distributed shear through the study areas [*Lewis and Stock*, 1998a].

Table 5.3. Paleomagnetic results from correlative tuffs in Baja California and Sonora.

Unit[a]	n/n$_0$	Dec.	Inc.	α_{95}	κ	R[b]	ΔR[c]	F[d]	ΔF[c]
				Mesa Cuadrada [*Lewis and Stock*, 1998a]					
				Locality MC, (30.53°N, 114.96°W)					
Tmrsf	5/6	218.3	-6.9	4.1	442.5	reference locality			
Tmr3b	3/3	9.5	53.9	8.9	129.8	reference locality			
Tmr4	8/10	348.8	50.3	2.6	482.7	reference locality			
				Sierra San Fermín [*Lewis and Stock*, 1998a]					
				Locality SFB (30.65°N, 114.79°W)					
Tmrsf	3/6	258.5	-3.1	9.1	178.4	40.2	8.0	-3.8	8.0
Tmr3b	9/9	27.1	50	6.2	61.5	17.6	14.0	3.9	8.7
Tmr4[e]	3/3	13.4	54.9	5.8	297.8	24.6	9	-4.6	5.1
				Locality SFD, (30.73°N, 114.85°W)					
Tmrsf	8/8	253	1.8	6.5	64	34.7	6	-8.7	6.1
				Locality SFE, (30.66°N, 114.83°W)					
Tmrsf	7/7	253.4	-2.8	5.7	93.3	35.1	6	-4.1	5.6
				Locality SFH, (30.55°N, 114.74°W)					
Tmrsf[6]	4/5	288.6	10.6	13.6	46.8	70.3	12	-17.5	11.4
Tmr3b	6/6	43.7	55.5	8.1	58	34.2	17	-1.6	9.6
Tmr4[e]	2/2	38.9	53.7	29.4	37.2	50.1	40	-3.4	23.6
				Locality SFI, (30.54°N, 114.83°W)					
Tmr4	11/12	42.4	42	3.4	165.3	53.6	5	8.3	3.4
Tmr5	12/12	41	41.1	4.9	71.5	-1.4	6.4	0.9	4.8
Tmr6[e]	2/6	75.8	49.1	2	7724.3	33.4	4.4	-7.1	3.2
				Locality SFJ, (30.54°N, 114.83°W)					
Tmrsf	6/6	255.4	-11.2	7.1	98.9	37.1	7	4.3	6.6
Tmr3b	5/6	33.1	52.4	6.7	105.5	23.6	15	1.5	8.9
Tmr4[6]	3/5	57.1	55.5	16.7	34.2	68.3	24	-5.2	13.5
				Locality SFK, (30.55°N, 114.79°W)					
Tmr4	6/6	42.1	52.7	6.1	101	53.3	9	-2.4	5.3
Tmr5	6/6	32.3	46.6	3.5	304.3	-9.8	9.0	6.7	5.6
Tmr6	4/6	48	55	3.9	418.7	5.9	9.7	-2.3	5.6
				Santa Rosa Basin [*Stock et al.*, 1999]					
				Locality SRB, (30.85°N, 114.97°W)					
Tmrsf	11/11	259.4	-11.5	2.7	261.6	41.1	4	4.6	3.9

Unit[a]	n/n_0	Dec.	Inc.	α_{95}	κ	R[b]	ΔR[c]	F[d]	ΔF[c]
		Santa Isabel Wash [*Stock et al.*, 1999; *Nagy*, 2000]							
		Locality SIW, (30.38°N, 114.92°W)							
Tmrsf	11/11	229.7	-9.1	2	497.7	11.4	4	2.2	3.6
Tmr3(2)	14/14	26.1	56	2.7	225	16.6	13	-2.1	7.4
Tmr4	9/10	2.1	43	5.3	99	13.3	7	7.3	4.7
		Isla Tiburón [*Oskin et al.*, 2001]							
		Locality SA, (29.18°N, 112.46°W)							
Tmrsf	6/7	235.1	-15.8	5.4	129	14.5	6	8.9	5.4
		Locality PR, (29.07°N, 112.49°W)							
Tmrsf	10/12	231.3	-1.3	4.6	101	10.7	5	-5.6	4.9
Tmr3	13/13	35.6	53.7	2.9	88	23.8	13	0.2	7.5
Tmr4[e]	5/10	358.1	38.3	5.9	177	7	7	12	5.2
		Locality PRS, (29.05°N, 112.49°W)							
Tmr3	11/12	40.9	61	2.8	241	29.1	13	-7.1	7.5
Tmr4	8/9	22.7	35.7	3.2	292	31.6	5	14.6	3.3
Tmr5	12/12	13.6	48.7	3.2	170	-9.1	5.0	-12.0	3.6
		Locality SM, (28.98°N, 112.46°W)							
Tmrsf	11/13	226	2.7	4	122	5.4	5	-9.6	4.6
Tmr3	11/12	23.8	55.6	4.7	96	12	14	-1.7	8.1
Tmr4	9/11	2.5	44.7	3.5	194	11.4	5	5.6	3.5
		Locality BV, (28.92°N, 112.47°W)							
Tmrsf[e]	16/18	232.9	16.4	7.8	23	12.3	7	-23.3	7.0
		Coastal Sonora [*Oskin et al.*, 2001]							
		Locality PC, (29.02°N, 112.08°W)							
Tmrsf	13/13	263	-11.6	2.2	338	42.4	4	4.7	3.7
		Locality BK, (28.88°N, 112.01°W)							
Tmrsf	10/11	245.6	-10.4	3.9	138	25	5	3.5	4.5
		Central Sonora[f]							
		Locality HE, (28.98°N, 111.00°W)							
Tmrsf?	5/7	202.5	-10	4.8	269	-18.1	5	3.1	5.1

[a] Tmrsf, Tuff of San Felipe; Tmr3 and Tmr4, Tuffs of Mesa Cuadrada; Tmr5 and Tmr6, Tuffs of Dead Battery Canyon.

[b] Rotation of Tmrsf, Tmr3, and Tmr4 relative to reference locality at Mesa Cuadrada. Clockwise values are positive. 2.3° subtracted from rotation values in Sonora to account for finite rotation of reference locality due to Pacific–North America plate displacement. Rotation of Tmr5 and Tmr6 calculated relative to Tmr4 at same sample locality to assess correlation (see text).

[c] Calculated according to *Beck* [1980] and *Demarest* [1983].

[d] Flattening of inclination relative to reference locality at Mesa Cuadrada for Tmrsf, Tmr3, and Tmr4. Flattening of inclination of Tmr5 and Tmr6 calculated relative to Tmr4 at sample locality to assess correlation (see text).

[e] Sample with high error values or less than 3 cores used in average.

[f] Probable correlative outcrop of the Tuff of San Felipe located 5 km south of Hermosillo (Fig. 5.1).

Paleomagnetism of the Tuff of San Felipe

Primary thermal remanent magnetization of the Tuff of San Felipe preserves an unusual low-inclination reversed polarity direction [*Stock et al.*, 1999]. Samples from correlative deposits of the Tuff of San Felipe on Isla Tiburón and coastal Sonora also yielded low-inclination reversed polarity vectors (Fig. 5.12, Table 5.3). This remanence direction differs substantially from the expected Miocene field direction and probably records an excursion or transitional phase of the geomagnetic field [*Stock et al.*, 1999]. Most sample localities of the Tuff of San Felipe in Baja California and Sonora yielded consistent results with evidence for clockwise vertical-axis rotation of up to 50° between sample localities [*Lewis and Stock*, 1998a; *Nagy*, 2000]. One sample locality within the central Sierra Menor (BV) yielded less consistent results from low-angle reversed to low-angle normal polarity. These results appear to be caused by a problem with structural correction in an area of distributed normal faulting and a change from west- to east-dipping strata. Overall, paleomagnetic results from outcrops of the Tuff of San Felipe in coastal Sonora and Isla Tiburón strongly support correlation of this deposit to the Tuff of San Felipe of Baja California.

Paleomagnetism of the Tuffs of Mesa Cuadrada

The Tuffs of Mesa Cuadrada display moderate-inclination normal polarity primary thermal remanent magnetization [*Lewis and Stock*, 1998a; *Nagy*, 2000]. These remanence directions are within the expected range of paleosecular variation of 10° to 15° about the geomagnetic pole and, unlike the low-inclination reversed remanence of

Figure 5.12. (next page) Magnetic inclination-declination summary plots for sample localities in northeastern Baja California, Isla Tiburón and coastal Sonora. Primary paleomagnetic remanance directions of the Tuff of San Felipe (black, sf), Tuffs of Mesa Cuadrada (grey, Tmr3 as 3, Tmr4 as 4) and the Tuffs of Dead Battery Canyon (open, Tmr5 as 5, Tmr6 as 6). Ellipses denote 95% confidence. Plots are lower hemisphere, equal area projection, with reversed polarity inclination results projected from upper hemisphere. See Table 5.3 for sources of data. MC is considered unrotated reference locality. All other localities show clockwise vertical-axis rotation.

Figure 5.12.

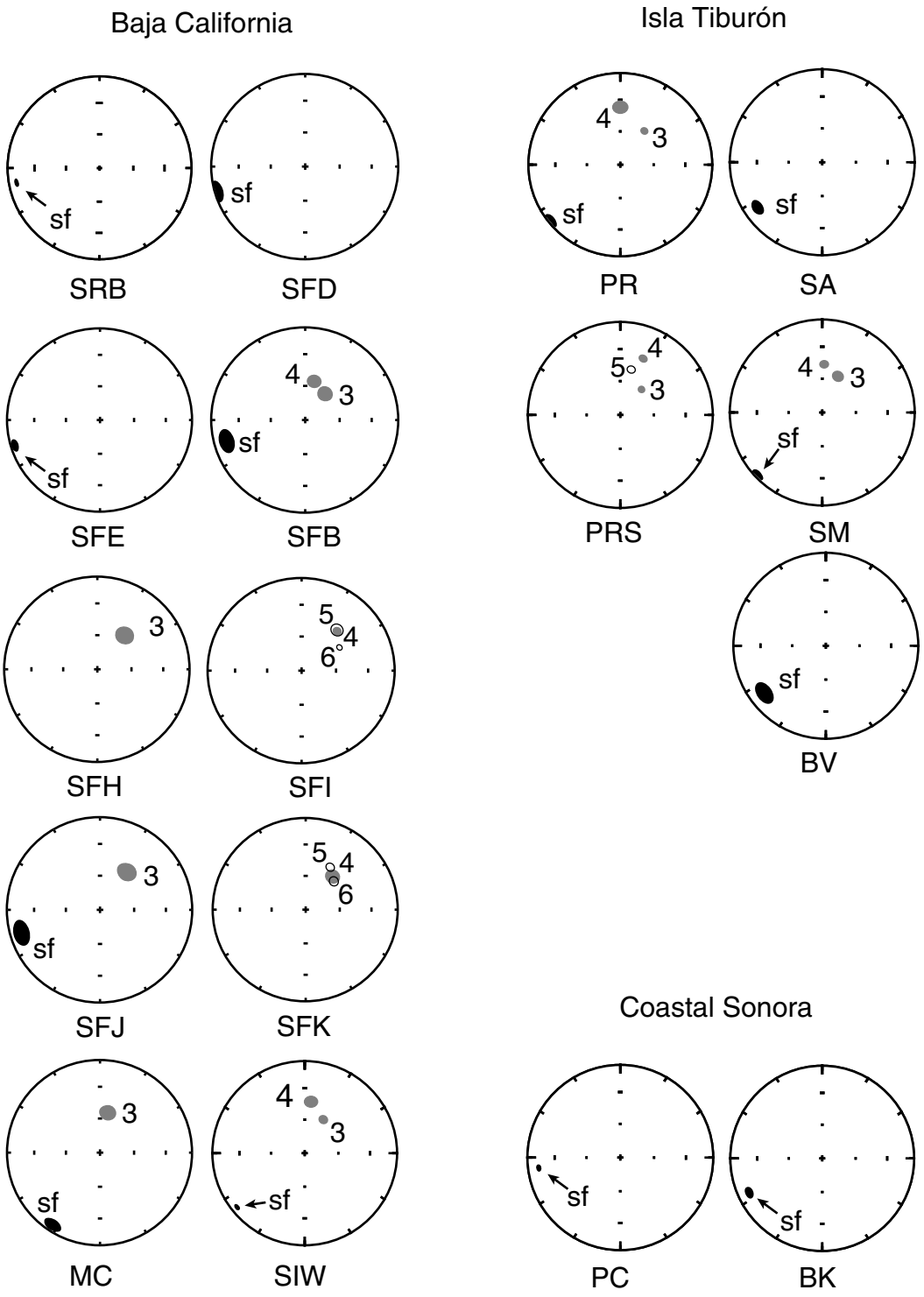
Baja California
Isla Tiburón
SRB
SFD
PR
SA
SFE
SFB
PRS
SM
BV
SFH
SFI
SFJ
SFK
Coastal Sonora
MC
SIW
PC
BK
sf
3
4
5
6

the Tuff of San Felipe, do not represent a distinctive fingerprint for correlation. However, since the Tmr4 member of the Tuffs of Mesa Cuadrada preserves a consistently shallower inclination and counterclockwise declination compared to the underlying Tmr3 member, paleomagnetism can be used to verify correlation of these deposits. Everywhere that each of these has been carefully sampled at the same locality, this correlation is robust (Fig. 5.12, Table 5.3).

Based on paleomagnetic measurements, *Nagy* [2000] suggested that units Tmr3 (type 1) and Tmr3 (type 2) of Santa Isabel Wash are not correlative to units Tmr3a and Tmr3b (Tmr3b was also mapped as just Tmr3) from the Sierra San Fermín. The average remanence directions for each of these cooling units differs from that of cooling unit Tmr4, supporting a hypothesis that Tmr3 (type 1), Tmr3 (type 2), Tmr3a, and Tmr3b are each paleomagnetically distinct cooling units [*Nagy*, 1997; *Nagy et al.*, 1999; *Nagy*, 2000]. Reexamination of individual sample localities reveals that the averaging technique used by *Nagy* [2000] included more samples of Tmr4 than Tmr3a or Tmr3b from a zone of greater clockwise vertical-axis rotation in the southern Sierra San Fermín [*Lewis*, 1994]. This biased the average declination for Tmr4 relative to the average declination of Tmr3b from the Sierra San Fermín. Due to this bias, Tmr3b appeared paleomagnetically distinct from Tmr3 (type 2) of Santa Isabel Wash. By using individual sample localities from the Sierra San Fermín instead of a range-wide average, the inclination and declination of Tmr3 (type 2) and Tmr3b relative to Tmr4 are shown to be consistent throughout the Baja California margin and consistent with outcrops on Isla Tiburón (Fig. 5.12, Table 5.3). Remanent paleomagnetic directions from unit Tmr3 (type 1) of Santa Isabel Wash and unit Tmr3a of the Sierra San Fermín remain distinctive from each other and from cooling unit Tmr4. Tmr3 (type 1) has not been mapped separately from Tmr3 (type 2) at Santa Isabel Wash and the actual distribution of these two units within the Tuffs of Mesa Cuadrada in the Puertecitos Volcanic Province is unknown.

Paleomagnetism of the Tuffs of Dead Battery Canyon

Correlation of the Tuffs of Dead Battery Canyon to outcrops on Isla Tiburón was tested by a method similar to that applied above to the Tuffs of Mesa Cuadrada. Cooling units Tmr5 and Tmr6 in Baja California both preserve normal-polarity, moderate-inclination paleomagnetic remanence directions, with Tmr6 steeper and clockwise of unit Tmr5 [*Lewis and Stock*, 1998a, Fig. 5.12 and Table 5.3]. Since only one cooling unit of the Tuffs of Dead Battery Canyon appears to be present of Isla Tiburón, the following analysis compares the paleomagnetic remanance of Tmr5 and Tmr6 to cooling unit Tmr4 of the Tuffs of Mesa Cuadrada, which is present at all localities where the Tuffs of Dead Battery Canyon were sampled. At locality SFK in the Sierra San Fermín, The remanence direction of unit Tmr4 of the Tuffs of Mesa Cuadrada overlaps Tmr5 and Tmr6 [*Lewis and Stock*, 1998a, Fig. 5.12 and Table 5.3]. These same units were also sampled at locality SFI in the Sierra San Fermín where structural control was less certain [*Lewis and Stock*, 1998a, Fig. 5.12 and Table 5.3]. At this locality, the pattern of Tmr4 and Tmr5 are again consistent, but the error ellipse for Tmr6 is steeper and clockwise of Tmr4. Note that remanance direction of Tmr6 is poorly constrained at locality SFI. Paleomagnetic remanence of the Tuffs of Dead Battery Canyon at locality PRS on Isla Tiburón is 9.1 ± 5.0° counterclockwise and 12.0 ± 3.6° steeper than cooling unit Tmr4 of the Tuffs of Mesa Cuadrada (Fig. 5.12 and Table 5.3). This remanance direction is consistent with the overall paleomagnetic directions of Tmr5 and Tmr6 from Baja California, but it is not distinctive of either Tmr5 or Tmr6 given the uncertainties present in the data. Although uncertain, paleomagnetic remanence does support correlation of the Tuffs of Dead Battery Canyon on Isla Tiburón to Isla Tiburón.

5.5 Correlation of conjugate rifted margins

The lithologic, geochemical, and paleomagnetic similarities of tuff outcrops in coastal Sonora and Isla Tiburón presented above confirm that these are displaced

parts of the tuffs known from northeastern Baja California. The outcrop area and facies relationships of these ignimbrites permit a precise restoration of the conjugate rifted margins of the northern Gulf of California. In the following sections, correlative stratigraphic features are matched across the Gulf of California and its surrounding extensional province (Figs. 5.13 and 5.14).

Stratigraphic evidence for the amount of dextral offset across the northern Gulf of California comes from groups one through five exposed in the study areas. Some of these offsets have been described from basement lithologies [*Gastil et al.*, 1991] and distinctive Middle Miocene age or older fluvial deposits [*Gastil et al.*, 1973]. The offset distributions of the Tuff of San Felipe and the Tuffs of the northern Puertecitos Volcanic Province significantly enhance the resolution of the amount and timing of dextral displacement. The facies and distribution of other volcanic and sedimentary strata intercalated with these ash-flow tuffs also support correlation. All of this evidence is summarized graphically as a series of tie lines for each margin study area (Figs. 5.13 and 5.14). The following sections summarize the evidence for each of these tie lines in stratigraphic order.

5.5.1 Group 1: Basement complex

Basement tie points are only broadly defined, at best. *Gastil* [1993] correlated a transition from shelf facies to slope and basin facies in Paleozoic and older metamorphosed sedimentary strata from eastern Sonora to the Sierra San Felipe (Fig. 5.2). This correlation is complicated by a lack of age control on most outcrops from the Sonoran coastline westward. Later margin-parallel basin formation in Permian or Mesozoic time [*Gastil et al.*, 1975, 1981; *Radelli*, 1989] may have deposited slope and basin-type deposits in a manner spatially unrelated to the correlation proposed by *Gastil* [1993]. *Silver and Chappell* [1988] show that the Cretaceous Peninsular Ranges Batholith is broadly correlated from eastern Baja California to coastal Sonora. Compositional trends in the batholith are parallel to the Gulf of California, however, making correlation of basement across the gulf necessarily imprecise [*L.T. Silver,*

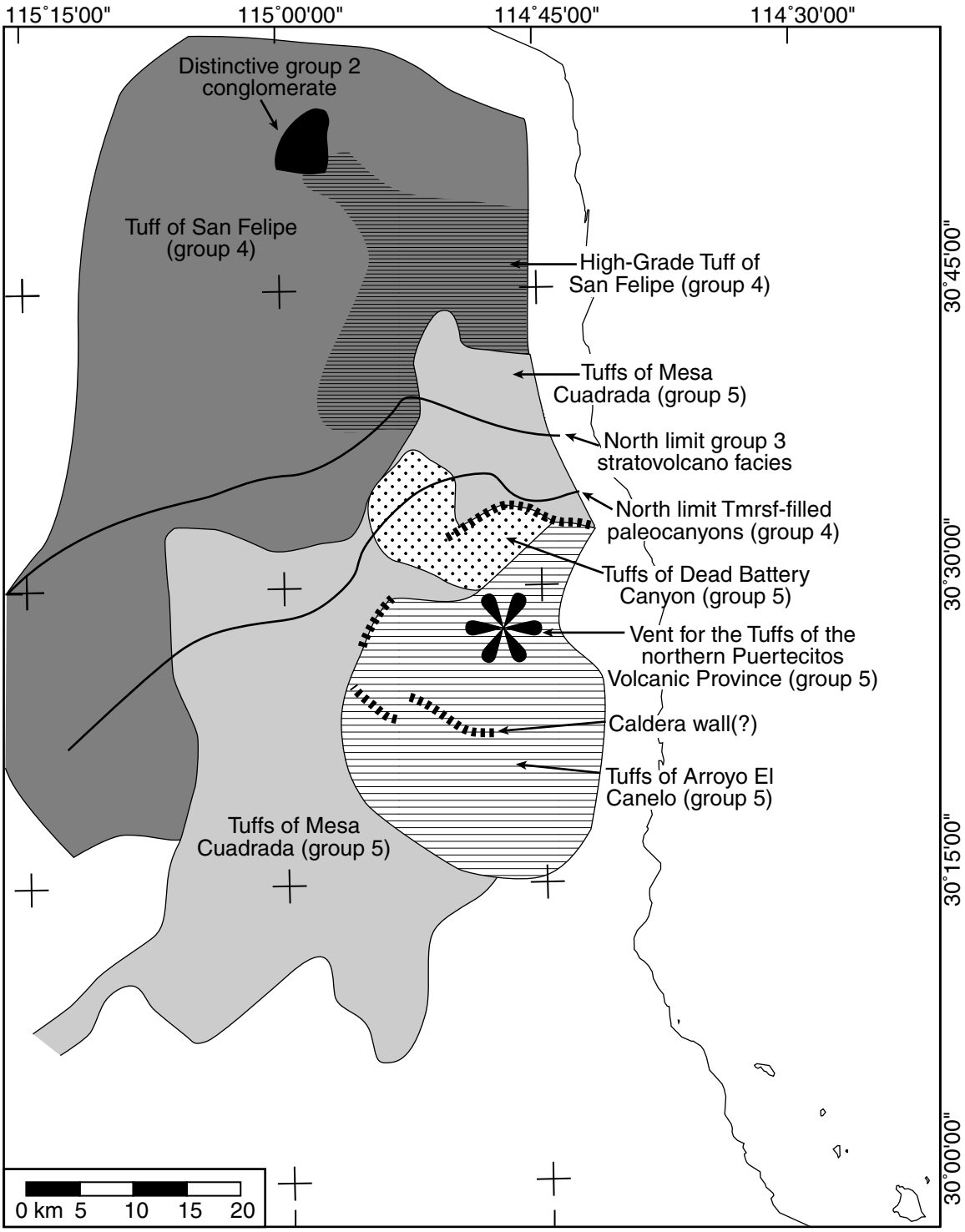

Figure 5.13. Correlative volcanic and sedimentary units in northeastern Baja California. Matching features from stratigraphic groups 1–5 shown. Probable caldera wall features outline group 5 vent area. Shoreline shown for reference only. Areas of ignimbrite distribution shown schematically, with some areas obscured by younger rocks.

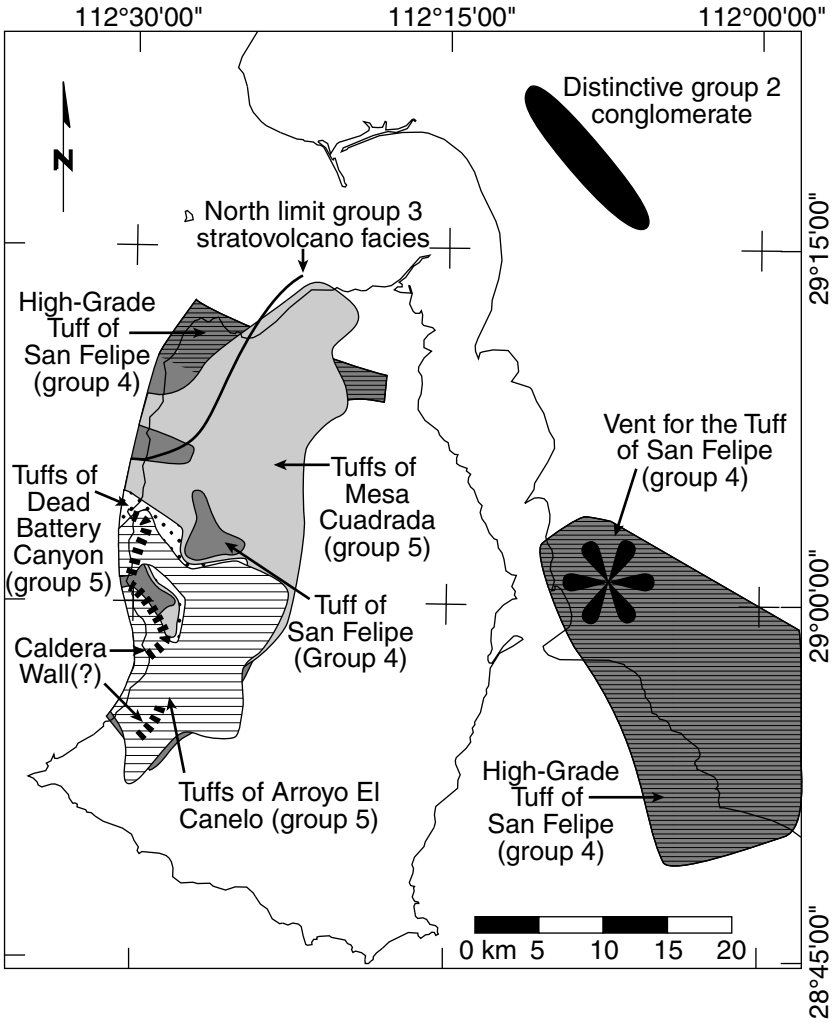

Figure 5.14. Correlative volcanic and sedimentary units on Isla Tiburón and coastal Sonora. Matching features from stratigraphic groups 1–5 shown. Speculative caldera wall features, partially covered by the Tuffs of Arroyo El Canelo, shown near the western shoreline of Isla Tiburón. Modern shoreline shown for reference only. Areas of ignimbrite distribution shown schematically, with some flows obscured by younger rocks.

personal communication, 1998]. Specific correlation of individual plutonic bodies, as has been applied to southern California (e.g., the Mount Lowe intrusive complex of *Dillon and Ehlig* [1993]) has not been attempted for the Gulf of California. Basement outcrops of the Sierra San Fermín and northern Isla Tiburón may prove fruitful for such work in the future.

5.5.2 Group 2: Tertiary basal sedimentary rocks

Tertiary sedimentary strata (group 2) described by *Gastil et al.* [1973] appear to be a robust geologic tie point across the northern Gulf of California. Inspection of the basement-cover transition over a large area of both northeastern Baja California and coastal Sonora confirms that outcrops of the distinctive conglomerate are limited to previously mapped areas [*Gastil and Krummenacher*, 1976; *Bryant*, 1986, distinctive conglomerate on Figs. 5.13 and 5.14]. Outcrop patterns in the Sierra Seri of coastal Sonora suggest a single southwest-directed channel (Figures 5.5 and 5.6). Outcrops in Baja California appear to have been isolated as a terrace deposit by 12.6 Ma. Correlation of these outcrops suggests ∼300 km of displacement across the Gulf of California. The uncertainty of this displacement is difficult to estimate because only remnant outcrops exist in Baja California and the transport distance between the correlative outcrops is unknown. The age of these outcrops is known only to be post-Mesozoic and pre-15 Ma [*Bryant*, 1986]. These strata therefore record the total amount of dextral offset in the Gulf of California since at least Middle Miocene time.

5.5.3 Group 3: Miocene volcanic arc

Arc-related volcanic strata deposited during Early- to Mid-Miocene time (group 3) also form a consistent outcrop pattern across the northern Gulf of California, with andesitic to dacitic eruptive centers in the northern Puertecitos Volcanic Province and southern Isla Tiburón. The northern extent of volcaniclastic deposits probably derived from these centers also matches across the Gulf of California (northern limit

of group 3 stratovolcano facies on Figs. 5.13 and 5.14).

5.5.4 Group 4: The Tuff of San Felipe

The Tuff of San Felipe (group 4) provides a robust match across the northern Gulf of California. It forms the largest volume pyroclastic flow in the study area, comprising 160 km^3 and covering over 4,000 km^2 (Fig. 5.4). This ignimbrite is likely to have erupted from near the present-day mainland Sonora coastline at Punta Chueca (Figs. 5.15 and 5.14). The 12.6 Ma age and stratigraphic position of the Tuff of San Felipe makes this ignimbrite ideal to measure the total dextral displacement across the Gulf of California since the onset of rifting after 11 Ma [*Stock et al.*, 1999].

Distribution of the Tuff of San Felipe west of coastal Sonora occurred through west-trending paleocanyons on Isla Tiburón and in the northern Puertecitos Volcanic Province. A single 3 km-wide paleocanyon in the northern Sierra Kunkaak is the only known pathway for the Tuff of San Felipe between coastal Sonora and western Isla Tiburón. Additional pathways may exist in unmapped areas of the Sierra Kunkaak or beneath the waters of the northern Infernillo channel. On western Isla Tiburón, the Tuff of San Felipe fills west-trending channels cut into volcanic and volcaniclastic strata in the south and basement in the north. On the southern part of the conjugate margin in northeastern Baja California, the Tuff of San Felipe also occupies paleocanyons cut into volcaniclastic strata (Fig. 5.15). Toward the northern Sierra San Fermín and the adjacent Sierra San Felipe, the Tuff of San Felipe formed a sheet ponded above sand dune and fluvial deposits. The thickest and highest-grade deposits of the Tuff of San Felipe occur in the northern Sierra San Fermín and adjacent parts of the Sierra San Felipe, northern Isla Tiburón, and mainland coastal Sonora (High-grade Tuff of San Felipe on Figs. 5.13 and 5.14). The southern limit of the Tuff of San Felipe may also correlate across the Gulf of California but a cover of younger volcanic rocks limits exposures (Figs. 5.13 and 5.14). The northern limit of the Tuff of San Felipe on the Sonoran margin appears to have been controlled by paleotopography. Outcrops north of Isla Tiburón may be flooded by the Gulf of California or

removed by erosion.

Figure 5.15. (next page) Distribution of the Tuff of San Felipe in Baja California, coastal Sonora and Isla Tiburón. stratigraphic thickness measurements in meters shown as numbers. Isopachs of tuff thickness shown as thin black lines. Dashed and dotted lines reflect uncertainty in isopach positions used to calculate tuff volume. 30 m contour interval. Outcrops of the Tuff of San Felipe fill west-trending paleocanyons on Isla Tiburón and the southern quarter of of outcrop area in Baja California. Thicker outcrops of the Tuff of San Felipe on coastal Sonora are related to a probable vent located east of Punta Chueca. The eastern boundary of these isopachs in coastal Sonora was arbitrarily placed east of all mapped outcrops of the Tuff of San Felipe on coastal Sonora. Additional deposits of the Tuff of San Felipe probably exist east of the mapped area.

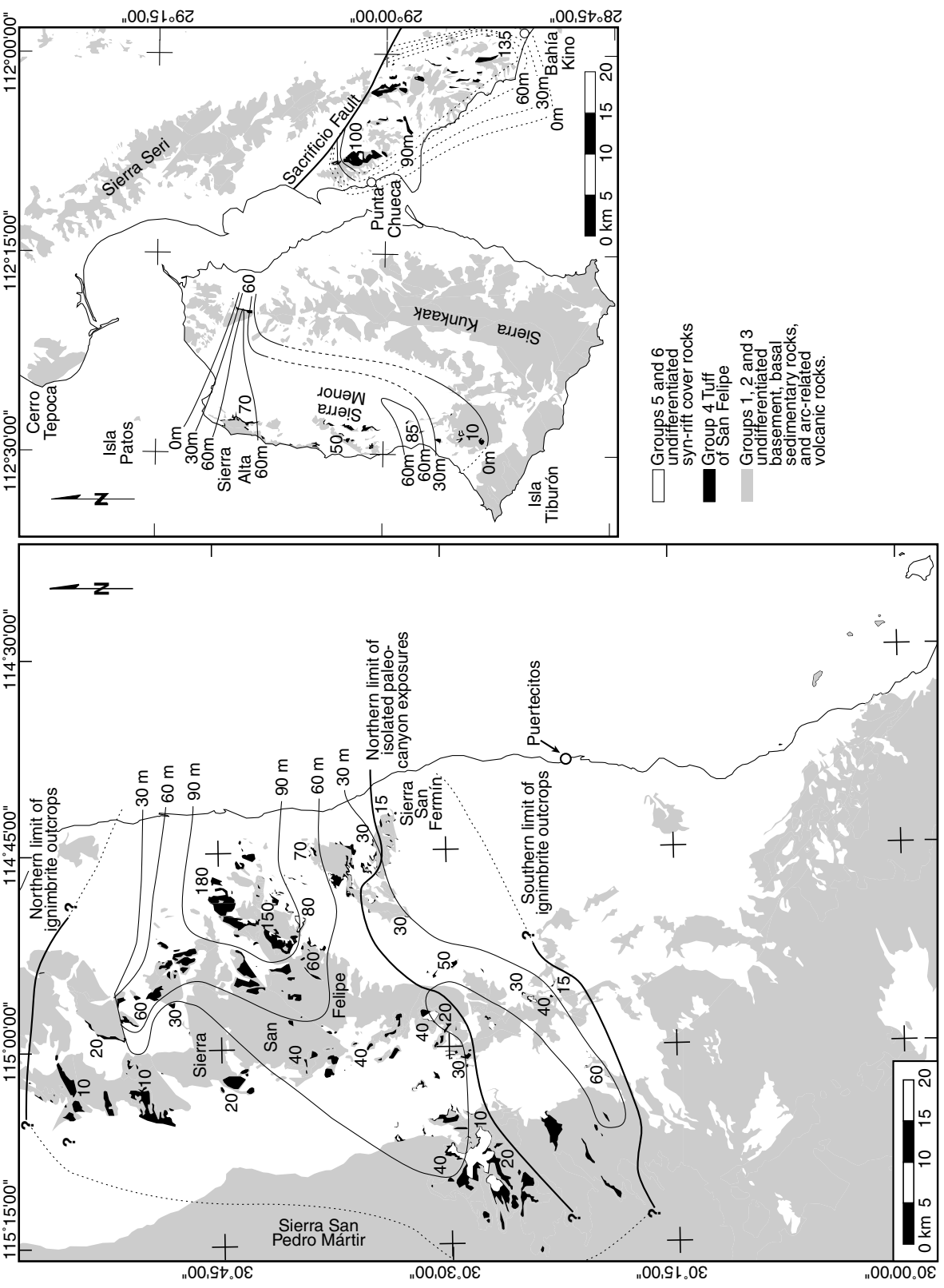
Sierra Seri
Sacrificio Fault
Punta Chueca
Bahía Kino
Cerro Tepoca
Isla Patos
Sierra Alta
Sierra Menor
Sierra Kunkaak
Isla Tiburón
Groups 5 and 6 undifferentiated syn-rift cover rocks
Group 4 Tuff of San Felipe
Groups 1, 2 and 3 undifferentiated basement, basal sedimentary rocks, and arc-related volcanic rocks.
Northern limit of ignimbrite outcrops
Northern limit of isolated paleo-canyon exposures
Puertecitos
Sierra San Fermín
Southern limit of ignimbrite outcrops
Sierra San Felipe
Sierra San Pedro Mártir
0 km 5 10 15 20

Figure 5.15.

Table 5.4. Summary of volume calculations of correlative tuffs.

Location	Maximum Thickness	Volume
	Tuff of San Felipe	
Baja California	180 m	118 km^3
Isla Tiburón	85 m	17 km^3
Coastal Sonora (west of 112°W)	135 m	25.2 km^3
Total (west of 112°W)		160 km^3
	Tuffs of Mesa Cuadrada	
Baja California	180 m	97 km^3
Isla Tiburón	190 m	22 km^3
Total		119 km^3
	Tuffs of Dead Battery Canyon	
Baja California	74 m	2.8 km^3
Isla Tiburón	38 m	1.0 km^3
Total		3.8 km^3
	Tuffs of Arroyo El Canelo	
Baja California	325 m	41 km^3
Isla Tiburón	60 m	9 km^3
Total		50 km^3
	Summary	
Tuffs of the Northern Puertecitos Volcanic Province:[1]		173 km^3
All correlative Tuffs (west of 112°W):		333 km^3

Note: See Tables 2.1 and 3.2 for details of these calculations. Volume measurements do not account for extension of the outcrop area after deposition and may overestimate the volume of tuffs by up to a factor of 2.

[1] The Tuffs of the Northern Puertecitos Volcanic Province include the Tuffs of Mesa Cuadrada, the Tuffs of Dead Battery Canyon, and the Tuffs of Arroyo El Canelo.

5.5.5 Group 5: Early syn-rift deposits

Early synrift volcanic and volcaniclastic deposits are variably useful for correlation across the northern Gulf of California. The Tuffs of the Northern Puertecitos Volcanic

Province each match in detail and are discussed separately in the following sections. Synrift sedimentary strata are confined to north-trending basins aligned parallel to the rift trend and thus are not useful for correlation. The southern termination of these basins at the Matomí accommodation zone in Baja California (Arroyo Matomí, Fig. 5.5) and the La Cruz fault on Isla Tiburón (Fig. 5.6) may indicate that these were once part of a connected transfer zone. Early synrift lava flows are concentrated in two discrete areas, one on western Isla Tiburón and the other in southern Valle Chico. Although these two outcrop areas could not have been juxtaposed originally, sporadic volcanism of this age in the Arroyo Matomí area may have linked them. These strata do not comprise a robust geologic tie point across the Gulf of California.

The Tuffs of Mesa Cuadrada

The distribution and facies of the Tuffs of Mesa Cuadrada correlate closely between northeastern Baja California and Isla Tiburón. These ignimbrites comprise the largest member of the Tuffs of the northern Puertecitos Volcanic Province in both volume and areal extent, covering over 2,000 km^2 with $\sim$120 km^3 of pyroclastic deposits (Table 5.4). The northern extent of outcrops is well exposed in the northern Sierra San Fermín and Sierra San Felipe of Baja California and the Sierra Alta of Isla Tiburón (Figs. 5.13, 5.14, and 5.16). The southern extent of outcrops is well exposed in the Sierra Menor of Isla Tiburón but obscured by younger volcanism in the Puertecitos area of Baja California. Thick, higher-grade deposits of the Tuffs of Mesa Cuadrada crop out adjacent to the eastern part of Arroyo Matomí, in the southern Sierra San

Figure 5.16. (next page) Distribution of the Tuffs of Mesa Cuadrada in Baja California and Isla Tiburón. Numbers denote combined stratigraphic thickness of Tmr3 and Tmr4 outcrops (in meters). Isopachs of tuff thickness labelled with 30 m contour interval. Three areas of non-deposition of the Tuffs of Mesa Cuadrada correspond to paleotopographic highs. Adjacent paleocanyons and basins are filled with up to 190 meters of the Tuffs of Mesa Cuadrada. Tuff thickness changes abruptly near proposed caldera wall features. The eastern edge of tuff distribution was probably controlled by fault-bounded relief east of the Tecomate basin (Fig. 5.6). Isopachs of tuff thickness are inferred to terminate against this boundary.

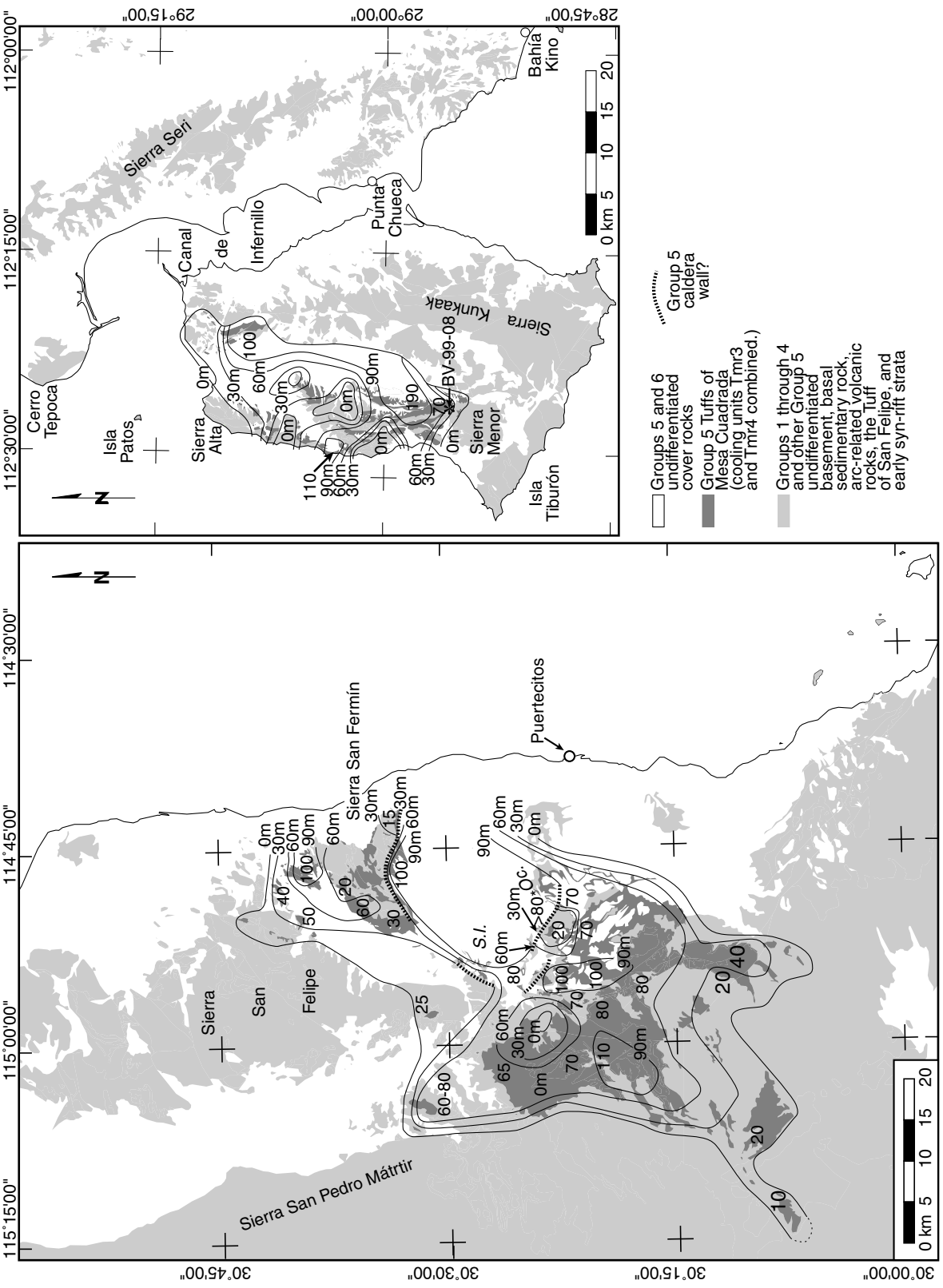
Sierra San Pedro Mártir
Sierra San Fermín
Sierra San Felipe
Puertecitos
S.I.
Oc
Groups 5 and 6 undifferentiated cover rocks
Group 5 Tuffs of Mesa Cuadrada (cooling units Tmr3 and Tmr4 combined.)
Groups 1 through 4 and other Group 5 undifferentiated basement, basal sedimentary rock, arc-related volcanic rocks, the Tuff of San Felipe, and early syn-rift strata
Group 5 caldera wall?
0 km 5 10 15 20
Sierra Seri
Canal de Infernillo
Punta Chueca
Bahía Kino
Isla Patos
Cerro Tepoca
Sierra Alta
Sierra Kunkaak
Sierra Menor
Isla Tiburón
BV-99-08

Figure 5.16.

Fermín, and in the Santa Isabel Wash area in Baja California and in the central Sierra Menor of Isla Tiburón.

Facies changes within the Tuffs of Mesa Cuadrada associated with younger rhyolitic volcanism suggest a vent for this ignimbrite located within a 20–30 km-diameter area centered at the eastern end of Arroyo Matomí. In Baja California, abrupt thickness changes in higher-grade Tmr4 occur southeast of Mesa Cuadrada, at Santa Isabel Wash, and in the southern Sierra San Fermín (Fig. 2.7). These abrupt thickness changes may reflect underlying topographic relief caused by subsidence due to a prior eruption (e.g., Tmr3) and are inferred here to overlie caldera-collapse structures (Figs. 5.13). This same region encloses an area of extensive rhyolite lava flows and Late Miocene and younger andesite volcanos than probably filled in the collapsed area (Fig. 5.5). The thickest deposits of the Tuffs of Mesa Cuadrada on Isla Tiburón are inferred to restore adjacent to this vent area, near the outlet of Arroyo Matomí.

Tuffs of Dead Battery Canyon

The Tuffs of Dead Battery Canyon cover a restricted area on both margins of the northern Gulf of California (Figs. 5.13, 5.14, and 5.17). The maximum thickness of these tuffs occurs where two cooling units (Tmr5 and Tmr6) are present in Baja California. Thick deposits of the Tmr5 cooling unit are present in the Punta Reina area of Isla Tiburón. The Tuffs of Dead Battery canyon are the lowest-volume member of the Tuffs of the Northern Puertecitos Volcanic Province that has been found to correlate across the northern Gulf of California. Known outcrops of the Tuffs of

Figure 5.17. (next page) Distribution of the Tuffs of Dead Battery Canyon in Baja California and Isla Tiburón. Numbers denote outcrop stratigraphic thickness measurements (in meters). Isopachs of tuff thickness labelled with 30 m contour interval. Paleotopography and limited tuff volume probably restricted distribution of the Tuffs of Dead Battery Canyon. Enclosed area of zero thickness indicates a paleotopographic high. A paleocanyon located northeast of this high and a basin located southeast of this high each contain eastward-thinning outcrops of the Tuffs of Dead Battery Canyon. Proposed caldera wall features correspond to abrupt thinning of these ignimbrites from >30 m to <5 m thickness.

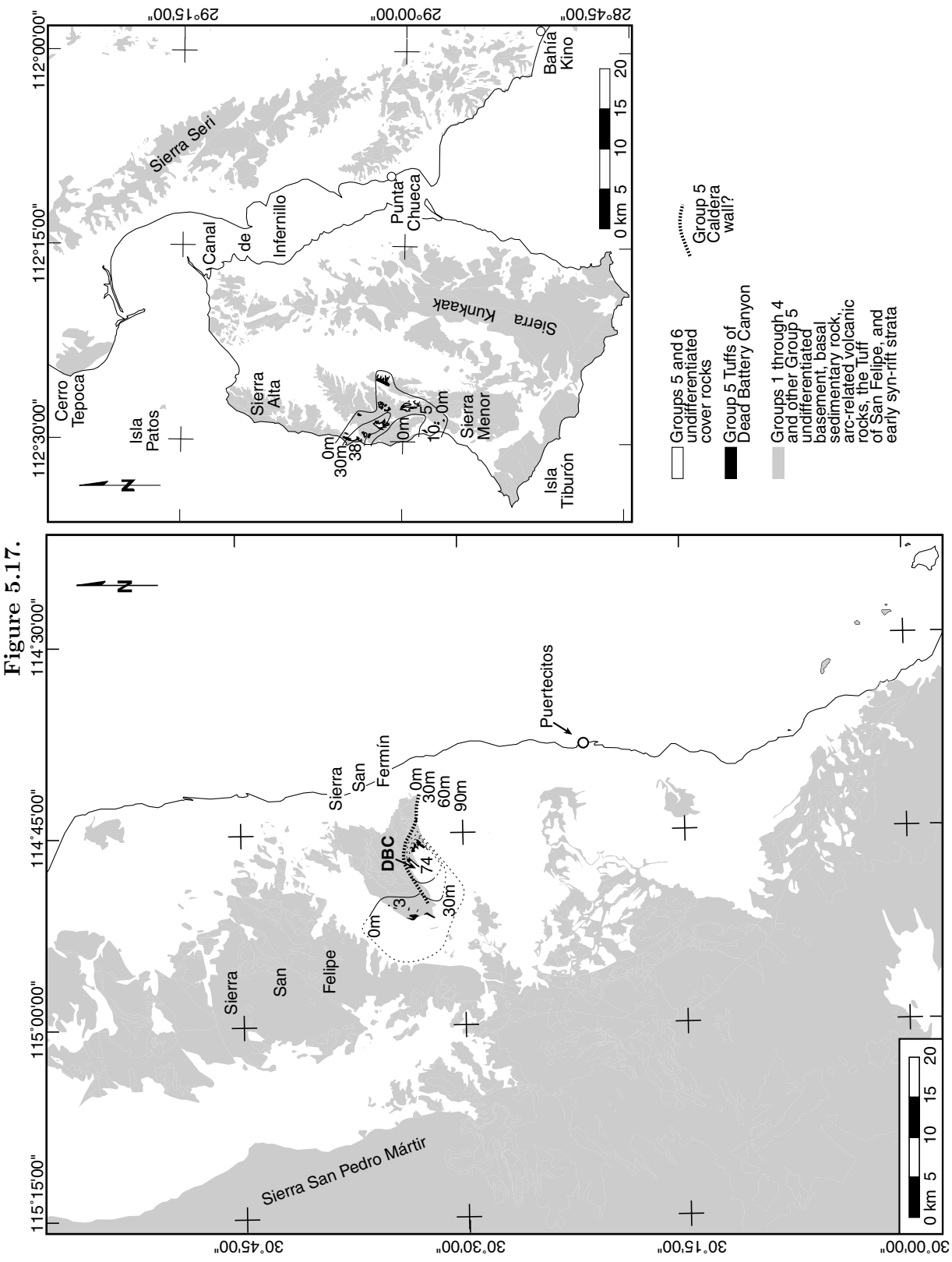
Sierra San Pedro Mártir
Sierra San Felipe
Sierra San Fermín
Puertecitos
DBC
0m
30m
60m
90m
74
3
Sierra Seri
Canal de Infernillo
Punta Chueca
Bahía Kino
Cerro Tepoca
Isla Patos
Sierra Alta
Sierra Kunkaak
Sierra Menor
Isla Tiburón
0 km 5 10 15 20
Groups 5 and 6 undifferentiated cover rocks
Group 5 Tuffs of Dead Battery Canyon
Groups 1 through 4 and other Group 5 undifferentiated basement, basal sedimentary rock, arc-related volcanic rocks, the Tuff of San Felipe, and early syn-rift strata
Group 5 Caldera wall?

Figure 5.17.

Dead Battery Canyon cover 170 km^2 with ∼4 km^3 of pyroclastic deposits (Table 5.4). The northern limit of the Tuffs of Dead Battery Canyon is well exposed in the central Sierra San Fermín of Baja California and the northern Sierra Menor of Isla Tiburón. These ignimbrites thin southward to zero thickness in the Sierra Menor and are buried by younger rhyolite lava flows south of the El Coloradito fault in the Sierra San Fermín. The Tuffs of Dead Battery Canyon do not appear to extend south of Arroyo Matomí in Baja California.

Tuffs of Arroyo El Canelo

The Tuffs of Arroyo El Canelo form the statigraphically highest and most complex member of the Tuffs of the Northern Puertecitos Volcanic Province. The five (or more?) cooling units of the Tuffs of Arroyo El Canelo cover 650 km^2 with ∼50 km^3 of pyroclastic deposits (Table 5.4). Outcrops of the Tuffs of Arroyo El Canelo occur south of the Tuffs of Dead Battery Canyon and partly overlap but extend southeast of the Tuffs of Mesa Cuadrada. This pattern is seen on both margins of the Gulf of California (Figs. 5.13, 5.14, and 5.18). In Baja California, the Tuffs of Arroyo El Canelo crop out primarily south of Arroyo Matomí, except for isolated exposures in the southern Sierra San Fermín. On Isla Tiburón, the Tuffs of Arroyo El Canelo crop out south of Punta Reina and within the central and southern Sierra Menor. On both margins, the northern outcrop limit of the Tuffs of Arroyo El Canelo lies south of the northern outcrop limit of the Tuffs of Dead Battery Canyon. Also, the Tuffs of Arroyo El Canelo crop out farther south than all other correlated ignimbrites. In

Figure 5.18. (next page) Distribution of the Tuffs of Arroyo El Canelo in Baja California and Isla Tiburón. Numbers denote combined stratigraphic thickness measurements of all cooling units (in meters). Isopachs of tuff thickness labelled with 30 m contour interval. Enclosed area of non-deposition of the Tuffs of Arroyo El Canelo corresponds to a paleotopographic high. Tuff thickness changes abruptly near proposed caldera wall features. The eastern edge of tuff on Isla Tiburón was probably controlled by fault-bounded relief east of the Tecomate basin (Fig. 5.6). Isopachs of tuff thickness are inferred to terminate against this boundary.

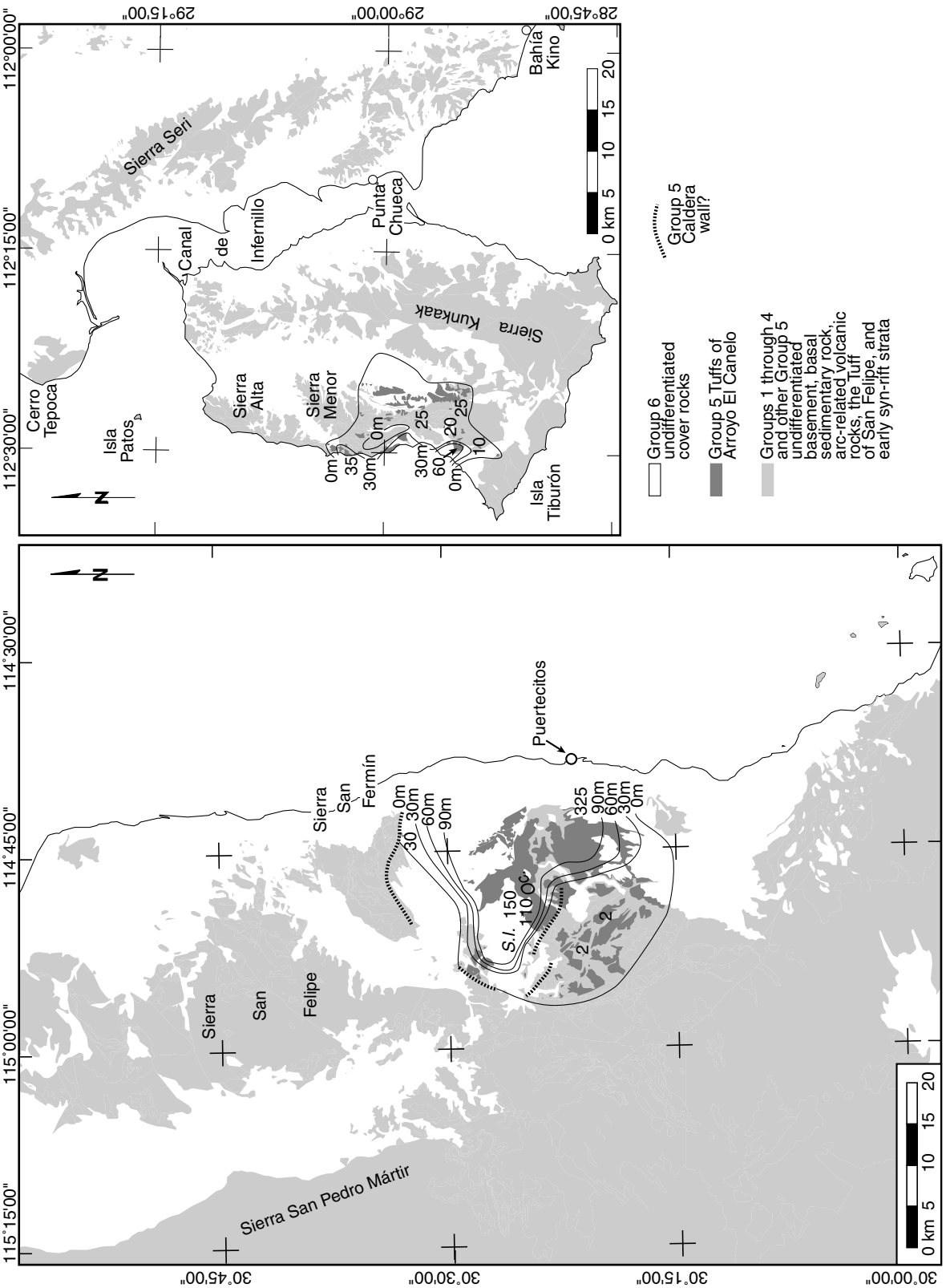
Sierra Seri
Bahía Kino
Punta Chueca
Canal de Infernillo
Sierra Kunkaak
Sierra Alta
Sierra Menor
Cerro Tepoca
Isla Patos
Isla Tiburón
0 km 5 10 15 20
Group 5 Caldera wall?
Group 6 undifferentiated cover rocks
Group 5 Tuffs of Arroyo El Canelo
Groups 1 through 4 and other Group 5 undifferentiated basement, basal sedimentary rock, arc-related volcanic rocks, the Tuff of San Felipe, and early syn-rift strata
Puertecitos
Sierra San Fermín
Sierra San Felipe
Sierra San Pedro Mártir
S.I. 150
110
325
0m
30m
60m
90m
25
20
10
35
2
112°00'00"
112°15'00"
112°30'00"
114°30'00"
114°45'00"
115°00'00"
115°15'00"
28°45'00"
29°00'00"
29°15'00"
30°00'00"
30°15'00"
30°30'00"
30°45'00"

Figure 5.18.

Baja California, the Tuffs of Arroyo El Canelo are mapped as far south as Arroyo Los Heme, west of Volcán Prieto. On Isla Tiburón, the Tuffs of Arroyo El Canelo are mapped as far south as the La Cruz fault.

Thicker, high-grade deposits of the Tuffs of Arroyo El Canelo form a more restricted distribution centered on outcrops of intra-caldera deposits in the eastern Arroyo Matomí area (Fig. 5.13). These deposits are buttressed against paleotopography formed during eruption of the Tuffs of Mesa Cuadrada (caldera wall(?) on Fig. 5.13). These thick deposits occur at least as far south as Arroyo La Cantera, west of Puertecitos. On Isla Tiburón, thick deposits of the Tuffs of Arroyo El Canelo crop out in two areas adjacent to the western coastline. Thick high-grade deposits occur near Bahiá Vaporeta, south of a paleotopographic barrier that was the southern limit of the Tuffs of Mesa Cuadrada. The Tuffs of Arroyo El Canelo may have ponded here on the south side of this barrier. Outcrops of thick, moderately to densely welded Tuff of Arroyo El Canelo occur adjacent to the coastline of Isla Tiburón from the northern part of Bahiá Vaporeta northwards to Punta Reina, where outcrops of this ignimbrite abruptly terminate (Fig. 5.18). These thick deposits are separated by normal faults and buttress unconformities from thinner sections to the east. The difference in stratigraphic thickness may indicate faulting after deposition of the Tuffs of Mesa Cuadrada, possibly related to caldera collapse (caldera wall(?) on Fig. 5.14).

5.6 Discussion

In the following discussion, offset of geologic features across the northern Gulf of California are used to restore Pacific–North America displacement. This analysis builds on the initial study of *Oskin et al.* [2001] which proposed 255 ± 10 km of opening of the Upper Delfín basin in the northern Gulf of California since the 6.3 Ma time of emplacement of Tmr3. Alternative restorations of 245 and 265 km are presented to illustrate the robustness of this reconstruction. Distributed dextral displacement of ignimbrite distributions is shown to support 41±13 km of additional plate bound-

ary motion between Baja California and mainland Sonora. By comparison of these results to plate motion circuit data, *Oskin et al.* [2001] showed that the Pacific–North America plate boundary localized in the Gulf of California during latest Miocene time. A revised compilation of these data presented here that includes distributed deformation of the continental margin further restricts the time of localization of the plate boundary. The record of plate boundary displacement from the Gulf of California is shown to place significant boundary conditions on models of the San Andreas fault system in southern California. Close restoration of conjugate rift margins is also shown to restrict tectonic models for early crustal evolution of the northern Gulf of California ocean basins.

5.6.1 Map-view restoration of conjugate rifted margins

Map-view restoration of conjugate rifted margins of the northern Gulf of California requires 255±10 km of opening of the Upper Delfín basin since eruption of the Tuffs of the Northern Puertecitos Volcanic Province at 6.1 to 6.3 Ma [*Oskin et al.*, 2001, Fig. 5.19 and 5.20]. The azimuths of the Tiburón Fracture Zone and Ballenas Transform faults (310° to 312°, Fig. 5.3, *Fenby and Gastil* [1991]) define the path of restoration. Sonora and Isla Tiburón are rotated 2.3° counterclockwise in map view relative to true north to account for rotation of 4.0° about a modified NUVEL-1A Pacific-North America Euler pole published by *DeMets and Dixon* [1999] (Lat. 50.5°N, Lon. 75.8°W). This restoration path is slightly counterclockwise of a 314° Pacific–North America plate motion vector at Puertecitos calculated with this same Euler pole. Distributed deformation of the Baja California margin described in [*Lewis and Stock*, 1998a] may account for this difference, as discussed later in the following section.

The amount and uncertainty of the 255 km restoration (Fig. 5.19 was determined by the limits of a reasonable fit between tie lines from the Tuffs of the Northern Puertecitos Volcanic Province (Fig. 5.13 and 5.14). The best fit of these tie lines is depicted on the map-view restoration (Fig. 5.19). Fits with 245 km and 265 km

of displacement illustrate the limits of the restoration (Fig. 5.20). The division of dextral displacement onto the Ballenas Transform and the Tiburón Fracture Zone (Fig. 5.3) depends upon the restoration of Isla Angel de la Guarda to an uncertain position south of Isla Tiburón [*Lonsdale*, 1989; *Stock*, 2000]. This uncertainty does not affect the summed dextral displacement measured here.

The distribution of the Tuffs of the Northern Puertecitos Volcanic Province constrains the amount and uncertainty of dextral displacement across the northern Gulf of California since Late Miocene time (Figs. 5.19 and 5.20). In particular, several stratigraphic transitions in the Arroyo Matomí and southern Sierra San Fermín region of Baja California correlate to the Punta Reina region of Isla Tiburón. Here, the Tuffs of Dead Battery Canyon and the Tuffs of Arroyo El Canelo abruptly pinch out above the Tuffs of Mesa Cuadrada. South of this line, thick, high-grade and intracaldera facies of the Tuffs of Mesa Cuadrada and the Tuffs of Arroyo El Canelo surround the inferred eruptive center at Arroyo Matomí. Thick deposits of these units in the central and southern Sierra Menor restore adjacent to the mouth of Arroyo Matomí. North of the southern Sierra San Fermín and Punta Reina, only the Tuffs of Mesa Cuadrada are present. Both the thickness and welding grade of cooling unit Tmr3 decrease northward in the Sierra San Fermín of Baja California and the Sierra Alta of Isla Tiburón.

The distribution of older volcaniclastic deposits preserved in the northern Puertecitos Volcanic Province and Isla Tiburón also matches in the map-view restoration (Figs. 5.19 and 5.20). The Tuff of San Felipe fills west-trending paleocanyons that crop out along the entire western coastline of Isla Tiburón. The Sierra San Fermín and the northern Puertecitos Volcanic Province contain similar paleocanyons filled by the Tuff of San Felipe. The precision of the map-view restoration is not enough to match individual paleocanyons; however, high-grade deposits of the Tuff of San Felipe in the northern Sierra Alta of Isla Tiburón and the northern Sierra San Fermín of Baja California are restored into proximity. A once-continuous cover of the Tuff of San Felipe in the Sierra San Felipe has no known correlative on coastal Sonora. Beneath the

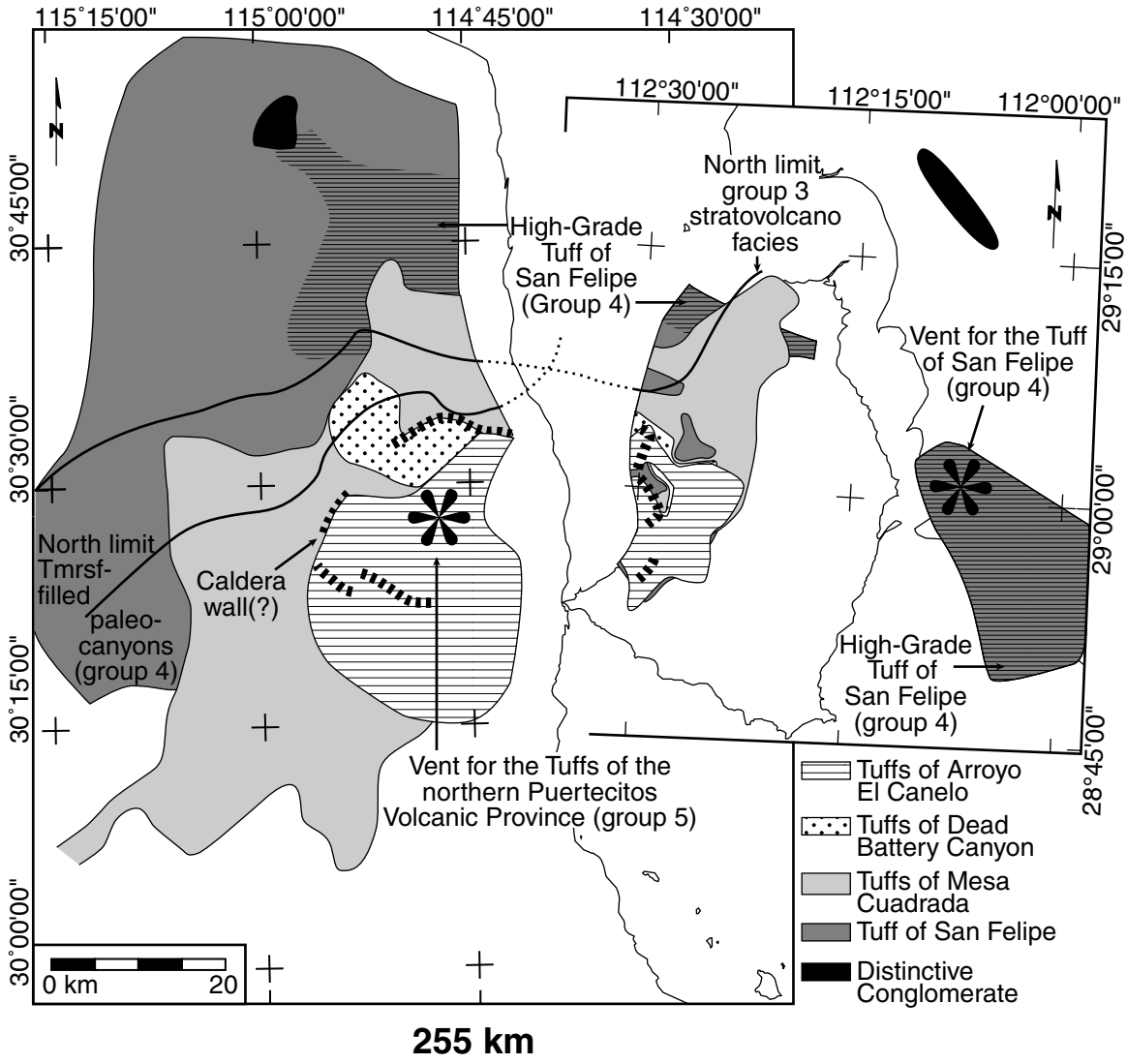

Figure 5.19. Preferred map-view restoration of conjugate rifted margins of the upper Delfín and Tiburón basins in the northern Gulf of California. 255 km of dextral displacement restored along an azimuth of 312° relative to Puertecitos, Baja California. Baja California held fixed. Coastal Sonora and Isla Tiburón shown rotated 2.3° clockwise to account for finite rotation during opening of the Gulf of California. This preferred restoration best matches features near opposite shorelines of the northern Gulf of California in an east-west alignment.

Tuff of San Felipe, volcaniclastic strata of the Early to Mid-Miocene arc also match in distribution on the map-view restoration. These deposits pinch out in the central and northern Sierra San Fermín of Baja California and the southern Sierra Alta of Isla Tiburón. Altogether, restoration of the Tuffs of the Northern Puertecitos Volcanic province also matches the distribution of older volcaniclastic deposits (Figs. 5.19 and 5.20). This result suggests no significant dextral motion between Isla Tiburón and Baja California prior to Late Miocene time.

The detailed reconstruction permitted by matching the distributions of the Tuffs of the northern Puertecitos Volcanic Province also limits the amount of upper continental crust that forms the seafloor of the northern Gulf of California. The width of Miocene continental surface area not accounted for between Isla Tiburón and Baja California is unlikely to exceed the 20–30 km radius of distribution of the Tuffs of Mesa Cuadrada. This unit is the most widespread of the Tuffs of the Northern Puertecitos Volcanic Province (Fig. 5.16). Preservation of the Tuffs of Dead Battery Canyon as a small-volume deposit on both rifted margins may require even less unaccounted crustal area. The gap between opposing rifted margins shown in the map-view restoration is approximately 20 to 25 km (Figs. 5.19 and 5.20), which is consistent with the radius of distribution of the correlative ignimbrites.

Figure 5.20. (next page) Alternative map-view restorations of conjugate rifted margins of the upper Delfín and Tiburón basins in the northern Gulf of California. 245 km and 265 km of dextral displacement restored along an azimuth of 312° relative to Puertecitos, Baja California. Baja California held fixed. Coastal Sonora and Isla Tiburón shown rotated 2.3° clockwise to account for finite rotation during opening of the Gulf of California. The 265 km restoration closely restores the edges of mapped outcrops but misaligns distributions of the Tuffs of Dead Battery Canyon and the Tuffs of Arroyo El Canelo. The 245 km restoration reasonably aligns the extent of correlative ignimbrites but requires a greater missing area of thick high-grade deposits between conjugate rift margins. See Fig. 5.19 for explanation of map symbols and patterns.

Figure 5.20.

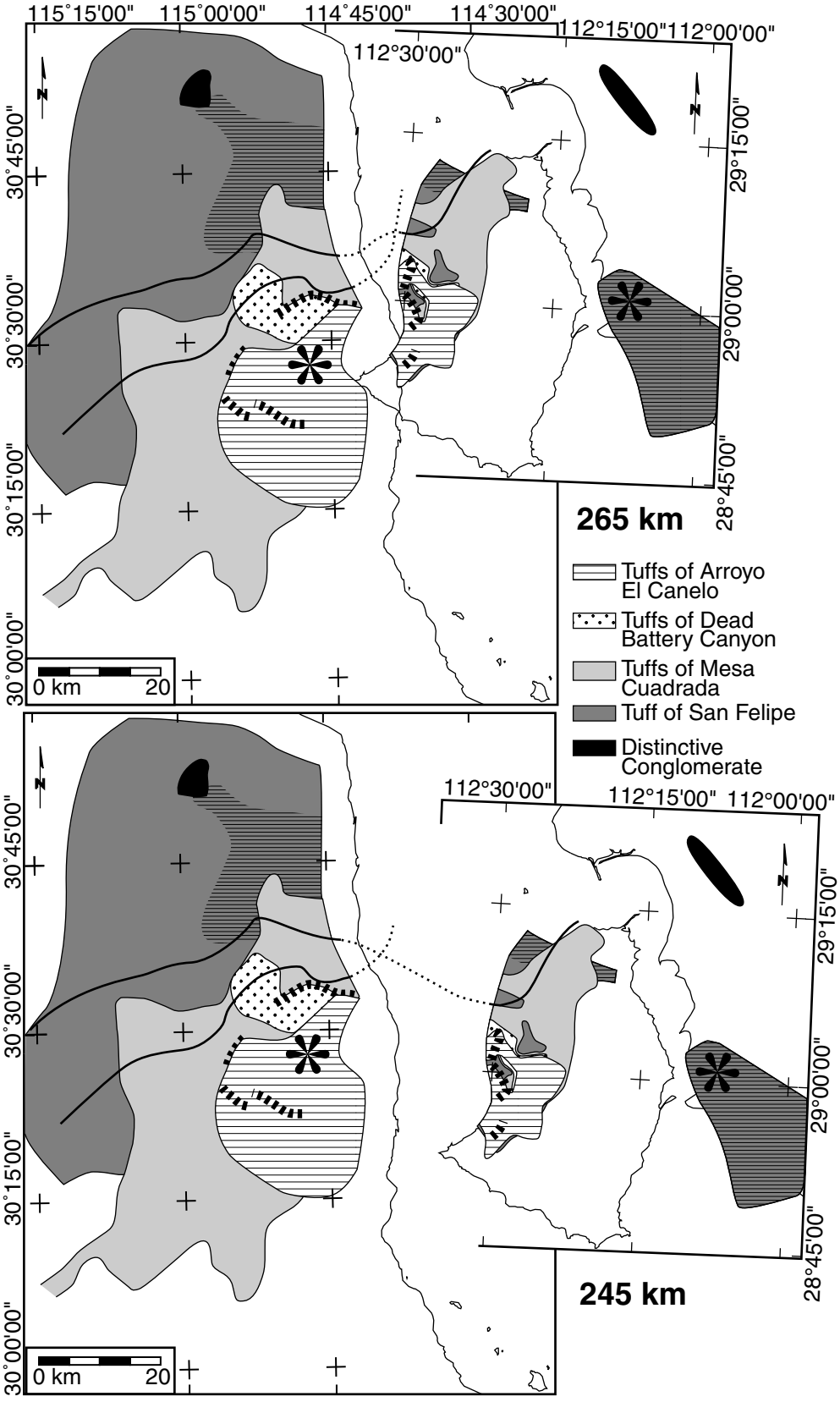
115°15'00"
115°00'00"
114°45'00"
114°30'00"
112°30'00"
112°15'00"
112°00'00"
30°45'00"
30°30'00"
30°15'00"
30°00'00"
29°15'00"
29°00'00"
28°45'00"
265 km
245 km
0 km
20
Tuffs of Arroyo El Canelo
Tuffs of Dead Battery Canyon
Tuffs of Mesa Cuadrada
Tuff of San Felipe
Distinctive Conglomerate

5.6.2 Distributed dextral displacement

Map-view restoration of 255±10 km of opening of the Upper Delfín basin between Isla Tiburón and the coastline of northeastern Baja California provides only a minimum estimate of the total dextral displacement across the Gulf of California Extensional Province. Outside this region, distributed deformation either west of the Baja California coastline or east of Isla Tiburón may have contributed to the total displacement across the Pacific-North America plate boundary. This section will review existing stratigraphic and paleomagnetic evidence to estimate the amount of distributed dextral displacement on both margin study areas (Fig. 5.21).

Two zones of discrete dextral displacement are proposed for the northeastern Baja California continental margin. The Valle de San Felipe fault [*Gastil et al.*, 1975; *Dokka and Merriam*, 1982, and Fig. 5.21] may carry dextral displacement from the Agua Blanca fault (Fig. 5.2) to a zone of distributed deformation in the Puertecitos Volcanic Province. Detailed studies of southern Valle Chico [*Stock*, 1993] correlate volcanic strata on both sides of this proposed fault, limiting significant dextral displacement here. Similarly, the west to northwest-trending Matomí accommodation zone [*Dokka and Merriam*, 1982; *Stock et al.*, 1991] appears to accommodate differential extension and rotation between the Puertecitos Volcanic Province and the Sierra San Felipe [*Nagy*, 2000] and does not carry significant dextral displacement.

Lewis and Stock [1998a] document distributed dextral displacement within the Baja California margin (Fig. 5.21). Their paleomagnetic and structural study proposes 23 ± 9 km of dextral displacement (along an azimuth of 340°) manifested by 30 ± 15° of localized clockwise rotation since eruption of the Tuffs of Mesa Cuadrada (cooling units Tmr3 and Tmr4) ca. 6.3 Ma. The western boundary of the rotating domain is pinned to the Valle de San Felipe fault. The eastern boundary of the rotating domain is proposed to lie just offshore of northeastern Baja California. This rotation occurs within the continental margin of Baja California west of correlative tuff outcrops on Isla Tiburón. When projected onto an azimuth of 314°, parallel to

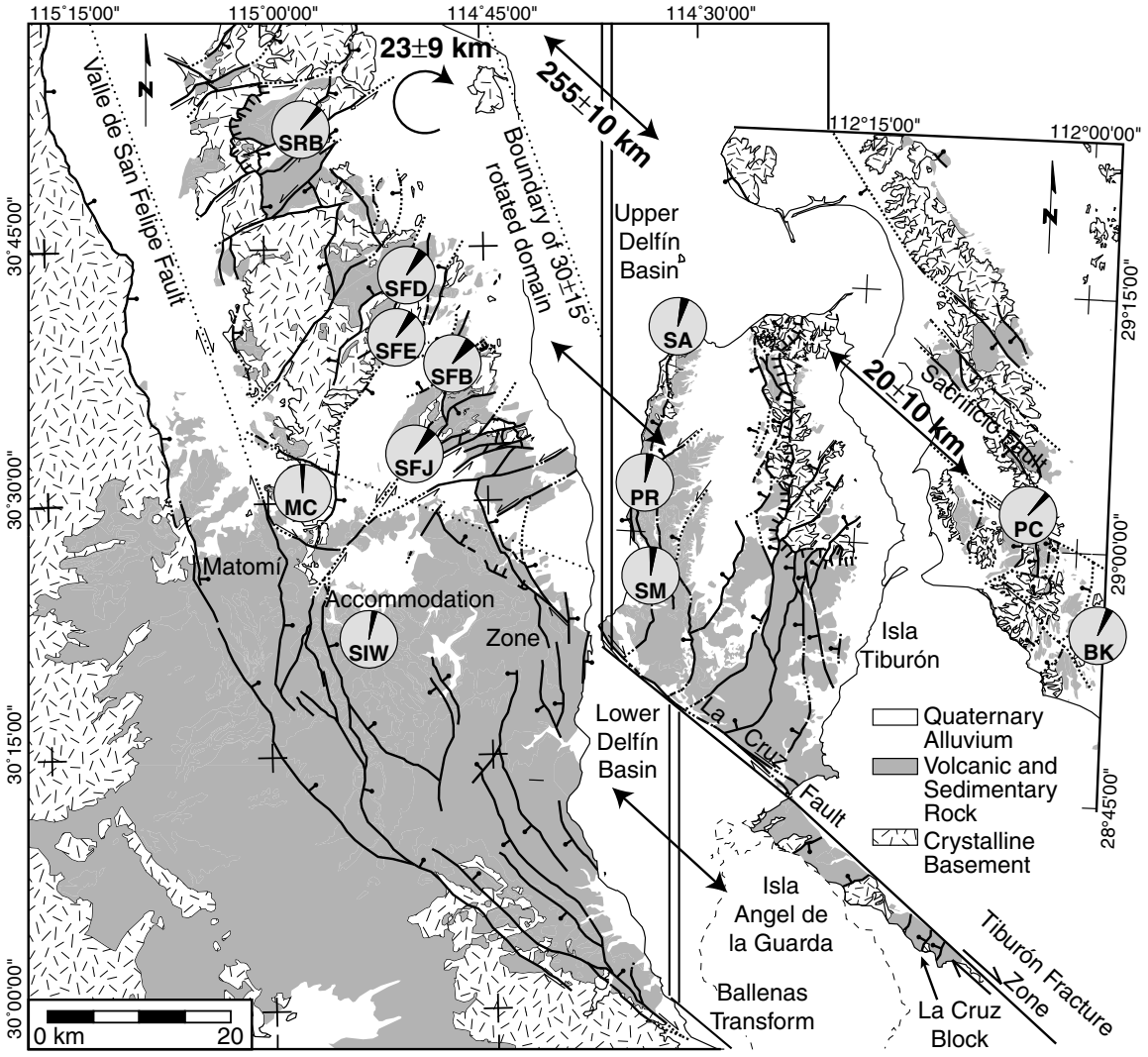

Figure 5.21. Distributed deformation of the continental margins of the Delfín basin. The Gulf of California is shown closed by 255 km between Isla Tiburón and the Baja California. Closure of the Lower Delfín basin shown by restoration of Isla Angel de La Guarda [*Lonsdale*, 1989; *Stock*, 2000]. The La Cruz block is shown restored southeast of Isla Tiburón, adjacent to Isla Angel de la Guarda. The original position of this block is poorly constrained. Paleomagnetic declination anomalies for the Tuff of San Felipe, relative to the MC reference site, shown by circular plots. See Table 5.3 for paleomagnetic remanence values and site names. Faulting on Baja California rift margin resulted in 30±15°of clockwise rotation of outcrops of the Tuff of San Felipe and the Tuffs of Mesa Cuadrada [*Lewis and Stock*, 1998a], which corresponds to 23±9 km of dextral shear along a 340° azimuth. Displacement of Tuff of San Felipe outcrops between Isla Tiburón and coastal Sonora resulted in 20±10 km of dextral displacement. Rotation of tuff outcrops in coastal Sonora is assumed to be a result of this displacement. Additional right-lateral displacement on the Sacrificio fault is unknown at present.

plate motion for northeastern Baja California, this amounts to 21 ± 9 km of displacement accommodated west of the Baja California coastline [*Lewis and Stock*, 1998a]. A vector sum of 23 ± 9 km of dextral displacement at an azimuth of 340° with 255 ± 10 km of opening of the Upper Delfín basin at an azimuth of 312° yields a combined slip vector of 276 ± 13 km (errors summed as root mean squares) at an azimuth of 314°, parallel to the modified Nuvel-1A direction of *DeMets and Dixon* [1999] for Puertecitos.

The La Cruz fault forms a zone of discrete dextral displacement mapped through southern Isla Tiburón. Neither the timing of motion nor the amount of offset across the La Cruz fault are well constrained. The only deposits to correlate across the fault zone are local group six pyroclastic deposits (Fig. 5.6). Group three deposits on either side of the La Cruz fault do not correlate and may indicate a larger amount of dextral and/or normal displacement. The La Cruz fault is interpreted here as an early strand of the Tiburón fracture zone that forms the southern margin of the Upper Delfín segment of the Gulf of California (Fig. 5.3). The block south of the La Cruz fault was probably transferred across the Tiburón Fracture Zone during the earliest stages of opening of the Upper Delfín basin (Fig. 5.21). Slip along this fault therefore should not be included as an additional component of the opening of the Upper Delfín basin.

Two parallel northwest-trending zones of dextral displacement have been inferred on the mainland Sonoran margin. One may underlie the Canal de Infernillo, between the mainland and Isla Tiburón. Offset of high-grade Tuff of San Felipe between Punta Chueca and the northern Sierra Kunkaak suggests 20±10 km of dextral displacement and/or northwest-directed extension across this zone. Basalt flows exposed in both of these areas may also correlate. Another zone of dextral displacement, the NW-striking Sacrificio fault, separates the Bahía Kino–Punta Chueca area on the southwest from the Sierra Seri on the northeast (Figs. 5.6 and 5.21). The total displacement across this structure is difficult to estimate, since none of the volcanic strata match across the fault. However, outcrops of a distinctive conglomerate in the Sierra Seri preclude

displacement on this structure that would sum with other offsets to exceed the ∼300 km estimated for the Gulf of California by *Gastil et al.* [1973]. Since 276±13 km and 20±10 km of displacement (296±17 km total) is already accounted for, strike-slip displacement on the Sacrificio fault is unlikely to exceed a few tens of km. Additional mapping on mainland coastal Sonora and in the Sierra Kunkaak could further constrain the amount of dextral displacement in this region.

Distributed dextral deformation may also be inferred from paleomagnetic declination data from Isla Tiburón and mainland coastal Sonora (Fig. 5.21). Localities on Isla Tiburón show 5–15° clockwise vertical-axis rotation of outcrops of the Tuff of San Felipe relative to reference localities in Baja California. One locality near Punta Reina (PRS on Fig. 5.8) also shows ∼30° rotation of the Tuffs of Mesa Cuadrada (Table 5.3). Overall, however, sample localities on Isla Tiburón show significantly less clockwise vertical-axis rotation than sample localities in Baja California. Therefore, no additional dextral displacement has been added from rotation of localities on western Isla Tiburón. Localities on coastal Sonora show 25–40° clockwise vertical-axis rotation of outcrops of the Tuff of San Felipe (Fig. 5.21). This rotation is here attributed to right-lateral shear in the coastal zone between the Sacrificio fault and Isla Tiburón. Dextral displacement accumulated by rotation of these localities is tentatively equated with displacement of correlative outcrops between Punta Chueca and the northern Sierra Kunkaak by 20±10 km.

In summary, the total distributed dextral displacement within the marginal continental areas of the Gulf of California rift adds 41±13 km of offset to the 255±10 km measured by map-view restoration of correlative ignimbrite strata (Fig. 5.21). 20±10 km is acquired from offset of the Tuff of San Felipe from Punta Chueca to the northern Sierra Kunkaak along an inferred shear zone beneath the Canal de Infernillo. Vertical-axis rotations documented by paleomagnetic studies add 21±9 km of dextral displacement from the Baja California margin [*Lewis and Stock*, 1998a, Fig. 5.21]. Additional dextral displacement contributed by the Sacrificio fault, located between the Sierra Seri and Punta Chueca, is unknown at present. However,

outcrops of a distinctive conglomerate in the Sierra Seri that correlate to outcrops in the Santa Rosa basin in Baja California [*Gastil et al.*, 1973] preclude a large dextral offset across the Sacrificio fault. Based upon the stratigraphic and paleomagnetic arguments presented here, the total amount of opening of the Upper Delfín segment of the northern Gulf of California is 296±17 km along an azimuth of ∼314°.

5.6.3 Timing of dextral displacement

Well-established isotopic ages for the Tuff of San Felipe and the Tuffs of the Northern Puertecitos Volcanic Province constrain timing of dextral displacement in the Gulf of California. Restoration of the Tuffs of the Northern Puertecitos Volcanic Province to Isla Tiburón indicates that this 255±10 km of offset accumulated after emplacement of the Tuffs of Mesa Cuadrada at 6.3±0.3 Ma and the Tuffs of Arroyo El Canelo at 6.1±0.5 Ma. Likewise, vertical axis rotations measured in the continental margin of Baja California also post-date emplacement of these ignimbrites [*Lewis and Stock*, 1998a]. Together, these displacements add up to 276±13 km since 6.1 to 6.3 Ma.

Dextral displacement from eastern Isla Tiburón to the Sacrificio fault accrued after emplacement of the Tuff of San Felipe at ∼12.6 Ma. *Calmus et al.* [2000] report apatite fission-track ages of 6 Ma and 10 Ma for basement exposures near Bahia Kino and the northern Sierra Kunkaak, thereby dating exhumation in this area. These dates may be relevant to the timing of dextral displacement. Other age control on deformation is difficult to obtain because of the lack of rocks younger than the Tuff of San Felipe in these areas. Close examination of synrift sedimentary strata and additional thermochronologic and structural studies of basement exposures are required to further define the post-Middle-Miocene record of deformation here. Displacement on the Sacrificio fault and the distribution of dextral displacement with time since 12.6 Ma are unconstrained.

Few areas of the northeastern Baja California or western Sonora study areas show any definitive evidence for substantial dextral displacement between 12.6 Ma and 6.3

Ma, despite widespread evidence for extension during this time period [*Stock and Hodges*, 1990; *Lee et al.*, 1996; *Lewis and Stock*, 1998b]. East- to northeast-directed extension during this time accommodated a component of displacement parallel to Pacific-North America plate motion [*Stock and Hodges*, 1989]. Locally, this effect was also manifested by minor distributed dextral displacement on the Matomí accommodation zone prior to 6.3Ma [*Nagy*, 2000, and Fig. 5.21]. The onset of clockwise rotation in the Sierra San Fermín [*Lewis and Stock*, 1998b] and opening of the Upper Delfín basin [*Oskin et al.*, 2001] both post-date 6.3 Ma. The consistent restoration of the Tuffs of San Felipe and the Tuffs of the Northern Puertecitos Volcanic province by the same 255±10 km reconstruction (Figs. 5.19 and 5.20) supports the onset of significant dextral displacement in the Gulf of California extensional province after 6.1 to 6.3 Ma [*Oskin et al.*, 2001].

In summary, timing information for dextral displacement between Baja California and mainland coastal Sonora supports substantial dextral displacement of at least 276±13 km from 6.1–6.3 Ma to the present. An additional 20±10 km of displacement occurred sometime between 12.6 Ma to the present in a region lacking dated rocks younger than 12.6 Ma. No evidence firmly supports substantial dextral displacement or opening of the Upper Delfín basin segment of the Gulf of California rift prior to 6.3 Ma, except for a component accommodated by northeast-directed continental extension from 12.6 Ma to 6.3 Ma.

5.6.4 Dextral Pacific–North America plate motion in the northern Gulf of California

Restoration of conjugate rifted margins of Upper Delfín basin of the northern Gulf of California defines the history of dextral plate motion in the Gulf of California (Fig. 5.22). Finite rotations derived from a plate circuit (Atwater and Stock, 1998) define the full Pacific–North America plate motion of ∼760 km along an average azimuth of 304° from 15.1 Ma (chron 5b, time scale of *Cande and Kent* [1995]) to present. Prior

to 12.5 Ma, the Magdelena microplate separated the Pacific plate from the North America plate offshore of southern Baja California [*Mammerickx and Klitgord*, 1982]. Subduction was dextral-oblique during this time [*Atwater*, 1989] and some component of dextral plate boundary motion may have been absorbed within the North American continent. Deposition of the Tuff of San Felipe as a pre-extensional marker indicates that plate-boundary motion probably did not occur within the northern Gulf of California west of coastal Sonora prior to ∼12.6 Ma. After 12.5 Ma, coast-parallel Pacific-North America plate displacement is divided into a component of dextral displacement accommodated across the Gulf of California, primarily after 6 Ma, and a second component of dextral displacement accommodated outside of the Gulf of California, primarily prior to 6 Ma. The age and offset of correlative ignimbrites across the northern Gulf of California and the record of seafloor spreading at the Alarcón basin in the southern Gulf of California (Fig. 5.1) define these components. Continental extension in the Gulf Extensional Province accommodated a significant component of the total plate motion [*Stock and Hodges*, 1989] but contributed little dextral displacement to the Gulf of California prior to 6 Ma.

Seafloor spreading at the Alarcón basin defines the slip history in the Gulf of California from 3.6 Ma to present (Fig. 5.22). *DeMets* [1995] documented that the rate of seafloor spreading here was 10%-15% less than the full Pacific-North America displacement rate prior to 1 Ma. This is shown as a deviation of the rate of motion across the Gulf of California from the Pacific-North America plate-circuit rate (Fig. 5.22). This discrepancy is significant relative to the error for these reconstructions by 3.6 Ma. The rate of seafloor spreading in the Gulf of California in the past one million years is indistinguishable from the full Pacific-North America rate within the uncertainty of recent reconstructions [*DeMets and Dixon*, 1999, and Table 5.5].

Restoration of the correlative ignimbrites across the northern Gulf of California (Figs. 5.19 and 5.21) requires that the Pacific-North America plate boundary and most of its motion was localized in the Gulf of California during or soon after eruption of the Tuffs of the Northern Puertecitos Volcanic Province. Opening of the Upper

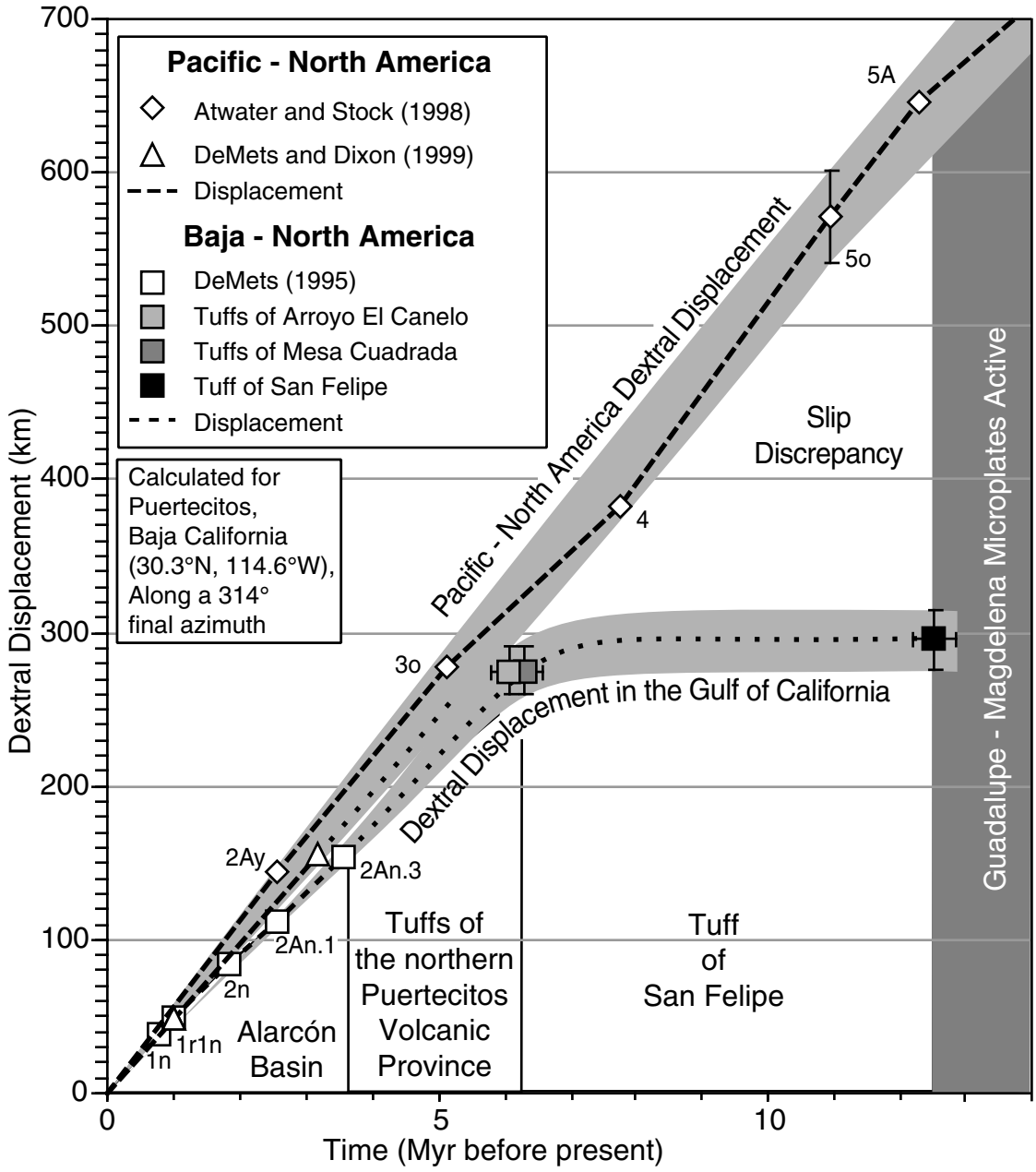

Figure 5.22. Dextral displacement in the Gulf of California relative to Pacific–North America plate motion. Lines on graph indicate displacement with time. Light grey fields indicate uncertainty. The majority of Pacific–North America plate motion since ∼6 Ma occurred in the Gulf of California as constrained by seafloor spreading at the Alarcón Basin [*Lonsdale*, 1989; *DeMets and Dixon*, 1999] and offset of the Tuffs of Northern Puertecitos Volcanic Province. Restoration of the Tuff of San Felipe indicates that Pacific–North America plate motion from 12.5 Ma to ∼6 Ma occurred outside of the Gulf of California. This slip discrepancy may be absorbed by dextral displacement west of the Baja California Peninsula [*Spencer and Normark*, 1979] and/or additional displacement within the southern Basin and Range Province [*Gans*, 1997].

Table 5.5. Comparison of Pacific–North America displacement rates applied to the northern Gulf of California.[1]

Rate[2] (mm/yr)	Time interval[3] (Ma)	Time to 275±13 km[4] (Ma)
Alarcon Rise [*DeMets*, 1995][5]		
47.9±2.1	0–1.03	
41.0±1.9	1.03–3.16[6]	6.6±0.6
Nuvel-1A [*DeMets and Dixon*, 1999][7]		
49.6±0.8	0–3.16[6]	5.5±0.4
Plate Circuit [*Atwater and Stock*, 1998][7]		
∼54	0–5.105	5.1±0.3

[1] Modified from *Oskin et al.* [2001].
[2] Rates calculated for Puertecitos, Baja California, 30.3°N, 114.6°W.
[3] Interval between magnetic anomalies used to calculate rate.
[4] Time required to accumulate 275±13 km between Isla Tiburón and the Puertecitos Volcanic Province.
[5] Motion of Baja California relative to North America measured from magnetic anomalies at the Alarcon Rise (Fig. 5.1).
[6] Rate extrapolated to time required to attain displacement of 275±13 km.
[7] Full Pacific–North America displacement rate.

Delfín basin since this time is at least 276±13 km (Fig. 5.22, Table 5.5). To accumulate this displacement measured from the offset ignimbrites requires extrapolation of the rate of seafloor spreading at the Alarcón basin back to 6.6±0.6 Ma (Table 5.5). This extrapolated age is indistinguishable from isotopic ages of the Tuffs of Mesa Cuadrada (6.3±0.3 Ma, Lewis, 1996) and the Tuffs of Arroyo El Canelo (6.1±0.5 Ma, Nagy et al., 1999). If the full Pacific-North America rate of motion [*DeMets and Dixon*, 1999] were accommodated in the Gulf of California, 276±13 km of displacement would have accumulated in 5.5±0.4 m.y. (Table 5.5). Separation of outcrops of the ∼12.6 Ma Tuff of San Felipe from Isla Tiburón to Baja California does not require any additional dextral offset here prior to 6.3 Ma. These results indicate that the Pacific-North America plate boundary localized in the Gulf of California during a short interval (1 to 2 m.y.) during latest Miocene time. Additional plate boundary slip measured within coastal Sonora and between coastal Sonora and Isla Tiburón may reduce the interval of localization of the plate boundary or be attributed to pre-6 Ma slip. However, the majority of Pacific-North America plate boundary motion from 12.5 Ma to 6.3 Ma must have occurred outside of the Gulf of California (Fig. 5.22).

The slip history presented here (Fig. 5.22) provides a test of existing models for opening of the Gulf of California. *Lonsdale* [1989] proposed that 50 km of seafloor spreading between Baja California and North America occurred at the Maria Magdalena Rise from 5 or 6 Ma until the onset of spreading at the Alarcón Rise at 3.6 Ma. The 276±13 km of offset measured across the northern Gulf of California requires 120±10 km more displacement than is recorded in the Alarcón basin. Seafloor spreading at the Maria Magdalena Rise, with additional displacement on the continental margins of the mouth Gulf of California during this time interval, would satisfy the amount of opening measured across the northern Gulf of California. *Umhoefer et al.* [1994] proposed acceleration of the Baja California-North America displacement rate at 3.5 Ma. A detailed resolution of dextral displacement in the Gulf of California prior to 3.5 Ma is not possible with the current geologic data. However,

the total amount of slip recorded in the northern Gulf of California since 6.1±0.5 Ma cannot accommodate significant acceleration of the displacement rate in the Upper Delfín basin at 1 Ma and 3.5 Ma [*Oskin et al.*, 2001]. In either case, the majority of Pacific-North America plate motion must have been accommodated in the Gulf of California since at least 5.5±0.4 Ma to 6.1±0.5 Ma.

5.6.5 Implications for dextral Pacific-North America plate motion in southern California

Models for the development of the Pacific-North America plate boundary in southern California imply a variety of displacement histories for the Gulf of California. This complexity increases uncertainty from addition of displacement from multiple transform faults and several zones of diffuse deformation [*Dickinson*, 1996, for example]. The slip history presented here for the northern Gulf of California (Fig. 5.22) provides a new constraint with which to evaluate these models, independent of the tectonic complexity of southern California. Recent efforts to summarize the amount of deformation in central California successfully reconcile Pacific-North America motion measured from continental deformation and plate circuit data [*Dickinson and Wernicke*, 1997; *Atwater and Stock*, 1998]. Similarly, displacement and timing information from the Gulf of California reconciles the majority of plate boundary motion in northwestern Mexico since ∼6 Ma (Fig. 5.22). In southern California, these data require that most of the dextral shear transmitted through the Transverse Ranges to the Salton Trough (Fig. 5.2) occurred after ∼6 Ma.

Most models of the San Andreas fault system in southern California are compatible with offsets and timing measured in the northern Gulf of California, despite a range of slip estimates for the southern San Andreas fault from 150–180 km [*Matti et al.*, 1992] to 240 km [*Ehlig et al.*, 1975]. When summed with additional displacement for other structures away from the San Andreas fault trace, both slip estimates overlap or exceed the 276±13 km of dextral displacement measured for the northern Gulf of

California since 6.1 to 6.3 Ma. The most significant of these additional displacements are 12±2 km of slip from the Elsinore fault [*Hull and Nicholson*, 1992], 45–75 km of shear by rotation of the Eastern Transverse Ranges [*Richard*, 1993; *Dickinson*, 1996], and possibly up to 22 km of slip on the Agua Blanca fault [*Allen et al.*, 1960]. Addition of slip from the Agua Blanca fault to the Gulf of California is problematic because this fault appears to terminate before reaching the Gulf Extensional Province [*Allen et al.*, 1960]. 26±2 km of slip on the San Jacinto fault [*Sharp*, 1967] is included with estimates for the San Andreas fault.

If only 150–180 km of slip has occurred on the southern San Andreas fault [*Matti et al.*, 1992], the total dextral displacement measured in the northern Gulf of California requires a considerable amount of slip on the San Gabriel fault. Adding 60±5 km of slip measured for the western San Gabriel fault [*Crowell*, 1974] yields a total of 289±18 to 300±21 km dextral displacement from southern California that would have been transferred into the Gulf of California [*Dickinson*, 1996]. These values overlap the 296±17 km total displacement estimate for the northern Gulf of California. An acceptable match is also obtained by adding only 22±1 km slip measured for the north branch of the San Gabriel fault [*Ehlig*, 1981], yielding a total of 269±13 to 280±16 km dextral displacement transferred into the Gulf of California [*Dickinson*, 1996]. These estimates both support the conclusion that dextral displacement in the Gulf of California from 12.5 Ma to 6.3 Ma probably does not exceed the 20±10 km estimate for displacement and rotation of outcrops of the Tuff of San Felipe east of Isla Tiburón.

Alternatively, higher estimates of displacement for the southern San Andreas Fault [*Ehlig et al.*, 1975; *Powell*, 1993] could require up to 390±20 km of dextral displacement in northwest Mexico [*Dickinson*, 1996]. To accommodate this slip would require ∼100 km of dextral displacement east of the Gulf of California, most of which would have had to occur prior to 6.3 Ma. Significant problems remain in reconciliation of this higher slip value in southern California [*Richard*, 1993]. Existing data from northwest Mexico cannot rule out substantial dextral displacement east of the Gulf

of California during Miocene time. Ultimately, up to 350 km of dextral displacement is required in northwest Mexico from 12.5 Ma to 6.3 Ma (slip discrepancy on Fig. 5.22). Most of this slip is usually assigned to the Tosco-Abreojos fault zone west of Baja California [*Spencer and Normark*, 1979; *Lyle and Ness*, 1991]. However, observations from southern California, and evidence for strike-slip faulting east of Isla Tiburón [*Gastil and Krummenacher*, 1977] and in southeastern Sonora [*Gans*, 1997], indicate that additional fieldwork is necessary to address the distribution of dextral shear during Mid- to Late-Miocene time.

5.6.6 Implications for crustal structure of the northern Gulf of California

Foundered upper continental crust forms only a small component of the crust of the Upper Delfín basin of the northern Gulf of California (Figs. 5.3 and 5.21). The proximity of restored conjugate rifted margins of the Upper Delfín basin segment of the rift indicates that the missing width of continental surface area is unlikely to exceed 25 km. This result implies that if uniform crustal stretching had occurred, a minimum of 1000% northwest-directed extension is required to form the present width of this segment of the northern Gulf of California. Seismic refraction and gravity studies of the northern Gulf of California indicate a crustal thickness of 13 to 21 km [*Phillips*, 1964; *Couch et al.*, 1991; *Gónzalez-Fernández et al.*, 2000; *Lewis et al.*, 2001]. To generate this thickness of new crust across the present width of the Gulf of California required a significant addition of crustal material. None of this material appears to be normal oceanic crust generated by seafloor spreading [*Lonsdale*, 1989]. Paradoxically, the crustal thickness of the northern Gulf of California is two to three times that of normal oceanic crust. Also, seismic P-wave velocity (6.4–6.8 km/s) and density estimates (2.75–2.85 g/cm^3) for most of this crust are too low to be oceanic lithosphere (Fig. 5.23). Some of the thickest crust in the northern Gulf of California (20 to 21 km) underlies the southeastern portion of the Delfín basin segment [*Phillips*,

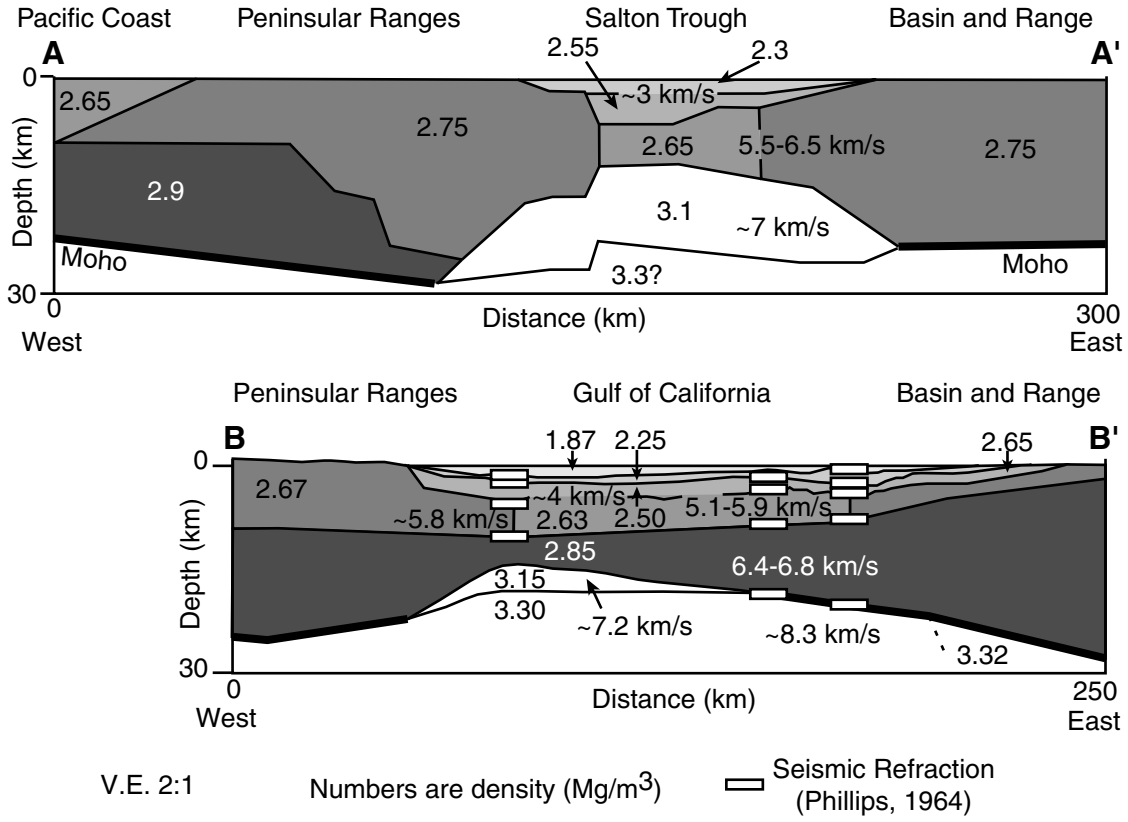

Figure 5.23. Crustal-scale cross sections of the Salton Trough and the northern Gulf of California. See Fig. 5.1 for cross-section locations. A-A' from *Fuis et al.* [1984], B-B' from *Couch et al.* [1991]. Numbers and shading indicate crustal density in g/cm^3 modeled from gravity and P-wave velocity. P-wave velocities shown in km/s. The crust of the northern Gulf of California ranges from 13–21 km thickness with a smooth transition to the continental margins of the Gulf of California.

1964; *Gónzalez-Fernández et al.*, 2000], which is proposed to be part of the earliest-formed crust in the northern Gulf of California [*Lonsdale*, 1989; *Stock*, 2000].

Several possible origins for generating new, thick crust beneath the northern Gulf of California have been proposed. Most models include significant areas of extended continental crust [*Curray et al.*, 1982; *Fuis et al.*, 1984; *Lonsdale*, 1989]. However, close correlation of conjugate rifted margins of the Upper Delfín basin of the northern Gulf of California precludes significant pure-shear type extension of the continent. *Fuis et al.* [1984] and *Lonsdale* [1989] also propose intercalation of sediments and basaltic melts to produce a composite crust beneath the Gulf of California and the Salton Trough. Similarly, *Nicholas* [1985] proposed that metasomatized upper mantle

in direct contact with metamorphosed sediments may form the crust of the Salton Trough.

Intercalation of sediments and basaltic melts to produce a composite crust is an appealing mechanism for Mid-Pliocene and later crustal formation in the Gulf of California. Large volumes of sediment necessary to at least double the thickness of normal igneous oceanic crust (from 7 to >14 km) require substantial sedimentary input from the Colorado River, which emptied into the Gulf of California by 4.3 Ma [*Winker and Kidwell*, 1986]. The catchment area, sediment discharge, and extent of recent sedimentary deposits from the Colorado River far exceeds those of other rivers in the northern Gulf of California drainage basin [*Van Andel*, 1964]. A crude estimate of the volume of sediment contained in the northern Gulf of California may be obtained by assuming an average thickness of 10 km of decompacted sediment in the Gulf basins from Isla Tiburón to the Salton Trough,

$$500km \times 120km \times 10km \quad = \quad 6.0 \times 10^5 km^3. \tag{5.1}$$

This estimate requires an average sedimentation rate of at least 2 mm/yr, which is consistent with measurements of Holocene sedimentation rate from a core in the Lower Delfín basin [*Van Andel*, 1964, core R-190 of the 'Sal Si Puedes basin'] and Pliocene sedimentation rates from the Fish Creek basin of the Salton Trough [*Johnson et al.*, 1983].

To check whether a large fraction of crust in the Northern gulf of California could have come from sediment carried by the Colorado River, the sedimentary input estimated above is compared to erosional denudation of the Colorado River drainage basin. The largest area of this basin is comprised of the Colorado plateau, and the sediment estimated to be contained in the northern Gulf of California is equivalent to 750 m of denudation, on average, of the Colorado Plateau by the Colorado River system,

Figure 5.24. (next page) Crustal sections of the Upper Delfín basin rift segment at ∼5 Ma illustrating three possible modes of early crustal formation in the northern Gulf of California. All solutions presented here are compatible with constraints from restoration of the Upper-Delfín basin. Continental margin cross sections based on *Stock* [1993], *Lewis* [1994], and Chapter 6 of this thesis. A, intercalation of sediments and basaltic intrusions with basaltic underplating [*Fuis et al.*, 1984]. *Nicholas* [1985] suggested a similar mechanism with metasomatized mantle in place of basaltic underplating. B, Normal oceanic crustal formation in a starved to moderately sedimented basin. This is similar to oceanic basins in the southern Gulf of California. C, Exhumation of middle to lower continental crust to form a metamorphic core complex.

$$800km \times 1000km = 8.0 \times 10^5 km^2, \tag{5.2}$$

$$\frac{6.0 \times 10^5 km^3}{8.0 \times 10^5 km^2} = 0.75km. \tag{5.3}$$

This is consistent with recent estimates of post-Eocene denudation of the Colorado Plateau by an average of 1.2 km [*Pederson*, 2000]. However, the analysis presented here assumes that most of the denudation of the Colorado Plateau has occurred since 4.3–5.5 Ma, i.e. since the time when the Colorado River first emptied into the northern Gulf of California [*Winker and Kidwell*, 1986, 1996]. Also unanswered from this analysis is how crustal formation occurred during the earliest opening of the Gulf of California, prior to arrival of the Colorado River.

Three alternative solutions are proposed here for formation of thick crust in the northern Gulf of California during Late Miocene and early Pliocene time (Fig. 5.24). The first alternative is that sediment supply from other river systems emptying into the nascent northern Gulf of California basins may have provided enough material to form transitional crust through the mechanisms proposed by *Fuis et al.* [1984] or *Nicholas* [1985]. These river systems would principally be those that drained the Sierra Madre Occidental (Fig. 5.1). Evidence suggests, however, that the sediment flux from these rivers was unlikely to have been able to contribute enough material to help generate ∼20 km-thick crust. Firstly, early sedimentary records from the northern Gulf of California indicate deep-water conditions and lower sedimentation

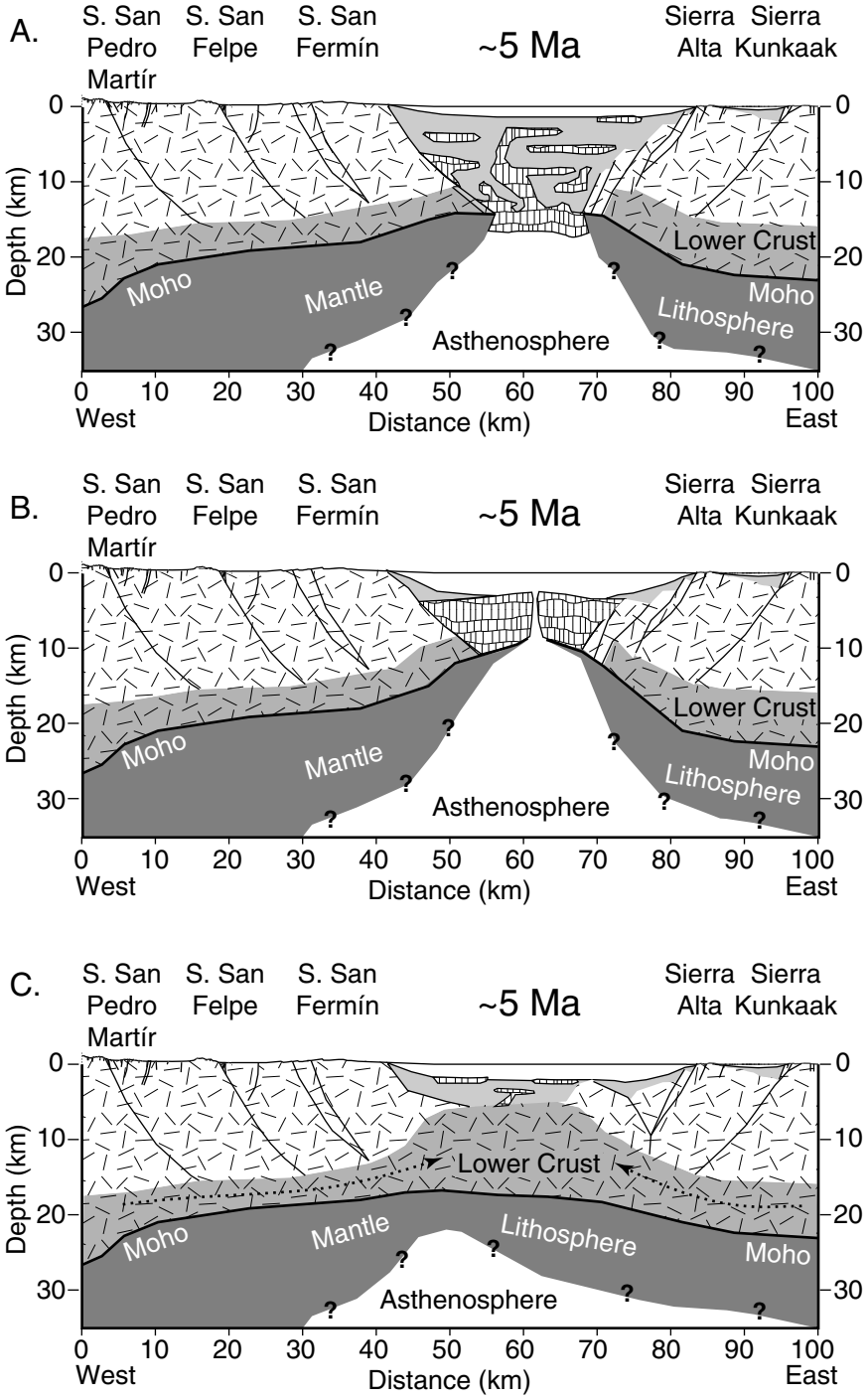
A.
S. San Pedro Martír
S. San Felpe
S. San Fermín
~5 Ma
Sierra Alta
Sierra Kunkaak
Depth (km)
Lower Crust
Moho
Mantle
Asthenosphere
Lithosphere
Moho
West
Distance (km)
East
B.
S. San Pedro Martír
S. San Felpe
S. San Fermín
~5 Ma
Sierra Alta
Sierra Kunkaak
Depth (km)
Lower Crust
Moho
Mantle
Asthenosphere
Lithosphere
Moho
West
Distance (km)
East
C.
S. San Pedro Martír
S. San Felpe
S. San Fermín
~5 Ma
Sierra Alta
Sierra Kunkaak
Depth (km)
Lower Crust
Moho
Mantle
Lithosphere
Asthenosphere
Moho
West
Distance (km)
East

Figure 5.24.

rate [*Boehm*, 1984; *Johnson et al.*, 1983; *Winker and Kidwell*, 1996]. Secondly, in the central and southern Gulf of California, where sediment input is only from rivers that drain the Sierra Madre Occidental, the crust is only 7 to 9 km thick [*Phillips*, 1964]. The crust of the southern Gulf of California is structured similar to normal oceanic crust, unlike the northern Gulf of California [*Phillips*, 1964].

A second alternative mechanism for crustal formation is that 7 to 9 km thick normal oceanic or transitional crust formed early in the history of the Gulf of California. This crust was then later overwhelmed by sedimentation by the Colorado River after ∼5 Ma. Seismic and gravity studies in the northern Gulf of California [*Phillips*, 1964; *Couch et al.*, 1991; *Gónzalez-Fernández et al.*, 2000] have yet to detect this crust, which would presumably be of higher density and P-wave velocity.

A third alternative is that large-magnitude continental extension may have exhumed an area of middle to lower continental crust to form part of the seafloor of the northern Gulf of California. This mechanism could produce new crustal area with the appropriate seismic velocity and density structure without loss of pre-extension crustal surface area. Mid-crustal rocks exposed in the Monte Blanco dome of northeastern Baja California [*Axen et al.*, 2000, see Fig. 5.1] are an example of this process. Predicted densities of mid-crustal rocks beneath the northern Gulf of California [*Couch et al.*, 1991] are similar to the density (2.8 to 2.9 g/cm^3) of the mid-crustal fluid layer proposed by *Wernicke* [1990]. However, P-wave velocities of the mid-crustal layer in the Gulf of California (6.4–6.8 km/s, *Phillips* [1964]) are slightly higher than for the middle crust beneath nearby continental metamorphic core complexes of southeastern California (6.35–6.5 km/s, *McCarthy et al.* [1991]).

If lower crustal flow has formed a significant volume of new crust beneath the northern Gulf of California then the consequences of this transfer of crustal material may be subtle. Strain partitioning by lower crustal flow is not necessarily expressed by equal amounts of upper and lower crustal extension and this extension may be unevenly distributed [*Wernicke*, 1990]. Thus, the record of faulting on the rift flank may not indicate transfer of a significant volume of lower- or mid-crustal material to

form the crust of the Gulf of California. Regional subsidence of the rift flank will result from removal of buoyant continental crust from below [*Driscoll and Karner*, 1998, for example]. In the case of the Gulf of California, thermal buoyancy or thermal subsidence from earlier basin and range extension may mask these effects. Only later in the rift history would regional subsidence indicate thinning of the lower crust beyond that accommodated by subaerially exposed fault systems.

One likely effect of exhumation of lower continental crust to form the crust beneath the northern Gulf of California would be thinning of the continental crust approaching the rift margin from outside the rift [*Wernicke*, 1985]. This would result because the pressure gradient driving lower crustal flow would be highest adjacent to the rift flank, thus drawing more material from regions closest to the Gulf of California. The length scale over which this process would operate is poorly known at present [*Wernicke*, 1990]. However, crustal thickness estimates for the Basin and Range province of southeastern California do indicate gradual thinning of the crust from 27 km to 22 km from the northeast side of the Chocolate Mountains to the Salton Trough [*Parsons and McCarthy*, 1996, and Figs. 5.1 and 5.23]. Moho depths beneath the Peninsular Ranges of southern California shallow from 37 km to 25 km approaching the Salton Trough from the west [*Ichinose et al.*, 1996; *Lewis et al.*, 2000; *Magistrale et al.*, 2000]. A similar step also exists beneath Peninsular Ranges of northeastern Baja California [*Couch et al.*, 1991; *Lewis et al.*, 2001]. Existing data from the Sonoran margin are too sparse to evaluate crustal thickness changes approaching the rift flank at this time. If crustal thickness variations observed on the rift flanks are related to extension, as suggested by *Lewis et al.* [2001], and these variations imply thinning of the crust in excess of that observed from the upper crustal extension of the rift flank after 6 Ma, then these features would require continental lower-crustal flow beneath the northern Gulf of California to accommodate lower crustal thinning. This mechanism would provide a viable continental origin for at least part of the crust of the northern Gulf of California that would conserve crustal surface area on the rift flanks.

In summary, several modes of crustal formation may have operated in the north-

ern Gulf of California. Together, all of these processes must conserve crustal surface area of the rift margins. Crustal structure of the most active, western half of the northern gulf of California [*Couch et al.*, 1991] and recent volcanism in the Salton Trough [*Herzig and Jacobs*, 1994] both support crustal formation in the absence of older continental crust. Crustal formation since middle Pliocene time has involved a substantial contribution of sediment from the Colorado River [*Fuis et al.*, 1984]. Other areas of crust in the northern Gulf of California, especially areas formed prior to ∼5 Ma, may be formed in part by exhumed middle to lower continental crust. Isotopic studies of volcanism within the northern Gulf of California basins may directly determine the presence of continental crust here. Additional field study of tectonism and subsidence of the rift margins and basins are required to comprehensively evaluate the relative contribution of lower crustal extension versus formation of new transitional oceanic crust in creating the northern Gulf of California.

5.7 Conclusions

Geologic investigations of northeastern Baja California, Isla Tiburón, and mainland coastal Sonora match Miocene volcaniclastic strata of conjugate rifted margins of the Upper Delfín basin. Stratigraphy comprised of four pyroclastic eruptive sequences, with a total of nine cooling units, is correlated from the northern Puertecitos Volcanic Province to Isla Tiburón and coastal Sonora. These eruptive sequences are the 12.6 Ma Tuff of San Felipe (1 cooling unit), the 6.3±0.3 Ma Tuffs of Mesa Cuadrada (2 cooling units), the Tuffs of Dead Battery Canyon (1 to 2 cooling units) and the 6.1±0.5 Ma Tuffs of Arroyo El Canelo (4 cooling units). The latter three units together comprise the Tuffs of the Northern Puertecitos Volcanic Province. Geochemistry, geochronology, and paleomagnetism of the Tuff of San Felipe and the Tuffs of Mesa Cuadrada confirm the proposed correlation. The Tuffs of the Northern Puertecitos Volcanic Province erupted from a vent adjacent to Arroyo Matomí near the eastern coastline of Baja California. The distribution of these ignimbrites is centered on this

source area. The vent for the Tuff of San Felipe is most likely located at Punta Chueca, on mainland coastal Sonora. The pyroclastic flow that deposited the Tuff of San Felipe flowed westward across Isla Tiburón through a system of paleocanyons before spreading out across northeastern Baja California.

The distribution of correlative ignimbrites permits restoration of dextral displacement across the northern Gulf of California. Restoration of the Tuffs of the Northern Puertecitos Volcanic Province indicates 255±10 km of dextral displacement, at an azimuth of 312°, between the northern Puertecitos Volcanic Province and western Isla Tiburón. This restoration also satisfies the distribution of the 12.6 Ma Tuff of San Felipe and Early to Middle Miocene volcaniclastic deposits. Outside of this region, offset pyroclastic flows and paleomagnetic declination anomalies indicate distributed deformation within northwest-trending zones on both margins of Upper Delfín basin. Measurements from these areas add 41±13 km of displacement, for a total 296±17 km of opening measured across the Upper Delfín basin segment of the northern Gulf of California. At least 276±13 km of this opening took place after eruption of the ca. 6.1 Ma to 6.3 Ma Tuffs of the Northern Puertecitos Volcanic Province.

As discussed in *Oskin et al.* [2001], these new geologic tie points define the slip history in the northern Gulf of California. Extension in this area from 12.6 Ma to 6.3 Ma was not accompanied by enough dextral shear to significantly displace outcrops of the Tuff of San Felipe, except possibly east of Isla Tiburón, where up to 20±10 km of dextral displacement may have occurred during this time interval. Eruption of the Tuffs of the Northern Puertecitos Volcanic Province marks the onset of significant plate-boundary slip in the Gulf of California. To accumulate the measured offset of these ignimbrites requires extrapolation of the rate of seafloor spreading at the mouth of the Gulf of California back to 6.6±0.6 Ma. This extrapolated age is indistinguishable from isotopic ages of the correlative ignimbrites. Even if the full Pacific-North America rate of motion is applied, the plate boundary must have localized in the Gulf of California by 5.5±0.4 Ma. These results indicate that the Pacific-North America plate boundary localized in the Gulf of California over a short

interval (1 to 2 m.y.) during latest Miocene time. Prior to 6.3 Ma, the majority of dextral Pacific-North America plate boundary motion must have occurred outside of the northern Gulf of California.

The slip history determined here for the northern Gulf of California requires that most of the activity of the southern San Andreas fault system in southern California occurred after ∼6 Ma. Reconciliation of a lower estimate of slip on the southern San Andreas fault (150–180 km, *Matti et al.* [1992]) added to slip from other sources (269±13 km to 300±21 km total, *Dickinson* [1996]) overlap the 275±13 km displacement measured for the northern Gulf of California since 6.1 to 6.3 Ma. Reconciliation of a higher estimate of displacement on the southern San Andreas fault (240 km, *Ehlig et al.* [1975]), in order to be compatible with offset measured in the northern Gulf of California, would require ∼100 km of additional dextral displacement east of Isla Tiburón prior to 6.3 Ma. Additional fieldwork in the Sonoran Basin and Range province is necessary to address this discrepancy.

Restoration of correlative distributions of the Tuffs of the Northern Puertecitos Volcanic Province accounts for all but a 15 to 25 km width of continental surface area between conjugate rifted margins of the Upper Delfín basin of the northern Gulf of California. This result indicates that at least 1000% extension has occurred in the this rift segment. Basically, the upper continental crust has ruptured near the present-day coastlines. To account for the 13 km to 21 km-thick crustal thickness of the northern Gulf of California requires a substantial input of new material beyond a typical 7 km-thick oceanic crustal section. Mixtures of basaltic melt or metasomatized upper mantle with sediment probably account for recent crustal formation here. These mechanisms of crustal formation may have been less likely to operate prior to the arrival of the Colorado River into the northern Gulf of California at ∼5 Ma. An alternative mechanism for crustal formation in the northern Gulf of California is exhumation of middle and/or lower continental crust as a metamorphic core complex. Thinning of the middle and lower continental crust beneath the rift margin may indicate that this process has occurred during opening of the northern Gulf of

California.

Chapter 6

Continental extension of conjugate rifted margins of the Delfín basin: Implications for continental rupture processes in the northern Gulf of California, Mexico

6.1 Abstract

Continental extension of the margins of the Delfín basin preceding and subsequent to localization of the Pacific–North America plate boundary here is assessed using correlative pre-rift and syn-rift ignimbrites as regional structural markers. The magnitude of extension of upper continental crust on the margins of the Upper and Lower Delfín basins of the northern Gulf of California ranges from <5% to ∼40% in most areas. More severe extension may have occurred in areas north of 30° 45′ in Baja California and east of Isla Tiburón in Sonora. The magnitude of upper crustal extension on the margins of the Delfín basin is much less than the factor of 2 to 2.5 thinning measured by *Lewis et al.* [2001] for the entire crustal column across the Main Gulf Escarpment of Baja California, which suggests that thinning must have been accommodated in part by lower crustal flow to areas elsewhere in the rift or outside of the rift margin. Extensional strain on the margins of the Gulf of California remained steady or increased after opening of the Upper Delfín basin, contrary to models of continental rift evolution that predict that strain should become localized within the ocean basin. Opening of the Upper Delfín basin may have been a response to a significant increase in strain rate, brought on by a change in boundary forces, rather than a response to weakening of the crust resulting from intracontinental extension.

6.2 Introduction

The transition from continental to oceanic crust on passive continental margins forms a fundamental yet poorly understood type of discontinuity in the lithosphere. Marine geophysical studies of passive margins reveal a variety of tectonic processes at the continent–ocean boundary. The transition from thick continental to thin oceanic lithosphere may be abrupt or gradual with or without a large volume of volcanism [*Cochran*, 1983; *Taylor and Hayes*, 1983; *Taylor et al.*, 1999; *Louden and Chian*, 1999]. Decoupled extension between the upper and lower continental crust [*Wernicke and*

Tilke, 1989; *Lister et al.*, 1991; *Driscoll and Karner*, 1998] or between the continental crust and sub-continental mantle lithosphere [*Nicholas*, 1985; *Beslier et al.*, 1990; *Whitmarsh et al.*, 2001] may control the kinematic evolution of rift development.

Origins for the variety of rifting geometries described for the continent-ocean boundary are incompletely understood. Narrow rifted continental margins are generally characterized as a result of a runaway process, where thinned continental crust localizes extensional strain and leads to continental break-up [*England*, 1983; *Buck*, 1991]. Wide rifted continental margins probably involved localized strain-dependent strengthening during continental extension, followed by a transition to narrow rifting and continental break-up [*Buck*, 1991; *Hopper and Buck*, 1996]. Critical boundary conditions for these processes are the rate of rifting and the pre-rift thickness and thermal state of the lithosphere. Changes in tectonic stress, sedimentation and volcanism may modify these conditions during rifting. Pre-existing weaknesses are likely to control the position of continental break-up [*Hopper and Buck*, 1996].

In most continental margins of the earth it is difficult to measure the simultaneous evolution of extensional strain on the rift margins and within the rift basin during continental break-up. Normally the continent-ocean boundary is obscured beneath several kilometers of passive margin-basin sediments and/or subsided deep beneath the ocean surface. Youthful ocean basins presently or recently undergoing continental break-up provide rare opportunities to study the transition from diffuse continental extension to focused oceanic rifting prior to deep burial and subsidence.

The Gulf of California, a youthful oceanic basin on the southwest margin of North America (Fig. 1.1) provides an exceptional opportunity to observe the structure of a continent-ocean boundary near sea level over a range of initial conditions. The continental margins of the Gulf of California were pre-conditioned by variable amounts of extension [*Stock and Hodges*, 1989; *Nagy and Stock*, 2000] and arc-related volcanism [*Hausback*, 1984; *Sawlan*, 1991]. The amount of sedimentation into the Gulf of California varies from very little adjacent to the central Baja California Peninsula to complete filling of the northern rift basins by the Colorado River delta [*Lonsdale*,

1989]. Extension direction has varied through the development of the Gulf of California rift. Early continental extension was orthogonal to the rift trend [*Angelier et al.*, 1981; *Stock and Hodges*, 1989; *Axen*, 1995; *Lewis and Stock*, 1998b]. At ∼6 Ma, the Pacific–North America plate boundary localized in the Gulf of California with at least 4 cm/yr of oblique rifting [*Oskin et al.*, 2001].

This chapter presents an overview of continental extension on conjugate rift margins of the Upper and Lower Delfín basins of the northern Gulf of California (Fig. 1.4). Extensional faulting in this region began between 11 and 12.6 Ma [*Stock and Hodges*, 1989; *Lee et al.*, 1996] and culminated in continental break-up in the Upper Delfín basin at ∼6 Ma and in the Lower Delfín basin by 2.6 Ma [*Oskin et al.*, 2001, and Chapters 5 and 7 of this thesis)]. Arc volcanism that preceded rifting here appears to have controlled the position of later rift-related faulting and volcanism [*Axen*, 1995; *Stock*, 2000]. Correlative pre-rift and syn-rift ignimbrite deposits present on both margins of the Upper Delfín basin provide regional structural markers that constrain the amount of extension preceding and subsequent to opening of this segment of the Gulf of California [*Oskin et al.*, 2001, and Chapter 5 of this thesis].

The record of extensional faulting is compiled here from new structural cross-sections of coastal western Sonora and Isla Tiburón (Plates I and III) and from previously published studies of northeastern Baja California. These records document the distribution and magnitude of upper-crustal extension from Miocene through Late Quaternary time. Variability in extension rate and Quaternary faulting is used to evaluate the degree of localization of rifting into the Upper and Lower Delfín basins. Comparison of upper crustal extension with geophysical estimates of crustal thinning by *Lewis et al.* [2001] is shown to support that vertical strain partitioning was active during continental rifting and break-up.

6.3 Regional stratigraphy and structural markers

Pre-rift and syn-rift volcanic and sedimentary strata are used to define the timing of fault displacement of the conjugate rift margin study areas. These strata were divided into five groups (groups 2 through 6) that overlie basement (group 1) in Chapters 2 and 3 of this thesis. Correlative ignimbrites on both margin study areas define region-wide stratigraphic markers. These ignimbrites are the ∼12.6 Ma Tuff of San Felipe [*Stock et al.*, 1999; *Oskin et al.*, 2001] and the 6.1–6.3 Ma Tuffs of the northern Puertecitos Volcanic Province (Figs. 6.1 and 6.2). The Tuff of San Felipe (group 4) occupies a transitional stratigraphic position above pre-rift sedimentary (group 2) and arc-related volcanic rocks (group 3) but below syn-rift volcanic and sedimentary rocks (groups 5 and 6). The Tuffs of the Northern Puertecitos Volcanic Province comprise a set of two to three principal ignimbrites, with several internal cooling units, that define the uppermost group 5 syn-rift deposits. The ∼6.3 Ma Tuffs of Mesa Cuadrada and the ∼6.1 Ma Tuffs of Arroyo El Canelo are the most volumetrically significant and areally extensive of these ignimbrites (Chapters 2, 3, and 5 of this thesis). A younger set of group 6 ignimbrites, the 2.6–3.3 Ma Tuffs of Los Heme, define a third set of stratigraphic markers on the Baja California margin [*Martín-Barajas et al.*, 1995, and *Melbourne, unpublished data*].

The Tuffs of the Northern Puertecitos Volcanic Province erupted at the temporal transition between intracontinental extension and localization of the Pacific–North America plate boundary in the northern Gulf of California. Correlation of these deposits across the northern Gulf of California indicates 255±10 km of displacement between Isla Tiburón and the east coast of Baja California [*Oskin et al.*, 2001]. Extrapolation of seafloor spreading and plate circuit records for the Pacific–North America plate boundary in the Gulf of California indicates that transfer of Baja California to the Pacific Plate occurred during latest Miocene time [*Oskin et al.*, 2001, and Chapter 5 of this thesis]. The emplacement of the Tuffs of the Northern Puertecitos Volcanic Province thus divides the behavior of the continental margin fault systems

Figure 6.1. (next page) Continental extension of the Baja California margin of the Upper Delfín basin. See text for discussion of stratigraphic groups depicted here. Geology based on detailed mapping of areas shown on Fig. 1.4 and *Gastil et al.* [1975], field reconnaissance in the Sierra San Felipe, and interpretation of a Landsat image (path 38 row 39) and aerial photography of the Puertecitos Volcanic Province. Percent extension depicted in boxes adjacent to cross-section lines. Sources of extension measurements: A, *Slyker* [1970]; B, *Bryant* [1986]; C, *Stock and Hodges* [1990]; D, *Stock et al.* [1991]; E, *Stock* [1993]; F, *Nagy* [1997]; G, *Lewis and Stock* [1998b]; H, field reconnaissance mapping; J, Chapter 7 of this thesis. Left-lateral fault offsets shown in boxes with arrows. Q's indicate faults with Quaternary scarps. Extensional accommodation zones abbreviated as follows: HAZ, Huatamote; DAZ, Delicias; MAZ, Matomí. Fault name abbreviations: S.R.N.F., Santa Rosa Narrows fault; E.C.F., El Coloradito fault; C.N.F., Cuervo Negro fault; S.I.F., Santa Isabel fault.

before (group 5) and after (group 6) initiation of opening of the Upper Delfín basin.

Late syn-rift volcanic and sedimentary rocks (group 6) may be used to constrain the behavior of continental margin fault systems during continental break-up. The Tuffs of Los Heme and its correlatives form the most widespread of these marker horizons on the northwest margin of the Delfín basin [*Stock et al.*, 1991; *Lewis*, 1994; *Martín-Barajas and Stock*, 1993; *Martín-Barajas et al.*, 1995, and Fig. 6.1]. This stack of at least 29 densely welded cooling units erupted from 3.3 to 2.6 Ma from a vent located to the east, offshore of the Puertecitos Volcanic Province of Baja California [*Martín-Barajas and Stock*, 1993; *Martín-Barajas et al.*, 1995, and *Melbourne, unpublished data*]. These eruptions may also mark the onset of rifting in the Lower Delfín basin [*Stock*, 2000]. Correlatives of the Tuffs of Los Heme are not known from western Sonora and have not been investigated on the conjugate margin of the Lower Delfín basin, Isla Angel de La Guarda. On the Sonoran continental margin study area, late syn-rift volcanic rocks are exposed only on southwest Isla Tiburón [*Gastil et al.*, 1999, and Chapter 3 of this thesis]. Offset late Quaternary alluvial fan deposits are used to define active fault systems on the continental margin study areas. While the exact ages of these deposits are unknown at present, these observations indicate where localization of plate boundary strain within the northern Gulf of California is incomplete.

Figure 6.1.

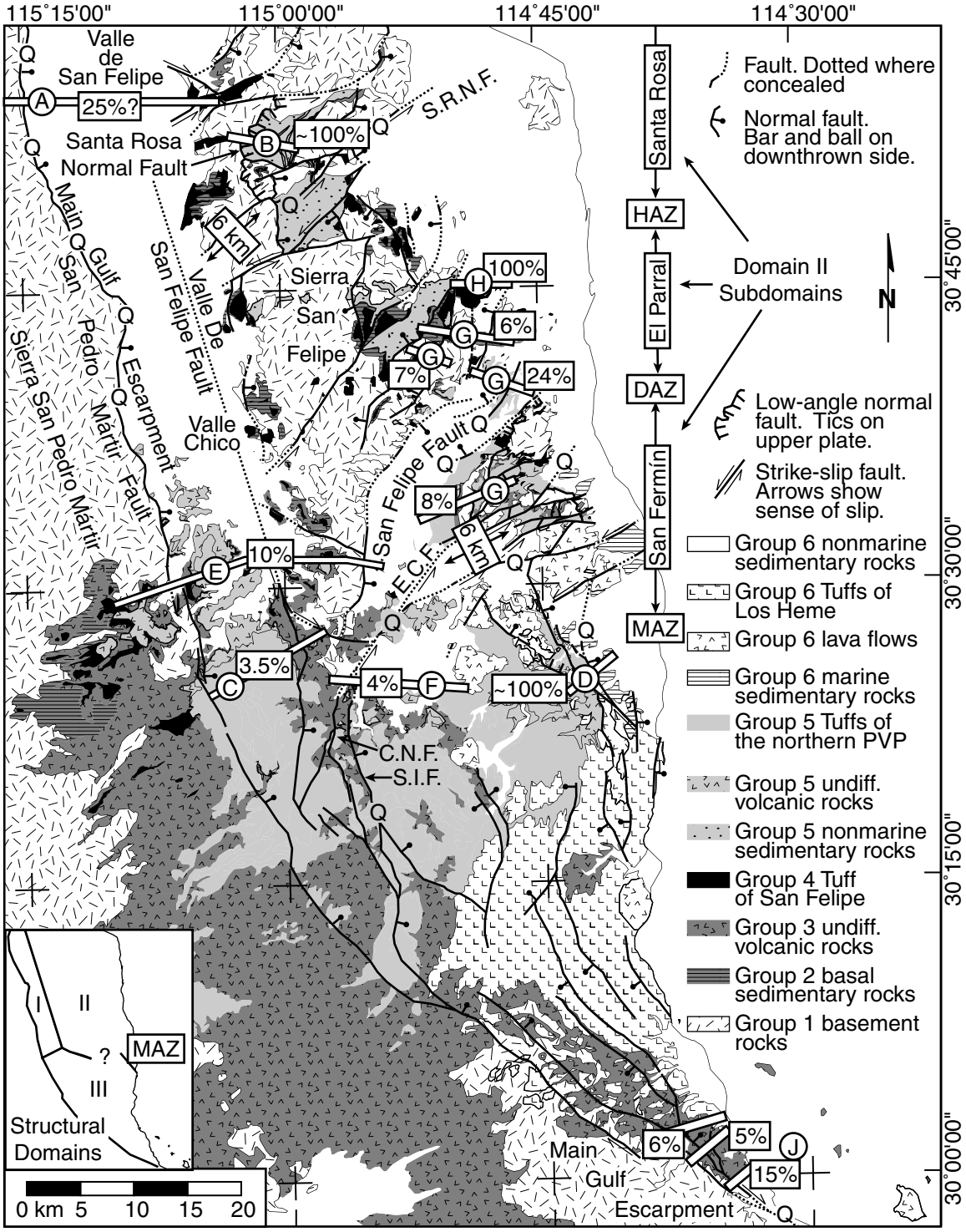
115˚15'00"
115˚00'00"
114˚45'00"
114˚30'00"
30˚45'00"
30˚30'00"
30˚15'00"
30˚00'00"
Valle de San Felipe
25%?
Santa Rosa Normal Fault
~100%
S.R.N.F.
Main Gulf Escarpment
Sierra San Pedro Mártir
Sierra San Pedro Mártir Fault
6 km
Valle De San Felipe Fault
Sierra San Felipe
100%
6%
7%
24%
Valle Chico
San Felipe Fault
8%
6 km
E.C.F.
10%
3.5%
4%
~100%
C.N.F.
S.I.F.
Santa Rosa
HAZ
El Parral
DAZ
San Fermín
MAZ
Fault. Dotted where concealed
Normal fault. Bar and ball on downthrown side.
Domain II Subdomains
N
Low-angle normal fault. Tics on upper plate.
Strike-slip fault. Arrows show sense of slip.
Group 6 nonmarine sedimentary rocks
Group 6 Tuffs of Los Heme
Group 6 lava flows
Group 6 marine sedimentary rocks
Group 5 Tuffs of the northern PVP
Group 5 undiff. volcanic rocks
Group 5 nonmarine sedimentary rocks
Group 4 Tuff of San Felipe
Group 3 undiff. volcanic rocks
Group 2 basal sedimentary rocks
Group 1 basement rocks
I
II
?
MAZ
III
Structural Domains
0 km 5 10 15 20
6%
5%
15%
Main Gulf Escarpment

6.4 Fault systems of the northeastern Baja California margin of the Upper Delfín basin

Fault systems of the northeastern Baja California study area are divided into three structural domains of extensional deformation [*Dokka and Merriam*, 1982]. Domain I comprises the east-dipping San Pedro Mártir fault and related structures of the Main Gulf Escarpment (Fig. 6.1). Down to the east displacement on the San Pedro Mártir fault has opened the Valle de San Felipe–Valle Chico composite basin which separates Domain I from Domain II. Domain II comprises exposures in the Sierra San Felipe and Sierra San Fermín, within the hanging wall of the San Pedro Mártir fault, east of Valle de San Felipe and Valle Chico (Fig. 6.1). Extension of domain II is complex [*Dokka and Merriam*, 1982] and involves distributed clockwise rotation of crustal blocks [*Lewis and Stock*, 1998a]. Domain III lies within the Puertecitos Volcanic Province, located to south of domains I and II. Extension in Domain III occurred on numerous closely-spaced normal faults without forming a significant basin and range-type physiography [*Dokka and Merriam*, 1982; *Stock and Hodges*, 1990]. The Matomí Accommodation Zone [*Dokka and Merriam*, 1982] separates Domain III from Domain II. The Ultima Esperanza fault zone (Fig. 6.1) is the best-exposed segment of the Accommodation zone [*Stock et al.*, 1991]. Dextral oblique faulting northwest of Puertecitos is interpreted here as the eastward continuation of the Matomí Accommodation Zone. Alternatively, this zone may instead strike southeasterly underneath a cover of younger rocks in the Puertecitos Volcanic Province [*Stock*, 2000; *Nagy*, 2000].

6.4.1 Domain I: San Pedro Mártir fault system

The San Pedro Mártir fault system (Domain I) forms part of the boundary between the tectonically stable central Baja California Peninsula and the Gulf Extensional Province [*Gastil et al.*, 1975; *Axen*, 1995]. This 110 km-long, NNW-striking normal

fault forms a prominent escarpment in granitic and metamorphic basement rocks rising up to 2.5 km in elevation above the surface of the adjacent rift basins. Vertical separation on the San Pedro Mártir fault system is estimated to reach a maximum of ∼5 km at the northwestern corner of Fig. 6.1 [*Slyker*, 1970; *Gastil et al.*, 1975] and diminishes to less than 1 km in southern Valle Chico [*Stock and Hodges*, 1990]. Part of the slip on the San Pedro Mártir fault passes southward into the Puertecitos Volcanic Province as two faults with at least 260 m of combined normal displacement [*Stock and Hodges*, 1990; *Stock*, 1993]. Normal slip on fault systems of southern Valle Chico was also transferred eastward to the Gulf of California by distributed right-lateral shear within the Matomí accommodation zone [*Dokka and Merriam*, 1982; *Stock and Hodges*, 1990; *Nagy and Stock*, 2000]. The dip of the San Pedro Mártir and related faults is at high angle (>60°) where mapped at the surface [*Stock and Hodges*, 1990]. Curvature of the fault trace and folding of the hanging wall strata indicate that the San Pedro Mártir fault is probably listric at depth [*Hamilton*, 1971; *Dokka and Merriam*, 1982; *Stock and Hodges*, 1990].

The Valle de San Felipe fault was proposed by *Gastil et al.* [1975] to lie within the Valle de San Felipe and Valle Chico with a strike parallel to the overall trend of the San Pedro Mártir fault. Much of the length of this fault is inferred since it does not cut the young valley fill of the Valle de San Felipe and Valle Chico [*Gastil et al.*, 1975]. *Stock and Hodges* [1990] observed strike slip fault striations on the Valle de San Felipe fault where it crops out in Arroyo Matomí (Fig. 6.1). Strike-slip displacements on the Valle de San Felipe Fault and other NNW-striking faults in southern Valle Chico are probably low because Late Miocene ignimbrite stratigraphy correlates well across this area [*Stock*, 1989, and Chapter 5].

The timing and amount of extension on the San Pedro Mártir fault is best constrained from southern Valle Chico, where *Stock* [1993] estimated ∼10% extension. At Mesa Cuadrada (Fig. 6.1) tilting of the Tuff of San Felipe (unit Mr1) is twice that of the Tuffs of Mesa Cuadrada (units Mr3 and Mr4), suggesting that extension has been evenly divided here both before and after ∼6.3 Ma [*Stock and Hodges*, 1990].

Extension across Valle Chico probably increases to the north, commensurate with increased displacement on the San Pedro Mártir fault. The magnitude of extension across most of Valle Chico and Valle de San Felipe is poorly constrained. An approximation may be made by setting the amount of extension equal to the normal separation on the San Pedro Mártir fault. This approximation yields ∼5 km, or 25% extension across the Valle de San Felipe. This amount of extension is compatible with moderate (30–40°) westward dips of volcanic and sedimentary rocks on the west side of the Sierra San Felipe [*Gastil et al.*, 1975]. Quaternary fault scarps along most of the length of the San Pedro Mártir fault indicate that this structure remains active [*Brown*, 1978].

6.4.2 Domain II: The Sierra San Felipe and Sierra San Fermín

The Siera San Felipe and Sierra San Fermín (Domain II) are a tectonically complex set of ranges located between the San Pedro Mártir fault and the Gulf of California. Two overall patterns of faulting are present in this region. N to NNW-striking normal faults are present throughout these ranges [*Gastil et al.*, 1975; *Lewis and Stock*, 1998b]. Some of these normal faults underlie intermontane basins (Fig. 6.1) and may have up to several kilometers of throw [*Bryant*, 1986]. These normal faults terminate at and/or are cut by NE to E-striking left-lateral strike-slip faults [*Gastil et al.*, 1975; *Dokka and Merriam*, 1982; *Lewis and Stock*, 1998b, a]. These strike-slip faults transect the Sierra San Fermín and Sierra San Felipe [*Gastil et al.*, 1975; *Dokka and Merriam*, 1982] and accommodate 30 ± 15 km of counterclockwise rotation of NE-striking fault-bounded blocks [*Lewis and Stock*, 1998a].

Normal fault systems

Normal fault systems within the Sierra San Fermín and Sierra San Felipe are divided here into three subdomains south of 31° latitude. All of these subdomains lie in the hanging wall of the San Pedro Mártir segment of the Main Gulf Escarpment of

Axen [1995]. The northern Santa Rosa subdomain and southern San Fermín subdomain comprise down-to-the-east normal faults. The El Parral subdomain separates these areas as a zone of down-to-the-west normal faulting. The diffuse Delicias Accomodation Zone separates the San Fermín and El Parral subdomain [*Lewis and Stock*, 1998b]. NE to ENE-striking strike slip faults in the Huatamote Accommodation Zone separate the opposing vergence of normal faulting between the Santa Rosa and El Parral subdomain.

The Santa Rosa and San Fermín subdomains both culminate in east-dipping master normal faults that bound intermontane basins. The Sierra San Felipe fault in the south bounds the Llanos de San Fermín basin. 800 m of normal separation has occurred on this fault east of Mesa Cuadrada [*Stock and Hodges*, 1990]. Most of the Sierra San Fermín lies within the hanging wall of the Sierra San Felipe fault and strata in the range tilt westward toward the fault. The Santa Rosa normal fault is a low-angle (18° to 20° eastward dip) normal fault that bounds the Santa Rosa basin [*Bryant*, 1986]. Strata of the Santa Rosa basin also dip westward toward the fault plane [*Gastil et al.*, 1975; *Bryant*, 1986]. Offset of the Tuff of San Felipe may indicate up to 5 km of normal separation on the Santa Rosa normal fault, similar to the San Pedro Mártir fault located 25 km to the west [*Bryant*, 1986, see Fig. 6.1]. The Huatamote basin is located south of and partially overlies the Santa Rosa basin (Chapter 2). Similar to the Santa Rosa basin, the Huatamote basin is bounded by a normal fault to the east. The relationship between this normal fault and the Santa Rosa normal fault is uncertain.

No single master normal fault is clearly evident for the El Parral subdomain of the Sierra San Felipe and northern Sierra San Fermín. Sedimentary rocks of the El Parral basin crop out within numerous north-trending fault blocks bounded by west-dipping normal faults. These faults are shown in simplified form on Fig. 6.1. Extension in this region is accommodated by distributed normal faulting [*Lewis and Stock*, 1998b]. The Ironwood Canyon fault, a low-angle normal fault in the northern Sierra San Fermín [*Lewis and Stock*, 1998b], is a possible fragment of a west-dipping

master normal fault for the El Parral subdomain.

The timing and amount of extension are variable throughout Domain II. The record is best constrained from the Sierra San Fermín, where *Lewis and Stock* [1998b] document 6% to 24% extension. Most normal faulting in the Sierra San Fermín appears to post-date the ∼6.3 Ma Tuffs of Mesa Cuadrada [*Lewis and Stock*, 1998b, Mr3 and Mr4]. Northeast of the Sierra San Fermín where latest Miocene ignimbrites are not present, extension is known only to post-date the ∼12.6 Ma Tuff of San Felipe [*Lewis and Stock*, 1998b]. The Tuff of San Felipe near the eastern range front of the El Parral subdomain of the Sierra San Felipe is locally extended by up to 100% and steeply tilted on closely-spaced moderately to shallowly dipping normal faults. In the Santa Rosa Basin, extension may also approach 100% [*Bryant*, 1986]. Late Miocene volcanic rocks present within syn-rift strata of the Santa Rosa basin are not present in the nearby Huatamote basin. These strata, and the observed overlap of Santa Rosa basin fill by younger Huatamote basin fill (Fig. 2.4), may indicate that extension in the Santa Rosa basin began and terminated earlier than in other areas of Domain II. Quaternary fault scarps are not present on the normal fault systems of Domain II except possibly for some of the scarps observed by *Lewis and Stock* [1998b] and *Dokka and Merriam* [1982] within the Llanos de San Fermín. Most notably, however, the master Sierra San Felipe normal fault that bounds the Llanos de San Fermín to the east appears to be inactive at present [*Stock and Hodges*, 1990]. Other significant normal faults of domain II also appear to be inactive.

Left-lateral strike-slip faults

E to NE striking left-lateral strike-slip faults transect the Sierra San Felipe and Sierra San Fermín with a 10–15 km spacing between principal fault systems [*Hamilton*, 1971; *Gastil et al.*, 1975; *Dokka and Merriam*, 1982; *Lewis and Stock*, 1998a]. These fault systems probably accommodate 30 ± 15 ° of vertical-axis rotation of fault blocks within the Sierra San Fermín and Sierra San Felipe [*Lewis and Stock*, 1998b, also Fig. 5.21]. Sinistral offset on the El Coloradito fault zone in the Sierra San Fermín may

be as much as 6 km [*Lewis and Stock*, 1998b]. A similar sinistral offset of 6 km occurs between outcrops of a pre-rift erosion surface and the Tuff of San Felipe at the southwestern end of the Santa Rosa Narrows fault (Fig. 6.1). These offsets are consistent with the amount of rotation documented by paleomagnetic declination anomalies in the Tuff of San Felipe (Mr1) and the Tuffs of Mesa Cuadrada (Mr3 and Mr4) [*Lewis and Stock*, 1998a]. Offsets on other left-lateral strike-slip faults in the region are uncertain but should be of similar magnitude if these faults collectively accommodate clockwise rotation [*Lewis and Stock*, 1998b].

Quaternary fault scarps are present on several NE-striking sinistral faults of Domain II. These scarps are especially well-documented on several strands of the El Coloradito fault [*Lewis*, 1994; *Lewis and Stock*, 1998b] and its continuation to the southwest [*Stock*, 1993]. The Delicias fault [*Lewis and Stock*, 1998b] and the Santa Rosa Narrows fault also cut Late Quaternary deposits. *Lewis and Stock* [1998b] noted that sinistral faults and clockwise rotation equally affect 6 Ma and 3 Ma strata in the Sierra San Fermín and that these faults did not affect depositional patterns in older basin deposits. From these relationships *Lewis and Stock* [1998b] conclude that dextral shear increased on the Baja California continental margin after ∼3 Ma. Observations from further north in the Sierra San Felipe, where sinistral faults are active but principal normal fault systems are inactive, support the conclusions of *Lewis and Stock* [1998b].

6.4.3 Domain III: The Puertecitos Volcanic Province

The Puertecitos Volcanic Province (Domain III) comprises a zone of diffuse east-west extension [*Dokka and Merriam*, 1982]. Principal fault systems of Domain III are NNW to NW-striking down-to-the-east normal faults and NW to NNE-striking, down-to-the-west normal faults [*Dokka and Merriam*, 1982, and Chapter 7 of this thesis]. Kinematic relationships between E and W-dipping faults suggest that E-dipping faults are the primary structures of domain III [*Dokka and Merriam*, 1982; *Nagy*, 2000, and Chapter 7 of this thesis].

Two principal E-dipping fault systems are exposed in the western half of Domain III [*Gastil et al.*, 1975; *Dokka and Merriam*, 1982; *Stock and Hodges*, 1990; *Nagy*, 2000]. A southern continuation of the San Pedro Mártir fault separates Domain III from the stable central Baja California Peninsula (Fig. 6.1). This fault system is continuous with structures of the San Pedro Mártir fault system further north, but with less normal displacement [*Stock and Hodges*, 1990]. The Cuervo Negro–Santa Isabel Fault forms a second principal fault system located 10–15 km east of the San Pedro Mártir fault [*Nagy*, 2000]. The Cuervo Negro–Santa Isabel Wash fault accommodates 500 m of down-to-the-east normal displacement with a sinistral component at Santa Isabel Wash [*Nagy*, 1997, 2000]. North of Domain III, the Cuervo Negro–Santa Isabel fault appears to curve northeastward to become the El Coloradito fault of the Sierra San Fermín [*Gastil et al.*, 1975, and Fig. 6.1]. Significant extension is required southeast of this fault trend to reconcile 6 km of principally sinistral displacement on the El Coloradito fault with 500 m of principally normal displacement on the Cuervo Negro–Santa Isabel Fault. The hypothesized link between these faults may have excised collapse-faults related to eruption of the Tuffs of the Northern Puertecitos Volcanic Province (Fig. 2.1 of Chapter 2). E-dipping fault systems of the western part of Domain III turn and merge southeastwards with a zone of oblique normal faults at the southeastern corner of the Puertecitos Volcanic Province with 1–2 km of dextral displacement (Chapter 7 of this thesis).

The timing of extension is relatively well constrained from the Puertecitos Volcanic Province. Conformable contacts between the Tuff of San Felipe and the Tuffs of the Northern Puertecitos Volcanic Province at Santa Isabel Wash [*Nagy*, 2000] and at Mesa El Avión [*Stock, unpublished mapping*] indicate that the majority of extension of Domain III occurred after 6.3 Ma. Scattered evidence exists for a small amounts of earlier extension [*Nagy*, 2000]. Faulting between $\sim$ 12.6 and 6.3 Ma is also indicated by thinning of the Tuffs of Mesa Cuadrada (Mr3 and Mr4) over fault-generated topographic relief at the southern continuation of the San Pedro Mártir fault system [*Stock and Hodges*, 1990]. Faulting at the southeastern end of the Puertecitos Volcanic

Province occurred mostly prior to 2.6 Ma but this timing is otherwise unconstrained (Chapter 7 of this thesis).

The amount of extension appears to be low throughout most of Domain III. *Stock and Hodges* [1990] document 3.5% of ENE-directed extension on the Matomí Plateau. *Nagy* [1997] documents a similar amount of extension (4%) from the Santa Isabel Wash area. Extension at the southeastern corner of Domain III is also low (5–15%, Chapter 7 of this thesis). Dextral displacement of 1–2 km on the faults at southwestern boundary of Domain III is consistent with the transfer of extension within the Puertecitos Volcanic Province to the Gulf of California (Chapter 7 of this thesis).

Exceptions to the low amounts of extension typical of Domain III occur at its eastern boundary. At or adjacent to the eastern end of the Matomí accommodation zone (Fig 6.1) *Stock et al.* [1991] document multiple generations of normal faulting that tilt the Tuffs of Arroyo El Canelo 50–75° to the southwest. These steeply tilted ignimbrites are overlain by flat-lying Tuffs of Los Heme and correlatives [*Stock et al.*, 1991; *Martín-Barajas et al.*, 1995]. *Stock et al.* [1991] and *Martín-Barajas and Stock* [1993] also document dextral-oblique normal faults along the range front here that offset both tuffs. Additional mapping is required to determine the total amount of extension from this area. High amounts of extension ($\sim$100%) are likely needed to explain the steep stratal tilts. This extension is constrained to have occurred primarily between emplacement of the Tuffs of Arroyo El Canelo at 6.1 $\pm$ 0.5 Ma [*Nagy et al.*, 1999] and the Tuffs of Los Heme at 3.3 Ma [*Martín-Barajas et al.*, 1995]. A second zone of high extension probably lies offshore of the southeastern Puertecitos Volcanic Province where the Isla Angel de la Guarda microplate separated from Baja California [*Stock*, 2000].

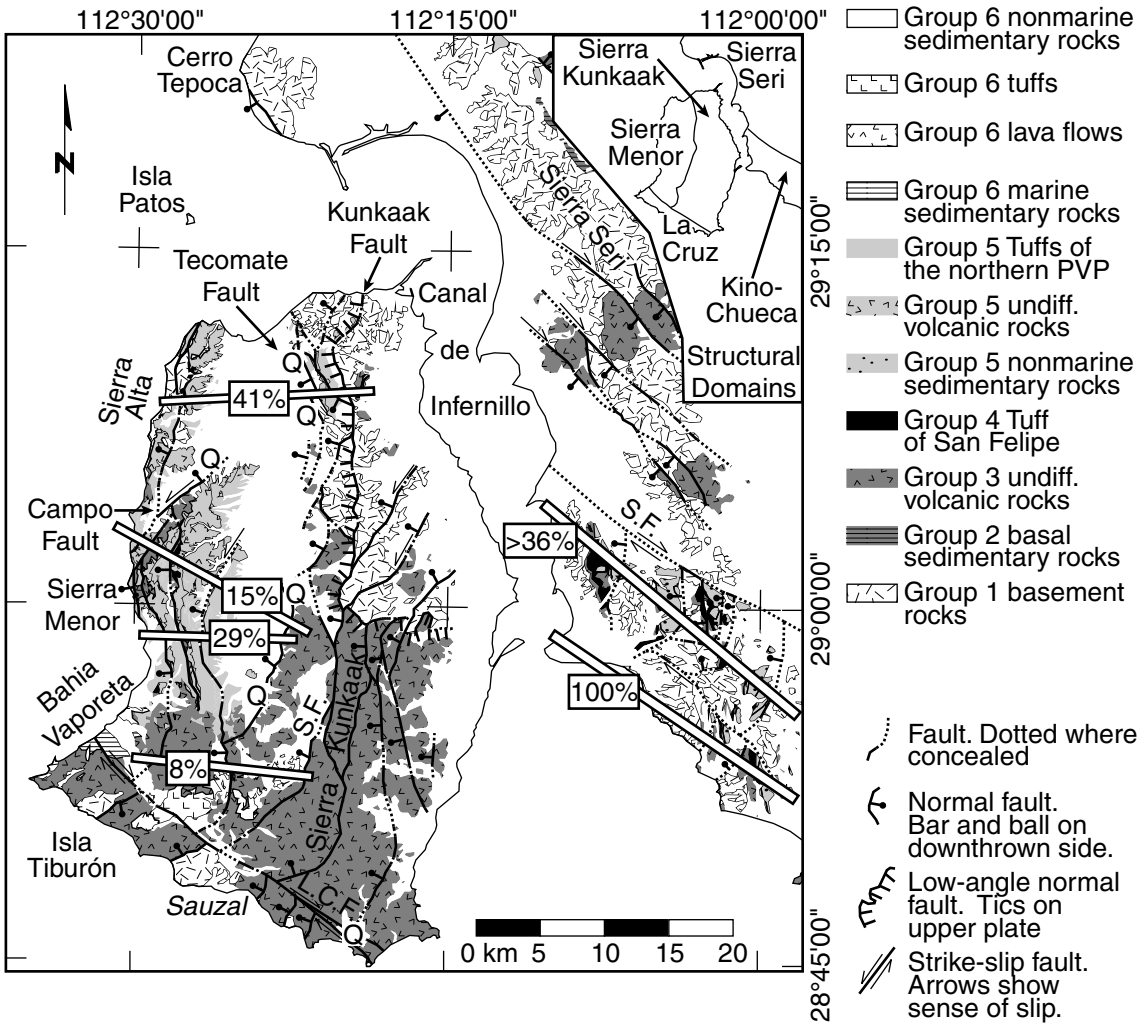

Figure 6.2. Continental extension of the Sonora margin of the Upper Delfín basin. Mapping generalized from plate I, plate II, *Gastil and Krummenacher* [1976], and *Gastil et al.* [1999] with additional field reconnaissance. A georeferenced Landsat Thematic Mapper image (path 36, row 40) was used as a base map. See text for discussion of the lithologic groups presented here. Percent extension depicted in boxes adjacent to cross-section lines from Plates I and III. Q's indicate faults with Quaternary scarps.

6.5 Fault systems of the western Sonora margin adjacent to the Upper Delfín basin

Fault systems of the western Sonora margin, adjacent to the Upper Delfín basin, are divided into five structural domains (Fig. 6.2). Each domain is characterized by different amounts of W and NW-directed extension. Each domain also contains unique pre-rift and syn-rift strata that have been juxtaposed by domain-boundary fault systems (Chapter 3). The three central domains, from west to east, are the Sierra Menor, Sierra Kunkaak, and Kino–Chueca domains. Outcrops of the Tuff of San Felipe are common to each of these domains (Fig. 6.2). Outcrops of the Tuffs of the Northern Puertecitos Volcanic Province are restricted to these domains on Isla Tiburón (Fig. 6.2). Right-lateral strike slip faults separate the two remaining domains from three central domains. On coastal mainland Sonora, the Sierra Seri domain is juxtaposed against the Kino–Chueca domain by the Sacrificio fault (Fig. 6.2). On southern Isla Tiburón, the La Cruz Domain is separated from the Sierra Menor and Sierra Kunkaak Domains by the La Cruz fault (Fig. 6.2).

6.5.1 The Sierra Menor Domain

The Sierra Menor Domain is comprised of two mountain ranges, the Sierra Menor and Sierra Alta, that lie adjacent to the western shoreline of Isla Tiburón. Broadly, the Sierra Menor domain and Sierra Alta are both tilted and slightly folded blocks in the hanging wall of the Tecomate fault system (Plates II and III). The Tecomate fault system is the westernmost of an array of structures that defines the western range front of the Sierra Kunkaak, east of the Sierra Menor domain. Normal slip on the Tecomate fault forms the Tecomate basin, a 5–10 km-wide N-striking alluvial valley through the center of Isla Tiburón. Most strata of the Sierra Menor and all strata of the Sierra Alta dip shallowly to the east, toward the Tecomate fault. Adjacent to Bahía Vaporeta, bedding dips to the west and forms a broad, faulted anticline (Plate

Figure 6.3. (next page) Restoration of normal slip on the Tecomate and Kunkaak faults, northern Isla Tiburón. Total normal offset on this fault system is 6.7 km, with 4.2 km of east-west extension. 60% of the total offset (4.0 km) and extension (2.5 km) occurred after 6.3 Ma. A. Present-day configuration of faults and basin deposits, with normal slip shown for time after deposition of the Tuffs of Mesa Cuadrada. Also refer to cross section A–A′ on Plates II and III. Deposition of Tmr3 eroded from the footwall of the Kunkaak fault indicates a minimum 0.9 km of slip post-6.3 Ma on the Kunkaak fault. No Tmr3 outcrops remain on the footwall block. B. Restoration of normal slip to the end of deposition of the Tuffs of Mesa Cuadrada (cooling unit Tmr4) at ∼6.3 Ma. Normal slip shown for time after deposition of the Tuff of San Felipe at 12.6 Ma but before 6.3 Ma. C. Restoration of normal slip to the time of deposition of the Tuff of San Felipe at 12.6 Ma. This ignimbrite was probably deposited before the onset of extension here.

II). This feature, as well as its curvilinear surface traces, indicates that Tecomate fault is probably listric beneath the Sierra Menor Domain. Normal offset on the Tecomate fault is 3.1 km east of the Sierra Alta (Plate III). Older strands of the Tecomate fault, including the low-angle Kunkaak fault, record an additional 3.5 km of offset (Fig. 6.3). Matching strata have not been identified between the footwall and hangingwall blocks of the Tecomate fault east of the central Sierra Menor. Restoration of the top of the Tuff of San Felipe to the surface along the fault trace restores 2.5 km of normal offset.

Secondary normal faults are common throughout the Sierra Menor Domain. NNW to NNE-striking down-to-the-west normal faults, each with 100–500 m of throw and set ∼2 km apart, are the dominant structural features within the central and southern Sierra Menor. This pattern is interrupted in the northern Sierra Menor, where the north-striking faults bend to the NE and may have an additional component of sinistral slip indicated by offset stratigraphic pinch-outs within the Tuffs of the Northern Puertecitos Volcanic Province. This oblique fault system culminates at the Campo fault, which displays 800 m of normal separation and forms a 3-km-wide alluviated valley between the Sierra Menor and Sierra Alta (Plate III). NNE-striking down-to-the-west normal faults reappear to the north as the dominant structures in the Sierra Alta. A sharp, NNE trending escarpment that forms the western coastline of the Sierra Alta is likely to correspond to an additional NNE-striking down-to-the-west normal fault just offshore. This hypothesized fault is labeled the Tiburón Escarpment

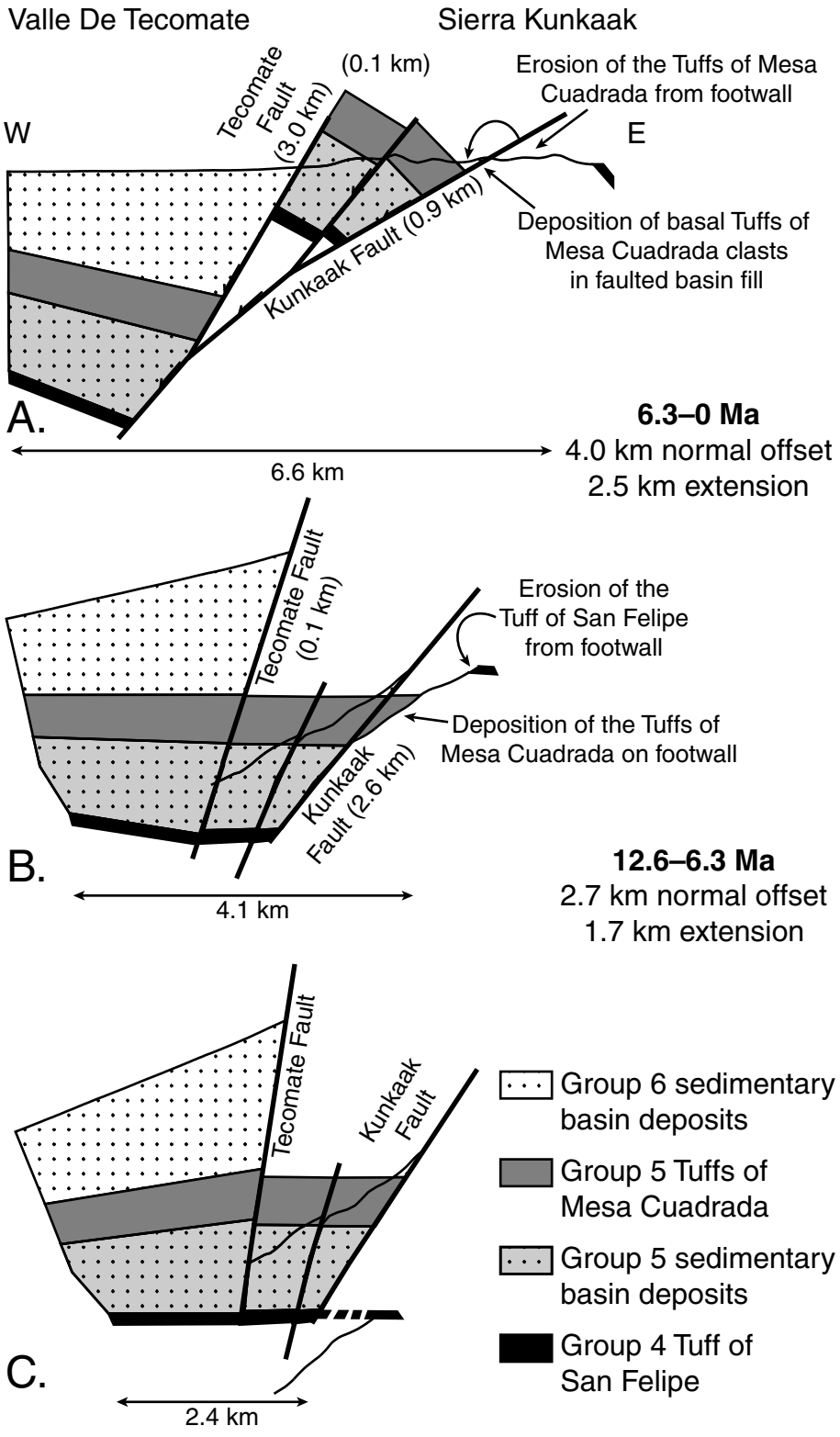
Valle De Tecomate
Sierra Kunkaak
Tecomate Fault (3.0 km)
(0.1 km)
Erosion of the Tuffs of Mesa Cuadrada from footwall
W
E
Deposition of basal Tuffs of Mesa Cuadrada clasts in faulted basin fill
Kunkaak Fault (0.9 km)
A.
6.3–0 Ma
4.0 km normal offset
2.5 km extension
6.6 km
Tecomate Fault (0.1 km)
Erosion of the Tuff of San Felipe from footwall
Deposition of the Tuffs of Mesa Cuadrada on footwall
Kunkaak Fault (2.6 km)
B.
12.6–6.3 Ma
2.7 km normal offset
1.7 km extension
4.1 km
Tecomate Fault
Kunkaak Fault
C.
2.4 km
Group 6 sedimentary basin deposits
Group 5 Tuffs of Mesa Cuadrada
Group 5 sedimentary basin deposits
Group 4 Tuff of San Felipe

Figure 6.3.

fault on Plate III.

The timing of extension in the Sierra Menor Domain is well constrained from new geologic mapping of correlative ignimbrites [*Oskin et al.*, 2001, and Plate II] and structural cross sections (Plate III). No fault movement or tilting appears to pre-date the Tuff of San Felipe in the Sierra Menor Domain. Angular unconformities between the ∼12.6 Ma Tuff of San Felipe and the ∼6.3 Ma Tuffs of Mesa Cuadrada indicate that about one-half to one-third of the tilting of the Sierra Menor Domain occurred prior to 6.3 Ma. In the southern Sierra Menor, the Tuff of San Felipe dips 22° to the east and is overlain by the Tuffs of Mesa Cuadrada dipping 15° to the east. On the western side of the Sierra Alta, Tuff of San Felipe dips 25–38° to the east, whereas on the eastern side of the Sierra Alta the Tuffs of Mesa Cuadrada dip only 14° to the east. In several localities adjacent to the western shoreline of Isla Tiburón, the Tuffs of the Puertecitos Volcanic Province directly overlie the Tuff of San Felipe with angular unconformity. For example, in the central Sierra Alta and at Punta Reina, the Tuffs of Mesa Cuadrada are deposited into paleocanyons cut into the Tuff of San Felipe and older strata ($^{3}54^{000}$,$^{32}\,15^{000}$ and $^{3}57^{000}$,$^{32}\,23^{000}$). Further east, within the Sierra Menor and Sierra Alta, an eastward-thickening wedge of group 5 strata separates these tuffs (Plate III).

Extension of the Sierra Menor domain increases from south to north. Normal separation on the Tecomate fault and on secondary normal faults within the Sierra Menor diminishes southward toward the La Cruz fault (Plate II). Extension across the southern Sierra Menor is estimated at 8–29% total, with up to 15% extension after 6.3 Ma (B–B′, C–C′, and D–D′, Plate III). These extension estimates across the southern part of the Tecomate basin are uncertain, however, because matching strata have not been mapped in the footwall of the Tecomate fault here. Extension was calculated west of the surface trace of the Tecomate fault by assuming that the appropriate matching horizons are located at or above the structural level of the trace. Further north, 41% (4.4 km) of extension total, with 2.6 km of extension after 6.3 Ma, is calculated by restoration of a cross section through the Sierra Alta

and northern Sierra Kunkaak (A–A′, Plate III). Here, matching strata are identified within the footwall of the Tecomate fault (plate II). Additional normal separation on the low-angle Kunkaak detachment fault is included with these estimates. The Tecomate and Kunkaak faults are interpreted to merge at depth.

Scarps in Quaternary deposits indicate that most of the fault systems of the Sierra Menor Domain are active. These include prominent fault scarps mapped along both the northern and southern segments of the Tecomate fault (Plate II). Quaternary alluvium is also cut by the Campo fault [*Gastil and Krummenacher*, 1977] and by other N-striking normal faults within the Sierra Menor (Plate II).

6.5.2 The Sierra Kunkaak Domain

The Sierra Kunkaak domain is comprised of the Sierra Kunkaak, a single chain of mountains forming the eastern half of Isla Tiburón. As a whole, the Sierra Kunkaak forms the footwall of the Tecomate and Sauzal basins (Plates II and III, Fig. 6.2). The Tecomate fault and the Sauzal fault are high-angle west-dipping normal faults that separate the Sierra Kunkaak from these basins. The eastern side of the Sierra Kunkaak descends gradually to sea level at the Canal de Infernillo (Fig. 6.2). This shallow channel, flooded by the Gulf of California, separates the Sierra Kunkaak Domain from the Kino–Chueca and Sierra Seri domains of coastal Sonora.

Internally, the Sierra Kunkaak displays a transition between two contrasting structural styles in coastal Sonora and Isla Tiburón. The southern Sierra Kunkaak are comprised of north-trending ridges of east-dipping volcanic strata bounded by smaller-offset west-dipping normal faults [*Gastil and Krummenacher*, 1976, Fig. 6.2]. This pattern is similar to the moderately-extended Sierra Menor Domain to the west. This north-trending structural grain is interrupted through the central Sierra Kunkaak where the strike of volcanic strata turns eastward [*Gastil and Krummenacher*, 1976]. North of this discontinuity, basement outcrops predominate and older fill of the Tecomate basin crops out at the crest of the Sierra Kunkaak in the footwall of the Kunkaak low-angle normal fault (cross section A–A′ of Plate III). This pattern is similar to

the highly-extended Kino–Chueca Domain to the east. The Kunkaak fault is inferred to turn eastward at the structural discontinuity and possibly underlie the southern Sierra Kunkaak (Fig. 6.2). Alternatively, the dip of the Kunkaak fault may steepen southward and continue as the Sauzal fault (cross section D–D′, Plate III). The abrupt transition from a thick volcanic cover in the southern Sierra Kunkaak to basement outcrops in the northern Sierra Kunkaak is probably a combined result of erosion and tectonic removal by the Kunkaak fault.

The timing and amount of extension over most of the Sierra Kunkaak Domain is poorly constrained, with the exception of the northern Sierra Kunkaak. Here, the Tuff of San Felipe has been displaced 6.7 km on the combined Kunkaak and Tecomate normal faults since ∼12.6 Ma (cross section A–A′ on Plate III, Fig. 6.3). Of this slip, at least 4.0 km occurred after deposition of the Tmr3 member of the Tuffs of Mesa Cuadrada at ∼6.3 Ma. Slip on the high-angle Tecomate strand and an intermediate splay east of the Tecomate fault occurred primarily after deposition of Tmr3 (3.1 of 3.2 km). At least 0.9 km of slip on the Kunkaak fault has also occurred after deposition of Tmr3, indicated by boulders of Tmr3 probably eroded from the footwall and deposited in unit Tmpal adjacent at the fault contact (Plate II). Some of these boulders show striated surfaces from shearing within the Kunkaak fault zone. Rotation of Tmr3 to dips of 45° in the hanging wall of the Kunkaak fault indicates that the shallow dip of this normal fault probably also post-dates 6.3 Ma (Plate II). Altogether, these structural and stratigraphic relationships indicate that 60% of the total extension (2.5 of 4.2 km) in the northern Sierra Kunkaak post-dates 6.3 Ma (Fig. 6.3). Percent extension is locally high within the Sierra Kunkaak (> 100%) across the Kunkaak low-angle normal fault. A sample from the northern Sierra Kunkaak that gave an apatite fission-track age of 10 Ma [*Calmus et al.*, 2000] probably was located in the footwall of the Kunkaak fault. Scarps in Quaternary deposits indicate that the high-angle Tecomate normal fault system is active (Plate II).

6.5.3 La Cruz Domain

The La Cruz domain occupies a 1–4 km wide strip along the southern coast of Isla Tiburón (Fig. 6.2). The right-lateral La Cruz fault forms the northern boundary of the La Cruz domain. Early to Middle Miocene volcanic strata of the La Cruz domain are distinctive from coeval strata of the adjacent Sierra Menor and Sierra Kunkaak domains, supporting significant displacement on this structure (Chapter 3 of this thesis). Late syn-rift strata of southwestern Isla Tiburón correlate across the La Cruz fault and indicate that slip on the fault occurred primarily before deposition of the lowest member of the Tuffs of Arroyo Sauzal (Tmprsz1) at ∼6 Ma (Chapter 3, also cross section D–D′, Plate III). Most likely, the La Cruz domain was transferred across the Tiburón fracture zone during the earliest stage of opening of the Upper Delfín basin (Chapter 3).

Extension within the La Cruz domain is poorly constrained, but probably moderate. Strata of the La Cruz domain are repeated across a series of southeast-dipping normal faults that crop out on the southern coastline of Isla Tiburón. Shallow dips of 10–25° measured by *Gastil et al.* [1999] on 11–21 Ma volcanic strata of the La Cruz domain further support low amounts of extension.

Right-lateral strike-slip displacement on the La Cruz fault may be 26 km or more, the length of the fault zone exposed on Isla Tiburón. No pre-rift nor early syn-rift strata are correlated across the La Cruz fault, based on reconnaissance observations along its trace. Thus, strata of the La Cruz domain probably originated southeast of Isla Tiburón and were juxtaposed across the La Cruz fault. Alternatively, the La Cruz fault may be a down-to-the-northeast normal fault that exposes strata on its footwall that lie burred beneath the hanging wall. This is less likely, however, because ignimbrites of the La Cruz domain as young as 11–12 Ma do not correlate with coeval strata north of the La Cruz fault. Quaternary activity of the La Cruz fault may be indicated by a subtle scarp and vegetation lineament on an alluvial fan on southeastern Isla Tiburón (Fig. 6.2).

6.5.4 Kino–Chueca Domain

The Kino–Chueca Domain is comprised of a series of narrow north-trending ridges of volcanic strata interspersed with more extensive areas of basement (Fig. 6.2). This domain is bounded on the west and south by the Gulf of California and on the east by the broad alluvial plain of the Rio Sonora. The Sierra Seri Domain abuts the northeastern boundary of the Kino–Chueca Domain along the Sacrificio fault, one of a family of right-lateral strike-slip faults within the Sonoran coastal zone [*Gastil and Krummenacher*, 1977]. The predominant structures within the Kino–Chueca domain are probably low-angle normal faults that underlie steeply dipping strata that is characteristic of this area. The positions of these faults are poorly constrained at present (Plate I). Fluvial conglomerates (unit Tmpal) unconformably overlying faulted volcanic rocks and basement may be remnants of a half-graben basin that existed here at one time during rifting.

Secondary structures within the Kino–Chueca domain are northwest-striking right-lateral strike-slip faults and high-angle, low-offset (10's of meters) north-striking normal faults. Both of these fault systems appear to be truncated by lower-angle(?) normal faults with greater amounts of offset (100's of meters, Plate I). Volcanic rocks of the southern and eastern parts of the Kino–Chueca domain dip steeply to vertical (65–89°) and form strike-parallel ridges. Dips become more moderate to shallow in the northwestern part of the domain near Punta Chueca. Some faulting in this northwestern area is closely associated with very densely welded Tuff of San Felipe and syn-tectonic infill by the Tuffs of Punta Chueca (Chapter 3 of this thesis). Two of these faults shown in cross section P–P′ on plate I are interpreted to be related to the vent for the Tuff of San Felipe.

Extension within the Kino–Chueca domain is probably moderate to high. Although measurement of the exact amount of extension is limited by a lack of detailed mapping here, steeply-dipping strata repeated at 2–10 km intervals require substantial amounts of extension (plate I). Outcrops of the Tuff of San Felipe, when restored

in cross section Q–Q′, suggest ∼100% extension. Structural control is very sparse in cross section P–P′. A preliminary estimate indicates at least 36% extension for this cross section. Clockwise vertical axis rotation of the Tuff of San Felipe by 25° and 40° was measured near Bahía Kino and Punta Chueca, respectively. These rotations are attributed to large-magnitude extension within a right-lateral shear zone. No Quaternary faulting is mapped in the Kino–Chueca domain.

Apparent right-lateral offset of 20±10 km between Punta Chueca and the northern Sierra Kunkaak is estimated from matching densely-welded near-vent facies of the Tuff of San Felipe and similar capping basalt flows (Chapter 3 of this thesis). Large-magnitude extension common to both of these areas suggests that this offset may result from northwest-directed extension. Lengthening of the region from Punta Chueca to the northern Sierra Kunkaak by 100% would have resulted in ∼10 km of northwest displacement. Lengthening of a larger region from Bahía Kino to the Sierra Kunkaak by 100% would have resulted in ∼20 km of northwest displacement. These displacements are within the range estimated in Chapter 3 from correlative volcanic strata.

6.5.5 Sierra Seri Domain

The Sierra Seri Domain consists of the Sierra Seri, a northwest-trending, northeast-tilted set of ranges that lie parallel to the Sonoran coastline north of Punta Chueca. Northwest-striking, southwest-dipping dextral oblique normal faults define the southwestern range front of the Sierra Seri (Fig. 6.2). None of these faults appears to cut Quaternary strata. The amount of extension within the Sierra Seri has not been measured, but is probably significant, based upon the moderate stratal dips (20° to 47°) within the range [*Gastil and Krummenacher*, 1977, and Plate I]. Extension between the Sierra Seri and adjacent ranges to the northeast or between the Sierra Seri and northern Isla Tiburón is unconstrained.

Right-lateral strike slip displacement on the Sacrificio fault, which lies between the Sierra Seri Domain and the Kino Chueca Domain, is also poorly constrained. A

distinctive conglomerate that crops out at the crest of the Sierra Seri and within the Sierra San Felipe of Baja California limits the amount of slip on the Sacrifico fault to a few tens of km (Chapter 5 of this thesis).

6.6 Discussion

The following discussion presents an overview of extension on the margins of the Delfín basin prior to and after opening of the upper and lower sub-basins (Fig. 6.4 and Table 6.1). This model is similar to ones presented by *Lonsdale* [1989], *Stock* [2000], and *Nagy and Stock* [2000] but with additional geologic constraints on the opening of the Upper and Lower Delfín basins from Chapters 5 and 7 of this thesis. The most important aspect of the Upper Delfín basin not accounted for by these previously published tectonic models is the surprisingly close restoration of the conjugate rift margins exposed in Baja California and Sonora. This close correlation of ignimbrite strata, presented by *Oskin et al.* [2001] and in Chapter 5, suggests that most of the upper crust on the conjugate margins of the Upper Delfín basin is accounted for by presently mapped outcrops. This information, combined with the record of continental extension from the margins, provides powerful constraints on the budget of continental crust and rift evolution in Upper Delfín segment of the Gulf of California. Similar constraints for the Lower Delfín basin require testing for the presence of correlative strata on northwestern Isla Angel de La Guarda. This uncertainty does not greatly affect the implications of the extensional record discussed here.

Table 6.1. Kinematic model for the tectonic evolution of the Upper and Lower Delfín basin.

A. Pre-Extensional Markers (<12 Ma)

- Arc Volcanism concentrated at the Puertecitos Volcanic Province and surrounding areas from 21–16 Ma (Chapter 2 of this thesis). Distribution of these rocks on Isla Angel de la Guarda is unconstrained.
- Distinctive conglomerate deposits in the Sierra San Felipe of Baja California and the Sierra Seri of coastal Sonora [*Gastil et al.*, 1973].
- Emplacement of the Tuff of San Felipe at ∼12.6 Ma; erupted from a vent located in coastal Sonora [*Stock et al.*, 1999; *Oskin et al.*, 2001].

B. Early Continental Extension (12–6.3 Ma)

- Beginning of extension on N-striking San Pedro Mártir [*Stock and Hodges*, 1990], San Felipe [*Stock et al.*, 1991], Santa Rosa [*Bryant*, 1986], and Tecomate normal faults.
- Probable beginning of extension on Ironwood Canyon fault [*Lewis and Stock*, 1998b], Campo fault, and in coastal Sonora.
- Beginning of distributed extension and shear on Matomí accommodation zone [*Stock and Hodges*, 1990], the La Cruz fault, and possibly the Sacrificio fault.
- Extensional roll-over fold forms in the Sierra Menor between opposite-polarity normal faulting on Isla Tiburón and Baja California.

C. Ignimbrite Volcanism in the northern Puertecitos Volcanic Province (6.3–6.1 Ma)

- Eruption of the Tuffs of Mesa Cuadrada and Tuffs of Dead Battery Canyon ca. 6.3 Ma from a vent located within the Matomí accommodation zone. Formation of caldera collapse features in the southern Sierra San Fermín and Santa Isabel Wash areas (Chapter 2 of this thesis).
- Eruption of the Tuffs of Arroyo El Canelo ca. 6.1 Ma from same vent area as the Tuffs of Mesa Cuadrada (Chapter 2 of this thesis).

Table. 6.1, continued

D. Opening of the Upper Delfín basin (∼6 Ma)

- Separation of Baja California from Isla Tiburón and coastal Sonora, forming Upper Delfín basin [*Oskin et al.*, 2001]. Large-magnitude oblique extension at the Puertecitos High Extension zone [*Stock et al.*, 1991] may be a fragment of a breakaway zone. Other breakaway zones probably exist offshore of Baja California and Isla Tiburón.
- Initiation of the Tiburón Fracture Zone at the junction of the Matomí accommodation zone and the La Cruz fault. Initial slip on the Tiburón Fracture Zone included significant (>26 km?) strike-slip displacement on the La Cruz fault. Slip rate on the La Cruz fault decreased by ∼4 Ma, leaving the La Cruz block as part of southern Isla Tiburón.

E. Ignimbrite Volcanism in the eastern Puertecitos Volcanic Province (3.3–2.6 Ma)

- Eruption of the Tuffs of Los Heme from 3.3 Ma to 2.6 Ma from a vent offshore east of the Puertecitos Volcanic Province [*Martín-Barajas et al.*, 1995]. The distribution of these ignimbrites on Isla Angel de la Guarda and in the Upper Delfín basin is unconstrained.
- Extension within the southern Puertecitos Volcanic Province and dextral-oblique extension on the Ballenas Tranform fault (Chapter 7 of this thesis).

F. Opening of the Lower Delfín basin (∼2.6 Ma)

- Northwestward jump in the locus of spreading in the Upper Delfín basin, abandoning spreading center adjacent to Isla Tiburón [*Lonsdale*, 1989].
- Separation of Isla Angel de la Guarda from Baja California, forming Lower Delfín basin [*Lonsdale*, 1989; *Stock*, 2000]. Breakaway zone may lie adjacent to northwest Isla Angel de la Guarda.
- Slowing and eventual stalling(?) of motion on the Tiburón Fracture Zone in favor of dextral displacement on the Ballenas Transform fault [*Stock*, 2000].
- Inception of left lateral faulting and clockwise vertical-axis rotation in Baja California [*Lewis and Stock*, 1998a].

6.6.1 Early continental extension

Early continental extension, prior to opening of the Upper Delfín basin, is generally of low magnitude where its record is well constrained by overlapping younger strata.

Figure 6.4. (next page) Kinematic model for opening of the Upper and Lower Delfín basins, Gulf of California. Based upon a model linking volcanism of the Puertecitos Volcanic Province and rift initiation proposed by *Stock* [2000] with additional geology from Isla Tiburón, coastal Sonora, and the southern Puertecitos Volcanic Province (Chapter 7 of this thesis). Eastern coastline of Baja California and the coasts of Isla Tiburón, Isla Angel de La Guarda, and Sonora shown as thin dashed lines. Active faults shown as solid thick lines. Faults that are about to become active shown as dashed thick lines. See Table 6.1 for summary of tectonic and volcanic events depicted here.

Several north-striking normal fault systems accommodated east-west extension during this time (Fig. 6.4b). Differential tilting between the ∼12.6 Ma Tuff of San Felipe and the 6.1–6.3 Ma Tuffs of the Northern Puertecitos Volcanic province is no more than 15° in most areas. Differential tilt may be as high as 24° in the Sierra Alta of northwestern Isla Tiburón, but cross sections across western Isla Tiburón indicate that the degree of differential tilting is lower overall (Plate III). Areas of the Puertecitos Volcanic Province south of the Matomí accommodation zone in Baja California were only slightly extended prior to 6 Ma [*Stock and Hodges*, 1990; *Nagy*, 2000].

Beyond the outcrop area of the Tuffs of the Northern Puertecitos Volcanic Province, areas of large-magnitude continental extension may pre-date opening of the Upper Delfín basin. The most-well constrained of these fault systems is the Santa Rosa normal fault, which underlies a nonmarine basin containing 8.9 Ma and older volcanic rocks [*Bryant*, 1986]. Extension as high as 100% across the El Parral subdomain may also pre-date 6.3 Ma. However, where the Tuffs of the Northern Puertecitos Volcanic Province are present in the southern half of this subdomain, extension occurred later than 6.3 Ma [*Lewis and Stock*, 1998b]. Extension and strike-slip faulting in coastal western Sonora may also pre-date opening of the Upper Delfín basin (Chapter 5 of this thesis), though apatite fission-track ages as young as 6 Ma from this region support a younger extensional history [*Calmus et al.*, 2000].

Minimal upper crustal extension, probably 10–20% overall, occurred on the margins of the Upper Delfín basin prior to ∼6.3 Ma. This appears to be a consistent result on both margins of the Upper Delfín basin (Figs. 6.1 and 6.2). More severe extension may have occurred prior to ∼6.3 Ma in areas north of 30° 45′ in Baja Cal-

Figure 6.4.

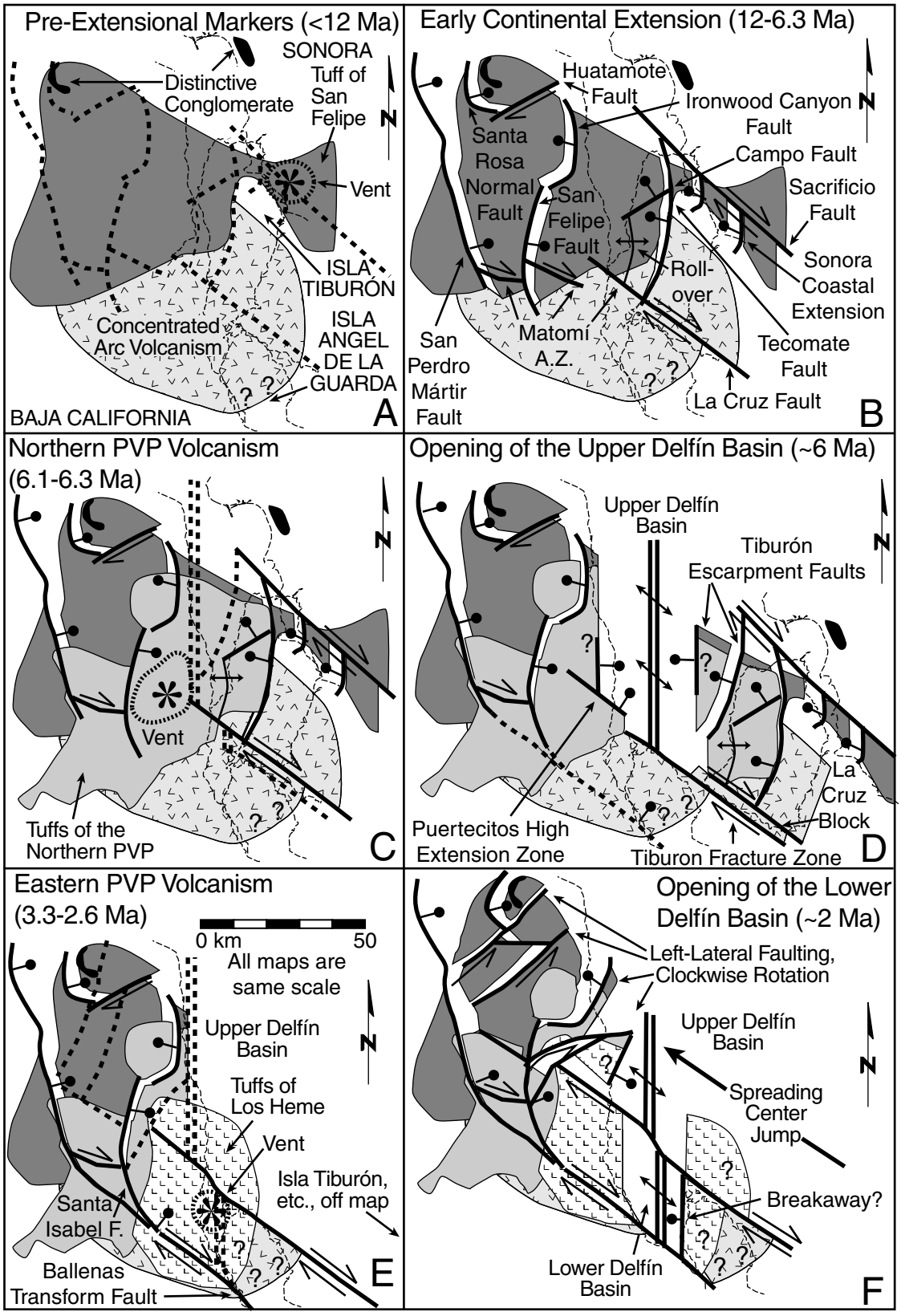
Pre-Extensional Markers (<12 Ma)
SONORA
Distinctive Conglomerate
Tuff of San Felipe
Vent
ISLA TIBURÓN
Concentrated Arc Volcanism
ISLA ANGEL DE LA GUARDA
BAJA CALIFORNIA
A
Early Continental Extension (12-6.3 Ma)
Huatamote Fault
Ironwood Canyon Fault
Santa Rosa Normal Fault
Campo Fault
San Felipe Fault
Sacrificio Fault
Roll-over
Sonora Coastal Extension
Matomí A.Z.
San Perdro Mártir Fault
Tecomate Fault
La Cruz Fault
B
Northern PVP Volcanism (6.1-6.3 Ma)
Vent
Tuffs of the Northern PVP
C
Opening of the Upper Delfín Basin (~6 Ma)
Upper Delfín Basin
Tiburón Escarpment Faults
La Cruz Block
Puertecitos High Extension Zone
Tiburon Fracture Zone
D
Eastern PVP Volcanism (3.3-2.6 Ma)
0 km
50
All maps are same scale
Upper Delfín Basin
Tuffs of Los Heme
Vent
Isla Tiburón, etc., off map
Santa Isabel F.
Ballenas Transform Fault
E
Opening of the Lower Delfín Basin (~2 Ma)
Left-Lateral Faulting, Clockwise Rotation
Upper Delfín Basin
Spreading Center Jump
Breakaway?
Lower Delfín Basin
F

ifornia and in areas east of Isla Tiburón in Sonora. Low amounts of extension in the region surveyed here may be partially explained by proximity to an accommodation zone in the continental rift system [*Faulds and Varga*, 1998]. Extension across the San Pedro Mártir fault segment diminishes southward and is presumably transferred to the southeast, through the Matomí accommodation zone, to an area of extension east of Isla Angel de la Guarda [*Stock and Hodges*, 1990; *Stock*, 2000, and Fig. 6.4b]. The La Cruz fault on Isla Tiburón may have originated as a continuation of this accommodation zone. Normal displacement on the San Felipe fault and the Tecomate fault also diminish southward towards the Matomí accommodation zone and the La Cruz fault, respectively.

6.6.2 Opening of the Upper Delfín basin

The opening of the Upper Delfín basin (Fig. 6.4c) is well constrained from multiple matching cooling units of the Tuffs of the Northern Puertecitos Volcanic Province [*Oskin et al.*, 2001, and Chapter 5]. Closely matched features of these deposits support that conjugate margins of the Upper Delfín basin were in close proximity prior to rupture near the present-day coastlines (Chapter 5 and Fig. 6.4c and 6.4d). North-striking normal fault systems established during prior continental extension continued to accommodate extension of the rift margin in Baja California [*Dokka and Merriam*, 1982; *Stock and Hodges*, 1990; *Lewis and Stock*, 1998b] and Sonora (Plates II and III).

The amount of extension that has occurred over most of the rift margin of the upper Delfín basin after ∼6.3 Ma is similar to the extension that occurred from 12.6 Ma to 6.3 Ma, probably also 10–30% on average. Where normal faults began to move prior to 6.3 Ma, the long-term rate of extension has either remained constant, as in southern Valle Chico [*Stock and Hodges*, 1990] or increased, as in the Sierra San Fermín [*Lewis and Stock*, 1998b] and on Isla Tiburón (Plate III and Fig. 6.3). Locally high amounts of extension occurred after 6.3 Ma in the northern Sierra San Fermín [*Lewis and Stock*, 1998b], adjacent to Puertecitos [*Stock et al.*, 1991], and in

the northern Sierra Kunkaak (Plates II and III). At least part of the large-magnitude extension of the Sonoran coastal area probably also post-dates 6 Ma [*Calmus et al.*, 2000].

Although the timing of opening of the Upper Delfín basin is well constrained, high-precision records of faulting during the initial stages of continental break-up are scarce on its continental margins. Locally high amounts of extension occurred between 6 and 3 Ma northwest of Puertecitos, Baja California (Puertecitos High Extension Zone of Fig. 6.4d, *Stock et al.* [1991]). This northwest-trending zone may have acted as an early strand of the Tiburón Fracture zone, which accommodated opening of the Upper Delfín basin. Other parts of the basin margin fault system have been modified by later faulting and vertical axis rotation in Baja California and may mostly lie offshore (Fig. 6.4f). The conjugate basin margin for the Upper Delfín basin west of Isla Tiburón probably also lies just offshore (Tiburón Escarpment fault of Plate III). Syntectonic sedimentation on the margins of Upper Delfín basin may provide additional high-precision records of extension rate during the initial stages of continental break-up. One location of such a sedimentary record of is the 'proto-gulf' marine basin on southwestern Isla Tiburón, which was deposited adjacent the La Cruz fault from ∼6 to 4 Ma (Chapter 8 of this thesis). Nearby, in the interior of Isla Tiburón, a correlative record of post-6 Ma rocks in the Sauzal basin may record motion of a continental margin fault system during initial opening of the Upper Delfín basin (Plate II and cross section D–D′ of Plate III).

It is uncertain which side of the Upper Delfín basin may have acted as the upper plate during continental break-up. Segmentation established during early continental rifting [*Axen*, 1995] appears to have been continuous across the Upper Delfín basin and probably influenced the position of the Tiburón Fracture Zone [*Stock*, 2000]. However, the polarity of rifting changes from east-directed to west-directed across the Upper Delfín basin, such that each side looks like a lower plate margin. This polarity reversal was established prior to opening of the basin (Plate III).

6.6.3 Opening of the Lower Delfín basin

The Tuffs of Los Heme record a change in tectonism on the Baja California margin of the Upper Delfín basin and possibly the beginning of opening of the Lower Delfín basin (Fig. 6.4e and Chapter 7 of this thesis). Paleomagnetic evidence from the Sierra San Fermín suggests that clockwise rotation of crustal blocks in northeastern Baja California post-dates the eruption of these ∼3 Ma tuffs [*Lewis and Stock*, 1998a, and Fig. 6.4f]. Left-lateral strike-slip faults that accommodate clockwise rotation of crustal blocks also post-date adjacent extensional basins that were active after 6.3 Ma [*Lewis and Stock*, 1998b]. This shift in tectonic activity may have culminated in opening of the Lower Delfín basin and separation of the Isla Angel de La Guarda Microplate from Baja California by 2.6 Ma [*Lonsdale*, 1989; *Stock*, 2000, and Chapter 7]. Further studies on Isla Angel de La Guarda are required to completely characterize the history of the Lower Delfín basin. The record of extension compiled here suggests that opening of the Lower Delfín basin may be as abrupt as that of the Upper Delfín basin.

Overall, extension in the Puertecitos Volcanic Province, which forms the northwest margin of the Lower Delfín basin, is very low (∼5%). Higher amounts of extension (15–29%) are observed locally where the rift margin narrows and at the intersection of east-dipping and west-dipping normal faults (Plate IV and Chapter 7). Extension began in the northern Puertecitos Volcanic Province prior to 6 Ma [*Stock and Hodges*, 1990; *Nagy*, 2000] and in the southeastern corner of the province before 2.6 Ma (Chapter 7 and Fig. 6.4d). These studies indicate that diffuse continental rifting preceded opening of the Lower Delfín basin. A zone of higher extension probably lies just offshore of the Puertecitos Volcanic Province where the Lower Delfín basin opened. Although the initial position of the southeast margin of the Lower Delfín basin (Isla Angel de la Guarda) is uncertain, the pattern of low amounts of continental extensional right up to the coastline is very similar in character to the margins of the Upper Delfín Basin. This similarity suggests, but does not prove, that the zone of

continental rupture may be as narrow in the Lower Delfín basin as observed in the Upper Delfín basin.

Reconnaissance geologic investigations of the southern Puertecitos Volcanic Province and Isla Angel de La Guarda suggest that the Puertecitos area acted as the upper plate during opening of the Lower Delfín basin [*Gastil et al.*, 1975]. The overall structure of the Puertecitos Volcanic Province is interpreted here as an extensional hanging wall rollover. This broad structural feature is evident from the elevation of the top of the Tuffs of Los Heme, which gradually drops from 700 m on the volcanic plateau of the central Puertecitos Volcanic Province to sea level at the Gulf of California. This elevation trend persists despite numerous small-offset west-dipping normal faults that elevate footwall blocks on the Gulf of California side. Although these normal faults sole into down-to-the-east dextral-oblique faults at the western and southwestern margin of the province, the normal offset on these fault systems is small [*Stock and Hodges*, 1990; *Nagy*, 2000, Chapter 7]. Basement exposures at the northeastern end of Isla Angel de La Guarda [*Gastil et al.*, 1975] indicate that the southeastern margin of the Lower Delfín basin may have been uplifted relative to the Puertecitos Volcanic Province. This conjugate margin is interpreted here as the lower plate of the Lower Delfín basin rift segment.

6.6.4 Summary of the kinematic evolution of the Upper and Lower Delfín basins

The tectonic history of opening of the Upper and Lower Delfín basins presented here (Fig. 6.4) confirms many aspects of the existing models for these basins [*Lonsdale*, 1989; *Stock*, 2000; *Nagy and Stock*, 2000]. Pulses of syn-rift ignimbrite volcanism in the Puertecitos Volcanic Province from 6.3–6.1 Ma and 3.3–2.6 Ma coincide with the opening of the Upper and Lower Delfín basins, respectively, as suggested by [*Stock*, 2000] and [*Nagy and Stock*, 2000]. Opening of the Upper Delfín basin commenced with localization of the Pacific–North America plate boundary at ∼6 Ma

[*Oskin et al.*, 2001], presaged by a period of diffuse continental extension that began by 11–12 Ma [*Stock and Hodges*, 1989; *Lee et al.*, 1996]. Significant plate boundary motion occurred initially only in the upper Delfín basin and on the Tiburón Fracture zone, bypassing the site of the Lower Delfín basin [*Lonsdale*, 1989; *Stock*, 2000]. Opening of the Lower Delfín basin was probably underway by 2.6 Ma (Chapter 7 of this thesis) and is likely to have coincided with a northwestward jump in the locus of spreading in the Upper Delfín basin [*Lonsdale*, 1989; *Stock*, 2000; *Nagy and Stock*, 2000]. The initial rate of spreading in the Lower Delfín basin was probably less than in the Upper Delfín basin, such that Isla Angel de la Guarda moved as an independent microplate, surrounded by transform faults and simultaneously active spreading centers (Chapter 7 of this thesis). Eventually, the spreading rate in the Lower Delfín equalled that of the Upper Delfín basin, shifting the plate boundary entirely to the west of Isla Angel de La Guarda [*Lonsdale*, 1989].

Existing models for the tectonic evolution of the Upper Delfín basin do not account for the close restoration of the conjugate rift margins presented by *Oskin et al.* [2001] and in Chapter 5 of this thesis. *Lonsdale* [1989], *Stock* [2000] and *Nagy and Stock* [2000] all conservatively restore ∼200 km of opening in the Upper Delfín basin, reserving a ∼100 km width of crustal area to account for subsided upper continental crust within the basin. These models account for this remaining ∼100 km displacement by a combination of east-west extension and dextral displacement in coastal Sonora. More regional tectonic restorations often closely align the shorelines of the northern Gulf of California in order to approximate the full ∼300 km offset estimated by *Gastil et al.* [1973] [*Gastil et al.*, 1979, for example]. It turns out that this approximation is somewhat closer to what has occurred in the northern Gulf of California, and that the Upper Delfín basin probably opened along a narrow north-striking breakaway zone (Chapter 5 of this thesis). Only minor changes to the models of *Lonsdale* [1989] and *Stock* [2000] are required to place a greater amount of divergence into the Upper Delfín basin. The Wagner Transition Zone model of *Nagy and Stock* [2000] must involve diffuse deformation of a substantial area of new transitional crust in the

northern Gulf of California, rather than submerged upper continental crust.

6.6.5 Implication for vertical strain partitioning

Crustal thickness estimates from passive seismic experiments across the Peninsular Ranges–Gulf of California transition zone indicate thinning by a factor of 2 to 2.5 across the rift flank [*Ichinose et al.*, 1996; *Lewis et al.*, 2000, 2001]. Moho depth reaches a maximum of ∼37 to 40 km beneath western Peninsular Ranges and shallows to ∼15 to 21 km beneath the northern Gulf of California and the Salton Trough. The steepest gradient in Moho depth underlies the high topography of the eastern Peninsular Ranges, directly adjacent to the extended continental margin of the northern Gulf of California. These observations led *Lewis et al.* [2000] to suggest that rifting has been accompanied by significant extension of the lower crust of the eastern Peninsular Ranges. If the continental crust on the margins of the Delfín basin has been extended on average in excess of 100%, as suggested above, then the modest amount of upper crustal extension measured here (Figs. 6.1 and 6.2) also requires that thinning has been decoupled between the upper and lower crust.

Overall, the amount of extension of the upper and lower continental crust must be balanced, so that an area of greater upper-crustal extension is required to offset decoupled large-magnitude lower crustal extension. There are two possible locations of compensatory extension of the upper continental crust in the vicinity of the Upper Delfín basin. One of these locations is the basin itself, where close correlation of the conjugate rift margins indicates that upper crustal extension has been localized and of large magnitude [*Oskin et al.*, 2001; *Lewis et al.*, 2001, and Chapter 5 of this thesis]. Lower crustal flow from the rift flanks towards the Upper Delfín basin would also help to explain formation of anomalously thick transitional crust in this area (Chapter 5 of this thesis). A second possible location of large-magnitude upper-crustal extension is the Sonoran continental margin east of Isla Tiburón. This region may contain a large proportion of the extension partitioned into the southern Basin and Range province during slip on the Tosco-Abreojos fault west of Baja California Sur [*Stock*

and Hodges, 1989]. Large magnitude extension measured here for the Sonoran coastal zone may be a small sample of the tectonism of this realm.

Alternatively, crustal thickness variations beneath the western margin of the Upper Delfín basin may be unrelated to extension after 12.6 Ma. One possibility is that the step in Moho depth beneath the eastern Peninsular Ranges is related to Late Cretaceous through Eocene compression that led to uplift and unroofing of the eastern Peninsular Ranges Batholith [*Ortega-Rivera et al.*, 1997; *Rothstein*, 1997; *Schmidt*, 2000]. This solution is unlikely, however, without a later extensional or delamination event, since an increase in Moho depth would be a more appropriate response to crustal thickening during compression. A second possibility is that pre-12 Ma extension induced lower-crustal thinning beneath the region. Although some early subsidence may be supported by shallow closed-basins preserved in pre-extensional continental sedimentary rocks (group 2, Chapter 2.1), subsidence of the Gulf Extensional Province appears to be mostly a more recent event. Pre-extensional fluvial systems drained west, across the peninsular ranges, as recently as the ∼12.6 Ma eruption of the Tuff of San Felipe [*Dorsey and Burns*, 1994; *Stock et al.*, 1999]. The modern elevations of the Gulf Extensional Province (0–0.5 km) and the western Peninsular Ranges (1.5–2 km) are consistent with isostatic compensation of the crustal thickness variations (10–15 km) described by *Lewis et al.* [2001]. Flexural rigidity [*Lewis et al.*, 2001] and/or lateral mantle density variations [*Wernicke et al.*, 1996; *Lewis et al.*, 2000] are only necessary to support the higher topography of the eastern Peninsular Ranges.

6.6.6 Rift localization in the Upper Delfín basin

Although the geometry of continental rifting appears to have affected the kinematic evolution of the Upper Delfín basin [*Stock*, 2000], the rate of upper crustal extension on the basin margins does not show a strong response to localization of strain in the rift basin. Mechanical models of continental rifting describe a runaway effect where rifting creates a zone of weakness that localizes strain [*England*, 1983;

Buck, 1991]. Field examples from East Africa and the Red Sea support this mechanism [*Cochran*, 1983; *Ebinger and Casey*, 2001]. The long term evolution of the Basin and Range Province in northwestern Mexico is also cited by *Buck* [1991] as an example of rift localization, where thinning of the crust eventually favored localization of rifting into the Gulf of California. The rifting history presented here for the margins of the Upper Delfín basin indicates that strain rate remained constant or increased at the onset of crustal rupture, rather than decreasing as the models would suggest.

Overall, the strain rate increased dramatically in the Gulf of California with localization of the Pacific–North America plate boundary here [*Oskin et al.*, 2001]. Proportionally, within the study area, the majority of this strain localized into the Upper Delfín basin and the fraction of the strain budget accommodated by the continental margin fault systems decreased dramatically. However, the long-term extension rate on individual continental normal fault systems changed little with the opening of the Upper Delfín basin. Quaternary faulting on most of the major continental normal fault systems on both margins of the Upper Delfín basin indicates that forces driving intracontinental extension persist to the present. This evidence suggests that rift localization into the Upper Delfín basin may have been a response to outside boundary forces resulting in a significant increase in strain rate, rather than a response to weakening of the crust resulting from intracontinental extension.

6.7 Conclusions

The magnitude of extension of upper continental crust on the margins of the Upper and Lower Delfín basins of the northern Gulf of California ranges from <5% to ∼40% in most areas. More severe extension may have occurred in areas north of 30° 45′ in Baja California and east of Isla Tiburón in Sonora. Higher percent extension is probably also associated with breakaway zones where the Upper and Lower Delfín basins opened. Overall, the magnitude of upper crustal extension on the margins of the Delfín basin is much less than the factor of 2 to 2.5 thinning of

the entire crustal column estimated from changes in Moho depth [*Lewis et al.*, 2001]. This result suggests that thinning was accommodated in part by lower crustal flow to areas elsewhere in the rift or outside of the rift margin. Localized, large-magnitude upper crustal extension in the Upper Delfín basin and/or in western Sonora may have accommodated this flow by exhumation of lower crust.

Evidence for the timing of opening of the Upper and Lower Delfín basins confirms, in general, the timing predicted by existing models [*Lonsdale*, 1989; *Stock*, 2000; *Nagy and Stock*, 2000]. Pulses of syn-rift ignimbrite volcanism in the Puertecitos Volcanic Province from 6.3–6.1 Ma and 3.3–2.6 Ma coincide with the opening of the Upper and Lower Delfín basins. However, a greater amount of divergence is required within the Upper Delfín basin than previously suggested to account for close restoration of its conjugate rifted margins.

Extensional strain on the margins of the Gulf of California remained steady or increased after opening of the Upper Delfín basin, contrary to models of continental rift evolution, which predict that strain should become localized within the ocean basin. Quaternary faulting on most of the major continental normal fault systems on both margins of the Upper Delfín basin indicates that forces driving intracontinental extension remain active. Rift localization into the Upper Delfín basin may have been a response to a significant increase in strain rate, brought on by a change in boundary forces, rather than a response to weakening of the crust resulting from intracontinental extension.

Chapter 7

Structural development of the Main Gulf Escarpment in the southern Puertecitos Volcanic Province, Baja California, Mexico

7.1 Abstract

The structural development of the Main Gulf Escarpment in the southern Puertecitos Volcanic Province is investigated here to determine the history of faulting leading to opening of the Lower Delfín basin of the Gulf of California. The Cinco Islas study area encompasses an unusually narrow reach of the Baja California continental margin where the Main Gulf Escarpment passes within 5 km of the coastline. Three families of normal faults are recognized at Cinco Islas. 1–2 km of dextral separation on northwest-striking dextral-oblique faults forms the Main Gulf Escarpment. This fault system appears to have accommodated extension within the interior of the Puertecitos Volcanic Province. North-striking, east-dipping and west-dipping normal faults originate at this dextral oblique fault zone. The majority of faulting at Cinco Islas pre-dates emplacement of the upper part of the Tuffs of Los Heme at ∼2.6 Ma. Fault activity may have migrated away from the Main Gulf Escarpment and localized within the Lower Delfín basin by this time. Opening of the Lower Delfín basin by 2.6 Ma would require that Isla Angel de La Guarda has acted as an independent microplate within the Gulf of California during part of its history, surrounded by simultaneously active spreading centers.

7.2 Introduction

Narrow continental rifts are thought to form by a runaway process, where crustal weaknesses localize extensional strain [*England*, 1983; *Buck*, 1991]. In contrast, intracontinental extension probably involves strain-dependant strengthening through crustal compensation of localized extension and/or buoyancy-driven restoring forces [*Buck*, 1991; *Hopper and Buck*, 1996]. These processes may represent a continuum of crustal rifting mechanisms with a tendency towards localization and continental rupture with time [*Buck*, 1991]. Once a continental rupture has been established, no mechanism has been proposed whereby seafloor spreading would be arrested in favor

of further continental rifting.

The midriff islands region of the northern and central Gulf of California presents an anomalous tectonic history of rift localization and abandonment. Rifting southeast of Isla Angel de La Guarda that formed the Tiburón basin later jumped north of this island, forming the lower Delfín basin [*Lonsdale*, 1989; *Stock*, 2000, Fig. 7.1]. This process appears to have produced two regions of continental rupture on the same rift segment, separated by a continental microplate, Isla Angel de la Guarda. Present-day Pacific–North America plate motion appears to be largely confined to the Lower Delfín basin and Ballenas Transform segments of the northern Gulf of California, bypassing the Tiburón fracture zone and Tiburón basin [*Henyey and Bischoff*, 1973; *Bischoff and Henyey*, 1974; *Ortlieb et al.*, 1989; *Lonsdale*, 1989; *Persaud et al.*, 1999].

Stock [2000] proposed that large-volume rhyolitic pyroclastic eruptions in the Puertecitos Volcanic Province correspond to the opening of the upper and lower Delfín rift segments in the northern Gulf of California. This hypothesis has been strengthened by restoration of displaced deposits of the ∼6.1 to 6.3 Ma Tuffs of the Northern Puertecitos Volcanic Province just prior to opening of the northern Delfín basin [*Oskin et al.*, 2001, and Chapter 5 of this thesis]. According to *Stock* [2000], eruption of the Tuffs of Los Heme between 3.3 Ma and 2.6 Ma [*Martín-Barajas et al.*, 1995, and Melbourne, unpublished data] would reflect the onset of opening in the Lower Delfín basin.

This study is designed to examine the record of opening of the Lower Delfín basin by documenting the faulting history on its continental margin in Baja California. The Cinco Islas study area (Fig. 7.1) is located along the northwestern projection of the Ballenas Transform fault (also called the Guaymas Transform fault) of the Gulf of California rift. This transform fault accommodates opening of the Lower Delfín basin. The southeast edge of the study area encloses a portion of the Main Gulf Escarpment, which separates the extended continental margin of the Gulf of California from the tectonically stable interior of Baja California. The Cinco Islas study area is unusual because the Main Gulf Escarpment passes within 5 km of the

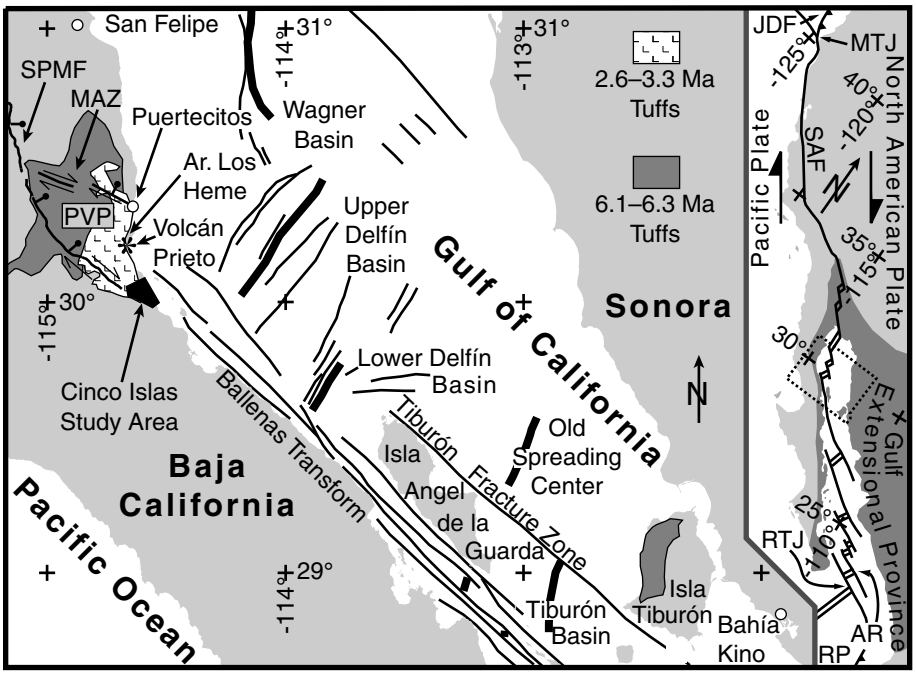

Figure 7.1. Location map of study area. Inset shows part of Pacific-North America plate boundary. AR, Alarcon Rise; JDF, Juan de Fuca plate; MTJ, Mendocino triple junction; RP, Rivera plate; RTJ, Rivera triple junction; SAF, San Andreas fault. Tuffs of the northern Puertecitos Volcanic Province in gray [*Oskin et al.*, 2001, and Chapter 5]. Tuffs of Los Heme shown with pattern [*Martín-Barajas et al.*, 1995; *Stock*, 2000, and Chapter 2]. Marine faults (thin lines) and axes of pull-apart basins (thick lines) are from *Fenby and Gastil* [1991]. 'Old Spreading Center' is an inferred former location of the axis of the Upper Delfín basin [*Fenby and Gastil*, 1991; *Lonsdale*, 1989; *Stock*, 2000]. MAZ, Matomí Accommodation Zone; PVP, Puertecitos Volcanic Province; SPMF, San Pedro Mártir Fault.

coastline here. Therefore, the history of faulting at Cinco Islas integrates the onshore record of rifting that has accompanied opening of the Lower Delfín basin into a narrow region. The Cinco Islas study area also corresponds to the southernmost outcrop area of the Tuffs of Los Heme. The relationship of these tuffs to fault movement at Cinco Islas thus provides a direct test of the chronology of rifting and volcanism proposed by *Stock* [2000]. The geology of this region also provides a potential geologic tie point to Isla Angel de la Guarda. The Cinco Islas study area was mapped previously in reconnaissance by *Gastil et al.* [1975]. *Gastil and Miller* [1993] describes several detailed studies of metasedimentary basement rocks along 30°N latitude and west of the area studied here. The northeast corner of mapping by *Phillips* [1993] overlaps the western corner of the area studied here by ∼0.5 km.

7.3 Stratigraphy

The strata exposed at Cinco Islas are divided here into four groups. These groups are the same as groups one, two, three, and six described in previous chapters of this thesis. This group numbering is maintained in the descriptions presented here. Group one forms the pre-Tertiary basement, which is almost entirely metasedimentary rocks in the study area. Group two comprises thin and discontinuous sedimentary deposits overlying the basement unconformity. Group three, Miocene arc-related volcanic and sedimentary rocks, forms the majority of outcrops in the Cinco Islas area. Group six comprises Pliocene age and younger rift-related volcanic and sedimentary rocks. The Tuffs of Los Heme [*Martín-Barajas et al.*, 1995] form the largest volume of group six rocks in Cinco Islas. The stratigraphic relationship of most interest here is the relationship of these tuffs to faulting and topographic relief formed in older strata.

7.3.1 Group 1: Pre-Tertiary basement

Pre-Tertiary basement of the Cinco Islas study area is almost entirely comprised of metasedimentary rocks of the Olvidada Formation [*Phillips*, 1993]. Within the

study area, these strata are mostly thinly-bedded pelitic schist with lesser amounts of marble, calc-silicate rock, and metachert. Quartzose lithologies are rare. These strata have been metamorphosed to amphibolite grade (andalusite-staurolite) and isoclinally folded [*Phillips*, 1993; *Rothstein*, 1997]. Foliation is consistently northwest-striking and dipping 50–70° to the northeast throughout the study area. Albian-Aptian fossils, including rudists, have been recovered from the Olvidada Formation [*Phillips*, 1993]. *Gastil* [1993] and *Phillips* [1993] interpret the Olvidada Formation as part of a back-arc basin, age-equivalent to the Alisitos Formation of western Baja California, that was closed during Late Cretaceous time. Southwest of Cinco Islas, the Olvidada Formation unconformably overlies Permian El Mármol, Zamora, and Cerro El Volcán Formations and Triassic De Indio Formation. These older strata are interpreted by *Buch and Delattre* [1993] as eugeoclinal (distal) strata derived from North America. Alternative interpretations of Baja California as an exotic terrane accreted in Cretaceous time [*Sedlock et al.*, 1993; *Dickinson and Lawton*, 2001] require an alternative origin for these formations.

Outcrops of pre-Tertiary basement are most common in the western and southern boundaries of the study area (unit Mzm, Plate IV). Volcanic and sedimentary rocks of groups two, three, and six cover an uneven pre-Miocene erosion surface. The paleoelevation of this surface may have been higher in the southwest, where group three volcanic rocks pinch out. Isolated, irregular basement outcrop patterns occur in some localities from exhumation of this uneven erosion surface. Isolated basement exposures also occur in a horst block in 'Dry Fall Canyon' ($^{7}27^{200}$E; $^{33}25^{700}$N, all locations are Universal Transverse Mercator, zone 11, NAD27 datum).

Outcrops of felsic intrusive rocks within the basement are rare and of small volume in the study area. These outcrops are not mapped on plate IV. These intrusions are assumed here to be part of the Cretaceous Peninsular Ranges batholith. Heat from this batholith was probably responsible for metamorphism of the metasedimentary rocks here [*Rothstein*, 1997]. A tonalite pluton of this batholith mapped by *Gastil et al.* [1975] crops out less than 1 km south of the study area.

7.3.2 Group 2: Tertiary Sedimentary Rocks

Group two sedimentary deposits unconformably overlie the Olvidada formation in 'Dry Fall Canyon.' These deposits are a 5–10 m thick, clast-supported, fluvial conglomerate mapped as unit Tcg on Plate IV. Clasts range in size from sand grains through small boulders, with cobbles most common. Clast lithologies are a mixture of volcanic lithologies with metamorphic and igneous basement. No distinctive lithologies were identified that might be exotic to the field area and surrounding region. Volcanic lithologies increase in abundance up-section, forming a gradational contact with overlying volcanic conglomeratic sandstone (unit Tmvcs). Unit Tcg is most likely Oligocene through Early Miocene age. Similar outcrops of basal sedimentary strata, located south and east of the study area, were assigned to the Mesa Formation by *Dorsey and Burns* [1994]. *Dorsey and Burns* [1994] recognized that these deposits underlie volcaniclastic rocks of the middle Miocene volcanic arc, and estimated an Oligocene to early Miocene age for the Mesa Formation. Similar basal sedimentary strata that crop out north of the Puertecitos Volcanic Province are described in Chapter 2.

7.3.3 Group 3: Miocene volcanic arc

Andesitic lava flows, tuffs, and volcaniclastic debris flows comprise the most voluminous lithologic group within the Cinco Islas study area. These deposits are correlated by lithologic similarity to Early to Middle Miocene age calc-alkaline arc volcanic rocks found throughout the Baja California peninsula [*Gastil et al.*, 1979; *Sawlan and Smith*, 1984]. Proximal facies of the Early to Middle Miocene volcanic arc, similar to the rocks exposed at Cinco Islas, are common in the Puertecitos Volcanic Province (Chapter 2 of this thesis). In Baja California Sur, equivalent arc-related volcanic rocks are known as the Comondú Formation [*Hausback*, 1984; *Sawlan*, 1991]. Within the study area, group three deposits of Cinco Islas are described as four separate packages and divided into 18 separate mappable units and subunits (Plate IV). Prox-

imal facies derived from two andesitic volcanic centers make up the majority of group three deposits. Two of these packages comprise an upper and lower vent complex with andesite lava flows, vent plugs, and cinders beds. Pyroclastic deposits, flow breccia, and debris flows form a middle package that crops out between lava flows from these two centers. Slightly more distal facies, represented by volcaniclastic sandstone, conglomerate, and a small-volume lava flow, crop out below and interfinger with the proximal deposits. Each of these four packages is described in greater detail in the following sections.

Volcaniclastic sandstone and conglomerate

Buff-colored, fine-grained ash and volcanic lithic sandstone and conglomerate form the base of Miocene age volcanic arc strata at Cinco Islas. Conglomeratic sandstone, mapped as unit Tmvcs, is the lowermost and most widespread of these rocks. Tmvcs forms a gradational contact with underlying group two conglomerate in 'Dry Fall Canyon.' Elsewhere, Tmvcs unconformably overlies group one basement. Tmvcs is overlain by lower andesite lava flows and related pyroclastic deposits. An at least 2 m thick andesite lava flow, with plagioclase and oxidized hornblende(?) phenocrysts crops out within Tmvcs, 1 km northwest of Arroyo Miramar (unit Tmva, $^{7}27^{500}$E, $^{33}24^{100}$N). In the northwestern part of the study area, conglomerate content within Tmvcs increases up-section, and a gradational contact is mapped between Tmvcs and an upper volcaniclastic conglomerate unit, Tmvcg. This conglomerate appears to be equivalent in composition and stratigraphic level to conglomerates mapped above the lower andesite and intermediate volcaniclastic deposits further to the west. From these relationships, it appears that medial to distal volcaniclastic rocks were deposited continuously adjacent to the proximal volcaniclastic rocks common to the rest of the Cinco Islas study area.

Lower andesite volcano and lava flows

Andesite flows and related small-volume pyroclastic deposits mark the onset of proximal volcanic deposition within the Cinco Islas study area. These deposits culminate in a ∼1 km diameter cinder cone with a 40 m diameter central andesite plug (unit Tmlav, $^{7}27^{400}$E, $^{33}25^{000}$N). An offset continuation of this volcano lies ∼2 km to the east ($^{7}29^{650}$E, $^{33}24^{500}$N). Three eruptive phases are recognized from this vent system. Each of these phases was initiated by pyroclastic deposition, followed by emplacement of andesite lava. Outside of the vent region, pyroclastic deposits typically comprise a 2 m or thinner layer of red scoria and andesitic lithic lapilli in a matrix of red to yellow coarse ash. These are overlain by massive dark-gray to dark purple andesite lava flows with plagioclase phenocrysts. Where these deposits cannot be subdivided into separate eruptive units, pyroclastic deposits are mapped as unit Tmlavr and the andesite lava is mapped as unit Tmla.

The lowermost eruption began by building a cinder cone and culminated in effusion of andesite lava flows. Proximal, cinder-cone-building pyroclastic deposits of yellow, red, and black andesitic scoria and lithic lapilli are mapped as unit Tmlavv. These deposits preserve primary dips at radiating away from the cinder cone and contain 2% elongate andesite bombs that flowed downhill after impact onto the cone surface (also known as cow-dung bombs). Tmlavv grades laterally into red to yellow ash, scoria and lithic lapilli mapped as unit Tmlavr1. Andesite lava flows, mapped as unit Tmla or Tmla1, erupted from a vent on the flank of the cinder cone preserved at the offset fragment ($^{7}29^{650}$E, $^{33}24^{500}$N). These pyroclastic deposits and associated Tmla1 lava flows occur together as far east as 'Travertine Wash' ($^{7}33^{800}$E, $^{33}21^{800}$N). These flows thin abruptly southwest of the cinder cone deposit ($^{7}26^{900}$E, $^{33}24^{400}$N), which suggests that this volcano may have been built on a northeast-facing paleo-slope.

A second eruption continued to build the lower andesite cinder cone and deposited a mantle of pyroclastic debris mapped as unit Tmlavr2. In most localities, these pyroclastic deposits are similar to unit Tmlavr1. A thicker section of Tmlavr2, with

a greater amount of ash beds and reworked deposits, occurs in 'Travertine Wash.' These deposits overlie a relatively thin lava flow of Tmla1, and may have ponded here against thicker lava flows to the northeast. A second andesite lava flow, mapped as unit Tmla2, erupted from a second vent on the flank of the cinder cone, located 1 km northwest of the first vent ($^{7}29^{050}$E, $^{33}25^{400}$N). This vent is very well exposed in the west canyon wall of Arroyo Miramar.

A third and final eruption of the lower andesite is confined to the area of the cinder cone. This eruption may have commenced by forming an explosion crater (or sector collapse?) that removed part of the Tmla1 and Tmla2 lava flows ($^{7}27^{700}$E, $^{33}25^{000}$N). The near-vertical walls of this crater are recognized by a mantle of bright red agglutinated spatter and scoria, mapped as unit Tmlavvr. These deposits are also present above lower andesite lava flows in the vicinity of the vent. The andesite lava plug in the center of the cinder cone (unit Tmlav) may have been emplaced into the bottom of the crater during this final eruption.

Middle volcaniclastic rocks

Andesitic tuffs, lahar deposits, and volcaniclastic breccias mark the second stage of proximal arc volcanism within the Cinco Islas study area. The thickness and proportion of primary deposits increases towards the southeastern part of the study area at 'Travertine Wash.' Most likely, these deposits were erupted from the same vent as the upper andesite lava flows which are also thickest in this area. A massive (0.4 km by 1 km) andesite plug, mapped as unit Tmuav, marks the location of this vent ($^{7}30^{300}$E, $^{33}23^{200}$N). This plug is offset about 1–2 km northwest of the thickest section of pyroclastic deposits and lava flows ($^{7}32^{300}$E, $^{33}22^{000}$N). The middle volcaniclastic rocks are subdivided into five members based upon significant changes in texture and bedding thickness. All five of these members are mapped in the most proximal position at 'Travertine Wash.' Two members are mapped in 'Camp Wash.' An undifferentiated member, Tmvbr, is mapped where the other members cannot be discerned because of talus cover. Unit Tmvbr is also mapped in the northwestern

part of the study area where reworked volcaniclastic debris flows and conglomerate predominate and the association to the other members is unclear. Conglomerate outcrops at the top of the volcaniclastic section in this area are correlated to unit Tmvcg, which is described above under the volcaniclastic sandstone and conglomerate heading.

Two members, each comprised predominantly of volcanic ash, form the lower part of the intermediate volcaniclastic rocks. A 2–5 m thick reworked volcaniclastic sandstone forms the lowermost member in 'Travertine Wash.' This sandstone is mapped as unit Tmvss and is made up of mostly coarse-grained, white volcanic ash and small pumice and lithic lapilli. Individual beds are 1–5 cm thick. The lower massive member, unit Tmvlm, forms the thickest and most extensive proximal member of the intermediate volcaniclastic rocks. Tmvlm is mapped from Arroyo Las Palmitas ($^{7}34^{100}$E, $^{33}20^{600}$N) to Arroyo Mirimar ($^{7}28^{800}$E, $^{33}25^{600}$N). Massive andesitic tuffs, each 10–30 m thick, are the dominant lithology of the lower massive member. These tuffs are 60–70% buff-colored ash, 20–30% andesitic lithic fragments, and 5–10% white pumice with plagioclase and hornblende phenocrysts. An andesite breccia is mapped between these tuffs at 'Travertine Wash' ($^{7}32^{550}$E, $^{33}21^{300}$N). Similar andesite breccias occur within lower massive member exposures in 'Camp Wash.' These small-volume breccia deposits are not mapped on plate IV.

Three members comprise the upper part of the intermediate volcaniclastic rocks. Two of these members, Tmvgb and Tmvug, are comprised of stacked 1–5 m thick beds of poorly sorted volcaniclastic breccia. These beds exhibit normal and reverse grading and are interpreted as both primary and reworked debris flows. Subrounded to angular clasts of plagioclase-phyric andesite are distinctive to these units. The phenocryst size (up to 1 cm) and content (up to 35%) of these clasts is much higher than in the associated upper andesite lava flows. This may indicate that a more viscous magma was involved during emplacement of the intermediate volcaniclastic rocks. The Upper Massive member (unit Tmvum) crops out between units Tmvgb and Tmvug at 'Travertine Wash' and north of Arroyo Las Palmitas. Unit Tmvum is

similar in texture and composition to the Lower Massive member, but with a greater proportion (25%) and larger-sized pumice. Outcrops of Tmvum are not mapped in 'Camp Wash.' A single, thicker section of graded beds mapped here as unit Tmvgb may contain laterally equivalent deposits to Tmvgb, Tmvum, and Tmvug mapped at 'Travertine Wash.'

Upper andesite volcano and lava flows

Andesite lava flows (unit Tmua) and a related andesite plug (unit Tmuav) form the uppermost group 3 deposits within the Cinco Islas study area (Plate IV). Both of these deposits are fine-grained, glassy, light to medium gray, orange-weathering andesite with 5% macroscopic plagioclase phenocrysts. Individual flow units within the upper andesite are marked by breccia concentration zones in outcrops at the head of 'Travertine Wash' ($^{7}32^{300}$E, $^{33}22^{000}$N) but are not prominent elsewhere. The presence of interflow breccia deposits and associated proximal pyroclastic deposits in the underlying intermediate volcaniclastic rocks indicates that a vent existed for these flows in the vicinity of 'Travertine Wash' and Arroyo Las Palmitas. Unit Tmuav marks the likely location of this vent offset 1–2 km dextrally on the Miramar fault. A fragment of this plug also crops out between two strands of the Miramar fault ($^{7}31^{300}$E, $^{33}23^{000}$N).

The upper andesite is a thick deposit but of local extent. Upper andesite flows exceed 100 m thickness between 'Camp Wash' and 'Travertine Wash.' Thinner deposits of upper andesite occur west of 'Camp Wash.' The upper andesite does not crop out north of 'Dry Fall Canyon.' The uppermost surfaces of the andesite lava flows are recognized from their subdued topography and by rare preservation of pahoehoe flow surfaces. These surfaces are mapped in localities where they are displaced by faults (e.g., $^{7}34^{000}$E, $^{33}22^{500}$N). Two outcrops of andesite directly overlying basement in the southern part of the study area are tentatively assigned to the upper andesite flow unit. These lava flows may also be part of the lower andesite or from a source outside of the study area.

7.3.4 Group 6: Syn-rift volcanic and sedimentary rocks

Syn-rift volcanic and sedimentary rocks of Cinco Islas are divided into three sequences separated by erosional unconformities. Two members of the Tuffs of Los Heme occur within the first and second of these sequences. Correlation of these four members to the ∼30 members present at Arroyo Los Heme [*Martín-Barajas et al.*, 1995] is discussed separately. At Cinco Islas, the canyons at 'Travertine Wash,' 'Camp Wash,' and Arroyo Miramar were all formed at the lowest unconformity beneath group six deposits. The lower group six sequence comprises the lower two cooling units of the Tuffs of Los Heme (Tprho and Tprhp) and an underlying Miocene(?) to Pliocene conglomerate (Tmpal). After emplacement of the Tprhp member of the Tuffs of Los Heme, a period of erosion partially removed these deposits from the canyons. The middle group six sequence, which partially refilled these canyons, is comprised of a basaltic cinder cone (unit Tpbc), overlain by the upper two cooling units of the Tuffs of Los Heme (units Tprhu and Tprhy), and capped by a small-volume basalt flow (unit Tpb). Erosion again removed these deposits from the canyons and downcutting has continued into the Quaternary period. The upper group six sequence comprises two generations of fluvial terraces of probable Quaternary age (units Qoal1 and Qoal2), as well as undifferentiated fluvial terraces (Qoal), active alluvium (Qal), talus (Qt and Qtv) and landslide deposits (Qls). An extensive travertine deposit (unit Qtr) mantles topography in the southern part of the study area at 'Travertine Wash' and Arroyo Las Palmitas. Each of these three sequences is described in greater detail in the following sections.

Lower sequence

Two cooling units of the Tuffs of Los Heme form the lower sequence of group six deposits. The lower cooling units of the Tuffs of Los Heme, units Tprho and Tprhp, form a distinctive pair throughout the interior of the southern Puertecitos Volcanic Province. The lowest of these units, Tprho, is a pink to orange partially welded to

non-welded ash-flow tuff with 15% pumice fiamme, 5% volcanic lithic fragments, and 1% plagioclase phenocrysts. The thickness of Tprho varies from 0 to 70 m in the Cinco Islas study area. This unit filled in paleotopography near the outlet of 'Camp Wash,' at Arroyo Miramar, and at 'Dry Fall Canyon.' At the northwest edge of the study area, Tprho covered fluvial conglomerates (Tmpal) and formed the base of a volcanic plateau in the southern Puertecitos Volcanic Province. Overlying Tprho, Tprhp is a densely welded ash-flow tuff with 5% pumice, 5% volcanic lithic fragments, and 2–4% plagioclase phenocrysts. Tprhp varies from 0–60 m thick in the study area. In deposits of Tprhp greater than 10 m thickness, the densest welding zone occurs at about one-third of the way up from the base of the flow. Tprhp appears to have been deposited from a higher-energy pyroclastic flow than Tprho, and deposits of Tprhp are plastered onto canyon walls in 'Camp Wash' and Arroyo Miramar. Densely welded Tprhp deposits also form a 1–2 m thick veneer of densely welded tuff on high mesas of upper andesite west of 'Camp Wash' and between Arroyo Miramar and 'Dry Fall' canyon. Tprhp also forms the southernmost mapped outcrop of the Tuffs of Los Heme, located within 'Travertine Wash' ($^{7}34^{000}$E, $^{32}16^{000}$N). Both the Tprho and Tprhp members of the Tuffs of Los Heme preserve a normal paleomagnetic polarity (Fig. 7.2 and Table 7.1).

Table 7.1. Paleomagnetic results from the Tuffs of Los Heme from Cinco Islas.

Unit	UTM E	UTM N	n/n$_0$	Dec.	Inc.	κ^a	$\alpha_{95}{}^a$	$\kappa_1{}^b$	$\alpha_{95}{}^b$	$\kappa_2{}^b$	$\alpha_{95}{}^b$
Tprho	$^{7}32^{100}$	$^{33}25^{750}$	7/7	356.0	52.1	1177	1.6	-955	1.2	-691	1.4
Tprhp	$^{7}32^{250}$	$^{33}25^{850}$	5/6	15.2	36.9	266	4.2	-544	1.9	-128	3.9
Tprhu	$^{7}32^{250}$	$^{33}25^{900}$	7/7	172.9	-45.4	414	2.8	-595	1.5	-184.7	2.8

[a] Fisher statistics.

[b] Bingham statistics.

Miocene(?) to Pliocene age fluvial conglomerate crops out below, between, and above units Tprho and Tprhp of the Tuffs of Los Heme. These conglomerate outcrops, mapped as unit Tmpal, are confined to the northwestern corner of the study area, adjacent to 'Dry Fall Canyon.' In this same region, extending to the northwest, the

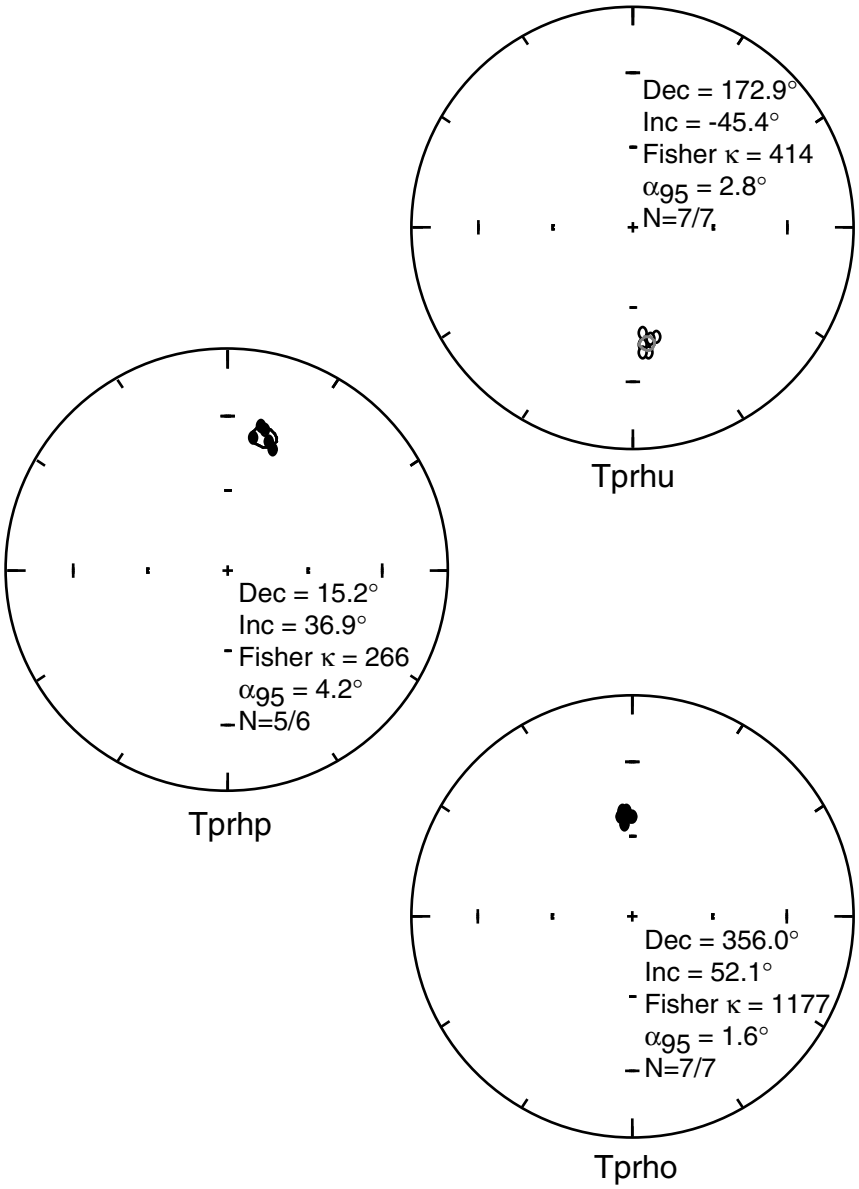

Figure 7.2. Inclination–declination plots from the Tuffs of Los Heme at Cinco Islas. Equal area projection. Cooling units Tprho and Tprhp from the lower part of the Tuffs of Los Heme at Cinco Islas are normal polarity. Cooling unit Tprhu from the upper part of the Tuffs of Los Heme at Cinco Islas is reversed polarity. Ellipses are α_{95}; Sample points for Tprho obscure small confidence ellipse for this unit. Fisher confidence cones centered on the means. See Appendix D for data acquisition and measurement techniques.

Tuffs of Los Heme formed a plateau that has been subsequently dissected by numerous east-flowing drainages. The association of conglomerate outcrops with the area of this plateau suggests that this area may have been a low-lying alluvial plain at the time of emplacement of the lower members of the Tuffs of Los Heme. This plain is present at the same unconformity as the northeast-draining canyons of Arroyo Miramar, 'Camp Wash,' and 'Travertine Wash.' The direction of topographic gradient on this plain would have most likely been down towards the northeast, similar to these canyons.

Middle sequence

The middle sequence of group six comprises basaltic andesite volcanic rocks intercalated with the upper two members of the Tuffs of Los Heme. A mafic pyroclastic deposit unconformably overlies unit Tprhp near the present-day coastline ($^{7}32^{900}E$,$^{33}\,26^{300}N$). Solid lava bombs as large as 50 cm diameter and the limited distribution of this deposit indicate that these outcrops are probably part of a local cinder cone. The composition of these rocks is probably basaltic andesite, similar to other syn-rift mafic rocks of the Puertecitos Volcanic Province [*Martín-Barajas et al.*, 1995].

Overlying the cinder deposit are the upper members of the Tuffs of Los Heme (units Tprhu and Tprhy). The lower of these units, Tprhu, is a pink to purple partially to densely welded ash-flow tuff with 1% pumice, 10% volcanic lithic fragments, and 2% plagioclase phenocrysts. Tprhu fills in a paleocanyon exposed in the west wall of 'Camp Wash' with 20 m of vapor-phase altered welded tuff. Outside of the paleocanyon, Tprhu forms a 1–3 m thick veneer of densely welded tuff. The uppermost unit of the Tuffs of Los Heme, unit Tprhpy, forms a 1–2 m thick veneer of densely welded tuff overlying unit Tprhu. Tprhy contains 10% pumice, 5–10% volcanic lithic fragments, and 10% plagioclase phenocrysts. Outcrops of Tprhu and Tprhy become thicker and more widespread adjacent to the coastal plain at Arroyo Miramar and further north. Both of these tuffs thin and pinch out ∼2 km inland of the coastal plain. The Tprhu member of the Tuffs of Los Heme preserves a reversed paleomag-

netic polarity (Fig. 7.2 and Table 7.1). Paleomagnetic measurements of the Tprhy did not produce a stable remanence direction. A thin basaltic andesite(?) flow outcrops above the Tuffs of Los Heme adjacent to the coastal plain (unit Tpb, $^{7}32^{000}$E, $^{33}27^{150}$N to $^{7}32^{700}$E, $^{33}26^{800}$N).

Upper sequence

The upper sequence of group six comprises Quaternary age alluvium, talus, landslides, and travertine. Travertine deposits at 'Travertine Wash' and Arroyo Las Palmitas are probably the oldest rocks of the upper sequence, since these are the only rocks of the upper sequence that are faulted. Travertine deposits, apparently precipitated from numerous springs in the area, mantle paleotopography formed in basement and group three volcanic rocks. Travertine deposits also form an elevated bench at the southern end of 'Travertine Wash.' Small cold springs present in this area today are probably a vestige of a once more vigorous hydrothermal system here.

The oldest fluvial deposits of the upper sequence are a pair of extensive terraces mapped as Qoal1. One of these terraces defines a 2 km wide paleovalley that followed the course of Arroyo Miramar. The other terrace forms a 20 m-high bench of deposits adjacent to the outlets of Arroyo Las Palmitas and Arroyo de Sagredo. Travertine deposits adjacent to Arroyo Las Palmitas are intercalated with the lower part of Qoal1. Younger fluvial terraces, smaller volume than Qoal1, are mapped as Qoal2 or Qoal. All of these older alluvium deposits are similar to active alluvium (unit Qal) mapped within presently active drainages.

Talus deposits mantle many of the steep canyon walls in the Cinco Islas study area. Where possible, contacts were mapped from scattered outcrops of rocks beneath talus. Where it completely obscures the underlying rocks, it is mapped as Qt on plate IV. A special talus unit, unit Qtv, is mapped where volcanic clasts are present in talus without an adjacent source of volcanic detritus. For example, Qtv deposits in the southeastern corner of the map overlie the original flow surface of the Tmua andesite ($^{7}35^{000}$E, $^{33}19^{000}$N). In this setting, this talus could not have been derived from the

underlying lava flow. The source rocks for this talus must have been completely eroded or transported away by strike-slip faulting.

A pair of 200 m diameter rotational landslides are recognized in the southern part of the Cinco Islas study area ($^{7}32^{000}$E, $^{33}21^{600}$N). These landslides transport a semi-intact stratigraphic section of group three volcanic rocks. Closed depressions have formed adjacent to the headwall of these landslides as the slide masses have moved to the southwest.

7.4 Structure

The Cinco Islas study area was chosen in order to understand interaction between northwest-striking faults of the Main Gulf Escarpment and north-striking faults within the Puertecitos Volcanic Province, and to relate this faulting history to opening of the Lower Delfín basin. The structures mapped in the Cinco Islas study area reflect the intersection of three groups of faults. The most significant of these fault groups is a set of northwest-striking, northeast-dipping, dextral-oblique normal faults that form the Main Gulf Escarpment in the southwest part of the study area. Subsidiary east-dipping and west-dipping groups of north-striking normal faults both terminate at the northwest-striking faults. Each of these fault groups is described separately below.

7.4.1 Northwest-striking dextral-oblique normal faults

Three northwest-striking, northeast-dipping dextral oblique normal faults transect the southwestern half of the Cinco Islas study area and form the Main Gulf Escarpment at this latitude. These structures are named the Sagredo fault, Palmitas fault, and Miramar fault on Plate IV. These faults strike parallel to foliation of the metasedimentary basement rocks, which may indicate that this segment of the Main Gulf Escarpment is controlled by a pre-existing structural discontinuity related to folding of the Olvidada Formation in Late Cretaceous time [*Phillips*, 1993]. Dextral

slip on the northwest-striking fault system is at least 1–2 km, measured from offset group three volcanic rocks across the Miramar fault. Vents of the lower andesite volcano are offset from Arroyo Miramar to 'Dry Fall Canyon' ($^{7}27^{400}$E, $^{33}25^{000}$N to $^{7}29^{650}$E, $^{33}24^{500}$N). The vent plug marking the probable source of the intermediate volcaniclastic rocks and the upper andesite is also dextrally offset 1–2 km from the most proximal facies of these rocks ($^{7}30^{300}$E, $^{33}23^{200}$N to $^{7}32^{300}$E, $^{33}22^{000}$N). Dextral displacement on the Palmitas and Sagredo faults is probably much less, since the lower andesite vent facies are not significantly offset across this fault trend. Apparent normal separation on the northwest-striking fault system increases from 250–300 m in the Arroyo Miramar drainage to at least 750 m in 'Travertine Wash.' The increase in normal offset is probably due to the addition of slip from north-striking, east-dipping faults (Plate IV). Slip on the northwest-striking dextral oblique faults has cut all pre-Quaternary rocks in the study area. Normal separation of the Tuffs of Los Heme in the western part of the study area is only 40 m on the Miramar fault and < 10 m on other northwest-striking faults, which is much less than the offset of older strata by these same fault strands.

7.4.2 North-striking, east-dipping normal faults

A family of north-striking, east-dipping normal faults control the structure of the eastern half of the Cinco Islas study area. The principal normal faults of this system underlie 'Camp Wash' and 'Travertine Wash,' each with 250–300 m of normal offset of group three volcanic rocks (Plate IV). Both of these normal faults are covered by unit Tprhp of the Tuffs of Los Heme ($^{7}31^{500}E$,$^{33}\,24^{400}N$ and $^{7}34^{000}E$,$^{32}\,21^{600}N$). The north-striking, east-dipping normal faults terminate at the northwest-striking dextral oblique fault system at 'Travertine Wash' and Arroyo Las Palmitas. The region of intersection is a complex of intersecting faults that accommodate a transition from east-directed extension to southeast-directed oblique extension. A zone of collapse adjacent to the Palmitas fault ($^{7}32^{400}E$,$^{33}\,21^{000}N$) may be explained by fragmentation of the block between northwest-striking and north-striking faults at this transition

zone (Fig. 7.3).

7.4.3 North-striking, west-dipping normal faults

North-striking, west-dipping normal faults control much of the structure of the eastern Puertecitos Volcanic Province [*Martín-Barajas and Stock*, 1993; *Martín-Barajas et al.*, 1995, and Chapter 2 of this thesis]. Within the northwestern part of the Cinco Islas study area, part of this west-dipping normal fault system terminates against northwest-striking dextral oblique normal faults of the Main Gulf Escarpment (Plate IV). Extension on the west-dipping normal faults began prior to deposition of the Tuffs of Los Heme and continued through emplacement of these units. Syn-depositional faulting is evident from thickening of the Tuffs of Los Heme across fault scarps ($^{7}28^{400}E,^{33}\,27^{250}N$ and $^{7}29^{100}E,^{33}\,27^{700}N$). No evidence for strike-slip separation was observed on these structures. The amount of normal offset on individual west-dipping normal faults mapped on Plate IV does not exceed 100 m in groups 1, 2 and 3 rocks and is less than 5–10 m in the Tuffs of Los Heme (Plate IV). The percent extension across the west-dipping normal faults is low, except at their intersections with east-dipping faults (cross section X-X′, plate IV). Faulting in the region of intersections involves multiple converging fault splays. At Arroyo Miramar, slip on a west-dipping normal fault in a zone of intersection has been inverted, resulting in a small amount of reverse faulting and folding of volcanic strata ($^{7}29^{200}E,^{33}\,24^{800}N$). This small fault block was probably isolated in the accommodation zone in a manner kinematically similar to the intersection of north-striking and northwest-striking east-dipping faults (Fig. 7.3). Reactivation of the west-dipping normal fault as a reverse fault probably occurred due to dextral slip on the irregular trace of the Miramar fault.

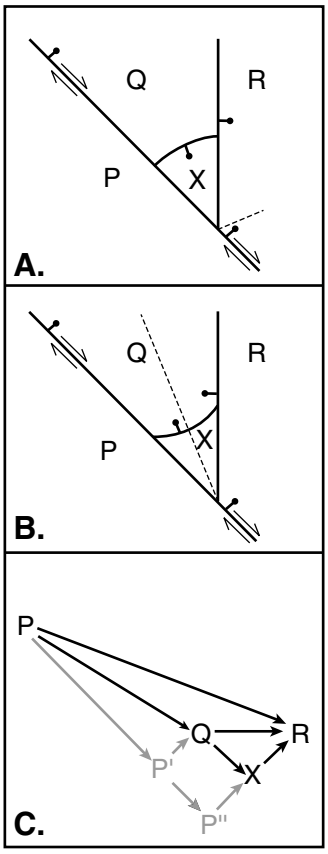

Figure 7.3. Kinematic model of the intersections of northwest-striking and north-striking normal faults. Diagrams A and B are kinematically similar fault configurations, featuring an east-dipping (A) and west-dipping (B) north-striking normal fault. Projection of fault intersection at depth shown as a thin dashed line. Modelled from locations ${}^{7}32^{500}E, {}^{33}\,21^{000}N$ and ${}^{7}28^{100}E, {}^{33}\,25^{200}N$ on Plate IV. Block X is a detached block at the triple junction between blocks P, Q, and R. Diagram C shows the relative motion of blocks in vector form. P′ and P″ are projections of point P along the northwest-striking fault trace that separate the strike-slip and normal components of motion relative to P. Motion of block X represents an intermediate rate of normal displacement between blocks P and R, but with a similar amount of dextral displacement as Block R relative to Block P. Block X may be thought of as 'sticking' between blocks P and R and detaching from block Q.

7.5 Discussion

7.5.1 Correlation of the Tuffs of Los Heme

Correlation of the Tuffs of Los Heme from the Puertecitos area to Cinco Islas provides a critical age constraint on the timing of deformation in the southern Puertecitos Volcanic Province. Four cooling units of the Tuffs of Los Heme comprise the majority of group six syn-rift rocks within the Cinco Islas study area. Reconnaissance mapping by *Stock* [2000] and similar mapping described in Chapter 2 correlate the Tuffs of Los Heme at Cinco Islas to tuffs described by *Martín-Barajas et al.* [1995] at Arroyo Los Heme (Fig. 7.1). However, correlation of the four individual cooling units at Cinco Islas to the 29 cooling units described by *Martín-Barajas et al.* [1995] is incomplete. Inspection of the area between Cinco Islas and Arroyo Los Heme by aerial photography and Landsat Imagery suggests that the Tprhu member of the Tuffs of Los Heme may be continuous with the uppermost ash-flow tuff (Tph29) described by *Martín-Barajas et al.* [1995]. Stratigraphic and paleomagnetic data, described below, support correlation of the unconformity beneath Tprhu at Cinco Islas to a similar unconformity beneath Tph29 at Volcán Prieto and Arroyo Los Heme.

The erosional unconformity between the second (Tprhp) and third (Tprhu) member of the Tuffs of Los Heme at Cinco Islas is correlated here to a depositional hiatus and angular unconformity beneath member Tph29 of the Tuffs of Los Heme described by *Martín-Barajas et al.* [1995] at Arroyo Los Heme. Basaltic andesite volcanism occurs at this unconformity at Volcán Prieto [*Martín-Barajas et al.*, 1995] and at Cinco Islas (unit Tpbc). Paleomagnetic measurements at Arroyo Los Heme [*Melbourne and Stock*, 1994, and Melbourne, unpublished data] found a change from normal to reversed polarity at this same stratigraphic level. Paleomagnetic measurements at Cinco Islas also document a reversal from normal to reversed polarity at the erosional unconformity between Tprhp and Tprhu (Fig. 7.2 and Table 7.1). At Arroyo Los Heme, this reversal occurs directly above a tuff dated at 2.65±0.02 Ma by *Martín-Barajas et al.* [1995] and is correlated to the C2An.1n to C2An.1r reversal at 2.58 Ma

[*Cande and Kent*, 1995, Melbourne, unpublished data]. The unconformity between the Tprhp and Tprhu members of the Tuffs of Los Heme at Cinco Islas probably also spans this polarity reversal at 2.58 Ma.

7.5.2 Timing and local tectonic setting of fault displacement

Stratigraphic and structural relationships in the Cinco Islas study area indicate that the majority of fault displacement here took place before emplacement of the Tuffs of Los Heme. Overlap of the north-striking, east-dipping normal faults by the Tuffs of Los Heme indicates that slip on this system must entirely pre-date 2.58 Ma. Exposures of northwest-striking dextral oblique normal faults and north-striking west-dipping normal faults that disrupt the Tuffs of Los Heme and older rocks cut the younger tuffs with only 15–20% of the total fault displacement (Plate IV). Strike-slip displacement of the Tuffs of Los Heme by the northwest-striking dextral oblique normal faults is less certain. However, the similar thickness of Tprho outcrops north and south of this fault system does not support substantial dextral displacement after emplacement of the Tuffs of Los Heme.

The onset and termination of faulting within the study is poorly constrained. None of the group three deposits within the study area show evidence for syndepositional faulting. Regional constraints on faulting in the Puertecitos Volcanic Province indicate that a small amount of extension took place as early as the period between 12.6 Ma and 6.7 Ma [*Stock and Hodges*, 1990; *Nagy*, 2000, and Chapter 6 of this thesis]. Faulting in the Cinco Islas area may have begun during this time. The latest faulting in the study area is indicated by displacement of the upper members of the Tuffs of Los Heme and by displacement of travertine deposits in the southeastern part of the study area. Quaternary fluvial terrace deposits (Qoal1, Qoal2, and Qoal) are not cut by faulting within the Cinco Islas study area.

The overall low amount of displacement on faults within the Cinco Islas study area indicates that this section of the Main Gulf Escarpment accommodates no more than the limited amount of extension documented within other areas of the Puertecitos

Volcanic Province. *Stock and Hodges* [1990] and *Nagy* [2000] estimate 3.5% and 4% of east-west extension, respectively, across parts of the northern Puertecitos Volcanic Province south of the Matomí Accommodation Zone. Extrapolating this percentage of extension across the ∼50 km-wide volcanic province would produce 1.8–2 km of net east-west separation. 1–2 km of strike-slip on the northwest-striking faults at Cinco Islas could accommodate 0.7–1.4 km of this east-west extension. These similar, low values of displacement allow for the possibility that the northwest-striking dextral oblique faults at Cinco Islas transfer extension from within the Puertecitos Volcanic Province onto the Ballenas Transform fault without any additional component of plate boundary displacement (Fig. 7.1).

7.5.3 Relationship of faulting at Cinco Islas to opening of the Lower Delfín basin

Opening of the Lower Delfín basin has been proposed as one of the youngest plate reorganization events within the Gulf of California [*Lonsdale*, 1989; *Stock*, 2000]. *Lonsdale* [1989] associated opening of the Lower Delfín basin with a change in transform fault geometries within the central and southern Gulf of California basins at ∼2 Ma. *Stock* [2000] noted that opening of the Lower Delfín basin could have started as late as 600 ka, which is the time required to produce the 30 km width of new crust generated at this basin [*Lonsdale*, 1989] at the full Pacific North–America rate of plate motion (48 mm/yr). Prior to the onset of rifting that led to opening of the Lower Delfín basin, the continental margin of the basin was probably outside of the area of Gulf extension [*Stock*, 2000]. The faulting history at Cinco Islas, which lies on the continental margin of the Lower Delfín basin, thus should reflect the timing of opening of this basin.

This history of faulting at Cinco Islas implies that rifting localized into the Lower Delfín basin before 2.58 Ma, since very little fault activity post-dates this time on the continental margin. A tectonic history compatible with opening the Lower Delfín

basin after 2 Ma would require faulting in the southern Puertecitos Volcanic Province to have been largely complete at least 600 ka earlier. While this possibility cannot be excluded without additional geological mapping of Isla Angel de La Guarda, opening of the Lower Delfín basin prior to 2.58 Ma is most compatible with the faulting history in the southern Puertecitos Volcanic Province.

The history of faulting at Cinco Islas thus suggests that there may have been simultaneous spreading within the Lower Delfín basin and the Tiburón basin for at least part of the past 2.6 Myr. In effect, Isla Angel de La Guarda must have acted as an independent microplate during part of its history, surrounded by transform faults and simultaneously active spreading centers. This is necessary because opening of the Lower Delfín basin cannot have occurred at the full Pacific–North America rate of motion during its entire history. Even if the shoreline of Isla Angel de Guarda is restored adjacent to Cinco Islas, closing the Lower Delfín basin by ∼100 km, this amount of opening would require only 2–2.3 Myr at the full rate of plate motion in the northern Gulf of California [*DeMets*, 1995; *Oskin et al.*, 2001].

The association of opening of the Lower Delfín basin with eruption of the Tuffs of Los Heme appears to closely match the timing proposed by *Stock* [2000]. The section of the Tuffs of Los Heme preserved at Cinco Islas correlates to the middle, normal polarity, and upper, reversed polarity sections of the Tuffs of Los Heme described by *Martín-Barajas et al.* [1995] and *Melbourne and Stock* [1994] at Arroyo Los Heme. A lower section of these tuffs is magnetically reversed [*Melbourne and Stock*, 1994, and unpublished data]. It is possible that this lower section of tuffs, which are as old as 3.3 Ma [*Martín-Barajas et al.*, 1995], may have erupted during the time when the majority of faulting was taking place at Cinco Islas. If this hypothesis is correct, then the entire sequence of the Tuffs of Los Heme, which range in age from 3.3 Ma to younger than 2.6 Ma, may record the start of opening of the Lower Delfín basin in great detail on its conjugate rifted margins.

7.6 Conclusions

Structural relationships recorded at Cinco Islas, Baja California, constrain the tectonic evolution of the Main Gulf Escarpment and part of the northwest margin of the Lower Delfín basin of the northern Gulf of California. Faulting at Cinco Islas accommodated extension within the interior of the Puertecitos Volcanic Province by 1–2 km of northwest-striking dextral oblique strike-slip faulting. North-striking normal faults originate at this dextral oblique fault zone. The majority of faulting at Cinco Islas pre-dates emplacement of the upper part of the Tuffs of Los Heme. A paleomagnetic polarity reversal within these tuffs at Cinco Islas and at Arroyo Los Heme [*Melbourne and Stock*, 1994] is correlated to the C2An.1n to C2An.1r reversal at 2.58 Ma [*Cande and Kent*, 1995]. These relationships indicate that the most of the faulting at Cinco Islas was complete by 2.58 Ma and, presumably, that faulting had localized within the Lower Delfín basin by this time. Opening of the Lower Delfín basin by 2.58 Ma would require that Isla Angel de La Guarda has acted as an independent microplate within the Gulf of California during part of its history, surrounded by simultaneously active spreading centers.

Chapter 8

Latest Miocene–Early Pliocene marine strata from southwest Isla Tiburón, Sonora, Mexico, and implications for the proto-Gulf of California marine incursion

8.1 Abstract

Emplacement mechanisms of volcanic strata on southwest Isla Tiburón are evaluated here to investigate the age of interstratified marine rocks. A non-welded rhyolitic ash-flow tuff, interpreted by previous workers as a sill and lava flow, was emplaced at the base of the marine rocks. This ash-flow tuff is dated at 5.7±0.2 Ma, 6.6±0.8 Ma, and 6.4±1.6 Ma. A Rhyodacite dike and its related lava flow, interpreted by previous workers as an ash-flow tuff and a separate dike, intrudes and overlies, respectively, the marine rocks. This dike and flow has been dated by previous workers as 11.2±1.3Ma, 3.7±0.9 Ma, and 4.2±1.8 Ma. The 11.2 Ma age, which was the core constraint for a Middle Miocene proto-Gulf of California origin for the underlying rocks, is discordant with all other isotopic dates and with the age of microfossils described by *Gastil et al.* [1999]. An alternative interpretation, utilizing all available geologic and geochronologic data except this discordant age, is shown to support that the proto-Gulf marine strata on southwestern Isla Tiburón are Latest Miocene to Early Pliocene age. Reinterpretation of the Isla Tiburón strata supports a simplified history of marine incursion into the Gulf of California. Marine rocks as old as 8.2 Ma in the southern Gulf of Califoria may indicate an early marine incursion over a region of more intense continental extension. Flooding of the entire Gulf of California basin by 6.3–6.5 Ma correlates to the onset of significant Pacific–North America plate boundary motion within the Gulf of California.

8.2 Introduction

The proto-Gulf of California is an enigmatic seaway proposed to have occupied the Gulf of California Extensional Province during the earliest stages of rifting from 12 Ma to ∼6 Ma. Marine incursion during this interval pre-dates localization of plate boundary motion in the Gulf of California and is associated with a proto-Gulf phase of east-west directed, basin and range-style extension [*Gastil and Krummenacher*, 1977;

Gastil et al., 1979; *Stock and Hodges*, 1989; *Smith*, 1991]. Evidence for extension during this early time period is abundant throughout the marginal basins of the Gulf of California [*Stock and Hodges*, 1989; *Lee et al.*, 1996; *Nagy and Stock*, 2000, and Chapter 6 of this thesis]. However, evidence for marine incursion into the Gulf of California during this period is sparse [*Helenes and Carreño*, 1999]. Faunal evidence supports that the Gulf of California has always connected to the Pacific Ocean at its southern end [*Smith*, 1991]. Paradoxically, the oldest evidence for proto-Gulf marine sedimentation is from Isla Tiburón, in the northern Gulf of California (Fig. 8.1). A 10 km^2 fossiliferous marine basin bounded by middle Miocene volcanic deposits located on the southwest corner of Isla Tiburon has been cited as evidence for marine incursion into the northern Gulf of California prior to 11 Ma [*Gastil and Krummenacher*, 1977; *Gastil et al.*, 1999].

The presence of marine strata provides an important constraint on the geodynamic setting of rifting in the Gulf of California. Continental extension elsewhere in the Basin and Range province of western North America has maintained elevations above sea level, with only isolated basins below sea level in the Death Valley region. Large-magnitude upper crustal extension in the Basin and Range province has been compensated by lower crustal flow, preserving crustal thicknesses of at least 24–30 km [*Wernicke et al.*, 1996, for example] and promoting diffuse extension [*Buck*, 1991]. If the crust of the Gulf of California was thinned such that the proto-Gulf marine incursion managed to infiltrate over a distance of 800–1200 km, then this may be evidence that lower crustal compensation in this region was significantly less effective. Localized, narrow rifting during the proto-Gulf stage may have been key to later rupture of the continent, allowing the Pacific–North America plate boundary to localize within the Gulf of California. A well-constrained record of early marine incursion is thus critical for understanding the mechanisms of continental rifting in the Gulf of California.

Middle Miocene marine sediments present on Isla Tiburón are the single most important evidence for the age and extent of the proto-Gulf of California [*Smith*, 1991].

Independent, well-constrained evidence for early marine sedimentation elsewhere in the Gulf of California is no older than 6.8 Ma north of Isla Tiburón, and no older than 8.2 Ma south of this island (Fig. 8.1 and Table 8.2, located at the end of this chapter). Attempts to duplicate the middle Miocene age constraint of the Isla Tiburón strata were unsuccessful [*Neuhaus*, 1989; *Gastil et al.*, 1999], calling into question the validity of the published ages of the proto-Gulf in the northern Gulf of California.

The purpose of this study is to reevaluate the age of the marine deposits of southwest Isla Tiburón. New geologic mapping of southwest Isla Tiburón and adjacent areas places this proto-Gulf basin within a tectonic context relative to other volcanic strata and sedimentary basins on the island. The emplacement mechanisms of volcanic rocks that directly underlie and overlie the proto-Gulf strata are reviewed and updated. Existing and new geochronology of each of these bounding deposits is presented, and the relative ages of these deposits are compared to their emplacement history. All of this data is shown to strongly support that one of these ages, an 11.2±1.3 Ma K–Ar age of a rhyodacite tuff and lava flow described by *Gastil and Krummenacher* [1977], is discordant. This age was the core constraint for a Middle Miocene proto-Gulf of California [*Smith*, 1991]. An alternative interpretation, in agreement with all available geologic and geochronologic data except this discordant age, is that the proto-Gulf marine strata on southwestern Isla Tiburón are Latest Miocene to Early Pliocene age. This reinterpretation of the Isla Tiburón strata also supports a simplified history of marine incursion in the Gulf of California that correlates well with other aspects of its tectonic history.

8.3 Geology of southwest Isla Tiburón

8.3.1 Previous studies

The geology of Isla Tiburón was first comprehensively described by *Gastil and Krummenacher* [1976] and *Gastil and Krummenacher* [1977]. These authors mapped

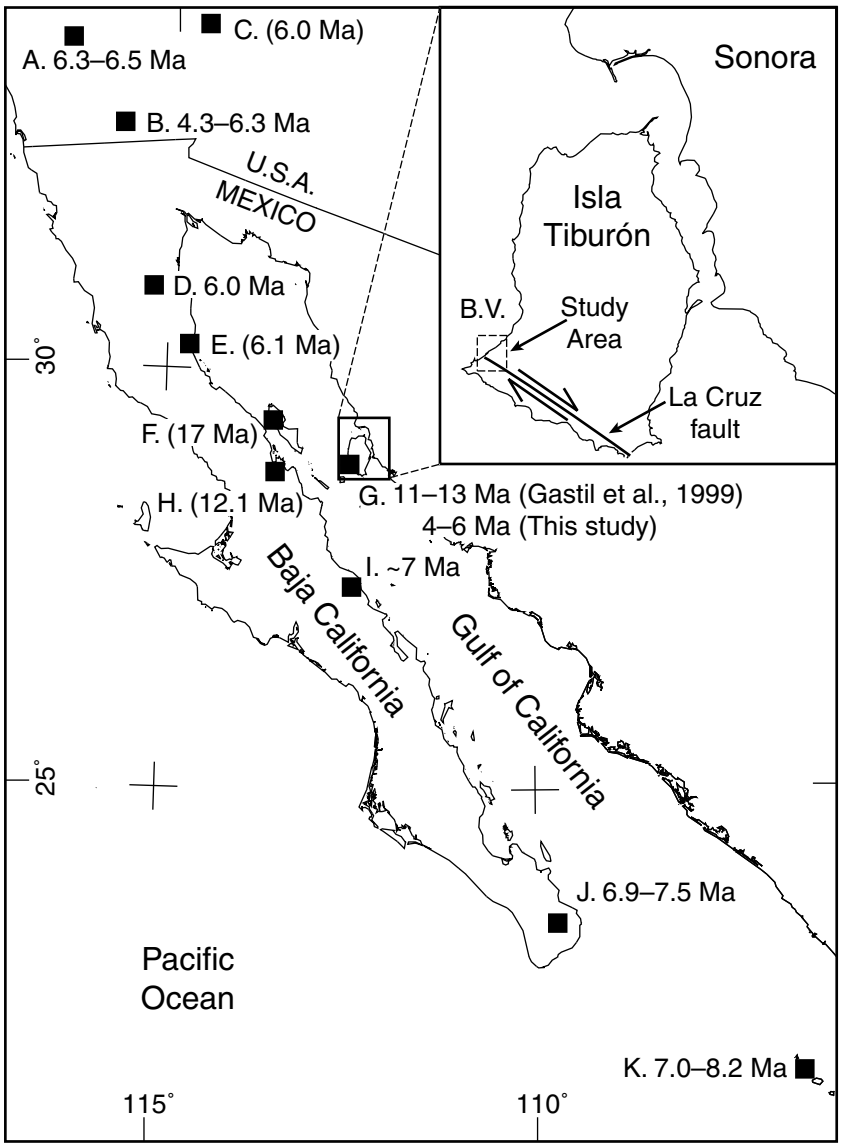

Figure 8.1. Miocene age marine rocks in the Gulf Extensional province. See Table 8.2 for sources of ages. Ages in parentheses are maximum constraints only. Inset map shows southwest Isla Tiburón study area and small square that was mapped in detail (Fig. 8.2). B.V., Bahía Vaporeta.

marine rocks on southwestern Isla Tiburón overlain by a 11.2±1.3 Ma rhyodacite ignimbrite (Table 8.1). Later studies documented a 12.9±0.4 Ma volcanic breccia (Table 8.1) intercalated with the marine rocks [*Smith et al.*, 1985; *Smith*, 1991; *Gastil et al.*, 1999]. Studies of the marine strata by *Cassidy* [1988] documented a ∼1.5 km thick section of fossiliferous conglomerate, with lesser amounts of sandstone. Mapping of volcanic rocks in this area by *Neuhaus* [1989] documented 21–15 Ma volcanic units beneath the marine rocks, as well as several 9 Ma and younger rhyolite tuffs, lava flows, breccia, and dikes that intrude and/or overlie the marine rocks. *Gastil et al.* [1999] summarizes all of this previous work, and includes descriptions and correlations of megafossils and microfossils from southwest Isla Tiburón. Megafossil assemblages at Isla Tiburón are similar to other pre-Pliocene marine fossils from the Gulf of California. Microfossil data support an age of deposition of the marine sandstone at southwestern Isla Tiburón between 6.4 and 4.0 Ma, which is discordant with the ages of bracketing volcanic rocks. This discordancy is not explained by *Gastil et al.* [1999].

Reevaluation of the marine rocks of southwest Isla Tiburón presented here was a result of detailed studies of the conjugate rifted margins the Upper Delfín basin of the Gulf of California [*Oskin et al.*, 2001, and Chapters 3 and 5 of this thesis]. These studies document 12.6 to 6.1 Ma welded ignimbrites on western Isla Tiburón that correlate to the Puertecitos Volcanic Province of Baja California. No marine rocks have been documented beneath these ignimbrites on either margin of the Upper Delfín basin [*Lewis*, 1994; *Stock et al.*, 1991, 1996; *Martín-Barajas et al.*, 1997, and Chapter 3 of this thesis]. Tilting and faulting of these rocks on Isla Tiburón started after 12.6 Ma and has continued through 6 Ma to Quaternary time (Chapter 6 of this thesis). These observations are contrary to the pre–11 Ma history of faulting and marine incursion on Isla Tiburón documented by *Gastil and Krummenacher* [1977] and *Gastil et al.* [1999]. Since the southern outcrop limit of the correlative ignimbrites lies adjacent to the proto-Gulf marine basin of southwest Isla Tiburón, the stratigraphic and structural relationships of these ignimbrites to the marine strata were investigated in detail to try to resolve these discrepancies in age and faulting.

Table 8.1. Geochronologic data from southwest Isla Tiburón.

Sample	Age	Method	Reference
Tmvlc: Arc volcanic rocks south of the La Cruz fault[1]			
A-1	20.5±0.5 Ma	K–Ar on hornblende	M2 andesite breccia of *Gastil et al.* [1999]
272	15.2±0.5 Ma	K–Ar on whole rock	Ma andesite of *Neuhaus* [1989]; M5 andesite of *Gastil et al.* [1999]
Tma1,Tmvs: Arc volcanic rocks north of the La Cruz fault			
284	17.7±0.2 Ma	$^{40}Ar/^{39}Ar$ on hornblende	Mand andesite of *Neuhaus* [1989]; M5 andesite of *Gastil et al.* [1999]
276	11.4±2.6 Ma	$^{40}Ar/^{39}Ar$ on feldspar	M7 andesite breccia of *Gastil et al.* [1999]
Tuff of El Canelo			
Tmrec	6.1 ± 0.5 Ma	$^{40}Ar/^{39}Ar$ on plagioclase	Age by lithologic correlation in Chapter 5[2]
275	6.1±1.8 Ma	K–Ar on whole rock	Mry of *Neuhaus* [1989]; M11 of *Gastil et al.* [1999][3]
Tmbr: Landslide breccia			
B2BS1260	12.9±0.4 Ma	K–Ar on plagioclase	Marine volcanic breccia of *Smith et al.* [1985][4]
5	9.0±1.2 Ma	$^{40}Ar/^{39}Ar$ on plagioclase	M10 of *Gastil et al.* [1999]
Tmprsz1: Member one of the Tuffs of Arroyo Sauzal			
51	5.7±0.2 Ma	K–Ar on alkali feldspar	Mr of *Neuhaus* [1989]; M10 of *Gastil et al.* [1999]
SWT-99-28	6.7±0.8 Ma	$^{40}Ar/^{39}Ar$ on alkali feldspar	Tmprsz1 of Chapter 3
TIB-98-11	6.4±1.6 Ma	$^{40}Ar/^{39}Ar$ on alkali feldspar	Tmprsz1 of Chapter 3
Tprcs: Rhyodacite of Cerro Starship			
S2B-27	11.2±1.3 Ma	K–Ar on plagioclase	M9 of *Gastil et al.* [1999][5]
S2G-13	3.7±0.9 Ma	K–Ar on plagioclase	M10 of *Gastil et al.* [1999][5]
10	4.2±1.8 Ma	K–Ar on whole rock	M9 'dike' of *Gastil et al.* [1999]

[1] Sample of oldest and youngest age from these rocks shown here. See *Gastil et al.* [1999] for additional isotopic ages.
[2] Correlated to the Tuff of Arroyo El Canelo of *Nagy et al.* [1999]. Not dated on Isla Tiburón.
[3] Mapped as Mry by *Neuhaus* [1989] as a separate unit underneath M11 of *Gastil et al.* [1999].
[4] Described as a debris flow within marine rocks by *Smith et al.* [1985]. Outcrop reinterpreted based on new field mapping as an erosional window into landslide breccia.
[5] First reported for unit T4x of *Gastil and Krummenacher* [1977].

Figure 8.2. (next page) Geologic map of southwest Isla Tiburón. See text for discussion of lithologies. Stratigraphic relationships of these groups are shown in Fig. 8.4. Geology based on *Neuhaus* [1989] and new field mapping. See Table 8.1 for ages corresponding to sample localities shown here. Tprcs dike outcrop northeast of Cerro Starship underlies sample locality marker for sample S2G-13.

Chapters 3.1 and 6 of this thesis provide a comprehensive description of the geology and structure of Isla Tiburón and coastal Sonora. The following sections describe the stratigraphy and structure in the vicinity of southwestern Isla Tiburón. The interpretations presented here often differ from previous workers. These differences are described in detail so as to make the reinterpretation of this important locality unambiguous.

8.3.2 Regional pre-basin stratigraphy

Basement rocks of southwest Isla Tiburón are granodiorite and tonalite plutons of the Cretaceous Peninsular Ranges batholith that intruded Paleozoic and Mesozoic metasedimentary rocks [*Gastil and Krummenacher*, 1976; *Silver and Chappell*, 1988; *Gastil et al.*, 1991]. Basement crops out south of the La Cruz fault, unconformably overlain by Miocene volcanic and sedimentary rocks (Fig. 8.2). North of the La Cruz fault, basement rocks do not crop out from beneath Miocene volcanic rocks in the study area.

Two distinctive domains of pre-rift, Early to Middle Miocene arc-related volcanic strata underlie the marine rocks on southwest Isla Tiburón. These domains are separated by the La Cruz fault, a northwest-striking, right-lateral strike-slip fault that transects the southernmost coastal area of Isla Tiburón [*Gastil and Krummenacher*, 1976]. This fault was recognized by *Gastil and Krummenacher* [1976] and *Neuhaus* [1989] to have cut the marine rocks and older volcanic rocks on southwest Isla Tiburón, but the magnitude of earlier strike-slip on this structure was not recognized by these authors. Detailed and reconnaissance studies have not located rocks older than ∼6 Ma that correlate across the fault trace (Chapter 3 of this thesis), suggesting that the

Figure 8.2.

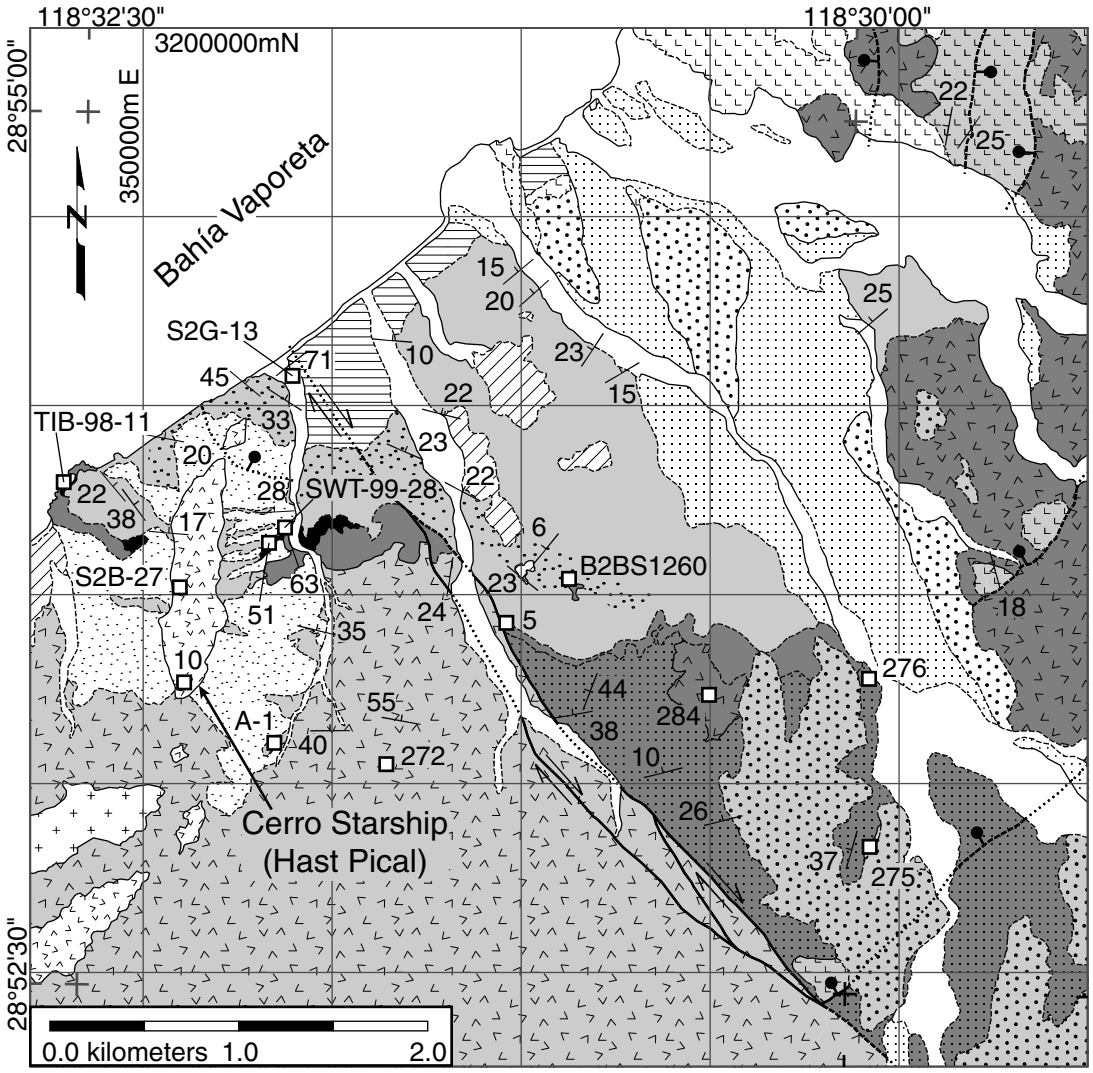
118°32'30"
118°30'00"
28°55'00"
28°52'30"
3200000mN
350000m E
N
Bahía Vaporeta
S2G-13
TIB-98-11
SWT-99-28
S2B-27
B2BS1260
A-1
Cerro Starship
(Hast Pical)
0.0 kilometers 1.0 2.0
55 Strike and dip of bedding
18 Strike and dip of eutaxitic foliation
276 Isotopic age sample locality
Qal, Qli: Active alluvial, littoral deposits
Qco: Colluvium
Qae: Sand Dunes
Qoal: Old Alluvium
Qmt: Marine Terrace
QTprbv: Tuff of Bahía Vaporeta
QTpal: Young nonmarine conglomerate
Tprcs: Rhyodacite of Cerro Starship
Tmpal: Old nonmarine conglomerate
Contact (Certain, uncertain, covered)
Fault (Certain, uncertain, covered)
Strike-slip fault
Normal fault
Tmpm: Marine (conglomeratic facies)
Tmpm: Marine (sandy facies)
Tmprsz1: Tuff of Arroyo Sauzal #1
Tmbr: Landslide breccia
Tmrec: Tuff of Arroyo El Canelo
Tmvs: Volcaniclastic deposits
Tma1: Andesite
Tmvlc: La Cruz volcanic rocks
Mzg: Granitic basement

La Cruz fault may have at least 26 km of earlier right-lateral displacement (Chapter 6 of this thesis).

Arc-related volcanic rocks of the Sierra Menor domain

Arc-related volcanic rocks north of the La Cruz fault comprise the southernmost part of the Sierra Menor Domain described in Chapter 3 of this thesis. These rocks are predominantly andesite lava and proximal andesitic debris-flow deposits (Fig. 8.2). Northeast of the outcrops of marine rocks, massive, orange-weathering andesite lava flows crop out in steep-sided ridges and are mapped as unit Tma1. These lava flows comprise part of a probable arc-related volcanic center in the southern Sierra Menor (Chapter 3.1). An isolated paleotopographic high of this andesite also crops out beneath the marine rocks ∼600 m northeast of the La Cruz fault. Surrounding this andesite outcrop, other outcrops beneath the marine basin strata are predominantly bedded volcaniclastic debris-flow deposits mapped as unit Tmvs. These are comprised of a mixed assemblage of subangular to subrounded, cobble-size grey, orange, and red plagioclase and hornblende phyric andesite lithic fragments supported by a matrix of pink to grey volcanic ash. Emplacement of these deposits was probably related to the adjacent andesitic volcanic center and/or other arc volcanic centers in the Sierra Menor and southern Sierra Kunkaak.

Two younger rhyolitic ignimbrites, the pre-rift ∼12.6 Ma tuff of San Felipe and the syn-rift 6.1±0.5 Ma Tuff of Arroyo El Canelo, also crop out adjacent to marine strata north of the La Cruz fault. Outcrops of the Tuff of El Canelo are shown on Fig. 8.2. Outcrops of the Tuff of San Felipe occur just north and east of the area mapped here. These ignimbrites are the oldest and youngest pyroclastic flows correlated to Baja California by *Oskin et al.* [2001] and in Chapter 5 of this thesis. Outcrops of these ignimbrites in the southern Sierra Menor are thin and discontinuous over paleotopography formed by Tma1 andesite lava flows (Chapter 3). Outcrops of the Tuffs of Arroyo El Canelo approach the La Cruz fault southeast of the marine rocks. One of these outcrops may have been dated by *Neuhaus* [1989] as 6.1±1.8 Ma (Table

8.1). These ignimbrites have not been mapped south of the La Cruz fault (Chapter 3 of this thesis).

Most of the earlier mapping of the region surrounding southwest Isla Tiburón did not differentiate volcanic rocks north and south of the La Cruz fault. Andesite lava flows north of the La Cruz fault are mapped as units T2 and T3 by *Gastil and Krummenacher* [1976]. Most of these lava flows crop out east of the area of detailed mapping by *Neuhaus* [1989] and *Gastil et al.* [1999]. The isolated paleotopographic high of andesite that crops out beneath marine strata is mapped as part of unit M5 by *Gastil et al.* [1999] and as unit Mand by *Neuhaus* [1989]. *Gastil et al.* [1999] report a 17.68±15 Ma age for this outcrop (Table 8.1). *Neuhaus* [1989] recognized this andesite as a separate unit, whereas *Gastil et al.* [1999] grouped it together with outcrops of basaltic andesite south of the La Cruz fault.

Volcaniclastic deposits mapped here as unit Tmvs were not recognized as a separate unit by *Neuhaus* [1989] or *Gastil et al.* [1999]. These authors grouped these deposits together with a dacitic andesite breccia (units M7 and Mbt, respectively) and a basal marine sedimentary breccia (unit M8a and Mbr, respectively). However, Tmvs outcrops are distinct from these other units. The dacitic andesite breccia, also described as a breccia tuff by *Neuhaus* [1989], is a younger deposit with abundant welded rhyolite ignimbrite clasts that was probably emplaced as a landslide. This breccia forms the base of marine basin deposits described below (unit Tmbr on Fig. 8.2). The basal marine sedimentary breccia is a clast-supported, occasionally fossiliferous conglomerate, unlike the ash-matrix-supported unfossiliferous debris flow deposits mapped as Tmvs on Fig. 8.2. *Gastil et al.* [1999] reported a 11.44±2.61 Ma age on feldspar separated from a clast within an andesite breccia within rocks mapped here as Tmvs (Table 8.1).

Arc-related volcanic rocks of the La Cruz domain

Pre-rifting volcanic rocks south of the La Cruz fault are dissimilar from coeval volcanic rocks on the rest of Isla Tiburón (Chapter 3 of this thesis). These strata

form a generally conformable sequence [*Gastil et al.*, 1999] that are grouped together here as the Volcanic Rocks of the La Cruz Block and mapped as unit Tmvlc. Based upon detailed mapping by *Neuhaus* [1989], *Gastil et al.* [1999] divided these strata into units M1-M6. The base of this section consists of thinly bedded lacustrine chert and carbonate rocks interbedded with fluvial arkose and conglomerate overlying basement (unit M1a of *Gastil et al.* [1999]). Basaltic to andesitic flows and breccias with red volcanic sandstone and tephra overlie these basal sedimentary rocks (units M1b-M5 of *Gastil et al.* [1999]). A dacite lava (unit M6 of *Gastil et al.* [1999]) caps the pre-marine basin section here. Several isotopic ages, ranging from 20.5±0.5 Ma to 15.2±0.5 Ma, are reported by *Neuhaus* [1989] and *Gastil et al.* [1999] for lava flows that underlie marine deposits south of the La Cruz fault.

Reconnaissance studies south of the La Cruz fault and east of the marine sedimentary outcrops reveal younger volcanic rocks that are also unique to the La Cruz Block (Chapter 3 of this thesis). These younger rocks are rhyolite lava flows, pumice flows, ash, and welded ash-flow tuffs. A sample of welded ash-flow tuff from Pico Colorado, 3 km southeast of the study area, yielded a 9.6±2.7 Ma age [*Stock and Oskin, in prep.*]. A second sample of welded ash-flow tuff from Ensenada de la Cruz, 20 km southeast of the study area, yielded a 11.3±2.0 Ma age [*Stock and Oskin, in prep.*].

8.3.3 Local basin stratigraphy

A diverse assemblage of volcanic, marine, and nonmarine rock units comprises a basin-filling sequence on southwest Isla Tiburón. Most of the units described in this section are unique to this region of the island. Unlike the volcanic rocks described above, most of the basin-filling sequence crops out both north and south of the La Cruz fault; thus, this section post-dates most of the displacement on this fault (Chapter 6 of this thesis). Rock units are described in the order of their emplacement *as observed during this study.* Earlier studies by *Neuhaus* [1989] and *Gastil et al.* [1999] interpreted that most of the younger volcanic rocks on southwest Isla Tiburón were

emplaced as dikes and sills. Thus the order of deposition and emplacement inferred by these authors differs from that described here.

Landslide breccia

The base of the southwest Isla Tiburón basin is comprised of one or more landslide breccia deposits. These breccias were emplaced unconformably on older volcanic rocks. Emplacement was probably subaerial, as there is is no evidence for marine strata beneath or involved with the landslide breccia. The landslide breccia, mapped as Tmbr on Fig. 8.2, ranges in thickness from 2 to >15 m, with the thickest deposits underlying Cerro Starship. Breccia lithologies are an irregular mixture of monolithologic, clast-supported zones of angular, densely welded tuff clasts intercalated with polylithologic zones of andesitic clast-supported and matrix-supported volcaniclastic breccia. Monolithologic zones of fragmented densely welded rhyolitic ignimbrite are the most common facies of Tmbr. The matrix of unit Tmbr is composed of pulverized angular fragments of breccia lithologies. Volcanic ash and pumice form part of the matrix of the polylithologic breccia. Outcrops of the base of the breccia display a cm-thick blackened zone of fragmental material with a sheared basal contact. Nonmarine volcaniclastic sediments underlying the breccia have not been altered except within the basal zone of sliding, which suggests that breccia lithologies were cooled before emplacement as a landslide.

The landslide breccia deposit at the base of the southwest Isla Tiburón marine basin was also mapped by *Neuhaus* [1989] and *Gastil and Krummenacher* [1976] as units M7 and Mbt, respectively, south of the La Cruz fault. North of the La Cruz fault, *Neuhaus* [1989] and *Gastil et al.* [1999] correlated these breccias to volcaniclastic debris flows mapped in this study as unit Tmvs. Although andesite clasts are common to both Tmvs and the landslide breccia, Tmvs has more rounded clasts, a greater proportion of ash matrix, and little or no pumice. Also, monolithologic zones of fragmented welded rhyolitic ignimbrite, which are the dominant facies of the landslide breccia, are absent from unit Tmvs. For this study, an alternative correlation of the

landslide breccia is mapped across the La Cruz fault to a 2 m thick breccia deposit previously mapped as unit Mr by *Neuhaus* [1989] and unit M10 by *Gastil et al.* [1999]. This breccia is comprised of fragments of welded rhyolite tuff that are organized into a recognizable welding zonation. These intriguing outcrops resemble a welded tuff that was fragmented in place. However, a sheared contact exposed at the base of these strata supports emplacement as a landslide. Since there is no evidence for in place coherent welded tuff outcrops, nor evidence for phreatic fragmentation of a partially cooled welded tuff, these outcrops are interpreted to have been emplaced by a landslide with the original stratigraphy of its source preserved by laminar flow.

Neuhaus [1989] and *Gastil et al.* [1999] interpreted a primary volcanic emplacement mechanism for units Mbt and M7, respectively, as an ash-flow breccia or breccia-tuff. Although the clasts within the breccia are entirely volcanic, emplacement of the breccia resulted in extensive brittle fragmentation that has cross-cut lava flow textures and eutaxitic foliation. Thus, emplacement of the breccia deposits into the southwest Isla Tiburón basin post-dates the volcanism that originally formed its clasts. Since there is no evidence for welding or flow of the breccia lithologies after emplacement, nor evidence for thermal alteration of underlying sedimentary strata, the clasts of this breccia deposit must have been cooled prior to emplacement. Correlative breccia north of the La Cruz fault, mapped as unit Mr by *Neuhaus* [1989] and unit M10 of *Gastil et al.* [1999], were interpreted by these authors as rhyolite flows and dikes. As described above, however, these rocks are actually comprised of fragments of densely welded tuff with a eutaxitic texture that was noted by both *Neuhaus* [1989] and *Gastil et al.* [1999]. This texture, formed from flattened pumice fragments, is indicative of an originally subaerial, pyroclastic emplacement mechanism for these rocks. After this primary volcanic emplacement, brittle fracture and probably transport as a landslide accompanied secondary emplacement of these rocks into the southwest Isla Tiburón basin.

Two clasts appear to have been dated from the landslide breccia. Both of these samples are from units mapped as Mr [*Neuhaus*, 1989] and M10 [*Gastil et al.*, 1999]

north of the La Cruz fault. *Gastil et al.* [1999] reported a 9.0±1.2 Ma age on plagioclase separated from unit M10. Since *Gastil et al.* [1999]'s unit M10 is interpreted by these authors to have intruded the marine sedimentary rocks, this age is cited as a second Middle Miocene age constraint on these proto-Gulf rocks. Reevaluation of the outcrops sampled by *Gastil et al.* [1999] reveals that this unit was in place prior to deposition of the marine strata and that clasts within this unit may have been transported from their original site of deposition. *Smith et al.* [1985]'s 12.9±0.4 Ma age for the marine strata may have also have sampled a clast from the landslide breccia. The outcrop from which their sample was obtained is mapped by *Neuhaus* [1989] as the same unit Mr as other nearby breccia deposits. This outcrop is interpreted here as an erosional window into the landslide breccia beneath the marine rocks (Fig. 8.2).

Member one of the Tuffs of Arroyo Sauzal

Member one of the Tuffs of Arroyo Sauzal is a non-welded to slightly welded ash-flow tuff that crops out at the base of Cerro Starship over an irregular paleotopographic surface formed by the Tmbr landslide breccia. This unit, mapped as Tmprsz1, contains 20% phenocrysts (alkali-feldspar $\gg$ clinopyroxene $\approx$ hornblende $\gg$ biotite $\approx$ plagioclase $\approx$ zircon) with <1% andesite and crystalline (basement?) lithic fragments. This unit is correlated in Chapter 3 to the lowest member of a section of four pyroclastic flows that crop out with fluvial sandstone and conglomerate in the Sauzal basin, located 10 km east of the study area and north of the La Cruz fault (Chapter 3.1). Tmprsz1 outcrops east of Cerro Starship are indurate and homogeneous in texture and appear to have been emplaced into a non-marine setting. Tmprsz1 outcrops west of Cerro Starship consist of an irregular zone of non-welded yellow pumice surrounding a discontinuous core of slightly welded red tuff. These textures suggest quenching of the ignimbrite and may indicate that this outcrop was emplaced in a shoreline setting. The outcrop of Tmprsz1 west of Cerro Starship is the earliest evidence for marine conditions in the southwest Isla Tiburón basin. Reworked pumice beds crop out within marine rocks adjacent to this outcrop.

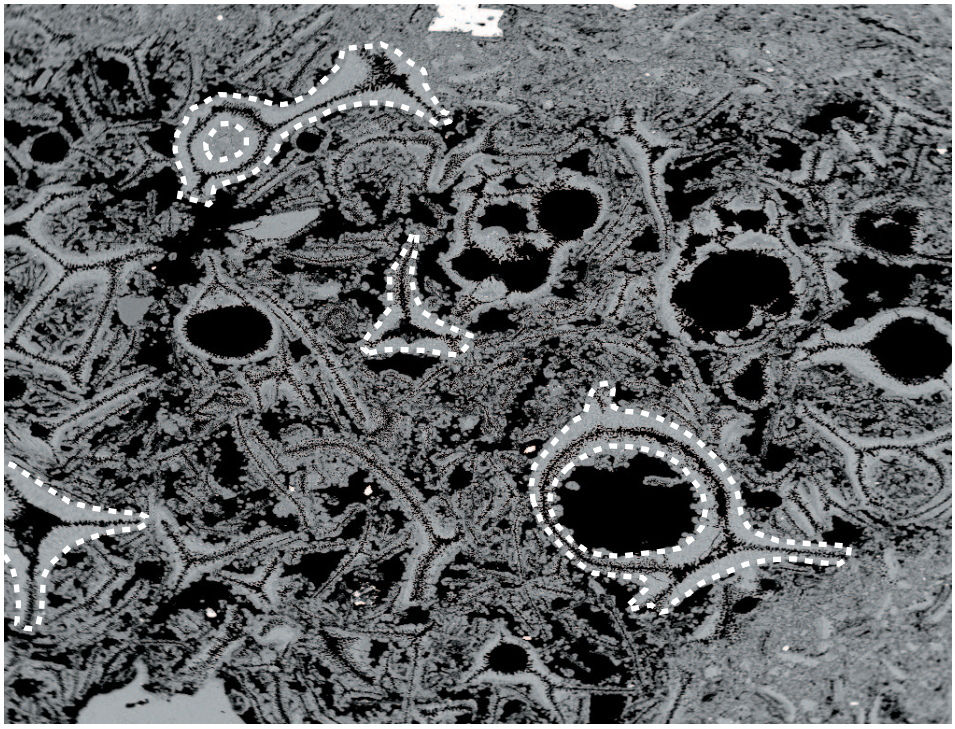

Figure 8.3. Scanning electron microscope image sample TIB-98-11 of member one of the Tuffs of Arroyo Sauzal showing pyroclastic texture. Field of view is 7 by 5 mm. Intersecting linear features are volcanic glass fragments formed by rupture of gas bubbles during explosive volcanism. White dashed lines outline some of these glass shards. Microscopic crystal growth has partially devitrified the glass, forming symmetric axiolitic texture of a devitrified light colored rim and dark glass core. Member one of the Tuffs of Arroyo Sauzal typically preserves delicate, partially intact spherical glass shards, as shown here.

Three isotopic ages of ∼6 Ma have been measured for samples of member one of the Tuffs of Arroyo Sauzal from southwest Isla Tiburón. A K–Ar date from alkali-feldspar separated from a sample from the outcrop east of Cerro Starship was reported by *Neuhaus* [1989] and *Gastil et al.* [1999] as 5.7±0.2 Ma (sample 51A, Table 8.1). A second date on feldspar separated from a sample from this outcrop yielded an age of 6.7±0.8 Ma (sample SWT-99-28, Table 8.1). Alkali feldspar separated from a sample from the slightly welded core zone of the outcrop west of Cerro Starship yielded an age of 6.4±1.6 Ma (sample TIB-98-11, Table 8.1).

Member one of the Tuffs of Arroyo Sauzal was mapped by previous workers as unit Mr [*Neuhaus*, 1989] and unit M10 [*Gastil et al.*, 1999]. *Neuhaus* [1989] interpreted this

unit as a rhyolite sill emplaced beneath the marine rocks. Petrographic examination if this unit reveals a delicate pyroclastic texture formed by fragmentation of a viscous, gaseous magma (Fig. 8.3). This texture, which is indicative of an ash-flow tuff, is unlikely to have been formed through intrusive processes. *Gastil et al.* [1999] reinterpreted the outcrops east of Cerro Starship as a rhyolite lava coulee emplaced onto the flank of this mountain. Neither the geologic map, which shows this unit as conformable beneath the marine rocks (Fig. 8.2), nor the pyroclastic texture of this unit (Fig. 8.3) support emplacement as a lava flow.

Marine and related non-marine conglomerate and sandstone

Fossiliferous marine conglomerate and sandstone that crop out over a 10 km^2 area of southwestern Isla Tiburón are grouped together here as unit Tmpm. These marine strata conformably overlie outcrops of landslide breccia and the member one of the Tuffs of Arroyo Sauzal (Fig. 8.2). The marine rocks of southwest Isla Tiburón consist primarily of clast-supported moderately well-sorted conglomerate [*Cassidy*, 1988]. Marine mollusk fossils are rare to abundant within the conglomerate [*Cassidy*, 1988; *Smith*, 1991; *Gastil et al.*, 1999]. These fossils appear to be mostly reworked, disarticulated shells in outcrops near the present-day coastline. Abundant oyster shells are observed near the base of the conglomerate north of the La Cruz fault. Sandstone is interbedded with the conglomerate beds adjacent to and beneath the Rhyodacite of Cerro Starship [*Cassidy*, 1988; *Neuhaus*, 1989; *Gastil et al.*, 1999]. Marine conglomerate outcrops north of the La Cruz fault are tilted 15–20° to the north [*Neuhaus*, 1989; *Gastil et al.*, 1999]. These outcrops are capped by discontinuous flat-lying, poorly-sorted to moderately-sorted marine or nonmarine conglomerate. The flat-lying beds both truncate and grade laterally into the tilted marine conglomerate. Thicker deposits of this nonmarine conglomerate are mapped as unit Tmpal (Fig. 8.2). These conglomerates are 1–10 m thick and also flat-lying. Outcrops of Tmpal occur inland (southeast) of the marine strata and as a series of high terraces unconformably overlying andesite.

Clasts within the marine conglomerate are predominantly andesite that are probably derived from local outcrops of lava flows and volcaniclastic debris flows [*Gastil et al.*, 1999]. A few distinctive clasts are also recognized within the marine conglomerate. Some of these distinctive clasts are derived from the Tuff of the Sierra Kunkaak, a welded tuff with a red glassy matrix and 50% angular aphanitic orange volcanic lithic fragments. This unit is distinctive to the Sierra Kunkaak, located 15 km east of the study area (Chapter 3). Clasts of the ∼12.6 Ma Tuff of San Felipe, a densely welded crystal-rich ignimbrite [*Stock et al.*, 1999; *Oskin et al.*, 2001], are also present within the marine conglomerate. Outcrops of the Tuff of San Felipe occur nearby in the Sierra Menor. Clasts of partially welded unit Tmr3 of the Tuffs of Mesa Cuadrada, a ∼6.3 Ma crystal-rich ash-flow tuff with abundant volcanic lithic fragments, are rare within the marine conglomerate. Most outcrops of Tmr3 on Isla Tiburón occur north of the paleotopographic high formed of Tma1 andesite lava flows north of the La Cruz fault. However, the distal partially welded facies of Tmr3, identical to the clasts present in the marine conglomerate, crops out 6 km east of the marine basin in the southern Sierra Menor (Chapter 3 of this thesis).

The marine rocks of southwest Isla Tiburón were mapped earlier as unit T3m by *Gastil and Krummenacher* [1976] and later subdivided into three subunits [*Cassidy*, 1988; *Neuhaus*, 1989; *Gastil et al.*, 1999]. These three subunits are a lower conglomerate member (Mbr and M8a), a middle sandstone member (Mss and M8c), and an upper conglomerate member (Mcgl and M8d). An additional member of rhyolite and andesite flows is mapped as unit M8b between the lower conglomerate and middle sandstone by *Gastil et al.* [1999]. This outcrop, which was first described as a breccia rather than a flow and dated at 12.9±0.4 Ma by *Smith et al.* [1985], is interpreted here as an erosional window into the landslide breccia beneath the marine rocks. Even if this outcrop is intercalated with the marine strata, it is not possible to lithologically differentiate this breccia from the landslide breccias underlying the marine rocks. Age-diagnostic microfossils are reported by *Gastil et al.* [1999] from sandstones interbedded within the marine conglomerate. Foraminifera fossils repre-

sent Late Miocene to Early Pliocene faunal zones N17B to N19, corresponding to an age of 6.4 to 4.0 Ma [*Gastil et al.*, 1999]. Calcareous nannoplankton microfossils also indicate a Late Miocene-early Pliocene age, with an early Pliocene age favored [*Gastil et al.*, 1999].

The depositional setting of the marine conglomerate is interpreted here as a shallow marine to littoral northwest-facing delta-fan built from arroyos draining southern Isla Tiburón. *Cassidy* [1988] first proposed a delta-fan origin for these rocks, based upon their coarse clastic composition and upward coarsening beds. Southeast-facing clast imbrications are cited by *Gastil et al.* [1999] to support a source for this fan from the northwest. However, the depositional architecture of the marine conglomerate and related non-marine capping conglomerates strongly resembles a northwest-facing set of delta-fan foreset beds capped by non-marine to marine transitional topset beds. Clasts derived from the Sierra Kunkaak, 15 km east of the southwest Isla Tiburón marine basin, further support an easterly source for these deposits. The 15–23° dip of these strata north of the La Cruz fault is interpreted as a primary depositional angle, and up-dip clast imbrications are interpreted to be the result of wave action in a nearshore to littoral setting.

Sandy facies of the marine strata probably represent offshore facies of the delta fan [*Gastil et al.*, 1999]. A lateral transition from nearshore marine conglomerate to offshore sandstone and sandy conglomerate is exposed in outcrops on the shoreline west of Cerro Starship. Well-sorted, rounded conglomerate overlying landslide breccia deposits is interpreted here as a littoral facies, similar to rocky shorelines present elsewhere on Isla Tiburón. The % sand matrix within the conglomerate increases northward, and sandstone interbeds appear. Sandstone is the dominant lithology in shoreline exposures north of Cerro Starship. Foraminifera from sandstone from southwest Isla Tiburón indicate an inner to outer neritic (50 to 150 m) water depth, [*Gastil et al.*, 1999], consistent with the stratigraphic association described here. Exposure of sand beds was probably enhanced by folding and tilting of these strata by deformation associated with the La Cruz fault.

Rhyodacite of Cerro Starship

The Rhyodacite of Cerro Starship, mapped as unit Tprcs on Fig. 8.2, caps marine rocks on southwestern Isla Tiburón [*Gastil and Krummenacher*, 1977; *Neuhaus*, 1989; *Gastil et al.*, 1999]. This flow contains 35% phenocrysts (plagioclase > hornblende > alkali-feldspar > opaques > biotite) and displays macroscopic flow foliation and trachytic alignment of plagioclase microphenocrysts in a glass matrix. The Rhyodacite of Cerro Starship was emplaced primarily as a 10 to 40 m thick lava flow that was emplaced subaerially over tilted marine rocks. This lava flow erupted from a north-striking dike that crops out intermittently on the eastern side of Cerro Starship. Components indicative of pyroclastic emplacement, such as eutaxitic foliation, pumice fragments, glass spicules or lithic fragments, are absent from the main body of the lava flow. A one- to two-meter–thick block-and-ash deposit underlies the main body of rhyodacite lava with a sharp contact. Locally, adjacent to the dike, these ash deposits have been compressed and welded by emplacement of the lava. The source dike for the Rhyodacite of Cerro Starship also crops out north of the flow in the base of the arroyo east of Cerro Starship (Fig. 8.2). The phenocrysts and texture of this dike are identical to the main body of the Rhyodacite of Cerro Starship.

The Rhyodacite of Cerro Starship was mapped as unit T4x by *Gastil and Krummenacher* [1976], units Mrt (flow) and Mgd (dike) by *Neuhaus* [1989] and units M9 (flow) and M10 (dike) by *Gastil et al.* [1999]. The flow was originally identified as an ash-flow tuff by *Gastil and Krummenacher* [1977]. *Neuhaus* [1989] recognized that the upper parts of this flow contained a highly variable foliation and were probably emplaced as 'an effusive phase' (lava flow?). *Neuhaus* [1989] and *Gastil et al.* [1999] interpreted the lower half of the flow as an ignimbrite. Although the flow foliation in the lower half of the Rhyodacite of Cerro Starship is usually parallel to its base, similar in appearance to an outcrop of eutaxiticaly foliated ignimbrite, all of this unit except the basal 1–2 m lacks evidence for pyroclastic emplacement.

Three samples of the Rhyodacite of Cerro Starship have been dated by K–Ar on

plagioclase. *Gastil and Krummenacher* [1977] report an age of 11.2±1.3 Ma (sample S2B-27, Table 8.1). This date has formed the basis of interpretation of marine strata on southwestern Isla Tiburón as evidence for a middle Miocene proto-Gulf of California [*Smith*, 1991]. *Gastil and Krummenacher* [1977] also dated an outcrop of the rhyodacite dike in the arroyo northeast of Cerro Starship at 3.7±0.9 Ma (sample S2G-13, Table 8.1). *Gastil and Krummenacher* [1977], *Neuhaus* [1989], and *Gastil et al.* [1999] interpreted this dike as a separate, younger unit. An attempt by *Neuhaus* [1989] to re-date the main body of the Rhyodacite of Cerro Starship from a sample from the top of the flow yielded a young age of 4.2±1.8 Ma (sample 10, Table 8.1). *Neuhaus* [1989] and *Gastil et al.* [1999] interpreted this sample as derived from a continuation of the of the younger rhyodacite dike through the center of Cerro Starship. New field mapping of this area did not reveal the dike mapped by *Neuhaus* [1989] and *Gastil et al.* [1999] through the crest of Cerro Starship. Instead, a dike was discovered on the eastern side of Cerro Starship in continuous exposure with the main body of the flow and on trend with the dike exposure to the north. As described above, these dikes are identical to the main body of the flow and clearly related to its emplacement. An attempt to re-date the Rhyodacite of Cerro Starship by $^{40}Ar/^{39}Ar$ was unsuccessful.

Nonmarine conglomerate

Younger nonmarine conglomerates, mapped as unit QTpal, post-date marine deposition on southwest Isla Tiburón. Unit QTpal forms a 2–4 m thick terrace deposit inset into the marine rocks and beneath the Tmpal terraces. Except for their geomorphic position, these conglomerates are identical to older conglomerates of unit Tmpal on southwest Isla Tiburón. This unit is locally overlain by the Tuffs of Bahía Vaporeta, a welded to non-welded lithic-rich rhyolitic tuff.

The Tuffs of Bahía Vaporeta

The youngest volcanic rocks exposed in the southwest Isla Tiburón basin are a series of 1 to 3 lithic-rich rhyolite tuffs mapped as unit QTprbv. These ignimbrites, designated the Tuffs of Bahía Vaporeta in Chapter 3 of this thesis, are small-volume non-welded to moderately welded pyroclastic flows exposed along the southwestern shoreline of Isla Tiburón. At least three five-meter-thick cooling units are exposed in a coastal mesa north of the marine conglomerate outcrops. A one- to two-meter-thick densely welded carapace of tuff overlies nonmarine conglomerate on southwestern Isla Tiburón. The Tuffs of Bahía Vaporeta may be recognized from their distinctive and abundant light- and dark-colored pumice and uncommon (1%) anorthoclase phenocrysts. Outcrops of the Tuffs of Bahía Vaporeta were mapped as Qm by *Gastil and Krummenacher* [1976], unit Mry by *Neuhaus* [1989] and M10 by *Gastil et al.* [1999]. These authors interpreted some of these outcrops as rhyolite dikes. No rhyolite dikes were observed in southwest Isla Tiburón during this study, except the rhyodacite dikes associated with the Rhyodacite of Cerro Starship, described above. The Tuffs of Bahía Vaporeta have not been dated.

Quaternary Deposits

Several types of Quaternary deposits are mapped on southwest Isla Tiburón (Fig. 8.2). These deposits include several alluvium-filled northwest-draining arroyos (unit Qal) separated by low-lying terraces (unit Qoal). A thick cover of colluvial deposits (Qco) mantles the steep slopes of Cerro Starship. Adjacent to the coastline of Bahía Vaporeta, sand dunes (Qae), marine terraces (Qmt), and littoral deposits (Qli) are mapped. The Quaternary fluvial deposits and their offshore equivalents probably comprise a depositional system very similar to that which emplaced the marine conglomerate and sandstone on southwest Isla Tiburón.

8.3.4 Faulting and tilting

Faulting has affected most of the volcanic and marine strata exposed on southwest Isla Tiburón. The principal structure through this area is the La Cruz fault. This right-lateral strike-slip fault transects the southern edge of Isla Tiburón [*Gastil and Krummenacher*, 1976, and Chapter 6 of this thesis]. *Neuhaus* [1989] and *Gastil et al.* [1999] both recognized that the La Cruz fault has dextrally displaced the marine strata by about 200 m. Earlier slip on the La Cruz fault may exceed 26 km (Chapter 6) because Early to Middle Miocene volcanic strata do not correlate across its trace (Chapter 3). North-striking normal fault systems of the Sierra Menor, north of the La Cruz fault, offset rocks as young as 6.1 Ma by >100 m (Chapter 6 of this thesis). These faults cannot be traced through the marine conglomerates (Fig. 8.2). This may be because there are few clear markers within the marine strata with which to trace offsets from these faults. A northeast-striking normal fault cuts across the northern end of Cerro Starship, dropping outcrops of the Rhyodacite of Cerro Starship on its north side by ∼20 m.

Tilting of the marine strata of southwest Isla Tiburón is interpreted here as a combination of primary tilt from deposition on a sloping delta-fan surface and tectonic tilt from deformation adjacent to the La Cruz fault. Stratal tilts north of the La Cruz fault remain under 25°, but the strike of bedding changes from northeast to northwest [*Neuhaus*, 1989; *Gastil et al.*, 1999, and Fig. 8.2]. Stratal tiles increase south of the La Cruz fault, locally approaching 45° along the coastline west of Cerro Starship. The 15–23° dips north of the La Cruz fault are interpreted here as depositional delta-fan or beach-face foreset beds that are associated with flat-lying transitional marine–nonmarine topset beds. The change in strike and steeper dip of bedding adjacent to and south of the La Cruz appear to be related to folding adjacent to the fault trace.

Figure 8.4. (next page) Schematic stratigraphic columns of southwest Isla Tiburón. Stratigraphic relationships of volcanic rocks and marine sediments according to *Gastil et al.* [1999] in upper frame and revised according to this study in the lower frame. See Table 8.1 for sources of isotopic ages and *Gastil et al.* [1999] for microfossil age. All volcanic rocks younger than 11.2 Ma are interpreted by *Gastil et al.* [1999] as intrusions and lava flows overlying older marine rocks. These relationships are simplified here into four distinctive units. A landslide breccia (Tmbr) and latest Miocene non-welded ash-flow tuff (Tmprsz1) underlie marine strata. Pliocene age dike and flow of the Rhyodacite of Cerro Starship (unit Tprcs) and the Plio-Quaternary(?) Tuffs of Bahía Vaporeta (unit QTprbv) overlie the marine rocks. See text for additional discussion of lithologies and relationships depicted here.

8.4 Discussion

8.4.1 Age of marine deposits of southwest Isla Tiburón

Existing microfossil evidence, together with geochronology for volcanic rocks both underlying and overlying marine strata on southwest Isla Tiburón, strongly support that marine deposition here occurred between 6 Ma and 4 Ma (Fig. 8.4). Arc-related volcanic strata beneath the southwest Isla Tiburón basin are 21–15 Ma south of the La Cruz fault and 17.7–11.4 Ma north of the La Cruz fault [*Gastil et al.*, 1999]. The lowermost basin-filling strata is a landslide breccia, containing clasts dated as 12.9 Ma and 9.2 Ma [*Smith et al.*, 1985; *Neuhaus*, 1989], and probably emplaced in a nonmarine setting. The first evidence for the presence of shallow marine conditions is from outcrops of partially-welded to non-welded member one of the Tuffs of Arroyo Sauzal. This tuff is isotopically dated at 5.7±0.2 Ma by *Neuhaus* [1989] and 6.7±0.8 Ma and 6.4±1.6 Ma during this study. Marine conglomerates depositionally overlie member one of the Tuffs of Arroyo Sauzal. Sandstone interbedded with the marine conglomerate contains microfossils from foraminiferal zones N17B to N19, corresponding to a 6.4–4.0 Ma age range [*Gastil et al.*, 1999].

The Rhyodacite of Cerro Starship overlies the marine rocks of southwest Isla Tiburón. This unit is predominantly a 10–40 m thick lava flow emplaced subaerially over tilted marine rocks. The dike that extruded the Rhyodacite of Cerro Starship crops out on the east side of the flow and within an arroyo northeast of the flow. A

Figure. 8.4

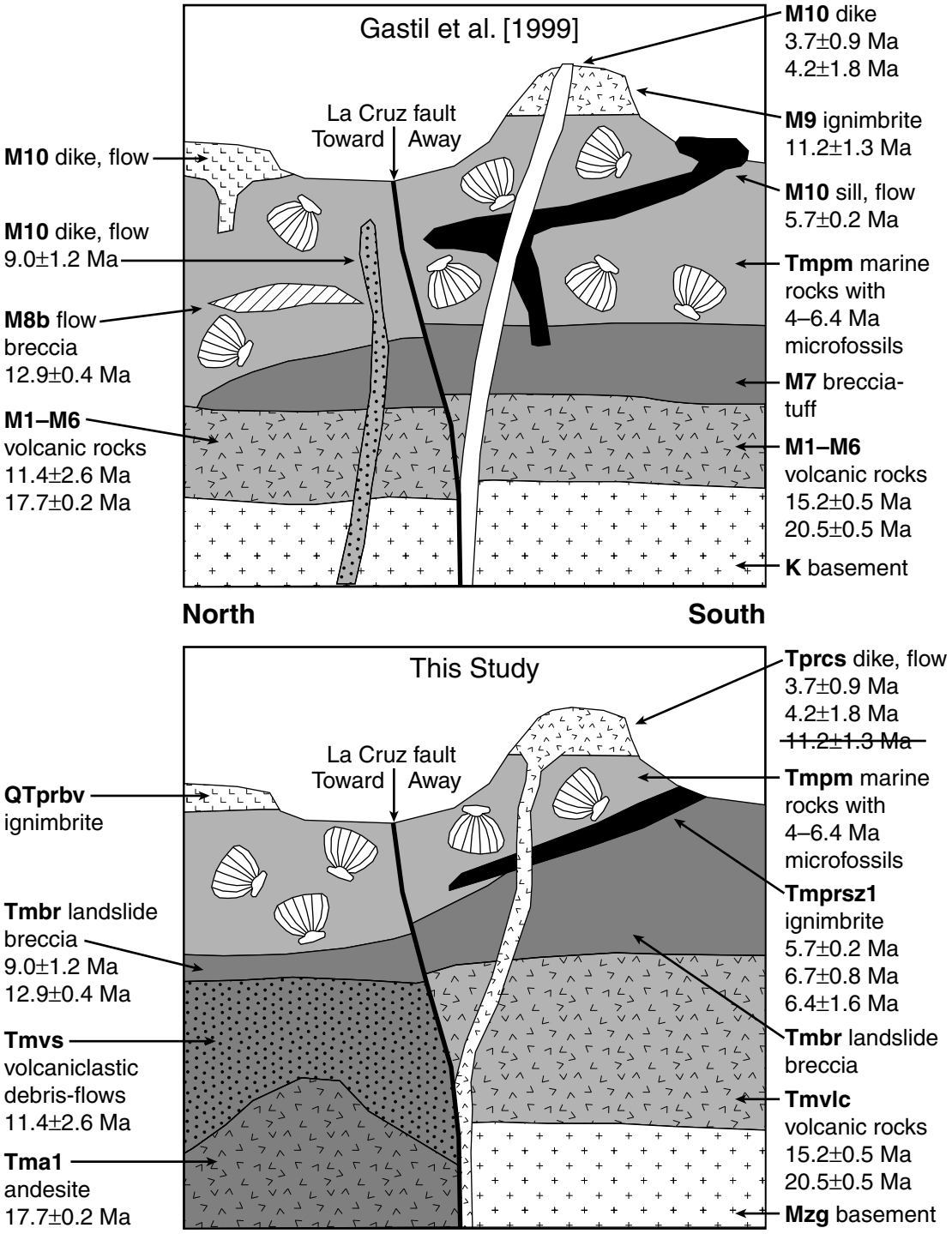
Gastil et al. [1999]
La Cruz fault
Toward
Away
M10 dike, flow
M10 dike, flow
9.0±1.2 Ma
M8b flow
breccia
12.9±0.4 Ma
M1–M6
volcanic rocks
11.4±2.6 Ma
17.7±0.2 Ma
M10 dike
3.7±0.9 Ma
4.2±1.8 Ma
M9 ignimbrite
11.2±1.3 Ma
M10 sill, flow
5.7±0.2 Ma
Tmpm marine
rocks with
4–6.4 Ma
microfossils
M7 breccia-
tuff
M1–M6
volcanic rocks
15.2±0.5 Ma
20.5±0.5 Ma
K basement
North
South
This Study
La Cruz fault
Toward
Away
QTprbv
ignimbrite
Tmbr landslide
breccia
9.0±1.2 Ma
12.9±0.4 Ma
Tmvs
volcaniclastic
debris-flows
11.4±2.6 Ma
Tma1
andesite
17.7±0.2 Ma
Tprcs dike, flow
3.7±0.9 Ma
4.2±1.8 Ma
11.2±1.3 Ma
Tmpm marine
rocks with
4–6.4 Ma
microfossils
Tmprsz1
ignimbrite
5.7±0.2 Ma
6.7±0.8 Ma
6.4±1.6 Ma
Tmbr landslide
breccia
Tmvlc
volcanic rocks
15.2±0.5 Ma
20.5±0.5 Ma
Mzg basement

1–2 m thick block and ash deposit at the base of the Rhyodacite of Cerro Starship has been partially welded by emplacement of the overlying lava flow. Of the three ages reported for the Rhyodacite of Cerro Starship and its associated dike, two of these ages have yielded consistent dates of ∼4 Ma. The 3.7 Ma date of the dike exposure north of Cerro Starship and the date of 4.2 Ma from the crest of the lava flow both agree with the stratigraphic position of the Rhyodacite of Cerro Starship above outcrops of the ∼6 Ma member one of the Tuffs of Arroyo Sauzal and marine sandstones containing 6.4–4.0 Ma microfossils. Only one age of 11.2±1.3 Ma determined by *Gastil and Krummenacher* [1977] for the Rhyodacite of Cerro Starship cannot be reconciled with these constraints.

Prior interpretations of southwest Isla Tiburón by *Neuhaus* [1989] and *Gastil et al.* [1999] explained the Latest Miocene and Pliocene volcanic rocks here as a series of dikes and lava flows that were emplaced into and above the marine rocks. Observations of the emplacement mechanisms of most of these rocks do not support their interpretations (Fig. 8.4). The only latest Miocene or younger volcanic unit of the southwest Isla Tiburón basin that was emplaced as a dike and lava flow is the Rhyodacite of Cerro Starship. The discordant 11.2±1.3 Ma age for this flow, originally reported by *Gastil and Krummenacher* [1977], has been maintained by *Neuhaus* [1989] and *Gastil et al.* [1999] even though microfossils from underlying marine strata and an additional dating attempt on this flow supported a younger age. Based upon new and existing stratigraphic and geochronologic evidence presented here, I conclude that the 11.2±1.3 Ma age originally reported by *Gastil and Krummenacher* [1977] cannot be correct. This 11.2±1.3 Ma age should be abandoned as a constraint on the proto-Gulf marine incursion. Likewise, the 12.9±0.4 age first reported by *Smith et al.* [1985] for a volcanic breccia intercalated with the marine strata appears to have been obtained from a sample from an underlying unit and is thus only a maximum constraint on the age of the marine rocks of southwest Isla Tiburón.

8.4.2 Depositional and tectonic setting of the southwest Isla Tiburón basin

The depositional and tectonic setting of marine sedimentary rocks of southwest Isla Tiburón is interpreted here as a shallow marine, fault controlled basin. The basin formed as a triangular-shaped embayment by a combination of opening of the Upper Delfín basin, west of Isla Tiburón, and dextral displacement on the La Cruz fault and the Tiburón fracture zone (Fig. 8.5). This embayment is present today as Bahía Vaporeta, just offshore of the study area. The southwest Isla Tiburón basin initially received landslide breccia emplaced into a nonmarine setting. The source for this breccia may be nearby outcrops of welded tuff at Cerro Colorado (3 km southeast of study area) or from outcrops that have been since displaced by the Tiburón fracture zone. Marine incursion into the southwest Isla Tiburón basin probably had occurred by the time of emplacement of member one of the Tuffs of Arroyo Sauzal above the landslide breccias. After emplacement of this ash-flow tuff, the basin began to be filled by streams draining southern Isla Tiburón. These streams built a delta-fan that prograded northwestward, filling the corner of the basin exposed today and spreading out into the more open waters of Bahía Vaporeta. Waning dextral displacement on the La Cruz fault cut and tilted these beds, exposing the lower, sandier facies of the delta-fan deposit. Eruption of the Rhyodacite of Cerro Starship covered some of these tilted beds south of the La Cruz fault. Moderate downcutting and northwestward progradation has continued to the present in the region north of the La Cruz fault, depositing sediment into Bahía Vaporeta.

The interpretation of the southwest Isla Tiburón basin as a shallow fault-controlled embayment differs considerably from previous workers. *Neuhaus* [1989] and *Gastil et al.* [1999] interpreted the southwest Tiburón basin as filling a collapse feature related to volcanism. These workers did not identify the structures or volcanic products associated with this collapse. The model presented here explains the wedge shape of the basin, northwest-facing foresets, and distinctive clasts contained within the ma-

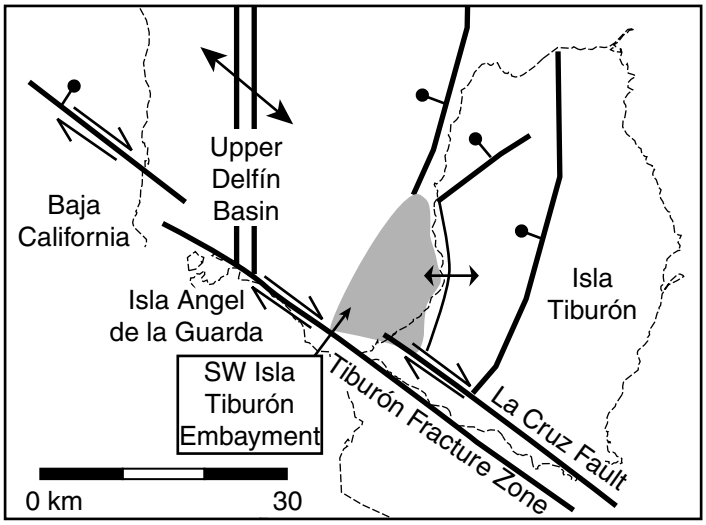

Figure 8.5. Tectonic origin of the southwest Isla Tiburón embayment. Opening of the Upper Delfín basin between Baja California and Isla Tiburón starts after ∼6 Ma [*Oskin et al.*, 2001]. Divergence across the Upper Delfín basin is transferred to the southeast by strike-slip on the La Cruz fault and the Tiburón Fracture zone. Southwest Isla Tiburón embayment formed north of the shear zone on southernmost Isla Tiburón on the partially subsided eastern continental margin of the Upper Delfín basin. Large-scale structural features of Isla Tiburón and coastal Baja California shown according to Chapter 6 of this thesis. Isla Angel de la Guarda, shown fixed to Baja California during initial opening of the Upper Delfín basin cf. [*Stock*, 2000].

rine sediments. The 4–6 Ma age of these marine deposits fits very well with the timing of opening of the Upper Delfín basin [*Oskin et al.*, 2001], normal faulting on Isla Tiburón, and significant displacement on the Tiburón Fracture Zone and La Cruz fault (Chapter 6).

The thickness of the marine deposit on southwest Isla Tiburón is probably much less than estimated by *Cassidy* [1988] and reported by *Smith* [1991] and *Gastil et al.* [1999]. *Cassidy* [1988] estimated up to 1.5 km of marine conglomerate in the northern part of the basin by interpreting a flat original dip for these beds. Evidence presented here indicates that these beds are delta-fan foresets deposited in a shallow marine to littoral setting, and that the dip of these beds is probably primary in exposures north of the La Cruz fault. The actual thickness of the basin-filling sequence on southwestern Isla Tiburón may be as little as 50 m, which is approximately the maximum height observed for individual foreset beds. Overall, the thickness of marine strata exposed in the onshore portion of the southwest Isla Tiburón basin probably does not exceed 300 m.

8.4.3 Implications for the proto-Gulf marine incursion

The presence of latest Miocene to Early Pliocene age rather than Middle Miocene age marine rocks on southwest Isla Tiburón significantly changes interpretation of the proto-Gulf of California marine incursion (Fig. 8.1). This new younger age, when combined with other well-constrained ages established through clear cross-cutting relationships and/or microfossil assemblages, supports marine incursion into the northern Gulf of California no earlier than 6.5 Ma (Table 8.2). South of Isla Angel de La Guarda and Isla Tiburón, well-constrained ages of marine rocks as old as 7.5–8.2 Ma indicate an earlier marine incursion here (Fig. 8.1 and Table 8.2). Rocks this old occur as far south as the San Jose Del Cabo basin and the Tres Marias Islands, adjacent to the mouth of the Gulf of California [*McCloy et al.*, 1988; *Molina-Cruz*, 1994]. This evidence suggests that the Gulf of California has always been connected to the Pacific Ocean near its present-day mouth. A hypothetical seaway across the

San Ignacio area of Baja Califronia Sur [*Helenes and Carreño*, 1999] is unnecessary to explain the distribution of well-constrained Miocene-age marine rocks in the Gulf of California.

Other Middle Miocene age (pre-11 Ma) proto-Gulf marine rocks have been proposed for the Boleo Formation of Baja California Sur [*Smith*, 1991], the Bahía de Los Angeles area of Baja California Norte [*Delgado-Argote et al.*, 2000b], and Isla Angel de La Guarda [*Delgado-Argote et al.*, 2000a]. In each of these cases, marine strata overlie isotopically dated Middle-Miocene or older volcanic rocks (Table 8.1). No sedimentary or volcanic textures associated with eruption underwater are reported from these rocks. Thus, the ages of these volcanic rocks only represent maximum ages of the overlying marine rocks. Further investigations of these marine rocks where intruded by or clearly overlain by isotopically dated volcanic rocks is necessary to definitively establish the presence of a Middle Miocene proto-Gulf of California.

Reworked Middle Miocene microfossils have been reported from otherwise Pliocene-age marine rocks in the northern Gulf of California [*Helenes and Carreño*, 1999, and references therein]. No source rocks have been identified for these fossils. After removing the constraint from Isla Tiburón, no other definitive evidence exists for Middle Miocene age marine rocks deposited by the proto-Gulf of California that could have been a source for these reworked fossils. The explanation for reworked Middle Miocene microfossils in Pliocene age rocks is presently unresolved.

Mollusk fossils from Isla Tiburón are correlated to the basal Imperial Formation of the Salton Trough [*Smith*, 1991]. Based upon this correlation, *Smith* [1991] suggests that parts of the basal Imperial formation may also be Middle Miocene age. Subsequent studies of microfossil assemblages of the basal Imperial Formation indicate a latest Miocene to Early Pliocene age for these sections [*McDougall et al.*, 1999; *Dean*, 1996]. These ages are the same as the revised age presented here for marine rocks on Isla Tiburón. Both the basal Imperial Formation and the marine rocks of southwest Isla Tiburón pre-date an increase in sedimentation rate into the Gulf of California that accompanied arrival of the Colorado River [*Johnson et al.*, 1983]. An alterna-

tive interpretation of the correlative macrofauna described by *Smith* [1991] and *Gastil et al.* [1999] for the basal Imperial formation and Isla Tiburón is that these fossils may be characteristic of the paleoenvironment of the Gulf of California prior to arrival of the Colorado River.

8.4.4 Tectonic implications of the proto-Gulf marine incursion

The extent of Miocene marine deposition in northwest Mexico provides an important constraint on crustal rheology preceding localization of the Pacific–North America plate boundary in the Gulf Extensional Province (southern Basin and Range province cf. *Henry and Aranda Gomez* [1992]). In most of the Basin and Range Province of southwest North America, large-magnitude intracontinental extension has been balanced by lower crustal flow, evening out crustal thickness over the province [*Wernicke*, 1990, for example] and preventing localization of a narrow zone of lithospheric necking [*Buck*, 1991]. This process has maintained most of the Basin and Range province at elevations above sea level. If marine deposition has occurred within the 1000 km-long Gulf Extensional Province since the onset of extension here ca. 12 Ma [*Stock and Hodges*, 1989; *Lee et al.*, 1996], then this would suggest that lithospheric necking was more localized and less compensated by lower crustal flow in the Gulf Extensional Province than elsewhere in the Basin and Range. The revised latest Miocene to Early Pliocene age of marine deposition on southwest Isla Tiburón removes the need to explain an early proto-Gulf marine incursion into the northern Gulf of California over a region of localized lithospheric necking. Instead, the history of marine incursion is consistent with the tectonic history of the Upper Delfín basin of the northern Gulf of California, which opened abruptly during latest Miocene time [*Oskin et al.*, 2001], probably in response to a change in boundary forces rather than by crustal weakening by intracontinental extension (Chapter 6 of this thesis).

Overall, the revised chronology presented here for initial marine incursion into the

Gulf of California is consistent with its extensional tectonic history. Regional plate tectonic reconstructions suggest that crustal attenuation from 12.5–6 Ma was more intense in the southern Gulf of California than in the northern Gulf of California [*Stock and Hodges*, 1989]. Marine incursion into the southern and central Gulf of California during Late Miocene time probably covered this region of more intense continental extension. Marine incursion into the northern Gulf of California and the Salton Trough after 6.5 Ma correlates closely with localization of Pacific–North America plate boundary motion here [*Oskin et al.*, 2001, and Chapter 5 of this thesis]. Although diffuse Basin and Range type extension of the continental margins of the northern Gulf of California was underway by 7.5–8.2 Ma [*Lee et al.*, 1996], the basins produced by this extension were either above sea level or isolated from the marine incursion to the south. Localization of the Pacific–North America plate boundary into the northern Gulf of California probably facilitated marine incursion here by creating a central region of intense continental rifting and by linking together isolated rift basins.

8.5 Conclusions

Reevaluation of volcanic rocks bounding marine strata exposed on southwest Isla Tiburón reveals that these marine deposits are latest Miocene to Early Pliocene age. The southwest Isla Tiburón marine basin overlies Early to Middle Miocene volcanic rocks juxtaposed by the La Cruz strike-slip fault. Landslide breccias containing clasts as young as 9 Ma mark the inception of basin sedimentation. Three separate constraints support a latest Miocene age for marine rocks that overlie these breccias. The first constraint is emplacement of member one of the Tuffs of Arroyo Sauzal above the landslide breccia at ∼6 Ma, coeval with the base of marine deposits. The second constraint on the age of the marine strata is the presence of latest Miocene to Early Pliocene age microfossils reported by *Gastil et al.* [1999]. The third constraint on the age of the marine strata is emplacement of the Rhyodacite of Cerro Starship

onto tilted marine rocks by a dike intrusion and subaerial lava flow. Two ages determined by *Gastil and Krummenacher* [1977] and *Neuhaus* [1989] for the Rhyodacite of Cerro Starship are ∼4 Ma. A third age of 11.2±1.3 Ma, first reported by *Gastil and Krummenacher* [1977], is discordant with other age constraints.

The southwest Isla Tiburón marine basin formed as a northwest-facing embayment controlled by opening of the Upper Delfín basin segment of the Gulf of California and by right-lateral strike slip on the La Cruz fault and Tiburón Fracture zones. Streams draining southern Isla Tiburón have partially filled the embayment with conglomerate and sandstone, forming a northwest-facing delta-fan. Bahía Vaporeta, located west of Isla Tiburón, is the offshore continuation of this northwest-facing embayment. The thickness of the marine deposits of southwest Isla Tiburón is much less the 1.5 km estimated by previous workers because much of the tilt of the marine strata represents primary deposition on a delta-fan slope and/or beach face. Waning dextral displacement on the La Cruz fault has offset and tectonically tilted the marine strata, which were then unconformably overlain by the ∼4 Ma Rhyodacite of Cerro Starship.

Since marine rocks as old as 7.5–8.2 Ma crop out adjacent to the mouth of the Gulf of California [*McCloy et al.*, 1988; *Molina-Cruz*, 1994], the Gulf has probably always been connected to the Pacific Ocean at its southern end. A hypothetical seaway across the San Ignacio area of Baja California Sur proposed is not required to explain the distribution of well-constrained Miocene-age marine rocks in the Gulf of California. Other proposed proto-Gulf marine rocks have been constrained only to overlie isotopically dated Middle-Miocene or older volcanic rocks and thus only have maximum ages. Investigations of these marine rocks where intruded by or clearly overlain by isotopically dated volcanic rocks are necessary to firmly establish their age.

The presence of latest Miocene to Early Pliocene age rather than Middle Miocene age marine rocks on southwest Isla Tiburón allows for new model of the proto-Gulf of California marine incursion. Early marine incursion into the southern and central Gulf of California as early as 8.2 Ma probably filled an area of more intense crustal

attenuation. Marine incursion over the entire length of the Gulf of California after 6.5 Ma corresponds to when the Pacific–North America plate boundary localized here. Localization of the plate boundary into the northern Gulf of California probably facilitated marine incursion by creating a central region of intense continental rifting and by linking together isolated rift basins. Latest Miocene marine incursion into the northern Gulf of California is consistent with the tectonic history of the Upper Delfín basin, which opened abruptly during latest Miocene, probably in response to a change in boundary forces rather than by crustal weakening by intracontinental extension.

Table 8.2. Miocene marine rocks from the Gulf of California.

Area (See Fig. 8.1)		Unit	Age [*Reference*][1]	Comments
A	San Gorgonio Pass	Imperial Formation	6.3–6.5 Ma [*McDougall et al.*, 1999]	Combined analysis of micropaleontology, paleoenvironment, and sea-level fluctuations with isotopic ages of bounding volcanic strata.
B	Imperial Valley	Fish Creek Gypsum	4.3–6.3 Ma [*Dean*, 1996]	Micropaleontology. Fish Creek Gypsum underlies the Imperial formation.
C	Colorado River Trough	Bouse Formation	(5.97±0.07 Ma) [*Spencer et al.*, 1998]	Tuff bed in Hualapai Limestone member of Muddy Creek formation. Precedes sedimentation from the Colorado River that was coeval with Bouse Formation. Bouse Formation may be of partially lacustrine origin [*Spencer and Patchett*, 1997].
D	Sierra San Felipe	San Felipe Diatomite	5.5–6.0 Ma [*Boehm*, 1984] (6.8±0.3 Ma) [*Stock*, 1997]	Micropaleontology and $^{40}Ar/^{39}Ar$ on alkali feldspar from detrital pumiceous material.
E	Arroyo Matomí	Puertecitos Formation	3.27±0.04 Ma [*Martín-Barajas et al.*, 1997] (6.1±0.5 Ma) [*Nagy et al.*, 1999]	Matomí mudstone member overlies ∼6.1 Ma Tuff of Arroyo El Canelo and underlies ∼3.3 Ma Tuff of Valle Curbina.
F	Isla Angel de la Guarda	Unnamed marine sedimentary rocks	(17±0.6 Ma) [*Delgado-Argote et al.*, 2000a]	Marine rocks overlie andesite lava flows. These ages are only a maximum constraint on the age of overlying marine sedimentary rocks.
G	Isla Tiburón	Southwest Isla Tiburón sedimentary rocks	4–6 Ma [*This study*]	Marine rocks underlain by ∼6 Ma member one of the Tuffs of Arroyo Sauzal and overlain by ∼4 Ma Rhyodacite of Cerro Starship. Microfossils indicate 6.4–4 Ma age [*Gastil et al.*, 1999].

Area (See Fig. 8.1)		Unit	Age [*Reference*][1]	Comments
H	Bahía de Los Angeles	Unnamed marine sedimentary rocks	(12.1±0.1 Ma) [*Delgado-Argote et al.*, 2000b]	Marine sedimentary rocks overlie andesite lava flows. Interpreted by *Delgado-Argote et al.* [2000b] as an intertidal environment through which local basaltic bodies rose as a peléan dome. However, because of lack of a clear cross-cutting relationship with marine strata, these ages are considered here as only a maximum constraint on the age of overlying marine sediments.
I	Santa Rosalía	Boleo Formation	∼7 Ma [*Holt et al.*, 2000] (7.7–8 Ma) [*Conly et al.*, 2000] (12.3 ± 0.4 Ma) (12.5 ± 0.4 Ma) [*Smith*, 1991]	$^{40}Ar/^{39}Ar$ age of 6.76±0.90 Ma on interstratified Cinta Colorada tephra combined with magnetostratigraphy. Ages in parentheses are for volcanic rocks that underlie the Boleo Formation.
J	San Jose del Cabo	Trinidad Formation	6.9 Ma [*Carreño*, 1992] 7.5 Ma [*Molina-Cruz*, 1994]	Benthic foraminifera and radiolarian microfossils, respectively, from the basal diatomite member of the Trinidad Formation.
K	Islas Tres Marias	Arroyo Hondo sediments	latest Miocene–Early Pliocene [*Carreño*, 1985] 7.0–8.2 Ma [*McCloy et al.*, 1988]	Calcareous microfossils (Planktonic foraminifera, ostracodes, and calcareous nannoplankton) and radiolaria, respectively.

[1] Ages in parentheses are maximum age constraints only.

Chapter 9

Active parasitic folds on the Elysian Park anticline: Implications for seismic hazard in central Los Angeles, California

Michael Oskin, Kerry Sieh	Seismological Laboratory, 252-21, California Institute of Technology, Pasadena, California 91125, USA
Thomas Rockwell	Department of Geological Sciences, San Diego State University, San Diego, California 92182, USA
Grant Miller	Advanced Earth Sciences, Incorporated, 13700 Alton Parkway, Suite 163, Irvine, California 92618, USA
Paul Guptill	GeoSyntec, 2100 Main Street, Suite 150, Huntington Beach, California 92648, USA
Matthew Curtis	Earth Technology Corporation, 100 West Broadway, Long Beach, California 90802, USA
Steve McArdle, Paul Elliot	Law/Crandall, Incorporated, 200 Citadel Drive, Los Angeles, California 90040, USA

From *Geological Society of America Bulletin*, vol. 112, no. 5, p. 693–707, Modified with permission of the publisher, the Geological Society of America, Boulder, Colorado, USA.

9.1 Abstract

We characterize the seismic hazard of the Elysian Park fault, a blind reverse fault beneath central Los Angeles, by analysis of the Elysian Park anticline, which overlies it. New shallow-subsurface geotechnical data, combined with other surficial stratigraphy and geomorphology, reveal that the Elysian Park anticline is an active, 20-km-long structure. From the style and rates of deformation of parasitic folds on the southern limb of the anticline, we estimate a contraction rate of 0.6 to 1.1 mm/yr. This rate provides a basis for estimating a rate of contraction of the entire Elysian Park anticline, which, in turn allows us to estimate a 0.8 to 2.2 mm/yr time-averaged rate of slip on the underlying fault. At this rate of slip, rupture of the Elysian Park fault could produce a nominal M_W 6.2 to 6.7 earthquake every 500 to 1300 years, on average. Although this Elysian Park earthquake would recur infrequently, its size and recurrence interval may be similar to those estimated for the sources of the destructive 1971 San Fernando and 1994 Northridge earthquakes.

9.2 Introduction

Three destructive earthquakes in modern times have shown that reverse faults are significant contributors to seismic hazard in the Los Angeles region (Figure 1). The San Fernando earthquake of 1971 (M_W 6.6), which produced significant damage on the northern outskirts of the metropolitan region, was generated by slip on a north-dipping reverse fault that ruptured to the surface [*Barrows*, 1975]. An adjacent, south-dipping blind thrust fault produced the 1994 Northridge earthquake (M_w 6.7) [*Hauksson et al.*, 1995]. The M_w 6.0 Whittier Narrows earthquake of 1987 also resulted from slip on a blind thrust fault [*Hauksson et al.*, 1988].

These destructive earthquakes have stimulated numerous attempts to assess the seismic potential of active structures within the metropolitan region [*Davis et al.*, 1989; *Hummon et al.*, 1994; *Shaw and Suppe*, 1996; *Schneider et al.*, 1996; *McNeilan*

et al., 1996; *Dolan et al.*, 1997; *Walls et al.*, 1998; *Rubin et al.*, 1998; *Shaw and Shearer*, 1999]. Nonetheless, characterization of seismic sources within the region is far from complete.

We investigate the Elysian Park anticline, a 20-km-long, 10-km-wide fold on the northern margin of the Los Angeles basin. Our goal is to assess the seismic hazard of the blind, Elysian Park fault that is producing this fold. The anticline is a modest feature, relative to the size of other folds and related reverse faults of the Transverse Ranges, or relative to the larger strike-slip faults of Southern California [*Davis et al.*, 1989; *Dolan et al.*, 1995], (Fig. 9.1). However, the blind Elysian Park fault may be large enough to produce an extraordinarily destructive earthquake in the densely populated metropolitan region. Because of the central location of this fault, losses from such an event would likely exceed the $40 billion [*Eguchi*, 1998] suffered from the Northridge earthquake, which struck the northern margin of the metropolitan region. A seismic source under the downtown area might result in collapse of some mid-level high-rise buildings [*Heaton et al.*, 1995].

The Elysian Park anticline has been a subject of two recently published studies regarding seismic hazards of blind thrust earthquakes. Publication of these studies followed the Whittier Narrows earthquake, which was produced by a blind thrust beneath the eastern terminus of the anticline. *Davis et al.* [1989] used the extensive surface and subsurface geologic record in the Los Angeles basin to predict thrust fault geometry and total convergence rate. In a separate study of the Elysian Park anticline, *Bullard and Lettis* [1993] develop and test several geomorphic criteria for characterizing active folds. Their study documents late Quaternary uplift, at 0.1 to 0.25 mm/yr, of a pair of smaller anticlines on the southern limb of the Elysian Park anticline. They conclude that these folds overlie southward-propagating segments of the Elysian Park fault.

We present a revised and expanded geomorphic interpretation of late Quaternary growth of the Elysian Park anticline. Similar to *Bullard and Lettis* [1993], we utilize the extent and deformation of multiple generations of fluvial terrace deposits to ex-

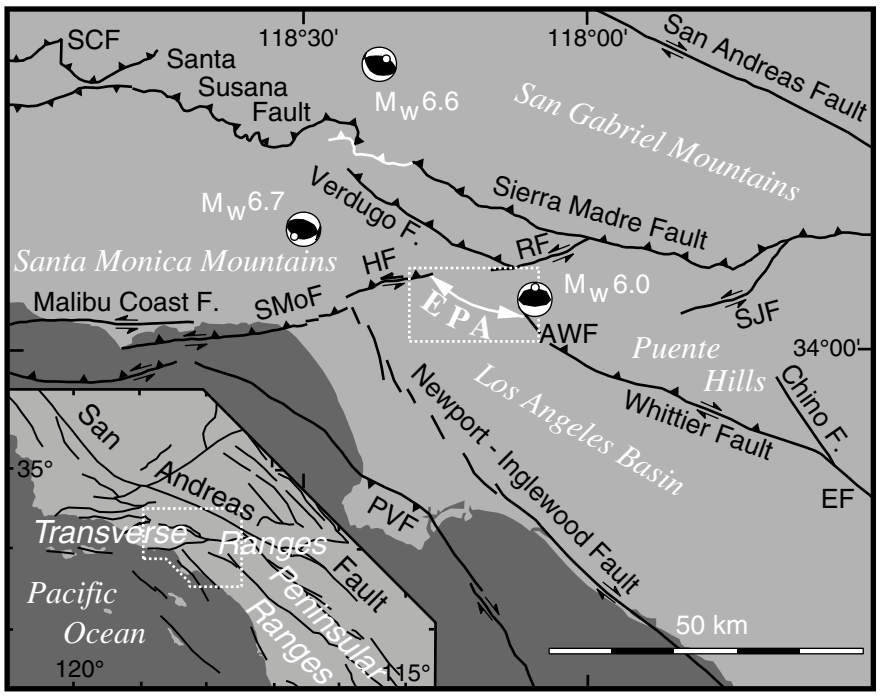

Figure 9.1. Index maps of principal active faults in the Los Angeles area. The Elysian Park anticline (EPA) is at the northern margin of the Los Angeles basin, at the juncture of northwest-trending, right-lateral strike-slip faults of the Peninsular Ranges and east-west trending, left-lateral, and reverse faults of the Transverse Ranges. Slip on a southwest-vergent, blind reverse fault is inferred to be forming the Elysian Park anticline. The surface trace of the reverse fault that produced the M_w 6.6 1971 San Fernando earthquake is shown as a white barbed line. The small white dots on each focal mechanism (lower hemisphere projection) indicate the slip vector. The white box in the center of the figure marks the corresponding coverage of the shaded relief map (Fig. 9.2) and geologic map (Fig. 9.3) of the Elysian Park anticline. AWF, Alhambra Wash fault; EF, Elsinore fault; HF, Hollywood fault; PVF, Palos Verdes fault; RF, Raymond fault; SCF, San Cayetano fault; SJF, San Jose fault; SMoF, Santa Monica fault.

amine parasitic folding. We complement this surficial data with a series of borehole transects across critical geomorphic features. These transects allow a more robust interpretation of the formation, correlation, and deformation of terrace surfaces. Our findings indicate higher rates of uplift, from 0.3 to 0.9 mm/yr for individual, parasitic folds. We also find that active parasitic folding is common to the entire, 20-kilometer length of the forelimb of the Elysian Park anticline. We propose that these parasitic folds manifest the majority of contraction from steepening of the forelimb of the active, primary (Elysian Park) anticline. To measure the contraction rate of the primary anticline, we sum the contractile components of deformation of these parasitic folds. Finally, we use this measure, in combination with the a spectrum of possible structural cross sections through the Elysian Park anticline, to estimate the seismic hazard posed by the blind Elysian Park fault.

9.3 Geologic setting

9.3.1 Regional framework

The Elysian Park anticline forms a segment of the southern boundary of the Transverse Ranges (Fig. 9.1). This boundary is contractional, due to transpressive motion of the Peninsular Ranges block against a wide restraining-bend in the San Andreas fault. The Los Angeles basin lies at the northwestern margin of the Peninsular Ranges block, and is overridden on the north and northeast by a set of contractile structures [*Wright*, 1991; *Schneider et al.*, 1996; *Shaw and Suppe*, 1996]. Within this convergent boundary, the Elysian Park anticline is a transitional structure that forms a kinematic link between the left-lateral-oblique uplift and extrusion of the Santa Monica Mountains [*Hoots*, 1930; *Dolan et al.*, 1997; *Walls et al.*, 1998] and the right-lateral-oblique uplift of the Puente Hills [*Yerkes et al.*, 1965]. The Elysian Park anticline lacks a surficially exposed frontal fault system. Rather, contraction is evident at the surface as fold growth.

9.3.2 Structure and physiography

The Elysian Park anticline forms a distinct structural and physiographic domain, within which there is a close association of topographic relief and fold structure (Fig. 9.2). Folded strata of the Elysian Park anticline are exposed in the Elysian and Repetto Hills, directly north and east of downtown Los Angeles. These hills are characterized by low elevations, (100–300 m) and low relief, (100–200 m) and are cut by a series of channels that trend across the anticlinal axis. The interfluves are generally steep-sloped parallel ridges between narrow canyons. This morphology contrasts with the southwest flank of the Elysian-Repetto Hills, where interfluves form an extensive set of low-relief fluvial terraces. Youthful, parasitic fold growth deforms these terraces into a series of east-trending topographic swells.

The Elysian Park anticline is structurally and physiographically separate from adjacent structural and geomorphic domains (Fig. 9.2). The axis terminates at both ends against surficially expressed, strike-slip and oblique-slip faults that cut Quaternary alluvium (Fig. 9.3). The Alhambra Wash fault separates the southeastern end of the Repetto Hills from the Whittier Narrows, a topographic and structural low point, where drainage from the north is constricted [*Davis et al.*, 1989]. The Hollywood fault separates the northern end of the Elysian Hills from the Santa Monica Mountains [*Hoots*, 1930; *Dibblee*, 1991]. The exposed Mesozoic basement rocks of the eastern Santa Monica Mountains form a higher-elevation (200 to 600 m), higher-relief domain that is physiographically distinct from the Elysian Hills. The northern limb of the Elysian Park anticline terminates against the Raymond fault, an active left-lateral structure [*Lamar*, 1970; *Jones et al.*, 1990]. The trace of the Raymond fault forms a distinct escarpment northeast of the Elysian Park anticline (Fig. 9.2). A series of east-west trending valleys connect the Raymond fault trend with the active trace of the Hollywood fault (Figs. 9.2 and 9.3). However, geomorphic indicators of Holocene faulting are absent along this trend [*Dolan et al.*, 1997]. The broad arc of the southern limb of the Elysian Park anticline terminates at a syncline, which

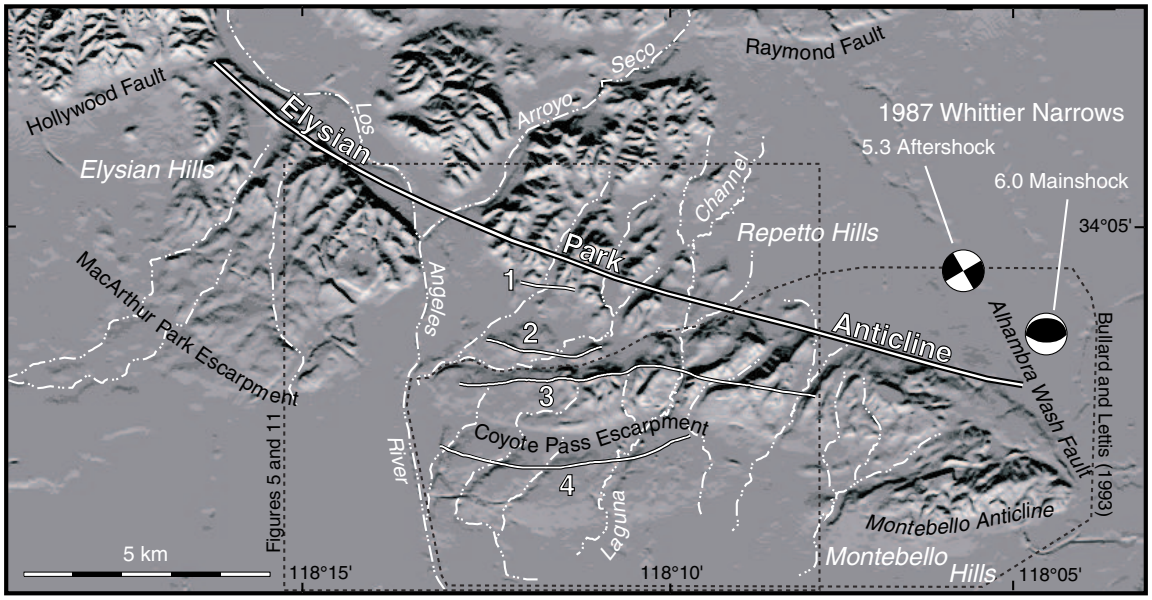

Figure 9.2. Shaded relief map of the Elysian Park anticline shows the relationship of topography to folding. Topographic relief correlates with the areal extent of the anticline and with the trends of parasitic secondary folds. Parasitic fold axes are depicted by thin white lines numbered 1 through 4. The Elysian Park anticlinal axis is delineated by the thicker white line. Drainages crossing all or part of the Elysian Park anticline are shown as white dash-dot lines. The box at the center of the figure surrounds the area of downtown and east Los Angeles detailed in Figs. 9.6 and 9.11. The irregular-shaped box at the lower right surrounds the area studied by *Bullard and Lettis* [1993]. This image is derived from 30m-pixel U.S.G.S. digital elevation models for the Hollywood, Los Angeles, and El Monte 7.5-minute quadrangles.

separates the Elysian Park anticline from the northern shelf of the Los Angeles basin [*Dibblee*, 1989; *Wright*, 1991]. The synclinal axis and the northern shelf are covered by alluvium, except at the extreme eastern end of the Elysian Park anticline. There, the syncline is more tightly constricted by the folding of the Montebello anticline, a northward-vergent fold formed within the northern shelf that is distinct from the Elysian Park anticline [*Quarles*, 1941; *Davis et al.*, 1989].

The structure of the Elysian-Repetto Hills is a double-plunging, south-vergent anticline, with numerous second-order parasitic folds and flexures (Fig. 9.3). Southward vergence is indicated by higher structural relief north of the fold axis and northward concavity of the axial trace. Structural relief of the Elysian Park anticline attains a maximum of 2.8 km at the center of the anticline, near the confluence of the Los Angeles River and the Arroyo Seco, and diminishes to less than 0.5 km near the Alhambra Wash fault [*Davis et al.*, 1989]. The southern limb, or forelimb, of the Elysian Park anticline is made up of several parasitic, south-vergent folds. These structures trend parallel to bedding planes, so the secondary fold axes converge eastward toward the plunging primary hinge.

9.3.3 Stratigraphic and structural history

The Neogene histories of the Elysian Park anticline and the Los Angeles basin are closely related. Marine strata exposed within the Elysian-Repetto Hills correlate with a thicker section within the Los Angeles basin [*Blake*, 1991]. Preceding contraction, the area of the Los Angeles central trough and the area later to become the Elysian Park anticline both formed as adjacent depocenters in a transtensional setting [*Wright*, 1991]. Strata of the Puente Formation, which antedate folding, thicken northward, toward the Elysian Park anticlinal axis (Fig. 9.4). Beginning in the earliest Pliocene Epoch, syn-tectonic thickening of Fernando Formation and younger strata record the rapid subsidence and filling of the Los Angeles central trough [*Schneider et al.*, 1996]. At the same time, structural inversion of the Elysian Park depocenter and formation of the Elysian Park anticline is recorded as a series

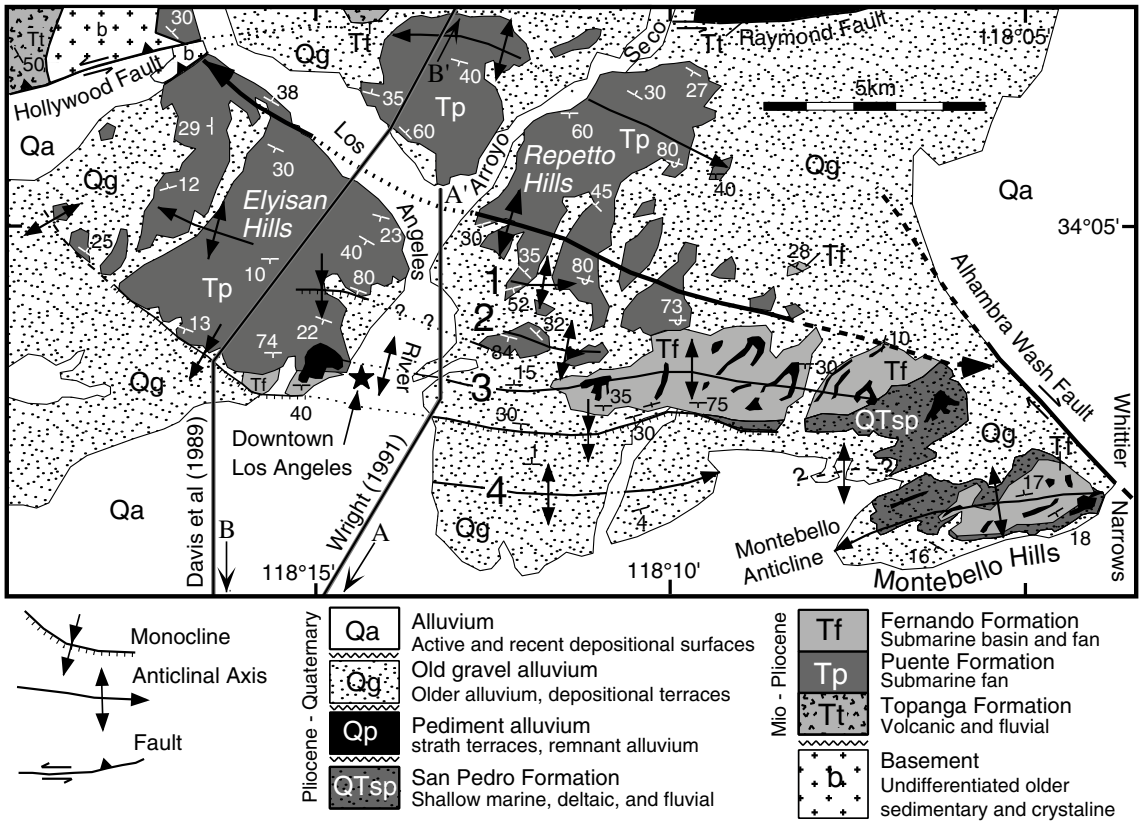

Figure 9.3. Geologic map of the Elysian Park anticline. The anticlinal axis and major bounding structures are depicted by thick black lines. Thinnest black lines represent trends of secondary folds. East-west trending, parasitic secondary anticlines in east Los Angeles are numbered 1 through 4. The Coyote Pass escarpment forms the southern limb of Structure 3. Two generations of older alluvium, Qg and Qp, are differentiated at the crest of Structure 3, whereas Structure 4 is capped by only Qg deposits. Compiled from *Bullard and Lettis* [1993], *Dibblee* [1989], *Dibblee* [1991], *Lamar* [1970], *Thomas et al.* [1961], *Quarles* [1941], and *Soper and Grant* [1932].

of angular unconformities within Fernando Formation and younger strata [*Soper and Grant*, 1932].

Recent uplift of the Elysian Park anticline is recorded by a series of fluvial deposits mantling the southeastern Elysian-Repetto Hills [*Bullard and Lettis*, 1993]. These deposits are formed of coarse, crystalline detritus, derived primarily from basement exposures within the San Gabriel Mountains (Fig. 9.1). We recognize three mappable allostratigraphic fluvial units in the Elysian-Repetto Hills: Qp, Qg, and Qa (Fig. 9.3). These units are differentiated on the basis of bounding unconformities that are recognizable throughout the study area. The oldest generation, Qp, forms isolated remnants of alluvium and, more commonly, basal strath surfaces that mantle the crest of the Elysian-Repetto Hills. The intermediate generation, Qg, consists of an extensive alluvial fill inset into the larger drainages of the Elysian-Repetto Hills and forming a pair of broad platforms east and west of downtown Los Angeles. The youngest generation, Qa, consists of youthful, low-relief terrace treads, and pre-urbanization stream beds and flood plains. Units Qp, Qg, and Qa correspond to the units Qp, Qg/Q1-Q2-Q3, and Q4-Q5, respectively, as mapped by *Bullard and Lettis* [1993].

9.3.4 Parasitic folding of the forelimb

Our study explores, in detail, parasitic folding of the forelimb of the Elysian Park anticline through downtown and east Los Angeles. In this area, a series of four, parallel, east-west trending parasitic anticlines deform both the Tertiary marine section and an extensive cover of Qp and Qg material. For clarity, we refer to these anticlines simply as Structures 1 through 4. However, most of these folds were given other names by previous workers: Structure 2, Boston Heights anticline [*Thomas et al.*, 1961]; Structure 3 (forelimb only), Coyote Pass escarpment [*Thomas et al.*, 1961]; Structure 4, Boyle Heights anticline [*Wissler*, 1943].

The degree of development of parasitic folds within the Tertiary marine units decreases systematically southwards from the Elysian Park anticline axis (Figs. 9.3

and 9.4). Structures 1 and 2, which lie closest to the axis of the Elysian Park anticline, appear as asymmetric folds in Tertiary sediments. Bedding attitudes of Tertiary marine strata underlying Structures 3 and 4 are shallower and deviate only slightly from the southward dips of the south limb of the Elysian Park anticline.

In contrast to the southward-diminishing expression of parasitic folding in the bedrock, topographic expression of late Quaternary parasitic fold growth increases southward, away from the Elysian Park anticline axis (Fig. 9.2). Structure 1 is not covered by Quaternary deposits and has no clear topographic expression. Structures 2, 3, and 4 each correspond with the topographically expressed highs of uplifted Qp and Qg deposits. Isolated and dissected remains of Qp deposits form the crests of Structures 2 and 3. A continuous extent of Qg deposits, capped by smooth, original depositional surfaces, form a set of fluvial terraces that are folded by Structures 3 and 4.

9.4 Methods of investigation

9.4.1 Mapping of geomorphic surfaces

To study the late Quaternary record of folding in downtown and east Los Angeles, we constructed a geomorphic map of Qp, Qg, and Qa fluvial deposits. Much of the geomorphic record is interpreted from a detailed topographic map, with 1.5- and 7.6-m (5- and 25-ft) contours. This contour map was digitized from archival, U.S.G.S. 6-minute, 1:24,000-scale, topographic quadrangles surveyed in the 1920's and published in the early 1930's (Fig. 9.5). Care was taken to investigate and remove anthropogenic features, such as roadcuts, from the geomorphic interpretation.

Using topographic and elevational continuity, we mapped the extent of preserved geomorphic surfaces of Qg and Qa. Breaks in slope, indicative of incision or deposition of a younger unit constrain the extent of surfaces. Due to greater relief and age, the Qp depositional surface is generally not preserved. Therefore, we mapped the strath

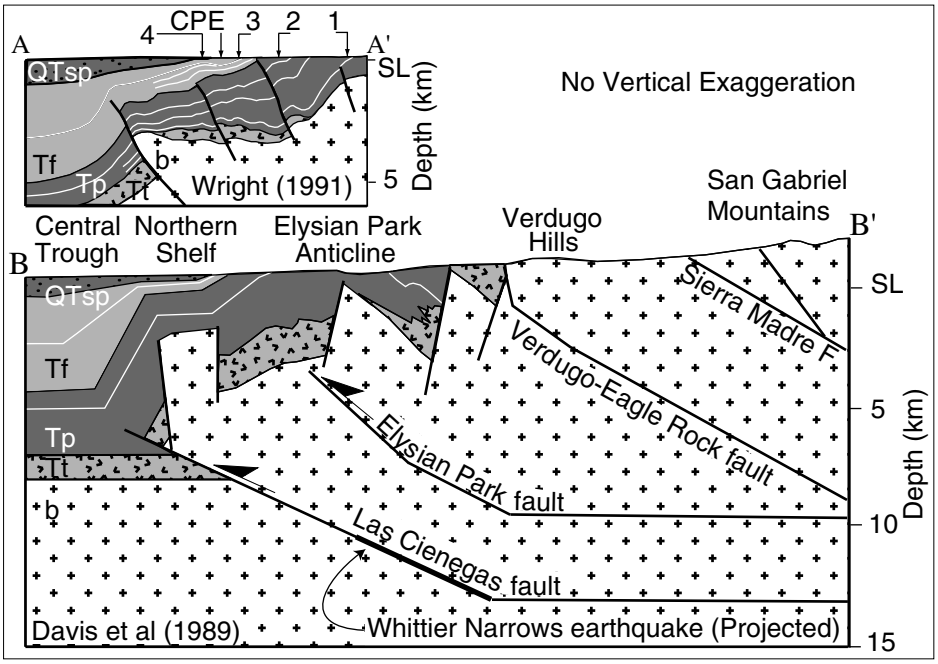

Figure 9.4. Cross sections through the northern Los Angeles basin and the Elysian Park anticline, adapted from *Wright* [1991] and *Davis et al.* [1989]. The Elysian Park anticline appears as a basement-involved fold in both sections. A blind-thrust-fault solution to folding of the Elysian Park anticline is presented in the generalized cross section B-B'. Parasitic folds and minor reverse faults on the southern limb of the Elysian Park anticline are depicted in greater detail by cross section A-A'. The locations of the Coyote Pass escarpment and the crests of Structures 1 through 4 are shown at the surface. Structures 1, 2, and 4 are correlated with steeply-dipping reverse faults and kinematically-related folds. Structure 3 occupies a position above a uniformly-dipping section bounded by Structure 2 and the Coyote Pass escarpment. Lithologic units are the same as in Figure 3. Units Qp, Qg and Qa are unable to be shown at this scale. Note that the assignment of the names, 'Elysian Park fault' and 'Las Cienegas fault' differs from *Davis et al.* [1989]. This was changed to reflect the kinematic relationship of blind thrusts to named surface fold structures. The Whittier Narrows earthquake rupture is projected along the Las Cienegas fault from 15 km east of cross section line.

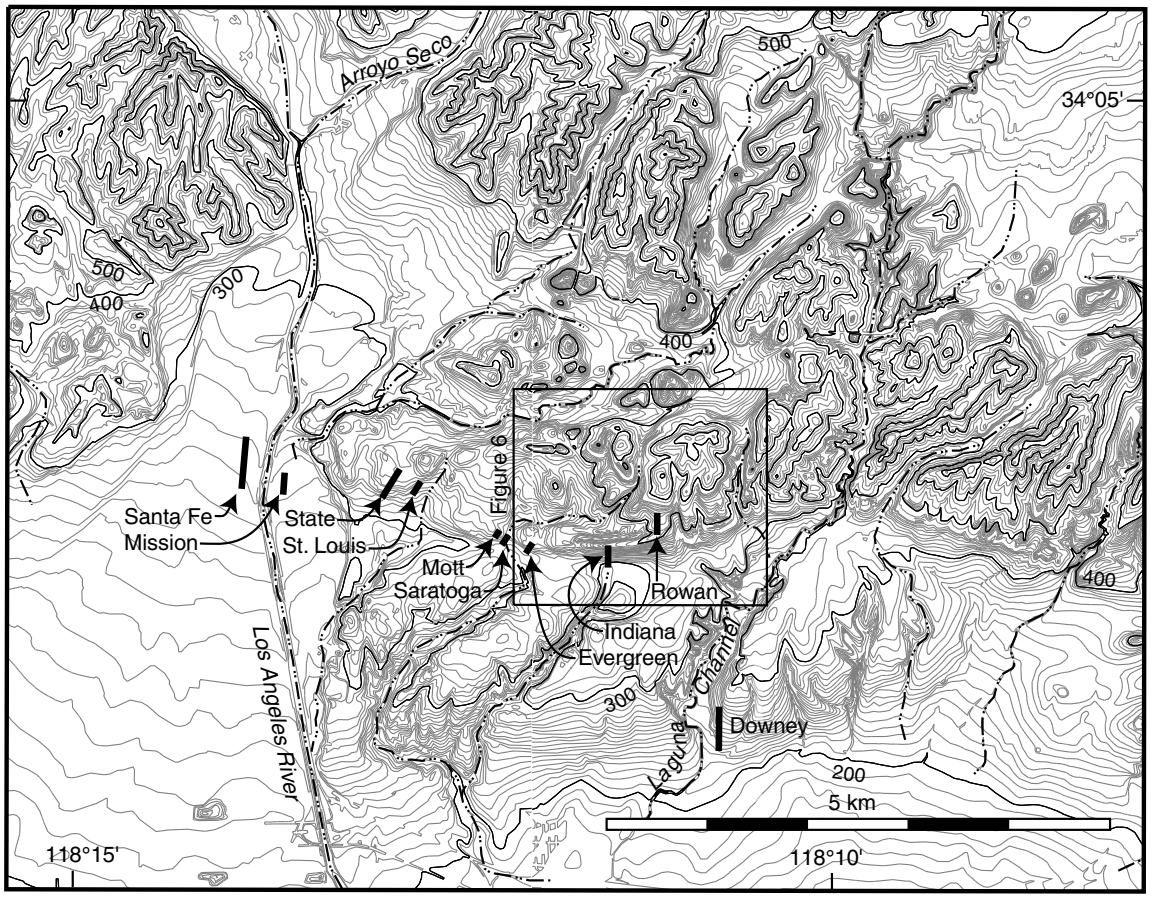

Figure 9.5. Topographic contour map of downtown and east Los Angeles, digitized from the 1926 Alhambra and 1928 Los Angeles 1:24,000 scale 6-minute quadrangles. Contour interval is 5 ft (1.5 m) up to 500 ft, and 25 ft (7.6 m) thereafter. Index contours at 100 ft (30 m) intervals denoted by heavy lines. Some very closely-spaced 5ft contours were discarded during digitization. The locations of nine borehole transects utilized in this study are shown [*GeoTransit Consultants*, 1996; *Law/Crandall*, 1997]. The Rowan, Evergreen, and Santa Fe transects are republished in this paper as Figs. 9.7, 9.9, and 9.10, respectively. Also, a trench investigation at Indiana Avenue *GeoTransit Consultants* [1996] is republished in this study as Fig. 9.8.

surface or contact at the base of Qp. Our mapping of Qp differs only slightly from *Bullard and Lettis* [1993], but our interpretation of the Qg and Qa terraces differs significantly from these previous workers.

The surface of Qg is divided into two members. The primary member, Qg1, forms the culmination of aggradation of the Qg deposit. Qg1 terraces are preserved throughout the study area. *Bullard and Lettis* [1993] mapped Qg1 as two separate surfaces, Qg/Q1 and Q2. Shallow subsurface investigations, detailed below, show that these form a single, deformed terrace. A second member, Qg2, forms a series of slightly younger terraces that closely follow the elevation of Qg1. The position of Qg2 relative to Qg1 varies locally, and Qg2 terraces can be traced locally from inset ($Qg2_i$) cut-and-fill deposits to superposed ($Qg2_f$) alluvial fans. Qg2 is roughly equivalent to Q3 of *Bullard and Lettis* [1993].

Similar to the surface of Qg, the surface of Qa is also divided into two members. Qa1 terraces formed where the culminating level of aggradation of unit Qa has been slightly incised. Where preserved, these terraces form low-relief risers that parallel the modern alluvial gradient. Qa1 is equivalent to Q4 and Q5 of *Bullard and Lettis* [1993]. The modern (pre-urbanization) stream beds form the youngest Qa surface. We have not mapped these surfaces in detail. However, we do map the thalwegs of significant stream channels.

9.4.2 Field investigation

To verify the topographic interpretation, shallow-subsurface field investigations were undertaken to evaluate critical geomorphic features. These investigations, which supplement the limited available outcrops, were crucial to our geomorphic interpretation. A total of nine continuous-core borehole transects, totaling over 130 separate cores, were undertaken as part of the seismic hazard study for the eastside extension of the Los Angeles subway [*GeoTransit Consultants*, 1994, 1996; *Law/Crandall*, 1997]. A selection of these transects, as well as a trench investigation, are republished in this paper to illustrate several important relationships between fluvial sedimentation,

folding, and our geomorphic interpretation (Figs 9.5 through 9.10).

Soil characteristics were not employed in our study to differentiate geomorphic surfaces. *Bullard and Lettis* [1993] used the maximum reddening of the soil horizon to help differentiate the various terrace members. Their published soil characteristics vary significantly between the major allostratigraphic units, Qa, Qg, and Qp. These units, however, are also recognizable from their topographic position and bounding unconformities. In contrast, Bullard and Lettis' total profile descriptions of the individual terrace members of Qg (Qg/Q1, Q2, Q3), including the color, thickness, and soil structure, are nearly equivalent. Thus, soil characteristics are not useful in differentiating these surfaces. We find that geomorphic interpretation, with the aid of shallow-subsurface field investigation, provides a more robust method to differentiate between the various allostratigraphic units and geomorphic surfaces.

9.5 Results

9.5.1 A geomorphically expressed active fold: Structure 3 in City Terrace

The City Terrace area of east Los Angeles illustrates our use of topography and shallow subsurface cross sections to constrain the distribution of Qg terrace remnants, and thus to interpret the timing of formation, abandonment, and folding of Qg deposits (Fig. 9.6). City Terrace is a topographic high that straddles the crest of Structure 3. The crest of City Terrace is capped by a Qp strath surface which cuts across moderately south-dipping Fernando Formation (Fig. 9.3). Cut into this high is a paleo-channel of Qg age. Currently, this abandoned channel forms a wind gap, and drainage from the north is diverted westward, between Structures 2 and 3 (Figs, 9.2, 9.5 and 9.6). A series of Qg1 terraces cap Qg deposits that fill the paleo-channel. These terraces are concordant with a Qg1 alluvial surface nested against the south flank of the hills. South of City Terrace, the Qg1 surface is deformed into a

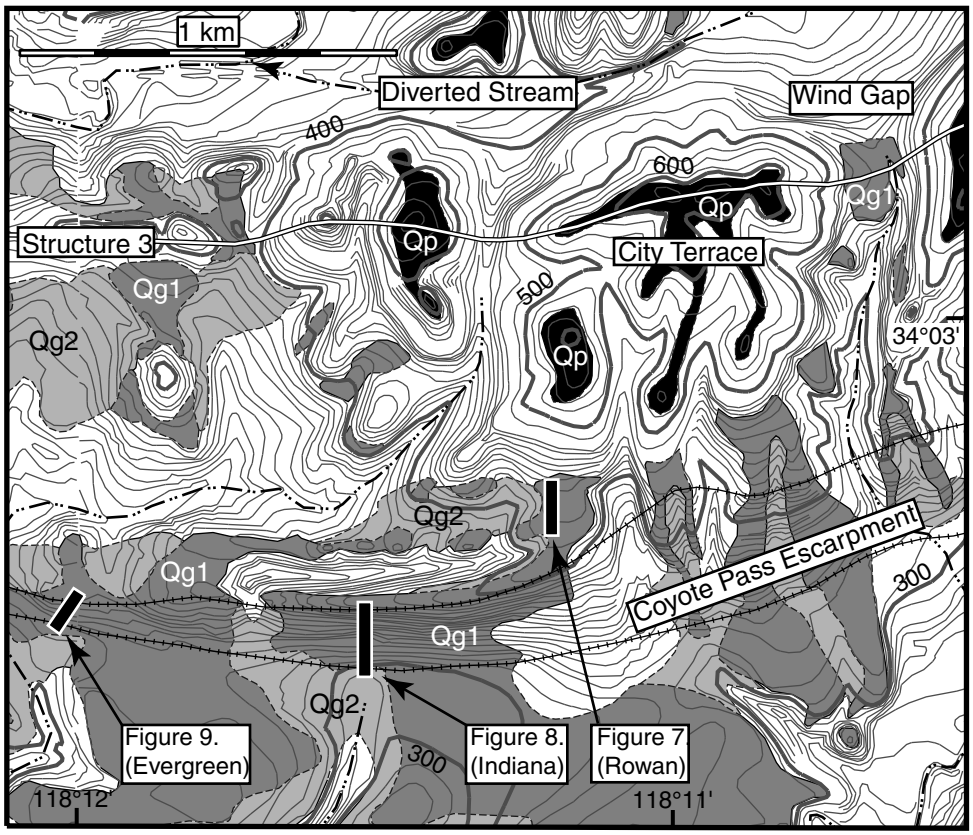

Figure 9.6. Topographic interpretation of the City Terrace area of east Los Angeles. Qp deposits cap the highest hills and Qg terraces are inset within the wind gap (upper right corner) and nested against the south and west flank of the hills. A borehole transect at Rowan Street (Fig. 9.7) illustrates an inset contact of Qg against a paleo-relief. A second borehole transect at Evergreen Avenue (Fig. 9.9) and a trench at Indiana Avenue (Figure 8) depict deformation of Qg deposits by the Coyote Pass monocline, which forms the Coyote Pass escarpment and the forelimb of Structure 3. Lithologic units same as Fig. 9.3.

monocline along the south limb of Structure 3, forming the Coyote Pass escarpment. Three shallow cross sections illustrate the depositional and deformational history of Qg deposits, and support our topographic correlation of the Qg1 remnants on either side of the escarpment.

The Rowan Street cross section (Fig. 9.7) depicts an abrupt, lateral lithologic change, between Qg deposits and adjacent strata of the Fernando Fm. This discontinuity, at the north end of the borehole transect, corresponds to south flank of the City Terrace topographic high (Fig. 9.6). The Qg section consists of a clean, coarse-grained, crystalline-source fluvial gravel deposit, capped by a 15 m-thick col-

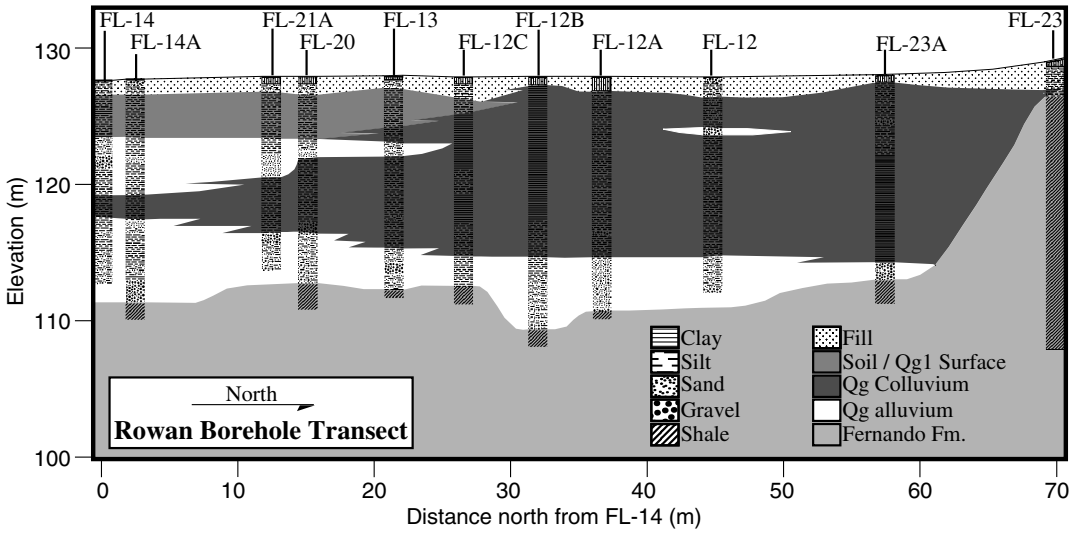

Figure 9.7. Rowan Street borehole transect illustrates an inset contact of Qg alluvial and colluvial deposits against steep paleo-relief. We interpret this contact as a collapsed paleo-channel wall. Borehole transect adapted from *GeoTransit Consultants* [1996].

luvial wedge of angular siltstone fragments. Based upon its extent and homogeneity, we interpret the colluvial deposit to represent rapid collapse of a steep paleo-channel wall, rather than an episodically eroded fault scarp.

From the geomorphic map (Fig. 9.6) and the Rowan Street borehole transect, we construct a history of Qg deposition for the City Terrace area. The paleo-channel wall beneath Rowan Street connects with the adjacent wind gap by a chain of nested Qg1 terrace remnants (Fig. 9.6). These remnants suggest that a southwest-flowing channel once emerged from the wind gap. This channel cut the paleo-cliff, and delivered the Qg gravel deposit at the base of the Rowan transect. Aggradation of up to 17 m of Qg deposits has partially filled this paleo-channel. The remaining, uncovered channel walls form the steeper topography surrounding the southern flank of City Terrace. Incision of Qg deposits has since renewed downcutting of the paleo-channel, leaving a paired string of topographically prominent Qg1 terraces.

A trench at Indiana Avenue (Fig. 9.8) illustrates the continuity of Qg deposits and the Qg1 surface across the Coyote Pass escarpment. The lowest level of the trench exposes alternating, discontinuous lenses of fine- and coarse-grained Qg alluvium.

Bedding dips in Qg are less than 3° at the base and crest of the fold limb, but steepen to as much as 26° mid-slope. Above the alluvium, a massive section of poorly sorted, fine-grained soil material with scattered gravel thickens towards the base of the escarpment. We interpret this wedge as a slope-wash colluvial deposit derived from higher up the escarpment. This wedge of colluvium, and a 5-10° discordance between the surface slope and steeper dipping strata in Qg, indicate a minor amount of erosion of the crest of the fold scarp, and redeposition at the base.

The Evergreen Avenue borehole transect depicts a series of fining-upward sequences of Qg alluvium draped across the Coyote Pass monocline. The laterally continuous graded beds, each capped by thin clay deposits, indicate an ephemeral, fluvial/lacustrine depositional environment. We define five beds, each consisting of a fining-upward set of strata. These beds are closely correlated between boreholes, based upon detailed characteristics of each fluvial/lacustrine sequence. Each are divided into a lower, fluvial package (white areas, Fig. 9.9), and grade up-section into a lacustrine package (gray areas, Fig. 9.9). The top of each package is defined by a correlated horizon, labeled C1, C2, etc., for lacustrine clay deposits and F1, F2, etc., for fluvial deposits. Generally, the abrupt transitions from lacustrine clay to coarser deposits form the most distinct and laterally continuous horizons, whereas the fluvial to lacustrine transitions are often gradational and sometimes discontinuous.

The Evergreen Avenue transect also demonstrates the continuity of Qg deposits across the Coyote Pass escarpment. No fault zones, nor fault repetition of stratigraphy, appear in any of the continuous cores. Uniform dip of these sequences between several very closely spaced boreholes precludes the existence of faults with significant offset hidden in the section. Thus, at least in the shallow subsurface, the Coyote Pass escarpment is formed by a tight, southward-vergent monocline, and the geomorphic surfaces on either side of the monocline are correlative.

As at Indiana Avenue, a wedge of massive, poorly-sorted material occupies the base of the monocline at Evergreen Avenue. We again interpret this material as colluvium that has eroded from the crest of the escarpment and been redeposited as

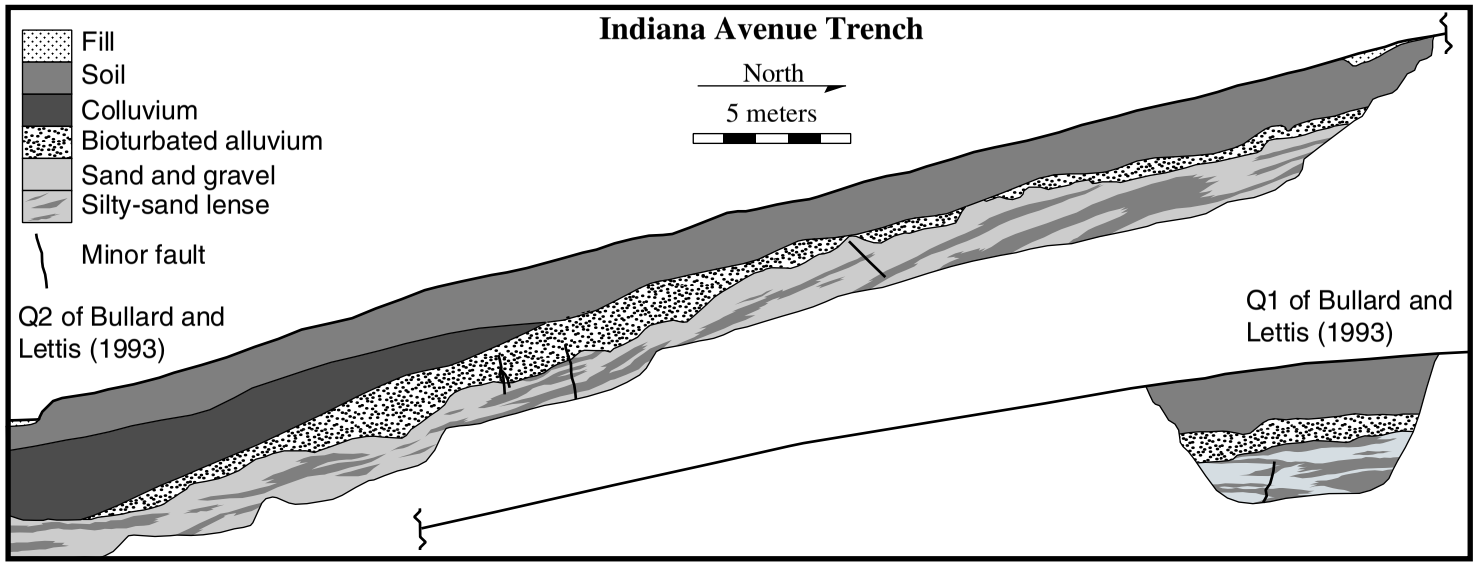

Figure 9.8. Map of the west wall of a trench cut into the Coyote Pass escarpment at Indiana Avenue shows that the structure is a monocline. The lower section is a continuation from the upper left corner. The lowermost unit of the trench depicts Qg deposits folded by the Coyote Pass monocline. Note that the fluvial beds are nearly parallel to the ground surface. Trench log adapted from *GeoTransit Consultants* [1996].

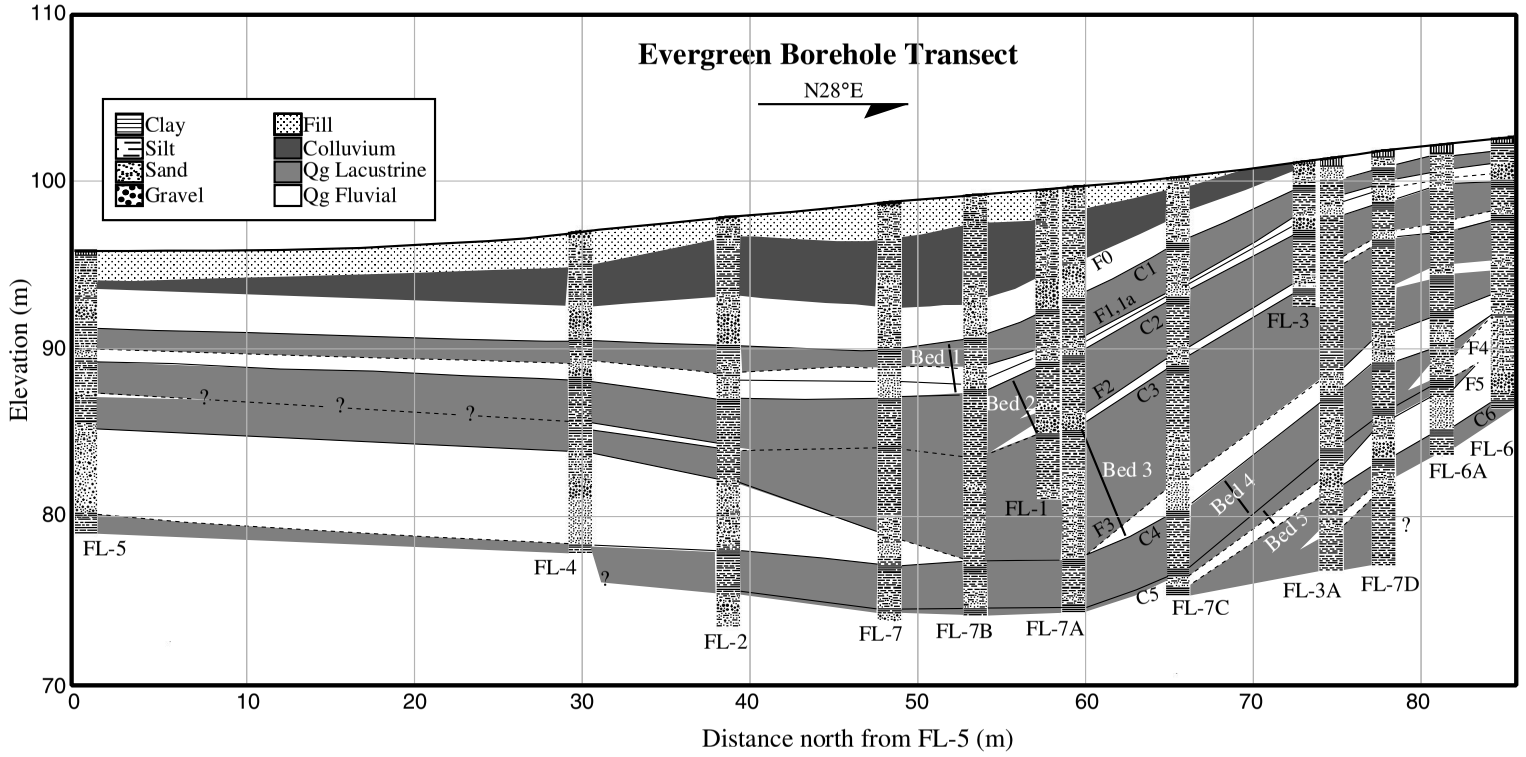

Figure 9.9. Evergreen Avenue borehole transect shows a sequence of lacustrine and fluvial Qg deposits folded across the Coyote Pass monocline. The thickness of fluvial/lacustrine deposits form the basis of correlations. These deposits show a repeated and distinct pattern of fining-upward packages. Secondary characteristics, especially the presence and grain size of fluvial deposits, as well as occasional smaller, distinctly colored or textured beds, provide secondary ties between boreholes. Horizons labeled C1, C2, C3, etc., represent the top of lacustrine layers, and horizons labeled F0, F1, F2, etc., represent fluvial to lacustrine transitions. Borehole transect adapted from *GeoTransit Consultants* [1996].

a colluvial wedge at the base. In both cross sections, the pronounced fold depicted at depth corresponds to a subdued topographic rise. Also, due to redistribution of sediment by erosion, the topographic expression of the south-facing fold limb is wider than the actual structure. However, we find that the topographic escarpment sufficiently represents the location and amplitude of the folded Qg1 surface.

9.5.2 A buried active fold: Structure 3 beneath the Los Angeles River

Beneath the broad floodplain of the Los Angeles River (Figs. 9.2 and 9.5) is an unconformable contact between alluvium and underlying marine strata [*Sieh*, 1997; *Law/Crandall*, 1997]. The Santa Fe Avenue borehole transect (Fig. 9.10) shows that this contact, and the overlying fluvial stratigraphy, form an asymmetric fold, with a shallow-dipping (0–2.5°) north limb and a moderate-dipping (up to 22°) south limb. The trend of this buried feature is perpendicular to the channel of the Los Angeles River, and aligned with Structure 3. At the crest of the fold, a 20 m-thick section of Qa is present above the unconformity cut on to marine strata. South of the crest, the unconformity steepens, and an older, Qg deposit may be preserved within the fluvial section. A cobble-rich horizon, dipping 1 to 3° southward from the crest of Structure 3, probably represents the base of the Qa deposit. Since the top of the Qa deposit is the historic floodplain of the Los Angeles River, surficial evidence of recent folding has probably been completely removed or buried.

9.5.3 Geomorphic surface map of downtown and east Los Angeles

The geomorphic map of downtown and east Los Angeles (Fig. 9.11) reflects many of the features visible in the shaded relief image (Fig. 9.2). The distribution of Qg, as depicted through geomorphic surfaces Qg1, and Qg2, corresponds to the areas of smooth, uplifted, flat topography, whereas the older Qp deposits are restricted to

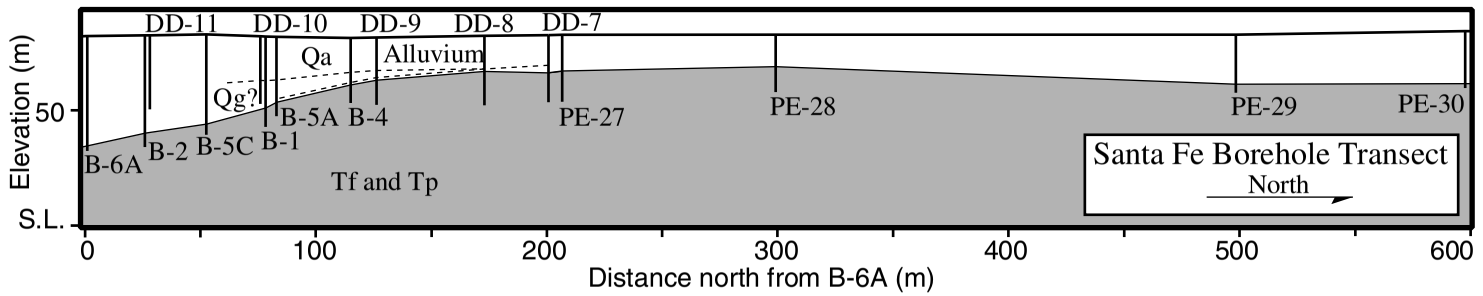

Figure 9.10. Santa Fe Avenue borehole transect across the westward projection of Structure 3, showing buried structural relief on the unconformity between Quaternary alluvium and Tertiary marine formations. Near the crest of the anticline, between boreholes DD–10 and DD–8, two contacts of cobble beds resting upon silty sand are denoted as thin dashed lines. Differential tilting of these horizons is attributed to growth of Structure 3 beneath the course of the Los Angeles River. Borehole transect adapted from *GeoTransit Consultants* [1996] and *Law/Crandall* [1997]. Lithologic units same as Fig. 9.3.

remnants that cap areas of higher elevation and relief. The pair of linear topographic inflections on the south limb of Structure 3 correspond to the escarpment formed by the Coyote Pass monocline. A discontinuity in the escarpment 1.5 km east of the Los Angeles River accommodates a change in near-surface structural style of the monocline, evident as a change in slope on Figure 9.5 [*Sieh*, 1998]. East of this discontinuity, the monocline forms a narrow flexure. To the west, the escarpment reflects a broader monocline that continues beneath Qa alluvial fill of the Los Angeles River (Fig. 9.10)[*Sieh*, 1997]. West of the river, this monocline reappears at the surface as the MacArthur Park escarpment.

Originally, both the Coyote Pass and MacArthur Park escarpments were interpreted to be faults, due to the abrupt topographic step and apparent stream deflections [*Thomas et al.*, 1961; *Dolan and Sieh*, 1994]. However, later investigations for the Los Angeles subway revealed that the Coyote Pass escarpment is actually a monocline [*GeoTransit Consultants*, 1996], which, in east Los Angeles, also forms the forelimb of Structure 3. Based upon the comparable surficial expression of the escarpments (Fig. 9.2), as well as the continuity of the folds beneath the floodplain of the Los Angeles River, we conclude that the combined MacArthur Park-Coyote Pass escarpment forms a 20-km-long fold that traverses most of the south limb of the Elysian Park anticline (Figs. 9.2 and 9.3).

9.5.4 Age of the Qg1 terrace

The age of the Qg1 terrace is constrained through radiometric and pedologic analyses. *Bullard and Lettis* [1993] published a U-Th age determination of 72±2 ka on a fossil bone collected at the Davidson Brick Quarry (from locality 'Q' in Figure 9.11), which they assigned to their geomorphic surface Q2. The U-Th age agrees with a second age determination of the Qg1 surface, which we obtained from analysis of soil development atop Qg deposits along Rowan Avenue (at locality 'R' in Figure 9.11). Two soil development indices were compared to other dated soil chronosequences in central and southern California [*Harden*, 1982; *Rockwell et al.*, 1985; *McFadden and*

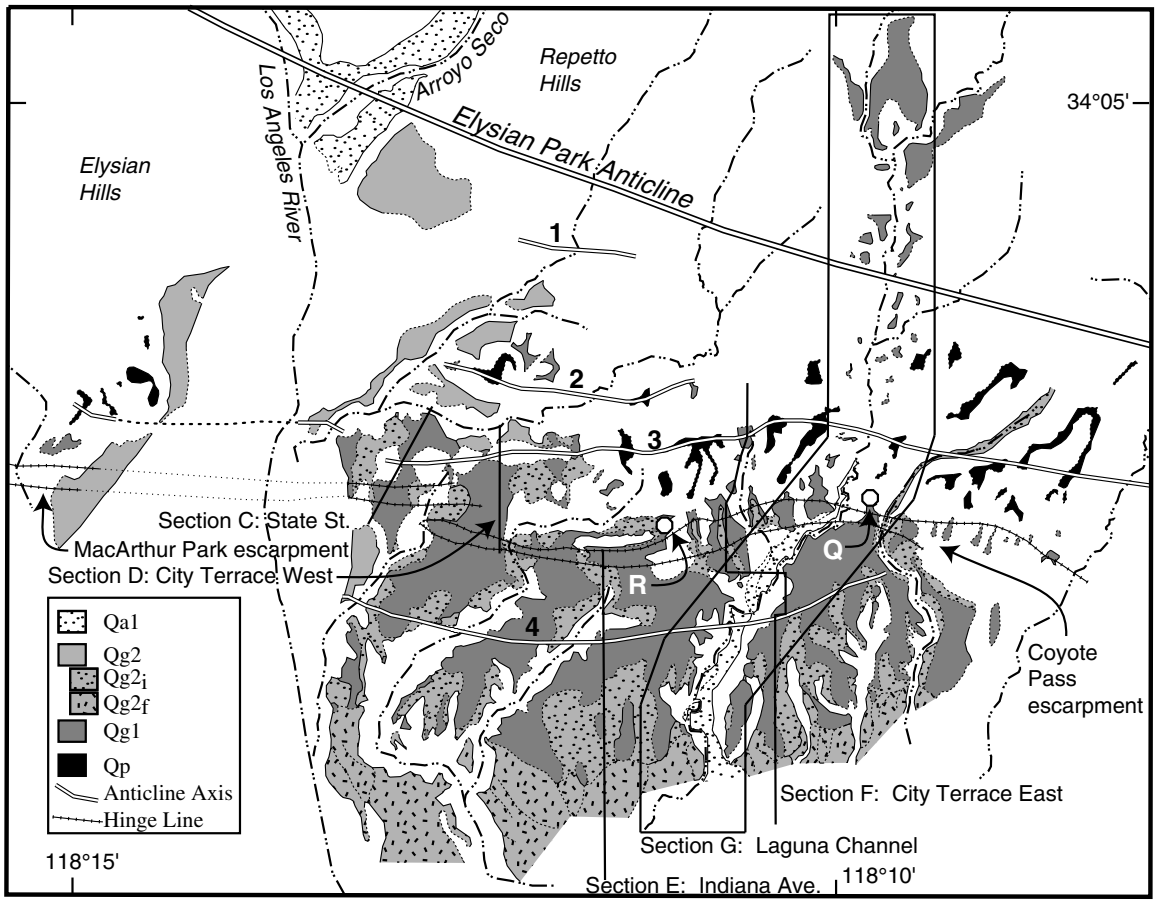

Figure 9.11. Geomorphic map of downtown and east Los Angeles, showing Qp deposits, and Qg and Qa surfaces. Axes of parasitic anticlines 2, 3, and 4 and the position of the Coyote Pass escarpment are interpreted from deformed surfaces. The locations of five topographic profiles of Qg surfaces are labeled C though G. Section G is a composite from terrace remnants within the strip surrounding Laguna Channel. Locations of samples that provide age estimates of the Qg1 surface: R., Rowan Street borehole transect; Q., Davidson Brick Quarry.

Weldon, 1987; *Rockwell et al.*, 1990, and Rockwell, unpublished data]. From comparison of the soil beneath Rowan Avenue with these chronosequences, we estimate soil development relative ages of 50–80 kyr and 50–70 kyr (See Tables E.1 and E.2 for soil description, index calculation and comparison). Based upon the soil development atop Qg, and the radiometric determination published by *Bullard and Lettis* [1993], we assign an abandonment age range of 50 to 74 ka to the Qg1 terrace.

9.5.5 Deformation rate of Qg terraces

To measure the spatial distribution and variability of uplift, and to calculate uplift rate, we use the geomorphic and topographic maps (Figs. 9.6 and 9.11) to construct five topographic cross sections of the folded Qg terraces and we subtract these profiles from a hypothetical undeformed alluvial gradient (Fig. 9.12). The cross sections depict several structural characteristics of Structures 3 and 4. Structure 4 is 2 to 2.5 km wide, approximately cylindrical, and exhibits uplift of the Qg1 surface in excess of 23 m, at an average rate of 0.3 to 0.5 mm/yr. Structure 3 is 1 to 1.5 km wide, asymmetric, and displays uplift of the Qg1 surface from 14 m near the Los Angeles River (cross section C) to 47 m at the Laguna Channel (cross section G). Uplift rate of Structure 3 must vary accordingly, from 0.2 to 0.3 mm/yr on the west, to 0.9 mm/yr on the east. The change in style of the Coyote Pass escarpment, described earlier, occurs between sections C and D, and is reflected in the narrower width of the southern flank of Structure 3 in sections D, E and G. Another change in the style of Structure 3 is expressed by the shape of the northern limbs between section F and G. This transition, from a nearly symmetric profile to a strongly asymmetric profile, corresponds to the eastward termination of the axis of Structure 2 between the converging axes of Structure 3 and the Elysian Park anticline (Figs. 9.2 and 9.3). We speculate that the eastward increase in uplift of Structure 3 near Laguna Channel may reflect the termination of Structure 2 and transfer of contraction onto Structure 3.

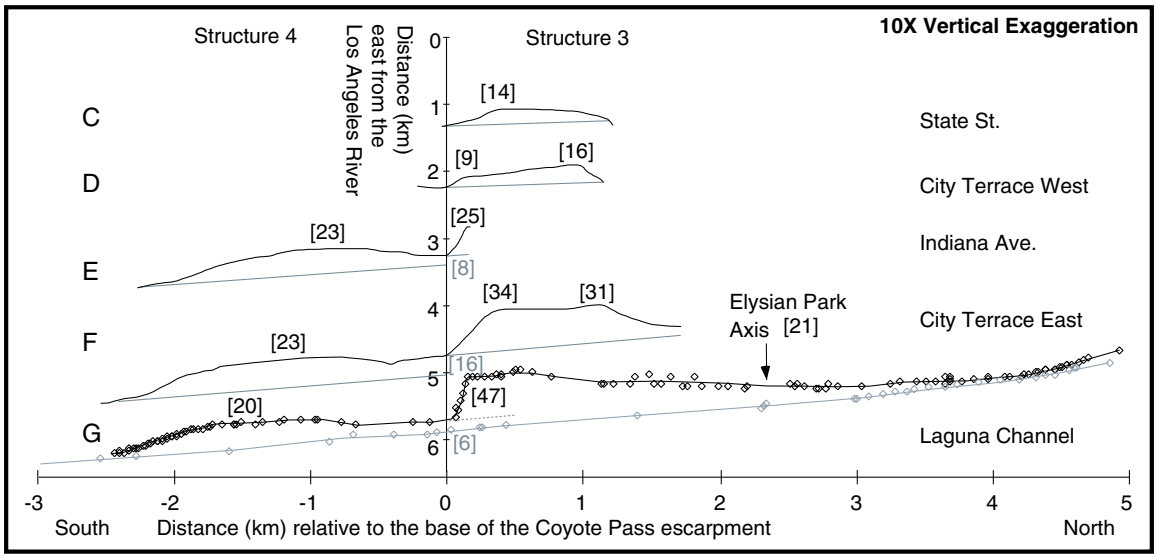

Figure 9.12. Topographic profiles of Qg surfaces through east Los Angeles. The vertical, central axis represents distance (in km) eastward along the trace of the lower hinge of the Coyote Pass escarpment from the Los Angeles River. Gray lines represent the modern stream gradient. The Los Angeles River gradient (0.004) is used for sections C and D, and the Laguna Channel gradient (0.009) is used for sections E and F. Section G is constructed from Qg1 terrace remnants on both sides of Laguna Channel, and compared directly with the modern stream elevation. Small diamonds indicate data points taken from the intersection of cross section lines and topogaphic contours. Dark numbers in brackets represent peak elevations of the Qg surfaces above the modern stream gradient. Gray numbers in brackets represent a net gain in elevation of the syncline between Structure 3 and Structure 4 at the Coyote Pass escarpment.

9.5.6 Large-magnitude cyclicity of base level of the Los Angeles River

Allostratigraphic units preserved in the Elysian-Repetto Hills indicate major changes in base level of the Los Angeles River system. The magnitude of aggradation over the crest of active folds requires a cyclic forcing of the fluvial system with the ability to far exceed tectonic base level uplift. For example, Structure 3 formed a positive topographic feature during aggradation of both Qg and Qa, as indicated by the preservation of uplifted Qg, and Qp deposits, respectively. Therefore, the uplift rate of Structure 3 exceeds the mean deposition rate of the Los Angeles River. Yet, up to 17 meters of Qg alluvium (Fig. 9.7) and 20 meters of Qa alluvium (Fig. 9.10) rest atop the crest of Structure 3. Clearly, short-term, periodic changes in the rate of aggradation, and similarly, rate of degradation of the river channel exceed the underlying tectonic uplift rate. Climate-induced changes in runoff and sediment load can greatly influence base level over short time scales [*Bull*, 1991]. The two most recent large-scale aggradation events preserved in east Los Angeles, Qa and Qg, probably represent climate-related base-level changes.

We speculate that these late Quaternary cycles may be regionally correlative. We tentatively correlate Qa and Qg with large-magnitude, climate-driven episodes of aggradation and terrace formation in the nearby Mojave Desert and Transverse Ranges, including the headwaters of the Los Angeles River. Inception of Qa deposition is probably contemporaneous with a period of regional aggradation and terrace formation that occurred approximately 7–14 ka, during the transition from late Pleistocene to Holocene climatic conditions [*Bull*, 1991]. We do not present any new numerical age data from Qa deposits. However, ages from deposits within the basal Gaspur aquifer beneath the Los Angeles Harbor range from 10 to 14 ka [*McNeilan et al.*, 1996]. This aquifer is restricted within a back-filled, incised channel of the Los Angeles River that correlates with Qa deposits in our study area [*Thomas et al.*, 1961]. The penultimate large aggradation event culminated with formation of thick,

extensive terrace deposits in the Transverse Ranges and the Mojave Desert of southern California about 50–60 ka [*Bull*, 1991; *Weldon*, 1986]. Qg aggradation in east Los Angeles appears to correlate with this regional event.

9.6 Discussion

9.6.1 Relationship of parasitic folding to the Elysian Park anticline

Based on the distribution and age of deformed late Quaternary fluvial deposits, we interpret that secondary folds on the southern limb of the Elysian Park anticline have been active over the past several tens of thousands of years. But how does their deformation relate to deformation of the Elysian Park anticline and slip on underlying Elysian Park Fault? In map view, Structures 1, 2, 3 and 4 are approximately parallel to the Elysian Park anticline, limited to its southern limb, and concave northeastward in map view. The growth of each parasitic fold contributes to the overall steepening and contraction of the larger forelimb. Thus, it appears that the folds we have mapped are secondary or parasitic folds, and that growth of these folds is directly associated to growth of the parent Elysian Park anticline.

The concentration of secondary contractile structures within the southern limb of the Elysian Park anticline may indicate whether the anticline is a fault-propagation fold or a fault-bend fold. Fault-bend anticlines occur where material is transported over a ramp-like step in a fault plane. These folds are characterized by structural relief that reflects the underlying ramp geometry [*Suppe*, 1983]. Fault-bend anticlines overlying thrust fault ramps consume only a small component of contraction, since fault slip is transferred, for the most part, from the lower flat through the fault ramp and onto the upper flat. Fault propagation folds, in contrast, consume the full component of fault slip by fold growth. The forelimb of a fold atop a blind thrust accommodates most of the horizontal component of shortening above the fault tip.

Contraction may be accommodated through a combination of asymmetric folding and penetrative shortening [*Suppe and Medwedeff*, 1990]. In east Los Angeles the steeply-dipping forelimbs of parasitic structures indicate that these are southward-vergent, fault-propagation folds (Figs. 9.3 and 9.9). The paralellism of the secondary fold axes with bedding strike on the southern limb of the Elysian Park anticline suggests that these parasitic folds are a mechanism to accommodate penetrative-style shortening, and therefore the Elysian Park anticline is also a southward-vergent, fault-propagation fold.

9.6.2 Relationship of folds to underlying blind thrust faults

Although most workers agree that active blind reverse faults exist beneath the Los Angeles urban region, opinions regarding the geometry of these faults vary widely. All interpretations are based principally on oil-well and seismic-reflection data. *Davis et al.* [1989] first proposed that slip on a stacked set of shallowly dipping thrust faults created fault-propagation folds (Fig. 9.4b). They ascribed the 1987 Whittier Narrows earthquake to rupture of a small section of the deepest of these structures (the Las Cienegas fault in Fig. 9.4b). *Shaw and Suppe* [1996] also endorsed shallowly dipping faults beneath the region, but concluded that the southernmost and deepest must extend southward across the basin as a flat thrust rather than terminate beneath the northern shelf. In their interpretation, the northern slope of the Central Trough is the limb of a fault-bend fold rather than a fault-propagation fold. *Schneider et al.* [1996] interpret the folded northern margin of the Central Trough to be a monoclinal flexure above a steeply dipping, southward-propagating reverse fault, which they have termed the "Los Angeles" fault.

Our data do not allow us to discriminate between these models of the major active faults, nor do they allow us to create a wholly new model. However, we are able to place additional constraints on the nature of at least one of these structures. The active folds that we have characterized lie above the tip of the Elysian Park fault, a blind thrust (originally named fault 'D') that *Davis et al.* [1989] proposed

to exist above the source of the Whittier Narrows earthquake (Fig. 9.4b). It is reasonable, then, to conclude that these secondary folds are being produced in response to reverse slip on the Elysian Park fault. In the following sections, we calculate the rate of folding across the secondary folds and attempt to extrapolate this rate to the Elysian Park fault. These calculations are necessarily speculative, but do allow for meaningful comparison of the seismic hazard of the Elysian Park fault with respect to analogous structures, and incorporation of the Elysian Park fault into regional hazard assessments [*Walls et al.*, 1998, for example].

9.6.3 Rigid-body rotation versus parasitic folding

To demonstrate that parasitic folds absorb the majority of the contraction of the forelimb of the Elysian Park anticline, we calculate the contractile component that would result if the entire forelimb tilted as a rigid body. Although as much as 53 m of uplift of the Qg1 surface is inferred from Figure 9.12, only 21 m of uplift is observed at the Elysian Park axis. To remove any higher-frequency effects from parasitic folds, we use the maximum uplift value. Only 0.6° of rotation of the 5km-length forelimb is necessary to produce 53 m of uplift. This same rotation value produces negligible (less than 1 m) north-south contraction. Hence, rigid-body rotation of the Qg1 surface contributes a negligible shortening, and therefore the contractile component of folding is reflected almost entirely by parasitic deformation.

9.6.4 Kinematic analysis of the Evergreen Avenue borehole transect

In this section, we focus our analysis on the Evergreen borehole transect across the Coyote Pass monocline, where we directly measure both the horizontal and vertical components of deformation of the forelimb of parasitic Structure 3. By generalizing the insights gained from this analysis, we use the deformed Qg1 terrace to estimate the summed contraction rate across the active parasitic folds on the forelimb of the

Elysian Park anticline.

The fluvial/lacustrine section beneath Evergreen Avenue (Fig. 9.9) provides a detailed set of correlations that traverse the Coyote Pass monocline. We carefully analyzed the thickness and length of the upper three fluvial/lacustrine beds in the Evergreen borehole transect to constrain the vector of deformation (Fig. 9.13). This vector represents the motion of the upper limb relative to the lower limb of the monocline, which is equivalent to motion of the crest of Structure 3 relative to the syncline between Structures 3 and 4. We present a summary of the results below and a complete description of the measurement technique in the accompanying data depository (Tables E.3 through E.11). For these analyses, we assume that the beds were originally horizontal and that deposition rate exceeded the uplift rate, such that folding was completely covered by concurrent deposition, and little or no fold-scarp-derived colluvium formed. Since each fluvial/lacustrine bed traverses the crest of the fold, these assumptions are reasonable. Also, since the geotechnical samples of these beds did not detect a systematic lateral change in porosity, we assume that differential compaction and shear-induced expansion are negligible.

To compute syndepositional uplift for bedding below the C1 level, we compare the differential thickness of bedding at the crest and base of the monocline between two pin lines (DV, Figure 9.13a). Continuously sampled boreholes provide a robust measure of bedding thickness to within a few ($\pm$ $\sim$3) centimeters. By comparing the bedding thicknesses outside the zone of deformation, at borehole FL-4, with the bedding thicknesses at the crest of the monocline, at borehole FL-6, we measure 3 m of uplift during deposition of Beds 1 through 3.

To measure syndepositional horizontal contraction across the monocline, we compare the bed length of the top and base of individual stratal packages (ΔH, Figure 9.13a). We again use boreholes FL-4 and FL-6 as our pin lines. Comparison of the length of horizon C1 and horizon C4 yields 2 m of contraction during deposition of Beds 1 through 3. This measure of sydepositional contraction is not as robust as the measurement of syndepositional uplift, since bedding planes are only sampled

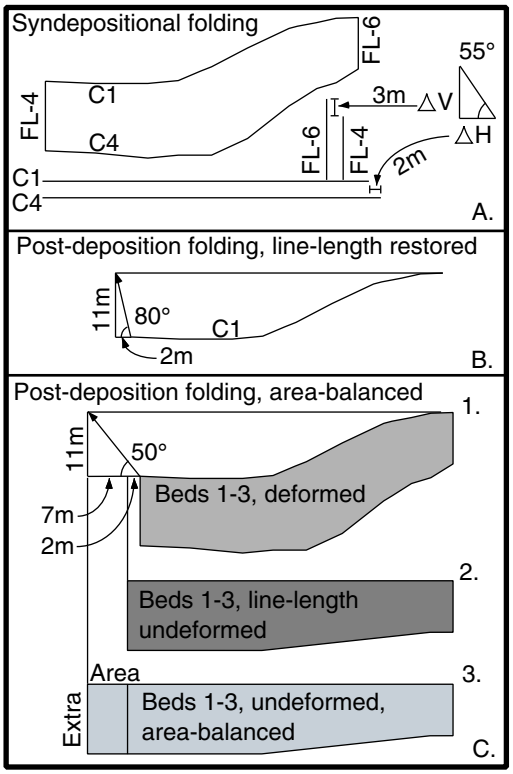

Figure 9.13. Illustration of methods used to derive the vector of deformation for the Coyote Pass monocline, using the stratigraphy documented in Fig. 9.9. A. Differential relief and line length between the C1 and C4 horizons are used to estimate a 55° vector for syndepositional folding. B. Determination of the contractional component of post-depositional folding requires accounting for both the deformed length of the C1 horizon and for tectonic thickening of bedding through the syncline. C. The first, light-gray panel depicts the deformed strata. The second, dark-gray panel depicts idealized growth strata. The third, light-gray panel depicts the idealized growth strata with an added length to match the cross-sectional area of the first, light-gray panel. Unstretching both the length of clay C1 and adding the additional thickening component yields a 50° vector for post-depositional folding.

at boreholes several meters apart. Because we use the shortest, straight-line distance between borehole correlations for our analysis, this is a minimum contraction estimate.

To characterize the vector of deformation, we resolve a ratio from the contraction and uplift measurements across the Coyote Pass monocline. The arccotangent of this ratio (shown in parentheses) is equivelant to the angle from horizontal of the displacement of the upper limb relative to the lower limb. Individual beds yield ratios from 0.4 (70°) to 1.2 (40°). This variation probably reflects the limitations of both our data and our assumptions about the original horizontally of the clay horizons. However, by grouping the beds together, we effectively 'stack' the syntectonic signal against the natural and measured 'error,' or variability, in bed thickness. Analyzed as a group, Beds 1 through 3 yield a ratio of 0.7 (55°) (Figure 9.13a).

A significant discrepancy arises when we compare Beds 1 through 3 with younger deformation (Figure 9.13b). The difference between line length and structural relief of the deformed C1 horizon and the length and structural relief of an idealized, horizontal line reveals 2 m of contraction and 11 m of uplift. These values yield a significantly lower ratio of 0.2 (80°). We interpret this discrepancy to be the result of penetrative contraction, which has altered the original length of bedding. We assume, and confirm below, that this penetrative component would yield little measurable effect during the deposition of Beds 1 through 3, since the magnitude of uplift between clay horizons is relatively small. However, the addition of 11 meters of uplift since deposition of the C1 horizon has allowed this penetrative component to absorb a considerable amount of the total contraction.

We propose that the majority of this penetrative contraction is absorbed through thickening in the syncline area, within and adjacent to the Coyote Pass monocline. Careful inspection of the Evergreen transect reveals evidence of this penetrative contraction component. There are two components to the syncline between Structures 3 and 4. Strata between boreholes FL-5 and FL-4 dip 1° northward. We interpret this as the northern limb of Structure 4. This limb forms a broad syncline between

Structures 3 and 4 which has partially filled with colluvial material. Strata between boreholes FL-4 and FL-7, however, are noticeably more steeply dipping, forming an additional, tighter, 30 meter-wide syncline at the foot of the monocline. Comparison of the deformed C1 and C4 horizons reveals that bedding within the tighter syncline is non-uniform. The C1 horizon is depressed by 0.3 meters at FL-7, whereas the C4 horizon is depressed by an additional 1.0 meters. If we assume that this thickening is due to entirely to syntectonic sedimentation over a growing fold, then the syncline must have grown significantly during deposition, and then nearly ceased to grow afterward. Alternatively, if the thickening is due to depositional processes alone, then fluvial/lacustrine sedimentation must have, at first, enhanced the shape of the depression at the syncline location, rather than filling it in. We propose that neither of these processes is principally responsible for the tight syncline at the base of the monocline. Rather, it is more plausible that the tighter syncline reflects penetrative contraction to accommodate rotation of the adjacent limb of the Coyote Pass monocline. This is a mechanically reasonable response of unlithified sediment to contraction within a developing fold hinge.

To measure the penetrative component of contraction, we use an area-balancing technique to restore thickened strata across the Coyote Pass monocline (Figure 9.13c). When both the line-length and penetrative components of contraction are accounted for, a consistent vector of deformation results. By restoring an additional 7 m (11%) of penetrative deformation, we estimate a total of 11 m of uplift and 9 m of contraction since deposition of C1, a ratio of 0.8 ($\sim$50°). This is nearly equivalent to the values measured above for syndepositional deformation. However, are the syndepositional values measured from differential line length accurate, in light of the significant contribution of penetrative contraction? To check this, we remove 11% of penetrative contraction and then recalculate the horizontal component. As a result, the syndepositional ratio for Beds 1 through 3 adjusts slightly, from 0.7 to 0.8. The convergence of these estimates leads us to conclude that a 0.7 to 0.8 ratio ($\sim$50 to 55°) is a reasonable representation of the vector of deformation for the Coyote Pass

monocline.

9.6.5 Summation of parasitic folding

To estimate the contraction rate of the forelimb of the entire Elysian Park anticline, we sum the contraction rates of active parasitic folds. We begin by summing the combined uplift of the Qg1 surface by these folds, estimated from the Laguna Channel topographic cross section ('G,' Fig. 9.12). Since this cross section passes eastward of the termination of Structures 1 and 2, we need only account for the uplift of Structure 3 (47 m) and Structure 4 (21 m). To estimate contraction, we assume that the contraction/uplift ratio determined at Evergreen Avenue can be applied in general to both structures. This approach is justified by the systematic geometry of parasitic folding in East Los Angeles displayed at the surface and in cross section (Figs 9.2, 9.3, and 9.4a). Using the ratio of 0.7 to 0.8, we estimate contraction of the Qg1 surface by 33 to 38 m from Structure 3, and 15 to 17 m from Structure 4. These estimates yield an overall contraction of 48 to 55 m, at a rate of 0.6 to 1.1 mm/yr, for the forelimb of the Elysian Park anticline in east Los Angeles.

9.6.6 Seismic hazard of the Elysian Park fault

The seismic hazard posed by a fault is a function of 1) the size of the fault, 2) its rate of slip, 3) the variability of recurrence intervals about the mean, 4) the time since the last major failure, 5) the range of earthquake sizes generated by a fault, and 6) the degree to which a fault fails in conjunction with neighboring structures. We place constraints on the first two parameters: The size of the source fault and its rate of slip. From these, we use the calculation methods employed by *Dolan et al.* [1995] to estimate the ranges of plausible earthquake magnitude and nominal recurrence interval. Because the *Dolan et al.* [1995] earthquake parameters and statistical regressions are well constrained, correlated, and fit specifically to Southern California, we maintain that these present a more accurate basis for estimating the hazard

Table 9.1. Elysian Park fault: Model earthquake magnitude.

Fault plane area[a] (km^2)	*Dolan et al.* [1995] M_w[b] (±0.1)	*Dolan et al.* [1995] M_0[c] (10^{26} ergs)	*Wells and Coppersmith* [1994] M_w[d] (±0.3)	*Wells and Coppersmith* [1994] M_0[c] (10^{26} ergs)
45°–30° model				
90	6.2	0.29	6.1	0.17
150	6.4	0.56	6.3	0.34
50° model				
150	6.4	0.56	6.3	0.34
210	6.6	0.86	6.4	0.54
60° model				
240	6.6	1.02	6.5	0.64
290	6.7	1.31	6.5	0.83

[a] Calculated fault plane area extending from 5 km depth, and 3 km depth, down to as much as 17km depth. Fault plane models are depicted on Fig. 9.14.

[b] Nominal magnitude calculated from the model fault plane area, using a regression for Southern California earthquakes, $M_w = 4.56 + 0.86 * Log(Area)$ from *Dolan et al.* [1995].

[c] Seismic moment calculated from the relation: $M_w = 2/3 * Log(M_0) - 10.7$ from *Hanks and Kanamori* [1979].

[d] Nominal magnitude calculated from the model fault plane area, using a regression for world-wide reverse-motion earthquakes, $M_w = 4.33 + 0.90 * Log(Area)$ from *Wells and Coppersmith* [1994].

of the Elysian Park fault than do global databases. For comparison, however, we also list results using the regression of global databases by [*Wells and Coppersmith*, 1994](Tables 9.1, 9.2, and 9.3).

Characteristic earthquake magnitude

We consider two classes of faults: Shallow-dipping thin-skinned faults and steeply dipping trans-crustal faults. If we adopt the geometry of the *Davis et al.* [1989] Elysian Park fault as a representative of thin-skinned geometries, we can use their cross section to calculate the area of the fault. In their model, the Elysian Park fault consists of an upper portion, with a dip of 45° and a down-dip length of 6

km, and a lower portion with a dip of 30° and down-dip length of 5 km (Figure 9.4, B-B'). We assume that the strike of these two planes is parallel to the trend of the MacArthur Park–Coyote Pass monocline, and that the Elysian Park fault (like the Elysian Park anticline) is bounded by the Hollywood, Alhambra Wash, and Raymond faults (Figure 9.14a). As alternatives, we also present steeper, 50° and 60° dipping reverse fault models (Figures 9.14b and 9.14c).

For each model, we also consider two classes of fault area: Rupture planes restricted to depths greater than 5 km, and rupture planes restricted to depths greater than 3 km. Due to the roughly conical model geometry of the Elysian Park fault, inclusion of the model fault plane from 3–5 km depth significantly increases the rupture area. The 45° to 30° fault plane restricted below 5 km has an area of 90 km^2, but has an area of 150 km^2 if the portion from 3 to 5 km depth is included. Similarly, the 50° model yields values of 150 km^2 and 210 km^2, and the 60° model yields even larger values of 240 km^2 and 290 km^2.

Now, we estimate a range of sizes for an earthquake generated by the Elysian Park fault (Table 9.1). Using the *Dolan et al.* [1995] regression of rupture area versus moment magnitude for southern California earthquakes, we estimate a M_w of 6.2 to 6.7 (6.1 to 6.7, including 1σ error in the regression) for failure of the Elysian Park fault. Using a similar regression by *Wells and Coppersmith* [1994], we derive a M_w range of 6.1 to 6.5 (5.9 to 6.7, with 1σ error).

To estimate average fault displacement per earthquake, we first translate the moment magnitude into seismic moment, using the relation $M_w = 3/2 * Log(M_0) - 10.7$ [*Hanks and Kanamori*, 1979]. Then, we solve the relation, $M_0 = \mu AD$, to estimate average displacement, D, from M_0, μ (crustal rigidity), and A (rupture area). Average displacement estimates vary over a small range, from 0.9 to 1.1 m for the 45° to 30° fault model, up to 1.2 to 1.4 m for the 60° model (Table 9.2).

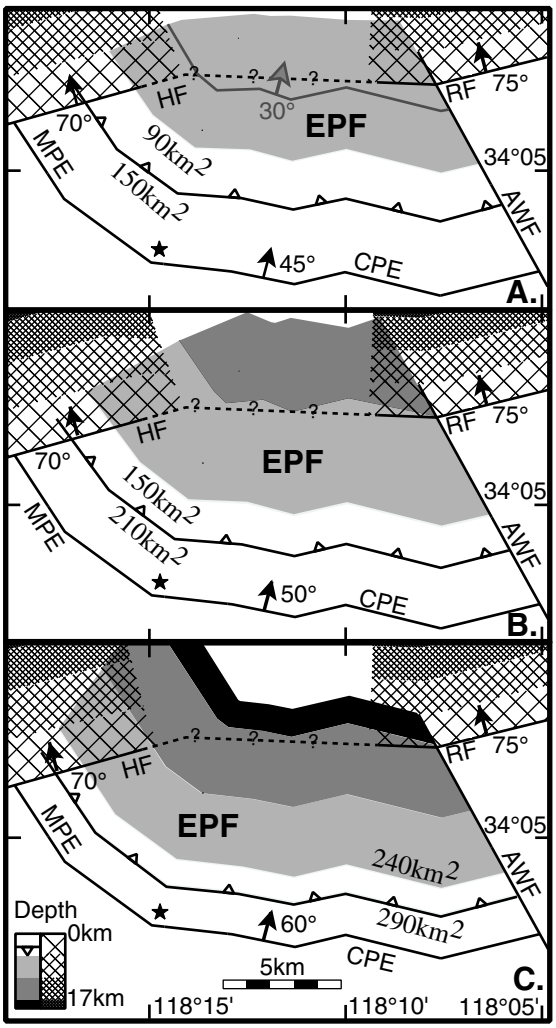

Figure 9.14. Three possible configurations for the Elysian Park fault. Each panel presents a shaded structure-contour image of the fault plane. A. Interpretation of the *Davis et al.* [1989] model, with a change in dip from 45° to 30° at 7.5 km depth. B., C. Steeper-dipping models with constant dip. The fault plane area between 5 km and 17 km depth, and 3 km and 17 km depth, are depicted in each panel. We restrict the extent of the Elysian Park fault by the location, and down-dip extension of bounding fault planes. Cross-hatch pattern denotes the down-dip extent of the Hollywood and Raymond faults. The star symbol in each panel indicates the location of downtown Los Angeles. AWF, Alhambra wash fault; CPE, Coyote Pass escarpment; EPF, Elysian Park fault; HF, Hollywood fault; MPE, MacArthur Park escarpment; RF, Raymond fault.

Table 9.2. Elysian Park fault: Model earthquake displacement.

Fault plane area[a] (km^2)	Rupture plane depth[b] (km)	Average Displacement[c] *Dolan et al.* [1995][d] (m)	*Wells and Coppersmith* [1994][e] (m)
45°–30° model			
90	10 to 5	0.9	0.6
150	10 to 3	1.1	0.8
50° model			
150	15 to 5	1	0.8
210	15 to 3	1.2	0.9
60° model			
240	17 to 5	1.2	0.9
290	17 to 3	1.4	1

[a] Calculated fault plane area extending from 5 km depth, and 3 km depth, down to as much as 17km depth. Fault plane models are depicted on Fig. 9.14.

[b] Vertical extent of rupture plane. See Fig. 9.14.

[c] Calculated from the relation, $M_0 = \mu AD$ [*Hanks and Kanamori*, 1979] where μ = crustal rigidity in dyne/cm^2, A = fault plane area, and D = average displacement.

[d] μ = 3.6 dyne/cm^2 for rupture up to 5 km depth, and μ = 3.3 dyne/cm^2 for rupture up to 3 km depth. [*Dolan et al.*, 1995].

[e] μ = 3.0 dyne/cm^2 for all rupture models. [*Wells and Coppersmith*, 1994].

Table 9.3. Elysain Park fault: Model earthquake recurrence interval.

Fault Plane Area[a]	Slip Rate[b]		Recurrence Interval *Dolan et al.* [1995][d]		Recurrence Interval *Wells and Coppersmith* [1994][c]	
	Low	High	Low	High	Low	High
(km^2)	(mm/yr)	(mm/yr)	(years)	(years)	(years)	(years)
45°–30° model						
90	0.8	1.6	1100	600	700	400
150	0.8	1.6	1300	700	900	500
50° model						
150	0.9	1.7	1100	600	800	400
210	0.9	1.7	1300	700	900	500
60° model						
240	1.2	2.2	1000	500	700	400
290	1.2	2.2	1100	600	800	400

[a] Calculated fault plane area extending from 5 km depth, and 3 km depth, down to as much as 17km depth. Fault plane models are depicted on Fig. 9.14.

[b] Calculated from the horizontal component contraction on the forelimb of the Elysian Park anticline, as determined from the summed contraction rate of parasitic folds in east Los Angeles.

[c] Calculated by dividing the average displacement by the slip rate. Average displacement estimates are listed in Table 9.2, as calculated using the parameters outlined in *Dolan et al.* [1995].

[d] Calculated by dividing the average displacement by the slip rate. Average displacement estimates are listed in Table 9.2, as calculated using the parameters outlined in *Wells and Coppersmith* [1994].

Recurrence interval of earthquakes

We use the average displacement estimates and the summed contraction estimate to speculate an average return period for rupture of the Elysian Park fault, independent of adjacent structures. We assume that the horizontal component of the slip rate on the Elysian Park fault matches the horizontal component measured from shortening of the forelimb of the overlying Elysian Park anticline. From the contractile component of 0.6 to 1.1 mm/yr estimated above, we calculate a slip rate of 0.8 to 1.6 mm/yr for the 45° segment of the 45° to 30° dipping fault model. For steeper-dipping reverse fault models, in order to match the observed contraction rate at the surface, we calculate higher slip rates of 0.9 to 1.7 mm/yr (50° model) and 1.2 to 2.2 mm/yr (60° model).

Dividing the coseismic slip values by the slip rate yields an estimate of average recurrence interval for an assumed rupture area (Table 9.3). For the 45° to 30° model, a nominal rupture of the entire area of the Elysian Park fault with M_w 6.2 to 6.4 should occur every 600 to 1300 years, on average. Similarly, a nominal rupture of the 50° fault plane model yields a M_w 6.4 to 6.6, also every 600 to 1300 years, and a nominal rupture of the 60° fault plane model yields a M_w 6.6 to 6.7, and an average recurrence interval 500 to 1100 years. Because the size of the model fault plane and the estimated slip rate both increase with fault dip, the range of calculated recurrence intervals do not vary greatly over a broad range of earthquake size.

9.6.7 Evaluation

The results of the above analysis present a wide array of seismic hazard estimates for the Elysian Park fault. At the low end, a restricted rupture beneath the core of the anticline could produce a relatively small M_w 6.2 earthquake. An event similar to the destructive, M_w 6.7 1994 Northridge Earthquake, however, is also plausible. A balanced model of the Elysian Park anticline and fault would restrict the range of these analyses by providing better constraints on the potential rupture area, as well as a more precise translation of the observable contraction rate at the surface into fault slip at depth. Such work is, unfortunately, beyond the scope of our current efforts.

Heaton et al. [1995] used a rectangular, shallow-dipping blind thrust fault beneath the Elysian Park anticline to estimate ground motions from a hypothetical earthquake. They assumed an area of 630 km^2, an average slip of 2.2 meters, and a magnitude of M_w 7.0. They were attempting to model an event on the Las Cienegas fault, which in Figure 9.4 B-B' resides below the Elysian Park fault. Our analysis suggests that the Elysian Park fault, by itself, is not capable of producing an earthquake as large as this. But, of course, even if our estimation of fault geometry is correct, the Elysian Park fault could fail in conjunction with neighboring structures, such as the Las Cienegas fault, the Whittier fault or the Hollywood fault, to generate

a significantly larger and more damaging earthquake.

Though we have documented surficial deformation, and related this surface record to the subsurface, we have not necessarily proven that the Elysian Park fault is seismogenic. Proving seismic behavior would be a difficult task, since a paleoseismic record of the fault may not be directly observable at the surface. However, growth of the parasitic folds on the forelimb of the Elysian Park anticline may preserve a record of seismicity. For example, if we multiply the post-Qg1 uplift rate of 0.2 mm/yr obtained for the Coyote Pass monocline at Evergreen Avenue by our recurrence interval estimate, we obtain a coseismic uplift estimate of 0.2 to 0.4 meters. These values approach the scale of structural relief resolved within individual lacustrine cycles at this site, which suggests that the Evergreen Avenue cross section may contain a stratigraphic record of seismically triggered folding. Other such records may exist within younger, Qa strata. Future investigation of these might further our understanding of the seismic potential of the Elysian Park anticline.

Finally, the parasitic folds on the forelimb of the Elysian Park anticline also present potential individual hazards. [*Hitchcock and Kelson*, 1999] note that surface deformation and zones of concentrated damage from the 1989 Loma Prieta earthquake correspond to zones of potentially fault-related secondary folds. The relationship of active folds on the forelimb of the Elysian Park anticline to the underlying thrust fault may lead to concentrated deformation and damage during an earthquake. The structure that is of most concern is the Coyote Pass monocline, which exhibits a narrow zone of uplift and tilting (Fig. 9.9) and passes directly beneath downtown Los Angeles (Figs. 9.3 and 9.11). The character of deformation across the Coyote Pass monocline is very similar to the concentrated zone of deformation surrounding an active fault zone, and it might be wise to take steps to mitigate this hazard.

9.7 Conclusions

This study represents an integrated application of geology and geomorphology to translate surficial fold deformation into a seismic hazard analysis of a blind thrust fault. We characterize youthful fold deformation of the Elysian Park anticline, a fault-related fold on the northern margin of the Los Angeles basin. To characterize the Elysian Park fault, we proceeded through several steps. First, we measured the youngest expression of fold deformation deduced from a series of parasitic anticlines located upon the forelimb of the Elysian Park anticline. This information was acquired through an integration of topographic analysis and shallow subsurface field investigations. By using the age and deformation of these deposits, we summarized the contraction rate of parasitic folding to obtain an estimate of contraction across the parent anticline. With the aid of a set of fault models, we then translated the surficially derived contraction estimate into a slip rate on the proposed blind reverse fault. Finally, we applied the slip rate and three-dimensional fault geometry to estimate the magnitude and recurrence interval of a nominal rupture of the Elysian Park fault.

Fault models of variable geometry give an array of seismic hazard estimates. Using a thin-skinned thrust fault model, based upon a regional cross section by *Davis et al.* [1989] we estimate that the Elysian Park fault slips at 0.8 to 1.6 mm/yr, and a nominal rupture of the entire length of this fault is capable of producing a M_w 6.2 to 6.4 earthquake. Steeper-dipping reverse fault models yield higher slip rates and magnitudes of 0.9 to 1.7 mm/yr, M_w 6.4 to 6.6, and 1.2 to 2.2 mm/yr, M_w 6.6 to 6.7. Estimates of an average recurrence interval for an event on the Elysian Park fault range from 500 to 1300 years. The range of these estimates would not be so broad if an updated, structurally balanced fault model existed. Also, larger earthquakes with longer return periods are possible, should the Elysian Park fault fail in conjunction with neighboring structures. Seismically triggered folding of individual parasitic folds, especially the Coyote Pass monocline, may locally increase the overall hazard.

9.8 Acknowledgments

This study is the product of a collaboration between Caltech scientists, geotechnical geologists, and the engineers and managers of the Engineering Management Consultant of the Metropolitan Transit Authority. We greatly appreciate the encouragement and financial support of the MTA. In particular, we are indebted to Bomi Ghadiali and James Monsees of Engineering Management Consultant for their logistical support and penetrating questions during the course of our work. Initial geomorphic investigation by James Dolan, of the University of Southern California, and later, independent research efforts with Karl Mueller, of the University of Colorado, and Andrew Meigs, of Oregon State University, contributed to the development of this paper. We are also indebted Jan Mayne and Anne Lilje for their painstaking efforts to digitize the detailed 1920's era topographic maps, and to Tony Soeller, for his expert G.I.S. advice. We thank Keith Kelson and Ernest Duebendorfer for their constructive reviews. This paper is contribution number 8588 of the Seismological Laboratory and contribution number 457 of the Southern California Earthquake Center. Partial support was provided by the Southern California Earthquake Center, a consortium of earthquake scientists funded by National Science Foundation Cooperative Agreement EAR-8920136 and U. S. Geological Survey Cooperative Agreements 14-08-0001-A0899 and 1434-HQ-97AG01718.

Appendix A

Measured stratigraphic sections of Isla Tiburón and coastal Sonora

Table A.1. Measured section, Sierra Menor South (SMS), Isla Tiburón.

Measured section of Tmal, Tmr3, Tmr4, Tmrec, southern Sierra Menor, Isla Tiburón. Base of section located at $^{3}58^{910}$E, $^{31}99^{840}$N. Measured using compass and jacob staff on March 29, 1999.

Thickness	Description
	Underlain by Tma1 andesite.
Tmal Basin-fill alluvium and air-fall deposits	
10 m	Small paleochannel, airfall fill of white pumice lappili. Beds 2 cm to 1 m thick. Rare blocks. Pinches out within 50 m along strike in either direction.
3 m	Boulder conglomerate, crudely bedded, clast up to 1 m across.
4 m	Orange ash and pumice flows. 10 cm beds, with one 2 m thick bed.
5 m	Boulder conglomerate, crudely-bedded.
22 m Total	(Tmal)
Tmr3 member of the Tuffs of Mesa Cuadrada	
0.2 m	Unwelded pumice lapilli and ash. 15% pumice and 5% volcanic lithic fragments.
1.3 m	Sintered/poorly welded massive ignimbrite with feldspar phenocrysts up to 2 mm size. Occasional black glass lenses up to 3 cm length. Grades from light orange to dark orange glass matrix.
1 m	More indurate, grading to moderately welded.
0.5 m	Black glass fragments/fiamme appear. Color trends upward from orange to brown. Perlitic fractures.
4 m	Black densely welded vitrophyre. Brown grading up to black in first meter. Upper part grades back to dark orange within 0.5 m, occasional brown intervals in upper part.
5 m	Orange welded tuff, 10% red and black volcanic lithic fragments.
46 m	Orange to red welded tuff. Indurate, with black fiamme grades upward gradually into white poorly welded tuff.
5 m	Slightly welded white ash-flow tuff. Non welded top of flow.
63 m Total	(Tmr3)
Tmr3t member of the Tuffs of Mesa Cuadrada	
∼3 m	Andesite cobbles in float. Deposit poorly exposed but must be from a thin congolomerate or colluvial lense between ash-flow tuffs.
0.5 m	Pumice lapilli, volcanic lithics, buff-colored basal airfall of Tmr4.
3.5 m Total	(Tmr3t)
Tmr4 member of the Tuffs of Mesa Cuadrada	
0.7 m	Greenish-brown pumice-rich moderately indurate poorly welded to non-welded basal glass. 5% Pumice, 1–2 cm, to 5 cm, ∼10% volcanic lithic fragments.

Measured section, Sierra Menor South (SMS), Isla Tiburón.

Thickness	Description
0.5 m	Incipiently welded brown glass, grading upward to welded at top. Orange pumice: 10%. Flattened glass fragments and volcanic lithic fragments: 5% Some large brown glass blobs (1 by 5 cm near top). Transitions over 10 cm to overlying densely welded vitrophyre.
12 m	Tan vitreous welded tuff grades to bright red densely welded tuff within 30 cm. Welding grade decreases gradually up-section.
7 m	White, non-welded to slightly welded tuff.
20.2 m Total	(Tmr4)
Tmal Basin-fill alluvium and air-fall deposits	
2 m	Poorly exposed andesite boulders and cobbles.
4.5 m	Poorly exposed pumice lapilli and ash airfall. Indurate red and black volcanic lithic bed at top.
0.5 m	Thin conglomerate bed.
7 m	(Tmal, too thin too map)
Tmrec Tuffs of Arroyo El Canelo	
1 m	Poorly exposed orange pumice lapilli ash-flow with black glassy volcanic lithic fragments.
7 m	Brown, moderately welded ash-flow tuff with 5% pumice fiamme and 10% lithic lapilli. Weathers to a rough pattern. Grades upward into a recessive ashy horizon with large pumice. Upper part welded by overlying ash-flow tuff with 5 cm thick orange vitrophyre overlain by a 25 cm thick layer rich in black fiamme.
0.3 m	Pink to red welded tuff with fiamme. Phenocrysts are concentrated into cm-scale concentration zones.
0.7 m	Purple vitreous welded tuff. Black fiamme up to 4 cm. Rich in feldspar phenocrysts. Welding decreases up-section.
2.5 m	Purple welded tuff with giant white vapor-phase altered pumice fiamme. Smaller black fiamme also present.
10 m	Vapor-phase altered welded tuff with large and small black pumice fiamme. Top eroded.
21.5 m Total	(Tmrec)

Table A.2. Measured section, Bahía Vaporeta South (BVS), Isla Tiburón.

Measured section of Tmrec, 5 km east of Bahía Vaporeta, Isla Tiburón. Base of section located at $^{3}56^{210}$E, $^{32}00^{290}$N. Measured using compass and hand levelling on March 31, 1999.

Thickness	Description
	underlain by Tmal Basin-fill alluvium and air-fall deposits.
Tmrec Tuffs of Mesa Cuadrada	
1 m	Purple densely welded vitrophyre. 25% phenocrysts with 10 cm-scale variations in concentration. 10% fiamme, 5% lithic fragments.
4 m	Purple welded tuff, rich in phenocrysts. Distinctive large white vapor-phase altered pumice. Becomes lighter purple and more vapor-phase altered up-section.
4 m	Scoriaceous red and black lithic horizon. Ash matrix disappears.
10 m	Upper welded tuff unit. Basal brown glassy ash with orange pumice lenses. Fragments only exposed, 10 cm max thickness. Overlain by purple welded tuff with vapor-phase altered pumice up to 20 cm length. Scoriaceous lithic inclusions common.
19 m Total	(Tmrec)

Table A.3. Measured section, Bahía Kino (BK), Sonora.

Measured section of Tmrsf, 3 km north of Bahía Kino, Sonora. Base of section located at $^{4}02^{100}$E, $^{31}95^{110}$N. Measured using tape and compass on April 2, 1999.

Thickness	Description
	Overlies Tmvs volcaniclastic deposits. Andesitic debris flow in red volcanic lithic sand matrix.
Tmrsf Tuff of San Felipe	
0.8 m	Ash and blocks (airfall?) Very pale orange colored matrix. Andesite and green altered ash blocks.
1 m	Black densely welded crystal-rich vitrophyre. Sharp basal contact. 10% feldspar phenocrysts. Orange alteration along fractures. Upper contact also sharp but often obscured by alteration along perlitic fractures.
1 m	Densely welded tuff with large lithophysal cavities (to 10 cm across). Moderate reddish orange matrix. Lithophysae decrease in size up-section.
0.5 m	Lithophysae flatten, begin to define platy cleavage. Vapor-phase alteration and resulting cavernous weathering begin.

Measured section, Bahía Kino (BK), Sonora.

Thickness	Description
5 m	Rare volcanic lithics with rolled foliation in surrounding tuff. Platy cleavage formed of eutaxitic foliation. Some large lenses up to 50 cm length may have been pumice. If so, then pumice may comprise more than 20% of rock.
5 m	Spherulites rare, lithophysae 10–40 cm range. Some 1 m long streaks may be pumice? Rheomorphic flow around rare cm-sized volcanic lithic fragments.
10 m	Foliation even more well-developed by extremely flattened pumice lenses. Pumice decreasing to 10% of rock.
17 m	Pumice up to 15%. Large and small lithophysae present. Large calcite crystals in lithophysae cavities. Rare distinctive black inclusions present, but difficult to locate.
8 m	Spherulites increasing rapidly in concentration, obliterating 10–15% of pyroclastic texture.
15 m	Spherulites increase to over 50%, coalescing to form bright white, crumbly, completely vapor-phase altered ash-flow tuff. Distinctive black rhyolite lithic fragments become more common, up to 20 cm in size.
63 m	Spherulitically devitrified welded ash-flow tuff. Locally up to 2% distinctive black inclusions. Inclusions easier to locate against white altered tuff.
5 m	Spherulites concentration drops to zero over 2 m distance. Up to 10% volcanic lithic fragments, orange to red as well as black. Up to 20% phenocrysts in bright red-orange matrix. Upper welded zone or just less-altered?
3.5m	non-welded to incipiently welded tuff. Buff-gray color. Small dark brown pumice up to 1 cm. 5% feldspar phenocrysts. Overlain by Tmrf2 rhyolite lava flow and basal block and ash deposits.
135 m Total	(Tmrsf)

Table A.4. Measured section, Punta Reina Footwall (PRF), Isla Tiburón.

Measured section of Tmrsf, 3 km southeast of Punta Reina, Isla Tiburón. Base of section located at $^{3}55^{430}$E, $^{32}12^{680}$N. Measured using compass and jacob staff on April 20, 1999.

Thickness	Description
Tmrsf Tuff of San Felipe	
0.7 m	Vitrophyre. Black to dark brown. 10–15% phenocrysts. Upper contact is a 3 cm gradation.
3.7 m	Spherulitic red densely welded tuff. Lithophysae up to 20 cm diameter. Large strung-out pumice to 30 cm length.
4 m	20–30% large strung-out pumice. Some exceeding 1 m length. First distinctive black inclusion encountered.
1.6 m	Transitional zone, 5% large pumice to 50 cm length, 5–10% spherulites.
11 m	Spherulitically devitrified welded tuff.
29 m	Spherulitically devitrified partially welded tuff. Pockets of distinctive lithic inclusions, each up to 4 cm long, forming up to 30% of rock locally. Capped by ∼5 m reworked ash and volcanic lithic fragments.
50 m Total	(Tmrsf)

Table A.5. Measured section, Sierra Menor (SM), Isla Tiburón.

Measured section of Tmrsf, Tmb2, Tmal, Tmr3, Tmr4, Tmrec, central Sierra Menor, Isla Tiburón. Base of section located at $^{3}57^{710}$E, $^{32}05^{710}$N. Measured using compass and jacob staff on April 16, 1999.

Thickness	Description
	Overlies Tmvs volcaniclastic conglomerate and debris-flow deposits.
Tmrsf Tuff of San Felipe	
0.8 m	Black densely welded vitrophyre with 15% feldspar phenocrysts.
0.3 m	Orange altered vitrophyre with small, 2–4 mm spherulitic crystal growths.
0.4 m	Spherulites increase to 10% of rock. Lithophysae present up to 4 cm diameter.
1 m	Orange to red densely welded tuff, lithophysae to 5 cm.
5 m	Pumice become increasingly flat up-section, approaching 1:20 aspect ratio. First distinctive black lithic inclusion.
19 m	Red densely welded tuff with prominent eutaxitic foliation and <10% spherulitic crystals.

Measured section, Sierra Menor (SM), Isla Tiburón.

Thickness	Description
8 m	Spherulites increase to 25% of rock. Foliation becomes difficult to resolve.
43 m	Spherulitically devitrified ash-flow tuff.
8 m	Upper, densely-welded and less altered zone. Up to 10% spherulites.
85.5 m	(Tmrsf)
Tmb2 Basalt	
3.5 m	Conglomerate of andesite clasts, gravel and sand.
7 m	Basalt lava flow, resistant base and recessive up-section.
5 m	Basaltic tephra, poorly exposed.
8 m	Resistant basalt flow, becoming more foliated up-section.
13 m	Basalt flow with thin basal tephra or autobreccia. Weathered and more foliated up-section.
6 m	Basaltic tephra, scoria, occasional bombs. Red, black and orange.
9 m	Basalt lava flow. Blocky base, then foliated and more weathered up-section.
3 m	Lithic lappili and block-sized scoria bed. May be a basal autobreccia to above flow.
2 m	Thin vesicular blocky basalt flow.
2 m	Scoria blocks.
10 m	Blocky, then foliated basalt lava flow.
9 m	Scoria and basaltic tephra, overlain by thin blocky basalt flow.
2 m	Basaltic tephra and scoria bed.
5 m	Foliated basalt with resistant blocky central interval.
7 m	Conglomerate, poorly exposed. Contains granitic basement cobbles.
7 m	Blocky basalt flow.
90.5 m Total	(Tmb2)
Tmal Basin-fill alluvium and air-fall deposits	
22 m	Unexposed beneath talus.
7 m	Poorly exposed sand-sized pumice and ash.
13 m	Bedded ash and pumice up to 1 cm size. 10–20 cm beds.
1 m	Poorly-sorted ash and pumice flow.
21 m	Bedded ash and pumice. Yellow to white, mostly reworked. Rare to uncommon volcanic lithic fragments.
42 m Total	(Tmal)
Tmr3 member of the Tuffs of Mesa Cuadrada	
3 m	Base of brown to orange slightly welded glass with orange pumice, cm-sized volcanic lithic fragments. Weldeing grade increases up-section. Fiamme to 5 cm. Grades into brown densely welded vitrophyre.
2 m	Black densely welded vitrophyre. 10–15% volcanic lithic lapilli.

Measured section, Sierra Menor (SM), Isla Tiburón.

Thickness	Description
3 m	Bright red welded ash-flow tuff. 5% black fiamme and 10% volcanic lithic fragments.
20 m	Bright red to orange welded crystal-rich ash-flow tuff, 10% volcanic lithic fragments. Pumice becoming less welded.
24 m	Gradational transition to light purple vapor-phase altered welded tuff. Weathers orange. 15% angular volcanic lithic fragments.
17 m	Central, resistant zone. Either more welded or less vapor-phase alteration. Bright red color returns. Lithophysae present.
27 m	Gradational transition back to light purple vapor-phase altered welded tuff.
9 m	Slightly welded, white ashy tuff. Recessive.
16 m	Non-welded pumice, lithic, and crystal-rich ash-flow tuff. Unwelded top of Tmr3.
118 m	(Tmr3)
Tmr4 member of the Tuffs of Mesa Cuadrada	
0.4 m	Brown glass, grading to light-dark brown.
0.2 m	Dark-brown to black glass with perlitic fractures.
0.5 m	Black glass. 5–10% sperulites, brown, 1–2 cm size.
0.5 m	Black glass, 10–50% spherulites to 1 cm.
0.5 m	Trending from brown to red. Rare spherulites to 10 cm.
9 m	Black to red matrix, spherulites increase in abundance, cavernous weathering.
15 m	Matrix becoming altered to white and purple in patches. Spherulites decrease to 5–10% of rock.
18 m	Purple densely welded tuff with up to 5% lithophysae.
9 m	Light purple less welded tuff.
18 m	Non-welded upper Tmr4. Recessive. Occasional large loose pumice in float. Poorly exposed overall.
71.1 m Total	(Tmr4)
Tmrec Tuffs of Mesa Cuadrada	
0.5 m	Dark purple basal vitrophyre.
1.5 m	Gradational dark purple to lighter purple welded crystal-rich tuff.
9 m	Light purple vapor-phase altered tuff with white altered pumice up to 30 cm across.
8 m	Matrix disappears. Dark to bright red scoria-like lithic fragments 5–20 cm length. Upper part of deposit welded by next welded tuff member.
0.7 m	Densely-welded and stretched pumice.
1.5 m	Densely welded glassy purple to reddish-brown tuff, 5% crystals, 5% lithic inclusions. Top of flow eroded.
21.3 m Total	(Tmrec)

Table A.6. Measured section, Punta Reina South (PRS), Isla Tiburón.

Measured section of Tmr3, Tmr4, Tmr5, Tmrec, 1 km south of Punta Reina, Isla Tiburón. Base of section located at $^{3}54^{080}$E, $^{32}14^{530}$N. Measured using compass and jacob staff on April 3, 2000.

Thickness	Description
	Section overlies Tmb2 basalt.
Tmr3 member of the Tuffs of Mesa Cuadrada	
3.5 m	Basalt breccia with ash matrix. Appears that base of Tmr3 has incorporated local basalt float. Steep paleotopography at contact apparent from adjacent outcrop relationships.
54.5 m	Non-welded at base. White ash matrix, 10% pumice lapilli, 10% volcanic lithic lapilli. Some cobble-size lithic fragments. Slightly welded to non-welded crystal and lithic-rich ash-flow tuff. Much of the lower exposure is covered by talus but well exposed on adjacent sea cliff. Phenocryst-rich zone present at 19 m and 28 m, 20% feldspar up to 3 mm size.
57 m Total	(Tmr3)
Tmr4 member of the Tuffs of Mesa Cuadrada	
0.3 m	Orange indurate ash.
0.3 m	Orange to black transitional non-welded to welded.
0.9 m	Welded black vitrophyre. Note that typical base of Tmr4 not well developed here, though present nearby. Rare feldspar phenocrysts.
10 m	Spherulitic densely welded red glassy crystal-poor tuff.
9 m	Densely-welded orange-red tuff, up to 10% vapor-phase recrystallized pumice. Up to 5% angular volcanic lithic fragments.
13 m	Slightly less welded. Pumice fiamme to 4 cm length. Lithic fragments up to 3 cm length.
19 m	More recessive, less welded ash-flow tuff. Light purple glassy to devitrified glassy matrix with 2–3% volcanic lithic fragments. Crystal poor.
22 m	Slightly welded to non welded upper part of Tmr4. Purple to white ash matrix, weathering to yellow.
74.5 m Total	(Tmr4)
Tmr5 member of the Tuffs of Dead Battery Canyon	
12 m	Basal densely welded purple glassy tuff. 10% plagioclase phenocrysts, 5% welded pumice.
20 m	Light purple devitrified crystal-rich welded tuff.
8 m	White vapor-phase altered welded tuff. Fiamme present.
40 m Total	(Tmr5)
Tmrec1 member of the Tuffs of Mesa Cuadrada	
1 m	Dark yellow to orange pumice flow. 15% lithic fragments, 2 mm common, up to 1 cm size.

Measured section, Punta Reina South (PRS), Isla Tiburón.

Thickness	Description
2 m	Dark red purple densely welded crystal-rich ash-flow tuff. Up to 20% feldspar phenocrysts and pumice to 1 cm altered to white. 5% lithic fragments.
1 m	Matrix becoming more purple, pumice increase in size to 10 cm, altered to white by vapor-phase recrystallization.
12 m	Purple-grey ash matrix. Welded vapor-phase recrystallized pumice up to 25%.
16 m Total	(Tmrec1)
Tmrec2 member of the Tuffs of Mesa Cuadrada	
1 m	Basal partially welded vitrophyre without spherulites, 15 cm thick, poorly exposed, black to dark brown with 20% phenocrysts to 2 mm, 5% volcanic lithic fragments. Overlain by dark brown weathered densely welded vitrophyre. Upper 50 cm with swiss-cheese texture from weathered cm-size spherulites.
15 m	Dark to light purple welded tuff, vapor-phase alteration increasing up-section. White altered pumice to 30 cm comprise up to 25% of rock. Upper part pumice weather as black fiamme in lighter purple matrix.
16 m Total	(Tmrec2)
Tmrfp member of the Tuffs of Mesa Cuadrada	
7 m	Transition to densely welded glassy red to purple ash-flow tuff (flagpole member). Transition very poorly exposed here. Basal 20 cm light partially welded glass zone seen in float.
7 m Total	(Tmrfp)

Table A.7. Measured section, Sierra Alta (SA), Isla Tiburón.

Measured section of Tmrsf, northern Sierra Alta, Isla Tiburón. Base of section located at $^{3}57^{360}$E, $^{32}28^{060}$N. Measured using compass and jacob staff on April 13, 2000.

Thickness	Description
	Section overlies 2–3 m of Tcg conglomerate on basement metasedimentary rocks.
Tmrsf Tuff of San Felipe	
1 m	Black densely welded vitrophyre. Orange altered zones surrounding perlitic fractures. Oxidized distinctive lithic fragments present.
0.3 m	Red to orange with lithophysae and spherulites.
0.4 m	Pink-purple densely welded zone with large flattened pumice.
68 m	Intensively spherulitically devitrified welded tuff. Distinctive lithics up to 60 cm length observed, comprising up to 30% of rock locally. Concentrations of these lithics at 5 m and 8–11 m. Lithics comprise ∼1% of rock overall for remainder of section.
69.7 m Total	(Tmrsf)

Appendix B

Microprobe analyses

Microprobe analyses were obtained with the California Institute of Technology, Division of Geological and Planetary Sciences JOEL-JXA-733 electron microprobe. Operating conditions were set at 15 kV accelerating potential and 25 nA probe current for all samples. Ten elements (Si, Al, Ca, Na, K, Fe, Mg, Ti, Mn, and Ba) were measured for all samples to within 0.1% concentration. K and Ba concentrations are below the detection limit for pyroxenes, as are Mg, Mn, and Ti concentration for feldspars. Samples measured for correlation were polished thin sections. Samples measured for geochronology were polished grain mounts.

The following pages are tables of microprobe measurements. Feldspar and pyroxene measurements are reprinted here from the Data Repository of *Oskin et al.* [2001] with permission of *Geology*. The last two tables, containing measurements of olivine in Tmr3 and of geochronology samples, have not been previously published.

Table B.1. Microprobe analyses of feldspar, Tuff of San Felipe, Baja California.

SiO_2 (Wt%)	FeO (Wt%)	CaO (Wt%)	Na_2O (Wt%)	Al_2O_3 (Wt%)	K_2O (Wt%)	BaO (Wt%)	Total[a] (Wt%)
Sample locality MA[b]							
66.8	0.2	1.5	7.9	20.1	4.4	0.1	101
67.3	0.2	1.3	7.9	20.1	4.6	0	101.5
65.9	0.2	3	8.8	21.8	1.8	0	101.6
67.7	0.1	0.5	6.2	19.4	7.7	0.1	101.6
67	0.1	0.6	6.3	19.3	7.4	0.1	100.8
67.8	0.2	0.5	6.2	19.3	7.6	0.1	101.7
67.2	0.2	1.2	7.6	20	4.9	0	101.2
67.3	0.2	1	7.4	19.6	5.3	0.1	100.9
67.1	0.2	0.6	6.4	19	7.2	0.1	100.5
67	0.2	1.5	8	20.2	4.3	0	101.1
67.2	0.2	1.2	7.6	20	5	0.1	101.3
67.5	0.2	1.3	7.5	20.1	5.1	0	101.7
66.7	0.2	1.6	8	20.4	4.1	0	100.9
66.7	0.1	1.7	7.8	20.5	4.1	0	101
67	0.2	1.7	8	20.4	4.2	0	101.5
67.1	0.1	0.6	6.5	19.3	7	0	100.7
67.4	0.2	0.5	6.1	19.1	7.7	0	101.1
66.6	0.2	0.5	6.2	19.1	7.9	0	100.5
57.6	0.1	9.3	6.2	27.3	0.3	0	100.9
58.7	0.1	8.4	6.6	26.6	0.3	0	100.7
59.6	0.1	7.9	7	26.1	0.4	0	101.1
67.1	0.1	0.8	7	19.7	6.4	0	101.1
67.2	0.2	0.9	7.2	19.7	5.9	0	101.1
67.9	0.1	0.6	6.2	19.3	7.4	0	101.6
66.5	0.2	1.1	7.6	19.7	5.2	0.1	100.4
67.8	0.2	0.5	6.2	19.1	7.7	0	101.4
67.2	0.1	0.8	6.9	19.5	6.5	0	101.1
67.6	0.1	0.6	6.4	19.2	7.3	0	101.2
67.2	0.1	1.2	7.6	19.8	5.1	0	101.1
66.9	0.1	1.2	7.6	20	5	0.1	100.8
66.9	0.1	1.6	7.9	20.1	4.2	0	100.9
67	0.1	1.2	7.7	19.8	5.1	0.1	101
66.9	0.1	1.5	7.8	20	4.6	0	100.9
67.1	0.1	1	7.5	19.7	5.4	0.1	101

Table B.1, continued.

SiO_2 (Wt%)	FeO (Wt%)	CaO (Wt%)	Na_2O (Wt%)	Al_2O_3 (Wt%)	K_2O (Wt%)	BaO (Wt%)	Total[a] (Wt%)
67.2	0.1	1.2	8.2	19.9	4.2	0.1	100.9
67.2	0.1	0.9	6.9	19.5	6.2	0	100.9
67.3	0.1	1	7.6	19.6	5.2	0	100.9
67.2	0.1	1.4	7.7	20	4.8	0.1	101.2
67.3	0.1	1.4	7.8	20.1	4.5	0.2	101.4
66.9	0.1	1.5	8	20.2	4.2	0	101
66.5	0.1	1.5	8	20	4.3	0.1	100.6
66.9	0.1	1.3	7.7	19.9	4.8	0	100.7
67.1	0.1	1.4	7.6	19.9	4.5	0	100.7
Sample locality SRB[c]							
66.9	0.2	0.9	7.3	19.4	5.8	0	100.5
67	0.1	0.5	6.1	19	7.8	0	100.5
67.1	0.1	0.5	6.3	19.1	7.5	0.1	100.7
66.8	0.2	0.9	7.3	19.5	5.7	0	100.4
66.3	0.2	1.4	7.8	19.9	4.4	0	100
66.4	0.2	1.3	7.8	19.7	4.5	0.1	100
66.5	0.2	0.9	7.2	19.4	6.1	0	100.2
66.4	0.2	1.3	7.8	19.9	4.7	0	100.3
66.5	0.2	1.2	7.7	19.7	5	0	100.3
66.7	0.2	0.6	6.3	19	7.3	0	100.1
66.8	0.2	0.6	6.4	19	7.2	0.1	100.2
67	0.1	0.5	6.3	19	7.3	0	100.3
66.5	0.2	1.2	7.5	19.6	5.2	0	100.2
66.4	0.2	1.3	7.7	19.7	4.7	0	100
66.6	0.1	1.1	7.5	19.5	5.3	0	100.2
Sample Locality SFD[d]							
66.8	0.1	0.5	6.3	19	7.5	0	100.4
66.5	0.2	1	7.3	19.5	5.7	0	100.2
66.9	0.2	0.6	6.4	19.1	7.3	0.1	100.6
66.5	0.2	1.2	7.8	19.9	4.9	0	100.6
66.4	0.2	1.2	7.8	19.8	4.9	0	100.4
66.4	0.2	1.5	8	20.2	4.2	0	100.6
66.4	0.1	0.5	6.2	18.8	7.4	0	99.5
66.4	0.2	0.7	6.5	18.9	6.8	0	99.5
66.5	0.2	0.5	6.1	18.7	7.7	0.1	99.7
66.9	0.2	0.5	6.1	19	7.9	0.1	100.8
67.1	0.2	0.6	6.5	19.2	7.1	0.1	100.8
66.5	0.2	1.3	7.5	19.8	5.1	0	100.5

Table B.1, continued.

SiO_2 (Wt%)	FeO (Wt%)	CaO (Wt%)	Na_2O (Wt%)	Al_2O_3 (Wt%)	K_2O (Wt%)	BaO (Wt%)	Total[a] (Wt%)
66.9	0.2	0.6	6.4	19.1	7.3	0	100.7
66.9	0.2	0.5	6.2	18.9	7.7	0	100.5
66.7	0.1	0.7	6.6	19.1	7.1	0.1	100.4
Sample locality SIW[e]							
66.7	0.2	0.7	6.3	19.1	7.2	0	100.2
67	0.1	0.6	6.3	19.1	7.3	0	100.5
67.1	0.2	0.6	6.4	19.1	7.3	0.1	100.6
66.5	0.1	1.4	7.7	19.9	4.4	0	100.2
66.4	0.1	1.5	8	20.1	4.4	0	100.6
67.1	0.2	0.6	6.3	19.1	7.3	0	100.5
66.7	0.1	0.5	6.1	18.9	7.8	0.1	100.2
66.9	0.1	0.5	6.2	19	7.6	0	100.4
66.9	0.2	0.5	6.2	19	7.7	0.1	100.7
66.7	0.2	1	7.3	19.6	5.6	0.1	100.5
66.4	0.2	1.1	7.3	19.6	5.6	0	100.4
66.4	0.2	1.4	7.9	20	4.6	0	100.5
66.9	0.2	1.3	7.7	19.8	4.8	0.1	100.9
66.4	0.1	1	7.4	19.5	5.4	0	100
66.9	0.1	0.5	6.2	18.9	7.5	0	100.3
Sample locality MC[f]							
65	0.2	1.5	8.1	19.7	3.9	0	98.4
65.2	0.2	1.2	7.7	19.3	4.7	0	98.3
64.8	0.1	1.4	7.9	19.5	4.2	0	98
65.6	0.1	0.6	6.4	18.7	7	0.1	98.5
65.5	0.2	0.6	6.5	18.8	6.9	0.1	98.6
65.1	0.1	1.2	7.4	19.2	4.9	0.1	98.1
65.3	0.1	0.7	6.6	18.8	6.6	0	98.2
64.9	0.2	1.4	8	19.6	4.1	0	98.2
65.1	0.1	1.3	7.8	19.5	4.4	0.1	98.3

Note: Each grouping of 1 to 3 analyses is from a single crystal. Additional microprobe analyses of feldspar from the Tuff of San Felipe published in *Stock et al.* [1999].

[a] Total of measured weight percent. Measurements with totals less than 98% or greater than 102% were discarded.

[b] First 24 analyses: Sample MT-92-14, 30.347° N 115.017° W. Second 19 analyses: Sample MT-92-20, 30.348°N 114.956° W.

[c] Sample number SRB-B316A, 30.849° N 114.963° W.

[d] Sample number SFD-4C, 30.708° N 114.840° W.

[e] Sample number PVPQ-306A, 30.410° N 114.806° W.

[f] Sample number MC-2, 30.529° N 114.968° W.

Table B.2. Microprobe analyses of feldspar, Tuff of San Felipe, Sonora.

SiO_2 (Wt%)	FeO (Wt%)	CaO (Wt%)	Na_2O (Wt%)	Al_2O_3 (Wt%)	K_2O (Wt%)	BaO (Wt%)	Total[a] (Wt%)
Sample locality BK[b]							
66.2	0.2	1.3	8	20.1	4.4	0.1	100.2
66.5	0.2	1.1	7.4	19.8	5.4	0	100.5
66.3	0.2	1.3	7.7	20.1	4.6	0	100.2
66.5	0.1	1.2	7.5	19.9	5	0	100.4
67.4	0.2	1	7.5	19.8	5.2	0	101.1
67	0.2	1.2	7.7	20	4.7	0	100.8
66.8	0.2	0.9	7	19.7	6.1	0.1	100.7
66.9	0.1	1.4	7.7	20.2	4.5	0	100.9
67.3	0.1	1.1	7.1	19.8	5.7	0	101.2
67.1	0.1	1.4	7.9	20.3	4.5	0	101.3
66.9	0.1	1.2	7.5	19.9	5.1	0	100.8
67	0.2	1.4	7.6	20.2	4.6	0	101
66.9	0.1	1.3	7.5	20.1	5.1	0	101
67.6	0.2	0.8	6.8	19.7	6.5	0.2	101.7
67.6	0.1	0.6	6.4	19.3	7	0	101.2
66.5	0.2	1.1	7.5	19.8	5.3	0	100.3
66.8	0.1	1.4	7.6	20.1	4.7	0	100.6
66.7	0.1	0.7	5.9	19.3	7.7	0.1	100.5
66.4	0.1	1.4	8.2	20.1	3.9	0.1	100.3
66.1	0.1	1.2	7.9	20	4.6	0.2	100.1
66.8	0.1	0.9	7	19.8	6.1	0	100.8
65.4	0.1	1.4	7.7	20.1	4.5	0	99.3
67	0	0.5	6.1	19.3	7.8	0	100.7
66.5	0	1.2	7.4	19.9	5.2	0	100.2
Sample locality PC[c]							
66.5	0.2	1.3	7.7	19.9	4.8	0.1	100.5
66.3	0.2	1.2	7.7	19.7	4.9	0.1	100.1
66.7	0.2	1.4	8.1	19.9	4.5	0	100.7

Table B.2, continued.

SiO_2 (Wt%)	FeO (Wt%)	CaO (Wt%)	Na_2O (Wt%)	Al_2O_3 (Wt%)	K_2O (Wt%)	BaO (Wt%)	Total[a] (Wt%)
Sample locality SM[d]							
67.2	0.1	0.6	6.5	19.3	7.3	0	101.2
66.9	0.2	1.2	7.8	19.9	4.9	0.1	101
67	0.2	0.9	7.4	19.6	5.8	0	100.8
67	0.1	1.2	7.5	19.9	5.1	0	100.9
66.9	0.2	1.4	7.8	20	4.7	0	101
66.8	0.2	1.1	7.6	19.8	5.3	0	100.8
66.5	0.2	1.6	8.1	20.3	4.1	0	100.9
66.5	0.2	1.8	8.4	20.5	3.6	0.1	101
66.8	0.2	1.1	7.4	19.6	5.4	0	100.5
66.4	0.1	0.9	7.1	19.5	6.2	0.1	100.4
66.6	0.2	1.4	7.9	20.1	4.5	0	100.7
65	0.2	1.5	8	20.1	4.2	0.1	99.2
64.4	0.1	1.4	7.9	20	4.6	0.1	98.6
66.6	0.2	1.2	7.7	19.9	5.1	0.1	100.7
66.7	0.1	1.6	8	20.2	3.9	0	100.6
67	0.2	1.2	7.8	19.9	5	0	101.2
67.1	0.1	1	7.4	19.7	5.6	0	100.9
66.7	0.2	1.5	8.1	20.2	4.3	0.1	100.9
66.7	0.1	1.3	8	20	4.6	0.1	100.9
66.8	0.2	0.9	7.1	19.4	6.3	0	100.6
67.5	0.2	0.8	7.2	19.3	6	0.1	101.2
67.2	0.1	0.6	6.7	19.3	7	0	101.1
67.1	0.2	1.2	7.8	19.8	4.8	0	100.9

Note: Each grouping of 2 to 4 analyses is from a single crystal.

[a] Total of measured weight percent. Measurements with totals less than 98% or greater than 102% were discarded.

[b] Sample number BK-98-13, 28.992° N 112.037° W.

[c] Sample number PC-98-18, 29.003° N 112.083° W.

[d] Sample number TIB-98-23, 28.974° N 112.460° W.

Table B.3. Microprobe analyses of pyroxene, Tuff of San Felipe, Baja California.

SiO_2 (Wt%)	MgO (Wt%)	FeO (Wt%)	CaO (Wt%)	Na_2O (Wt%)	TiO_2 (Wt%)	Al_2O_3 (Wt%)	MnO (Wt%)	Total[a] (Wt%)
Sample locality MA[b]								
49.6	2.6	27.1	19.9	0.3	0.2	0.4	0.9	101.2
49	2.7	27.1	19.7	0.3	0.2	0.4	1	100.4
49.7	2.8	26.4	19.9	0.3	0.2	0.4	1	100.8
49.3	2.8	27.2	19.6	0.3	0.1	0.4	1	100.9
49.3	2.8	27	19.8	0.3	0.2	0.4	1	100.8
49.5	2.8	27.4	19.4	0.4	0.2	0.4	1	101.1
49.6	3	26.4	19.9	0.3	0.1	0.4	1	100.9
49.4	2.8	26.9	19.8	0.3	0.2	0.4	0.9	100.7
49.6	2.7	26.7	19.6	0.3	0.1	0.4	1	100.5
49.6	2.9	26.7	19.8	0.4	0.2	0.4	0.9	101
49.3	2.9	26.7	19.3	0.4	0.1	0.5	1	100.3
49.3	2.7	27.5	19	0.3	0.2	0.5	1.1	100.5
49.5	2.8	26.9	19.5	0.4	0.2	0.4	1	100.8
49.4	2.9	27.2	19.6	0.3	0.2	0.5	1	101.2
49.2	2.7	27.8	19	0.4	0.2	0.5	1	100.7
49.5	3	26.5	19.8	0.3	0.2	0.4	0.9	100.7
49.5	2.9	26.9	19.7	0.3	0.2	0.4	0.9	100.9
49.6	2.8	26.9	19.6	0.3	0.1	0.4	1	100.8
49.8	2.9	26.5	19.9	0.3	0.1	0.4	1	101
49.4	2.7	27.3	19.5	0.4	0.2	0.4	1	100.9
49.5	2.7	26.9	19.5	0.3	0.2	0.4	1	100.6
49.5	2.9	26.9	19.6	0.4	0.1	0.4	1	100.9
49.3	7.4	39.4	1.7	0.1	0.1	0.6	1.6	100.2
50.1	5.3	22.8	19.4	0.4	0.2	0.6	0.9	99.9
49.7	2.6	27.5	19.8	0.3	0.2	0.4	1	101.5
48.9	2.3	27.8	19.5	0.3	0.2	0.5	0.9	100.6
49.5	2.7	26.8	19.9	0.3	0.2	0.4	0.9	100.8
49.3	2.7	27.1	19.5	0.4	0.2	0.4	0.9	100.5
49.2	2.6	27.2	19.8	0.3	0.1	0.4	0.9	100.6
48.9	2.1	27	19.8	0.3	0.1	0.4	0.8	99.6
49.2	2.8	24.8	19.7	0.3	0.2	0.4	0.7	98.1
49.4	3	24.3	19.8	0.3	0.2	0.4	0.7	98.1

Table B.3, continued.

SiO_2 (Wt%)	MgO (Wt%)	FeO (Wt%)	CaO (Wt%)	Na_2O (Wt%)	TiO_2 (Wt%)	Al_2O_3 (Wt%)	MnO (Wt%)	Total[a] (Wt%)
48.5	1.6	26.4	19.2	0.4	0.3	0.6	0.9	98.1
48.4	1.5	28.6	18.9	0.4	0.4	0.7	1.2	100.3
49.3	2.7	26.4	19.5	0.4	0.2	0.4	0.9	99.9
49.3	2.9	26.3	19.4	0.3	0.2	0.5	0.9	100
49.5	2.9	24.5	19.2	0.3	0.2	0.6	1	98.3
49.3	2.9	23.1	19.7	0.3	0.2	0.4	1	97
Sample locality SRB[c]								
49.3	2.7	27.4	19.8	0.3	0.2	0.4	1	101.2
49.5	2.9	27.3	18.7	0.4	0.2	0.5	0.9	100.4
49	2.8	27.6	19.1	0.4	0.2	0.4	0.9	100.4
48.8	2.3	27.8	17.1	0.8	0.2	0.5	0.9	98.6
49	2.4	28.3	18.5	0.5	0.2	0.4	0.9	100.4
50.4	7.6	19.8	19.8	0.4	0.3	0.9	1	100.3
50.7	7.6	20.1	19.6	0.4	0.4	0.8	1.1	100.7
50.4	7.5	19.8	19.7	0.4	0.4	0.8	1	100
51.2	9.4	17.6	19.5	0.4	0.4	1	0.9	100.4
51.3	9.5	18.2	19.5	0.4	0.4	0.9	0.9	101.2
51.4	9.6	17.2	19.4	0.4	0.5	1	0.9	100.5
49.2	2.4	29	16.8	0.7	0.2	0.7	0.8	100.1
Sample Locality SFD[d]								
49.1	2.7	27.4	19.9	0.3	0.2	0.5	1	101.1
49.2	2.7	27.6	20	0.3	0.2	0.4	1	101.5
49.3	2.8	27.5	19.8	0.3	0.2	0.4	0.9	101.4
49.2	2.9	27.8	19.8	0.3	0.2	0.5	0.9	101.6
49.3	2.7	27.6	19.8	0.3	0.2	0.4	0.9	101.2
49.3	3	28	19.6	0.4	0.2	0.4	0.9	101.8
49	2.6	27.8	18.7	0.4	0.2	1	1	100.7
49.2	2.8	27.3	19.8	0.3	0.2	0.4	1	101.1
49.4	2.8	27.2	19.6	0.3	0.2	0.4	1	101.1
49.4	3	27.3	19.8	0.3	0.2	0.4	1	101.4
49.3	2.9	27.5	19.4	0.4	0.1	0.6	1	101.2

Table B.3, continued.

SiO_2 (Wt%)	MgO (Wt%)	FeO (Wt%)	CaO (Wt%)	Na_2O (Wt%)	TiO_2 (Wt%)	Al_2O_3 (Wt%)	MnO (Wt%)	Total[a] (Wt%)
Sample locality SIW[e]								
49.4	2.7	27.4	20	0.3	0.2	0.4	1	101.4
49.1	2.9	26.9	19.8	0.4	0.2	0.5	1	100.7
49.3	2.9	27.8	19.7	0.3	0.2	0.4	0.9	101.7
49.5	2.7	27.7	19.6	0.3	0.2	0.5	1	101.5
49.3	2.7	28	19.5	0.3	0.1	0.5	1	101.5
49.5	2.7	28.1	19.6	0.3	0.2	0.4	1	101.9
52.5	19.4	27.7	0.8	0	0.1	0.4	0.6	101.7
52.1	19.1	26.5	1.5	0	0.2	0.8	0.6	100.9
53.4	16.7	25.8	0.8	0.1	0.1	0.8	0.6	98.4
48.5	2.6	27.4	19.8	0.3	0.2	0.5	1	100.4
48.7	2.8	26.7	19.9	0.3	0.1	0.4	0.9	99.8
48.8	2.8	26.2	20	0.3	0.2	0.4	0.9	99.8
Sample locality MC[f]								
48.1	3	26.6	18.7	0.3	0.1	0.4	1	98.3
48.3	3.1	25.8	19.2	0.3	0.2	0.4	0.9	98.3
47.9	3.1	26.3	19.2	0.4	0.1	0.4	1	98.4

Note: Each grouping of 1 to 4 analyses is from a single crystal.

[a] Total of measured weight percent. Measurements with totals less than 98% or greater than 102% were discarded.

[b] First 22 analyses: Sample MT-92-14, 30.347° N 115.017° W. Second 16 analyses: Sample MT-92-20, 30.348°N 114.956° W.

[c] Sample number SRB-B316A, 30.849° N 114.963° W.

[d] Sample number SFD-4C, 30.708° N 114.840° W.

[e] Sample number PVPQ-306A, 30.410° N 114.806° W.

[f] Sample number MC-2, 30.529° N 114.968° W.

Table B.4. Microprobe analyses of pyroxene, Tuff of San Felipe, Sonora.

SiO_2 (Wt%)	MgO (Wt%)	FeO (Wt%)	CaO (Wt%)	Na_2O (Wt%)	TiO_2 (Wt%)	Al_2O_3 (Wt%)	MnO (Wt%)	Total[a] (Wt%)
Sample locality BK[b]								
48.4	2.7	26.9	19.4	0.3	0.2	0.4	0.9	99.2
48.4	2.6	27.4	19.4	0.4	0.2	0.5	0.9	99.8
48.6	2.7	26.9	19.1	0.3	0.2	0.4	1	99.2
48.7	2.8	26.7	19.7	0.4	0.2	0.4	1	99.9
48.7	2.7	26.4	19.4	0.3	0.2	0.4	0.9	99.2
49.9	3.6	24.9	19.1	0.3	0.2	1	1	100.2
49.2	2.7	26.6	19.3	0.3	0.1	0.5	1.1	100
49.3	3	25.5	19.9	0.3	0.2	0.4	1	99.8
49.4	2.6	26.8	20.1	0.3	0.1	0.4	0.9	100.8
49.2	2.6	27.1	19.8	0.3	0.2	0.5	1	101
49.1	2.6	26.6	20.1	0.3	0.2	0.4	1	100.3
50.5	6	21.6	20.1	0.4	0.2	0.7	1	100.5
49.3	3.1	25.7	19.9	0.3	0.2	0.4	1	100.1
48.5	2.8	25.9	19.8	0.3	0.2	0.4	1.1	99.1
48.4	2.7	26.8	20	0.3	0.2	0.4	1.1	99.9
49	2.7	26.4	20	0.3	0.2	0.4	1.1	100
49.1	2.8	26.4	19.9	0.3	0.2	0.4	1.1	100.3
49.3	2.6	27.1	20	0.3	0.2	0.5	1.1	101
49.4	2.6	27.5	19.6	0.4	0.2	0.5	1.1	101.4
49.6	2.9	26.2	20	0.3	0.2	0.4	1.1	100.8
49	2.7	26.7	20	0.3	0.1	0.4	1.1	100.4
49	2.7	26.5	19.9	0.4	0.2	0.4	1	100.1
49.1	2.7	26.4	20	0.3	0.2	0.4	1	100.3

Table B.4, continued.

SiO_2 (Wt%)	MgO (Wt%)	FeO (Wt%)	CaO (Wt%)	Na_2O (Wt%)	TiO_2 (Wt%)	Al_2O_3 (Wt%)	MnO (Wt%)	Total[a] (Wt%)
Sample locality PC[c]								
48.7	2.3	27.9	19.2	0.4	0.2	0.5	1	100.2
48.6	2.6	27.5	19.6	0.3	0.2	0.4	1	100.1
48.6	2.5	27.5	19.5	0.4	0.3	0.5	0.9	100.3
Sample locality SM[d]								
49.4	2.7	27.1	19.6	0.4	0.2	0.5	1	100.8
49.4	2.7	27.3	19.5	0.3	0.2	0.4	1	100.8
49.8	2.7	27.2	19	0.4	0.2	0.5	1	100.9
49.4	2.9	27.2	19.4	0.3	0.2	0.4	1	100.8
49.4	2.9	26.9	19.6	0.3	0.2	0.4	0.9	100.7
49.2	2.8	27	19.3	0.4	0.2	0.4	1.1	100.4
49.3	2.6	27.8	19.3	0.3	0.2	0.5	1	100.9
49.1	2.8	27	19.6	0.3	0.2	0.4	1	100.5
49	2.8	27.1	19.5	0.4	0.2	0.4	1	100.3
48.7	3	26.4	19.2	0.3	0.1	0.6	1	99.4
49	2.9	27.1	19.2	0.3	0.2	0.4	1	100.2
49.1	2.8	27	19.4	0.3	0.2	0.5	1	100.4
49.1	3.1	27.1	19.1	0.4	0.2	0.4	1	100.3
49	2.6	27.4	19.4	0.3	0.2	0.4	1	100.3
49.3	2.7	27.6	19.2	0.4	0.2	0.4	1	100.8
49.1	2.7	27.5	19.3	0.4	0.1	0.4	0.9	100.6
49.2	3	27	19.5	0.3	0.2	0.4	0.9	100.5

Note: Each grouping of 2 to 3 analyses is from a single crystal.

[a] Total of measured weight percent. Measurements with totals less than 98% or greater than 102% were discarded.

[b] First group (3 analyses): Sample BK-98-03, 28.883° N 112.008° W. Second group (20 analyses): Sample BK-98-13, 28.992°N 112.037°W.

[c] Sample number PC-98-18, 29.003° N 112.083° W.

[d] Sample number TIB-98-23, 28.974° N 112.460° W.

Table B.5. Microprobe analyses of feldspar, Tmr3 ignimbrite, Baja California.

SiO_2 (Wt%)	FeO (Wt%)	CaO (Wt%)	Na_2O (Wt%)	Al_2O_3 (Wt%)	K_2O (Wt%)	BaO (Wt%)	Total[a] (Wt%)
Sample locality VC[b]							
67.8	0.2	0.4	7.7	19.5	5.9	0.3	101.9
68	0.2	0.4	7.6	19.3	5.9	0.3	101.7
68	0.2	0.5	8	19.5	5.4	0.5	102
68.1	0.2	0.5	7.8	19.5	5.6	0.2	101.8
68	0.2	0.4	7.6	19.4	5.9	0.4	101.8
68.1	0.2	0.3	7.5	19.4	6.1	0.2	101.9
67.3	0.2	0.4	7.6	19.4	5.6	0.4	100.9
66.7	0.2	0.5	7.8	19.2	5.5	0.3	100.1
66.8	0.2	0.5	7.5	19.4	5.5	0.4	100.4
67.2	0.2	0.5	7.6	19.3	5.6	0.4	100.7
63.1	0.1	4.9	8.7	23.6	0.8	0.3	101.4
60.3	0.2	6.4	8	24.7	0.6	0.2	100.3
67.4	0.2	0.5	8	19.2	5.1	0.5	100.8
66.7	0.2	0.9	8.4	19.7	4.2	0.3	100.4
62.1	0.2	5	8.5	23.4	0.8	0.3	100.2
62.2	0.2	4.9	8.5	23.4	0.7	0.4	100.4
Sample locality SFE[c]							
64.2	0.1	1.6	8.8	20.7	3.1	0.7	99.3
63.9	0.1	1	7.6	20.1	4.9	1.4	99.1
64.4	0.1	1.3	8.7	20.5	3.5	1.3	99.7
66.2	0.1	0.3	7.6	19	5.9	0.3	99.4
65.7	0.1	0.4	7.6	19.2	5.9	0.3	99.3
65.7	0.2	0.3	7.6	19.1	6	0.3	99.1
65.2	0.1	0.6	8.3	19.5	4.6	0.3	98.8
65.7	0.2	0.3	7.7	19.2	5.8	0.3	99.2
65.8	0.2	0.4	8.1	19.3	5.2	0.4	99.3

Table B.5, continued.

SiO_2 (Wt%)	FeO (Wt%)	CaO (Wt%)	Na_2O (Wt%)	Al_2O_3 (Wt%)	K_2O (Wt%)	BaO (Wt%)	Total[a] (Wt%)
Sample Locality SIW[d]							
66.8	0.2	0.3	7.5	19.5	6.1	0.4	100.9
66.2	0.2	0.4	7.7	19.5	5.8	0.3	100.1
66.6	0.1	0.4	7.8	19.5	6	0.2	100.6
66.8	0.2	0.3	7.6	19.4	6.3	0.2	100.9
66.8	0.2	0.3	7.6	19.4	6.2	0.3	100.7
66.6	0.2	0.3	7.3	19.3	6.5	0.2	100.5
65.9	0.2	0.3	7.3	19.1	6.3	0.3	99.5
65.8	0.2	0.3	7.2	19.2	6.4	0.2	99.2

Note: Each grouping of 1 to 3 analyses is from a single crystal.

[a] Total of measured weight percent. Measurements with totals less than 98% or greater than 102% were discarded.

[b] Sample number VC-86-148, 30.523° N 115.102° W.

[c] Sample number SF-00-11, 30.649° N 114.856° W.

[d] Sample number PVPL-231A, 30.384°N, 114.917° W.

Table B.6. Microprobe analyses of feldspar, Tmr3 ignimbrite, Sonora.

SiO_2 (Wt%)	FeO (Wt%)	CaO (Wt%)	Na_2O (Wt%)	Al_2O_3 (Wt%)	K_2O (Wt%)	BaO (Wt%)	Total[a] (Wt%)
Sample locality SM[b]							
67.7	0.2	0.3	7.5	19.1	6.4	0.3	101.5
67.9	0.2	0.3	7.5	18.8	6.5	0.2	101.3
68	0.2	0.3	7.4	19.1	6.5	0.2	101.6
67	0.2	0.3	7.4	18.9	6.2	0.4	100.5
66.6	0.2	0.8	8.1	19.6	4.9	0.7	100.9
66.4	0.2	0.5	7.9	19.2	5.3	0.5	100.1
66.7	0.2	0.6	8.2	19.5	4.8	0.4	100.5
66.9	0.2	0.3	7.4	18.9	6.6	0.3	100.4
66.8	0.2	0.3	7.3	18.9	6.4	0.2	100.1
67.1	0.2	0.3	7.5	18.9	6.2	0.3	100.5
66.8	0.2	0.3	7.2	18.6	6.4	0.2	99.7
66.8	0.2	0.3	7.3	18.7	6.5	0.2	100
66.8	0.1	0.3	7.4	18.9	6.3	0.2	100
66.4	0.2	0.3	7.4	18.9	6.3	0.3	99.8
67.3	0.2	0.3	7.5	18.9	6.2	0.3	100.7
66.5	0.1	0.7	8.3	19.3	4.9	0.4	100.2
64.9	0.2	0.4	7.4	19	5.9	0.3	98.1
65.1	0.1	0.3	7.3	18.8	6	0.3	98
65	0.2	0.5	7.6	19.1	5.5	0.4	98.4
65.3	0.2	0.4	7.5	18.9	5.7	0.3	98.2
65.4	0.2	0.4	7.6	19	5.7	0.2	98.4
65.2	0.2	0.3	7.2	18.9	6.3	0.3	98.5
65.4	0.2	0.3	7.3	18.9	6.2	0.3	98.6
65.5	0.2	0.3	7.4	19	6.2	0.3	98.8
66.1	0.2	0.3	7.6	19	6	0.2	99.3
66	0.2	0.3	7.5	19.1	5.9	0.3	99.3
65.9	0.2	0.3	7.5	19.2	6	0.3	99.4

Table B.6, continued.

SiO_2 (Wt%)	FeO (Wt%)	CaO (Wt%)	Na_2O (Wt%)	Al_2O_3 (Wt%)	K_2O (Wt%)	BaO (Wt%)	Total[a] (Wt%)
Sample locality PR[c]							
67	0.2	0.3	7.3	19.3	6.5	0.4	100.9
66.9	0.2	0.4	7.6	19.5	6	0.3	100.8
67	0.1	0.4	7.7	19.6	5.7	0.2	100.9
66.5	0.2	0.3	7.4	19.3	6.2	0.3	100.1
66.3	0.2	0.4	7.8	19.6	5.4	0.3	100.1
66.2	0.2	0.4	7.8	19.4	5.6	0.4	99.9
65.9	0.1	0.4	7.6	19.2	5.6	0.3	99.2
65.7	0.2	0.5	7.7	19.5	5.2	0.4	99.3
66	0.1	0.4	7.7	19.2	5.4	0.3	99.1
Sample Locality SK[d]							
66.5	0.2	0.3	7.3	19.2	6.4	0.4	100.3
66.6	0.2	0.3	7.4	19.4	6.2	0.2	100.5
66.6	0.2	0.4	7.9	19.6	5.4	0.4	100.6
67.3	0.2	0.3	7.5	19	5.6	0.4	100.3
66.6	0.2	0.4	7.8	19.6	5.5	0.3	100.4
66.7	0.2	0.3	7.4	19.4	6.3	0.3	100.6
66.6	0.2	0.3	7.6	19.4	5.8	0.2	100
66.5	0.2	0.4	8.2	19.6	5	0.3	100.2
66.4	0.2	0.5	8.2	19.8	4.8	0.4	100.3
65.9	0.2	0.3	7.4	18.9	5.8	0.3	98.9
65.7	0.2	0.3	7.3	19	5.8	0.2	98.5
65.7	0.2	0.3	7.5	19.1	5.7	0.2	98.7
65.7	0.2	0.4	7.5	19	5.7	0.4	98.9
65.5	0.2	0.4	7.9	19	5.1	0.3	98.4
65.7	0.2	0.3	7.5	18.8	5.8	0.3	98.7

Note: Each grouping of 1 to 3 analyses is from a single crystal.

[a] Total of measured weight percent. Measurements with totals less than 98% or greater than 102% were discarded.

[b] First 16 analyses: Sample TIB-98-12, 28.979° N 112.458° W. Second 11 analyses: Sample BV-99-08: 28.924°N, 112.446° W.

[c] Sample number PRS-309, 29.052° N 112.500° W.

[d] Sample number BA-99-13, 29.171° N 112.358° W.

Table B.7. Microprobe analyses of pyroxene, Tmr3 ignimbrite, Baja California.

SiO_2 (Wt%)	MgO (Wt%)	FeO (Wt%)	CaO (Wt%)	Na_2O (Wt%)	TiO_2 (Wt%)	Al_2O_3 (Wt%)	MnO (Wt%)	Total[a] (Wt%)
Sample locality VC[b]								
49.6	3.5	26.8	19.4	0.5	0.2	0.3	0.7	101
49.2	2.5	28.4	19.3	0.6	0.3	0.3	0.7	101.3
49.4	2.6	28.3	19.3	0.5	0.1	0.2	0.8	101.3
52.7	18.5	26.9	1.6	0	0.2	0.7	0.7	101.4
52.9	19.4	25	1.5	0	0.2	1	0.7	100.9
51.1	15.2	31.4	1.5	0	0.3	0.8	0.9	101.4
49	7.4	41.7	1.6	0	0.1	0.2	1.3	101.5
50.3	4.1	26.3	19.4	0.5	0.2	0.4	0.7	101.9
50.6	6.9	22.8	18.4	0.5	0.4	1.1	0.8	101.5
50.2	6.3	23.1	19	0.4	0.2	0.5	0.7	100.6
50.3	6.7	23.5	18.4	0.3	0.2	0.5	0.7	100.6
50.6	6.7	22.6	19.2	0.4	0.1	0.5	0.7	100.9
50.8	7.6	21.8	18.7	0.4	0.2	0.7	0.7	100.9
50.6	6.5	22.9	19.3	0.4	0.1	0.5	0.7	101.2
50.6	7.8	22.8	18	0.4	0.3	0.7	0.7	101.3
50.4	6.7	23.8	18.5	0.4	0.2	0.6	0.7	101.5
49.8	3	27.3	19.6	0.5	0.2	0.3	0.7	101.5
50.1	3.2	26.8	19.3	0.5	0.1	0.5	0.6	101.2
48.5	7.3	41.4	1.4	0	0.2	0.2	1.3	100.3
48.8	7.6	40.3	1.8	0	0.1	0.1	1.3	100.2
50.3	5.7	24.1	19.2	0.5	0.2	0.4	0.8	101.2
49.5	3.9	26.4	19.4	0.5	0.1	0.3	0.7	100.8
49.7	3.8	26.2	19.6	0.5	0.1	0.3	0.7	100.9
49.5	10.8	37.1	1.3	0	0.1	0.4	1	100.3
49.2	9.5	39.1	1.2	0	0.1	0.4	1.1	100.6
49.6	3.4	27.1	19.6	0.5	0.1	0.3	0.7	101.3
49.9	3.4	27.2	19.6	0.5	0.2	0.3	0.8	101.8
49.7	3.2	27.4	19.6	0.5	0.2	0.3	0.7	101.6
49.7	3.2	27.5	19.7	0.5	0.1	0.3	0.7	101.8
49.7	4.1	26.5	19.4	0.5	0.1	0.4	0.7	101.5
49.4	9.2	39.3	1.3	0.1	0.1	0.4	1.2	101.2
49.1	8.1	41.1	1.3	0	0.1	0.2	1.3	101.3
49.8	7.7	36.2	5.8	0.2	0.1	0.3	1.1	101.1
49.9	2.9	27.7	19.9	0.5	0.2	0.3	0.7	102
49.4	3.3	26.7	19.3	0.5	0.1	0.3	0.7	100.4

Table B.7, continued.

SiO_2 (Wt%)	MgO (Wt%)	FeO (Wt%)	CaO (Wt%)	Na_2O (Wt%)	TiO_2 (Wt%)	Al_2O_3 (Wt%)	MnO (Wt%)	Total[a] (Wt%)
49.1	2.8	27.6	19.2	0.5	0.2	0.3	0.7	100.5
49.5	3.4	26.5	19.7	0.5	0.2	0.3	0.7	100.7
49.3	2.9	27.4	20	0.5	0.2	0.3	0.7	101.2
48.5	3.3	27	19.3	0.5	0.1	0.4	0.7	100
49.8	2.7	27.4	19.9	0.5	0.1	0.2	0.8	101.6
49.9	2.9	27.3	19.6	0.5	0.1	0.3	0.7	101.4
49.6	3	27.4	18.7	0.5	0.1	0.4	0.7	100.5
50.7	7.5	21.5	19.1	0.3	0.2	0.6	0.6	100.6
49.8	6.4	22.8	19.1	0.4	0.1	0.6	0.6	99.9
49	3.8	25.9	19	0.4	0.2	0.4	0.7	99.4
49.9	5	23.9	19.2	0.5	0.2	0.6	0.7	100
48.7	5.9	23.9	18.5	0.5	0.2	0.6	0.6	99.1
Sample locality SF[c]								
49.5	4.3	26.4	19.8	0.5	0.2	0.4	0.7	101.8
49.1	3.6	27.1	19.7	0.5	0.2	0.3	0.8	101.4
49.2	3.8	26.5	19.6	0.5	0.1	0.3	0.7	100.8
48.8	9.6	40.1	1.4	0	0.2	0.2	1.5	101.8
48.6	9	40	1.5	0	0.2	0.2	1.4	101
48.6	8.5	40.5	1.5	0	0.1	0.2	1.3	100.8
49	3.9	27.4	19.6	0.5	0.1	0.3	0.7	101.5
48.4	3.7	26.6	19.5	0.5	0.2	0.3	0.8	99.9
47.9	2.7	27.6	19.6	0.5	0.2	0.2	0.7	99.7
48.6	2.7	27.8	20	0.5	0.2	0.2	0.7	100.7
48.6	3.2	27	19.6	0.5	0.1	0.3	0.8	100.2
48.6	3.5	27.3	19.1	0.5	0.1	0.3	0.7	100.2
48.3	3.7	26.9	19.2	0.5	0.2	0.3	0.7	99.9
48.5	4	26.3	19.3	0.5	0.2	0.3	0.7	99.8
48.6	3.9	26.6	19.3	0.5	0.1	0.3	0.7	100
48.4	3.3	27.1	19.3	0.5	0.1	0.3	0.7	99.8

Table B.7, continued.

SiO_2 (Wt%)	MgO (Wt%)	FeO (Wt%)	CaO (Wt%)	Na_2O (Wt%)	TiO_2 (Wt%)	Al_2O_3 (Wt%)	MnO (Wt%)	Total[a] (Wt%)
Sample locality SIW[d]								
48.7	3.6	27	19.4	0.5	0.1	0.3	0.7	100.4
48.7	3.7	27	19.4	0.4	0.2	0.3	0.7	100.5
48.7	3.9	26.5	19.3	0.5	0.1	0.3	0.7	100
48.8	10.8	37	1.4	0	0.1	0.2	1.1	99.7
47.6	7.6	41.3	1.9	0	0.2	0.4	1.3	100.1
48.8	3.9	26.1	19.3	0.5	0.2	0.3	0.8	99.8
48.9	4	26.3	19.1	0.5	0.1	0.3	0.7	100
49.7	12.6	35.4	1.3	0	0.1	0.4	1.1	100.7
49.9	6.7	24.2	18.4	0.4	0.2	0.5	0.8	101.1
49.6	5	25.9	19.3	0.5	0.2	0.4	0.8	101.6
49.6	3.9	26.6	19.7	0.5	0.1	0.3	0.8	101.4
49.2	9.5	40	1.4	0	0.1	0.2	1.3	101.9
49	9.2	40.3	1.5	0	0.1	0.2	1.4	101.9
48.3	7.9	41.9	1.4	0	0.1	0.2	1.3	101.3
49.6	4.6	26.6	19.2	0.5	0.1	0.3	0.8	101.8
49.4	3.9	26.8	19.7	0.5	0.1	0.3	0.7	101.5
49.4	3.6	27	19.9	0.4	0.2	0.3	0.8	101.8

Note: Each grouping of 2 to 10 analyses is from a single crystal.

[a] Total of measured weight percent. Measurements with totals less than 98% or greater than 102% were discarded.

[b] Sample number VC-86-148, 30.523° N 115.102° W.

[c] Sample number SF-00-11, 30.649° N 114.856° W.

[d] Sample number PVPL-231A, Tmr3-type II, 30.384°N, 114.917° W.

Table B.8. Microprobe analyses of pyroxene, Tmr3 ignimbrite, Sonora.

SiO_2 (Wt%)	MgO (Wt%)	FeO (Wt%)	CaO (Wt%)	Na_2O (Wt%)	TiO_2 (Wt%)	Al_2O_3 (Wt%)	MnO (Wt%)	Total[a] (Wt%)
Sample locality SM[b]								
48.9	3.3	26.4	19.7	0.5	0.2	0.3	0.7	99.8
49.8	4.1	25.8	20	0.4	0.2	0.3	0.7	101.4
49.6	2.2	27.1	19	0.5	0.2	0.6	0.7	100
49.8	3.9	26.2	19.6	0.5	0.1	0.3	0.8	101.3
49.3	3.1	27	19.6	0.5	0.2	0.3	0.7	100.9
49.7	3.8	26.5	19.6	0.5	0.1	0.3	0.7	101.3
49.5	3.8	26	19.6	0.5	0.1	0.3	0.7	100.6
49.5	4.6	26.4	19.6	0.5	0.1	0.3	0.7	101.7
49.8	3.9	27	19.6	0.5	0.2	0.3	0.7	101.9
49.4	3.7	26.4	19.5	0.5	0.2	0.3	0.7	100.9
48.8	12.2	36.3	1	0	0.2	0.9	1	100.4
47.4	7.3	42.7	1.3	0	0.2	0.3	1.4	100.6
48.8	3.8	27.3	19.6	0.5	0.2	0.3	0.7	101.2
48.9	3.3	27.5	19.7	0.5	0.1	0.3	0.7	101.1
47.8	3.9	26.8	19.3	0.5	0.1	0.3	0.7	99.5
48.8	9.2	40.5	1.3	0	0.1	0.2	1.3	101.6
49.2	9.7	39.7	1.4	0	0.1	0.2	1.4	101.9
48.7	8.6	41.3	1.4	0	0.1	0.2	1.4	101.8
49.5	4.4	27.2	18.8	0.5	0.1	0.3	0.8	101.6
49.3	3.9	26.9	19.6	0.5	0.2	0.3	0.7	101.4
48.7	10.3	39.3	1	0	0.1	0.7	1.1	101.4
49.3	12.1	36.8	1	0	0.2	0.8	1	101.3
49	3.3	26.4	19.2	0.5	0.2	0.3	0.8	99.8
48.6	2.4	27.8	19.5	0.5	0.2	0.2	0.7	100
48.5	2.5	27.8	19.4	0.5	0.2	0.2	0.8	99.8
48.2	3.8	25.9	18.9	0.5	0.1	0.3	0.7	98.6
48.3	3.6	25.9	18.8	0.4	0.1	0.3	0.7	98.2
48.5	3.9	25.6	19.1	0.4	0.2	0.3	0.7	98.8
48.4	3.8	25.1	19.2	0.5	0.1	0.3	0.7	98.2
47.8	2.6	27	19.2	0.5	0.2	0.2	0.7	98.3
47.9	2.7	26.7	19	0.6	0.2	0.3	0.7	98.1
48.8	3.2	26.6	19.1	0.5	0.2	0.3	0.6	99.3
48.8	2.8	27	19.5	0.5	0.2	0.3	0.7	99.7
48.8	3.5	26.2	19.5	0.5	0.1	0.3	0.6	99.5

Table B.8, continued.

SiO_2 (Wt%)	MgO (Wt%)	FeO (Wt%)	CaO (Wt%)	Na_2O (Wt%)	TiO_2 (Wt%)	Al_2O_3 (Wt%)	MnO (Wt%)	Total[a] (Wt%)
Sample locality PR[c]								
48.8	3.9	26.4	19	0.5	0.2	0.3	0.7	99.9
48.5	3.2	27	19.4	0.5	0.1	0.3	0.7	99.8
49.9	6.1	24.1	18.9	0.4	0.2	0.4	0.8	100.9
50	6	24.4	18.8	0.4	0.1	0.4	0.8	101
49.8	5	25.2	19.3	0.4	0.1	0.4	0.7	101
48.9	3.1	27.5	19.5	0.6	0.2	0.3	0.7	100.8
48.6	2.6	28.1	19.8	0.5	0.2	0.2	0.8	100.8
48.5	3.3	27.4	19.9	0.5	0.2	0.3	0.7	100.7
48.9	1.9	29.3	19.5	0.6	0.2	0.2	0.9	101.6
49	2.6	28.1	19.6	0.6	0.2	0.2	0.8	101.1
48.7	3	27.5	19.4	0.5	0.1	0.3	0.8	100.4
48.5	4.1	26	19.1	0.4	0.2	0.4	0.7	99.4
48.4	2.4	27.9	19.6	0.5	0.2	0.2	0.7	100
48.3	2.2	28.4	19.8	0.6	0.2	0.2	0.8	100.5
48.1	3.2	26.3	19.1	0.5	0.2	0.3	0.7	98.6
48.8	3.9	26.6	19	0.5	0.1	0.3	0.8	100.1
48.6	3.9	26.4	19	0.5	0.2	0.3	0.8	99.7
48.9	4.7	25.6	18.9	0.5	0.2	0.4	0.8	99.9
49	4.2	26.1	19.4	0.4	0.1	0.3	0.7	100.3
49.2	4.6	25.7	19.1	0.5	0.2	0.4	0.8	100.6

Table B.8, continued.

SiO_2 (Wt%)	MgO (Wt%)	FeO (Wt%)	CaO (Wt%)	Na_2O (Wt%)	TiO_2 (Wt%)	Al_2O_3 (Wt%)	MnO (Wt%)	Total[a] (Wt%)
Sample Locality SK[d]								
47.9	2.3	28.9	18.5	0.5	0.2	0.3	0.8	99.4
48.6	2.7	27.6	19.3	0.5	0.1	0.3	0.8	99.8
48.7	3.9	26	19.1	0.5	0.2	0.3	0.7	99.4
48.2	4	25.4	19.2	0.4	0.2	0.3	0.7	98.5
49.2	4.6	25.4	18.9	0.4	0.1	0.5	0.7	99.8
48.9	4	26	19.1	0.4	0.1	0.4	0.7	99.9
49.3	3.7	26.1	19.3	0.5	0.1	0.3	0.7	100
49.2	3.4	26.8	19.1	0.5	0.1	0.3	0.7	100.3
49	3.3	26.5	19.6	0.5	0.1	0.3	0.7	100
49	2.9	27.4	19.5	0.5	0.1	0.3	0.8	100.5
48.8	2.6	27.6	19.2	0.6	0.2	0.3	0.7	99.9
48.3	2.8	27.2	19.1	0.5	0.1	0.3	0.8	99
48.4	3	27.2	19.1	0.5	0.2	0.3	0.7	99.3
47.1	6.5	41.7	1.6	0	0.1	0.2	1.4	98.5
48.2	3.1	26.8	19.4	0.4	0.1	0.2	0.7	99
48.3	3.5	26.7	19.3	0.5	0.2	0.3	0.7	99.4
48.5	3.4	26.7	19.3	0.5	0.2	0.3	0.7	99.6
48.3	3.2	26.5	19.7	0.5	0.1	0.3	0.8	99.4

Note: Each grouping of 1 to 5 analyses is from a single crystal.

[a] Total of measured weight percent. Measurements with totals less than 98% or greater than 102% were discarded.

[b] First 22 analyses: Sample TIB-98-12, 28.979° N 112.457° W. Second 13 analyses: Sample BV-99-08: 28.924°N, 112.446° W.

[c] Sample number PRS-309, 29.052° N 112.500° W.

[d] Sample number BA-99-13, 29.171° N 112.358° W.

Table B.9. Microprobe analyses of olivine, Tmr3 ignimbrite, Baja California and Sonora.

MgO (Wt%)	SiO_2 (Wt%)	CaO (Wt%)	TiO_2 (Wt%)	MnO (Wt%)	FeO (Wt%)	Total[a] (Wt%)	Fo[b]	Fa[b]
Sample Locality SF[c]								
2.7	28.6	0.2	0.0	3.0	64.3	99.1	0.07	0.90
2.6	30.0	0.2	0.0	1.9	66.9	101.6	0.06	0.93
2.7	29.9	0.2	0.1	2.1	67.0	102.0	0.07	0.93
Sample Locality SM[d]								
2.3	30.3	0.2	0.0	1.9	66.9	101.7	0.06	0.93
2.3	29.6	0.2	0.0	1.9	66.9	101.0	0.06	0.93
2.4	29.8	0.2	0.0	1.9	65.7	100.0	0.06	0.91
2.4	29.8	0.2	0.0	1.9	65.8	100.1	0.06	0.92
2.4	30.0	0.2	0.0	1.8	65.6	99.9	0.06	0.91
2.6	29.7	0.2	0.0	1.7	64.9	99.2	0.06	0.90
2.8	29.8	0.3	0.0	2.0	63.8	98.7	0.07	0.89
2.5	30.0	0.2	0.0	1.8	65.4	99.9	0.06	0.91
2.5	29.9	0.2	0.0	1.8	65.2	99.6	0.06	0.91
2.4	30.0	0.2	0.0	1.9	65.7	100.2	0.06	0.91
Sample Locality SK[e]								
2.3	29.6	0.2	0.0	1.8	65.3	99.2	0.06	0.91
2.3	29.7	0.2	0.0	1.9	65.6	99.7	0.06	0.91
2.4	29.6	0.2	0.0	2.0	65.0	99.4	0.06	0.91
2.3	29.7	0.2	0.1	1.9	66.3	100.6	0.06	0.92
2.4	29.7	0.2	0.0	1.9	65.2	99.4	0.06	0.91
2.4	29.7	0.2	0.0	1.9	65.3	99.5	0.06	0.91
2.4	29.9	0.2	0.0	1.8	65.2	99.5	0.06	0.91
2.4	29.9	0.2	0.0	1.9	65.5	99.9	0.06	0.91
2.3	29.8	0.2	0.0	1.8	64.9	99.1	0.06	0.90

Note: Each grouping of 1 to 3 analyses is from a single crystal.

[a] Total of measured weight percent. Measurements with totals less than 98% or greater than 102% were discarded.

[b] Fraction of Forserite (Fo) and Fayalite (Fa) olivine end members.

[c] First 2 analyses: Sample TIB-98-12, 28.979° N 112.457° W. Second 8 analyses: Sample BV-99-08: 28.924°N, 112.446° W.

[d] Sample number PRS-309, 29.052° N 112.500° W.

[e] Sample number BA-99-13, 29.171° N 112.358° W.

Table B.10. Microprobe analyses of crystal separates for geochronology.

Al_2O_3 (Wt%)	SiO_2 (Wt%)	CaO (Wt%)	K_2O (Wt%)	Na_2O (Wt%)	Total (Wt%)	Mineral
Sample SWT-99-25			Tmpm clast	28.904°N, 112.533°W		
19.4	67.4	0.7	7.2	6.9	101.8	anorthoclase
19.6	68.2	0.6	7.4	6.7	102.6	anorthoclase
20.3	66.8	1.5	4.5	8.5	101.7	anorthoclase
19.6	67.6	0.8	6.3	7.5	102.1	anorthoclase
20.4	67.1	1.4	4.5	8.4	102.1	anorthoclase
20.1	66.9	1.4	4.8	8.2	101.6	anorthoclase
20.1	66.9	1.4	4.6	8.4	101.6	anorthoclase
20.2	66.5	1.4	4.6	8.2	101.2	anorthoclase
0.0	100.3	0.0	0.0	0.0	100.4	quartz
0.0	101.1	0.0	0.0	0.0	101.2	quartz
20.2	67.0	1.4	4.6	8.4	101.7	anorthoclase
20.3	66.8	1.5	4.6	8.4	101.7	anorthoclase
20.0	65.9	1.2	7.6	6.3	101.2	anorthoclase
20.5	66.2	1.5	6.9	6.7	101.9	anorthoclase
Sample BV-99-08			Tmr3	28.917°N, 112.447°W		
19.5	66.6	0.7	4.4	8.9	100.8	anorthoclase
21.2	65.1	2.4	1.5	10.2	100.8	anorthoclase
19.5	66.9	0.7	4.6	8.8	101.2	anorthoclase
19.4	67.0	0.7	4.6	8.8	101.2	anorthoclase
18.9	67.6	0.3	5.9	7.9	101.1	anorthoclase
19.0	67.4	0.3	5.9	8.0	101.1	anorthoclase
18.8	67.0	0.3	6.3	7.6	100.5	anorthoclase
19.0	66.9	0.3	6.3	7.7	100.7	anorthoclase
18.8	67.5	0.2	6.4	7.6	100.9	anorthoclase
19.0	66.9	0.4	6.0	7.9	100.7	anorthoclase

Table B.10, continued.

Al_2O_3 (Wt%)	SiO_2 (Wt%)	CaO (Wt%)	K_2O (Wt%)	Na_2O (Wt%)	Total (Wt%)	Mineral
Sample SWT-99-11[a]			Tprcs	28.924°N, 112.446°W		
24.1	60.6	6.5	0.5	8.1	100.2	plagioclase
24.2	61.0	6.5	0.6	8.2	100.8	plagioclase
24.0	61.1	6.0	0.6	8.2	100.3	plagioclase
24.0	60.7	6.1	0.6	8.3	100.1	plagioclase
25.4	59.1	7.7	0.4	7.5	100.4	plagioclase
25.2	59.4	7.6	0.5	7.4	100.5	plagioclase
24.5	61.0	6.5	0.6	8.1	100.9	plagioclase
25.8	58.4	8.3	0.4	7.2	100.8	plagioclase
26.0	58.4	8.3	0.4	7.1	100.6	plagioclase
Sample BV-99-30			Tmrsf	28.956°N, 112.470°W		
19.4	68.0	0.5	7.9	6.3	102.3	anorthoclase
19.6	67.6	0.6	7.4	6.5	101.9	anorthoclase
20.3	67.5	1.4	4.9	7.9	102.2	anorthoclase
19.9	67.7	1.2	5.4	7.8	102.2	anorthoclase
20.3	68.0	1.2	5.4	7.5	102.5	anorthoclase
20.2	68.0	1.2	5.4	7.6	102.7	anorthoclase
19.6	68.1	0.7	6.9	6.8	102.5	anorthoclase
19.8	68.0	0.9	6.3	7.3	102.4	anorthoclase
20.2	67.3	1.3	4.7	8.2	101.9	anorthoclase
20.4	68.0	1.2	5.1	7.9	102.7	anorthoclase
Sample BV-99-20[a]			Tma2	28.991°N, 112.476°W		
0.0	103.4	0.0	0.0	0.0	103.4	quartz
0.0	103.3	0.0	0.0	0.0	103.4	quartz
0.0	103.3	0.0	0.0	0.0	103.4	quartz
0.0	103.0	0.0	0.0	0.0	103.1	quartz
0.0	102.8	0.0	0.0	0.0	103.0	quartz
0.0	102.1	0.0	0.0	0.0	102.1	quartz
24.5	62.5	6.1	0.6	8.1	101.9	plagioclase
25.1	61.5	6.4	0.6	7.8	101.5	plagioclase
0.0	102.4	0.0	0.0	0.0	102.5	quartz
0.0	101.9	0.0	0.0	0.0	102.0	quartz

Table B.10, continued.

Al_2O_3 (Wt%)	SiO_2 (Wt%)	CaO (Wt%)	K_2O (Wt%)	Na_2O (Wt%)	Total (Wt%)	Mineral
Sample TIB-98-02			Tmvlc	28.766°N, 112.351°W		
20.1	67.1	1.3	4.8	8.3	101.8	anorthoclase
19.8	67.3	1.3	4.7	8.3	101.8	anorthoclase
20.1	67.1	1.4	4.7	8.3	101.9	anorthoclase
20.3	67.7	1.5	4.6	8.1	102.2	anorthoclase
19.6	67.7	0.7	6.9	7.0	102.2	anorthoclase
19.6	67.5	0.7	7.0	6.9	101.9	anorthoclase
19.4	67.1	0.5	7.6	6.5	101.3	anorthoclase
19.4	67.1	0.5	7.5	6.7	101.5	anorthoclase
19.8	67.2	1.0	6.0	7.5	101.8	anorthoclase
19.3	67.9	0.4	8.0	6.1	101.9	anorthoclase
Sample TIB-98-25			Tmrcc	28.840°N, 112.488°W		
20.1	67.3	1.2	5.2	8.1	102.1	anorthoclase
19.8	67.7	1.0	5.2	8.1	101.8	anorthoclase
20.6	66.9	1.6	4.0	8.7	102.0	anorthoclase
20.3	67.1	1.4	4.4	8.4	101.8	anorthoclase
20.8	66.4	1.9	3.5	8.8	101.6	anorthoclase
20.2	67.1	1.3	4.8	8.2	101.9	anorthoclase
20.3	66.9	1.6	4.4	8.4	101.7	anorthoclase
20.5	67.3	1.5	4.4	8.3	102.3	anorthoclase
20.0	67.0	1.2	4.9	8.1	101.4	anorthoclase
19.6	67.3	0.9	6.3	7.3	101.6	anorthoclase

Table B.10, continued.

Al_2O_3 (Wt%)	SiO_2 (Wt%)	CaO (Wt%)	K_2O (Wt%)	Na_2O (Wt%)	Total (Wt%)	Mineral
Sample TIB-98-11			Tmprsz1	28.899°N, 112.542°W		
19.3	67.6	0.4	5.7	7.9	101.5	anorthoclase
19.3	67.1	0.4	5.5	8.3	101.2	anorthoclase
19.0	67.5	0.3	6.1	7.8	101.3	anorthoclase
19.1	68.0	0.3	6.1	7.8	101.8	anorthoclase
23.9	61.9	5.2	0.7	8.8	100.9	plagioclase
23.9	62.1	5.2	0.7	9.1	101.4	plagioclase
19.2	67.5	0.4	5.4	8.2	101.3	anorthoclase
19.5	68.1	0.4	5.7	7.9	102.1	anorthoclase
19.3	67.9	0.4	5.4	8.2	101.6	anorthoclase
19.5	68.0	0.4	5.3	8.1	101.9	anorthoclase
19.4	67.7	0.5	5.5	8.2	101.8	anorthoclase
19.3	67.9	0.4	5.7	8.0	101.8	anorthoclase
22.9	63.1	4.1	0.9	9.3	100.9	plagioclase
23.1	62.9	4.4	0.8	9.3	101.0	plagioclase
Sample TIB-98-23			Tmrsf	28.974°N, 112.460°W		
19.2	67.8	0.5	7.7	6.5	102.0	anorthoclase
19.6	68.0	0.7	7.1	6.6	102.3	anorthoclase
19.8	67.8	1.0	5.8	7.6	102.2	anorthoclase
19.5	67.9	0.6	7.4	6.7	102.3	anorthoclase
20.1	67.8	1.2	5.6	7.5	102.3	anorthoclase
20.2	67.6	1.2	5.0	7.8	101.9	anorthoclase
20.4	67.5	1.3	4.8	7.9	102.1	anorthoclase
20.3	67.0	1.3	4.8	8.1	101.9	anorthoclase
20.4	67.4	1.5	4.7	8.0	102.2	anorthoclase
20.5	67.1	1.5	4.4	8.3	102.1	anorthoclase

Table B.10, continued.

Al_2O_3 (Wt%)	SiO_2 (Wt%)	CaO (Wt%)	K_2O (Wt%)	Na_2O (Wt%)	Total (Wt%)	Mineral
Sample BK-99-05			Tmrsf	28.880°N, 112.023°W		
20.5	67.3	1.5	4.4	8.3	102.2	anorthoclase
20.5	68.0	1.5	4.5	8.2	102.7	anorthoclase
20.5	67.9	1.3	4.7	8.0	102.7	anorthoclase
19.3	67.2	0.7	7.1	7.0	101.7	anorthoclase
19.4	67.9	0.6	7.6	6.4	102.0	anorthoclase
19.5	67.7	0.7	6.9	6.9	101.9	anorthoclase
19.3	67.9	0.5	7.9	6.2	102.0	anorthoclase
19.4	68.2	0.5	7.7	6.4	102.3	anorthoclase
20.2	67.2	1.4	4.6	8.1	101.7	anorthoclase
19.4	67.6	0.6	7.5	6.5	101.7	anorthoclase
Sample SWT-99-28			Tmprsz1	28.898°N, 112.530°W		
0.0	102.3	0.0	0.0	0.0	102.4	quartz
0.0	102.6	0.0	0.0	0.0	102.6	quartz
19.5	67.3	0.5	5.5	8.3	101.4	anorthoclase
19.4	67.6	0.5	5.5	8.2	101.7	anorthoclase
19.1	67.6	0.3	6.2	7.9	101.4	anorthoclase
19.2	67.8	0.3	6.1	7.6	101.7	anorthoclase
19.2	67.7	0.3	6.1	7.9	101.6	anorthoclase
19.1	67.2	0.4	6.0	8.0	101.1	anorthoclase
19.3	67.7	0.4	5.8	7.9	101.6	anorthoclase
19.0	68.1	0.3	6.1	7.7	101.6	anorthoclase
Sample SZ-98-04[a]			Tpth3	28.867°N, 112.467°W		
24.6	61.2	6.5	0.4	8.0	101.3	plagioclase
24.4	62.0	5.9	0.5	8.4	101.6	plagioclase
25.7	60.0	7.7	0.4	7.4	101.5	plagioclase
25.4	59.9	7.5	0.3	7.6	101.1	plagioclase
25.7	59.7	7.7	0.3	7.4	101.3	plagioclase
27.5	57.2	9.7	0.2	6.4	101.5	plagioclase
27.0	57.1	9.6	0.2	6.5	100.9	plagioclase
27.8	55.9	10.6	0.2	6.0	101.0	plagioclase
26.5	58.1	8.8	0.3	6.8	101.0	plagioclase
23.9	62.3	5.7	0.5	8.5	101.2	plagioclase

Table B.10, continued.

Al_2O_3 (Wt%)	SiO_2 (Wt%)	CaO (Wt%)	K_2O (Wt%)	Na_2O (Wt%)	Total (Wt%)	Mineral
Sample TIB-98-09[b]			Tmbr	28.897°N, 112.531°W		
0.0	0.1	56.7	0.0	0.0	56.8	calcite?
24.3	62.4	6.0	0.6	8.1	101.7	plagioclase
24.1	62.6	5.8	0.6	8.3	102.0	plagioclase
24.2	62.1	6.0	0.6	8.1	101.5	plagioclase
0.0	0.1	58.4	0.0	0.0	58.6	calcite?
0.0	0.1	58.6	0.0	0.0	58.8	calcite?
23.8	62.9	5.6	0.6	8.5	101.9	plagioclase
24.0	62.5	5.7	0.6	8.3	101.7	plagioclase
0.0	0.1	56.7	0.0	0.0	56.9	calcite?
0.0	0.0	57.4	0.0	0.0	57.6	calcite?
Sample TIB-98-12			Tmr3	28.979°N, 112.457°W		
18.6	67.2	0.3	6.2	7.5	100.1	anorthoclase
18.6	66.8	0.3	6.2	7.5	99.8	anorthoclase
18.7	65.1	0.3	5.6	7.6	98.0	anorthoclase
18.8	65.2	0.4	5.7	7.8	98.5	anorthoclase
19.1	67.5	0.3	5.7	8.0	101.2	anorthoclase
19.4	68.3	0.4	5.4	7.9	102.0	anorthoclase
27.4	56.9	9.4	0.3	6.6	100.9	plagioclase
27.3	57.0	9.9	0.3	6.3	101.0	plagioclase
19.3	68.2	0.3	6.0	7.7	101.9	anorthoclase
19.3	68.7	0.4	6.1	7.7	102.4	anorthoclase
Sample SZ-98-08			Tmprsz1	28.885°N, 112.384°W		
19.3	67.8	0.4	5.6	8.0	101.6	anorthoclase
19.4	68.3	0.4	5.5	8.0	102.1	anorthoclase
19.6	68.4	0.5	5.0	8.4	102.4	anorthoclase
19.6	68.3	0.5	4.9	8.3	102.1	anorthoclase
19.4	67.7	0.4	5.5	7.9	101.6	anorthoclase
19.5	67.8	0.4	5.5	8.1	101.8	anorthoclase
0.0	103.0	0.0	0.0	0.0	103.1	quartz
0.0	102.7	0.0	0.0	0.0	102.7	quartz
19.3	68.5	0.3	5.6	8.0	101.9	anorthoclase
19.6	68.4	0.4	5.8	7.6	102.4	anorthoclase

Note: Each grouping of 2 analyses is from a single crystal.

[a] Samples containing significant plagioclase were not successfully dated in this study.

[b] Calcite accidentally separated, sample discarded.

Appendix C

$^{40}Ar/^{39}Ar$ Geochronology

Separates of feldspar were prepared from all samples. Separation of feldspar was by dry mechanical techniques. Altered rinds of hand-samples were chipped away and the remaining unaltered sample was processed through a jaw crusher. The resulting rock chips were inspected to remove lithic fragments from the sample. The remaining chips were then fed through a pulverizer, washed, dried and sifted to separate a 30# to 80# (0.59 mm to 0.177 mm) fraction. Highly magnetic particles were removed using a hand magnet and the remaining was sample placed into an ultrasound bath to dislodge glass particles from feldspar phenocrysts. The nonmagnetic fraction of each sample was concentrated using a Frantz isodynamic separator. The non-magnetic fraction, which consists mostly of non-Fe bearing phenocrysts, was again placed into an ultrasound bath to dislodge glass particles. Samples were then washed and dried for handpicking.

Handpicking employed the method of gamma-ray irradiation to differentiate feldspars from quartz [*Rose et al.*, 1994]. This method uses a ^{137}Cs source to irradiate the sample. This does not alter the chemical composition nor impart radioactivity to the phenocrysts but does cause a minor amount of damage to the crystal lattice. This damage imparts a 'smoky' color to the crystals in proportion to the number of Si-O bonds. Quartz darkens the fastest whereas plagioclase darkens the slowest. Alkali-feldspar darkens at an intermediate rate. After a short period of exposure to gamma rays, each type of feldspar and quartz may be differentiated by color. With additional exposure, eventually, all phenocrysts will become opaque. Application of this method by *Nagy* [1997] showed that gamma-irradiation does not affect isotopic age measurements.

Final separation procedures for each sample followed irradiation by gamma rays for 3 to 5 days. 100 to 200 mg of crystals of the irradiated sample were handpicked to remove impurities of quartz, plagioclase, and phenocrysts with attached glass. A few crystals from each sample were mounted and polished for microprobe analyses (Table 3.1). Handpicking techniques were most effective for selecting alkali-feldspar. Calcite was accidentally selected for the breccia clast (unit Tmbr) and the andesite sample was contaminated by quartz (Tma2) possibly derived from lithic inclusions. K and Ca content were measured by microprobe for a few crystals from each sample (Appendix B, Table B.10).

Handpicked separates were prepared for $^{40}Ar/^{39}Ar$ dating by the following procedures. Each sample was washed with ethanol, water, and acetone. Samples readied for dating were sealed and shipped to McMaster University nuclear reactor in Hamilton, Ontario, Canada for irradiation. Samples were encased in commercial grade Al foil, packed into nine aluminum disks which were stacked vertically, and wrapped in Cd to reduce neutron-induced production of ^{40}Ar. The samples irradiated for 7.0 hrs for a total of 14.0 MWhrs in position 5C of the McMaster University nuclear reactor. Fish Canyon sanidine [*Renne et al.*, 1994, 27.95 Ma] was used as a flux monitor.

Measurements of Ar isotopes were made at the Massachusetts Institute of Technology CLAIR laboratory by Dr. Joann Stock. This facility uses laser fusion to release Ar from the sample. Six to eight crystals of K-feldspar were placed in each sample well. Ten sets of measurements were attempted for each sample, although in some cases the sample did not fuse. These results are summarized in Tables 3.1 and 5.2.

The following pages contain petrographic descriptions of samples used for geochronology.

Sample:	SWT-99-25	$^{3}50^{520}E, ^{31}98^{130}N$
Unit:	Tmpm	rounded tuff clast from marine conglomerate
Description:	somewhat altered; phenocryst-rich welded tuff clast from marine conglomerate from southwest Isla Tiburón	
Components:	%	Note
glass shards	40	0.5-1 mm, welded
phenocrysts	20	1-2 mm, common large crystals, generally subhedral-anhedral
pumice	35	0.1-1 cm, large
lithic fragments	5	1-4 mm, rare to uncommon
Phenocrysts:	%	Note
alkali feldspar	90	1-2 mm, anhedral
clinopyroxene	5	0.5 mm, green in plane light
plagioclase	trace	1-2 mm, ragged edges
mafic opaque	5	∼0.2 mm
olivine?	trace	0.1 mm, high relief cluster
Lithic fragments:	andesite, tuff(?)	
Alteration:	axiolitic replacement fabric in glass shards and pumice, silicified groundmass	
Structure:	eutaxitic foliation, fiamme, section cut 45 degrees oblique to foliation	

Sample:	BV-99-08	$^{3}59^{090}E, ^{32}\,00^{240}N$
Unit:	Tmr3	Tmr3 member, Tuffs of Mesa Cuadrada
Description:	Very clean glassy welded tuff with clean phenocrysts.	
Components:	%	Note
glass	70	0.1-1 mm, light orange shards
pumice	5	0.5-1 cm, finely laminated
lithic fragments	5	
phenocrysts	20	0.2-2 mm
Phenocrysts:	%	Note
alkali feldspar	80	0.5-2 mm, clean
clinopyroxene	5	0.3-1 mm, clean
biotite	trace	0.5 mm, small thin crystals
zircon?	trace	0.2 mm, high relief
hornblende	trace	light brown
mafic oxide	15	0.1-0.2 mm, small
Lithic fragments:	altered andesite lithic fragments and a plagioclase-rich glomerocryst	
Alteration:	altered lithics, otherwise a very clean sample	
Structure:	eutaxitic foliation, welding	

Sample:	SWT-99-11	$^{3}50^{400}E,^{31}\,97^{120}N$
Unit:	Tprcs	Rhyodacite of Cerro Starship
Description:	rhyodacite lava flow.	
Components:	%	Note
glass matrix	50	dark brown color
microlites	25	0.1–0.3 mm, acicular plagioclase with glass cores indicative of quenching; defines trachytic flow texture
phenocrysts	25	0.2–3 mm
lithic fragments	trace	andesite lithic fragment observed
Phenocrysts:	%	Note
plagioclase	70	0.5–3 mm, zoned euhedral, sometimes as glomerocrysts with mafic silicates and oxides, others as single elongate crystals with conspicuous brown glass inclusisons
hornblende	5	0.5–2 mm, brown to olive color, equant, blocky, subhedral to euhedral; common in glomerocrysts
orthopyroxene	5	0.5–2 mm, light green, equant to acicular, subhedral, common association with mafic oxides; not pleochroic
mafic oxide	15	0.05–0.5 mm, elongate and equant, common as small crystals disseminated through matrix
quartz	5	up to 3 mm, uncommon, anhedral crystals with common internal glass pockets
Lithic fragments:	andesite lithic observed in hand sample and cut into thin section; overall lithic inclusions are very rare	
Alteration:	embayed mafic silicates and quartz, random oxidized grains may be olivine	
Structure:	trachytic flow texture defined by microlites; no evidence for pyroclastic texture	

Sample:	BV-99-20	$^{3}56^{740}E, ^{32}03^{790}N$
Unit:	Tma2	early syn-rift andesite lava flow
Description:	glassy, plagioclase crystal-rich andesite lava flow	
Components:	%	Note
matrix glass	25	
matrix microlites	25	0.01–0.05 mm, Non-aligned, high-aspect ratio plagioclase; devitrification effect of cooling flow(?)
phenocrysts	50	0.1-1 mm, equiangular plagioclase, rare large feldspar or quartz with disequilibrium texture
Phenocrysts:	%	Note
plagioclase	60	0.1–0.5 mm, equant blocks to tabular lathe-shape, some zoned extinction
biotite	30	0.1-0.3 mm small tabular books, slightly ragged and altered edges; common as small single flakes
hornblende	10	0.5-1 mm
Lithic fragments:	xenocrysts or large embayed phenocrysts of quartz or feldspar; no multi-grain lithics in thin section	
Alteration:	moderate to low overall. Devitrification of glass matrix	
Structure:	little to no flow lamination apparent from crystal alignment	

Sample:	TIB-98-02	$^{3}68^{150}E,^{31}\,82^{640}N$
Unit:	Tmvlc	Welded Tuff of Ensenada de la Cruz
Description:	densely welded crystal-rich ash-flow tuff	
Components:	%	Note
glass shards	65	1 mm, clear interior, opaque and recrystallized rims
phenocrysts	20	
lithic fragments	15	
Phenocrysts:	%	Note
alkali feldspar	90	0.25-3 mm, anhedral-subhedral blocks, untwinned or simple twins
pyroxene	10	0.5 mm, non-pleochroic green, sometimes simple twins, anhedral
plagioclase	trace	rare, possibly lithic-derived
Lithic fragments:	andesite up to 3 mm	
Structure:	welded glass	

Sample:	TIB-98-25	$^{3}54^{770}E,^{31}\,91^{030}N$
Unit:	Tmrcc	Welded Tuff of Cerro Colorado
Description:	alkali feldspar- and pyroxene-phyric welded tuff vitrophyre; sampled to test correlation to Tmr3; orange-colored glass with clear reduced rims; two prominent orange splotches in section correspond to areas of extensive recrystalization of glass (but not spherulitic overgrowths)	

Components:	%	Note
welded glass	75	0.2-0.5 mm, orange cores
phenocrysts	15	0.1-1 mm, large blocky K-spar (some exceeding 1 mm) smaller mafic silicates and oxides
lithic fragments	5	0.3-1 mm, angular
pumice	5	0.2-5 mm, fine-textured fiamme. 10:1 aspect ratio. One smaller pumice may preserve an olivine phenocryst (see below)

Components:	%	Note
alkali feldspar	85	0.5-2 mm, tartan extinction
pyroxene	5	0.5 mm, green-brown pleochroism, equant angular crystal cross sections
opaque	5	0.1-0.3 mm, equant, square cross sections
hornblende	5	0.2 mm, small, altered
olivine(?)	trace	0.1 mm, one crystal in section

Lithic fragments:	orange altered lithic: plagioclase, red oxidized and recrystallized zones
Alteration:	some alteration of mafic phenocrysts (Hornblende>pyroxene); devitrification zones cross eutaxitic foliation at high angles
Structure:	eutaxitic foliation defined by prominent welding of glass shards and pumice

Sample:	TIB-98-11	$^{3}49^{630}E, ^{31}97^{550}N$
Unit:	Tmprsz1	Tuffs of Arroyo Sauzal #1
Description:	non-welded to slightly welded ash-flow tuff, brecciated	
Components:	%	Note
groundmass	35	
glass shards	50	up to 1 mm, non-compacted, cuneiform-like bubble walls
fine matrix glass	50	
phenocrysts	15	0.3-2 mm
breccia	50	brecciated non-welded ash-flow tuff, with different textural composition than matrix
glass shards	64	1 mm, non-compacted, cuneiform-like bubble walls
fine matrix glass	16	
phenocrysts	13	
Phenocrysts:	%	Note
alkali feldspar	0.3-2 mm	anhedral-subhedral, simple twins occasionally
clinopyroxene	0.2-1 mm	green (sodic?)
Lithic fragments:	<1% rhyolite and andesite clasts	
Alteration:	some iron oxides stain on fine glass matrix, otherwise very clean	
Structure:	Brecciated sample from pumice-enclosed exposure that may have interacted with seawater during emplacement; petrographic texture of cm-size clasts of non-welded tuff contained in a matrix of additional tuff; matrix glass is finer-grained than clasts.	

Sample:	Tib-98-23	$^{3}57^{730}E, ^{32}\,05^{760}N$
Unit:	Tmrsf	Tuff of San Felipe
Description:	moderately devitrified crystal-rich welded tuff vitrophyre	
Components:	%	Note
glass shards	80	0.1–1mm, brown color
red oxides	12	form spherulites
phenocrysts	7	
Phenocrysts:	%	Note
anorthoclase	98	<1mm
augite	trace	weakly pleochroic green
hornblende	trace	strongly pleochroic brown
magnetite	1	
Alteration:	devitrified glass; reduced rims of glass shards; spherulites up to 1 mm	
Note:	sample BV-99-30 from same outcrop as sample TIB-98-23	

Sample:	BK-99-05	$^{4}00^{250}E,^{31}\,94^{900}N$
Unit:	Tmrsf	Tuff of San Felipe
Description:	densely-welded crystal-rich ignimbrite vitrophyre with aphanitic lithic fragments and rare pumice fiamme	
Components:	%	Note
welded glass	65	0.2–0.5 mm, densely welded with round perlitic fractures
lithic fragments	10	0.5 mm-1 cm, a group of similar aphanitic volcanic lithic fragments with plagioclase microlites; abundance exaggerated because of one large lithic in thin section
pumice	2	2–4 mm, welded pumice with fiamme texture
other glass	8	0.5-1 mm, rounded, dense lenses; may be cognate glass droplets or other pumice(?)
phenocrysts	15	
Phenocrysts:	%	Note
anorthoclase	94	0.2–2 mm, mottled extinction, tartan extinction poorly developed, simple angular twins rare, cleavage well developed, angular (fractured?) hacky crystal edges common
augite	3	0.2–0.5 mm, green (sodic?) subangular, weakly pleochroic
mafic oxide	3	$<$ 0.1 mm, black angular crystals, magnetite(?)
Lithic fragments:	aphanitic lithic fragments with plagioclase microlites in groundmass–andesite(?)	
Alteration:	devitrification along fracture, otherwise absent	
Structure:	densely welded, eutaxitic foliation defined by pumice and other glass lenses	

Sample:	SWT-99-28	$^{3}50^{530}E,^{31}98^{140}N$
Unit:	Tmprsz1	Tuffs of Arroyo Sauzal #1
Description:	crystal-rich non-welded ash-flow tuff	
Components:	%	Note
glass	79	0.4–1 mm, large undeformed glass spicules, often containing recognizable fragments of bubble walls, sometimes with two bubble-wall triple junctions preserved
lithic fragments	1	0.3–0.7 mm, andesite and other aphanitic volcanic lithologies
Phenocrysts:	%	Note
alkali feldspar	90	0.3–3 mm, subhedral to anhedral, some large fragments with intact crystal faces. untwinned or simple twins
clinopyroxene	6	0.2–0.4 mm, subhedral, rarely euhedral, light-yellowish green to brownish green weak pleochroism
biotite	1	0.3 mm
magnetite	3	0.1 mm, euhedral to subhedral cubes and octahedra sections
plagioclase	trace	0.5–1 mm, rare, present as glomerocrysts with biotite
hornblende	trace	0.1–0.3 mm, oxidized, especially oxidized cores, euhedral rims, dark brown
Lithic fragments:	andesite, aphanitic volcanic, glomerocrysts may be tonalite lithic fragments	
Alteration:	axiolitic recrystallization of glass spicules, darker silicified areas of matrix	
Structure:	delicate pyroclastic texture of glass fragments, no foliation discerned at petrographic scale	

Sample:	SZ-98-04	$^{3}57^{030}E, ^{31}93^{780}N$
Unit:	Tpth3	Air-fall tuff of Hipat Mesa #3
Description:	welded pumice air-fall tuff	
Components:	%	Note
glass groundmass	15	glass shards
pumice	55	welded
lithic fragments	15	andesite and other aphanitic volcanic rock.
phenocrysts	15	
Phenocrysts:	%	Note
alkali feldspar	20	simple twins
plagioclase	70	some zoned
hornblende	10	equant cross section
Lithic fragments:	andesite lithics very common	
Alteration:	pumice fiamme with some spherulites	
Structure:	welding/foliation texture strongly developed in crushed pumice	

Sample:	TIB-98-09	$^{3}50^{750}E$,$^{31}\,97^{380}N$
Unit:	Tmbr	welded tuff clast from Tmbr landslide breccia
Description:	densely welded, moderately devitrified crystal-rich ash-flow tuff clast	
Components:	%	Note
glass shards	77	welded, distinctive separate pyroclastic fragments, define eutaxitic foliation; approximately 1/2 devitrified
phenocrysts	15	up to 2 mm, occasional larger glomerocrysts
pumice	6	welded fiamme
lithic fragments	2	andesite up to 5 mm
Phenocrysts:	%	Note
plagioclase	90	0.5-4 mm, clean crystals, zoned, albite twins
augite	8	up to 3 mm, green
magnetite	2	0.1–0.3 mm, subhedral to euhedral cubic crystals
Lithic fragments:	mafic-augite-feldspar glomerocrysts, andesite	
Alteration:	embayed augites, devitrified groundmass welding texture	
Structure:	welding texture, indicative of a primrary subaerial emplacement as an ash-flow tuff prior to secondary emplacement as a landslide	

Sample:	TIB-98-12	28.979° N 112.457° W.
Unit:	Tmr3	Tmr3 member, Tuffs of Mesa Cuadrada
Description:	lithic and crystal-rich moderatley welded tuff	
Components:	%	Note
lithics	5	andesite, tuff(?)
pumice fiamme	5	up to 5 mm, fine glass froth matrix
glass shards	77	1-2 mm, reduced rims
phenocrysts	13	
Phenocrysts:	%	Note
anorthoclase	89	up to 5 mm, clean
augite	8	euhedral-subhedral
magnetite	3	
Lithic fragments:	andesite, tuff(?)	
Alteration:	oxidized glass (tuff lithic fragment?) some devitrification of glass, otherwise very clean sample	
Structure:	welding of glass, crushed pumice	

Sample:	SZ-98-08	$^{3}65^{000}E, ^{31}95^{910}N$
Unit:	Tmprsz1	Tuffs of Arroyo Sauzal #1
Description:	low grade welded to non-welded crystal-rich ash-flow tuff	

Components:	%	Note
glass shards	80	0.5-2 mm, flattened
lithic fragments	trace	<1 mm, rare andesite lithic fragments
phenocrysts	20	0.5-3 mm, large, dominantly feldspar

Components:	%	Note
alkali feldspar	90	0.5-3 mm, subhedral to anhedral
clinopyroxene	5	1 mm, cross section view observed
hornblende	5	1 mm, cross section view observed
biotite	trace	1 mm, one crystal observed
plagioclase?	trace	1 mm, one albite twinned crystal, zoned
zircon	trace	0.5 mm, one high-relief, high interference bipyramidal crystal observed

Lithic fragments:	andesite (?) <1 mm and very crystalline, may alternatively be crystalline basement (tonalite?)
Alteration:	some glass devitrification
Note:	glass shards resemble similar large shards and phenocryst assemblage also resembles samples TIB-98-11 and SWT-99-28 from southwest Isla Tiburón

Appendix D

Paleomagnetic sampling and analysis

Each sample locality at Isla Tiburón, coastal Sonora, and Cinco Islas was selected after careful field study of its structural setting (Plates I, II, and IV). Structural control for each sample locality was measured from stratified sedimentary deposits or reworked pyroclastic deposits at the base of each flow. Eutaxitic foliation, although present, was not used because it was found to be an unreliable indicator of paleohorizontal due to differential compaction over paleotopography and post-depositional rheomorphic flow. Sample localities for the Tuff of San Felipe and the Tuffs of Mesa Cuadrada listed for Baja California were studied by previous workers [*Lewis and Stock*, 1998a; *Stock et al.*, 1999; *Nagy*, 2000]. Sampling strategies followed by these authors are similar to this study, although eutaxitic foliation was employed where extensive sheets of ignimbrite deposits appeared unaffected by local paleotopography in Baja California.

Sampling strategy varied according to the lithology of each ash-flow tuff. In all cases, samples with minimal post-depositional hydrothermal alteration were targeted. Samples of the dark-brown to black basal vitrophyre were acquired for the Tuff of San Felipe and unit Tmr3 of the Tuffs of Mesa Cuadrada. Non-welded samples were acquired for the lower units of the Tuffs of Los Heme and Tmr3 at one locality (PRS, Fig. 5.8). Extensive perlitic fracturing of the vitrophyre of cooling unit Tmr4 of the Tuffs of Mesa Cuadrada required sampling of the thin partially welded basal brown glass instead. A similar horizon was sampled for the Tuffs of Dead Battery Canyon where an exceptionally hard vitrophyre prevented drilling.

At each sample locality, 6 to 18 cores were drilled for each unit. For every locality except site SA, cores were drilled using a gasoline-powered drill with a 25.4mm (1 in)

diameter drill bit cooled with water. Core samples were oriented in the field using an azimuthal Brunton compass and a brass orienting sleeve with attached frontal plate. A sun compass was also used to check the orientation of each core if possible. A brass strip was used to mark the top of each core and the cores were then broken from the outcrop and removed. Cores that became loose during drilling were measured if they could be refit into their holes. The top of each core was marked with a line and arrows that point outward to the outcrop surface. Oriented block samples were collected from locality SA and for some samples from unit Tmr4 at locality PRS. These blocks were later drilled in the lab and oriented relative to lines of known strike and dip marked in the field on each block sample. Core sections 12.8 mm (0.5 in) in length were cut from each core for measurement at the Caltech Paleomagnetics Laboratory.

Based upon previous paleomagnetic studies of the Tuff of San Felipe, Tuffs of Mesa Cuadrada (Tmr3 and Tmr4), and the Tuffs of Dead Battery Canyon, alternating-field (AF) demagnetization was applied to all samples. *Lewis* [1994] and *Nagy* [1997] examined demagnetization strategies for these ash-flow tuffs. These studies found that single-domain magnetite is the dominant magnetic carrier, with a component of hematite present in proportion to the amount of vapor-phase alteration of samples. These studies also found that alternating field (AF) demagnetization removed secondary magnetic overprints more efficiently than thermal demagnetization. The most common magnetic overprint encountered in this study is a viscous remanent magnetization (VRM) imparted from the present-day magnetic field. Less commonly, an overprint of chemical remanent magnetization (CRM) or induced remanent magnetization (IRM) was present in the cores. Sampling strategy was designed to avoid the most common types of these overprints, i.e., altered samples with a CRM component and samples from ridge-tops with a high probability for lightning-induced IRM. Probable lightening-induced overprints were found in Tmr4 at locality PR and Tphry at locality CI. Both of these units at these sampling localities were located at ridge tops. Prepared core samples were measured in a computer-controlled cryo-

Figure D.1. (next 11 pages) Representative demagnetization plots from the Tuff of San Felipe and Tuffs of the northern Puertecitos Volcanic Province on Isla Tiburón and coastal Sonora. Also shown are representative demagnetization plots from the Tuffs of Los Heme at Cinco Islas, Baja California. Zjiderveld plot (at left) shows measured declinations and inclinations with progressive demagnetization. Lower hemisphere plot of this data also shown at right, solid points directed downward. Grey-shaded circle shows present-day magnetic field at the sampling locality. Normalized magnetic intensity plot (box at right) shows magnetic intensity (normalized to initial intensity) with progressive demagnetization (curve) and a histogram showing the fraction of the total intensity removed at a given demagnetization step.

genic SQUID (Superconducting Quantum Interference Device) magnetometer in a magnetically shielded m-metal room. A series of closely spaced low-intensity AF demagnetization steps from 5 mT to 100 mT usually removed a VRM component, leaving a single-component magnetization present up to the limit of AF demagnetization (700 to 800 mT) interpreted as a primary thermal magnetic remanence. The results of these measurements are summarized in Figure D.2 as equal area inclination-declination plots for each ash-flow tuff described in Chapter 5. Inclination-declination plots for Cinco Islas are shown in Figure 7.2.

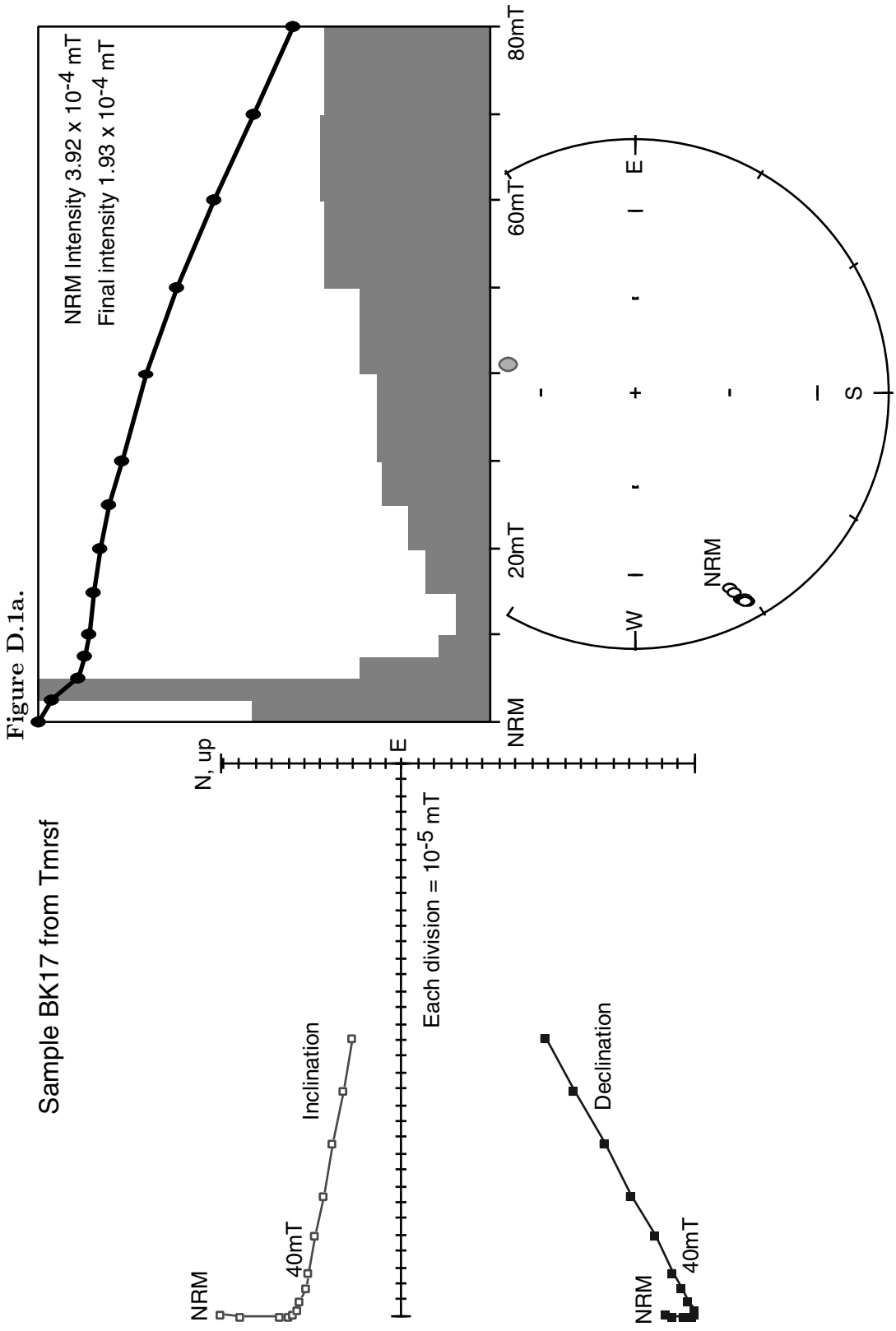
Sample BK17 from Tmrsf
NRM Intensity 3.92 x 10-4 mT
Final intensity 1.93 x 10-4 mT
NRM
20mT
60mT
80mT
N, up
E
Each division = 10-5 mT
NRM
40mT
Inclination
Declination
W
E
S
NRM

Figure D.1a.

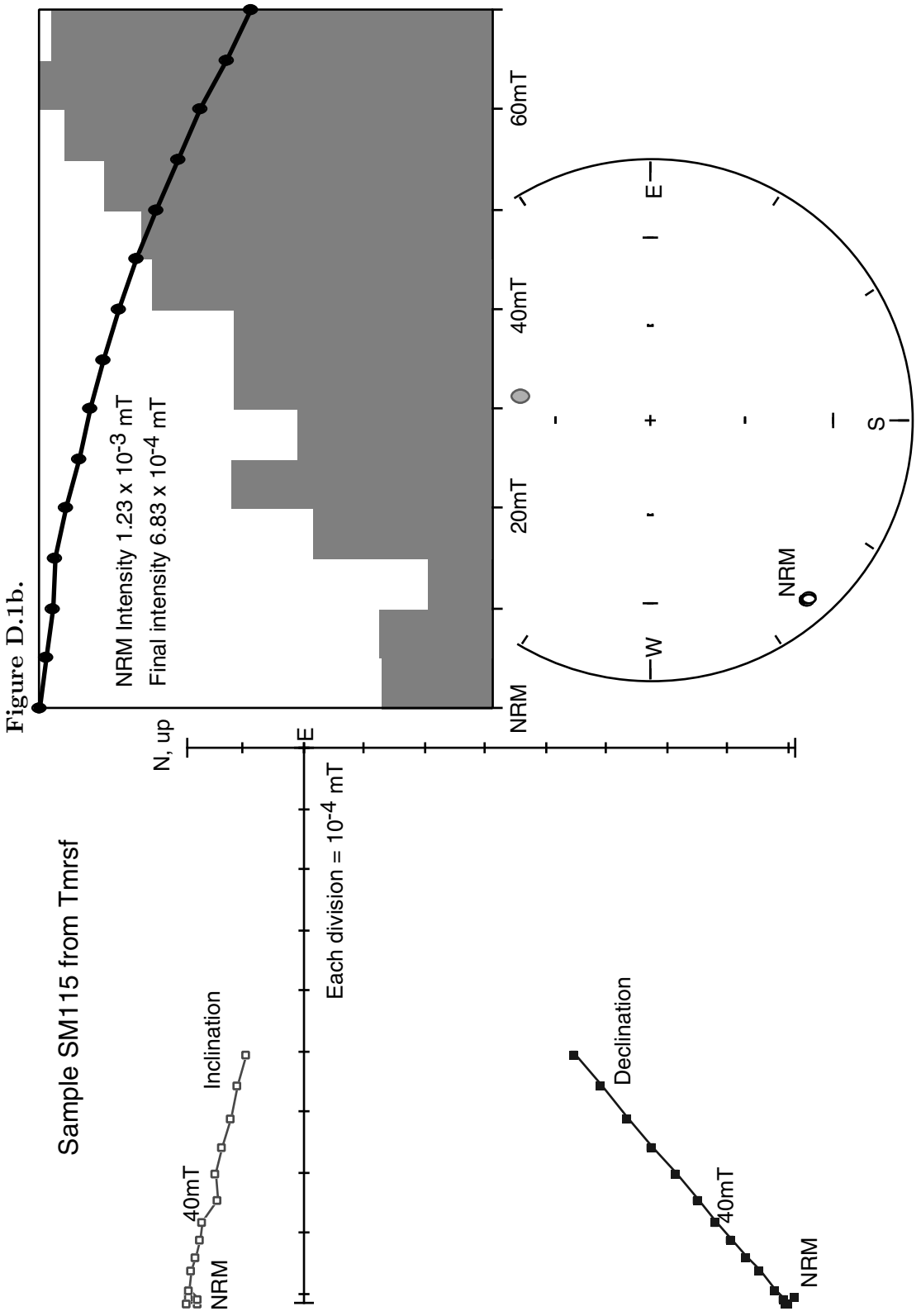
Sample SM115 from Tmrsf
NRM Intensity 1.23 x 10-3 mT
Final intensity 6.83 x 10-4 mT
N, up
E
Each division = 10-4 mT
NRM
20mT
40mT
60mT
W
E
S
NRM
Inclination
40mT
NRM
Declination
40mT
NRM

Figure D.1b.

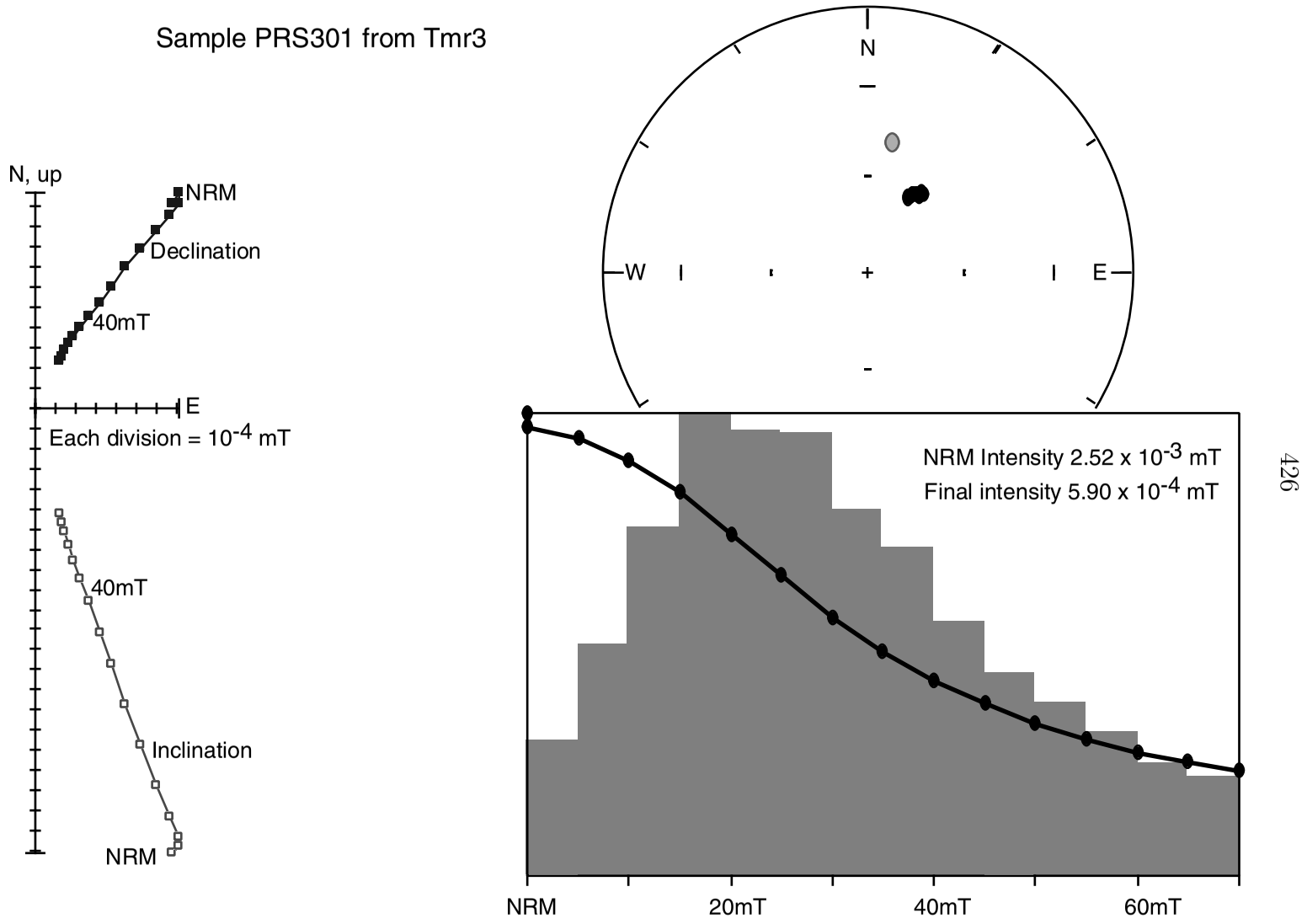
Sample PRS301 from Tmr3
N, up
NRM
Declination
40mT
E
Each division = 10-4 mT
40mT
Inclination
NRM
N
W
E
NRM Intensity 2.52 x 10-3 mT
Final intensity 5.90 x 10-4 mT
NRM
20mT
40mT
60mT

Figure D.1c.

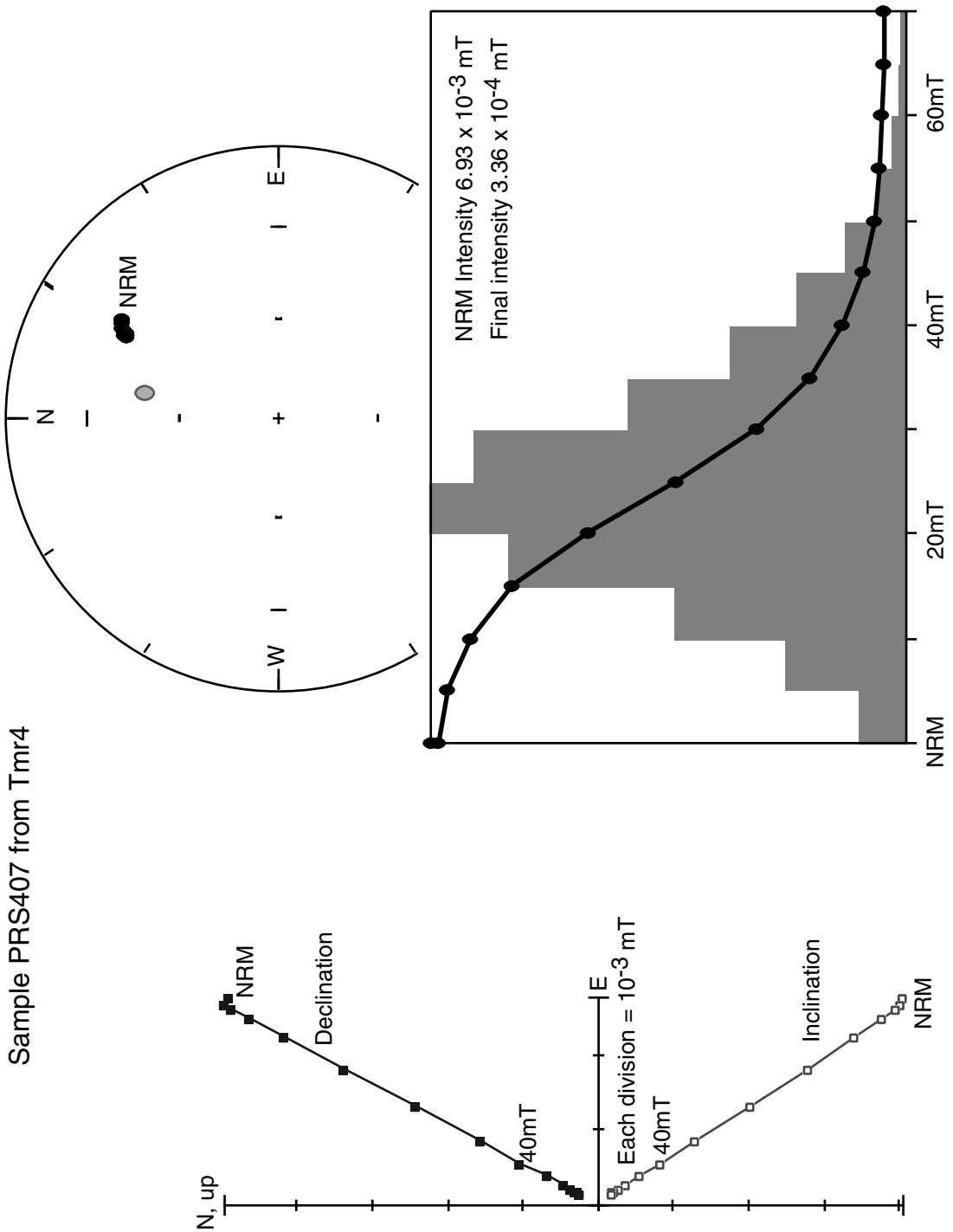
Sample PRS407 from Tmr4
N
E
W
NRM
NRM Intensity 6.93 x 10-3 mT
Final intensity 3.36 x 10-4 mT
NRM
20mT
40mT
60mT
N, up
NRM
Declination
40mT
E
Each division = 10-3 mT
40mT
Inclination
NRM

Figure D.1d.

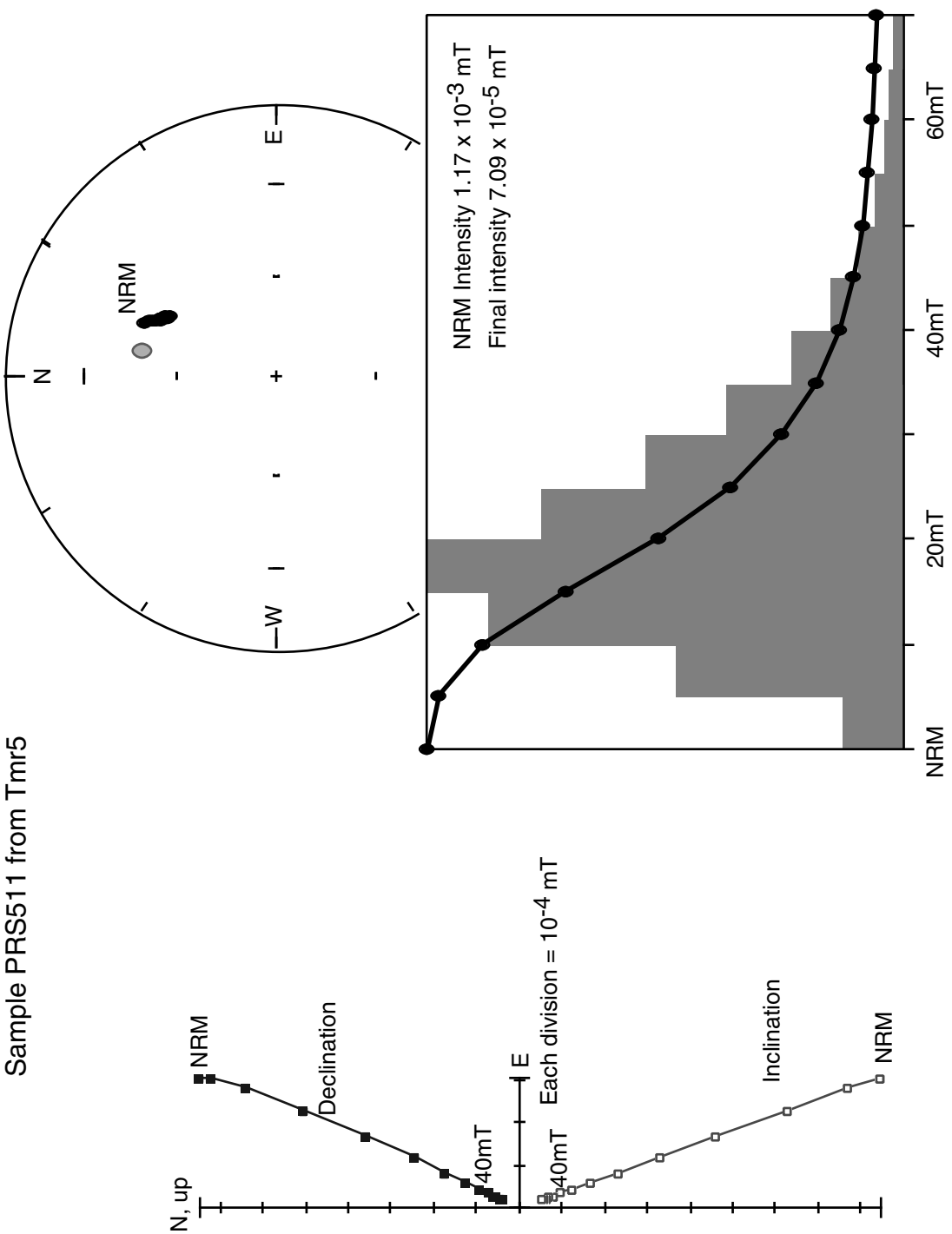
Sample PRS511 from Tmr5
N, up
NRM
Declination
40mT
E
Each division = 10-4 mT
40mT
Inclination
NRM
N
E
W
NRM
NRM Intensity 1.17 x 10-3 mT
Final intensity 7.09 x 10-5 mT
NRM
20mT
40mT
60mT

Figure D.1e.

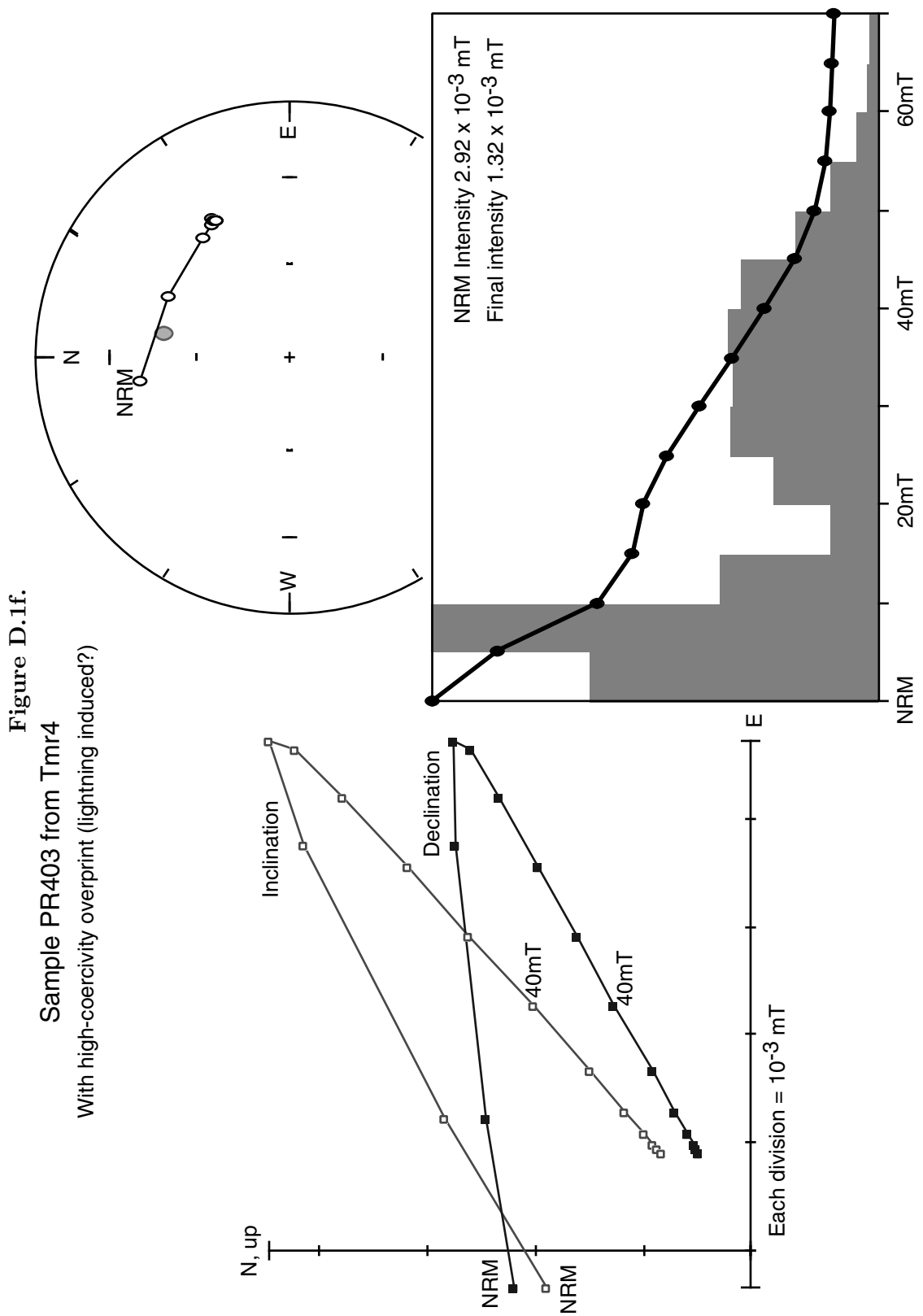
Sample PR403 from Tmr4
With high-coercivity overprint (lightning induced?)
N
W
E
NRM
NRM Intensity 2.92 x 10-3 mT
Final intensity 1.32 x 10-3 mT
NRM
20mT
40mT
60mT
N, up
Inclination
Declination
40mT
40mT
NRM
NRM
E
Each division = 10-3 mT

Figure D.1f.

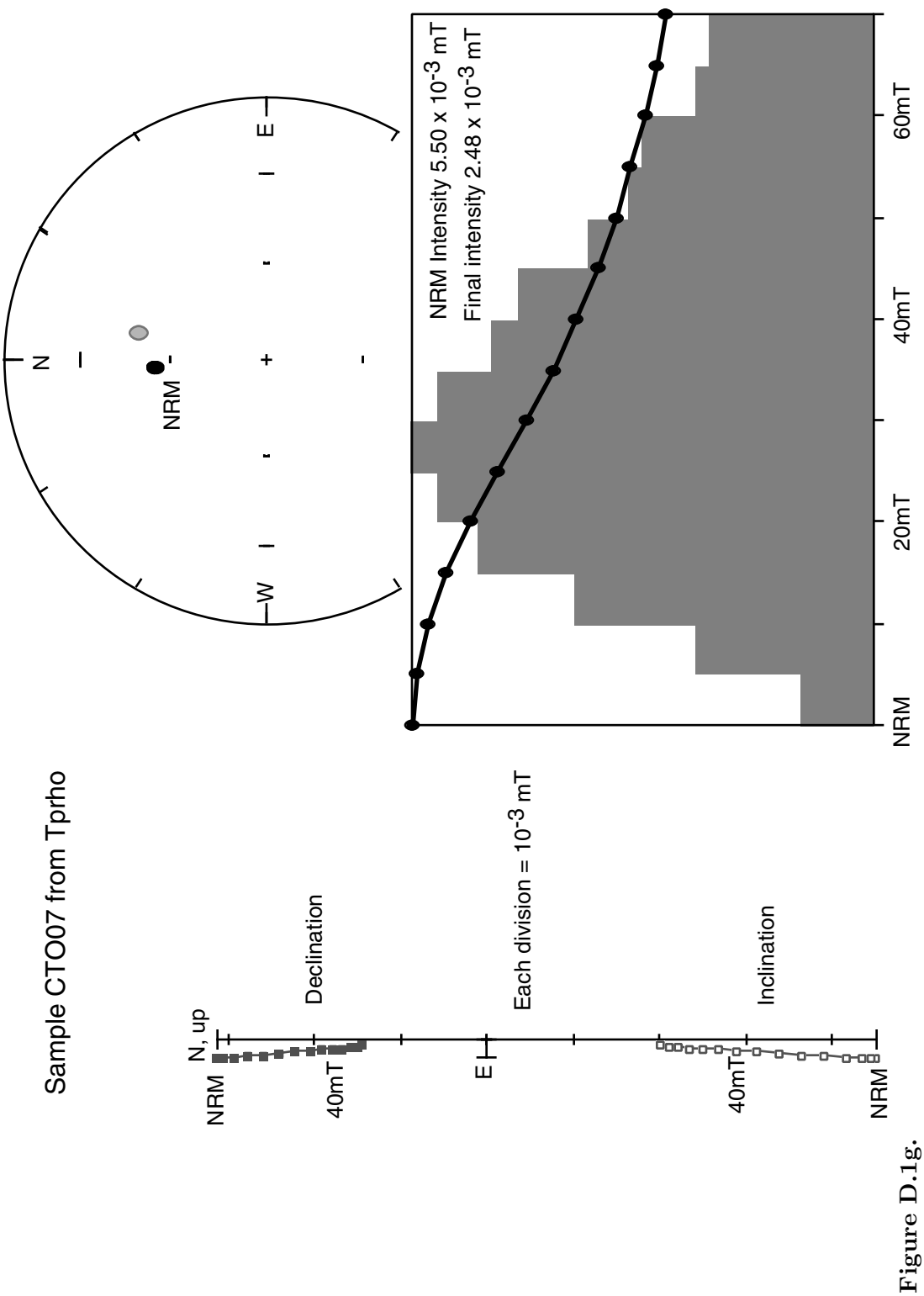
Sample CTO07 from Tprho
N, up
NRM
40mT
Declination
E
Each division = 10-3 mT
40mT
Inclination
NRM
N
E
W
NRM
NRM Intensity 5.50 x 10-3 mT
Final intensity 2.48 x 10-3 mT
NRM
20mT
40mT
60mT

Figure D.1g.

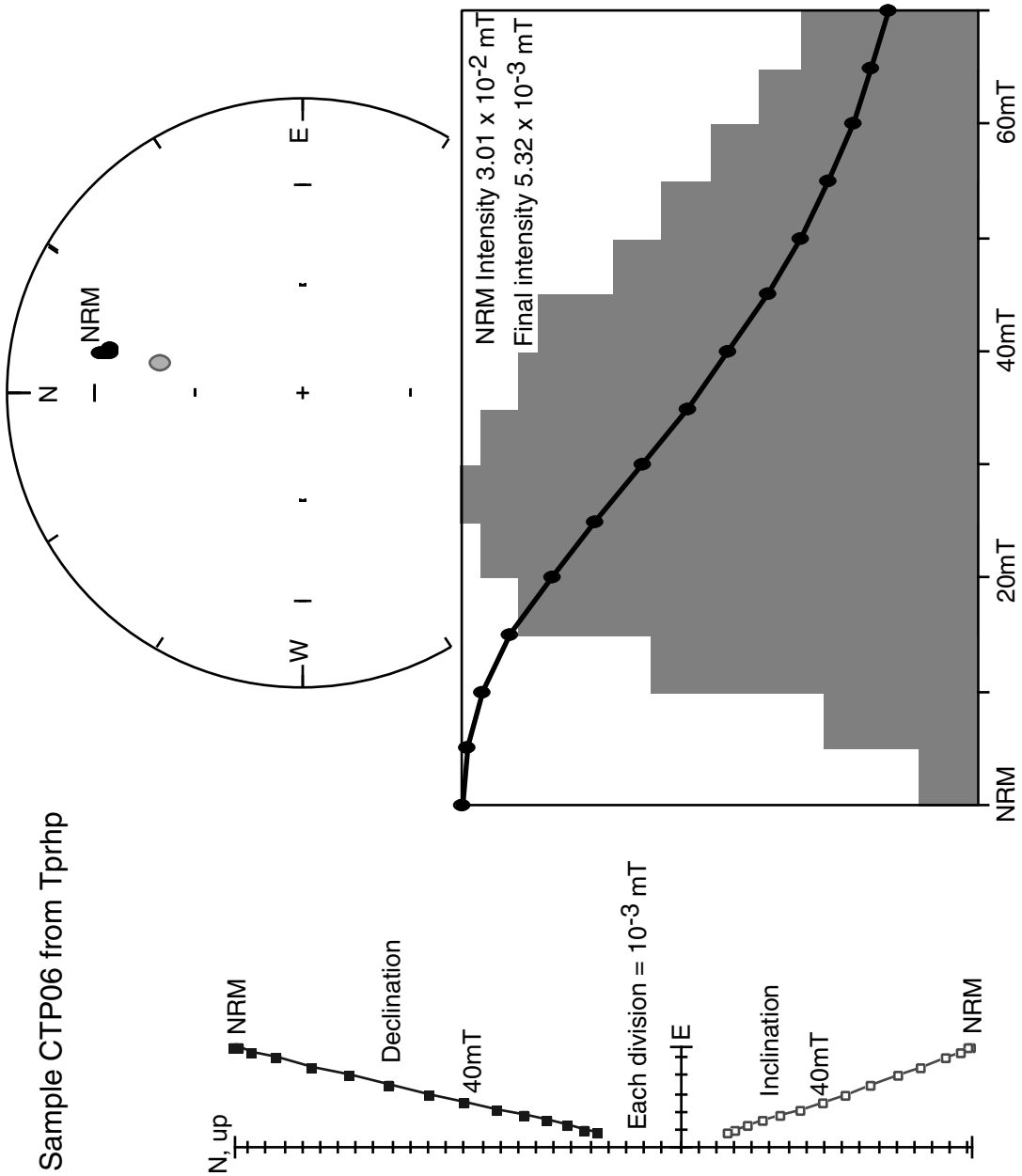
Sample CTP06 from Tprhp
N
E
W
NRM
NRM Intensity 3.01 x 10-2 mT
Final intensity 5.32 x 10-3 mT
NRM
20mT
40mT
60mT
N, up
NRM
Declination
40mT
Each division = 10-3 mT
E
Inclination
40mT
NRM

Figure D.1h.

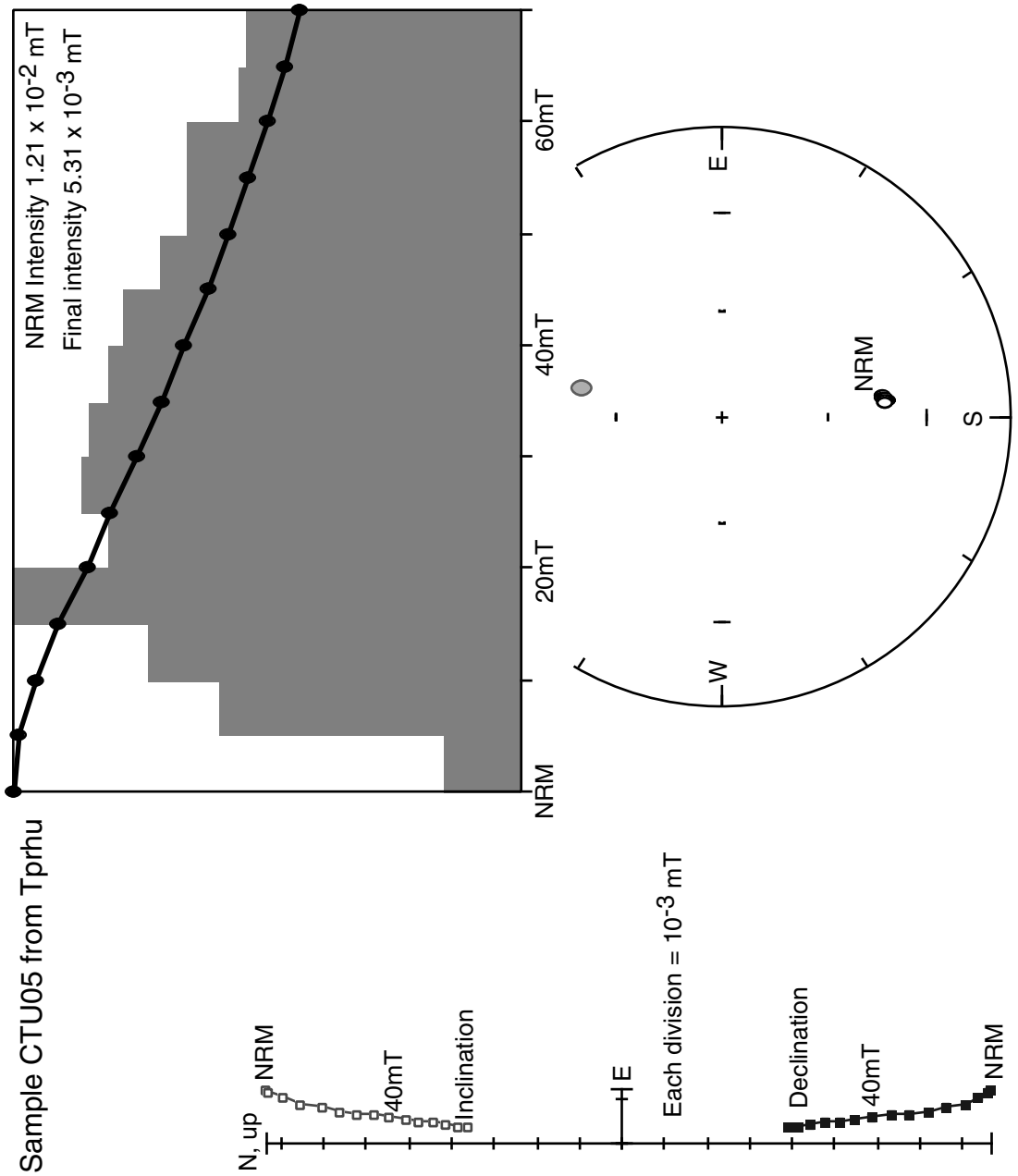
Sample CTU05 from Tprhu
NRM Intensity 1.21 x 10-2 mT
Final intensity 5.31 x 10-3 mT
NRM
20mT
40mT
60mT
W
E
S
NRM
N, up
NRM
40mT
Inclination
E
Each division = 10-3 mT
Declination
40mT
NRM

Figure D.1i.

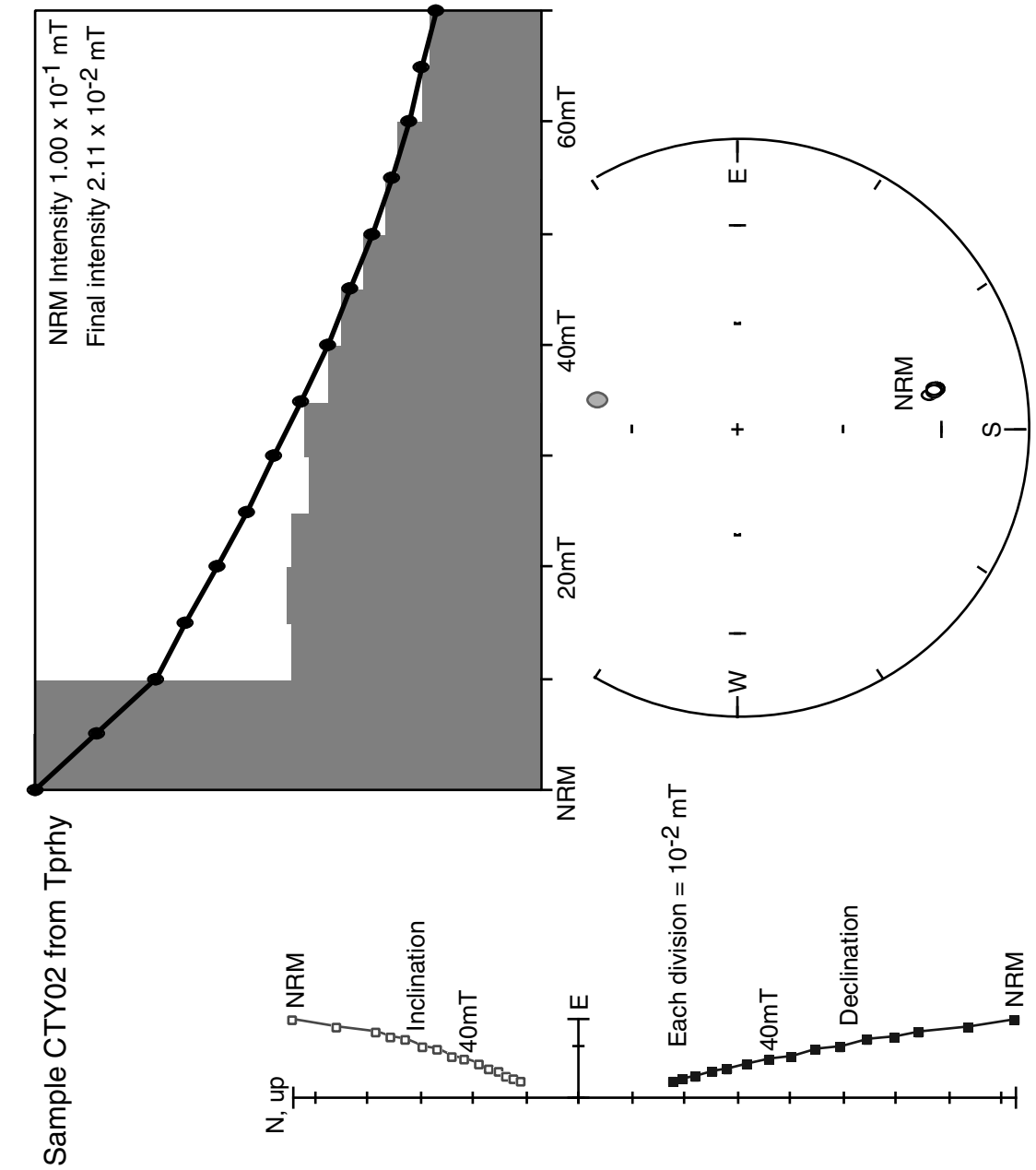
Sample CTY02 from Tprhy
NRM Intensity 1.00 x 10-1 mT
Final intensity 2.11 x 10-2 mT
NRM
20mT
40mT
60mT
W
E
S
NRM
N, up
NRM
Inclination
40mT
E
Each division = 10-2 mT
40mT
Declination
NRM

Figure D.1j.

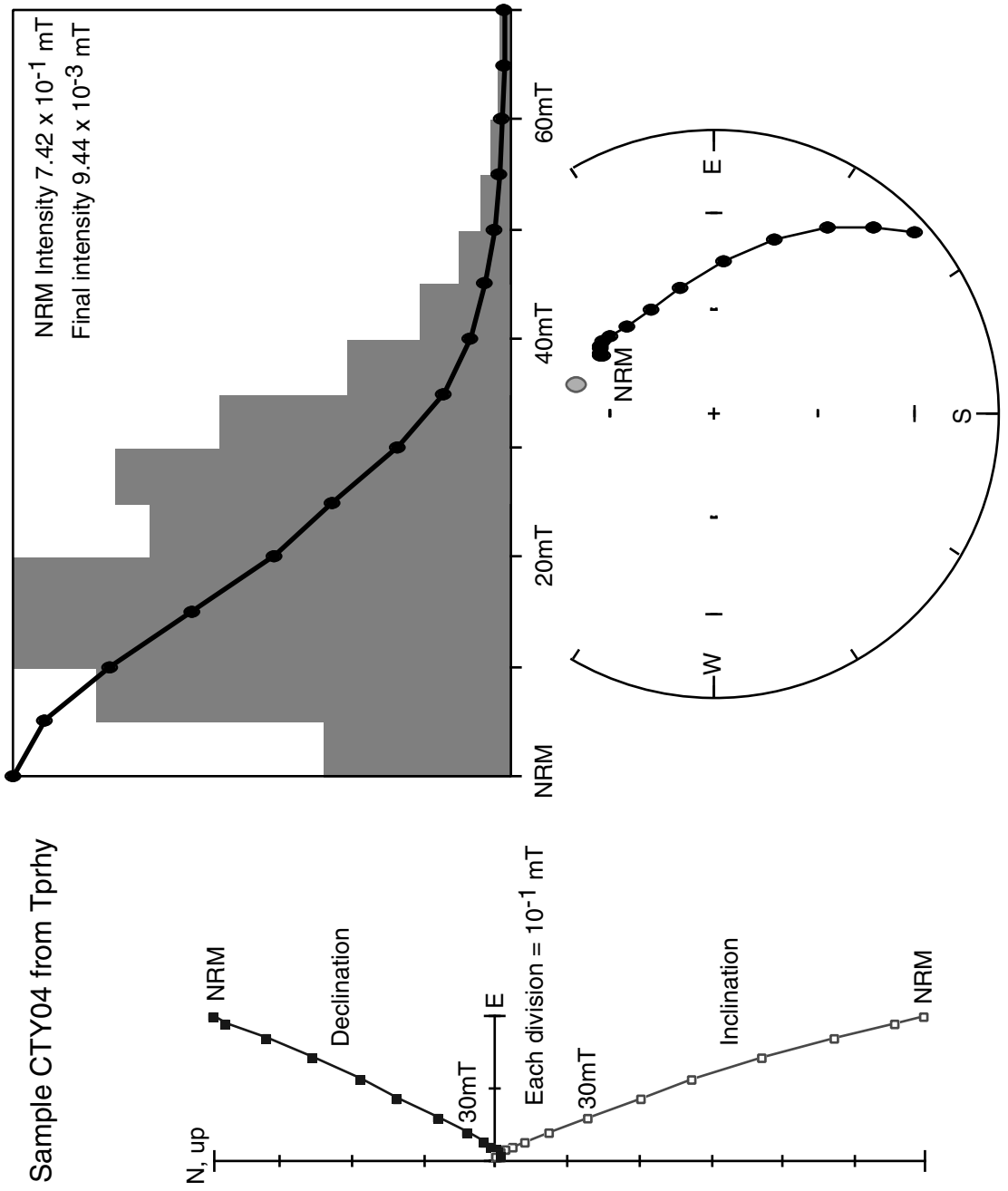
Sample CTY04 from Tprhy
NRM Intensity 7.42 x 10-1 mT
Final intensity 9.44 x 10-3 mT
NRM
20mT
40mT
60mT
W
N
E
S
NRM
N, up
Declination
30mT
E
Each division = 10-1 mT
30mT
Inclination
NRM

Figure D.1k.

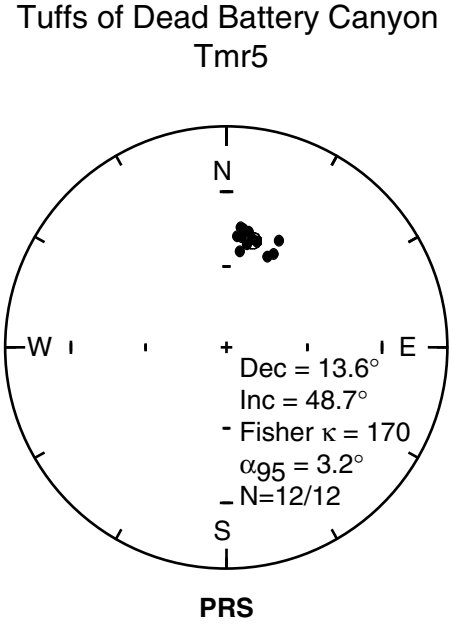

Figure D.2. (3 pages) Representative demagnetization plots from correlative tuffs on Isla Tiburón and coastal Sonora. Cooling unit Tmr5 of the Tuffs of Dead Battery Canyon, cooling units Tmr3 and Tmr4 of the Tuffs of Mesa Cuadrada, and the Tuff of San Felipe shown. Ellipses are $\alpha_9 5$. Fisher confidence cones centered on the means. Sample HE is from a locality 5 km south of Hermosillo, Sonora (Fig. 1.3) in a tuff described by *Paz-Moreno et al.* [2000] that is chemically and lithologically similar to the Tuff of San Felipe.

Figure D.2, continued.

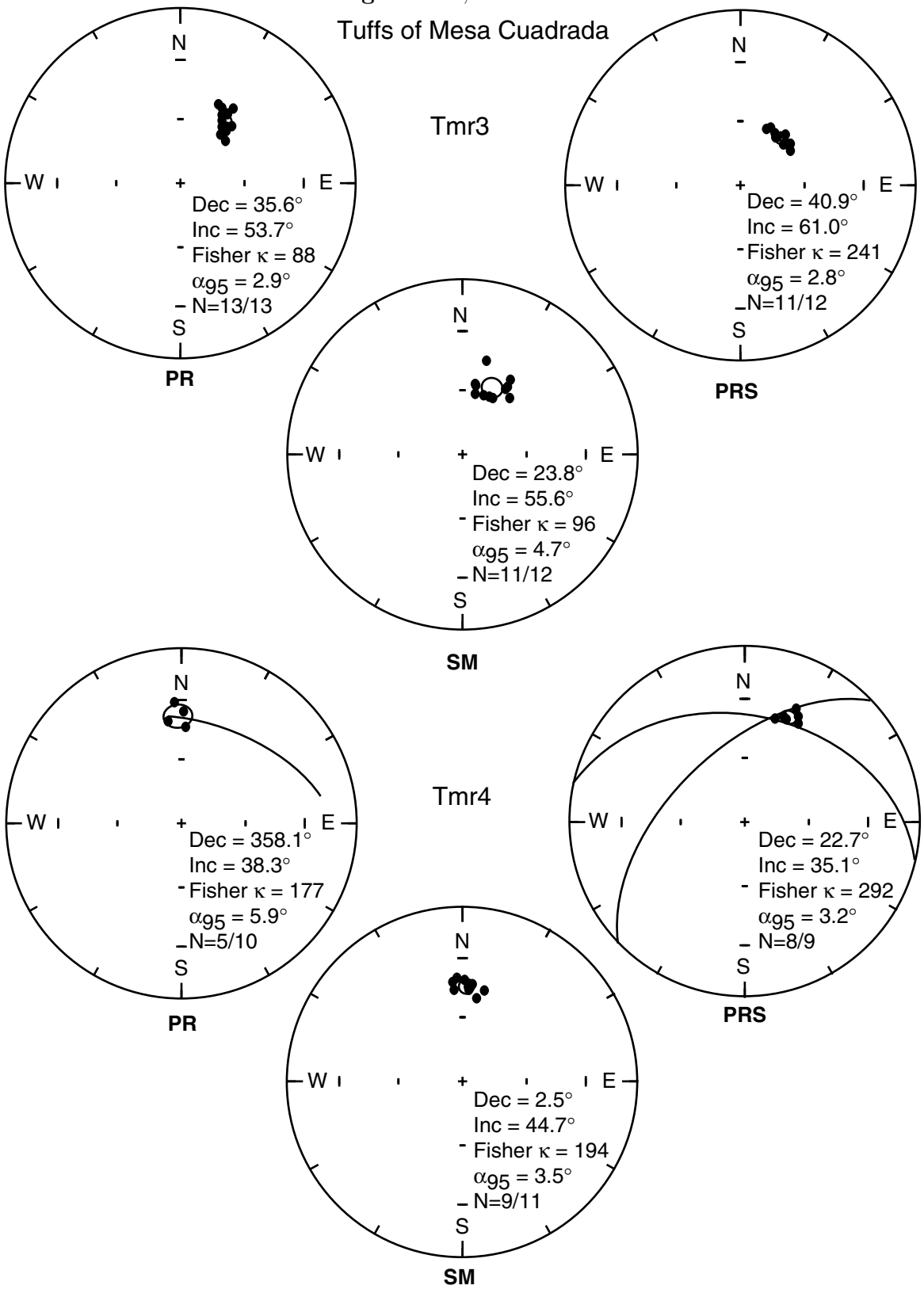

Figure D.2, continued.

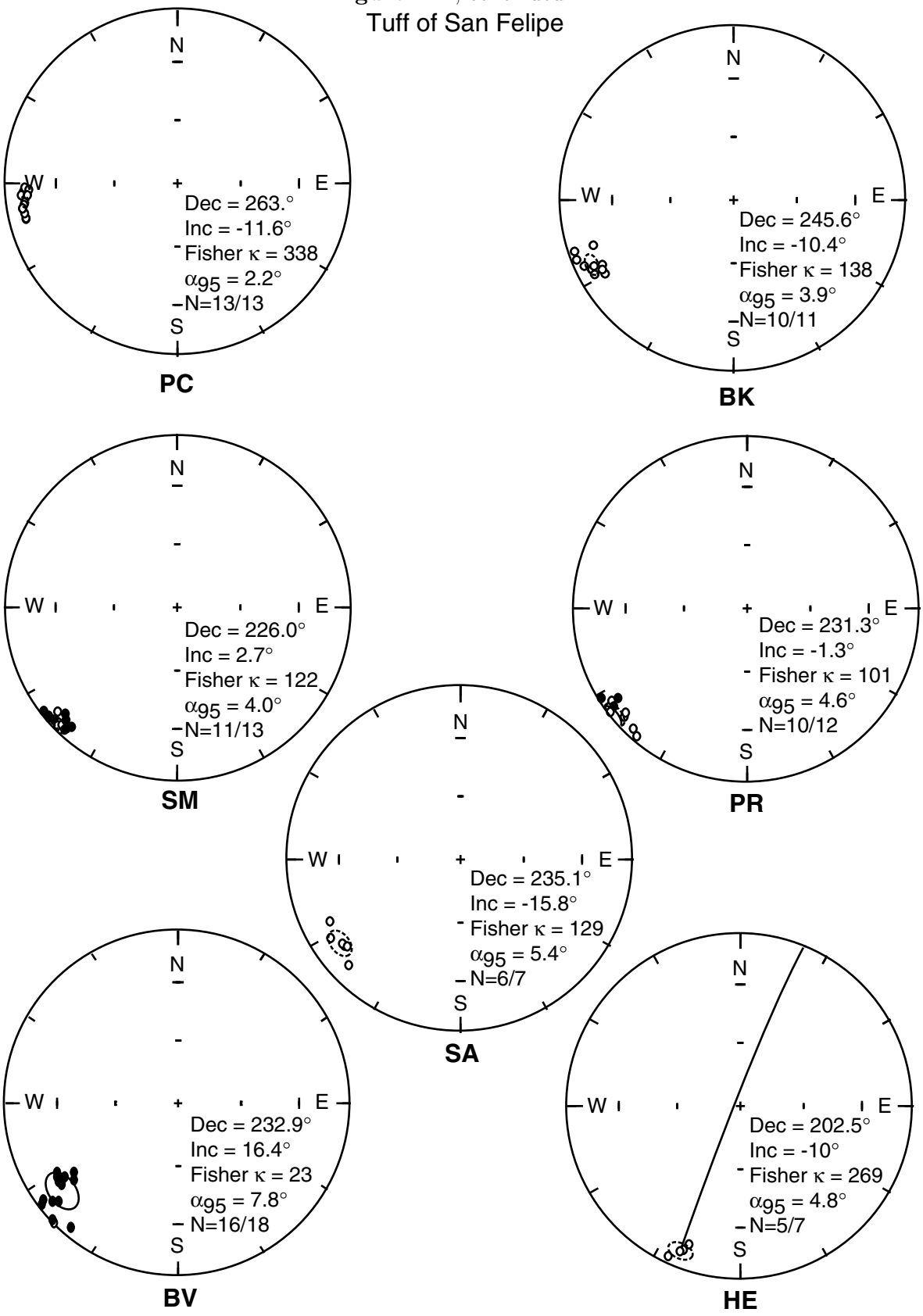

Appendix E

Data Repository tables from 'Active parasitic folds on the Elysian Park anticline: Implications for seismic hazard in central Los Angeles, California'

Table E.1. Soil description of Qg1 terrace surface from beneath Rowan Avenue.

Horizon	Depth (cm)	Thickness (cm)	Color dry ; moist	Texture	Structure	Consistency Dry	Wet
Pedon FL-14A							
Fill?	61-69	8	10YR4/3.5; 10YR3/3	CL	3g-1msbk	so	s, vp
			0.13	N/A	0	0	0.75
Bt	69-132	63	10YR5/3; 10YR4/2	SCL	2-3mabk	h	vs, vp
			0.05	0.25	0.5	0.5	1
2Bt	132-204	72	10YR5/4; 10YR4/2	SL	2mpl;2msbk	h	s, p
			0.1	0	0.2	0.5	0.5
3Bt	204-229	25	10YR6/5; 10YR4/3	SCL	2mabk	vh	vs, p
			0.2	0.25	0.4	0.75	0.75
3Bt2	229-320	91	10-7.5YR5/4; 10-7.5YR4/3	SC	2-3mpr	eh	vs, vp
			0.08	0.5	0.7	1	1
3Bt3	320-381	61	10YR5/6; 10YR4/4	SC-C	3mpr	eh	vs, vp
			0.3	0.63	1	1	1
4BC11	381-452	71	10YR-2.5Y5/4; 10YR-2.5Y4/3	SCL	m-1msbk	vh	ss, p
			0.2	0.25	0	0.75	0.25
4BC12	452-528	76	10YR-2.5Y5/4; 10YR-2.5Y4/3	SCL	m-sg	vh	ss, p
			0.2	0.25	0	0.75	0.25
4BC2	528-577	49	2.5Y5/4; 2.5Y4/3	SL-LS	m-1msbk	lo-so	so, po
			0.25	0.13	0	0	0
4C	577-610	33	10YR6/2.5; 10YR4/2	S	m	lo	so, po
			0.03	0	0	0	0

Table E.1, continued.

Horizon	Depth (cm)	Thickness (cm)	Color dry ; moist	Texture	Structure	Consistency Dry	Wet
Pedon FL-18							
A	31-71	10	10YR5.5/4; 10YR3/2.5	SiL	3mabk	h-vh	s, p
			0.13	0	0.6	0.63	0.5
E	71-80	9	10YR5/6; 10YR4/3	SiL	3mabk	sh	s, ps
			0.25	0	0.6	0.25	0.25
Bt	80-122	42	10YR4/4; 10YR3/3	CL	3mpr	eh	vs, vp
			0.15	0.5	1	1	1
Bt2	122-177	55	10YR4/5; 10YR3/4	CL	3mabk	eh	vs, p
			0.25	0.5	0.6	1	0.75
BC	177-241	64	7.5YR4/6; 7.5YR4/4	SCL	2mabk	sh-vh	s, p
			0.35	0.33	0.4	0.5	0.5
2BC	241-329	88	10YR5/6; 10YR4/6	SCL	2msbk	sh	ss, po
			0.4	0.33	0.17	0.25	0
2Bbeta	329-333	4	10YR4/4; 10YR4/5	SCL	2msbk	sh	ss, po
			0.25	0.2	0.17	0.25	0.13
3BC	333-386	53	10YR5/5; 10YR4/4	SCL	2fabk	sh-h	s, ps
			0.25	0.2	0.33	0.38	0.25
3BC2	386-472	86	10YR5/4; 10YR4/4	SL	m-1fsbk	lo-so	ss, po
			0.2	0	0.1	0	0.08
3C	472-589	117	10YR6/2.5; 10YR4/3	SL	m-sg	lo	so, po
			0.08	0	0	0	0

Note: Soil descriptions, with soil development index beneath. Soils are described according to SCS *Staff* [1975]. Horizon and soil development indexes calculated according to *Harden* [1982] and *Ponti* [1985]. Sample Fl-14A is taken from the borehole of the same identity located on Figure 7. Sample and borehole FL-18 is located 120m south of the section shown in Figure 7. Parent soil material is interpreted to be sand to sandy loam, with a primary clay component added for the uppermost portion of each profile.

Table E.1, continued.

Horizon	Clay films	Boundary	Horizon Index (H.I.)	H.I. X Thickness (cm)	Notes
Pedon FL-14A					
Fill?	None	a			Gravelly mat w/ripped up Bt and
	0		0.02	0.17	tar chunks
Bt	2kpo, 2mkpo; 2npf	c-g			
	0.67		0.33	20.65	
2Bt	3kpo, 2stgr	a			Structure may reflect post-soil
	0.63		0.24	17.2	Compaction
3Bt	3kpo	a			Very few mangans
	0.53		0.36	8.89	
3Bt2	3kpo, 3mkpf	c-g			Mangans, carb-coating 40-70% of pfs
	0.67		0.49	44.62	
3Bt3	4mkpo, 3kpo; 3mkpf	c			Rootlets, some mangans,
	0.8		0.62	37.87	carb in some pores
4BC11	2npo; 2stgr; v1-1npf; 1nbr				Some (10±%) pebble-sized gravel
	0.62		0.3	21.5	
4BC12	v1npo; 1stgr	g			Some (10±%) pebble-sized gravel
	0.37		0.26	19.84	
4BC2	None	c-g			
	0		0.06	3.06	
4C	none	?			
	0		0	0	
		Maximum Horizon Index:	0.62		
		Soil Development Index at 400cm:	153.24		
		Soil Development Index at 549cm:	173.8		

Table E.1, continued.

Horizon	Clay films	Boundary	Horizon Index (H.I.)	H.I. X Thickness (cm)	Notes
Pedon FL-18					
A	none	a			Top of A cut off
	0		0.23	2.25	
E	none	a			
	0		0.18	1.65	
Bt	4mkpo, 3kpo; 3stgr; 3npf	g			Mangans
	0.93		0.6	25.08	
Bt2	1n-mkpo; 3stgr; 2npf	d			Mangans, carb lining some pores
	0.63		0.5	27.35	
BC	1npo; 3stgr; 1nbr	g			Mangans
	0.6		0.36	23.29	
2BC	4stgr, 1nco; 3nbr	a			Mangans lining some pores;
	0.73		0.31	27.62	mottles in upper portion of profile
2Bbeta	4stgr, 2nco, 3mkbr	a			
	0.77		0.27	1.09	
3BC	v1npo; v1npf	g			
	0.3		0.24	12.88	
3BC2	v1stgr	g			
	0.27		0.09	8.12	
3C	none	a			
	0		0.01	1.46	
		Maximum Horizon Index:	0.6		
		Soil Development Index at 400cm:	128		
		Soil Development Index at 549cm:	130.8		

Table E.2. Comparison of Qg1 soil to dated chronosequences.

Chronosequence member	Mean maximum horizon index	Mean soil development index (cm)	Age (ka)
Ventura Basin[a]			
Q1	0	0	<0.02
Q2	0.1	N.D.	0.08 to 0.2
Q3	0.21	N.D.	0.5 to 5
Q4	0.36	56	8 to 12
Q5a	0.48	70	15 to 20
Q5b	0.57	106	25 to 30
Q6a	0.61	147	∼38
Q6b	0.61	153	44 to 64
Q6c	0.74	162	79 to 105
Q7a	0.85	193	160 to 200
Cajon Pass[b]			
RW-9	0.11	N.D.	0.05
RW-10&18	0.08-0.14	N.D.	0.3
RW-12	0.17	9	5.9
RW-15	0.19	7.6	7.15
RW-13	0.18	13	8.35
RW-6	0.36	18.5	11.5
RW-17	0.29	33	12.4
RW-11	0.58	73	55
RW-14	0.7	251	500

Table E.2, continued.

Chronosequence member	Mean maximum horizon index	Mean soil development index (cm)	Age (ka)
Merced River[c]			
Post Modesto	0.05-0.14	N.D.	3
Late Modesto	0.1-0.25	15	10
Early Modesto	0.48	57	40
Upper Riverbank	0.64	92	120
Lower Riverbank	0.7	N.D.	250
Anza[d]			
Q3b	0.23	26	9.5
Altadena[e]			
	0.46	104	29
East Los Angeles[f]			
FL-14A	0.62	153	50 to 80
FL-18	0.6	128	50 to 60

Note: Maximum Horizon and Soil Development Indices from three dated soil chronosequences and two additional dated soil samples developed under xeric, mediterranean climates in central and southern California. Most of these chronosequence members have several descriptions each. Thus, the index values are means. Estimate of soil development age of Qg1 surface derived from comparison of the index values measured for the Qg1 terrace soil with these chronosequences. See Table E.1 for index calculation of Qg1 terrace soil samples FL-14A and FL-18.

[a] *Rockwell et al.* [1985].

[b] *McFadden and Weldon* [1987].

[c] *Harden* [1982].

[d] *Rockwell et al.* [1990].

[e] Rockwell, unpublished data.

[f] This study.

Table E.3. Surveyed positions and logged correlations, Evergreen borehole transect.

Borehole	Position north of FL-5 (feet)	Elevation borehole top (feet)	Clay deposit, depth beneath surface			
			C1 (feet)	C2 (feet)	C3 (feet)	C4 (feet)
FL-5	0	314	14.5	20.5	N.C.	50.5
FL-4	97	318	21	28.3	38	60.5
FL-2	126	321	25	35	44.5	64.5
FL-7	157.5	324	28	37.7	47.3	70.5
FL-7B	174.3	325	27.5	38	50.5	70
FL-1	188	326	23	33	47	N.D.
FL-7A	193.5	327	21.5	32.5	47	72
FL-7C	214.7	329	12.8	23.1	36	64.25
FL-3	239	332	5	13	24.5	N.D.
FL-3A	242.5	332	3.5	11.4	N.C.	46
FL-7D	254.4	334	3.5	9.5	17	41
FL-6A	266.3	336	3	8	17.5	39.5
FL-6	277.8	336	2.5	8	15	32

Borehole logs published in *GeoTransit Consultants* [1996]. Some correlations are modified from the original report. N.C.=no correlation N.D.=No data.

Table E.4. Correlation elevations.

Borehole	Position north of FL-5 (m)	Elevation borehole top (m)	Clay deposit elevation C1 (m)	C2 (m)	C3 (m)	C4 (m)
FL-5	0	95.7	91.3	89.5	86.7[a]	80.3
FL-4	29.6	96.9	90.5	88.3	85.3	78.5
FL-2	38.4	97.8	90.2	87.2	84.3	78.2
FL-7	48	98.8	90.2	87.3	84.4	77.3
FL-7B	53.1	99.1	90.7	87.5	83.7	77.7
FL-1	57.3	99.4	92.4	89.3	85	77.7[a]
FL-7A	59	99.7	93.1	89.8	85.3	77.7
FL-7C	65.4	100.3	96.4	93.2	89.3	80.7
FL-3	72.9	101.2	99.7	97.2	93.7	86.4[a]
FL-3A	73.9	101.2	100.1	97.7	94.4	87.2
FL-7D	77.5	101.8	100.7	98.9	96.6	89.3
FL-6A	81.2	102.4	101.5	100	97.1	90.4
FL-6	84.7	102.4	101.7	100	97.8	92.7

Note: Clay horizons C1, C2, C3, and C4 on Fig. 9.9 are equivalent to a graph of these correlations.

[a] Elevation extrapolated between neighboring boreholes.

Table E.5. Line length of correlative clay horizons.

Borehole to borehole segment	Correlative clay deposit line length C1 (m)	C2 (m)	C3 (m)	C4 (m)
FL-5 to FL-4	29.6	29.6	29.6	29.6
FL-4 to FL-2	8.8	8.9	8.9	8.8
FL-2 to FL-7	9.6	9.6	9.6	9.6
FL-7 to FL-7B	5.1	5.1	5.2	5.1
FL-7B to FL-1	4.5	4.6	4.4	4.2
FL-1 to FL-7A	1.8	1.7	1.7	1.7
FL-7A to FL-7C	7.2	7.3	7.6	7.1
FL-7C to FL-3	8.1	8.4	8.6	9.3
FL-3 to FL-3A	1.2	1.2	1.3	1.3
FL-3A to FL-7D	3.7	3.8	4.3	4.2
FL-7D to FL 6A	3.7	3.8	3.7	3.8
FL-6A to FL-6	3.5	3.5	3.6	4.2

Table E.6. Bed thickness.

Borehole	Bed 1[a] (m)	Bed 2[b] (m)	Bed 3[c] (m)	Bed 1 + 2 + 3[d] (m)
FL-5	1.8	2.8	6.4	11
FL-4	2.2	3	6.9	12
FL-2	3.1	2.9	6.1	12
FL-7	3	2.9	7.1	13
FL-7B	3.2	3.8	5.9	13
FL-1	3.1	4.3	7.3	14.6
FL-7A	3.4	4.4	7.6	15.4
FL-7C	3.1	3.9	8.6	15.7
FL-3	2.4	3.5	7.4	13.3
FL-3A	2.4	3.3	7.2	13
FL-7D	1.8	2.3	7.3	11.4
FL-6A	1.5	2.9	6.7	11.1
FL-6	1.7	2.1	5.2	9

[a] Elevation of C2 horizon subtracted from the elevation of C1 horizon.

[b] Elevation of C3 horizon subtracted from the elevation of C2 horizon.

[c] Elevation of C4 horizon subtracted from the elevation of C3 horizon.

[d] Summed thickness of bed 1, bed 2, and bed 3.

Table E.7. Syndepositional folding.

Bed	Uplift			Contraction			Dip of shear plane	
	Thickness of bed at FL-4 (m)	Thickness of bed at FL-6 (m)	Uplift (Difference) (m)	Bottom of bed line length (m)	Top of bed line length (m)	Contraction (Difference) (m)	Angle (°)	Ratio (contraction / uplift)
Bed 1	2.2	1.7	0.6	58	57.3	0.6	41	1.2
Bed 2	3	2.1	0.8	58.7	58	0.8	47	0.9
Bed 3	6.9	5.2	1.7	59.4	58.7	0.7	67	0.4
Bed 1+2+3	12	9	3.1	59.4	57.3	2.1	55	0.7
Colluvium[a]	11.1	0	11.1	57.3	55.1	2.2	79	0.2

[a] Deformation occurring after deposition of C1 horizon determined by comparison with an idealized, horizontal surface.

Table E.8. Bed cross-sectional area.

Borehole to borehole segment	Bed 1 (m^2)	Bed 2 (m^2)	Bed 3 (m^2)	Bed 1 + 2 + 3 (m^2)
FL-4 to FL-2	23.3	25.9	57.3	106.4
FL-2 to FL-7	28.8	27.9	63.3	120
FL-7 to FL-7B	15.8	17.2	33.4	66.3
FL-7B to FL-1	13.1	16.9	27.7	57.6
FL-1 to FL-7A	5.4	7.3	12.5	25.2
FL-7A to FL-7C	201	27	52.4	100.4
FL-7C to FL-3	20.7	27.5	59.2	107.4
FL-3 to FL-3A	2.6	3.7	7.8	14
FL-3A to FL-7D	7.7	10.2	26.3	44.2
FL-7D to FL-6A	6.1	9.4	25.4	40.9
FL-6A to FL-6	5.6	8.8	20.8	35.3
Sum FL-4 to FL-6	149.9	181.7	386.1	717.7

Note: Cross-sectional area of each segment calculated from the straight line distance between boreholes, multiplied by the average thickness between boreholes.

Table E.9. Post-depositional penetrative contraction.

Bed	Pre-deformation model length[a]				Pre-deformation model area[b]				Measured cross-section area[c] (m^2)	Measured model area (m^2)	Extra length needed to balance area[d] (m)
	Lower flat (m)	Middle limb (m)	Upper flat (m)	Sum length (m)	Lower panel (m^2)	Middle panel (m^2)	Upper panel (m^2)	Sum area (m^2)			
Bed 1	23.6	30.2	3.5	57.3	52.5	59	5.9	117.3	149.9	32.6	14.6
Bed 2	23.6	30.8	3.5	58	69.9	78.4	7.5	155.8	181.7	25.9	8.8
Bed 3	28.1	30.7	0	58.7	192.5	184.6	0	377.2	386.1	9	1.3
Bed 1+2+3	23.6	30.2	3.5	57.3	284	317.9	31.6	633.4	717.7	84.3	7

[a] The upper, deformed boundary horizon of each bed, or beds, is used to construct an idealized section of growth strata, with a thicker section at the base of the monocline, tapering to a thinner section over the crest of the fold.

[b] Upper and lower bed thicknesses taken from boreholes FL-6, and FL-4, respectively. See table E.8 for thickness measurements. Model area calculated as a rectangular panel for the upper and lower flat area, and a trapezoidal area over the reach of the middle limb. See figure 9.14b for example.

[c] Sum from bottom of Table E.8.

[d] Measured cross-sectional area in excess of the model cross-sectional area reflects penetrative contraction and thickening of bedding at the base of the monocline. We convert this thickening into an additional length by dividing the excess area by the model bed thickness at the base of the monocline.

Table E.10. Post-depositional folding summary.

Bed	Uplift[a]	Contraction					Dip of shear plane	
		Undeformed section length[b]	Deformed section length[c]	Line length contraction[d]	Penetrative contraction[e]	Sum contraction	Angle	Ratio (contraction / uplift)
	(m)	(m)	(m)	(m)	(m)	(m)	(°)	
Bed 1	11.1	57.3	55.1	2.2	14.6	16.9	33	1.5
Bed 2	11.7	58	55.1	2.9	8.8	11.6	45	1
Bed 3	12.5	58.7	55.1	3.6	1.3	4.9	68	0.4
Bed 1+2+3	11.1	57.3	55.1	2.2	7	9.2	50	0.8

[a] Uplift calculated from the difference in elevation of the top of each bed at FL-4 and at FL-6.
[b] The line length of the deformed top of each bed.
[c] The modern difference in horizontal position between FL-4 and FL-6.
[d] Deformed length of section subtracted from the undeformed length of section.
[e] From farthest right column of Table E.9.

Table E.11. Revised syndepositional deformation.

Bed	Uplift	Contraction					Adjusted dip of vector	
		Undeformed section length[a]	Penetrative contraction[a]	Penetrative contraction[b]	Original estimate[c]	Revised contraction[d]	Angle	Ratio (contraction / uplift)
	(m)	(m)	(m)	(strain)	(m)	(m)	(°)	
Bed 1	0.6	57.3	14.6	0.2	0.6	0.8	34	1.5
Bed 2	0.8	58	8.8	0.13	0.8	0.9	43	1.1
Bed 3	1.7	58.7	1.3	0.02	0.7	0.7	67	0.4
Bed 1+2+3	3.1	57.3	7	0.11	2.1	2.4	52	0.8

Note: Penetrative contraction after deposition modifies the original length of each horizon. We revise the syndepositional contraction estimate by an additional length to compensate for post-depositional strain.

[a] From Table E.10.

[b] (Undeformed line length + Penetrative contraction) / Penetrative contraction.

[c] From Table E.7.

[d] Original contraction estimate / (1-Penetrative contraction strain).

Bibliography

Abbott, P. L., and T. E. Smith, Sonora, Mexico, Source for the Eocene Poway Conglomerate of Southern California, *Geology*, *17*(4), 329–332, 1989.

Allen, C. R., L. T. Silver, and F. G. Stehlie, Agua Blanca Fault–a major transverse structure of northern Baja California, Mexico, *Geological Society of America Bulletin*, *71*, 457–482, 1960.

Anderson, P. V., Prebatholithic stratigraphy of the San Felipe area, Baja California Norte, Mexico, in *GSA Special Paper 279: The prebatholithic stratigraphy of peninsular California*, edited by R. G. Gastil and R. H. Miller, pp. 1–10, Geological Society of America, 1993.

Angelier, J., B. Colletta, J. Chorowicz, L. Ortlieb, and C. Rangin, Fault tectonics of the Baja Califoria Peninsula and the opening of the Sea of Cortez, Mexico, *Journal of Structural Geology*, *5*(4), 347–357, 1981.

Argus, D. F., et al., Shortening and thickening of metropolitan Los Angeles measured and inferred by using geodesy, *Geology*, *27*(8), 703–706, 1999.

Atwater, T., Implications of plate tectonics for the Cenozoic evolution of western North America, *Geological Society of America Bulletin*, *81*, 3513–3536, 1970.

Atwater, T., Plate tectonic history of the northeast Pacific and western North America, in *The Eastern Pacific Ocean and Hawaii*, edited by E. L. Winterer, D. M. Hussong, and R. W. Decker, vol. N, pp. 21–72, The Geological Society of America, Boulder, Colorado, 1989.

Atwater, T., and J. M. Stock, Pacific North America plate tectonics of the Neogene

southwestern United States: An update, *International Geology Review*, *40*(5), 375–402, 1998.

Axen, G. J., Extensional segmentation of the Main Gulf Escarpment, Mexico and the United States, *Geology*, *23*, 515–518, 1995.

Axen, G. J., M. Grove, D. Stockli, O. M. Lovera, and D. A. Rothstein, Thermal evolution of Monte Blanco dome: Low-angle normal faulting during Gulf of California rifting and late Eocene denudation of the eastern Peninsular Ranges, *Tectonics*, *19*(2), 197–212, 2000.

Barrows, A. G., Surface effects and related geology of the San Fernando earthquake in the foothill region between Little Tujunga and Wilson canyons, *Bulletin - California, Division of Mines and Geology*, *196*, 97–118, 1975.

Beck, M. E., Paleomagnetic record of plate-margin tectonic processes along the western edge of North America, *Journal of Geophysical Research*, *85*, 7115–7131, 1980.

Beslier, M. O., J. Girardeau, and G. Boillot, Kinematics of peridotite emplacement during North Atlantic continental rifting, Galicia, northwestern Spain, *Tectonophysics*, *184*, 321–343, 1990.

Bischoff, J. L., and T. L. Henyey, Tectonic elements of the central part of the Gulf of Califronia, *Geological Society of America Bulletin*, *85*(12), 1893–1904, 1974.

Blake, G. H., Review of the Neogene biostratigraphy and stratigraphy of the Los Angeles Basin and implications for basin evolution, in *Active margin basins*, edited by K. T. Biddle, vol. 52 of *Memoir*, pp. 135–184, American Association of Petroleum Geologists, 1991.

Boehm, M. C., An overview of the lithostratigraphy, biostratigraphy, and paleoenvironments of the late Neogene San Felipe Marine Sequence, Baja California, Mexico, in *Geology of the Baja California Peninsula*, edited by V. A. Frizzell, vol. 39, pp.

253–265, Society of Economic Paleontologists and Mineralogists, Pacific Section, Los Angeles, California, 1984.

Branney, M. J., and B. P. Kokelaar, A reappraisal of ignimbrite emplacement: Changes from particulate to non-particulate flow during progressive aggradation of high-grade ignimbrite, *Bulletin of Volcanology*, *54*, 504–520, 1992.

Brown, L. G., Recent Fault Scarps Along the Eastern Escarpment of the Sierra San Pedro Mártir, Baja California, Master's thesis, California State University, San Diego, 1978.

Bryant, B. A., Geology of the Sierra Santa Rosa Basin, Baja California, Mexico, Master's Thesis, San Diego State University, 1986.

Buch, I. P., and M. P. Delattre, Permian and Lower Triassic stratigraphy along the 30th parallel, eastern Baja California Norte, Mexico, in *GSA Special Paper 279: The prebatholithic stratigraphy of peninsular California*, edited by R. G. Gastil and R. H. Miller, pp. 77–90, Geological Society of America, 1993.

Buck, R. W., Modes of continental extension, *Journal of Geophysical Research*, *96*, 20161–20178, 1991.

Bull, W. B., *Geomorphic responses to climatic change*, Oxford Univ. Press, New York, 1991.

Bullard, T. F., and W. R. Lettis, Quaternary fold deformation associated with blind thrust faulting, Los Angeles Basin, California, *Journal of Geophysical Research*, *98*(B5), 8349–8369, 1993.

Burchfiel, B. C., P. W. Lipman, and M. L. Zoback, eds., *The Cordilleran Orogen: Conterminous U. S.*, vol. G-3 of *The Geology of North America*, Geological Society of America, Boulder, Colorado, 1992.

Butler, R. L., *Paleomagnetism*, Blackwell Scientific Publications, Cambridge, MA, 1992.

Calmus, T., G. Poupeau, J. Defaux, and E. Labrin, Basin and range and Gulf of California tectonics: Contribution of an apatite fission track study, in *Cuarta Reunion Sobre La Geologia Del Noroeste de Mexico y Areas Adyacentes*, edited by T. Calmus and E. Pérez-Segura, vol. 2, pp. 13–14, National Autonomous University of Mexico and the University of Sonora, Hermosillo, Sonora, Mexico, 2000.

Cande, S. C., and D. V. Kent, Revised calibration of the geomagnetic polarity timescale for the late Cretaceous and Cenezoic, *Journal of Geophysical Research*, *100*, 6093–6096, 1995.

Carreño, A. L., Biostratigraphy of the Late Miocene to Pliocene on the Pacific island Maria Madre, Mexico, *Micropaleontology*, *31*(2), 139–166, 1985.

Carreño, A. L., Neogene microfossils from the Santiago Diatomite, Baja California Sur, Mexico, *Paleontología Mexicana*, *59*, 1992.

Cassidy, M. E., Marine Stratigraphy and paleontology of southwestern Isla Tiburón, Master's, San Diego State University, 1988.

Clark, R. N., Spectroscopy of rocks and minerals and principles of spectroscopy, in *Remote Sensing for the Earth Sciences*, edited by A. N. Rencz, vol. 3 of *Manual of Remote Sensing*, 3rd ed., pp. 1–58, John Wiley and Sons, New York, 1998.

Cochran, J. T., A model for development of Red Sea, *American Association of Petroleum Geologists Bulletin*, *67*(1), 41–69, 1983.

Coney, P. J., Structural aspects of suspect terranes and accretionary tectonics in western North America, *Journal of Structural Geology*, *11*(1-2), 107–125, 1989.

Conly, A. G., S. D. Scott, and H. Bellon, The Boleo Cu-Co-Zn deposit of Baja California Sur: Can it be syngenetic?, in *Cuarta Reunion Sobre La Geologia Del*

Noroeste de Mexico y Areas Adyacentes, edited by T. Calmus and E. Pérez-Segura, vol. 2, National Autonomous University of Mexico and the University of Sonora, Hermosillo, Sonora, Mexico, 2000.

Couch, R. W., G. E. Ness, O. Sánchez-Zamora, G. Calderón-Riveroll, P. Doguin, T. Plawman, S. Coperude, B. Huenn, and W. Gumma, Gravity anomolies and crustal structure of the Gulf and Peninsular Province of the Californias, in *American Association of Petroleum Geologists Memoir 47: The Gulf and Peninsular Province of the Californias*, edited by J. P. Dauphin and B. R. T. Simoneit, vol. 47, pp. 25–45, Amercan Association of Petroleum Geologists, Tulsa, Oklahoma, 1991.

Crowell, J. C., The San Gabriel fault and Ridge Basin, southern California, in *San Andreas fault in southern California, California Division of Mines And Geology Special Report 118*, edited by J. C. Crowell, pp. 208–221, California Division of Mines an Geology, Sacramento, CA, 1974.

Crowell, J. C., An outline of the tectonic history of southeastern California, in *The geotectonic development of California*, edited by W. G. Ernst, vol. 1 of *Rubey*, pp. 583–600, Prentice-Hall, Englewood Cliffs, New Jersey, 1981.

Curray, J. R., D. G. Moore, K. Kelts, and G. Einsele, Tectonics and geological history of the passive continental margin at the tip of Baja California, in *Initial Reports of the Deap Sea Drilling Project, Leg 64*, edited by J. R. Curray and D. G. Moore, vol. 64, pp. 1089–1116, U.S. Government Printing Office, Washington, D. C., 1982.

Davis, T. L., J. Namson, and R. F. Yerkes, A cross section of the Los Angeles area: Seismically active fold and thrust belt, the 1987 Whittier Narrows earthquake, and earthquake hazard, *Journal of Geophysical Research*, *94*(B7), 9644–9664, 1989.

Dean, M. A., Neogene Fish Creek Gypsum and associated stratigraphy and paleontology, southwestern Salton Trough, California, in *Sturzstroms and detachment faults, Anza-Borrego Desert State Park, California*, edited by P. L. Abbott and

D. C. Seymour, vol. 24 of *Annual Field Trip Guidebook*, pp. 123–148, South Coast Geological Society, San Diego, CA, 1996.

Delgado-Argote, L. A., F. J. Escalona-Alcázar, M. E. Vázquez-Jaimes, and M. López-Martinez, Temporal relationship of the volcanic activity and sedimentation in the regions of Bahia de Los Angeles, Bahia Las Animas, and San Lorenzo Archipelago, Gulf of California, *Memorias, V Reunión sobre Geologia de la Peninsula de Baja California*, *5*, 2000a.

Delgado-Argote, L. A., M. López-Martínez, and M. C. perrilliat, Geologic reconnaissance and age of volcanism and associated fauna from sediments of Bahia de Los Angeles Basin, central Gulf of California, in *Cennezoic tectonics and volcanism of Mexico*, edited by J. Stock, G. Aguirre, and H. Delgado, vol. 334 of *Geological Society of America Special Paper*, pp. 111–121, Geological Society of America, Boulder, CO, 2000b.

Demarest, H. H., Error analysis for the determination of tectonic rotation from paleomagnetic data, *Journal of Geophysiscal Research*, *88*, 4321–4328, 1983.

DeMets, C., A reappraisal of seafloor spreading lineations in the Gulf of California: Implications for transfer of Baja California to the Pacific plate and estimates of Pacific-North America motion, *Geophysical Research Letters*, *22*(24), 3545–3548, 1995.

DeMets, C., and T. H. Dixon, New kinematic models for Pacific-North America motion from 3 Ma to present, I: Evidence for steady motion and biases in the NUVEL-1A model, *Geophysical Research Letters*, *26*(13), 1921–1924, 1999.

DePaolo, D. J., A neodymium and strontium isotopic study of the Mesozoic calc-alkaline granitic batholiths of the Sierra Nevada and Peninsular Ranges, California, *Journal of Geophysical Research*, *86*(10470-10488), 1981.

Dibblee, T. W. J., Geologic map of the Los Angeles Quadrangle, Los Angeles County, California, 1989.

Dibblee, T. W. J., Geologic map of the Hollywood and Burbank South 1/2 quadrangles, Los Angeles County, California, 1991.

Dickinson, W. R., *Kinematics of Transrotational Tectonism in the California Transverse Ranges and its Contribution to Cumulative Slip Along the San Andreas Transform Fault System, Geological Society of America Special Paper 305*, Geological Society of America, Boulder, Colorado, 1996.

Dickinson, W. R., and T. F. Lawton, Carboniferous to Cretaceous assembly and fragmentation of Mexico, *Geological Society of America Bulletin*, *13*(9), 1142–1160, 2001.

Dickinson, W. R., and B. P. Wernicke, Reconciliation of San Andreas slip discrepancy by a combination of interior Basin and Range extension and transrotation near the coast, *Geology*, *25*(7), 663–665, 1997.

Dillon, J. T., and P. L. Ehlig, Displacement on the southern San Andreas fault, in *The San Andreas fault system: Displacement, palinspastic reconstruction, and geologic evolution: Geological Society of America Memoir 178*, edited by R. E. Powell, I. Weldon, R. J., and J. C. Matti, pp. 199–216, Geological Society of America, Boulder, CO, 1993.

Dixon, T., F. Farina, C. DeMets, F. Suarez-Vidal, J. Fletcher, B. Marquez-Azua, M. Miller, O. Sancjez, and P. Umhoefer, New kinematic models for Pacific-North America motion from 3 Ma to present, II: Evidence for a 'Baja California shear zone', *Geophysical Research Letters*, *27*(23), 3961–3964, 2000.

Dokka, R. K., and R. H. Merriam, Late Cenozoic extension of northeastern Baja California, Mexico, *Geological Society of America Bulletin*, *93*(5), 371–378, 1982.

Dolan, J. F., and K. E. Sieh, Paleoseismology and geomorphology of the northern Los Angeles Basin: Evidence for Holocene activity on the Santa Monica fault and identification of new strike-slip faults through downtown Los Angeles, *American Geophysical Union Fall Meeting Abstracts with Programs*, *73*, 589, 1994.

Dolan, J. F., K. E. Sieh, T. K. Rockwell, R. Yeats, J. Shaw, J. Suppe, G. Huftile, and E. Gath, Prospects for larger or more frequent earthquakes in the Los Angeles metropolitan region, *Science*, *267*, 199–205, 1995.

Dolan, J. F., K. E. Sieh, T. K. Rockwell, P. Guptill, and G. Miller, Active tectonics, paleoseismology and seismic hazards of the Hollywood fault, southern California, *Geological Society of America Bulletin*, *109*(12), 1595–1616, 1997.

Dorsey, R. J., and B. Burns, Regional stratigraphy, sedimentology, and tectonic significance of Oligocene-Miocene sedimentary and volcanic rocks, northern Baja California, Mexico, *Sedimentary Geology*, *88*, 231–251, 1994.

Driscoll, N. W., and G. D. Karner, Lower crustal extension across the Northern Carnarvan basin, Australia: Evidence for an eastward dipping detachment, *Journal of Geophysical Research*, *103*(B3), 4975–4991, 1998.

Ebinger, C. J., and M. Casey, Continental breakup in magmatic province: An Ethiopian example, *Geology*, *29*(6), 527–530, 2001.

Eguchi, R. T., Direct economic losses from the Northridge Earthquake: a 3 year post-event perspective, *Earthquake Spectra*, *14*(2), 20, 1998.

Ehlig, P. L., Origin and tectonic history of the basement terrane of the San Gabriel Mountains, central Transverse Ranges, in *The Geotectonic Development of California; Rubey Volume 1*, edited by W. G. Ernst, pp. 253–283, Prentice-Hall, Englewood Cliffs, NJ, 1981.

Ehlig, P. L., K. W. Ehlert, and B. M. Crowe, Offset of the upper Miocene Caliente and Mint Canyon Formations along the San Gabriel and San Andreas Faults, in *San*

Andreas Fault in Southern California: California Division of Mines and Geology Special Report 118, edited by J. C. Crowell, pp. 83–92, California Division of Mines and Geology, Sacremento, 1975.

England, P., Constraints on extension of continental lithosphere, *Journal of Geophysical Research*, *88*, 1145–1152, 1983.

Faulds, J. E., and R. J. Varga, The role of accommodation zones and transfer zones in the regional segmentation of extended terranes, in *Accommodation Zones and Transfer zones: the Regional Segmentation of the Basin and Range Province*, edited by J. E. Faulds and J. H. Stewart, vol. 323 of *Geological Society of America Special Paper*, pp. 1–46, Geological Society of America, Boulder, CO, 1998.

Fenby, S. S., and R. G. Gastil, A seismo-tectonic map of the Gulf of California and surrounding areas, in *The Gulf and Peninsular Provinces of the Californias , American Association of Petroleum Geologists Memoir 47*, edited by J. P. Dauphin and B. R. Simoneit, pp. 79–83, American Association of Petroleum Geologists, 1991.

Fuis, G. S., W. D. Mooney, J. H. Healy, G. A. McMechan, and W. J. Lutter, A seismic refraction survey of the Imperial Valley Region, California, *Journal of Geophysical Research*, *89*, 1165–1189, 1984.

Gabb, W. M., Notes on the Geology of Lower California, in *Geology*, edited by J. Whitney, vol. 2, pp. 137–148, Calfornia Geological Survey, Sacramento, CA, 1882.

Gans, P. B., Large-magnitude Oligo-Miocene extension in southern Sonora: Implications for the tectonic evolution of northwest Mexico, *Tectonics*, *16*(3), 388–408, 1997.

Gastil, G., G. Morgan, and D. Krummenacher, The tectonic history of peninsular California and adjacent Mexico, in *The Geotectonic Development of California,*

Rubey Volume 1, edited by W. Ernst, pp. 285–306, Prentice-Hall, Englewood Cliffs, New Jersey, 1981.

Gastil, G. R., and R. H. Miller, *The prebatholithic stratigraphy of peninsular California*, vol. 279 of *Geological Society of America Special Paper*, Geological Society of America, 1993.

Gastil, G. R., J. Neuhaus, M. Cassidy, J. T. Smith, J. C. Ingle, and D. Krummenacher, Geology and paleontology of southwestern Isla Tiburón, Sonora, Mexico, *Revista Mexicana de Ciencias Geológicas*, *16*(1), 1–34, 1999.

Gastil, R. G., Prebatholithic history of peninsular California, in *The prebatholithic stratigraphy of peninsular California, Geological Society of America Special Paper 279*, edited by R. G. Gastil and R. H. Miller, vol. 279, pp. 145–156, Geological Society of America, Boulder, CO, 1993.

Gastil, R. G., and D. Krummenacher, Reconnaissance geologic map of coastal Sonora between Puerto Lobos and Bahia Kino, GSA Map and Chart Series MC-16, 1976.

Gastil, R. G., and D. Krummenacher, Reconnaissance geology of coastal Sonora between Puerto Lobos and Bahia Kino, *Geological Society of America Bulletin*, *88*(2), 189–198, 1977.

Gastil, R. G., D. V. Lemone, and W. J. Stewart, Permian fusulinids from near San Felipe, Baja California, *AAPG Bulletin*, *57*, 746–747, 1973.

Gastil, R. G., R. P. Phillips, and E. C. Allison, *Reconnaissance geology of the State of Baja California, Geological Society of America Memoir 140*, Memoir - Geological Society of America, Geological Society of America, Boulder, CO, 1975.

Gastil, R. G., G. Morgan, and D. Krummenacher, Mesozoic history of peninsular California and related areas east of the Gulf of California, in *Mesozoic paleogeography of the western United States*, edited by D. G. Howell and K. McDougall,

pp. 107–115, American Association of Petroleum Geologists, Sacramento, Calif., United States, 1978.

Gastil, R. G., D. Krummenacher, and J. A. Minch, The record of Cenozoic volcanism around the Gulf of California, *Geological Society of America Bulletin*, *90*(9), 839–857, 1979.

Gastil, R. G., et al., The relation between the Paleozoic strata on opposite sides of the Gulf of California, in *Studies of Sonoran Geology: Geological Society of America Special Paper 254*, edited by E. Perez-Segura and C. Jacques-Ayala, pp. 7–16, Geological Society of America, Boulder, CO, 1991.

GeoTransit Consultants, Geotechnical Investigation for: Preliminary engineering program eastside extension Metro Red Line project, *Tech. Rep. 94-1100*, GeoTransit Consultants, 1994.

GeoTransit Consultants, Final fault investigation for: Engineering design program eastside extension Metro Red Line project, *Tech. Rep. 95-8347-18*, GeoTransit Consultants, 1996.

Gónzalez-Fernández, A., J. J. Dañobietia, D. Córdova, L. A. Delgado-Argote, R. Carbonell, R. Bartolomé, and F. Michaud, Lithospheric structure of the upper Gulf of California using deep seismic and gravity data, in *Memorias, V Reunión sobre Geologia de la Peninsula de Baja California*, edited by L. C. Magaña, vol. 5, pp. 69–70, Universidad Autonoma de Baja California, Loreto, Baja California Sur, 2000.

Hamilton, W., Recognition on space photographs of structural elements of Baja California, *Professional Paper 718*, U.S. Geological Survey, 1971.

Hanks, T. C., and H. Kanamori, A moment magnitude scale, *Journal of Geophysical Research*, *84*(B5), 2348–2350, 1979.

Harden, J. W., A quantitative index of soil development from field descriptions: Examples from a chronosequence in Central California, *Geoderma*, *28*, 1–28, 1982.

Hauksson, E., L. Jones, T. L. Davis, K. Hutton, A. Brady, P. Reasenberg, A. Michael, and R. F. Yerkes, The 1987 Whittier Narrows earthquake in the Los Angeles metropolitan area, California, *Science*, *239*, 1409–1412, 1988.

Hauksson, E., L. Jones, and K. Hutton, The 1994 Northridge earthquake sequence in California: Seismological and tectonic aspects, *Journal of Geophysical Research*, *100*(B7), 12,335–12,355, 1995.

Hausback, B., et al., Isla San Luis Volcano, Baja California, Mexico–Timing of Volcanic Activity, in *American Geophysical Union 2000 Fall Meeting*, edited by Anonymous, vol. 81, p. 1359, American Geophysical Union, San Francisco, CA, 2000.

Hausback, B. P., Cenozoic volcanic and tectonic evolution of Baja California Sur, Mexico, in *Geology of the Baja California Peninsula*, edited by J. Frizzell, Virgil A., vol. 39, pp. 219–236, Pacific Section of the Economic Paleontologists and Mineralogists, Los Angeles, California, 1984.

Heaton, T., J. Hall, D. Wald, and M. Halling, Response of High-Rise and Base-Isolated Buildings to a Hypothetical Mw7.0 Blind Thrust Earthquake, *Science*, *267*, 206–211, 1995.

Helenes, J., and A. L. Carreño, Neogene sedimentary evolution of Baja California in relation to regional tectonics, *Journal of South American Earth Sciences*, *12*, 589–605, 1999.

Henry, C. D., and J. J. Aranda Gomez, The real southern basin and range: Mid Cenozoic to Late Cenozoic extension in Mexico, *Geology*, *20*(8), 701–704, 1992.

Henyey, T. L., and J. L. Bischoff, Tectonic elements of the northern part of the Gulf of California, *GSA Bulletin*, *84*, 315–330, 1973.

Herzig, C. T., and D. C. Jacobs, Cenozoic volcanism and two–stage extension in the Salton Trough, southern California and northern Baja California, *Geology*, *22*, 991–994, 1994.

Hitchcock, C. S., and K. I. Kelson, Growth of late Quaternary folds in southwest Santa Clara Valley, San Francisco Bay area, California: Implications of triggered slip for seismic hazard and earthquake recurrence, *Geology*, *27*(5), 391–394, 1999.

Holt, J. W., J. M. Stock, and E. W. Holt, An age constraint on Gulf of California rifting from the Santa Rosalía basin, Baja California Sur, Mexico, *GSA Bulletin*, *112*(4), 540–549, 2000.

Hook, S. J., E. A. Abbott, C. Grove, A. B. Kahle, and F. D. Palluconi, Multispectral thermal infrared data in geological studies, in *Remote Sensing for the Earth Sciences*, edited by A. N. Rencz, vol. 3 of *Manual of Remote Sensing*, 3rd ed., pp. 1–58, John Wiley and Sons, New York, 1998.

Hoots, H. W., Geology of the eastern part of the Santa Monica Mountains, Los Angeles county, California, *U.S. Geological Survey Professional Paper*, *165-C*, 82–134, 1930.

Hopper, J. R., and W. Buck, Effect of lower crustal flow on continental extension and passive margin formation, *Journal of Geophysical Research*, *101*(B9), 20,175–20,194, 1996.

Hull, A. G., and C. Nicholson, Seismotectonics of the northern Elsinore fault zone, southern California, *Bulletin of the Seismological Society of America*, *82*, 800–818, 1992.

Hummon, C., C. Schneider, R. Yeats, J. F. Dolan, K. E. Sieh, and G. Huftile, The Wilshire Fault: Earthquakes in Hollywood?, *Geology*, *22*, 291–294, 1994.

Ichinose, G. A., S. Day, H. Magistrale, T. Prush, F. Vernon, and A. Edelman, Crustal

thickness variations beneath the Peninsular Ranges, southern California, *Geophysical Research Letters*, *23*, 3095–3098, 1996.

Johnson, N. M., C. B. Officer, N. D. Opdyke, G. D. Woodard, P. K. Zeitler, and E. H. Lindsay, Rates of late Cenezoic tectonism in the Vallecito-Fish Creek basin, western Imperial Valley, California, *Geology*, *11*, 664–667, 1983.

Jones, L., K. E. Sieh, E. Hauksson, and K. Hutton, The 3 December 1988 Pasadena, California earthquake: Evidence for strike-slip motion on the Raymond fault, *Seismological Society of America Bulletin*, *80*, 474–482, 1990.

Krummenacher, D., G. R. G., J. Bushee, and J. Doupont, K-Ar apparent ages, Peninsular Ranges batholith, southern California and Baja California, *Geological Society of America Bulletin*, *86*, 760–768, 1975.

Lamar, D. L., Geology of the Elysian Park-Repetto Hills area, Los Angeles County, California, *California Division of Mines Special Report*, *101*, 45, 1970.

Larson, R. L., H. W. Menard, and S. M. Smith, Gulf of California: a result of ocean floor spreading and transform faulting, *Science*, *161*, 781–784, 1968.

Law/Crandall, Report of Seismic Hazard Investigation, Proposed East Side Line Extension, Metro Red Line, Santa Fe Avenue, *Tech. rep.*, Law/Crandall, 1997.

Lee, J., M. Miller, R. Crippen, B. Hacker, and J. Ledesma-Vazquez, Middle Miocene extension in the Gulf extensional province, Baja California: Evidence from the southern Sierra Juárez, *GSA Bulletin*, *108*(5), 505–525, 1996.

Lewis, C. J., Constraints on extension in the Gulf extensional province from the Sierra San Fermín, northeastern Baja California, Mexico, Ph.D. Thesis, Harvard University, 1994.

Lewis, C. J., Stratigraphy and geochronology of Miocene and Pliocene volcanic rocks in the Sierra San Fermín and southern Sierra San Felipe, Baja California, Mexico, *Geofisica Internacional*, *35*, 1–31, 1996.

Lewis, C. J., and J. M. Stock, Paleomagnetic evidence of localized vertical-axis rotation during Neogene extension of the Sierra San San Fermín, northeastern Baja California, Mexico, *JGR*, *103*, 2455–2470, 1998a.

Lewis, C. J., and J. M. Stock, Late Miocene to recent transtensional tectonics in the Sierra San Fermín, northeastern Baja California, Mexico, *J. Structural Geology*, *20*, 1043–1063, 1998b.

Lewis, J. L., S. M. Day, H. Magistrale, J. Eakins, and F. Vernon, Regional crustal thickness variations of the Peninsular Ranges, southern California, *Geology*, *28*(4), 303–306, 2000.

Lewis, J. L., S. M. Day, H. Magistrale, R. R. Castro, L. Astiz, C. Rebollar, J. Eakins, F. L. Vernon, and J. N. Brune, Crustal thickness of the Peninsular Ranges and Gulf Extensional Province in the Californias, *Journal of Geophysical Research*, *106*(B7), 13,599–13,611, 2001.

Lister, G. S., M. A. Etheridge, and P. A. Symonds, Detachment models for the formation of passive continental margins, *Tectonics*, *10*(5), 1038–1064, 1991.

Lonsdale, P., Geology and tectonic history of the Gulf of California, in *The Eastern Pacific Ocean and Hawaii, Geology of North America, Volume N*, edited by E. L. Winterer, D. M. Hussong, and R. W. Decker, pp. 499–521, Geological Society of America, Boulder, CO, 1989.

Lonsdale, P., Structural Patterns of the Pacific Floor offshore of Peninsular California, in *American Association of Petroleum Geologists Memoir 47: The Gulf and Peninsular Province of the Californias*, edited by J. P. Dauphin and B. R. T. Simoneit, vol. 47, pp. 87–143, American Association of Petroleum Geologists, Tulsa, Oklahoma, 1991.

Louden, K. E., and D. Chian, The deep structure of non-volcanic rifted continental

margins, *Philosophical Transactions of the Royal Society of London*, *357*, 767–804, 1999.

Lyle, M. W., and G. E. Ness, The opening of the southern Gulf of California, in *The Gulf and Peninsular Province of the Californias: American Association of Petroleum Geologists Memoir 47*, edited by J. P. Dauphin and B. R. T. Simoneit, vol. 47, pp. 403–423, American Association of Petroleum Geologists, Tulsa, Oklahoma, 1991.

Magistrale, H., S. Day, R. W. Clayton, and R. Graves, The SCEC southern California reference three-dimensional seismic velocity model version 2, *Bulletin of the Seismological Society of America*, *90*(6B), S65–S76, 2000.

Mahon, K. I., The new "York" regression: application of an improved statistical method to geochemistry, *International Geology Review*, *38*, 293–303, 1996.

Mammerickx, J., and K. D. Klitgord, Northern East Pacific Rise: Evolution from 25 m.y. B.P. to the present, *JGR*, *87*(B8), 6751–6759, 1982.

Martín-Barajas, A., and J. M. Stock, Estratigrafía y petrología de la secuencia volcánica de Puertecitos, Noreste de Baja California. Transición de un arco volcánico a rift, in *Contribuciones a la Tectónica del Occidente de México. Monografía No. 1 de la Unión Geofísica Mexican*, edited by L. A. Delgado-Argote and A. Martín-Barajas, vol. 1, pp. 66–89, Mexican Geophysical Union, Mexico City, Mexico, 1993.

Martín-Barajas, A., J. M. Stock, P. Layer, B. Hausback, P. Renné, and M. Martínez-López, Arc-rift transition volcanism in the Puertecitos Volcanic Province, northeastern Baja California, Mexico, *GSA Bulletin*, *107*(4), 407–424, 1995.

Martín-Barajas, A., M. Tellez-Duarte, and J. M. Stock, The Puertecitos Formation: Pliocene volcaniclastic sedimentation along an accommodation zone in northeastern Baja California, in *Pliocene Carbonate and Related Facies Flanking the Gulf of*

California, Baja California, Mexico: Geological Society of America Special Paper 318, edited by M. E. Johnson and J. Ledesma-Vasquez, pp. 1–24, Geological Society of America, 1997.

Matti, J. C., M. M. Douglas, and B. F. Cox, The San Andreas Fault system in the vicinity of the central Transverse Ranges Province, southern California, *Open-File Report 92-354*, U.S. Geological Survey, 1992.

McCarthy, J., S. P. Larkin, G. S. Fuis, R. W. Simpson, and K. A. Howard, Anatomy of a metamorphic core complex: Seismic refraction/wide-angle reflection profiling in southeastern California and western Arizona, *Journal of Geophysical Research*, *96*(B7), 12,259–12,291, 1991.

McCloy, C., J. C. Ingle, and J. A. Barron, Neogene stratigraphy, foraminifera, diatoms, and depositional history of Maria Madre Island, Mexico: Evidence of early Neogene marine conditions in the southern Gulf of California, *Marine Micropaleontology*, *13*(3), 193–212, 1988.

McDougall, K., R. Poore, and J. Matti, Age and environment of the Imperial Formation near San Gorgonio Pass, California, *Journal of Foraminiferal Research*, *29*(1), 4–25, 1999.

McFadden, L., and R. Weldon, Rates and processes of soil development on Quaternary terraces in Cajon Pass, California, *Geological Society of America Bulletin*, *98*, 280–293, 1987.

McNeilan, T., T. K. Rockwell, and G. Resnick, Style and rate of Holocene slip, Palos Verdes fault, southern California, *Journal of Geophysical Research*, *101*(B4), 8317–8334, 1996.

Melbourne, T. L., and J. Stock, Evidence for differential fault block rotation within the Puertecitos Volcanic Province, NE Baja California, Mexico, in *Abstracts, Ge-*

ological Society of America, Cordilleran Section Meeting., edited by Anonymous, vol. 3, p. 73, Geological Society of America, Boulder, CO, 1994.

Merrill, R. T., and M. W. McElhinny, *The Earth's Magnetic Field: Its History, Origin, and Planetary Perspective*, Academic Press, London, 1983.

Minch, J. A., The Late Mesozoic-Early Tertiary framework of continental sedimentation, northern Peninsular Ranges, Baja California, Mexico, in *Eocene Depositional Systems*, edited by J. A. Minch, pp. 43–68, Pacific Section, Society of Economic Minerologists and Paleontologists, Los Angeles, California, 1979.

Molina-Cruz, A., Biostratigraphy and paleoceanographic significance of the radiolarians from the protomouth of the Gulf of California, *Ciencias Marinas*, *20*(4), 441–465, 1994.

Muehlberger, W. R., A. R. Moustafa, and P. R. Tauvess, Tectonic map of North America, 1996.

Nagy, E. A., Extensional deformation and volcanism within the northern Puertecitos volcanic province, Sierra Santa Isabel, Baja California, Mexico, Ph.D. Thesis, California Institute of Technology, 1997.

Nagy, E. A., Extensional deformation and paleomagnetism at the western margin of the Gulf Extensional Province, Puertecitos Volcanic Province, northeastern Baja California, Mexico, *GSA Bulletin*, *112*(6), 857–870, 2000.

Nagy, E. A., and J. M. Stock, Structural controls on the continent-ocean transition in the northern Gulf of California, *Journal of Geophysical Research*, *105*(B7), 16,251–16,269, 2000.

Nagy, E. A., M. Grove, and J. M. Stock, Age and stratigraphic relationships of pre- and syn-rift volcanic deposits in the northern Puertecitos Volcanic Province, Baja California, Mexico, *Journal of Volcanology and Geothermal Research*, *93*, 1–30, 1999.

National Imagery and Mapping Agency, Digital Terrain Elevation Data (Northwest Mexico), 1993.

Neuhaus, J. R., Volcanic and Nonmarine Stratigraphy of Southwest Isla Tiburón, Gulf of California, Mexico, Master's, San Diego State University, 1989.

Nicholas, A., Novel type of crust produced during continental rifting, *Nature*, *315*, 112–115, 1985.

Ortega-Rivera, A., et al., Chronological constraints on the thermal and tilting history of the Sierra San Pedro Mártir Pluton, Baja California, Mexico, from U/Pb, ^{40}Ar/^{39}Ar, and fission-track geochronology, *GSA Bulletin*, *109*(6), 728–745, 1997.

Ortlieb, L., Quaternary vertical movements along the coasts of Baja California and Sonora, in *The Gulf and Peninsular Province of the Californias*, edited by J. P. Dauphin and B. R. T. Simoneit, vol. 47 of *AAPG Memoir*, pp. 447–480, The American Association of Petroleum Geologists, Tulsa, Oklahoma, 1991.

Ortlieb, L., J. C. Ruegg, J. Angelier, B. Colletta, M. Kasser, and P. Lesage, Geodetic and tectonic analyses along an active plate boundary: The central Gulf of California, *Tectonics*, *8*(3), 429–441, 1989.

Oskin, M., J. Stock, and A. Martín-Barajas, Rapid localization of Pacific-North America plate motion in the Gulf of California, *Geology*, *29*(5), 459–462, 2001.

Parsons, T., and J. McCarthy, Crustal and upper mantle velocity structure of the Salton Trough, southeast California, *Tectonics*, *15*(2), 456–471, 1996.

Paz-Moreno, F., A. Demant, and R. Ornelas-Solís, Las ignimbritas hiperalcalinas neogenas de la region de Hermosillo, Sonora, Mexico: Mineralogia y geoquimica, in *Cuarta Reunion Sobre La Geologia Del Noroeste de Mexico y Areas Adyacentes*, edited by T. Calmus and E. Pérez-Segura, vol. 2, pp. 90–91, National Autonomous University of Mexico and the University of Sonora, Hermosillo, Sonora, Mexico, 2000.

Paz-Moreno, F. A., and A. Demant, The recent Isla San Luis volcanic centre: petrology of a rift-related suite in the northern Gulf of California, Mexico, *Journal of Volcanology and Geothermal Research*, *93*, 31–52, 1999.

Pederson, J. L., How much rock uplift in the Colorado Plateau can be attributed to post-Laramide erosion and isostatic response?, in *Geological Society of America Annual Meeting : Abstracts with Programs*, edited by Anonymous, vol. 7, pp. A–41, Geological Society of America, Reno, Nevada, 2000.

Persaud, P., A. Gonzalez-Fernandez, M. S. Steckler, J. M. Stock, A. Martin-Barajas, G. S. Mountain, and J. B. Diebold, Multichannel seismic imaging of active tectonics, NW Gulf of California, *EOS Transactions, AGU Fall Meeting Abstracts*, 1999.

Phillips, J. R., Stratigraphy and structural setting of the Mid-Cretaceous Olvidada Formation, Baja California Norte, Mexico, in *The Prebatholithic Stratigraphy of Peninsular California*, edited by R. G. Gastil and R. H. Miller, vol. 279 of *Geological Society of America Special Paper*, pp. 97–106, Geological Society of America, Boulder, CO, 1993.

Phillips, R. P., Seismic refraction studies in Gulf of California, in *Marine Geology of the Gulf of California: American Association of Petroleum Geologists Memoir 3*, edited by T. Van Andel and G. G. Shor, pp. 90–121, American Association of Petroleum Geologists, Tulsa, Oklahoma, 1964.

Ponti, D. J., The Quaternary alluvial sequence of the Antelope Valley, California, *Geological Society of America Special Paper*, *203*, 79–96, 1985.

Poole, F. G., W. B. Berry, and R. J. Madrid, Ordovician eugeoclinal rocks on Turner Island in the Gulf of California, Sonora, Mexico, in *Simposio de la Geologia de Sonora y Areas Adjacentes*, edited by C. Gonzalez-Leon and E. L. Vega-Granillo, vol. 3, University of Sonora (UNISON) and the National Autonomous University of Mexico (UNAM), Hermosillo, MX, 1993.

Powell, R. E., Balanced palinspastic reconstruction of pre-late Cenezoic paleogeology, southern California: Geologic and kinematic constraints on evolution of the San Andreas fault system, in *The San Andreas fault system: Displacement, palinspastic reconstruction, and geologic evolution: Geological Society of America Memoir 178*, edited by R. E. Powell, I. Weldon, R. J., and J. C. Matti, pp. 1–106, Geological Society of America, Boulder, CO, 1993.

Quarles, M. J., Geology of the Repetto and Montebello hills (California), Master's, California Institute of Technology, 1941.

Radelli, L., The ophiolites of Caimalli and the olvidada nappe of northeastern Baja California and west-central Sonora, Mexico, in *Geologic studies in Baja California*, edited by P. L. Abbott, vol. 63, pp. 79–85, Society of Economic Paleontologists and Mineralogists, Pacific Section, 1989.

Reid, H. F., Mechanics of the earthquake, in *The California Earthquake of 1906, Volume II*, edited by A. C. Lawson, p. 192, Carnegie Institute of Washington, Washington, D.C., 1910.

Renne, P. R., A. L. Deino, R. C. Walter, B. D. Turrin, C. C. I. Swisher, T. A. Becker, G. H. curtis, W. D. Sharp, and A. R. Jaouni, Intercalibration of astronomical and radioisotoic time, *Geology*, *22*, 783–786, 1994.

Rhodes, J. M., Geochemistry of the 1984 Mauna Loa eruption: Implications for magma storage and supply, *Journal of Geophysical Research*, *93*(B5), 4453–4466, 1988.

Richard, S. M., Palinspastic reconstruction of southeastern California and southwestern Arizona for the Middle Miocene, *Tectonics*, *12*(4), 830–854, 1993.

Rockwell, T. K., D. L. Johnson, E. A. Keller, and G. R. Dembroff, A late Pleistocene-Holocene soil chronosequence in the central Ventura Basin, southern California,

U.S.A., in *Geomorphology and Soils*, edited by K. Richards, R. Arnett, and S. Ellis, pp. 309–327, George Allen and Unwin, 1985.

Rockwell, T. K., C. Loughman, and P. Merifield, Late Quaternary rate of slip along the San Jacinto fault zone near Anza, southern California, *Journal of Geophysical Research*, *95*, 8593–8605, 1990.

Rose, T. P., R. E. Criss, and G. R. Rossman, Irradiative coloration of quartz and feldspars with application to preparing high-purity mineral separates, *Chemical Geology*, *114*, 185–189, 1994.

Rothstein, D., Metamorphism and Denudation of the Eastern Peninsular Ranges Batholith, Baja California Norte, Mexico, Ph.D., University of California, Los Angeles, 1997.

Rubin, C. M., S. C. Lindvall, and T. K. Rockwell, Evidence for large earthquakes in metropolitan Los Angeles, *Science*, *281*(5375), 398–402, 1998.

Sabins, F. F., *Remote sensing: Principles and interpretation*, 3rd ed., W. H. Freeman and Company, New York, 1996.

Sawlan, M. G., Magmatic evolution of the Gulf of California rift, in *The Gulf and Peninsular Province of the Californias*, edited by J. P. Dauphin and B. R. T. Simoneit, vol. Memoir 47, pp. 301–370, The American Association of Petroleum Geologists, Tulsa, OK, 1991.

Sawlan, M. G., and J. G. Smith, Petrologic characteristics, age, and tectonic setting of Neogene volcanic rocks in northern Baja California, in *Geology of the Baja California Peninsula*, edited by V. A. Frizzell, vol. 39, pp. 237–251, Pacific Section of the Society of Economic Paleontologists and Mineralogists, Los Angeles, California, 1984.

Schmidt, K. L., Investigation of Arc Processes: Relationships Among Deformation, Magmatism, Mountain Building, and the Role of Crustal Anisotropy in the Evolu-

tion of the Peninsular Ranges Batholith, Baja California, Ph.D. Thesis, University of Southern California, 2000.

Schneider, C., C. Hummon, R. Yeats, and G. Huftile, Structural evolution of the northern Los Angeles Basin, California, based on growth strata, *Tectonics*, *15*(2), 341–355, 1996.

Sedlock, R. L., F. Ortega-Gutierrez, and R. F. Speed, *Tectonostratigraphic terranes and tectonic evolution of Mexico*, vol. 278 of *Geological Society of America Special Paper*, Geological Society of America, Boulder, CO, 1993.

Sharp, R. V., San Jacinto fault zone in the Peninsular Ranges of southern California, *Geological Society of America Bulletin*, *78*, 705–729, 1967.

Shaw, J. H., and P. M. Shearer, An elusive blind-thrust fault beneath metropolitan Los Angeles, *Science*, *283*, 1516–1518, 1999.

Shaw, J. H., and J. Suppe, Earthquake hazards of active blind-thrust faults under the central Los Angeles Basin, California, *Journal of Geophysical Research*, *101*(B4), 8623–8642, 1996.

Sieh, K., Prehistoric large earthquakes produced by slip on the San Andreas fault at Pallet Creek, California, *Journal of Geophysical Research*, *83*(B8), 3907–3939, 1978.

Sieh, K. E., Addendum report: Supplemental subsurface investigation of potential for seismic deformation of the Metro Red Line Eastside Extension by the Coyote Pass structure, *Tech. rep.*, Earth Consultants International, 1997.

Sieh, K. E., Investigation of the Coyote Pass structure at Cummings and St. Louis Streets, *Tech. rep.*, Earth Consultants International, 1998.

Silver, L. T., and B. W. Chappell, The Peninsular Ranges Batholith: an insight into the evolution of the cordilleran batholiths of southwestern North America, *Transactions of the Royal Society of Edinburgh: Earth Sciences*, *79*, 105–121, 1988.

Silver, L. T., H. P. Taylor, and B. W. Chappell, Some petrological, geochemical, and geochronological observations of the Peninsular Ranges batholith near the international border of the U.S.A. and Mexico, in *Mesozoic Crysalline Rocks: Peninsular Ranges Batholith and Pegmatites, Point Sal Ophialite: Geological Society of America Annual Meeting Guidebook*, edited by P. L. Abbott and V. R. Todd, pp. 83–110, Geological Society of America, Boulder, CO, 1979.

Slyker, R. G., Geologic and Geophysical Reconnaissance of the Valle De San Felipe Region, Baja California, Mexico, Masters, California State University, San Diego, 1970.

Smith, J. T., Cenozoic marine mollusks and paleogeography of the Gulf of California, in *The Gulf and Peninsular Province of the Californias: American Association of Petroleum Geologists Memoir 47*, edited by J. P. Dauphin and B. R. T. Simoneit, vol. 47, pp. 637–666, American Association of Petroleum Geologists, Tulsa, Oklahoma, 1991.

Smith, J. T., J. G. Smith, J. C. J. Ingle, R. G. Gastil, M. C. Boehm, Q. J. Roldan, and R. E. Casey, Fossil and K-Ar age constraints on upper middle Miocene conglomerate, SW Isla Tiburon, Gulf of California, *The Geological Society of America, Cordilleran Section, 81st annual meeting*, *17*(6), 409, 1985.

Soper, E. K., and U. S. Grant, Geology and Paleontology of a portion of Los Angeles, California, *Geological Society of America Bulletin*, *43*, 1041–1068, 1932.

Spencer, J. E., and W. R. Normark, Tosco-Abreojos fault zone: A Neogene transform plate boundary within the Pacific margin of southern Baja California, *Geology*, *7*, 554–557, 1979.

Spencer, J. E., and P. J. Patchett, Sr isotope evidence for a lacustrine origin for the upper Miocene to Pliocene Bouse Formation, lower Colorado River trough, and implications for timing of Colorado Plateau uplift, *GSA Bulletin*, *109*(6), 767–778, 1997.

Spencer, J. E., L. Peters, and W. C. McIntosh, 6 Ma 40Ar / 39Ar date from the Hualapai Limestone and implications for the age of the Bouse formation and Colorado River, *GSA Rocky Mountain Section abstracts with programs*, *30*(6), 37, 1998.

Staff, S. S., *Soil Taxonomy*, vol. 436 of *U.S. Department of Agriculture Handbook*, U.S. Government Printing Office, Washington, D.C., 1975.

Stewart, J. H., Regional characteristics, tilt domains, and extensional history of the later Cenozoic Basin and Range Province, western North America, in *GSA Special Paper 323: Accommodation zones and transfer zones; the regional segmentation of the Basin and Range Province*, edited by J. E. Faulds and J. H. Stewart, vol. 323, pp. 47–74, Geological Society of Ameica, 1998.

Stock, J., A. Martín-Barajas, and M. Tellez-Duarte, Early rift sedimentation and structure along the northeast margin of Baja California, in *Field Conference Guide 1996*, edited by P. L. Abbott and J. D. Cooper, vol. 80, pp. 337–372, Pacific Section of the American Association of Petroleum Geologists and the Pacific Section of the Society of Economic Mineralogists and Paleontologists, San Diego, CA, 1996.

Stock, J. M., Sequence and geochronology of Miocene rocks adjacent to the main gulf escarpment: Southern Valle Chico, Baja California Norte, Mexico, *Geofisica Internacional*, *28*(5), 851–896, 1989.

Stock, J. M., Geologic map of southern Valle Chico and adjacent regions, Baja California, Mexico, *Map and Chart Series (Geological Society of America)*, *76*, 11, 1993.

Stock, J. M., Age and source of pumice lapilli within the San Felipe marine sequence, northeast Baja California, *International meeting on the Geology of the Baja California Peninsula, Ensenada, Baja California Norte, April 6-9, 1997*, 1997.

Stock, J. M., Relation of the Puertecitos Volcanic Province, Baja California, to development of the plate boundary in the Gulf of California, in *Cenozoic Tectonics and*

Volcanism of Mexico, Geological Society of America Special Paper 334, edited by H. Delgado-Granados, G. Aguirre-Diaz, and J. M. Stock, pp. 143–155, Geological Society of America, Boulder, Colorado, 2000.

Stock, J. M., and K. V. Hodges, Pre-Pliocene extension around the Gulf of California and the transfer of Baja California to the Pacific Plate, *Tectonics*, *8*(1), 99–115, 1989.

Stock, J. M., and K. V. Hodges, Miocene to Recent structural development of an extensional acommodation zone, northeastern Baja California, Mexico, *Journal of Structural Geology*, *12*(3), 315–328, 1990.

Stock, J. M., and P. Molnar, Uncertainties and implications of the Late Cretaceous and Tertiary position of North America relative to the Farallon, Kula, and Pacific plates, *Tectonics*, *7*(6), 1339–1384, 1988.

Stock, J. M., A. Martín-Barajas, F. Suárez-Vidal, and M. M. Miller, Miocene to Holocene extensional tectonics and volcanic stratigraphy of northeastern Baja California, Mexico, in *Guidebook for the 1991 Annual Meeting of the Geological Society of America, San Diego, California*, edited by M. Walawender and B. Hanan, pp. 44–67, Geological Society of America, Boulder, Colorado, 1991.

Stock, J. M., C. J. Lewis, and E. A. Nagy, The Tuff of San Felipe: an extensive middle Miocene pyroclastic flow deposit in Baja California, Mexico, *Journal of Volcanology and Geothermal Research*, *93*, 53–74, 1999.

Suppe, J., Geometry and kinematics of fault-bend folding, *American Journal of Science*, *283*, 684–721, 1983.

Suppe, J., and D. A. Medwedeff, Geometry and kinematics of fault-propagation folding, *Ecologae Geologicae Helvetiae*, *83/3*, 409–454, 1990.

Taylor, B., and D. E. Hayes, Origin and history of the South China Sea basin, in *The Tectonic and Geologic Evolution of Southeast Asian Seas and Islands: Part*

2, edited by D. E. Hayes, vol. 27 of *Geophysical Monograph*, pp. 23–56, American Geophysical Union, Washington, D. C., 1983.

Taylor, B., A. M. Goodliffe, and F. Martinez, How continents break up: Insights from Papua New Guinea, *Journal of Geophysical Research*, *104*(B4), 7497–7512, 1999.

Thatcher, W. R., Strain accumulation on the northern San Andreas Fault zone since 1906, *Journal of Geophysical Research*, *80*(35), 4873–4880, 1975.

Thomas, R. G., J. J. Landry, R. J. Turney, J. R. Cummings, J. F. LoBue, J. T. Scheliga, and E. H. Gilmour, Planned utilization of the ground water basins of the coastal plain of Los Angeles County; Appendix A: Ground water geology, *Tech. rep.*, California Department of Water Resources, 1961.

Umhoefer, P. J., R. J. Dorsey, and P. Renne, Tectonics of the Pliocene Loreto basin, Baja California Sur, Mexico, and evolution of the Gulf of California, *Geology*, *22*(7), 649–652, 1994.

Valencia-Moreno, M., P. P. Vargas-Navarro, and M.-E. Barcía-Rivera, Geologia y geochemica del batolito costero de sonora, in *Cuarta Reunion Sobre la Geologia del Noroeste de Mexico y Areas Adyacentes*, edited by T. Calmus and E. Pérez-Segura, vol. 2, pp. 138–139, National Autonomous University of Mexico and the University of Sonora, Hermosillo, MX, 2000.

Van Andel, T., Recent marine sediments of Gulf of California, in *Marine Geology of the Gulf of California: American Association of Petroleum Geologists Memoir 3*, edited by T. Van Andel and G. G. Shor, pp. 216–310, American Association of Petroleum Geologists, Tulsa, Oklahoma, 1964.

Walls, C., T. Rockwell, K. Mueller, Y. Bock, S. Williams, J. Pfanner, J. F. Dolan, and P. Fang, Escape tectonics in the Los Angeles metropolitan region and implications for seismic risk, *Nature*, *394*, 356–360, 1998.

Weaver, S. D., I. L. Gibson, B. F. Houghton, and C. J. N. Wilson, Mobility of rare earth and other elements during crystallization of peralkaline silicic lavas, *Journal of Volcanology and Geothermal Research*, *43*, 57–70, 1990.

Weldon, R., The late Cenozoic geology of Cajon Pass: Implications for tectonics and sedimentation along the San Andreas fault, Ph.D., California Institute of Technology, 1986.

Weldon, R. J., K. E. Meisling, and J. Alexander, A speculative history of the San Andreas fault in the central Transverse Ranges, California, in *The San Andreas fault system: Displacement, palinspastic reconstruction, and geologic evolution: Geological Society of America Memoir 178*, edited by R. E. Powell, I. Weldon, R. J., and J. C. Matti, pp. 161–198, Geological Society of America, 1993.

Wells, D. L., and K. J. Coppersmith, New empirical relationships among magnitude, rupture length, rupture width, rupture area, and surface displacement, *Seismological Society of America Bulletin*, *84*(4), 974–1002, 1994.

Wernicke, B. P., Uniform-sense normal shear of the continental lithosphere, *Canadian Journal of Earth Sciences*, *22*, 108–125, 1985.

Wernicke, B. P., The fluid crustal layer and its implications for continental dynamics, in *Exposed Cross-Sections of the Continental Crust*, edited by M. H. Salisbury and D. M. Fountain, pp. 509–544, Kluwer Academic Publishers, Amsterdam, Netherlands, 1990.

Wernicke, B. P., and P. G. Tilke, Extensional tectonic framework of the U. S. central Atlantic passive margin, in *Extensional Tectonics and Stratigraphy of the North Atlantic Margins*, edited by A. J. Tankard and H. R. Balkwill, vol. 46 of *American Association of Petroleum Geologists Memoir*, pp. 7–22, American Association of Petroleum Geologists, Tulsa, OK, 1989.

Wernicke, B. P., et al., Origin of high mountains in the continents: The southern Sierra Nevada, *Science*, *271*, 190–193, 1996.

Whitmarsh, R. B., G. Manatschal, and T. A. Munshull, Evolution of magma-poor margins from rifting to seafloor spreading, *Nature*, *413*, 150–154, 2001.

Wilson, C. J. N., and W. Hildreth, The Bishop Tuff: New insights from eruptive stratigraphy, *Journal of Geology*, *105*, 407–439, 1997.

Winker, C. D., and S. M. Kidwell, Paleocurrent evidence for lateral displacement of the Pliocene Colorado River delta by the San Andreas fault system, southeastern California, *Geology*, *14*, 788–791, 1986.

Winker, C. D., and S. M. Kidwell, Stratigraphy of a marine rift basin: Neogene of the western Salton Trough, California, in *Field Conference Guide 1996*, edited by L. A. Patrick and J. D. Cooper, vol. 73, pp. 295–336, American Association of Petroleum Geologists, Pacific Section, San Diego, California, 1996.

Wissler, S. G., Stratigraphic formations of the producing zones of the Los Angeles Basin oil fields, in *Geologic Formations and Economic Development of the Oil and Gas Fields of California*, edited by O. P. Jenkins, vol. 118 of *California Department of Natural Resources, Division of Mines Bulletin*, pp. 209–234, California Department of Natural Resources, Sacramento, CA, 1943.

Wright, T. L., Structural geology and tectonic evolution of the Los Angeles Basin, California, in *Active margin basins*, edited by K. T. Biddle, vol. 52 of *Memoir*, pp. 35–134, American Association of Petroleum Geologists, 1991.

Yerkes, R. F., T. H. McCulloh, J. E. Schoellhamer, and J. G. Vedder, Geology of the Los Angeles Basin, California, *U. S. Geological Survey Professional Paper*, *420-B*, 62, 1965.